Phase Equilibrium Studies of Some Basalt-like Compositions in the System $CaO-MgO-Al_2O_3-SiO_2-Na_2O-Fe-O_2$

by

David John Humphries, B.A.

Thesis presented for the Degree of Doctor of Philosophy of the University of Edinburgh in the Faculty of Science

1975

EDINBURGH UNIV. EX BIBL.

ABSTRACT

The geologically relevant phase equilibria in the system $CaO-MgO-Al_2O_3-SiO_2$ involving the phases anorthite, forsterite, diopside, enstatite, spinel and silica are well known. Each of these phases, except silica, is a member of a solid solution series; changing the ratios of the end members of these series will change the phase equilibria. Parts of two larger systems have been studied to evaluate these changes, - $CaO-MgO-Al_2O_3-SiO_2-Na_2O$, in which the albite/anorthite ratio of the plagioclase feldspar can be varied; and $CaO-MgO-Al_2O_3-SiO_2-Fe-O_2$ in which the FeO/MgO ratio of the olivine, pyroxene and spinel solid solution series can be varied.

Relationships in a system with more than three components cannot be simply represented on a sheet of paper; a data reduction scheme was therefore employed to reduce the number of components to four, from which projections could be used to portray the equilibria. The data reduction scheme was so arranged that all members of each of the solid solution series had coordinates in the pseudoquaternary system $XO-YO-R_2O_3-ZO_2$, identical with those of the analogous crystal structure in the system $CaO-MgO-Al_2O_3-SiO_2$. The changes in the phase equilibria could then be evaluated independently of those changes conditioned by the differing molecular weights of the analogous constituents.

In the system $CaO-MgO-Al_2O_3-SiO_2-Na_2O$, anorthite was replaced by molecularly equivalent amounts of albite at

three bulk CIPW normative plagioclase ratios - $An_{68}Ab_{32}$, $An_{51.5}Ab_{48.5}$, and $An_{34.6}Ab_{65.4}$. As a result, the normative plagioclase content of the liquids in equilibrium with the phases forsterite, diopside, enstatite, plagioclase and silica, diopside, enstatite, plagioclase increases. When this is represented in a forsterite projection, the liquids in the equilibria appear to become more R_2O_3-rich. At the same time, the reaction nature of the equilibrium forsterite+spinel+plagioclase+liquid changes to one of coprecipitation, influencing the possible variations which can be achieved in residual liquids during equilibrium or fractional crystallisation. An analysis of the changes for olivine saturated equilibria is presented, and shows that bulk compositions having albite-rich normative plagioclase ratios and which are peraluminous in the CIPW norm, are unable to produce the silica saturated residual liquids which bulk compositions having more anorthite-rich normative plagioclase ratios could produce.

In the system $CaO-MgO-Al_2O_3-SiO_2-Fe-O_2$, MgO was replaced by molecularly equivalent amounts of FeO at several ratios, and the pO_2 of the atmosphere of the experiments was controlled at about the pO_2 of the Ni/NiO and Fe/FeO equilibria. The changes in the phase fields as the FeO/MgO ratio increased is gradual, more marked changes occurring at high FeO/MgO mole ratios (greater than 3), due to the instability of the pyroxenes in the MgO-poor systems. The instability of fayalitic olivine at the pO_2 of the Ni/NiO equilibrium also contributed to these changes, along

with the increased stability of a spinel phase as the atmosphere became more oxidising. The effect on the normative composition of the liquids depended on the pO_2 of the atmosphere - at low pO_2 conditions, the normative anorthite content of the liquids decreased with increasing FeO/MgO ratio, but in olivine projection this was shown also as a decrease in R_2O_3 content; in more oxidising conditions, the normative anorthite content of the liquids again decreased, but in the olivine projection this was now shown as an increase in R_2O_3 content. The reaction nature of the equilibrium olivine+spinel+anorthite+liquid remained throughout, enabling the variation in residual liquid compositions obtainable, to be as equally variable with changing FeO/MgO ratio, as in the iron-free system.

Similar trends of iron enrichment or silica enrichment depending on the pO_2 conditions of crystallisation outlined by previous studies on simpler systems are still present in the more complex system. The precise delineation of crystallisation histories could not be attempted until information on the phase compositions and liquid compositions is obtained. The low variance equilibria within the system are postulated, two inferred univariant equilibria being those involving olivine+silica+low-Ca pyroxene+anorthite+high-Ca pyroxene+spinel+liquid and olivine+silica+low-Ca pyroxene+anorthite+high-Ca pyroxene+iron metal + liquid.

The data obtained are then combined with previous data on the system $CaO-MgO-Al_2O_3-SiO_2-Na_2O-Fe-O_2$ to predict phase relations as the albite/anorthite and FeO/MgO ratios

changed together. The results are then compared to results for a series of natural compositions from terrestrial (Reunion Island, Indian Ocean) and lunar sources studied under the same conditions. The comparison revealed that although the agreement was better than when the system $CaO-MgO-Al_2O_3-SiO_2$ was used alone, there was still some disagreement, the major cause of which was thought to be due to the TiO_2 content of the natural samples. A comparison was also made of crystallisation histories from simple synthetic systems and natural melting studies, the previous discrepancies being explained by using realistic comparisons in the synthetic systems.

CONTENTS

Volume 1

		Page
CHAPTER 1	INTRODUCTION	
1.1	Introduction	1
1.2	Scope of this research	4
CHAPTER 2	EXPERIMENTAL TECHNIQUE	
2.1	Introduction	6
2.2	Preparation of compositions	8
	2.2.1 Synthetic compositions	8
	2.2.2 Natural compositions	14
2.3	Furnace operation	15
2.4	Temperature control	21
2.5	Atmospheric control	27
2.6	Containers	38
2.7	Length of experiments	42
2.8	Identification of phases	44
CHAPTER 3	METHOD OF PRESENTATION OF RESULTS	
3.1	The problem	48
3.2	The data reduction scheme	50
3.3	Shorthand notation	58
3.4	Interpretation of diagrams	59
CHAPTER 4	THE SYSTEM $CaO-MgO-Al_2O_3-SiO_2$	
4.1	Introduction	66
4.2	Previous research	67
4.3	Experimental results	69
4.4	Discussion	73

		Page
CHAPTER 5	THE SYSTEM $CaO-MgO-Al_2O_3-SiO_2-Na_2O$	
5.1	Introduction	75
5.2	Previous research	77
5.2.1	The system $MgO-Al_2O_3-SiO_2-Na_2O$	77
5.2.2	The system $CaO-MgO-Al_2O_3-SiO_2-Na_2O$	79
5.3	Experimental results	82
5.4	Discussion	87
CHAPTER 6	THE SYSTEM $CaO-MgO-Al_2O_3-SiO_2-Fe-O_2$	
6.1	Introduction	93
6.2	Previous research	94
6.2.1	Introduction	94
6.2.2	The system $MgO-SiO_2-Fe-O_2$	94
6.2.3	The system $CaO-MgO-SiO_2-Fe-O_2$	96
6.2.4	The system $CaO-MgO-Al_2O_3-SiO_2-Fe-O_2$	99
6.3	Experimental results	103
6.4	Discussion	112
CHAPTER 7	THE SYSTEM $CaO-MgO-Al_2O_3-SiO_2-Na_2O-Fe-O_2$	
7.1	Introduction	118
7.2	Previous research	119
7.3	Discussion	122
CHAPTER 8	MELTING STUDIES ON NATURAL ROCKS	
8.1	Introduction	124
8.2	Previous melting studies	126
8.2.1	Terrestrial samples	126
8.2.2	Lunar samples	130
8.3	Experimental results	132
8.4	Discussion	135

Page

CHAPTER 9 CONCLUSIONS

9.1 Summary 143

9.2 Future studies 145

ACKNOWLEDGEMENTS 146

REFERENCES 147

APPENDIX A ABBREVIATIONS A1

APPENDIX B COMPOSITIONS OF STARTING MATERIALS

B.1 Compositions studied in the system $CaO-MgO-Al_2O_3-SiO_2$ B1

B.2 Compositions studied in the system $CaO-MgO-Al_2O_3-SiO_2-Na_2O$ B4

B.2.1 Anorthite:albite CIPW normative ratio = 67.97:32.03 Wt% B4

B.2.2 Anorthite:albite CIPW normative ratio = 51.48:48.52 Wt% B7

B.2.3 Anorthite:albite CIPW normative ratio = 34.66:65.34 Wt% B10

B.3 Compositions studied in the system $CaO-MgO-Al_2O_3-SiO_2-Fe-O_2$ B13

B.4 Natural compositions B24

APPENDIX C DETAILS OF FURNACE OPERATIONS

C.1 Furnace operations involving compositions in the system $CaO-MgO-Al_2O_3-SiO_2$ and $CaO-MgO-Al_2O_3-SiO_2-Na_2O$ C1

C.2 Furnace operations involving compositions in the system $CaO-MgO-Al_2O_3-SiO_2-Fe-O_2$ and natural samples C11

APPENDIX D DETAILS OF ATMOSPHERIC CONTROL D1

Page

APPENDIX E RESULTS OF QUENCHING EXPERIMENTS

E.1 Compositions in the system $CaO-MgO-Al_2O_3-SiO_2$ E1

E.2 Compositions in the system $CaO-MgO-Al_2O_3-SiO_2-Na_2O$ E5

E.2.1 Compositions with CIPW normative anorthite: albite ratio = 67.97:32.03 E5

E.2.2 Compositions with CIPW normative anorthite:albite ratio = 51.48:48.52 E8

E.2.3 Compositions with CIPW normative anorthite:albite ratio = 34.66:65.34 E11

E.3 Compositions in the system $CaO-MgO-Al_2O_3-SiO_2-Fe-O_2$ E14

E.3.1 Results at the FeFeO equilibrium E14

E.3.2 Results at the NiNiO equilibrium E38

E.3.3 Results in air atmosphere E53

E.4 Natural compositions E56

APPENDIX F CALCULATION OF CO-ORDINATES IN PROJECTION DIAGRAMS F1

APPENDIX G PUBLISHED PAPERS G1

FIGURES Volume 2

CHAPTER 1

INTRODUCTION

1.1 Introduction

Basaltic rocks are chemically very complex - that is, the chemical system in which their complete chemical analysis can be expressed, involves a large number of oxides. The detailed experimental study of such a system is unrealisable at present. Fortunately, approximately 80-85% of the total chemical analysis of any such rock can be represented in the synthetic system $CaO-MgO-Al_2O_3-SiO_2$ (CMAS*). It is also fortunate that the most common minerals in basaltic rocks - members of the plagioclase, pyroxene, olivine and spinel solid solution series - all have a structural representative or analogue in this system.

Study of the system CMAS experimentally at atmospheric pressure could therefore provide important clues to the origins, mechanisms of evolution and relationships between the many widely different igneous rock types. The study of parts of this system has been undertaken over the past decades by many researchers (for example, Bowen, Schairer and co-workers at the Geophysical Laboratory, Washington; Osborn and co-workers at The Pennsylvania State University), who have presented many points of interpretation of basalt and peridotite petrogenesis on the basis of their results.

At the same time, the problem has been approached, to a limited extent only, by experiments on the natural rocks

---

* Abbreviations in Appendix A.

themselves - melting studies - to determine the equilibrium phase relations (for example, Tilley, Yoder and Schairer (1963, 1964, 1965, 1967, 1968); Thompson (1972) and references therein). While in general, the same phases occur in the natural rocks as in the melting experiments, their order of appearance often does not agree with that determined from petrographic study, for example, the Snake River and Skye lavas (Thompson (1972)). The order also does not in general agree with that predicted from the synthetic system CMAS for a molecularly equivalent composition (see O'Hara (1968), Jamieson (1969, 1970)).

One reason for the discrepancy is obvious - the remaining 15-20% of the analysis contains oxides which have a pronounced effect on the order and temperatures of appearance of the phases. Indeed, those representatives of the solid solution series mentioned above, that are not in the system CMAS, contain oxides present in this "minor" fraction of the analysis - in the plagioclase series Na_2O (albite), in the pyroxene and olivine series FeO (hedenbergite, ferrosilite, fayalite), and in the spinel series FeO, Fe_2O_3, and TiO_2 (hercynite, ilmenite, haematite). Other constituents also occur in these solid solution series, but these are the important ones.

Several studies have been undertaken on systems involving these additional components (for example, the simplified basalt tetrahedron (Yoder and Tilley (1962); the join Anorthite-Forsterite-Silica-Fe-O_2 (Roeder and Osborn (1966)), but even these works add up to only a small portion of those data needed to describe a more complete

natural basalt system. Since many of the constituents of a basalt are present in only very small quantities, a better simplification than that previously used is to consider the main eight components: CMASNKT-Fe-O_2.

The experimental study of the geologically relevant portion of such a synthetic system will yield results more applicable to the natural system than those previously obtained, and possible processes operating in nature can then be evaluated with more precision.

1.2 Scope of this research

Before the eight component synthetic basalt system can be completely portrayed and its secrets revealed, the simpler subsystems must be adequately examined experimentally. To this end, the system CMASN-Fe-O_2 is considered in this thesis, by studying the two further subsystems CMASN and CMAS-Fe-O_2. Behaviour in that part of the six component synthetic system relevant to basalts is then inferred from these results. At the same time data from natural rocks - both terrestrial and lunar - melted under the same conditions in this laboratory by co-workers is used to attempt to relate more closely the behaviour in synthetic and natural systems.

Because of the complexities of representing more than three components graphically, the following approach was taken. Joins which had already been studied in the system CMAS were chosen as a base. Selected compositions in these joins were used as generating points for a series of modified compositions; in the system CMASN, the anorthite content of each original CMAS composition was replaced by a molecularly equivalent amount of plagioclase with a fixed albite/anorthite ratio; in the system CMAS-Fe-O_2, the MgO content was replaced by a molecularly equivalent amount of MgO plus FeO having a fixed MgO/FeO ratio. By application of an isostructural molecularly equivalent data reduction scheme (O'Hara (1968); Jamieson (1969)), these analyses were reduced to four components equivalent to CaO, MgO, Al_2O_3, SiO_2, after which, each altered composition had identical co-ordinates in the reduced system as the original unaltered

composition had in the system CMAS. The effect of albite/anorthite and MgO/FeO changes on phase relations can then be examined independently of any effects due to changes in the molecular weights.

It was an aim of this study that the more accurate prediction of the crystallisation behaviour of a basaltic rock composition at atmospheric pressure should be achieved, and the validity of established theories on the behaviour of basaltic liquids in the presence of additional components examined.

CHAPTER 2

EXPERIMENTAL TECHNIQUE

2.1 Introduction

In terms of phase equilibrium research, a number of different techniques are available for studying at atmospheric pressure any desired chemical system. The value of the results obtained by an experimenter using one technique, in comparison with those obtained by another using a different technique, will depend largely on the researchers' understanding and complete knowledge of his technique and apparatus, and those of others. It is therefore essential that the means by which the results were obtained be stated as fully and clearly as possible.

Concentration of phase equilibria research in a few centres, has meant that several researchers can use similar apparatus to study different systems, leading to some intra-laboratory consistency in the approach to the study of phase equilibria. Evaluation of each particular feature of the technique is therefore only required to be undertaken once and need only be repeated for major changes in technique. Thus many of the facets of the technique used in this laboratory have already been reported in the literature in many diverse places, by various authors (see sections below). In order to state clearly and fully the technique used here, the important points are combined in this Chapter with some new information.

Much of the precise information presented for this laboratory has not been given by other workers for their

techniques. Inter-laboratory comparisons are, therefore, made difficult, and differences in the conditions reported for a particular equilibrium should be interpreted with caution.

2.2 Preparation of compositions

2.2.1 Synthetic compositions

The first requirement for any phase equilibria research in synthetic systems is accurately prepared, homogeneous compositions on which to conduct the study. To this end, synthetic compositions have been prepared in four possible states for use in experiments in the past: glass, devitrified glass, mixed oxides and "gels". In recent years, differing results on identical compositions prepared differently, has led to the investigation and comparison of some of these methods of preparation and an analysis of the different results obtained (for example, Hamilton and Henderson (1968); Biggar and O'Hara (1969a); Biggar, O'Hara, Humphries, and Peckett (1972)).

Glasses, though very homogeneous, have been shown to be poor starting materials because of delayed nucleation of phases even in long run lengths, and also suffer from loss of volatile oxides during preparation (for example, Na_2O,K_2O (Schairer and Bowen (1955,1956))). Crystal sizes in the run products are also fairly small. Devitrified glasses suffer similarly though to a lesser degree. Mixed oxides suffer from the possibility of non-homogeneity, unless ground very finely and intimately mixed, and even then sampling errors are possible. "Gels" are submicroscopically homogeneous, very fine-grained, have no nucleation problems with respect to glasses, and grow moderately large, euhedral crystals. The physical state and homogeneity of "gel" starting materials has been examined and found very satisfactory by Hamilton and Henderson (1968) and Biggar and

O'Hara (1969a). "Gels" were therefore considered the most satisfactory starting material, being moderately easy to prepare accurately and involve no loss by volatilization during preparation of alkali-bearing compositions.

The precise method of preparation of a "gel" composition has varied. The basic method is to obtain a solution containing one salt of each element, such that after addition of an excess of ammonium hydroxide, the hydroxides of each element are precipitated. The resulting precipitate is then dried, and roasted until constant weight is achieved.

Thus, Roy (1956) and Luth and Ingamels (1965) volumetrically mixed nitrate solutions of the elements, added silica as ethylorthosilicate or ludox (varying sodium contamination), and then hydrolysed with ammonium hydroxide. Volumetric dispensation was not considered entirely satisfactory by them, suggesting weight burettes as a better alternative. Hamilton and Henderson (1968) and Elsdon, Hamilton and Nolan (1972) mixed weighed amounts of suitable solid starting materials for each element, added sufficient dilute nitric acid to form a nitrate solution, followed by tetraethylorthosilicate and ammonium hydroxide for hydrolysis. This method is good for the preparation of small numbers of compositions. Hamilton and MacKenzie (1960) used a slight variation, mixing the nitrate solution of the elements with previously prepared silica (made by hydrolysing tetraethylorthosilicate and roasting). The resultant mixture was then dried out and roasted. This method has the advantage of no production of ammonium nitrate and the avoidance of the low, possibly variable, yield of silica

from tetraethylorthosilicate. The decomposition of nitrates to the oxides is probably equally satisfactory to the decomposition of the hydroxides, but the possible advantage of the "gel" structure, obtained by the precipitation of the hydroxides, is lost. Biggar and O'Hara (1969a) mixed nitrate solutions of each element by weight, added silica as tetraethylorthosilicate and hydrolysed with ammonium hydroxide. This method involved the use of a more concentrated nitric acid than previously, requiring more ammonium hydroxide for hydrolysis with consequent production of large amounts of potentially explosive ammonium nitrate. The drying process therefore was extended compared to the previous methods. However, this method is the most convenient for preparing large numbers of "gels" from stock standard solutions of the elements.

The problem of preparing iron-bearing "gels" - the difficulty of preventing precipitation of ferric hydroxide when iron is dissolved in dilute nitric acid - was overcome by Heald, Reaker and Herrington (1969) by the use of a standardised solution of ferric benzoate in N,N-dimethyl formamide. Preparation of this solution is however somewhat tedious. Elsdon, Hamilton and Nolan (1972) suggested dissolving iron filings in dilute nitric acid in an ice bath, and adding to the nitrate solution of the other elements at the last moment to avoid precipitation. Biggar and O'Hara (1969a), however, had little difficulty in dissolving iron sponge in an excess of 45% nitric acid to make a stable standard solution.

The method of preparation described by Biggar and O'Hara (1969a) was therefore followed. Stock solutions of each of the elements, except silicon, were prepared at concentrations below the solubility of the nitrates at room temperature, using 45% nitric acid prepared from AnalaR concentrated nitric acid and distilled water.

a) Magnesium solutions: Approximately 14.8 gms of Magnesium crystals (Spectrographic pure; Johnson, Matthey and Co. Ltd.), plus 30 mls of distilled water, were slowly dissolved in 180 mls 45% nitric acid in a conical flask, in an ice tray, on a magnetic stirrer.

b) Calcium solutions: Calcium carbonate (AnalaR; 99.5% minimum assay) was dried at 400°C for at least one hour. Approximately 45 gms $CaCO_3$, plus 80 mls distilled water, were dissolved in 110 mls 45% nitric acid in a conical flask.

c) Aluminium solutions: Approximately 7.5 gms of Aluminium dust (99.99% assay; The British Aluminium Co. Ltd.), were slowly dissolved in 210 mls 45% nitric acid in a conical flask. The flask was then kept at 60-90°C on a water bath until all the powder had dissolved.

d) Iron solutions: Approximately 18.5 gms of iron sponge (99.995% assay; Johnson, Matthey and Co. Ltd.), plus 10 mls of distilled water, was very slowly dissolved in 140 mls 45% nitric acid in a conical flask, in an ice tray. After the reaction had slowed, the flask was kept at 60-90°C on a water bath for several days until the iron sponge was entirely dissolved.

e) Sodium solutions: Sodium carbonate (AnalaR; 99.9% assay after heating) was dried at 400°C for at least one hour.

Approximately 10 gms Na_2CO_3, plus 30 mls of distilled water, were dissolved in 40 mls of 45% nitric acid in a conical flask.

Once dissolved, each solution was very carefully transferred to a 250 ml volumetric flask and made up to 250 mls with distilled water. The weight of solution required to give one gram of the relevant oxide was then calculated. The concentration of each solution, together with a measure of the possible errors introduced by the accuracy of the weighing balance, are summarised in table 2.1. It is readily apparent from this tabulation that the major source of error in the preparation of the standard solution is in the accuracy of weighing the original solid component sources. This accuracy was considered sufficient for the compositions required in this study, but a more accurate weighing balance must be used if very accurate compositions, for example, stoichiometric compositions, are required.

A 10 gm batch of each composition required was prepared by weighing, into a 500 ml polythene container with an air-tight lid, the appropriate amount of each of the stock standard solutions of each element. Each solution was added from a burette reserved solely for nitrate solutions of that element, the readings before and after being noted for use in cases of poor recovery postmortems. 40 mls of ethanol was then added to ensure complete miscibility between the nitrate solution and the organic silica source. The required amount of tetraethylorthosilicate was added, followed by an excess of AnalaR 0.88 ammonium hydroxide to produce a thick precipitate. The mixture was gently shaken

Table 2.1 A measure of the errors in the calculation of the grams of standard solution required to give one gram of each oxide. The calculation is based on a solution weight of 300 gms, except for sodium (250 gms), and a weighing balance accuracy of ± 0.01 gms at each weighing.

Solution	Approx. amt of oxide in solution (gms)	Oxide calc. error (gms)	Gms std soln/gm oxide			
			no errors	soln wt error only	oxide calc error only	max errors
Mg	25	± 0.01658	12.0	± 0.0004	± 0.008	± 0.008
Ca	25	± 0.00560	12.0	± 0.0004	± 0.003	± 0.003
Al	14	± 0.01889	21.4	± 0.0007	± 0.029	± 0.030
Fe	24	± 0.01286	12.5	± 0.0004	± 0.007	± 0.007
Na	6	± 0.00585	41.6̇	± 0.0016̇	± 0.040	± 0.041

during addition of the ammonium hydroxide to ensure complete mixing. The lid was fitted and the "gel" left overnight to complete the precipitation of all the hydroxides.

The "gel" was transferred to a 250 ml Pyrex glass beaker, using an ethanol-distilled water (1:1) mixture as a wash liquid, and dried out slowly at about 60-80°C. Once dry, the "gel" was heated slowly to 200°C, left overnight at 400°C and then transferred to a Palau basin to be left overnight at 900°C to ensure maximum removal of any remaining nitrate. Palau basins which had previously been saturated with iron were used for the iron-bearing compositions. The yield was determined and the sample ground for 10 minutes in an amalgamator.

Later preparations utilised a 250 ml P.T.F.E. beaker with a tightly fitting nylon lid, the "gels" only being transferred to glass beakers after drying out at 200°C. This reduced the problem of "gels" drying out and becoming firmly attached to the glass beaker, leading to a possible source of contamination during removal and poor recoveries.

Recoveries varied depending on the presence or absence of iron. Iron-free "gels" generally achieved 9.93 to 10.02 gms, most being better than 9.97 gms (see Appendix B.1 and B.2). Iron-bearing "gels" had a more variable yield, generally in the range 9.8 to 10.1 gms (all iron recalculated as Fe_2O_3), this value depending on the oxidation state of the iron in each sample in air (see Appendix B.3 for recoveries).

Sources of variability in the weight recovered during the preparation, occur during the transfer of the "gel" from

the polythene container/PTFE beaker to the glass beaker, and then to the Palau basin. No allowance was also made for less than 100% recovery from a standard solution, but allowance was made for the low silica yield (99.7%) determined for the tetraethylorthosilicate by Biggar and O'Hara (1969a). A similar recovery was reported by Hamilton and Henderson (1968) for tetraethylorthosilicate. Biggar and O'Hara (1969a) obtained 99.7-100.1% yields from similar metal nitrate solutions to those used in this study.

Table 2.1 summarised the errors possible during the preparation of the standard solutions; Table 2.2 uses these calculations to estimate the magnitude of the errors possible during the addition of each component during the "gel" preparation. It is apparent therefore that there is between 0.11% and 0.29% error possible in each element added at the 1 gm level. This error will decrease if more than one gram is required, and increase if less than one gram is required.

2.2.2 Natural compositions

The natural samples studied were from Reunion Island, Indian Ocean, and were supplied by Dr. B.G.J. Upton. Each sample was supplied ready ground from the XRF analysis sample, but was reground under acetone until the particle size was less than approximately 20 μm.

Table 2.2 A measure of the errors in the preparation of a "gel" composition, in terms of grams per one gram of each oxide. Calculation based on weighing accuracy of ± 0.01 gms at each weighing.

Solution	Correct std soln calc. Weighing error only	Max std soln error No weighing error	Max std soln error plus weighing error
Mg	± 0.0008	± 0.0006	± 0.0014
Ca	± 0.0008	± 0.0002	± 0.0011
Al	± 0.0005	± 0.0014	± 0.0019
Fe	± 0.0008	± 0.0005	± 0.0013
Na	± 0.0002	± 0.0010	± 0.0012
Si	± 0.0029		± 0.0029

2.3 Furnace operation

The equipment used to conduct experiments at atmospheric pressure to determine phase equilibrium diagrams by the observation and recognition of the appearance of phases versus temperature for particular compositions, has either been a "quenching" furnace (notably used by Bowen, Schairer at the Geophysical Laboratory, Washington (details in Shepherd, Rankin and Wright (1909))), or in recent years on a smaller scale, hot-stage microscopes. The latter suffer from the disadvantage that only very small single samples can be used at a time, and temperature control and calibration is not as satisfactory as in quenching furnaces, but have the advantage of being able to view the phases growing as temperature decreases.

The quenching furnace, however, has been used successfully over a long period of time, the advantage being in the ability to load more than one sample at a time; a larger amount of each sample can be used in individual capsules which can be quenched sufficiently fast to preserve the phase assemblage; better temperature measurement and calibration can be maintained; and it is possible to maintain longer runs at approximately constant temperature. This type of furnace was used in this study.

Precise data on the thermal characteristics of quenching furnaces and the assembly used to contain the charges, is only available for the furnaces used in this laboratory (Biggar and O'Hara, 1969b). The thermal behaviour of a furnace and its sample assembly is unique to each furnace, and varies with the temperature and atmosphere

of the furnace. The most important characteristic is the temperature maximum in the thermal profile of these furnaces. Its location must be determined to avoid the superheating of the charge.

All experiments were carried out in the vertical, V25B, furnaces described in detail by Biggar and O'Hara (1969b). The basic design is one of an impervious alumina tube surrounded by a furnace element wound with Pt10%Rh. At either end is attached a water cooling jacket, to carry the gas inlet tube and quenching flask at the bottom, and the gas outlet tube and probe assembly fixture at the top. Each furnace was constructed gas-tight using neoprene O-rings, and the quenching fluid used was water in all cases, which remained in the flask during each run. Temperature control was achieved by a Pt:Pt13%Rh thermocouple built into the furnace element at approximately one third of the length of the element. The thermocouple was linked to a controller, a West Instruments Ltd. Viscount potentiometric controller, which was able to keep the control thermocouple within $\pm$ 2 μV ($\pm$ 0.14^{o}C) of a set point over long periods of time.

The probe assembly used to carry the charges was almost identical to that described by Biggar and O'Hara (1969b). An alumina tube enclosed two heavy duty quench wires and a thermocouple sheath (of alumina tube), which projected approximately 1.5 cm beyond the end of the tube. The assembly containing the charges was attached to this projection by a thin quench wire attached to the main permanent

quench wires, such that the tip of the thermocouple sheath was just above the top of the capsules. The bases of the capsules were about 1 cm below this point, therefore, during each experiment.

The thermocouple used for the measurement of the temperature of the run was contained within the sheath permanently, and was protected from any possible foreign contamination from the charges, and from the harmful atmospheres used in some of the runs. Using this assembly it was possible, having calibrated the thermocouple (section 2.4), to measure the temperature of the run at any time. This procedure was considered much more preferable to that in which the thermocouple measuring the temperature is inserted into the furnace after the run to prevent contamination (Roeder and Osborn (1966), Presnall (1966)).

Very early runs utilised the cemented type of capsule assembly described by Biggar and O'Hara (1969b); later runs however used an improved non-cemented design enabling a more uniform assembly to be maintained. A bucket was constructed out of scrap platinum capsules, slightly taller than the size of the sample containers (1 cm). This bucket was suspended by a suspension wire on an alumina spacer, which in turn was suspended by the quench wire on the end of the thermocouple projection as with the cemented assembly. The advantage of this assembly was in a greater capacity of capsules - up to 18 per experiment run; re-use of the bucket eliminating differences in size of the cemented assembly and therefore different thermal conductivity; and rejection of a possible and likely source of contamination

of the charges by the alumina cement used. No loss in temperature gradient accuracy was found during trial gold calibration experiments (Biggar, personal communication). The thermal gradient within and between capsules in this type of assembly is less than $\frac{1}{2}^{o}C$ at the melting point of gold (1064.43°C).

Various furnaces were used throughout this study. Each furnace was investigated to determine its thermal profile, and frequent temperature calibrations were conducted independently of the other furnaces. The thermal profile of a furnace varies with temperature due to the design of the windings of the element, which were commercially supplied (Johnson, Matthey and Co. Ltd.). Each element had an upper and lower closely wound zone separated by a sparsely wound central zone. The depth at which the upper temperature maximum occurred was determined in each furnace at various temperature extremes by lowering the probe assembly, with a dummy capsule assembly, 1 cm per 45 minutes and recording the emf of the axial thermocouple in the probe. With increasing temperature this maximum moves to higher levels in the furnace (figure 2.1). In those furnaces in which the atmosphere was to be controlled, the appropriate gas flow and gas mixture was used for the determination of the profile. The appropriate running depth was then selected for the temperature range of proposed operations, to avoid superheating of the capsule assembly during insertion of the probe. The running depth is only valid for a particular temperature range, because of migration of the temperature maximum. It is probable

that differently wound furnace elements will produce different thermal profiles to those reported here.

Each experiment was therefore conducted in the following manner. The furnace temperature was set at least four hours, preferably overnight, before the start of a run, following the findings of Biggar and O'Hara (1969b). In controlled atmosphere experiments, the gas mixture required was set up (section 2.5). The probe was lowered gradually in 5 cm/15 minute steps from the cold upper water cooler, into the upper hot zone, until the assembly was 2.5 cm above its final running depth. After at least one hour at this depth, the probe was lowered 1 cm/10 minutes twice and 0.5 cm/10 minutes once to the final mark, where the probe was centred in the furnace by means of a clamping screw at the top of the probe assembly. Visual inspection was possible through the quenching fluid by means of a mirror placed underneath. Run length was calculated from the time the probe reached the final marker.

The thermal history of the measuring thermocouple, and by assumption the charge assembly, was recorded for several runs from the time the probe reached the final mark, using this lowering technique. It was found that no detectable overshoot of the final temperature occurred during the heating period of approximately 1 to 2 hours required for the assembly to reach a constant temperature (figure 2.2). Thermal shock effects on the probe were also reduced with this technique.

At the end of a run, the quench wire was fused enabling the charge assembly to drop into the quench fluid. The

charges were recovered and dried immediately. The probe was then slowly raised, to reduce thermal shock, to the top of the furnace, and the gas supply terminated.

2.4 Temperature control

The emf produced by a thermocouple placed in a furnace varies with temperature and can easily be measured. Reference tables relating temperature and emf for various perfect thermocouple types have been produced. Thus an emf reading for a thermocouple within a furnace can be converted to a precise temperature; a true temperature if the thermocouple junction were perfect. However, it is extremely difficult to produce a perfect thermocouple, and recrystallisation and contamination of the wires involved, require that it is necessary to calibrate the thermocouple against the melting points of well-known and convenient metals or compounds.

The temperature of each experiment was determined by measuring the emf of the axial Pt:Pt13%Rh thermocouple in the probe assembly, using a galvanometer and potentiometer with ice junction. The emf measured was converted to degrees Celsius using the conversion tables supplied by Johnson, Matthey and Co. Ltd.

Calibration of this thermocouple was frequently carried out, using the same probe and capsule assembly to that used in the experiments except that "dummy" capsules, made from scrap platinum capsule material, were loaded into the platinum bucket. The same number of capsules were used in calibration and during runs. The calibrants used were:

Gold	1064.43°C
Lithium metasilicate	1207.9°C
Diopside	1395.3°C

the temperatures being based on the 1968 IPTS Temperature

Scale, following the discussion given by Biggar (1972). In the calibration runs, gold wire (Grade 1; Johnson, Matthey and Co. Ltd.) was contained in a small ceramic sheath in a platinum capsule, since gold forms a low melting temperature alloy with platinum. Lithium metasilicate and Diopside (the same materials as used by Biggar (1972)) were contained in platinum capsules. The melting temperatures were found to be independent of furnace atmosphere by G.M. Biggar (personal communication).

Recent work at this laboratory, and confirmed by Kushiro (1973), has shown that Diopside has a melting interval (Biggar and O'Hara (1969c)); however, for practical purposes the amount of liquid at temperatures below the liquidus is very small, and it is not the appearance of liquid which is taken as the calibration point. Lithium metasilicate probably behaves similarly, or the composition of the mixture is slightly in error, because easily detectable amounts of liquid are observed up to 10°C below the disappearance of the last primary crystal. The very accurate preparation of compositions is a necessity if these compounds are to be used as calibrants. The difficulty of preparation of a stoichiometric composition was highlighted by the study of the Akermanite composition by Biggar (1972a), where most samples of this alleged composition were probably non-stoichiometric. Lithium metasilicate also suffers from quenching growth problems, such that an interpretation of the texture of the run product is necessary, thus introducing a further element of error into the results.

In theory, a calibrant as desirable as a perfectly melting compound would be an isobaric invariant liquid composition, in which total conversion from crystals to liquid occurs at the temperature of the isobaric invariant equilibrium. Such a composition would show a large increase in the amount of the liquid phase, which can be easily recognised, and interpretational ambiguity should therefore be dismissed, so long as quench phases do not appear upon quenching. In practice, an increase of more than 50% liquid is required for unambiguous optical interpretation. This places some restraints on possible calibrants: the temperature contours on the liquidus surfaces about the invariant liquid composition must not be closely spaced; and the composition proposed for the calibrant must not lie in an unfavourable position with regard to the actual first liquid produced and the corresponding subsolidus assemblage, especially if the composition is found not to be the actual isobaric invariant liquid composition. Despite these disadvantages, a greater tolerance in preparation is still possible, and makes these types of compositions practical calibration points.

Two compositions of this type have been investigated: the isobaric invariant liquid compositions for the assemblages Anorthite-Wollastonite-Gehlenite (AWG) and Anorthite-Wollastonite-Silica (AWT) in the system $CaO-Al_2O_3-SiO_2$. The compositions of these liquids has been determined previously by Rankin and Wright (1915), and "gels" were prepared using these compositions (table 2.3).

Table 2.3 The compositions of the calibrants Anorthite-Wollastonite-Gehlenite (AWG) and Anorthite-Wollastonite-Silice (AWT), from Rankin and Wright (1915).

	AWG	AWT
CaO	38.00	23.25
Al_2O_3	20.00	14.75
SiO_2	42.00	62.00
Yield	9.96 gm	9.97 gm

All silicates for use as calibrants must be crystallised to their stable sub-solidus assemblage at as high a temperature as practical. This reduces the possibility of false melting of metastable assemblages, for example, cristobalite instead of tridymite. Thus the AWG composition was prepared at 1100°C for 40 hours, and the AWT composition at 1050°C for 40 hours.

Rankin and Wright, based on an unspecified calibration scale, determined the melting temperatures to be: AWG - 1265°C, AWT - 1170°C, both ± 5°C. The new temperatures determined here are: AWG - 1275.8°C ± 2.2°C and AWT - 1185.6°C ± 0.7°C. The furnace operation details and run results for these compositions are given in table 2.4.

Neither composition studied was the actual isobaric invariant liquid composition. The calibration temperature is taken as the point at which there is a large increase in the amount of liquid, and this was not the point at which the last primary crystal disappeared. The AWG composition was found to melt to the assemblage an+woll+liq but there was a sufficient increase in the percentage of liquid for it to be satisfactory as a calibrant. Later runs have shown that wollastonite is the liquidus phase, this composition having a melting history lasting about 4°C.

The AWT composition melted to the assemblage woll+sil+liq and there was only a small increase in the amount of liquid in the runs conducted over a temperature range of 6°C. The determination of the amount and presence of liquid in these runs was hindered by the small crystal size and the low relief of the crystals in the glass where

Table 2.4 Furnace operation details and run results for the calibrants Anorthite-Wollastonite-Gehlenite (AWG) and Anorthite-Wollastonite-Silica (AWT).

a) Anorthite-Wollastonite-Gehlenite (AWG)

Run	Time hrs.mins	axial emf	calc. temp. ^{o}C	calibrant	result	
8-127	3.00	15881	1389.0	Di	solid	
8-128	3.00	15899	1390.2	Di	solid	
8-129	3.00	15908	1390.8	Di	solid	Mean = $1390.9^{o}C$
8-130	3.15	15911	1391.0	Di	liquid	i.e. + 4.4 ± $0.1^{o}C$
8-131	3.15	13243	1201.5	L_2S	solid	
8-132	3.00	13253	1202.2	L_2S	solid	Mean = $1202.7^{o}C$
8-133	3.00	13268	1203.3	L_2S	liquid	i.e. + 5.2 ± $0.5^{o}C$
8-136	18.15	14233	1272.6	AWG	liquid*	Mean = $1270.8^{o}C$
8-137	18.15	14181	1268.9	AWG	solid	± $1.8^{o}C$

Correction value for $1270.8^{o}C$ is + 5.0 ± $0.4^{o}C$

Anorthite-Wollastonite-Gehlenite melting temperature = 1275.8 ± $2.2^{o}C$

* Assemblage present is an+woll+liq

Table 2.4 (continued)

b) Anorthite-Wollastonite-Silice (AWT)

Run	Time hrs.mins.	axial emf	calc. temp. °C	calibrant	Result	
8-206	3.15	13222	1200.0	L_2S	liquid	
8-207	3.10	13188	1197.5	L_2S	solid	
8-208	3.00	13180	1197.0	L_2S	solid	Mean = 1199.6°C
8-209	3.00	13211	1199.2	L_2S	solid	i.e. + 8.3 ± 0.4°C
8-210	3.00	12768	1167.2	AWT	solid	
8-211	3.00	12848	1173.0	AWT	solid	
8-212	3.00	12912	1177.6	AWT	liquid*	
8-213	3.00	12934	1179.2	AWT	liquid*	Mean = 1173.3°C ± 0.3°C
8-214	3.05	12991	1183.3	AWT	liquid*	
8-215	171.10	12904	1177.0	AWT	solid	

Correction value for 1173.3°C is + 8.3 ± 0.4°C

Anorthite-Wollastonite-Silica melting temperature = 1185.6 ± 0.7°C

* Assemblage present is woll+sil+liq

Abbreviations: Di = Diopside, L_2S = Lithium metasilicate.

present. The small increase in the amount of liquid is only to be expected from an examination of the closeness of the temperature contours about this isobaric invariant liquid (Rankin and Wright (1915), figure 8). This composition was therefore not considered a satisfactory calibrant.

A calibration correction value was determined at each calibration point as necessary, by obtaining one "solid" result (unmelted gold wire or unmelted anorthite-wollastonite-gehlenite; primary crystals of lithium metasilicate or diopside present) and one "liquid" result (melted gold wire, lithium metasilicate or diopside; the appearance of glass (liquid) in anorthite-wollastonite-gehlenite), for a small change in temperature. Occasionally a "melting interval" result was interpreted when the gold wire contained melted beads, or when only one or two primary crystals of lithium metasilicate or diopside were found in the charge.

The correction value varied at each calibration point. Biggar and O'Hara (1969b) and Biggar (1972) showed that the correction values approximate to a very shallow curve. Insufficient calibrations were determined to confirm this behaviour; it was therefore assumed that the calibration value changed in a linear manner between calibration points. Each correction value could also be assigned an error range depending upon the closeness of solid and liquid results. In most cases the correction value to be applied was a positive value, it ranging from up to +17°C to +0°C, the actual value increasing at each calibration point with the age of the thermocouple (all other things remaining

constant).

The quoted temperature of each experiment was determined as follows: the apparent temperature was calculated from the emf measurement using the Pt:Pt13%Rh thermocouple conversion tables. For runs intermediate to calibration determinations, the correction value was calculated by linear interpolation of the correction values at the calibration points. For runs near to calibration determinations, the correction value at that point was often used. The calibration value used, and the calibration determinations on which it is based, for each run are given in Appendix C. The error range for each run was calculated in a similar manner.

2.5 Atmospheric control

Systems involving components which have only one oxidation state are studied at atmospheric pressure in stagnant air atmospheres. Those systems involving components with variable oxidation states, for example iron, require that the atmosphere in which the experiments are conducted be controlled by some means.

The most commonly used method is that of mixing two gases which are relatively inert to the compositions under study, to produce a particular partial pressure of oxygen (pO_2*) in the furnace atmosphere at the run temperature. The one gas dissociates to release a constant amount of oxygen at constant temperature; the other gas combines with some of this oxygen thereby reducing the amount of oxygen in the atmosphere. By varying the proportions of the gases, a varying pO_2, lower than that of the pure dissociating gas, can be obtained.

Common gas mixtures used are CO_2+H_2, CO_2+CO, and H_2O+H_2. The latter mixture is usually preferred for very low pO_2 studies, but imposes the constraint that the gas stream must be kept hot enough to prevent the condensation of the steam. Both of the CO_2-bearing mixtures have been widely used with satisfactory results. However, CO_2+CO mixtures (not pure CO_2) could precipitate carbon in cooler parts of the furnace, depending on the flow rate used and the thermal profile of the furnace, by the dissociation of the CO portion of the mixture. Mixtures of CO_2+H_2 were used

---

* The term pO_2 is used in preference to the more thermodynamically rigorous term fugacity.

here, carbon precipitation from these mixtures only being possible at very low temperatures, and then only from a restricted range of mixtures (Cairns and Tevebaugh (1964)).

Another common technique has been to contain the sample in a container composed of the metal having the variable oxidation state (for example, iron capsules) in an evacuated sealed silica tube. In this method, the phases present are always in equilibrium with the metal concerned (Fe), and the pO_2 is fixed at an unknown value lower than that at which the element is stable with its oxide form in the element-oxygen system.

A further technique has been used in the study of the melting relations of some natural compositions. Here the sample is contained in sealed "inert" capsules in an air atmosphere or in open "inert" capsules in an inert atmosphere, and creates its own individual pO_2 within the capsule by the release of oxygen from the high oxidation state oxides in the sample (for example Fe_2O_3). The process continues until equilibrium is reached between the gas phase and the FeO/Fe_2O_3 ratio in the sample. The actual atmosphere obtained is unknown, and will also be strongly dependent on the amounts of H_2O and CO_2 in the sample. This technique is discussed further in Chapter 8 in connection with the melting studies on natural samples, since none of the synthetic compositions have a predetermined FeO/Fe_2O_3 ratio.

The selection of an appropriate atmosphere to use in iron-bearing systems when gas mixing is used, is extremely important. Various possibilities have been tried previously -

constant pO_2 at all temperatures, constant mixing ratio of the gases at all temperatures, or adjusting the mixture to produce the pO_2 of a particular well-known equilibria at each temperature required - the latter not being very popular. Constant pO_2 was used because regular sections could be studied from oxidising to reducing conditions. Constant mixing ratio is similar, but has the advantage of approaching the pO_2 versus temperature relationship that a buffer possesses. In almost all the previous controlled atmosphere experiments using these two methods, the atmosphere in the furnace in contact with the capsules has not been calibrated. Reliance has always been placed on analysis of the gas at room temperature prior to entry into the furnace. In this study it was decided to conduct the experiments at oxygen partial pressures near to those of recognised equilibria at which the pO_2 is well defined, and where it can be calibrated in the actual experimental configuration to be used.

Having chosen this type of controlled atmosphere experiments, a pO_2-temperature relationship of a known equilibria appropriate to the range of pO_2 measured in a cooling magma lake (Sato and Wright (1966)) and inferred from the study of the opaque minerals in lavas (Anderson (1968)) was chosen. This relationship approximates that for the oxidation of Nickel to Nickel oxide (Ni/NiO) as shown in figure 2.3. The pO_2 versus temperature relationship for this equilibrium has been determined by Campbell and Roeder (1968), Hahn and Muan (1961) and Larimer (1968) and Eugster and Wones (1962) present an equation relating

pO_2 and temperature for this equilibrium. Oxygen partial pressures in this equilibrium are moderately oxidising, being at a higher pO_2 than the oxidation curve for FeO to Fe_3O_4 in the system Fe-O_2; the ratio of Fe_2O_3:FeO in the run products is therefore probably quite high. A pO_2-temperature relationship yielding more reducing conditions was also chosen, this being more appropriate to that of lunar samples; that of the equilibrium between Iron and Iron oxide (Fe/FeO). The ratio of Fe_2O_3:FeO in the run products at this equilibrium will be very small, but no iron metal should appear in the charges. The pO_2 versus temperature relationship for this equilibrium (shown in figure 2.3) has been determined by Darken and Gurry (1945) and Eugster and Wones (1962) present an equation based on this data. Suitable containers are also available to contain the iron-bearing charges at these two pO_2-temperature relationships (see section 2.6).

To determine the calibration correction value at each equilibrium, a sample of Fe_2O_3 (Specpure; Johnson, Matthey and Co. Ltd.), or a Ni+NiO mixture (Specpure; Johnson, Matthey and Co. Ltd.) was included in many experiments (see Appendix D). A mixture of Ni+NiO, in the proportions 90% NiO and 10% Ni, was used following the findings of Hahn and Muan (1961), in order to avoid the presence of large quantities of metal phase which has a tendency to impair attainment of equilibrium. In this sample, the loss of Ni metal should be easily observed on the oxidising side of the equilibrium. The Fe/FeO equilibrium calibrations were conducted exclusively in furnaces 5 and 7; the Ni/NiO

equilibrium calibrations were conducted in furnaces 3 and 5.

The sample of Fe_2O_3 was contained in iron foil packets, the product being either light grey very hard magnetic iron, or a very soft darker nonmagnetic wustite. In some runs a mixture was obtained. In furnace 5 the results were moderately consistent, despite the use of different platinum buckets and new probes due to corrosion (figure 2.4); in furnace 7 the results are slightly more erratic (figure 2.5) possibly due to an even higher corrosion rate at the higher temperatures used. A further possible source of error is in the random positioning of the calibrant capsule in the charge assembly and possible pO_2 gradients within this assembly. The pO_2 gradients within the assembly have not been investigated, but are inferred to be very small if the zone determined for the equilibrium in each furnace is caused by this feature. However, since the pO_2 only varies very slightly for large changes in the $\%H_2$ in the mixture at the 60-70% H_2 level, a line was drawn as a best fit to the data, to determine the calibration curve. The deviation from the true curve is quite large in terms of $\%H_2$, but is small in terms of the pO_2.

The determination of the Ni/NiO calibration was carried out in a similar manner. The sample of Ni+NiO was contained in Nickel packets within a platinum shield to prevent alloying between the Ni and Silver-Palladium capsules. The product was either grey metallic nickel or

light green soft nickel oxide. In a number of runs a mixture was obtained indicating either larger pO_2 gradients than at the Fe/FeO equilibrium or a slow oxidation or reduction rate through the material. In furnace 3, the results (figure 2.6) indicate that the equilibrium could again only be determined as a zone rather than a sharp boundary. A best fit line through the data is used to determine the calibration curve. Again the deviation is only small in terms of pO_2, the control of the $\%H_2$ in the gas mixture being more precise than that used in the Fe/FeO equilibrium calibrations, by using a smaller capillary. (see below). The few results obtained from furnace 5 show a similar relationship (figure 2.7).

The method by which the gas mixtures required were obtained was as follows and is diagrammatically shown in figure 2.8. Commercially supplied CO_2 and H_2 (Air Products Ltd.) were used as the source of the gases. Each gas supplied to each furnace was connected to a manometer tube with a capillary to restrict the flow to measurable amounts. The precise volume of gas passing through the capillary was controlled by the depth of a dip tube in a water tank, through which the excess gas pressure was relieved, the depth of the dip tube being reflected in a measurable pressure drop (in cms) on the manometer tube. In order to relate this measurement to the volume of gas passing through the capillary, each capillary was approximately calibrated by measuring the flow rate per minute for that gas. This enabled the volume per cm measured pressure drop on the

manometer tube to be calculated for each capillary. The composition of the gas and the total volume of flow for any combination of pressure drop measurements could then be calculated. Various sizes of capillary were used, since the dip tubes had a maximum depth of about 20 cms and the accuracy of gas composition required at the two operating conditions was different.

Having attained the correct volume of each gas required passing through the individual capillaries, the two gases were mixed and passed into the furnace. The calculated composition was also periodically checked by analysis of the gas mixture, prior to entry to the furnace, using a Cambridge Instrument Co. Ltd. temperature controlled Katharometer. Approximate agreement was found, the error depending on the calibration value assigned to the capillaries for the calculated composition. Since the gas was not analysed during each run the calculated compositions are used throughout, and calibration is therefore essential.

The gas flow was always up the furnace. The linear flow rate required was chosen to be about 1 cm/sec within the furnace, following the recommendations of Darken and Gurry (1945). The flow of gas up the furnace tube required to maintain this flow rate was calculated to be about 240 ccs/minute.

Calculation of the pO_2 for a particular CO_2/H_2 mixture was performed by computer using a program slightly modified from that described by Biggar (1969). CO_2 and H_2 gases

react according to the following reactions:

$$2CO_2 = 2CO + O_2 \qquad (1)$$

$$2H_2O = 2H_2 + O_2 \qquad (2)$$

which can be combined when both gases are present to give the water-gas reaction:

$$CO_2 + H_2 = CO + H_2O \qquad (3)$$

The equilibrium constants for these reactions, K_1, K_2, and K_3, are related

$$\sqrt{\frac{K_1}{K_2}} = K_3 \qquad (4)$$

Values for K_1 and K_3 were reported by Darken and Gurry (1945) and were used by Biggar (1969) to define computational equations relating K_1 and K_3 to temperature. Values for K_2 were then determined by the above relationship (4).

The pO_2 for an r% volume of H_2 in the gas mixture was calculated by Biggar (1969) as follows:

a) Calculate pCO and pH_2O at equilibrium in the water-gas equilibrium.

Let pCO at equilibrium = x

$$CO_2 + H_2 = CO + H_2O \qquad (5)$$

(100-r-x)(r-x)(x) (x)

$$K_3 = \frac{(x)(x)}{(100-r-x)(r-x)}$$ and solve for x.

b) Insert the volumes of CO_2 (100-r-x) and CO(x) at equilibrium into the CO_2 dissociation reaction:

$$2CO_2 = 2CO + O_2 \qquad (6)$$

(100-r-x) (x)

$$pO_2 = \frac{(K_1)(100-r-x)^2}{(x)^2}$$

Using this method Biggar (1969) noted impossible values for pO_2 at low $\%H_2$ levels. The discrepancy was in the amount of pCO calculated to be in the equilibrium mixture. At low $\%H_2$ levels, the CO_2 dissociation contributes a significant proportion of CO to the equilibrium mixture. The calculation was revised to include the amount of CO produced from the CO_2 reaction assuming no H_2 was present:

a) Let pCO from pure CO_2 = y. Water-gas reaction (5) now becomes

$$\underset{(100-r-x-y)}{CO_2} + \underset{(r-x)}{H_2} = \underset{(x+y)}{CO} + \underset{(x)}{H_2O} \qquad (7)$$

$$K_3 = \frac{(x+y)(x)}{(100-r-x-y)(r-x)} \quad \text{and solve for x.}$$

b) pO_2 calculation now becomes:

$$\underset{(100-r-x-y)}{2CO_2} = \underset{(x+y)}{2CO} + O_2 \qquad (8)$$

$$pO_2 = \frac{(K_1)(100-r-x-y)^2}{(x+y)^2}$$

It has since become apparent that this equation is still not satisfactory when applied to high $\%H_2$ levels because the pCO value (y) from pure CO_2 dissociation was still included in the equations. The amount of pCO from this source was a large proportion of, or even greater than, that generated from the small CO_2 percentage actually in the mixture. It was therefore necessary to use the above equations (7) and (8) up to 50% H_2 mixtures and use equations (4) and (2) at higher levels. The pO_2 for equation (2) is given by

$$\underset{(x)}{2H_2O} = \underset{(r-x)}{2H_2} + O_2 \qquad (9)$$

$$pO_2 = \frac{(K_2)(x)^2}{(r-x)^2}$$

This change was also necessary because of the limits of computational accuracy when dealing with very small numbers at the extreme percentage values.

The calculation of the pCO from CO_2 dissociation at low $\%H_2$ levels was also improved further by a re-iteration procedure. Initially the pCO value (y) is calculated from the $\%CO_2$ in the mixture and the pCO at equilibrium (x) is calculated. The amount of CO_2 at equilibrium is then used to recalculate (y) and (x). The process continues until the value of pCO at equilibrium (x) remains constant.

In the experiments, the furnace atmosphere also contains additional water vapour from the quenching fluid. Biggar (1969) noted this has only a very small effect on the pO_2 at low $\%H_2$ levels. The effect is more marked at high $\%H_2$ levels:

1300°C	10% H_2	0% water	$\log_{10}(pO_2) = -7.85$
		10% water	$\log_{10}(pO_2) = -7.80$
	90% H_2	0% water	$\log_{10}(pO_2) = -12.46$
		10% water	$\log_{10}(pO_2) = -11.81$

A further possible source of error is in the readings on the manometer tubes used to calculate the percentage of H_2 in the mixture. A measure of the errors from this source is given for two typical mixtures in table 2.5.

Values for the equilibrium constants K_1, K_2, and K_3 have also been given by Wagman et al. (1945). A check on the effect this has on the final pO_2 was carried out and

Table 2.5 A measure of the errors in the calculation of the gas composition from the readings on the manometer tubes.

a) Fe/FeO equilibrium region

Assume CO_2 flowrate through capillaries = 13.61 ccs/minute

H_2 flowrate through capillaries = 8.56 ccs/minute

Based on manometer readings:

CO_2 reading = 5.5 cm; H_2 reading = 20.4 cm

$\%H_2$ calculated = 70.00% $\log_{10}(pO_2)$ = -12.17 at 1207.9°C

Assume ± 0.1 cm CO_2 reading error

$\%H_2$ calculated error = ± 0.38% $\log_{10}(pO_2)$ error = ± 0.02

Assume ± 0.1 cm H_2 reading error

$\%H_2$ calculated error = ± 0.11% $\log_{10}(pO_2)$ error = ± 0.01

Assume maximum error

$\%H_2$ calculated error = ± 0.49% $\log_{10}(pO_2)$ error = ± 0.03

b) Ni/NiO equilibrium region

Assume CO_2 flowrate through capillaries = 13.82 ccs/minute

H_2 flowrate through capillaries = 0.368 ccs/minute

Based on manometer readings:

CO_2 reading = 17.2 cm; H_2 reading = 14.3 cm

$\%H_2$ calculated = 2.166% $\log_{10}(pO_2)$ = -7.56 at 1207.9°C

Assume ± 0.1 cm CO_2 reading error

$\%H_2$ calculated error = ± 0.012% $\log_{10}(pO_2)$ error = ± 0.01

Assume ± 0.1 cm H_2 reading error

$\%H_2$ calculated error = ± 0.015% $\log_{10}(pO_2)$ error = ± 0.01

Assume maximum error

$\%H_2$ calculated error = ± 0.027% $\log_{10}(pO_2)$ error = ± 0.01

found to be insignificant: less than $\pm$0.01 in the $-\log_{10}(pO_2)$ value.

It should also be noted that various assumptions regarding the gaseous components are made to simplify these calculations. These have been fully discussed by Nafziger, Ulmer and Woermann (1971).

2.6 Containers

A universal capsule material to satisfactorily contain geologically relevant charge compositions during the experiments has not been found. In systems not involving iron, platinum has been proved suitable and has been used for all types of studies in quenching furnaces. Reaction with the container has not been reported, nor has loss of any oxides other than alkalis by volatilization.

However, containers for iron-bearing systems has always been a problem. Early studies of such systems utilised iron containers, the phases present always being in contact with metallic iron at a low unknown pO_2 (for example Bowen and Schairer (1935)). Later studies in an air atmosphere utilised platinum containers successfully, noting only small iron losses (Muan (1957)) as expected from the data of Taylor and Muan (1962) on the Pt-Fe system.

Between these two extremes, experiments were rarely conducted until Muan (1963) investigated silver-palladium alloys as containers. Silver is a very good container, absorbing very little iron even at an iron activity of 1.0, but has the severe limitation of a low melting point (961.93°C). Addition of palladium (melting point 1554°C) raises the melting point of the alloys which, however, then absorb more iron at a given activity of the metal, leading to greater iron loss from the charge to the container. However, Muan (1963) found that these alloys up to $Ag_{40}Pd_{60}$ were more suitable than platinum, depending on the oxygen potential of the system. At each temperature there is an

optimum composition of alloy to be used as container for iron oxide. The upper temperature and lower pO_2 limits at which silver-palladium alloys of optimum composition can be used was determined by Muan (1963) and is shown in figure 2.3. From this it can be seen that the alloys $Ag_{40}Pd_{60}$ and $Ag_{70}Pd_{30}$ are suitable containers for experiments at and about the Ni/NiO equilibrium. The maximum temperatures at which the alloys can be used are 1240°C and 1170°C respectively. Platinum must still be used at the highest temperatures though.

Under more reducing conditions, at the pO_2 of the Fe/FeO equilibrium, the silver-palladium alloys are unsuitable. Biggar (1970) has found molybdenum to be a suitable container at this low pO_2. Molybdenum metal is stable only at low pO_2, and its oxidation to MoO_2 occurs at approximately the same oxygen partial pressures as the Fe/FeO equilibrium. Thus molybdenum can be used at and below the pO_2 of the Fe/FeO equilibrium. The behaviour of iron-bearing charges in molybdenum containers has been discussed by Biggar (1970), who found only negligible loss of iron to the container occurred at the Fe/FeO equilibrium. Losses increased however at much lower pO_2 levels.

The behaviour of elements other than iron in the charges, in the various capsule materials has not been fully investigated. No reaction was noted between the charges and the platinum or silver-palladium alloys. Reaction did occur, however, between high CaO compositions and molybdenum containers, resulting in black needles.

appearing in a few charges. No reaction was noted in the geologically relevant compositions. Loss of constituents by volatility has also not been adequately investigated and may be significant at low oxygen pressures, particularly in the case of alkalis. A few preliminary runs were conducted to gauge the possible magnitude of this loss and the results are given in table 2.6.

The platinum and silver-palladium capsules were cut 1 cm in length from 3 mm diameter tube supplied by Johnson, Matthey and Co. Ltd. The base of each section of tube was squeezed together and welded, to form the capsule. Molybdenum capsules were made by cutting molybdenum sheet (99.9%; Koch-light Laboratories Ltd.) into 1 cm square pieces, folding in half and welding the base and side in an argon box.

Since up to 18 capsules were run together, a system of tick welds on the top of the capsules, combined with squeezing of the weld on the platinum and silver-palladium capsules, was used to identify each capsule. After filling each capsule, the capsule was tapped several times to ensure the material was all at the base of the capsule, and the inside top of the capsule cleaned with a pipe-cleaner. Platinum and silver-palladium capsules were coated with MgO powder suspended in Xylene to prevent their welding together during the run. After each run the outsides were cleaned on a metal brush, and the capsules opened as follows:

a) Platinum and silver-palladium capsules: the base was

Table 2.6 Results of preliminary runs to determine loss of volatile oxides during an experiment.

Composition	Run	Temp. °C	Hours	Container	pO_2	Na_2O initial	Na_2O final	% Recovery
H5	6-37	1300	264	Pt	air	0.026[f]	0.070[f]	269
A7	6-37	1300	264	Pt	air	4.86[f]	4.39[f]	90
Re 2	3-238	1300	2	Pt	air	3.36[f]	3.49[p]	104
Re 2	7-214	1300	5	Mo	Fe/FeO	3.36[f]	2.57[p]	76
Re 2	7-215	1300	24	Mo	Fe/FeO	3.36[f]	1.82[p]	54
Re 1	5-236	1150	44	Mo	Fe/FeO	6.35[f]	5.68[p]	89

f flame photometry analyses - M.J. Saunders

p electron probe analyses - P.D. Dixon

cut off with scissors just above the weld, then one side, and the charge extracted.

b) Molybdenum capsules: the capsule was broken along the side weld and along the base.

It was generally easy to recover almost all the charge from the platinum and silver-palladium capsules. In the molybdenum capsules however, the charge had generally migrated up the welded side of the capsule, either during the run or during quenching, and it was more difficult to recover all the charge.

2.7 Length of Experiments

The length of run considered necessary for the charges to reach equilibrium was determined by the system studied. In iron-free systems, the longer the run length, the more confident the experimenter can be in reaching equilibrium in the charges. Long runs are especially important when subsolidus runs or runs with small amounts of liquid present are being conducted. In the systems studied, run lengths of about 7 days were considered necessary, this being much longer than experiments carried out by other workers on similar compositions. Agreement with previous results in these systems indicates that either equilibrium was achieved or the length of time required to reach equilibrium is very much longer than 7 days.

In iron-bearing systems, runs of such length were not considered necessary. Maintenance of a constant gas mixture for such lengths of time is difficult and previous research on similar systems has indicated that only a short time is needed to achieve equilibrium. A gas mixture passed through the furnace will act as an oxygen reservoir and oxygen will be fairly rapidly added to or subtracted from the charges as necessary. The length of time this takes has not been fully investigated, but Presnall (1966) established by experiment that 3 hours were sufficient for a close approach to equilibrium of the ratio Fe_2O_3:FeO and the gas mixture. Fudali (1965), however, using natural samples, showed that 36-48 hours was required

to establish the Fe_2O_3:FeO ratio at $\log_{10}(pO_2) = -6$ at 1200°C and at least 12-24 hours at $\log_{10}(pO_2) = -8$ at 1200°C. This difference was ascribed to intergranular air trapped in the sample and that the equilibrium time was a function of the amount of H_2 present in the gas mixture.

Since longer experiments may lead to other serious compositional changes, a compromise is necessary. Early experiments were limited to 5 hours duration, until confidence in the apparatus was achieved, when overnight runs (17-18 hours) were used. In no case did runs of the two lengths produce contradictory results.

2.8 Identification of phases

After opening the capsules, the charges were broken into smaller pieces using an agate mortar and pestle. A part of the ground material was then mounted on a glass slide and covered with 1.640 refractive index oil. The remainder was retained. All charges were then examined by optical microscope using transmitted light.

A few charges were also examined using X-ray diffraction equipment, $CuK_{\alpha 1}$ radiation. X-ray examination, however, is only a useful confirmatory tool, being effective only when greater than 10-15% of a phase is present in the charge. The method cannot be used to determine the accurate incoming of a phase.

Since the size of individual crystals within experimental charges is generally only about 20 μ or less, not all the standard petrographic microscope techniques can be applied to identifying the phases encountered. Emphasis has to be placed on those properties easily determined: refractive index, crystal habit, birefringence, extinction angle and twinning. Using these properties it was usually possible to distinguish the phases in this study. Difficulty was encountered, however, when two phases differed only in their crystal habit, for example forsterite and diopside.

The optical properties of a phase also vary with the system studied due to the effects of solid solution in that phase. The crystal habit also depends on the amount of liquid present in the charge: the greater the amount of liquid present, the larger and more well-developed the

phases appear. A short description of the phases and the properties used for their identification is therefore relevant.

a) Olivine (fo,ol): The olivines appeared similar in all the systems studied. The usual crystal habit was one of colourless well rounded crystals, but occasionally euhedral crystals occurred especially when abundant liquid was present. In compositions near the spinel stability field, and in the natural charges, inclusions were often noted in the centre of the crystals. Quench margins were also found on crystals from very iron rich compositions in the system CMAS-Fe-O_2. Actual quench olivine crystals, if present, could not be detected optically from, presumably, equilibrium crystals. The refractive index of the crystals was higher than that of the glass and the birefringence was strong.

b) Clinopyroxene (di,cpx): The usual crystal habit was one of short narrow lath-like crystals, often simply twinned. Near the liquidus, these crystals grew as very large broad lath plates. In compositions near the low-Ca pyroxene stability field in the system CMAS-Fe-O_2, the clinopyroxenes were recognised as very small subrounded crystals and not the usual lath-like crystals. Quench crystals were found in some charges along with primary crystals, these crystals occurring as long very thin needles. The refractive index of the crystals was higher than that of the glass, and the birefringence was moderate to strong. Inclined extinction was often recognised.

The incoming of clinopyroxene was usually marked by a rapid increase in the percentage of crystals present in the charge. This fact was taken into account when attempting to distinguish clinopyroxene from olivine in some of the natural charges when a moderately large percentage of olivine was already present.

c) Low-Ca pyroxenes (pen,pig,pyx): Two crystal habits were noted:

i) moderately large, weak birefringence, straight extinction, plate-like crystals. These were interpreted to be of orthorhombic type.

ii) euhedral prismatic crystals, having weak birefringence and a low extinction angle - interpreted to be of monoclinic, pigeonite type.

Only a few compositions encountered these phases, the complete description and extent of their stability fields was therefore not attempted. In both cases, the refractive index was greater than that of the glass. Quench margins were only noted on crystals in charges from high iron compositions in the system CMAS-Fe-O_2.

d) Plagioclase (an,plag): In the synthetic systems, the crystal habit was one of very small, colourless laths. Refractive index was always lower than that of the glass and twinning usually occurred. Birefringence was very weak, and extinction was inclined. In the natural charges, the feldspar occurred as irregular plate-like crystals with weak birefringence. Albite twinning was common. Refractive index was again usually lower than that of the

glass, but in the more siliceous compositions it was often greater than the glass, reflecting the higher Na_2O content of the charges.

e) Spinel (sp): The appearance of spinel varied with the system studied. In the systems CMAS and CMASN spinel occurred as very small, colourless, isotropic, rounded crystals. In the system CMAS-Fe-O_2 and in the natural charges at the FeFeO equilibrium, the spinel occurred only as a very late phase as very dark irregular crystals, but at more oxidising pO_2 occurred as euhedral crystals, isotropic, and black. The colourless spinels were probably of the MA compositional type, the FeFeO equilibrium spinels of the ilmenite or hercynite type, and the more oxidised spinels of the magnetite type. The composition of none of the spinels was determined.

f) Silica (sil): The crystal habit of the silica phase was quite distinctive: either as irregular rounded crystals or as Y-shaped twins - cristobalite or tridymite. Generally the two habits occurred together and a boundary between the two polymorphs could not be determined. The refractive index was very much lower than that of the glass, and the birefringence was very weak.

g) Wollastonite (woll): Occurred as very small plates having one refractive index lower and one higher than the glass to give a twinkling effect. The birefringence was very weak.

CHAPTER 3

METHOD OF PRESENTATION OF RESULTS

3.1 The problem

The problem of representing a system with more than three components has been inherent in phase equilibria work from the earliest synthetic experimental studies. For many decades, the problem was not serious since sufficient convenient joins in synthetic systems could be studied utilising the stoichiometric phase compositions as end members of the join. However, as more complex synthetic systems were studied, the phase compositions encountered could not be represented on the join studied - "pseudo"-binary and "pseudo"ternary joins resulted. This meant that crystallisation paths of compositions entering equilibria containing the "foreign" phase could not be followed on the original join.

The relationship of phase equilibria in one join to that in another join was also not considered, except in the construction of "flow diagrams" (Schairer (1954)), this being the only graphical representation considered feasible. This approach aided the interpretation of crystallisation trends within a system and still has use as a simple means of showing invariant and univariant equilibria in any system (for example, the CMAS flow sheet (Humphries, Biggar and O'Hara (1972)). It is used as such in this thesis to show the relationships between isobaric invariant and univariant equilibria.

To consider the geometrical relationships between

equilibria and the compositions of the phases in those equilibria, and to examine the consistency of the phase equilibria data from the various sections studied, projections from phases common to many of the equilibria were utilised. In this way the bounding surfaces of the liquidus phase volume of the projection phase can be portrayed on convenient planes which intersect the system. The calculation of the projection co-ordinates is discussed in Appendix F.

Thus, O'Hara (1969) discussed part of the forsterite-bearing equilibria in the system CMAS; O'Hara and Biggar (1970) discussed the periclase projection and its relation to basic refractories; Biggar (1971) discussed part of the C_2S projection in CMAS relevant to cements; and Humphries (1972) has presented diagrams for all the bounding surfaces of the C_2S and spinel (MA) volumes in CMAS.

This type of projection simplifies a four component system to two dimensions, enabling the crystallisation paths (fractional or equilibrium) of any composition saturated with the projection phase throughout its crystallisation interval, to be easily followed. A more quantitative approach is therefore possible in a much wider context using such techniques.

3.2 The data reduction scheme

Since the projections mentioned previously only remove one dimension from the problem of visual representation, an extremely useful means was developed by O'Hara (1968) and Jamieson (1969), whereby all or a large proportion of an analysis of a rock or synthetic composition, was reduced to four "components" equivalent to CaO, MgO, Al_2O_3, SiO_2. This reduced system is here called $XO-YO-R_2O_3-ZO_2$ after Jamieson (1969).

The primary objective of the scheme is that all the members of a single solid solution series - Forsterite-Fayalite olivines, Diopside-Hedenbergite pyroxenes, Enstatite-Ferrosilite pyroxenes, or the Albite-Anorthite-Orthoclase feldspars - should each have co-ordinates in the pseudo-quaternary system identical with those of the analogous crystal structure in the system CMAS.

The objective was achieved by developing equations which converted iso-structural molecules into the equivalent weight of the analogous CMAS molecule. Thus in the case of the simple elemental substitutions, for example MgO replaced by FeO (as in the olivine, pyroxene and spinel solid solution series), this is accomplished by the simple recasting of the molar proportions of the substituting elemental oxide into that of the analogous CMAS oxide.

The more complex feldspar molecules are dealt with in a similar manner: the "plagioclase" molecule is based on 8 oxygens. The chemical formula of anorthite (CAS_2) involves only 8 oxygens; the chemical formula of albite (NAS_6)

involves 16 oxygens. Therefore in the plagioclase solid solution series, the albite formula (NAS_6, two plagioclase molecules) is equivalent structurally to two anorthite molecules. In the reduction scheme one NAS_6 thus converts to two CAS_2 molecules. The same procedure applies to orthoclase (KAS_6).

This very simple manipulation will therefore reveal changes in the liquid compositions in equivalent equilibria other than those conditioned by the differing molecular weights of the analogous constituents.

The equations used in this scheme are repeated here again from O'Hara (1968) and Jamieson (1969) for completeness.

Wt % XO = (mol props. $CaO-3\frac{1}{3}P_2O_5+2Na_2O+2K_2O$) x 56.08

Wt % YO = (mol props. $MgO+FeO+MnO+NiO-TiO_2$) x 40.311

Wt % R_2O_3 = (mol props. $Al_2O_3+Cr_2O_3+(Fe_2O_3)+TiO_2+Na_2O+K_2O$) x 101.961

Wt % ZO_2 = (mol props. $SiO_2-2Na_2O-2K_2O$) x 60.085

Although Fe_2O_3 is included in these equations, all the compositions studied in the system CMAS-Fe-O_2 and the natural rock samples studied, were reduced to their pseudoquaternary co-ordinates with all the iron calculated as FeO. In this way the effect of changing pO_2 on the phase relations can be observed. The FeO/Fe_2O_3 ratio in the run products was not determined but the ratio can be considered very high at iron/wustite conditions and still greater than one at Ni/NiO conditions.

After application of the reduction scheme, projections can be developed in the same manner as for the system CMAS.

UNIV. EDINBURGEN. EX BIBL.

The $2YO.ZO_2$ (olivine) projection into $XO.ZO_2$-$YO.ZO_2$-R_2O_3 (CS-MS-A) and the $XO.YO.2ZO_2$ (clinopyroxene) projection into $XO.R_2O_3$-YO-ZO_2 (CA-M-S) are used widely in this study. Similar projection diagrams have been drawn for each system studied, to compare the changes in position in projection of the liquids in selected equilibria as the MgO/FeO or albite/anorthite ratios vary. These two projections have also been previously used to describe behaviour in the natural rock groups melted (Jamieson (1970), Humphries (1972a), Biggar, O'Hara, Humphries and Peckett (1972)).

The tetrahedron XO-YO-R_2O_3-ZO_2 is shown in figure 3.1 with the location of the phases encountered in this study and the names of their CMAS counterparts. Figure 3.2 shows the $XO.ZO_2$-$YO.ZO_2$-R_2O_3 (CS-MS-A) plane and the positions of relevant compositions, piercing points and joins mentioned in the text; figure 3.3 shows the $3XO.R_2O_3$-YO-ZO_2 (C_3A-M-S) plane similarly.

In many of the figures presented and parts of the text, the reduction scheme has been used. In order to avoid confusion with the CMAS system and when the scheme has not been used, the XO-YO-R_2O_3-ZO_2 notation has been used to indicate the phase names when the scheme applies, a common phase name equivalent to that particular XO-YO-R_2O_3-ZO_2 composition being placed afterwards in parenthesis.

The features of the reduction scheme of importance to the two synthetic systems under consideration are:

1. The superposition of the two systems CMAS and NMAS after application of the reduction scheme involves a portion of

NMAS occurring in negative space in the pseudoquaternary system. In allowing the albite and anorthite structural equivalence, the reduction equations result in Na_2O alone reducing to negative co-ordinates ($2XO.R_2O_3.-2ZO_2$). As a result, the join SiO_2 to Na_2O after reduction enters negative space at the point $2XO.R_2O_3$ (equivalent to NS_2 before reduction); all co-ordinates in the volume $N-A-NS_2-M$ ($2XO.R_2O_3.-2ZO_2:R_2O_3:2XO.R_2O_3:YO$) are therefore negative; and the volume $XO-2XO.R_2O_3-YO-ZO_2$ of the pseudo-quaternary system is unused. This feature is important when the system NMAS is considered in Chapter 5.

2. Because all members of a solid solution series plot at one point, and each synthetic system studied involves only one type of isostructural substitution, the systems can be conveniently studied at constant bulk composition ratios. For example, in CMASN at constant bulk CIPW normative plagioclase (Ab/An) ratios, and in CMAS-Fe-O_2 at constant bulk MgO/FeO ratios. Liquidus and projection diagrams can then be drawn for each bulk ratio considered.

3. The relationship of the reduction scheme to the CIPW norm is relatively simple as far as the constituents under discussion here are concerned. O'Hara and Yoder (1967) presented a normative plot of values for compositions in part of the plane CS-MS-A in CMAS, and O'Hara (1969) described in a forsterite projection, the change in the ratio of the normative constituents in the forsterite-bearing liquids in CMAS during different types of crystallisation, using these values. In order to extend this type of treat-

ment, using olivine projections, to the systems studied here, it is necessary to define the manner in which the ratios of the normative constituents change for molecularly equivalent compositions. The ratios of the normative constituents will change because the CIPW norm calculation makes use of the different molecular weights of each of the individual constituents of each solid solution series, whereas the data reduction scheme does not.

In the system CMAS, the plane CS-MS-A can be subdivided into several areas, compositions in each area having similar CIPW normative minerals present (figure 3.4). The CIPW norm of the Anorthite-Forsterite ($CAS_2.M_2S$ or $XO.R_2O_3.2ZO_2$-$2YO.ZO_2$) piercing point determines the normative ratio distribution in the join CS-MS-A ($XO.ZO_2$-$YO.ZO_2$-R_2O_3), and has Anorthite 66.4, Forsterite 33.6 wt %. The normative ratios in the geologically interesting part of the join are shown in detail in the figure. Three areas of normative types can be distinguished on the diagram: compositions have "saturated" norms - An+Fo+Di+En; those having "undersaturated" norms - Larnite- or Wollastonite-bearing norms, but no Corundum; and those having "peraluminous" norms - Corundum-bearing norms.

In the system CMASN, similar areas can be delimited (figure 3.5), but the "undersaturated" areas about the Plagioclase-Forsterite piercing point, do not have Larnite in the norm, having Nepheline instead, due to the mechanics of the norm calculation. More $XO.ZO_2$ (Wollastonite)-rich compositions have a norm involving Larnite, Wollastonite,

Sodium metasilicate or Nepheline depending on the Na_2O/CaO ratio. Chayes and Yoder (1971) have proposed possible modifications to the CIPW norm calculation to deal with these unusual compositions, and relate the norm to the modal mineralogy more accurately.

The equivalent $XO.R_2O_3.2ZO_2$-$2YO.ZO_2$ (Albite-Forsterite) piercing point ($NAS_6.2M_2S$ before reduction) has a CIPW norm Albite 65.1, Forsterite 34.9 wt %. There are thus small changes in the ratios of the normative minerals for molecularly equivalent compositions in the geologically interesting part of the join. The reason for the small change has been mentioned previously: the molecular weight of the albite formula (NAS_6) is almost twice that of the anorthite formula (CAS_2) molecular weight, but since one albite formula is equivalent to two plagioclase molecules, the reduction scheme molecular albite/anorthite ratio and the CIPW normative wt % plagioclase ratio are almost the same.

The slight normative change results in the plagioclase/dippside and plagioclase/enstatite ratios in the CIPW norm for the same molecularly equivalent composition gradually decreasing as the bulk plagioclase composition becomes more sodic in the system CMASN.

A much more complex situation exists in the system CMAS-Fe-O_2, where the olivine forms part of a solid solution series, and therefore has a changing molecular weight as far as the CIPW norm is concerned. Similar areas of like normative assemblages (figure 3.6) occur to those in CMAS, the only change being in the actual proportions of the CIPW norm minerals for a molecularly equivalent composition.

Thus the $XO.R_2O_3.2ZO_2$-$2YO.ZO_2$ (Anorthite-Fayalite) piercing point ($CAS_2.(FeO)_2S$ before reduction) in the system CaO-FeO-Al_2O_3-SiO_2, has a norm Anorthite 57.7, Fayalite 42.3 wt %. If this were the only solid solution change involved, this would result in the anorthite/diopside and anorthite/hypersthene normative ratios decreasing for molecularly equivalent compositions in the system CMAS-FeO. However, since the diopside-Hedenbergite and enstatite-ferrosilite solid solution series are also involved, with molecular weight increases as the FeO/MgO ratio increases, the normative ratios decrease further. The normative ratio diopside/hypersthene also decreases with FeO/MgO increase for molecularly equivalent compositions.

Change of pO_2 in this system, results in a lower FeO/Fe_2O_3 ratio as more oxidising conditions prevail. In CAS-Fe-O_2 this will be displayed in a lowering of the amount of FeO-bearing normative minerals, and the appearance of magnetite and hematite as normative minerals, as molecularly equivalent compositions become more oxidised. In the system CMAS-Fe-O_2 the effect will also be seen in the production of more MgO-rich ferromagnesian normative minerals (but less of them).

The effect on a molecularly equivalent composition can be deduced only if the FeO/Fe_2O_3 ratio is known. In this study the ratio was not determined; therefore, only a general statement on the effect can be made. Any increase in the Fe_2O_3 amount in a molecularly equivalent composition, will result in magnetite increasing in the norm, with the

removal of an equivalent amount of FeO from that available for the silicates. This will reduce the Fe/Mg ratio in the ferromagnesian minerals and allow a more siliceous normative assemblage.

Ian Abernathy Bond

3.3 Shorthand notation

The modified shorthand notation c n E f p is used to abbreviate the long and potentially tiresome descriptions of equilibria; c represents the number of components in the system; f is the number of degrees of freedom of the equilibrium using the full Phase Rule (P + F = C + 2); n is the number of phases resorbed as heat is extracted from the system; and p the number of phases present, which is normally replaced by a list of the phases participating in that equilibrium. If n is included those phases being resorbed are indicated by overlines; if n is not known or is unimportant, it is omitted along with resorption overlining. As an example:

4 2 E 2 fo, $\overline{\text{sp}}$, an, $\overline{\text{liq}}$ describes the divariant equilibrium forsterite + spinel + anorthite + liquid in a four component system, in which the two phases spinel and liquid are decreasing in amount as heat is extracted from the system. Another way to look at this is that spinel is in reaction relationship with the liquid to produce anorthite and forsterite.

A further abbreviation to describe the liquid or any other phase in an equilibrium is in general: X. c n E f p where X represents the phase being discussed. For example: L. 4 2 E 2 fo, $\overline{\text{sp}}$, an, $\overline{\text{liq}}$ describes the liquid in the equilibrium given as an example above.

3.4 Interpretation of diagrams

The manner in which the liquidus diagrams presented are interpreted is similar to that used in any other pseudo-binary or pseudoternary system. Crystallisation of mixtures within any phase volume in these non-projected diagrams can be traced if the actual phase composition involved lies in the join depicted. Many early published articles include descriptions of the crystallisation histories of compositions - for example, Rankin and Wright (1915) and Bowen and Schairer (1935) - and Ehlers (1972) deals with this subject in detail.

The interpretation of projection diagrams in a four-component system has been extensively described by O'Hara (1969). Essentially, projection figures can be treated as a type of pseudoternary diagram, noting that

a) the projection phase is present in all equilibria;

b) the liquids during crystallisation do not lie in the plane of projection.

Their absolute compositions can only be determined by knowledge of the amount of the projection phase which must be added to or subtracted from, the co-ordinates of the particular liquid in question, in the projection plane. If however, the same liquid composition is represented in two projections from different phases, its composition can be calculated from the projection co-crdinates in the two planes (see Appendix F);

c) the behaviour of the projection phase in invariant or univariant equilibria is best determined in a projection

from one of the other phases in the equilibrium. In general terms the relationship can be expressed: if the liquid composition can be exactly and uniquely represented in terms of the compositions of the crystalline phases co-existing with it at equilibrium, the equilibrium is univariant. Any crystalline phase used in negative amount must be in a reaction relationship with the liquid as heat is extracted.

If no unique solution is possible, but many unique solutions become possible as one of the crystal species is eliminated in turn, it is a true invariant equilibrium. If no solution is possible, the equilibrium has two or more degrees of freedom. Reaction relationship can then only be calculated from the expression of where the tangent to the sense of the liquid change cuts the figure of the solid phases.

The extension of the interpretation of projection diagrams in four component systems to that of projection diagrams for specific bulk ratios (of specific components) in five component systems is simple. The only change, as far as the systems CMASN and CMAS-Fe-O_2 studied here are concerned, is that one or more of the phases in the projection diagram and sometimes the projection phase, becomes a member of a solid solution series.

In both these systems, this is reflected in the fact that the liquids in equilibria involving a solid solution phase always contain a lower ratio of anorthite/albite or MgO/FeO, as the case may be, than that of the relevant solid

solution actually crystallising. This can easily be demonstrated in the simpler systems Forsterite-Fayalite (Bowen and Schairer (1935)) and Anorthite-Albite (Bowen (1913)). A discussion of the $2YO.ZO_2$ (olivine) projections for each of the systems studied will indicate what effect this relationship has on the interpretation of the diagrams.

In the system CMASN, those equilibria involving plagioclase have the relationship mentioned above. Each olivine projection diagram shows only those liquids on the surface of the olivine volume which have the anorthite/albite ratio stated for that diagram. Thus, during the crystallisation of any composition having a particular anorthite/albite bulk ratio and which projects into the field of olivine + plagioclase crystallisation, only the liquid at the instant plagioclase commences crystallisation is represented in projection on that diagram. Further plagioclase crystallisation will lower the anorthite/albite ratio in the liquid; at some later stage during crystallisation, this liquid may be represented on an olivine projection diagram for compositions having a lower anorthite/albite bulk plagioclase ratio. Without knowledge of the compositions of the plagioclases crystallising in relevant equilibria, the exact crystallisation trends for any composition once plagioclase crystallises cannot be determined. A general sense of types of crystallisation trend can still be deduced however.

Those compositions which project into any other field of crystallisation (for example, olivine + diopside) can have their crystallisation paths traced on the projection

diagram relevant to their anorthite/albite ratio, until they reach a plagioclase-bearing equilibrium. This is because extraction of these phases does not affect the anorthite/albite ratio of the liquid. Since olivine, the projection phase, affects the liquid composition in a similar manner to these phases, any compositions within the olivine phase volume can be used to draw the projection diagrams. The actual composition of the liquids on the bounding surfaces of the olivine volume need not therefore be known.

This is in contrast to behaviour in the system CMAS-Fe-O_2 where olivine is also a member of an MgO/FeO-bearing solid solution series. Any composition, having any bulk MgO/FeO ratio, upon crystallisation of olivine will immediately develop a liquid with a lower MgO/FeO ratio. Two possible types of olivine projection diagram are therefore possible at any selected MgO/FeO ratio.

1) Projection diagrams showing those liquids on the surface of the olivine volume which have the particular MgO/FeO ratio stated. This type of presentation was used for the system CMASN. In the system CMAS-Fe-O_2, however, this requires knowledge of the actual composition of the liquids on the bounding surfaces. Compositions within the olivine volume cannot be used to draw these diagrams, the olivine crystallisation having altered the MgO/FeO ratio of the liquid such that at the instant the second phase appears, the MgO/FeO ratio is no longer that of the initial bulk composition ratio. This type of diagram could not be drawn

for this system in this work, since no liquid compositions were determined.

2) Projection diagrams showing the second phase to crystallise after olivine for compositions in a particular join. This type of diagram is equivalent to the first type of diagram when the projection phase is not a member of a solid solution series, as in CMASN. In the system CMAS-Fe-O_2, however, since olivine is a member of a solid solution series, this is the type of diagram used to present the data. The MgO/FeO ratio of the liquids on the bounding surface of the olivine volume are not uniform on each diagram; the ratio is always lower than that stated for the diagram. The precise ratio at each projection position depends on the initial MgO/FeO ratio of the bulk compositions used, the particular "plane" of compositions used and the amount of olivine crystallisation which has occurred from liquids at different points in that plane before a second solid phase appears.

No matter which type of presentation is used, once the crystallisation of any composition reaches the second crystalline phase, the liquid attains lower MgO/FeO ratios and leaves the initial projection diagram. The tracing of precise crystallisation paths requires much detailed knowledge of the compositions of the phases in relation to the liquid compositions. General types of trend can still be postulated, using the projection diagrams purely as a means of presentation of the relationship of the equilibria to their relevant crystalline phases.

Only the ferrous oxide of iron was mentioned above. As

the pO_2 is changed, a different series of diagrams is then relevant. At this stage, therefore, the projection diagrams presented in Chapter 6 are purely a means of presentation of the results obtained. Only with a great deal more research can precise crystallisation trends be traced in the complex system; general trends can, however, be outlined. As an example of a different approach to the problem in iron-bearing systems, the reader is referred to Presnall (1964).

While the above text applied to olivine projections, the same comments apply also to $XO.YO.2ZO_2$ (clinopyroxene) projections. In the latter, however, a further point to remember is that the projection composition only very roughly approximates that of the actual clinopyroxene crystallising. In the case of the olivine projections, there is much better agreement, there being only slight solid solution range outside the forsterite-fayalite join in those equilibria relevant here. The clinopyroxene projection is, however, useful in relating the olivine-bearing equilibria to the silica-bearing equilibria, especially important when discussing fractional crystallisation trends.

Use of a $XO.R_2O_3.2ZO_2$ (plagioclase) projection overcomes some of the problems involved when only MgO/FeO substitutions are considered, since crystallisation of the projection phase alone does not affect the MgO/FeO ratio of the liquid. However, once a second phase appears which involves MgO/FeO solid solution, similar comments apply to this projection as to the olivine projection for the CMASN system. Use of

a plagioclase projection in the system CMASN involves the same problems as an olivine projection in CMAS-Fe-O_2, since plagioclase crystallisation involves a changing anorthite/albite ratio in the liquid. Only generalised plagioclase projection diagrams are presented, since few suitable compositions were studied. The relevance of these diagrams to basalts is doubtful, but they are of use when considering more evolved rocks having a higher FeO/MgO ratio.

CHAPTER 4

THE SYSTEM $CaO-MgO-Al_2O_3-SiO_2$

4.1 Introduction

Studies in this system have formed the basis of research into the behaviour of possible magma compositions during their evolution. One member of each of the important solid solution series is present in the system - anorthite (plagioclase), diopside and enstatite (pyroxenes), forsterite (olivine) and spinel (spinels). It is thus appropriate that it also forms the base upon which the more complex systems studied here are constructed.

Consistency between the data for the systems studied is obviously necessary. Interlaboratory errors in the temperature and compositional range of important equilibria are possible, especially in view of the differences of experimental technique (Chapter 2). A limited amount of research was therefore considered necessary to establish the important equilibria using the experimental techniques of this laboratory.

4.2 Previous research

The geologically important subsystem Forsterite-Diopside-Anorthite-Silica has received much attention, and the phase equilibria determined (Andersen (1915): An-Fo-SiO_2; Osborn and Tait (1952): An-Di-Fo; Kushiro (1972): Di-Fo-SiO_2; and references contained therein). The olivine-bearing equilibria, which occupy a large portion of this subsystem were summarised and extensively discussed by O'Hara (1969), using a forsterite projection into the plane CS-MS-A. This summary was based entirely upon the published and unpublished data of other workers using techniques different from that used in this laboratory.

It was one of the earliest tasks of workers in this laboratory to confirm the data for some of these important equilibria. To accomplish this, the joins C_3A-M-S (O'Hara and Biggar (1969), Biggar and O'Hara (1972)) and Enstatite-Grossular (Ford and O'Hara (1972)) have been studied using identical experimental technique to that used here. Essentially agreement was found in most parts of interest to this study, the stability of diopside + spinel (O'Hara and Biggar (1969a)), however, was in contradiction to previous knowledge, and has recently been confirmed (Schairer and Yoder (1970) and comments by Humphries (1972)).

Recent work by Yang and Foster (1972), Kushiro (1972) and Yang (1973), has revealed the stability of an iron-free pigeonite in this system. This phase was not recognised by previous workers at this laboratory because runs were not conducted in the temperature range in which iron-free pigeonite

is stable; their phase diagrams must therefore be revised to include this new phase field.

The position of 4 E 1 fo,di,pig,pen,liq in a forsterite projection can be approximately located from the data of Yang (1973). Projected in figure 4.3 are those compositions (labelled 3-6) from Yang (table 1, page 489) that involve forsterite crystallisation, and also the pigeonite and protoenstatite compositions obtained by probe analysis of the experimental charges of these compositions (table 2, page 493). Since 4 E 3 fo,pig,liq is present only near 4 E 3 fo,di,liq and does not cover the pigeonite composition in projection, 4 E 2 fo,pig,pen,liq involves resorption of protoenstatite. From the quenching results for composition number 6, following forsterite crystallisation, protoenstatite crystallises followed by pigeonite, the protoenstatite not being completely resorbed in 4 E 2 fo,pig,pen,liq before diopside (di) appears at 4 E 1 fo,pig,pen,di,liq at 1276°C. In consequence, the zone in which 4 E 1 fo,pig,pen,di,liq can project is quite restricted.

The presence of iron-free pigeonite precludes diopside+protoenstatite from occurring in any composition lying in the forsterite volume and projecting to the enstatite-rich side of 4 E 2 fo,pig,di,liq, above a temperature of 1276°C. The non-stability of forsterite +anorthite+iron-free pigeonite can be clearly seen.

4.3 Experimental results

In order to confirm more accurately the temperature and location of 4 E 2 fo, di, an, liq in a forsterite projection into the plane CS-MS-A, and to establish approximate temperature contours on the 4 E 3 fo, di, liq and 4 E 3 fo, an, liq surfaces, a limited number of new compositions were prepared in the join CS-MS-A. The compositions lie on the joins Diopside-MAS (includes the Anorthite-Forsterite piercing point in the join CS-MS-A and forms part of the join Anorthite-Diopside-Forsterite), Diopside-$M_5A_3S_5$ and Diopside-$M_7A_3S_7$. Five compositions were also prepared about the piercing point of 4 E 2 fo, di, an, liq in the plane Anorthite-Diopside-Forsterite to confirm the results of Osborn and Tait (1952). Appendix B.1 contains the compositional data; Appendix C.1 contains details of the furnace operations; Appendix E.1 the results of the runs conducted in this system.

The results of runs on the compositions lying in the plane Anorthite-Diopside-Forsterite were used to modify slightly the liquidus diagram of Osborn and Tait (1952). The revised diagram (figure 4.1) contains only a slight repositioning of the piercing point of 4 E 2 fo, di, an, liq and lies within the experimental error of the data of Osborn and Tait (see Biggar, O'Hara, Humphries and Peckett (1972)). The temperature of this piercing point is revised from 1270 $\pm$ 5°C (corrected to 1272°C) of Osborn and Tait, to 1278°C in this work.

Those compositions on the join Diopside-MAS are also shown in figure 4.1. Their position within the forsterite

volume indicates at least 100°C of forsterite crystallisation prior to second phase entry. Expressed slightly differently, c.13% of forsterite has crystallised in that composition in the join which enters 4 E 2 fo, an, di, liq following 4 E 4 fo, liq crystallisation. The liquidus diagram for CS-MS-A (figure 4.2) constructed from previously published data from many sources, indicates that the forsterite liquidus temperature and the extent of the forsterite phase volume increases from the Diopside-MAS join to more enstatite-rich compositions. Compositions on the join Diopside-$M_7A_3S_7$, for example, will therefore crystallise much more than 13% forsterite prior to second phase entry. Compositions lying in the join CS-MS-A are therefore not the ideal compositions in which to identify accurately the incoming of a second phase, especially when that phase can be very similar optically to forsterite as in the case of diopside.

The temperature at which 4 E 2 fo, di, an, liq is attained by compositions in the Diopside-MAS join is at least 1280°C (see Appendix E.1), while those compositions nearer to 4 E 2 fo, di, an, liq in the Anorthite-Diopside-Forsterite join did not enter this equilibrium until 1278°C. The explanation for this inconsistency is that the experimental technique cannot be claimed more accurate than $\pm$ 3°C when runs from different experiments and different furnaces are compared. A closer comparison of results on different compositions can only be achieved by running all compositions to be compared at the same time, as was necessary to identify the diopside + spinel stability by O'Hara and Biggar (1969a).

A closer comparison of results from different runs must be achieved using the same furnace with very strict calibration control.

A forsterite projection into the plane CS-MS-A (figure 4.3) is used to present the results on those compositions in the join CS-MS-A, since they all have a forsterite liquidus (not actually determined for all compositions in this study). The location in projection of 4 E 2 fo, an, di, liq is confirmed as similar to that presented by O'Hara (1969). Temperature contours are indicated on 4 E 3 fo, di, liq and 4 E 3 fo, an, liq from this work, by extrapolation from results to be presented in the systems CMASN (Chapter 5) and CMAS-Fe-O_2 (Chapter 6), and from previously published data.

O'Hara (1969) did not contour the 4 E 3 surfaces, but indicated in the text (page 136) a temperature of c. 1275°C for 4 E 2 fo, di, an, liq on the Diopside-Pyrope join. Hytonen and Schairer (1960, 1961) reported 1262 ± 5°C (1264°C corrected) for the piercing point of 4 E 2 fo, an, di, liq in the join Enstatite-Anorthite-Diopside. In figure 4.3 this piercing point projects at the point where 4 E 2 fo, di, an, liq becomes silica saturated (indicated by the dotted line). The temperature of 4 E 2 fo, di, an, liq in Diopside-$M_7A_3S_7$ (above 1264°C) is in agreement within the range of experimental error with that of Hytonen and Schairer. In consequence, the temperature drop on 4 E 2 fo, di, an, liq from the maximum of 1280°C to c. 1265°C on Diopside-$M_7A_3S_7$ is slightly steeper than that of O'Hara (1969), but it is

Why no mention of 1280° on $M_5A_3S_5$? page E3

still significant to remember that for a small temperature drop (15°C) initially from the maximum, the residual liquid increases rapidly its Enstatite/Diopside normative ratio. The rapid decrease in temperature in 4 E 2 fo, di, an, liq to the enstatite-rich side of the join Diopside-$M_7A_3S_7$ in projection is still present and results in the enstatite/diopside normative ratio increasing more slowly while the temperature drops to 1241°C at 4 E 1 fo, di, an, pen, liq.

Revised phase diagrams including the pigeonite field can now be drawn for the joins Enstatite-Grossular (figure 4.4) and C_3AS_{15}-M (figure 4.5), and a liquidus diagram for the join C_3A-M-S based on these data and those of Biggar and O'Hara (1972) presented (figure 4.6). The insertion of the pigeonite field does not contravene any of the runs previously reported in these diagrams. While the extent of 4 E 3 fo, pig, liq has been proposed above, the corresponding 4 E 3 sil, pig, liq extent is unknown. The assumption in drawing figures 4.5 and 4.6 is that the pigeonite field extends to the same extent against the forsterite and silica phase volumes. If this assumption is incorrect, it will only require minor modification to the diagrams.

Based on all available information, a diopside projection (which is commonly used in dealing with natural rock melting data), (figure 4.7), an anorthite projection (figure 4.8) and a flow sheet for equilibria in the geological part of this system (figure 4.9), are also presented.

4.4. Discussion

The essential features of the crystallisation of forsterite-saturated bulk compositions in this system has been described by O'Hara (1969) by means of a discussion of the crystallisation histories of various individual compositions. A summary of this information can be made by delimiting areas of like crystallisation histories under perfect equilibrium and perfect fractional crystallisation (figures 4.10, 4.11). The crystallisation histories for each area are presented in tables 4.1 and 4.2.

A similar treatment of the diopside projection shows the relationship between the forsterite-bearing equilibria and the silica-bearing equilibria, not shown by the forsterite projection (figures 4.12, 4.13; crystallisation histories in tables 4.3 and 4.4.).

The most important features of the forsterite-saturated crystallisation histories is the dependence of the final product of those compositions about the Anorthite-Forsterite piercing point on the reaction nature of the equilibrium 4 E 2 fo,sp,an,liq and the type of crystallisation involved. Thus, forsterite-saturated bulk compositions within the shaded area of figures 4.10, 4.11 can yield either melilite+spinel-bearing (perfect equilibrium) or silica+protoenstatite-bearing (perfect fractional) or forsterite+protoenstatite-bearing (intermediate equilibrium/fractional) end products. The CIPW norm of the residual liquid can thus be either undersaturated or saturated from the same bulk starting composition.

Table 4.1 The generalised equilibrium crystallisation histories of like areas of forsterite saturated compositions presented in figure 4.10.

Area	Equilibrium crystallisation history
1	4 E 4 fo,liq; 4 E 3 fo,sp,liq; 4 E 2 fo,sp,an,liq (not all spinel is lost by reaction with liquid); 4 E 1 fo,sp,an,di, liq. Solidifies, or continues by 4 E 2 fo,di,sp,liq to 4 E 1 fo,di,sp,mel,liq depending on bulk composition.
2	4 E 4 fo,liq; 4 E 3 fo,sp,liq; 4 E 2 fo,sp,an,liq (all spinel is lost by reaction with liquid); 4 E 3 fo,an,liq; 4 E 2 fo, an,di,liq; 4 E 1 fo,sp,an,di,liq. Solidifies, or continues by 4 E 2 fo,di,sp,liq to 4 E 1 fo,di,sp,mel,liq depending on bulk composition.
3	4 E 4 fo,liq; 4 E 3 fo,sp,liq; 4 E 2 fo,sp,an,liq (all spinel is lost by reaction with liquid); 4 E 3 fo,an,liq; 4 E 2 fo,an,di, liq; 4 E 1 fo,an,di,pen,liq. Solidifies.
4	4 E 4 fo,liq; 4 E 3 fo,sp,liq; 4 E 2 fo,sp,an,liq (all spinel is lost by reaction with liquid); 4 E 3 fo,an,liq; 4 E 2 fo,an, di,liq or 4 E 2 fo,an,pen,liq; 4 E 1 fo,an,di,pen,liq. Solidifies.
5	4 E 4 fo,liq; 4 E 3 fo,sp,liq; 4 E 2 fo,sp,an,liq (not all spinel is lost by reaction with liquid); 4 E 1 fo,sp,an,cord,liq. Solidifies.
6	4 E 4 fo,liq; 4 E 3 fo,sp,liq; 4 E 2 fo,sp,an,liq (not all spinel is lost by reaction with liquid); 4 E 1 fo,sp,an,cord,liq (all spinel remaining is lost); 4 E 2 fo,an,cord,liq; 4 E 1 fo,an,cord, pen,liq. Solidifies.
7	4 E 4 fo,liq; 4 E 3 fo,sp,liq; 4 E 2 fo,an,sp,liq (all spinel is lost by reaction with liquid); 4 E 3 fo,an,liq; 4 E 2 fo,an,cord, liq or 4 E 2 fo,an,pen,liq; 4 E 1 fo,an,cord,pen,liq. Solidifies.

Table 4.1 (continued).

Area	Equilibrium crystallisation history
8	4 E 4 fo,liq; 4 E 3 fo,an,liq; 4 E 2 fo,an,pen,liq or 4 E 2 fo,an,cord,liq; 4 E 1 fo,an,cord,pen,liq. Solidifies.
9	4 E 4 fo,liq; 4 E 3 fo,an,liq; 4 E 2 fo,an,di,liq or 4 E 2 fo,an,pen,liq; 4 E 1 fo,an,di,pen,liq. Solidifies.
10	4 E 4 fo,liq; 4 E 3 fo,di,liq; 4 E 2 fo,an,di,liq; 4 E 1 fo, an,di,pen,liq. Solidifies.
11	4 E 4 fo,liq; 4 E 3 fo,di,liq; 4 E 2 fo,an,di,liq; 4 E 1 fo, an,di,sp,liq. Solidifies, or continues by 4 E 2 fo,di,sp,liq to 4 E 1 fo,di,sp,mel,liq depending on bulk composition.
12	4 E 4 fo,liq; 4 E 3 fo,an,liq; 4 E 2 fo,an,di,liq; 4 E 1 fo, an,di,sp,liq. Solidifies, or continues by 4 E 2 fo,di,sp,liq to 4 E 1 fo,di,sp,mel,liq depending on bulk composition.

Note

1. Some compositions in areas 2,3,9,10,11 and 12 will solidify in 4 E 2 fo,an,di,liq due to diopside solid solution.

Table 4.2 The generalised perfect fractional crystallisation histories of like areas of forsterite saturated compositions presented in figure 4.11.

Area	Perfect fractional crystallisation history
1	4 E 4 fo,liq; 4 E 3 fo,sp,liq; (4 E 2 fo,sp,an,liq); 4 E 3 fo,an,liq; 4 E 2 fo,an,di,liq; (4 E 1 fo,an,di,sp,liq); 4 E 3 di,sp,liq; 4 E 2 di,an,sp,liq; 4 E 1 di,an,sp,mel,liq.
2	4 E 4 fo,liq; 4 E 3 fo,sp,liq; (4 E 2 fo,an,sp,liq); 4 E 3 fo, an,liq; 4 E 2 fo,an,di,liq or 4 E 2 fo,an,pen,liq; (4 E 1 fo, an,di,pen,liq); 4 E 2 an,di,pen,liq; 4 E 1 an,di,pen,sil,liq.
3	4 E 4 fo,liq; 4 E 3 fo,sp,liq; (4 E 2 fo,an,sp,liq or 4 E 3 fo, sp,cord,liq); 4 E 3 fo,an,liq or 4 E 3 fo,cord,liq by various routes to (4 E 1 fo,an,cord,pen,liq); fo and cord then lost; 4 E 3 an,pen,liq; by various routes to 4 E 1 an,pen,cord,sil,liq.
4	4 E 4 fo,liq; 4 E 3 fo,an,liq; 4 E 2 fo,an,di,liq; (4 E 1 fo, an,di,sp,liq); 4 E 3 di,sp,liq; 4 E 2 di,an,sp,liq; 4 E 1 di, an,sp,mel,liq.
5	4 E 4 fo,liq; 4 E 3 fo,an,liq; 4 E 2 fo,an,di,liq or 4 E 2 fo, an,pen,liq; (4 E 1 fo,an,di,pen,liq); 4 E 2 an,di,pen,liq; 4 E 1 an,di,pen,sil,liq.
6	4 E 4 fo,liq; 4 E 3 fo,an,liq; 4 E 2 fo,an,cord,liq or 4 E 2 fo,an,pen,liq; (4 E 1 fo,an,pen,cord,liq); 4 E 3 an,pen,liq to 4 E 1 an,pen,cord,sil,liq.
7	4 E 4 fo,liq; 4 E 3 fo,di,liq; 4 E 2 fo,di,an,liq; (4 E 1 fo, an,di,sp,liq); 4 E 3 di,sp,liq; 4 E 2 di,an,sp,liq; 4 E 1 di,an, sp,mel,liq.
8	4 E 4 fo,liq; 4 E 3 fo,di,liq; 4 E 2 fo,an,di,liq or 4 E 2 fo, di,pen,liq or 4 E 2 fo,di,pig,liq. By various routes to (4 E 1 fo,di,pen,an,liq); 4 E 2 an,di,pen,liq; 4 E 1 an,di,pen,sil,liq.

Table 4.2 (continued).

Notes

1. Not all the crystallisation history can be seen on figure 4.11. Once fo is lost from the sequence, a different projection is required. Those areas involving spinel crystallisation can be seen on the spinel projection presented by Humphries (1972).

2. Equilibria enclosed in brackets are encountered instantaneously only, one or more phases being in reaction relationship with liquid.

Table 4.3 The generalised equilibrium crystallisation histories of like areas of diopside saturated compositions presented in figure 4.12.

Area	Equilibrium crystallisation history
1	4 E 4 di,liq; 4 E 3 di,sil,liq; 4 E 2 di,sil,an,liq; 4 E 1 di, sil,an,pen,liq. Solidifies.
2	4 E 4 di,liq; 4 E 3 di,sil,liq; 4 E 2 di,sil,pen,liq; 4 E 1 di, sil,pen,an,liq. Solidifies.
3	4 E 4 di,liq; 4 E 3 di,sil,liq; 4 E 2 di,sil,pig,liq; 4 E 1 di, sil,pig,pen,liq; 4 E 2 di,sil,pen,liq; 4 E 1 di,sil,pen,an,liq. Solidifies.
4	4 E 4 di,liq; 4 E 3 di,pig,liq; 4 E 2 di,pig,sil,liq; 4 E 1 di, sil,pig,pen,liq; 4 E 2 di,sil,pen,liq; 4 E 1 di,sil,pen,an,liq. Solidifies.
5	4 E 4 di,liq; 4 E 3 di,pig,liq; 4 E 2 di,pig,pen,liq; 4 E 3 di,pen, liq; 4 E 2 di,pen,sil,liq; 4 E 1 di,sil,pen,an,liq. Solidifies.
6	4 E 4 di,liq; 4 E 3 di,pig,liq; 4 E 2 di,pig,pen,liq; 4 E 3 di, pen,liq; 4 E 2 di,pen,an,liq; 4 E 1 di,sil,pen,an,liq. Solidifies.
7	4 E 4 di,liq; 4 E 3 di,pen,liq; 4 E 2 di,pen,sil,liq; 4 E 1 di, pen,sil,an,liq. Solidifies.
8	4 E 4 di,liq; 4 E 3 di,pen,liq; 4 E 2 di,pen,an,liq; 4 E 1 di,pen, an,sil,liq. Solidifies.
9	4 E 4 di,liq; 4 E 3 di,an,liq; 4 E 2 di,an,sil,liq; 4 E 1 di,an,sil, pen,liq. Solidifies.
10	4 E 4 di,liq; 4 E 3 di,an,liq; 4 E 2 di,an,pen,liq; 4 E 1 di,an, pen,sil,liq. Solidifies.
11	4 E 4 di,liq; 4 E 3 di,an,liq; 4 E 2 di,an,fo,liq; 4 E 1 di,an, fo,pen,liq; 4 E 2 di,an,pen,liq; 4 E 1 di,an,pen,sil,liq. Solidifies.

Table 4.3 (continued).

Area	Equilibrium crystallisation history
12	4 E 4 di,liq; 4 E 3 di,an,liq; 4 E 2 di,an,fo,liq; 4 E 1 di,an, fo,pen,liq. Solidifies.
13	4 E 4 di,liq; 4 E 3 di,an,liq; 4 E 2 di,an,fo,liq; 4 E 1 di,an, fo,sp,liq. Solidifies.
14	4 E 4 di,liq; 4 E 3 di,fo,liq; 4 E 2 di,fo,an,liq; 4 E 1 di,fo, an,sp,liq. Solidifies.
15	4 E 4 di,liq; 4 E 3 di,fo,liq; 4 E 2 di,fo,an,liq; 4 E 1 di,fo, an,pen,liq. Solidifies.
16	4 E 4 di,liq; 4 E 3 di,fo,liq; 4 E 2 di,fo,an,liq; 4 E 1 di,fo, an,pen,liq; 4 E 2 di,an,pen,liq; 4 E 1 di,an,pen,sil,liq. Solidifies.
17	4 E 4 di,liq; 4 E 3 di,fo,liq; 4 E 2 di,fo,pen,liq; 4 E 1 di,fo, pen,an,liq. Solidifies.
18	4 E 4 di,liq; 4 E 3 di,fo,liq; 4 E 2 di,fo,pen,liq; 4 E 1 di,fo, pen,an,liq;4 E 2 di,an,pen,liq; 4 E 1 di,an,pen,sil,liq. Solidifies.
19	4 E 4 di,liq; 4 E 3 di,fo,liq; 4 E 2 di,fo,pen,liq; 4 E 3 di, pen,liq; 4 E 2 di,pen,an,liq; 4 E 1 di,pen,an,sil,liq. Solidifies.
20	4 E 4 di,liq; 4 E 3 di,fo,liq; 4 E 2 di,fo,pig,liq; 4 E 1 di,fo, pig,pen,liq;4 E 2 di,fo,pen,liq; 4 E 1 di,fo,pen,an,liq. Solidifies.
21	4 E 4 di,liq; 4 E 3 di,fo,liq; 4 E 2 di,fo,pig,liq; 4 E 1 di,fo, pig,pen,liq;4 E 2 di,fo,pen,liq; 4 E 1 di,fo,pen,an,liq; 4 E 2 di,pen,an,liq; 4 E 1 di,pen,an,sil,liq. Solidifies.
22	4 E 4 di,liq; E 3 di,fo,liq; 4 E 2 di,fo,pig,liq; 4 E 1 di,fo, pig,pen,liq; 4 E 2 di,fo,pen,liq; 4 E 3 di,pen,liq; 4 E 2 di,pen, an,liq; 4 E 1 di,pen,an,sil,liq. Solidifies.

Table 4.3 (continued).

Area	Equilibrium crystallisation history
23	4 E 4 di,liq; 4 E 3 di,fo,liq; 4 E 2 di,fo,pig,liq; 4 E 3 di,pig, liq; 4 E 2 di,pig,pen,liq; 4 E 3 di,pen,liq; 4 E 2 di,pen,an,liq; 4 E 1 di,pen,an,sil,liq. Solidifies.
24	4 E 4 di,liq; 4 E 3 di,fo,liq; 4 E 2 di,fo,pig,liq; 4 E 3 di,pig, liq; 4 E 2 di,pig,pen,liq; 4 E 3 di,pen,liq; 4 E 2 di,pen,sil,liq; 4 E 1 di,pen,sil,an,liq. Solidifies.
25	4 E 4 di,liq; 4 E 3 di,fo,liq; 4 E 2 di,fo,pig,liq; 4 E 3 di,pig, liq; 4 E 2 di,pig,sil,liq; 4 E 1 di,pig,sil,pen,liq; 4 E 2 di,sil, pen,liq; 4 E 1 di,sil,pen,an,liq. Solidifies.

Notes.

1. The composition of diopside crystallisaing has been assumed to be stoichiometric diopside, that is the projection composition.
2. The compositions of pen and pig plot at EN stoichiometric composition.

Removal of these simplifications will affect only the delineation of the areas.

Table 4.4 The generalised perfect fractional crystallisation histories of like areas of diopside saturated compositions presented in figure 4.13.

Area	Perfect fractional crystallisation history
1	4 E 4 di,liq; 4 E 3 di,sil,liq; 4 E 2 di,sil,an,liq; 4 E 1 di, sil,an,pen,liq.
2	4 E 4 di,liq; 4 E 3 di,sil,liq; 4 E 2 di,sil,pen,liq; 4 E 1 di, sil,pen,an,liq.
3	4 E 4 di,liq; 4 E 3 di,sil,liq; 4 E 2 di,sil,pig,liq; (4 E 1 di, sil,pig,pen,liq); 4 E 2 di,sil,pen,liq; 4 E 1 di,sil,pen,an,liq.
4	4 E 4 di,liq; 4 E 3 di,pig,liq; 4 E 2 di,pig,sil,liq; (4 E 1 di, sil,pig,pen,liq); 4 E 2 di,sil,pen,liq; 4 E 1 di,sil,pen,an,liq.
5	4 E 4 di,liq; 4 E 3 di,pig,liq; (4 E 2 di,pig,pen,liq); 4 E 3 di, pen,liq; 4 E 2 di,pen,an,liq; 4 E 1 di,pen,an,sil,liq.
6	4 E 4 di,liq; 4 E 3 di,pen,liq; 4 E 2 di,pen,sil,liq; 4 E 1 di,pen, sil,an,liq.
7	4 E 4 di,liq; 4 E 3 di,pig,liq; (4 E 2 di,pig,pen,liq); 4 E 3 di,pen, liq; 4 E 2 di,pen,an,liq; 4 E 1 di,pen,an,sil,liq.
8	4 E 4 di,liq; 4 E 3 di,pen,liq; 4 E 2 di,pen,an,liq; 4 E 1 di,pen, an,sil,liq.
9	4 E 4 di,liq; 4 E 3 di,an,liq; 4 E 2 di,an,sil,liq; 4 E 1 di,an, sil,pen,liq.
10	4 E 4 di,liq; 4 E 3 di,an,liq; 4 E 2 di,an,pen,liq; 4 E 1 di,an, pen,sil,liq.
11	4 E 4 di,liq; 4 E 3 di,an,liq; 4 E 2 di,an,fo,liq; (4 E 1 di,an, fo,pen,liq); 4 E 2 di,an,pen,liq; 4 E 1 di,an,pen,sil,liq.
12	4 E 4 di,liq; 4 E 3 di,an,liq; 4 E 2 di,an,fo,liq; (4 E 1 di,an, fo,sp,liq); 4 E 3 di,sp,liq; 4 E 2 di,sp,an,liq; 4 E 1 di,sp, an,mel,liq.

Table 4.4 (continued).

Area	Perfect fractional crystallisation history
13	4 E 4 di,liq; 4 E 3 di,fo,liq; 4 E 2 di,fo,an,liq; (4 E 1 di,an, fo,sp,liq); 4 E 3 di,sp,liq; 4 E 2 di,sp,an,liq; 4 E 1 di,sp,an, mel,liq.
14	4 E 4 di,liq; 4 E 3 di,fo,liq; 4 E 2 di,fo,an,liq; (4 E 1 di,fo, an,pen,liq); 4 E 2 di,an,pen,liq; 4 E 1 di,an,pen,sil,liq.
15	4 E 4 di,liq; 4 E 3 di,fo,liq; (4 E 2 di,fo,pen,liq); 4 E 3 di,pen, liq; 4 E 2 di,pen,an,liq; 4 E 1 di,pen,an,sil,liq.
16	4 E 4 di,liq; 4 E 3 di,fo,liq; (4 E 2 di,fo,pig,liq); 4 E 3 di,pig, liq; (4 E 2 di,pig,pen,liq); 4 E 3 di,pen,liq; 4 E 2 di,pen,an,liq; 4 E 1 di,pen,an,sil,liq.
17	4 E 4 di,liq; 4 E 3 di,fo,liq; (4 E 2 di,fo,pig,liq); 4 E 3 di,pig, liq; (4 E 2 di,pig,pen,liq); 4 E 3 di,pen,liq; 4 E 2 di,pen,sil,liq; 4 E 1 di,pen,sil,an,liq.
18	4 E 4 di,liq; 4 E 3 di,fo,liq; (4 E 2 di,fo,pig,liq); 4 E 3 di,pig, liq; 4 E 2 di,pig,sil,liq; (4 E 1 di,pig,sil,pen,liq); 4 E 2 di,pen, sil,liq; 4 E 1 di,pien,sil,an,liq.

Notes

1. Equilibria enclosed in brackets are encountered instantaneously only, one or more phases being in reaction relationship with liquid.

2. The compositions of di, pen, and pig have been assumed to be stoichiometric. Removal of this simplification will only affect the delineation of the areas.

The normative behaviour of the residual liquids can be determined by following the crystallisation histories of various bulk starting compositions with reference to figure 3.4. The behaviour is summarised for each compositional area in the figures.

CHAPTER 5

THE SYSTEM $CaO-MgO-Al_2O_3-SiO_2-Na_2O$

5.1 Introduction

The effects on geologically important phase equilibria, when the plagioclase solid solution representative is gradually altered from anorthite (Chapter 4, the system CMAS) to albite, without altering the other solid solution representatives, is a further step in the study of the larger synthetic basalt system. This is accomplished by the addition of Na_2O to the system CMAS.

From a general viewpoint of joins studied with anorthite and albite as the plagioclase end member, it is readily apparent that when the feldspar is albite, the plagioclase liquidus phase volume is much reduced in its extent, in comparison with the situation when anorthite is the plagioclase present. Coincident with this contraction, the temperatures of equivalent equilibria are substantially lowered.

As an example of this, in the join Anorthite-Forsterite-Silica (Andersen (1915)), the anorthite volume extends to compositions with approximately 50% anorthite, and the temperature of the piercing point of L. 4 E 2 fo,an,pyx,liq in this plane is 1260 °C. In the equivalent join Albite-Forsterite-Silica (Schairer and Yoder (1961)), the albite liquidus phase volume is found only in compositions with greater than 69% albite, and the temperature of the piercing point of L. 4 E 2 fo,ab,pyx,liq in this plane is 1045 °C.

A study of these changes at intermediate bulk normative plagioclase ratios in the system CMASN would be very desirable, especially the effect on the composition and temperature of L. 4 E 2 fo,plag,di,liq, since this equilibrium is encountered by the majority of natural rocks at some stage during their evolution.

5.2. Previous research

5.2.1 The system $MgO-Al_2O_3-SiO_2-Na_2O$

A small amount of data is available in the literature for this system. The liquidus phase fields in the plane $XO.ZO_2-YO.ZO_2-R_2O_3$ (CS-MS-A) can be predicted from the few joins studied, and are indicated in figure 5.1. Within the enlarged olivine phase volume (as compared to that of CS-MS-A), the second phase to appear is indicated in the appropriate areas. This $2YO.ZO_2$ (forsterite) projection graphically depicts the forsterite-bearing equilibria presented as part of the flow diagram for the system MASN by Schairer (1957). The unusual appearance of the diagram is due to the manner of calculation of the co-ordinates in the pseudoquaternary system (Chapter 3).

The L. 4 E 3 surfaces present in the forsterite projection (figure 5.1) are forsterite + liquid plus one of cordierite, albite, enstatite, spinel, nepheline or NMS compounds as indicated, and four L. 4 E 1 can be approximately located in the projection: L. 4 E 1 fo,sp,ab,ne,liq L. 4 E 1 fo, sp,ab,cord,liq, L. 4 E 1 fo,cord,ab,pyx,liq, and L. 4 E 1 fo,ab,pyx,NM_5S_{12},liq. Data for L. 4 E 2 involving forsterite + nepheline + liquid generally project to the low silica side of the plane $XO.ZO_2-YO.ZO_2-R_2O_3$ (CS-MS-A); the only data point projecting into the plane being that for the maximum on L. 4 E 2 fo,ab,ne,liq at 1058 °C in the join Forsterite-Nepheline-Silica (Schairer and Yoder (1961)).

The important points to note are the small extension of the L. 4 E 3 fo,ab,liq to the R_2O_3-rich side of the piercing point of the forsterite-albite join in the projection, and the much larger extent of the L. 4 E 3 fo,ab,liq towards the N-M-S join than that of L. 4 E 3 fo,an,liq in CMAS (figure 4.3). All the geologically important forsterite-bearing equilibria are present in MASN as in CMAS, indicating complete solid solution of plagioclases in these equilibria in the system CMASN.

Thus the maximum on 4 E 2 fo,ab,sp,liq corresponds to that on 4 E 2 fo,an,sp,liq in CMAS, but while the latter equilibrium involves resorption of spinel, 4 E 2 fo,ab,sp,liq does not. The change from reaction to non-reaction occurs within CMASN, therefore, and has a very important bearing on the equilibrium and fractional crystallisation histories of compositions of geological interest (section 5.4).

The presence of L. 4 E 1 fo,sp,ab,cord,liq and L. 4 E 1 fo,cord,ab,pyx,liq in MASN and L. 4 E 1 fo,sp,an,cord,liq and L. 4 E 1 fo,cord,an,pyx,liq in CMAS indicates the probability that these equilibria form two 5 E 2 involving complete plagioclase solid solution from the anorthite-bearing to the albite-bearing end of the CMASN system. The L. 5 E 2 fo,sp,plag,cord,liq and L. 5 E 2 fo,plag,cord,pyx,liq therefore meet no 5 E 1 within CMASN.

Within the five component system, 5 E 2 fo,sp,plag,cord,liq must alter its behaviour. 4 E 1 fo,sp,an,cord,liq in CMAS is a reaction point at which spinel is resorbed (i.e. it is 4 2 E 1 fo,$\overline{\text{sp}}$,an,cord,$\overline{\text{liq}}$) while 4 E 1 fo,sp,ab,cord,liq in

MASN is an isobaric eutectic (i.e. 4 1 E 1 fo,sp,ab,cord,$\overline{liq}$). For reasons discussed later, this change in behaviour within CMASN is believed to occur at a very low anorthite/albite ratio.

L. 4 E 1 fo,ab,cord,pyx,liq (MASN) and L. 4 E 1 fo,an,cord,pyx,liq (CMAS) are both silica saturated; forsterite reaction with liquid therefore probably occurs within the complete extent of 5 E 2 fo,plag,cord,pyx,liq. The major effect of these changes is that it is not possible in MASN to proceed from forsterite-spinel-bearing assemblages to enstatite-silica-bearing assemblages during any type of crystallisation, whereas it is possible in CMAS.

5.2.2 The system $CaO-MgO-Al_2O_3-SiO_2-Na_2O$

Previous knowledge of this system is limited. The joins Diopside-Albite-Forsterite (Schairer and Morimoto (1958)) and Diopside-Albite-Enstatite (Schairer and Morimoto (1959)) are pierced by L. 5 E 3 fo,plag,di,liq at approximately 1130 ^{o}C. A $2YO.ZO_2$ (forsterite) projection of this information (figure 5.2) shows the proposed positions of some of the forsterite-bearing equilibria when the bulk normative plagioclase in the system is albite and diopside is still present as a phase. The locations of L. 5 E 3 fo,plag,pyx,liq and L. 5 E 3 fo,cord,pyx,liq with L. 5 E 2 fo,plag,pyx,cord,liq are drawn at slightly more enstatite-rich compositions in the projection than for the MASN system. The piercing point of L. 5 E 2 fo,plag,sp,cord,liq is drawn at a very much more enstatite-rich point in projection than that of the MASN position (L. 4 E 1 fo,ab,sp,cord,liq) for reasons noted

later (section 5.3).

The proposed position in projection of the piercing point of L. 5 E 2 fo,plag,di,pyx,liq at this position in the system has been estimated. This is its most sodic proposed position known; complete solid solution of plagioclase occurs in this equilibrium within CMASN, and its termination 5 E 1 at a very low CaO region probably involves the NM_5S_{12} compound (possibly 5 E 1 fo,plag,pyx,di,NM_5S_{12},liq). Since L. 5 E 2 fo,plag,di,pyx,liq is silica saturated throughout its known range, forsterite reaction occurs throughout, silica-bearing equilibria being the goal of any compositions involving complete forsterite resorption during equilibrium or fractional crystallisation.

The very narrow extent of L. 5 E 4 fo,plag,liq to the diopside-rich side of the forsterite-plagioclase join should be noted. The areal extent of this locus decreases with decreasing anorthite/albite bulk ratio. However, its enlarged extent in MASN indicates that the locus must enlarge from its minimum extent at the anorthite/albite ratio of the 5 E 1 involving diopside.

Studies on systems involving anorthite/albite mixtures are limited to Diopside-Albite-Anorthite (Bowen (1915)) and Forsterite-Albite-Anorthite (Schairer and Yoder (1967)). Complete plagioclase solid solution is present in these joins. The join Forsterite-Albite-Anorthite is pseudoternary in that a spinel liquidus occurs within the join at high anorthite/albite ratios. The disappearance of spinel as a liquidus phase occurs at $An_{59}Ab_{41}$(wt%) and 1290 ^{o}C. This is the

anorthite/albite ratio which determines the change from spinel resorption to spinel co-precipitation in 5 E 3 fo,sp,plag,liq. When the plagioclase crystallising from the liquid reaches this normative ratio, the tangent to the sense of movement of L. 5 E 3 fo,sp,plag,liq will intersect the plagioclase-spinel join, indicating co-precipitation. The effect of this change is noted below.

It should also be noted that temperatures along L. 5 E 4 di,plag,liq and L. 5 E 4 fo,plag,liq in these two sections decrease gradually as the plagioclase becomes more albitic. However, as the plagioclase moves nearer to albite the temperatures drop much more rapidly into a very low temperature region in the pure albite join.

The join Diopside-Enstatite-$Albite_{40}Anorthite_{60}$ (mole %; Emslie (1971)), locates L. 5 E 3 fo,plag,di,liq at the bulk normative plagioclase ratio of $An_{61.4}Ab_{38.6}$ at 1235 $\pm$ 5 °C. Its location in a $2YO.ZO_2$ (forsterite) projection (see figure 5.14) is in agreement with the present data.

Eggler (1974) has presented an analysis of L. 5 E 3 fo,plag,pyx,liq and L. 5 E 3 sil,plag,pyx,liq in the join $MgO-SiO_2$-$Anorthite_{50}Albite_{50}$ (normative ratio). The location of the forsterite-bearing liquid is in agreement with that inferred from this work (see figure 5.8).

5.3 Experimental results

To determine the effects of changing the anorthite/albite ratio of the plagioclase end member on the location and temperature of the forsterite-bearing equilibria, compositions were prepared such that after application of the data reduction scheme these compositions had co-ordinates within the join $XO.ZO_2$-$YO.ZO_2$-R_2O_3 (CS-MS-A). Within this join they also lay on the joins $XO.YO.2ZO_2$-$YO.R_2O_3.ZO_2$ (Diopside-MAS), $XO.YO.2ZO_2$-$5YO.3R_2O_3.5ZO_2$ (Diopside-$M_5A_3S_5$) and $XO.YO.2ZO_2$-$7YO.3R_2O_3.7ZO_2$ (Diopside-$M_7A_3S_7$). The molecular anorthite/albite ratios of 2,1, and 0.5 (corresponding to bulk normative plagioclase ratios An_{68}, $An_{51.5}$ and $An_{34.6}$, wt%) were chosen for the compositions. The compositional data are given in Appendix B.2; furnace operation details involving these compositions in Appendix C.1; run details and products obtained in Appendix E.2.

In order to show the relationships between the results on the various joins at the various ratios studied the results are graphically displayed in a variety of ways:

1. The join $XO.R_2O_3.2ZO_2$ - $XO.YO.2ZO_2$ - $2YO.ZO_2$ (Plagioclase-Diopside-Forsterite) is drawn for each anorthite/albite ratio studied (figures 5.3 to 5.5). The join Anorthite-Diopside-Forsterite was presented as figure 4.1. The join Albite-Diopside-Forsterite (Schairer and Morimoto (1958)) is also shown, recalculated according to the data reduction scheme, for comparison purposes (figure 5.6). Data from the join $XO.YO.2ZO_2$-$YO.R_2O_3.ZO_2$ (Diopside-MAS) together with data read from Forsterite-Albite-Anorthite (Schairer and Yoder (1967))

and Diopside-Albite-Anorthite (Bowen (1915)) was used to construct the diagrams.

2. Since all the compositions studied have forsterite as liquidus phase (liquidus temperature not determined for all compositions), a $2YO.ZO_2$ (forsterite) projection into $XO.ZO_2$-$YO.ZO_2$-R_2O_3 (CS-MS-A) is drawn for each anorthite/albite ratio studied (figures 5.7 to 5.9). By this means the results on each join studied are related to each other, to provide a picture of the geometrical relationships of the forsterite-bearing equilibria at each anorthite/albite ratio. Interpolation between the CMAS and MASN systems was used to locate approximately the forsterite-cordierite-bearing equilibria.

3. The data for each anorthite/albite ratio for each join, are combined to show the continuous manner of change, in temperature and location in the join, of the forsterite-bearing equilibria which intersect the join. (figures 5.10 to 5.12).

4. Summary diagrams are drawn to show the change in temperature and composition of the equilibria encountered as the bulk normative plagioclase changes from anorthite to albite in the starting mixtures.

a) In the join $XO.R_2O_3.2ZO_2$-$XO.YO.2ZO_2$-$2YO.ZO_2$ (Plagioclase-Diopside-Forsterite), the position and temperatures of L. 5 E 3 fo,plag,di,liq, L. 5 E 3 fo,plag,sp,liq, L. 5 E 4 fo,di,liq, L 5 E 4 fo,plag,liq, L. 5 E 4 fo,sp,liq and L. 5 E 4 plag,sp,liq are shown versus anorthite/albite ratio (figure 5.13).

b) A $2YO.ZO_2$ (forsterite) projection into $XO.ZO_2$-$YO.ZO_2$-R_2O_3 (CS-MS-A) shows the position in projection and temperature

changes of L. 5 E 3 fo,plag,di,liq, L. 5 E 3 fo,plag,pyx,liq and L. 5 E 2 fo,plag,di,pyx,liq versus anorthite/albite ratio (figure 5.14).

c) A $XO.YO.2ZO_2$ (diopside) projection into the plane $XO.R_2O_3 - YO - ZO_2$ (CA-M-S) shows the relationship between the forsterite-diopside equilibria and the silica-diopside equilibria as the anorthite/albite ratio changes (figure 5.15). This is a graphical representation of part of the suggested flow sheet for compositions in CMASN given by O'Hara and Biggar (1969a). Individual diopside projections at each anorthite/albite ratio studied were not attempted because of insufficient limiting data.

The results presented in these diagrams show that the change from anorthitic to albitic plagioclase, is reflected in a gradual change in the location of the liquid compositions in the equilibria, from those appropriate to the pure anorthite-bearing system to those appropriate to the most albite known positions, except for the behaviour of L. 5 E 2 fo,cord,plag,sp,liq. Thus L. 5 E 2 fo,plag,pyx,di,liq moves to more aluminous compositions, that is higher plagioclase/enstatite and plagioclase/diopside normative ratios in projection, as the ratio becomes more albitic. The region of potential L. 5 E 4 fo,plag,liq compositions in projection thus decreases in size, while the L. 5 E 4 fo,di,liq and L. 5 E 4 fo,pyx,liq regions correspondingly expand.

The Plagioclase-Diopside-Forsterite joins (figures 5.3 to 5.6 and the summary in figure 5.13) show the change in the

relative sizes of the phase volumes. Thus the forsterite phase volume expands at the expense of the plagioclase volume, the diopside volume remaining only near the Plagioclase-Diopside join. The spinel volume disappears from the join at the Forsterite-Plagioclase join.

The disappearance of spinel from the Forsterite-Anorthite-Albite join at An_{59} is also shown by the contraction of L. 5 E 3 fo,sp,plag,liq to more aluminous compositions. As a result of this, the spinel reaction in this equilibrium will cease, becoming one of co-precipitation of forsterite, spinel, and plagioclase. This behaviour was not confirmed in this study nor was the albite/anorthite ratio in the liquid at which the change occurs determined. It would however require extensive, most unlikely, solid solution changes to prevent its occurrence. The contraction of L. 5 E 4 fo,sp,liq decreases rapidly once this change has occurred, such that very little change in its projected position occurs.

The behaviour of L. 5 E 2 fo,cord,plag,sp,liq is not a simple, gradual change from L. 5 E 2 fo,cord,an,sp,liq (CMAS) to L. 5 E 2 fo,cord,ab,sp,liq (MASN). Results on the $XO.YO.2ZO_2$-$7YO.3R_2O_3.7ZO_2$ (Diopside-$M_7A_3S_7$) join at $Ab_{65.4}$ ratio, indicate that liquids in this equilibrium have not yet passed through this join. The assumption was therefore made that the position in projection of the liquid in this equilibrium probably changes very rapidly at very low anorthite/albite ratios to achieve its projected position in the system MASN (figure 5.1). The projected position at the most albitic ratio known (figure 5.2) was drawn on the basis of this assumption.

Accompanying these changes, is a lowering of temperatures generally; thus L. 5 E 2 fo,plag,pyx,di,liq decreases from 1241°C (An_{100}) to c.1230°C (An_{68}), c.1220°C ($An_{51.5}$) and then decreases much more rapidly to less than 1100°C at the almost pure albite position. This behaviour in the temperature decrease is similar to that encountered in the Plagioclase-Forsterite and Plagioclase-Diopside joins mentioned above.

The composition of L. 5 E 3 fo,plag,di,liq at $An_{61.4}$ (normative ratio) in the plane Plagioclase-Diopside-Enstatite from Emslie (1971) was projected from forsterite and is included in figure 5.14. Its position in projection agrees very well with the present results. Slight disagreement on the temperature is understandable: Emslie quotes 1235 $\pm$5°C on an unstated technique, while the temperature by interpolation in this study is c. 1245°C.

The composition of L. 5 E 3 fo,plag,pyx,liq at An_{50} (normative ratio) in the plane Plagioclase-MgO-SiO_2 from Eggler (1974) was also projected from forsterite and is shown on figure 5.8. Its position in projection agrees fairly well with that estimated for An_{50} in this work. The temperature however is lower: Eggler quotes 1228°C, while interpolation here gives c. 1240°C. Again the technique is unknown, as is the temperature brackets on the runs which give that result.

The expansion of the olivine volume with more albitic plagioclase ratio is also reflected in the area in olivine projection in which the liquids are silica saturated. The anorthite and albite bulk ratio silica saturation areas,

together with the change in projection of the point on L. 5 E 3 fo,plag,di,liq at which silica saturation occurs, are shown in figure 5.14. It is readily apparent that the area expands and at high albite ratios the area of olivine normative L. 5 E 3 fo,plag,di,liq is very restricted.

The change in extent of the iron-free pigeonite volume with changing bulk plagioclase ratio could not be studied with the compositions available. If the pigeonite field extends to meet the plagioclase field only small alterations to the figures will be required to accommodate the changes.

5.4. Discussion

As was noted in Chapter 4 in the system CMAS, the equilibrium involving forsterite, anorthite, spinel and liquid provided the means by which residual liquids which are both saturated* and undersaturated* in the CIPW norm, could be derived from the same bulk starting composition, depending upon the degree of fractionation involved. The new results and their analysis, presented previously in section 5.3, showed that as the plagioclase was changed from anorthite to albite, the analogous equilibrium, 5 E 3 plag, fo, sp, liq within CMASN, altered its nature from one involving spinel reaction with the liquid, to one of co-precipitation of plagioclase, forsterite and spinel. This change in nature has a decisive effect on the crystallisation histories of molecularly equivalent bulk compositions having different anorthite/albite ratios.

To consider this change at its simplest, the relationship of 5 E 3 plag, fo, sp, liq to the volume Forsterite-Albite-Anorthite-Spinel is fundamental. To display this relationship, a forsterite projection into the plane Albite-Anorthite-Spinel extended is sketched in figure 5.16. In this figure, the piercing point of L. 5 E 3 plag, fo, sp, liq in this plane is also shown. Using this diagram, a similar analysis of like crystallisation histories can be attempted,

---

* In the following discussion, the term saturated is taken to represent those compositions which would not contain corundum, larnite, and nepheline in the CIPW norm; and undersaturated represents those compositions which would contain corundum, and/or larnite and/or nepheline in the norm.

as was used in Chapter 4 for forsterite saturated bulk compositions. Thus the figures 5.17, 5.18 show the areas of similar crystallisation histories under equilibrium and fractional types of crystallisation and tables 5.1, 5.2 give the details of the histories of each area.

Under equilibrium crystallisation conditions (figure 5.17), only bulk compositions which project in areas 1 and 2 can produce residual liquids which are saturated in the CIPW norm during crystallisation. While they encountered 5 E 3 plag, fo, sp, liq at a point while spinel is still in reaction relationship with the liquid, not all the spinel is lost before crystallisation ceases within this equilibrium. Bulk compositions in area 1 will solidify with the last liquid being saturated in the CIPW norm, but those in area 2 will solidify only when the liquid has become undersaturated again in the CIPW norm.

Bulk compositions projecting in area 3 will encounter 5 E 3 plag,fo,sp,liq while spinel is still in reaction relationship, but the liquids are undersaturated in the CIPW norm. Prior to solidification, however, spinel will cease reaction with the liquid and commence to precipitate. Bulk compositions projecting in area 4 will never yield liquids in which spinel is in reaction relationship in 5 E 3 plag,fo,sp,liq and the liquids are always undersaturated in the CIPW norm.

Bulk compositions projecting in area 5 are the only compositions saturated in the CIPW norm to yield spinel as a phase during crystallisation. Crystallisation will persist in 5 E 3 plag,fo,sp,liq while spinel is resorbed

Table 5.1 The generalised equilibrium crystallisation histories of like areas of forsterite saturated compositions presented in figure 5.17. Further discussion in the text.

Area	Equilibrium crystallisation history
1	5 E 5 fo,liq; 5 E 4 fo,sp,liq; 5 E 3 fo,sp,plag,liq; Solidifies before all spinel has reacted, and the anorthite/albite ratio of liquid is less than $An_{59}Ab_{41}$.
2	5 E 5 fo,liq; 5 E 4 fo,sp,liq; 5 E 3 fo,sp,plag,liq; Solidifies before all spinel has reacted, and the anorthite/albite ratio of liquid is greater than $An_{59}Ab_{41}$.
3	5 E 5 fo,liq; 5 E 4 fo,sp,liq; 5 E 3 fo,sp,plag,liq. Spinel is initially in reaction relationship, but later precipitates before solidification.
4	5 E 5 fo,liq; 5 E 4 fo,sp,liq; 5 E 3 fo,sp,plag,liq. Spinel is never in reaction relationship. Solidifies.
5	5 E 5 fo,liq; 5 E 4 fo,sp,liq; 5 E 3 fo,sp,plag,liq (complete spinel resorbtion occurs); 5 E 4 fo,plag,liq; 5 E 3 fo,plag,di,liq; 5 E 2 fo,plag,di,pyx,liq. Solidifies.
6	5 E 5 fo,liq; 5 E 4 fo,plag,liq; 5 E 3 fo,plag,di,liq; 5 E 2 fo, plag,di,pyx,liq. Solidifies.
7	5 E 5 fo,liq; 5 E 4 fo,plag,liq; 5 E 3 fo,plag,sp,liq; Solidifies.
8	5 E 5 fo,liq; 5 E 4 fo,sp,liq; 5 E 3 fo,sp,plag,liq (all spinel is resorbed); 5 E 4 fo,plag,liq. Compositions having bulk anorthite/albite ratios greater than $An_{59}Ab_{41}$ solidify; others continue to 5 E 3 fo,plag,sp,liq and then solidify.

Table 5.2 The generalised perfect fractional crystallisation histories of like areas of forsterite saturated compositions presented in figure 5.18. Further discussion in the text.

Area	Perfect fractional crystallisation history
1 and 2	5 E 5 fo,liq; 5 E 4 fo,sp,liq; (5 E 3 fo,sp,plag,liq); 5 E 4 fo, plag,liq; 5 E 3 fo,plag,di,liq; (5 E 2 fo,plag,di,pyx,liq); 5 E 3 plag,di,pyx,liq; 5 E 2 plag,di,pyx,sil,liq.
3	5 E 5 fo,liq; 5 E 4 fo,plag,liq; 5 E 3 fo,plag,di,liq; (5 E 2 fo,plag,di,pyx,liq); 5 E 3 plag,di,pyx,liq; 5 E 2 plag,di,pyx, sil,liq.
4	5 E 5 fo,liq; 5 E 4 fo,sp,liq; (5 E 3 fo,sp,plag,liq); 5 E 4 fo, plag,liq; 5 E 3 fo,sp,plag,liq.
5	5 E 5 fo,liq; 5 E 4 fo,plag,liq; 5 E 3 fo,plag,sp,liq.
6	5 E 5 fo,liq; 5 E 4 fo,sp,liq; 5 E 3 fo,sp,plag,liq.

Note

1. Equilibria enclosed in brackets are encountered instantaneously only, one or more phases being in reaction relationship with liquid.

and the liquid increases its albite/anorthite ratio. Complete resorbtion will occur and crystallisation will then continue to diopside-bearing equilibria (5 E 3 plag,fo,di, liq). Compositions projecting in area 6 follow this latter course also, but do not crystallise spinel at any point in their histories. Residual liquids produced by compositions in areas 5 and 6 are always saturated in the CIPW norm. Compositions undersaturated in the CIPW norm projecting in area 7 produce residual liquids which are always undersaturated even though plagioclase is crystallising. The plagioclase crystallisation interval will always be long and the liquid path through the system curved. Eventually 5 E 3 plag,fo,sp,liq is encountered and spinel precipitates.

Bulk compositions projecting in the small area 8, which are undersaturated in the CIPW norm, have a very varied history. Initially L. 5 E 4 fo,sp,liq are undersaturated in the CIPW norm but become saturated before reaching L. 5 E 3 plag,fo,sp,liq. The latter liquids later become undersaturated, spinel resorption occurring throughout. At the appropriate point all the spinel is lost and these compositions enter 5 E 4 plag,fo,liq having liquids always undersaturated in the norm. Those compositions having bulk anorthite/albite ratios greater than An_{59}, will solidify in this equilibrium. Compositions more albite rich, reprecipitate spinel when 5 E 3 plag,fo,sp,liq is reached and then solidify in this equilibrium.

The possible crystallisation paths are thus very varied depending on the initial bulk composition.

Fractional crystallisation of compositions in area 1 (figure 5.18) initially produces residual liquids undersaturated in the CIPW norm, becoming saturated prior to entering 5 E 3 plag,fo,sp,liq. Spinel is then lost and the residual liquids eventually lose olivine and later encounter equilibria containing a silica-bearing mineral (not shown in this section). Compositions in area 2 are similar, except that no liquids undersaturated in the norm are produced, but spinel occurs as a phase within the history. Area 3 compositions are also similar but develop no spinel in their crystallisation histories. The range of compositions producing end products which precipitate a silica mineral is, therefore, extensive.

The bulk compositions undersaturated in the CIPW norm, in areas 4, 5, 6, can never produce saturated liquids by means of diopside or enstatite precipitating histories (they may reach liquids which precipitate a silica mineral by the cordierite precipitating histories though - see below). Compositions in area 4 cease precipitating spinel at 5 E 3 plag,fo,sp,liq, but reprecipitate spinel after some fractionation in 5 E 4 fo,plag,liq. Compositions in areas 5 and 6 are straightforward, their fractional crystallisation involving no reaction relations.

Extension of this simple discussion must now be made to include compositions richer in diopside or enstatite components. To do this graphically is impossible without a simplification being made. The simplification chosen is to consider a forsterite projection of all bulk compositions at a particular anorthite/albite ratio (as was done in effect in the system CMAS - with An_{100} bulk ratios).

The diagrams for equilibrium and fractional crystallisation areas when the bulk ratio was An_{100} (figures 4.10, 4.11), can be used equally well for general consideration of all bulk compositions with anorthite/albite ratios greater than An_{59}, provided the previous discussion is kept in mind for compositions encountering 5 E 3 plag,fo,sp,liq.

Bulk compositions more albite rich than An_{59} have much simpler crystallisation histories. Like areas can again be outlined for equilibrium (figure 5.19) and fractional (figure 5.20) types of crystallisation. The details of the crystallisation histories are given for these areas in tables 5.3, 5.4. Those compositions entering 5 E 3 plag, fo,sp,liq must be treated in a similar manner to those for the simple system discussed above.

The most important feature of these figures is that bulk compositions undersaturated in the norm, can no longer yield residual liquids saturated in the norm via diopside+ forsterite or enstatite+forsterite crystallisation. Cordierite-precipitating liquids provide the only means to reach residual liquids which precipitate a silica mineral. The range of variation of residual liquid compositions is, therefore, much reduced for these bulk compositions.

The behaviour shown by those bulk compositions lying within area 8 (figure 5.17) under equilibrium crystallisation must extend into the larger system. However, the limited knowledge of the system is insufficient to determine the extent and direction of the extension at present.

There is another way which may produce variation in residual liquids in this system. The thermal maximum of,

Table 5.3 The generalised equilibrium crystallisation histories of like areas of forsterite saturated compositions presented in figure 5.19.

Area	Equilibrium crystallisation history
8	5 E 5 fo,liq; 5 E 4 fo,plag,liq; 5 E 3 fo,plag,cord,liq or 5 E 3 fo,plag,pyx,liq; 5 E 2 fo,plag,cord,pyx,liq. Solidifies.
9	5 E 5 fo,liq; 5 E 4 fo,plag,liq; 5 E 3 fo,plag,di,liq or 5 E 3 fo,plag,pyx,liq; 5 E 2 fo,plag,di,pyx,liq. Solidifies.
10	5 E 5 fo,liq; 5 E 4 fo,di,liq; 5 E 3 fo,di,plag,liq or 5 E 3 fo,plag,pyx,liq; 5 E 2 fo,plag,pyx,di,liq. Solidifies.
11	5 E 5 fo,liq; 5 E 4 fo,di,liq; 5 E 3 fo,di,plag,liq. Solidifies in unknown nepheline or melilite bearing equilibria.
12	5 E 5 fo,liq; 5 E 4 fo,plag,liq; 5 E 3 fo,plag,di,liq. Solidifies in unknown nepheline or melilite bearing equilibria.
13	5 E 5 fo,liq; 5 E 4 fo,plag,liq; 5 E 3 fo,plag,sp,liq. Solidifies in unknown nepheline or melilite bearing equilibria.
14	5 E 5 fo,liq; 5 E 4 fo,plag,liq; 5 E 3 fo,plag,sp,liq; 5 E 2 fo, plag,sp,cord,liq; 5 E 3 fo,plag,cord,liq; 5 E 2 fo,plag,cord,pyx, liq. Solidifies.

Table 5.4 The generalised perfect fractional crystallisation histories of like areas of forsterite saturated compositions presented in figure 5.20.

Area	Perfect fractional crystallisation history
4	5 E 5 fo,liq; 5 E 4 fo,plag,liq; 5 E 3 fo,plag,di,liq; to ??
5	5 E 5 fo,liq; 5 E 4 fo,plag,liq; 5 E 3 fo,plag,di,liq or 5 E 3 fo,plag,pyx,liq; (5 E 2 fo,plag,pyx,di,liq); 5 E 3 plag, pyx,di,liq; 5 E 2 plag,pyx,di,sil,liq.
6	5 E 5 fo,liq; 5 E 4 fo,plag,liq; 5 E 3 fo,plag,cord,liq or 5 E 3 fo,plag,pyx,liq; (5 E 2 fo,plag,pyx,cord,liq); 5 E 4 plag, pyx,liq to 5 E 2 plag,pyx,cord,sil,liq ?
7	5 E 5 fo,liq; 5 E 4 fo,di,liq; 5 E 3 fo,di,plag,liq; to unknown nepheline or melilite bearing equilibria.
8	5 E 5 fo liq; 5 E 4 fo,di,liq; 5 E 3 fo,di,plag,liq; (5 E 2 fo, di,plag,pyx,liq); 5 E 3 di,plag,pyx,liq; 5 E 2 plag,di,pyx,sil,liq.
9	5 E 5 fo,liq; 5 E 4 fo,plag,liq; 5 E 3 fo,plag,sp,liq; to unknown nepheline or melilite bearing equilibria.
10	5 E 5 fo,liq; 5 e 4 fo,plag,liq; 5 E 3 fo,plag,sp,liq; (5 E 2 fo, plag,sp,cord,liq); 5 E 3 fo,plag,cord,liq; (5 E 2 fo,plag,cord, pyx,liq); 5 E 4 plag,pyx,liq; to 5 E 2 plag,pyx,cord,sil,liq ?

Note

1. Equilibria enclosed in brackets are encountered instantaneously only, one or more phases being in reaction relationship with liquid.

for example, 5 E 3 plag,fo,di,liq will involve a different diopside solid solution at different plagioclase compositions, that is, the thermal divides themselves change position as the Na/Ca ratio varies. It is thus possible for a bulk composition to begin crystallisation producing liquids which would have become undersaturated in the norm, if the thermal divides were in a fixed position in the projection, but because the effective position of the thermal divide may move through the bulk composition in the projection as the Na/Ca ratio rises, the liquids produced could then become saturated in the norm.

This situation will most probably exist about the maximum on L. 5 E 3 fo,plag,di,liq but the exact changes which occur are unknown because the diopside compositions are unknown. It is entirely possible that saturated compositions may change to produce undersaturated liquids, but this is unlikely since no temperature maximum was located on L. 5 E 3 plag,fo,di,liq in the area studied.

In summary, the variation in residual liquids outlined for the system CMAS is continued into CMASN to moderate An/Ab bulk ratios. Change in the nature of 5 E 3 plag,fo,sp,liq however, reduces the extent of variation in more albite rich bulk compositions. In terms of CIPW normative constituents, all olivine-bearing equilibria become more plagioclase-rich as the An/Ab bulk ratio reduces.

CHAPTER 6

THE SYSTEM $CaO-MgO-Al_2O_3-SiO_2-Fe-O_2$

6.1 Introduction

The ionic substitution of Fe for Mg is found in the pyroxene, olivine and spinel solid solution series. The next logical step in the study of the subsystems of the basalt system is, therefore, to introduce iron. The addition of iron, however, involves the addition of two components, because iron is stable in two co-existing oxide forms - FeO and Fe_2O_3 - whose ratio depends, among other things, on the partial pressure of oxygen (in the atmosphere equilibrated with the sample).

That the phase equilibria relations are strongly dependent on the pO_2 of the atmosphere in iron-bearing systems, has been ably demonstrated for the simpler joins, such as SiO_2-Fe-O_2 (Muan (1955)) and $MgO-SiO_2-Fe-O_2$ (Muan and Osborn (1956)). However, the effect of pO_2 and changing Fe/Mg ratio on the composition and temperature of the geologically important olivine-clinopyroxene-anorthite-liquid equilibrium has escaped attention up to this time.

6.2 Previous research

6.2.1 Introduction

The complexity of the system requires that a large amount of data must be obtained to completely describe equilibria within it. Previously published data are available for several joins in the system, much of the work being carried out by a technique using iron crucibles, which affords a convenient means of controlling the pO_2. Phase equilibria assemblages reported are, therefore, in equilibrium with metallic iron and the pO_2 thus defined is lower than that of the iron-wustite equilibrium in the system Fe-O_2. Several important studies have, however, been undertaken in which the pO_2 has been an independent variable.

6.2.2 The system MgO-SiO_2-Fe-O_2

Based on the studies of SiO_2-Fe-O_2 (Muan (1955)) and MgO-SiO_2-Fe-O_2 (Bowen and Schairer (1935); Muan and Osborn (1956)), Speidel and Nafziger (1968) presented an intensive variable plot of $\log_{10}(pO_2)$ versus temperature for the system MgO-SiO_2-Fe-O_2 (redrawn as figure 6.1), defining L. 6 E 3 ol,pyx,sil,Fe,liq (OPSIL)* to occur at 1305°C, $pO_2 = 10^{-11.8}$ and L. 6 E 3 ol,pyx,sp,sil,liq (OPMSL) to occur at 1255°C, $pO_2 = 10^{-7.1}$. Intensive variable plots do not, however, show the equilibria in relation to the composition axes.

---

* In this chapter, to shorten figure notations, the following symbols are used on the diagrams and after the equilibria in the text:
S = sil; O = ol; P = pyx,pig or pen; I = iron metal;
L = liq; M = sp; D = cpx; W = woll; A = An.

To overcome this, the L. 6 E 4 data from SiO_2-Fe-O_2 (Muan (1955)) and MgO-SiO_2-Fe-O_2 (Bowen and Schairer (1935); Muan and Osborn (1956) plus interpolations given by Presnall (1966)) are recalculated with all iron as FeO, and plotted in the join MgO-FeO-SiO_2 (figure 6.2). The composition of L. 6 E 3 ol,pyx,sp,sil,liq (OPMSL) is, therefore, defined (with all the iron expressed as FeO), as are the compositions of the L. 6 E 4, as a function of pO_2. The inferred composition of L. 6 E 3 ol,pyx,sp,sil,liq (OPMSL) agrees with that quoted by Muan and Osborn (1956) with all the iron recalculated as FeO. It should be noted, however, that the data for this system given by Speidel and Osborn (table 1, p. 1142; 1967) are not consistent with those of Muan and Osborn (1956), or figure 6.2.

This multi-pO_2 MgO-SiO_2-Fe-O_2 plot (figure 6.2) clearly shows the influences of pO_2 on the phase equilibria. At any given pO_2 the phase equilibrium diagram for this system can be drawn by determining the liquid compositions on the 6 E 4 equilibria which exist at that pO_2. Thus in figure 6.2 the phase equilibria boundaries are shown at pO_2 = air and pO_2 = Fe just present. In air, the magnetite phase volume occupies much of the more iron-rich portion of the diagram. As the pO_2 becomes more reducing, the magnetite volume contracts to higher Fe/Mg ratios, the olivine and pyroxene volumes increasing in extent. At $pO_2 = 10^{-7.1}$ and 1255°C, 6 E 5 pyx,sp,liq is replaced by 6 E 5 ol,sil,liq. Thereafter, the magnetite phase volume continues to contract to more iron rich compositions with the olivine volume expanding to replace it. The pyroxene

volume, however, contracts slightly to the boundaries shown at pO_2 = Fe just present.

Utilising the information on this figure, the phase equilibrium diagram for the join at the pO_2 of the Ni/NiO (figure 6.3) and Fe/FeO (figure 6.4) equilibria can be constructed. It should be noted that the Ni/NiO equilibrium diagram intersects L. 6 E 3 ol,pyx,sp,sil,liq (OPMSL). From these two diagrams, the phase equilibria information for the join ZO_2-YO(S-M) at the various Fe/Mg ratios studied can be determined.

Also from figure 6.2, information can be obtained to construct a liquidus phase diagram for the join Enstatite-Ferrosilite versus pO_2 (figure 6.5). This figure shows the liquidus phase present for each composition in the join at any pO_2. The Ni/NiO and Fe/FeO equilibria pO_2 curves are drawn on the diagram for reference.

6.2.3 The system CaO-MgO-SiO_2-Fe-O_2

The accumulation of data for this system by the addition of CaO to the MgO-SiO_2-Fe-O_2 system has been attempted by a number of studies. The phase diagram for the iron-free system CMS is known from Ferguson and Merwin (1919), redrawn by Osborn and Muan (1960) to incorporate later work. More recent data on the geologically important join Diopside-Forsterite-Silica is available from Kushiro (1972) and Yang and Foster (1972).

Part of the MgO-free system CaO-SiO_2-Fe-O_2, has been studied in contact with metallic iron crucibles by Bowen, Schairer and Posnjak (1933), who determined L. 6 E 3

ol,woll,sil,Fe,liq (OWSIL) at 1105°C and L. 6 E 3 ol,woll, pwoll,Fe,liq at 1193°C. The same system was studied in air by Phillips and Muan (1959), who determined the absence of an olivine volume but L. 6 E 4 hem,sp,sil,liq and L. 6 E 4 hem,pwoll,sil,liq were found. Intermediate pO_2 studies have not been conducted.

Data for variable Fe/Mg ratios is obtainable from Presnall (1966), who studied the join Diopside-Iron oxide-Forsterite between air and $pO_2 = 10^{-8}$ atmospheres. On the basis of these results, Presnall postulated the existence of L. 6 E 3 pyx,cpx,sp,sil,liq (PDMSL) and L. 6 E 3 ol,pyx, sp,cpx,liq (OPMDL) at pO_2 between air and 10^{-6} at least. The temperature of these equilibria were not determined.

Nafziger (1970) studied the join Diopside-Iron oxide-Silica at a constant CO_2/H_2 mixing ratio = 50 (this ratio approximates that of the Ni/NiO equilibrium; see figure 6.1). On the basis of these results, Nafziger postulated the existence of L. 6 E 3 ol,sil,cpx,sp,liq (OSDML), L. 6 E 3 sil,cpx,pyx,sp,liq (SDPML) and L. 6 E 3 ol,cpx,pyx,sp, liq (ODPML) which would result in the unusual situation of L. 6 E 4 ol,cpx,sp,liq (ODML) existing separately twice, and the existence of two separate olivine volumes. This feature is most unlikely in sections where the pO_2 changes regularly, but is not impossible for other pO_2 sections that change irregularly.

A more likely interpretation when this join is considered as part of the larger $CaO-MgO-SiO_2-Fe-O_2$ system, and since Nafziger determined experimentally that L. 6 E 3 ol,sil,cpx,sp,liq (OSDML) does occur at this ratio between

1090 and 1144°C, is shown in the sketch of the system (figure 6.6). In this interpretation L. 6 E 3 ol,sil, cpx,sp,liq (OSDML) occurs outside the tetrahedron portrayed, but probably within Diopside-Hedenbergite-Fe_3O_4-SiO_2-Forsterite, and L. 6 E 3 ol,sil,cpx,pyx,liq (OSDPL) and L. 6 E 3 ol,sil,pyx,sp,liq (OSPML) occur within the tetrahedron. A sketch of the pO_2 versus temperature relationships for these data is shown as figure 6.7, postulating the existence of L. 6 E 2 sil,ol,pyx,cpx,sp,liq (SOPDML) at a slightly more oxidising pO_2 than that of the Ni/NiO equilibrium.

Ricker (reported in Muan and Osborn (1965)), studied the system in contact with metallic iron, reporting L. 6 E 2 sil,cpx,ol,woll,Fe,liq (SDOWIL) at 1100°C and FeO/(FeO+MgO) ratio = 0.64 (mole), as the only geologically significant equilibria. The presence of L. 6 E 2 sil,ol,pyx,cpx,Fe,liq (SOPDIL) was not reported possibly due to the difficulty of distinguishing the two pyroxenes, but it must exist in this system.

Turnock (1962) presented a diagram for the join Diopside-Hedenbergite at the pO_2 of the Fe/FeO equilibria. Yoder, Tilley and Schairer (1963) utilising data from several sources, including Turnock, constructed a liquidus diagram for the join CS-MS-FS in equilibrium with metallic iron. Roedder (1965) studied MS-FS-CMS_2-CFS_2 in contact with metallic iron, and presented a similar diagram. Minor differences were ascribed to the low angle at which the equilibria intersect the join studied and the possible

silica deficiency of some of Roedder's compositions (Roedder (1965):p.702). Three important equilibria were thought on the basis of these diagrams to have piercing points in this quadrilateral: L. 6 E 3 cpx,ol,pyx,Fe,liq (DOPIL), L. 6 E 3 cpx,pyx,sil,Fe,liq (DPSIL), and L. 6 E 3 sil,cpx,woll,Fe,liq (SDWIL).

However, a multi-Fe/Mg ratio plot of the system CMS-Fe-O_2, at the pO_2 at which metallic iron is present (figure 6.8), shows the inferred positions of the L. 6 E 2 and L. 6 E 3 of importance to this study, and indicates that L. 6 E 3 sil,cpx,woll,Fe,liq (SDWIL) is unlikely to pierce the pyroxene quadrilateral. It is possible, however, that at the pO_2 of the Fe/FeO equilibrium (a more oxidising pO_2), this equilibrium does pierce the plane as suggested by the data of Turnock (1962). In figure 6.8, the position of L. 6 E 2 sil,ol,cpx,pyx,Fe,liq (SODPIL) is postulated, while L. 6 E 3 ol,cpx,woll,Fe,liq (ODWIL) links to melilite-bearing equilibria (Ricker, reported in Muan and Osborn (1965),p.145).

6.2.4 The system CaO-MgO-Al_2O_3-SiO_2-Fe-O_2

Data for the iron-free system CMAS has been presented in Chapter 4. Several joins in the MgO-free system, CAS-Fe-O_2, were studied by Schairer (1942) in contact with metallic iron containers. These data are utilised in the MgO-free diagrams to be presented.

A few studies, only, have been made on intermediate Fe/Mg ratios within the system. Muan, Hauck and Löfall (1972) studied the join Anorthite-Diopside-Fayalite in

contact with metallic iron containers, finding the results similar to those for Anorthite-Diopside-Forsterite, though much lower liquidus temperatures were encountered over most of the system.

A major contribution to the data on the system was the study of MgO-Anorthite-SiO_2-Fe-O_2 (Roeder and Osborn (1966)), utilising anorthite saturation (projection) diagrams. The anorthite saturated L. 6 E 3 data from the various pO_2 sections studied by Roeder and Osborn, have been recalculated with all iron as FeO, and plotted as an anorthite projection onto the join MgO-FeO-SiO_2 (figure 6.9). The composition of the L. 6 E 3 as a function of pO_2, and the composition of L. 6 E 2 ol,pyx,sil,sp,an,liq (APOMSL) piercing point in this join is approximately located.

Addition of the data for the system MS-Fe-O_2 (above), with no anorthite present, enables the same equilibria and the adjacent anorthite-free equilibria, to be presented on the diagram $XO.R_2O_3.2ZO_2$-YO-ZO_2 (An-M-S) as a multi-Fe/Mg ratio and multi-pO_2 diagram (figure 6.10), and to show how the percentage of anorthite in the liquid phase varies in each of the equilibria. An approximate $\log_{10}(pO_2)$ versus temperature plot of the same equilibria (figure 6.11) was used to determine the relationship between the L. 6 E 3 equilibria and the pO_2 conditions used in the present experiments.

Thus, the anorthite saturation diagrams at the pO_2 of the Ni/NiO (figure 6.12) and Fe/FeO (figure 6.13) equilibria were constructed, as were the $XO.R_2O_3.2ZO_2$-YO-ZO_2 (Anorthite-M-S) multi-Fe/Mg ratio plots at the same pO_2 conditions

(figures 6.14,6.15). Liquidus diagrams for the join $YO.ZO_2$-$XO.2YO.R_2O_3.3ZO_2$ piercing point in the plane $XO.ZO_2$-$YO.ZO_2$-R_2O_3 (En-AnFo piercing point in CS-MS-A) at the pO_2 of the Ni/NiO (figure 6.16) and Fe/FeO (figure 6.17) equilibrium could then be drawn.

In view of the necessity to draw $2YO.ZO_2$ (olivine) projection diagrams for compositions that lie in a specific join (in this case $XO.ZO_2$-$YO.ZO_2$-R_2O_3 (CS-MS-A)) as was discussed in Chapter 3, the K_D relationship determined by Roeder and Emslie (1970) for olivine and liquid was used to calculate those bulk compositions on the join which would produce L. 6 E 4 straight from L. 6 E 6 ol,liq. A value of 0.33 was taken for K_D following the discussion of Cawthorn, Ford, Biggar, Bravo and Clarke (1973). The results are presented in figures 6.18,6.19. Also included are the olivine projections of the boundaries of the olivine volume assuming no prior olivine crystallisation has occurred. These boundaries naturally project at higher Fe/Mg ratios since no olivine, with a higher Mg/Fe ratio, has crystallised.

The extensive study of Anorthite-MgO-SiO_2-Fe-O_2 by Roeder and Osborn (1966), therefore, only provides data for a small part of the complete system.

A recent study by Merrill, Williams and Akella (1975) on the plane An-En-FS, at a pO_2 near that of the Fe/FeO equilibrium, indicated that L. 6 E 4 ol,an,pyx,liq (OAPL) pierces this plane. This data is not supported by the findings of Roeder and Osborn (1966) or the previously

presented analysis of that data at the pO_2 of the Fe/FeO equilibrium (figures 6.13, 6.15), in which L. 6 E 4 ol,an,pyx,liq (OAPL) always lies to the silica-rich side of this plane, at these pO_2. A possible explanation for this inconsistency lies in the use of Pt support wire for the charges, resulting in the bulk composition losing iron and becoming more SiO_2-rich and therefore encountering L. 6 E 4 ol,an,pyx,liq (OAPL). Further support for this reasoning comes from the data of Schairer (1942), who found L. 6 E 4 ol,an,sil,Fe,liq to occur on the join An-FS suggesting that the olivine phase volume in An-En-FS extends to much higher Fe/Mg ratios than found by Merrill, Williams and Akella (1975).

Results on some of the compositions used in this study have already been reported by Clarke and Biggar (1972) in connection with Ca-poor pyroxene compositions. The determination of cpx entry, however, was not undertaken, and these charges have been incorporated into this study and re-examined.

6.3 Experimental results

The elucidation of the phase equilibria relationships for a larger area of the geologically interesting part of the system at varying pO_2, was undertaken by preparing compositions having variable Fe/Mg ratios, and whose bulk recalculated compositions (all FeO treated as equivalent weight of MgO) lay on one of several joins which had already been studied in the iron-free system, CMAS (Chapter 4).

Compositions were prepared on the joins $XO.YO.2ZO_2$-$YO.R_2O_3.ZO_2$ (Diopside-MAS) and $XO.YO.2ZO_2$-$5YO.3R_2O_3.5ZO_2$ (Diopside-$M_5A_3S_5$) having FeO/MgO mole ratios of 0.18, 0.5 and 1.0. Further compositions were prepared on the joins $YO.ZO_2$-$3XO.R_2O_3.3ZO_2$ (En-Gross) and $3XO.R_2O_3.15ZO_2$-YO (C_3AS_{15}-M) lying in the plane $3XO.R_2O_3$-YO-ZO_2 (C_3A-M-S) at FeO/MgO mole ratios of 0.2, 0.33, 0.5, 1.0, 2.0, 3.0 and X (MgO-free). Several other individual compositions were prepared at intermediate FeO/MgO mole ratios on the latter joins and within other parts of the plane $3XO.R_2O_3$-YO-ZO_2 (C_3A-M-S), to assist interpretation. The compositions prepared are given in Appendix B.3.

Those compositions lying within the $3XO.R_2O_3$-YO-ZO_2 (C_3A-M-S) plane have names coded:

FeO/MgO mole ratio - Moles MgO - 3 - 1 - Moles SiO_2

Thus, 0.5-9-3-1-15 refers to the composition having an FeO/MgO mole ratio of 0.5, having 9 moles of MgO, 3 moles of CaO, 1 mole of Al_2O_3, and 15 moles of SiO_2. The moles of FeO present is 4.5 (0.5 times 9). After recalculation,

this composition would be equivalent to 13.5-3-1-15 in the system $YO-XO-R_2O_3-ZO_2$. The MgO-free compositions have X as the moles of MgO and the moles of FeO as the FeO/MgO ratio.

In order to vary the FeO/Fe_2O_3 ratio in the charges, the experiments were conducted at two values of pO_2 - those of the Fe/FeO and Ni/NiO equilibria. The conditions at the Fe/FeO equilibrium would be moderately reducing, the majority of the iron in the charge being present as FeO. At Ni/NiO equilibrium more of the iron present would be as Fe^{3+} and these pO_2 values approximately bracket those assumed to occur in natural conditions (see Chapter 8 and Section 2.5).

The furnace operation details of these experiments are given in Appendix C.2; the atmospheric control details in Appendix D; and the results of the experiments in Appendix E.3.

The results are presented as groups of diagrams for each pO_2 studied, showing the effect of change of Fe/Mg ratio on each join. The relevant figure for each join mentioned below can also be found by reference to table 6.1. The groups of diagrams are:

1. The joins $XO.YO.2ZO_2-YO.R_2O_3.ZO_2$ (Diopside-MAS) and $XO.YO.2ZO_2-5YO.3R_2O_3.5ZO_2$ (Diopside-$M_5A_3S_5$) as T-X sections for the FeO/MgO mole ratios 0.18, 0.5 and 1.0 (figures 6.20-6.22 and 6.25-6.27 for Fe/FeO; figures 6.62-6.64 and 6.67-6.69 for Ni/NiO). A liquidus and second phase diagram for each join shows the relationship between the results at different Fe/Mg ratios (figures 6.23-6.24 and 6.28-6.29 for

Table 6.1 A reference table giving the figure numbers for each of the joins studied in the system $CaO-MgO-Al_2O_3-SiO_2-Fe-O_2$ at the pO_2 of the Fe/FeO and Ni/NiO equilibria, and in air.

Join studied	Fe/FeO	Ni/NiO	air
$XO.YO.2ZO_2-YO.R_2O_3.ZO_2$ (Diopside-MAS)			
mole ratio FeO/MgO = 0.18	6.20	6.62	
" = 0.50	6.21	6.63	
" = 1.00	6.22	6.64	
Liquidus diagram	6.23	6.65	
Second phase diagram	6.24	6.66	
$XO.YO.2ZO_2-5YO.3R_2O_3.5ZO_2$ (Diopside-$M_5A_3S_5$)			
mole ratio FeO/MgO = 0.18	6.25	6.67	
" = 0.50	6.26	6.68	
" = 1.00	6.27	6.69	
Liquidus diagram	6.28	6.70	
Second phase diagram	6.29	6.71	
$YO.ZO_2-3XO.R_2O_3.3ZO_2$ (En-Gross)			
mole ratio FeO/MgO = 0.20	6.30	6.72	
" = 0.33	6.31	6.73	
" = 0.50	6.32	6.74	
" = 1.00	6.33	6.75	
" = 2.00	6.34	6.76	
" = 3.00	6.35	6.77	
" = X (MgO-free)	6.36	6.78	
Liquidus diagram	6.37	6.79	
Second phase diagram	6.38	6.80	
$3XO.R_2O_3.15ZO_2-YO$ (C_3AS_{15}-M)			
mole ratio FeO/MgO = 0.50	6.39	6.81	
" = 1.00	6.40	6.82	
" = 2.00	6.41	6.82	
Liquidus diagram	6.42	6.84	6.99
Second phase diagram	6.43	6.85	

Table 6.1 continued.

Join studied	Fe/FeO	Ni/NiO
$XO.ZO_2$-$YO.ZO_2$-R_2O_3 (CS-MS-A)		
mole ratio FeO/MgO = 0.50	6.44	6.86
" = 1.00	6.45	6.87
" = 2.00	6.46	6.88
" = 3.00	6.47	6.89
" = X (MgO-free)	6.48	6.90
$3XO.R_2O_3$-YO-ZO_2 (C_3A-M-S)		
mole ratio FeO/MgO = 0.50	6.49	6.91
" = 1.00	6.50	6.92
" = 2.00	6.51	6.93
" = 3.00	6.52	6.94
" = X (MgO-free)	6.53	6.95
$2YO.ZO_2$ (olivine) projections into $XO.ZO_2$-$YO.ZO_2$-R_2O_3 (CS-MS-A)		
mole ratio FeO/MgO = 0.50	6.54	6.86
" = 1.00	6.55	6.87
" = 2.00	6.56	-
" = 3.00	6.57	-
" = X (MgO-free)	6.58	-
Summary diagrams		
$XO.ZO_2$-$YO.ZO_2$-R_2O_3 (CS-MS-A)	6.59	6.96
$3XO.R_2O_3$-YO-ZO_2 (C_3A-M-S)	6.60	6.97
$2YO.ZO_2$ (olivine) projection	6.61	6.98

Fe/FeO; figures 6.65-6.66 and 6.70-6.71 for Ni/NiO).

2. The join $YO.ZO_2$-$3XO.R_2O_3.3ZO_2$ (En-Gross) as T-X sections for the FeO/MgO mole ratios of 0.2, 0.33, 0.5, 1.0, 2.0, 3.0, and X (MgO-free) (figures 6.30-6.36 for Fe/FeO; figures 6.72-6.78 for Ni/NiO). The data are combined together in the form of a liquidus and a second phase diagram (figures 6.37-6.38 for Fe/FeO; figures 6.79-6.80 for Ni/NiO).

3. The join $3XO.R_2O_3.15ZO_2$-YO (C_3AS_{15}-M) as T-X sections for the FeO/MgO mole ratios of 0.5, 1.0, and 2.0 together with the liquidus and second phase diagrams for the join (figures 6.39-6.43 for Fe/FeO; figures 6.81-6.85 for Ni/NiO).

The previous groups of diagrams concentrated on displaying the Fe/Mg relationships in individual sections. To portray the relationships between the various joins studied at constant Fe/Mg ratios, the following groups of diagrams are presented:

1. Liquidus diagrams of the low-R_2O_3 portion of the plane $XO.ZO_2$-$YO.ZO_2$-R_2O_3 (CS-MS-A) shows the relationship between the joins $XO.YO.2ZO_2$-$YO.R_2O_3.ZO_2$ (Diopside-MAS), $XO.YO.2ZO_2$-$5YO.3R_2O_3.5ZO_2$ (Diopside-$M_5A_3S_5$) and $YO.ZO_2$-$3XO.R_2O_3.3ZO_2$ (En-Gross) at the FeO/MgO mole ratios 0.5, 1.0, 2.0, 3.0 and X (MgO-free)(figures 6.44-6.48 for Fe/FeO; figures 6.86-6.90 for Ni/NiO).

2. Liquidus diagrams of the plane $3XO.R_2O_3$-YO-ZO_2 (C_3A-M-S) shows the relationship between the joins $YO.ZO_2$-$3XO.R_2O_3.3ZO_2$ (En-Gross) and $3XO.R_2O_3.15ZO_2$-YO (C_3AS_{15}-M) at the FeO/MgO mole ratios 0.5, 1.0, 2.0, 3.0 and X (MgO-free) (figures 6.49-6.53 for Fe/FeO; figures 6.91-6.95 for Ni/NiO).

3. Projections from $2YO.ZO_2$(olivine) into the plane $XO.ZO_2$-$YO.ZO_2$-R_2O_3 (CS-MS-A) using the data from compositions lying in that plane itself, indicates lower variance equilibria which probably exist in this system. The FeO/MgO mole ratios 0.5, 1.0, 2.0, 3.0, and X (MgO-free) are shown for the pO_2 of the Fe/FeO equilibria (figures 6.54-6.58), where olivine occurs on the liquidus of the plane at all FeO/MgO ratios, but only for the ratios 0.5 and 1.0 at the pO_2 of the Ni/NiO equilibria (figures 6.86-6.87), where olivine does not appear on the liquidus at higher FeO/MgO mole ratios. Also shown are the olivine projection boundaries for more olivine-rich compositions than those in this plane, to show the change in projection position of the equilibria more clearly and over a greater compositional area.

4. Summary diagrams showing multi-FeO/MgO ratio relationships are given for the liquidus diagrams $XO.ZO_2$-$YO.ZO_2$-R_2O_3 (CS-MS-A) (figure 6.59 for Fe/FeO; figure 6.96 for Ni/NiO), and $3XO.R_2O_3$-YO-ZO_2 (C_3A-M-S) (figure 6.60 for Fe/FeO; figure 6.97 for Ni/NiO), and for the $2YO.ZO_2$ (olivine) projection into $XO.ZO_2$-$YO.ZO_2$-R_2O_3 (CS-MS-A) (figure 6.61 for Fe/FeO; figure 6.98 for Ni/NiO).

Throughout the study of the system CMAS-Fe-O_2, the identification of the low Ca pyroxene polymorph present was doubtful. The polymorph present was thought to be pigeonite in most cases, but a full examination of the distribution of the polymorphs was beyond the scope of this study and the compositions prepared. Where the polymorph was considered doubtful the abbreviation pyx has been used.

The important points to note from the collection of diagrams for the results at the pO_2 of the Fe/FeO equilibrium are:

1. Those characteristics present in the iron-free system (FeO/MgO = 0) remain until high iron ratios (FeO/MgO > 3) are achieved. Thus, the majority of changes in liquidus fields and subliquidus phase equilibria occur at FeO/MgO ratios greater than 3. Prior to these major changes, the phase fields contract or expand with increasing iron content. Those liquidus fields involving a phase of variable Fe/Mg ratio generally contract and disappear prior to the MgO-free (X) system, except for the olivine (and magnesiowustite) solid solution series which, at these low pO_2, still have phase fields present in the MgO-free (X) system. Those phases not involving variable Fe/Mg ratio (for example, anorthite and silica), generally expand their phase volumes and occupy substantially larger volumes in the MgO-free (X) system.

Accompanying these changes is a lowering of temperatures as the Fe/Mg ratio increases, temperatures in the MgO-free system being less than 1100°C for compositions in the join FS-Grossular having an olivine liquidus. The temperature of L. 6 E 4 ol,cpx,an,liq in this join also decreases from 1255°C (FeO/MgO = 0) to 1070°C (FeO/MgO > 7) (figure 6.38).

2. The $2YO.ZO_2$ (olivine) projection diagrams (figures 6.54-6.58) show that as the Fe/Mg ratio increases the position in projection of L. 6 E 4 ol,an,cpx,liq, L. 6 E 4 ol,an,pig, liq and L. 6 E 3 ol,an, cpx,pig,liq becomes marginally less R_2O_3-rich. Also shown is L. 6 E 4 ol,an,sp,liq

becoming more R_2O_3-rich, the extent of L. 6 E 5 ol,an,liq correspondingly increasing in the more iron-rich compositions.

The summary $2YO.ZO_2$ (olivine) projection diagram (figure 6.61) shows the projected position of two divariant equilibria which pierce this "constant" pO_2 plane through the system. These are the lowest variance equilibria that can exist at "constant" pO_2 at atmospheric pressure. The two piercing points are L. 6 E 2 ol,sil,pig,an,cpx,liq (OSPADL) and L. 6 E 2 ol,an,woll,cpx,sil,liq (OAWDSL); their temperatures and compositions at this pO_2 are not known from the data presented here.

At the pO_2 of the Ni/NiO equilibrium, however, the distribution of phases has altered considerably. One possible cause of part of these changes is the method used to project the bulk compositions - namely, calculating all iron in the charge as FeO and then projecting. In effect, this procedure produces diagrams which are projections from oxygen along oxygen control lines. The presence of any Fe_2O_3 in a charge would, therefore, result in compositions appearing richer in non-iron oxides than they should in fact be. All equilibria are thus slightly more iron-rich ($FeO + Fe_2O_3$) than they appear.

The following features are important to note:

1. The pattern of phase fields present in the iron-free system changes much more rapidly as the iron content increases than at the pO_2 of the Fe/FeO equilibria. The olivine volume contracts rapidly being replaced by larger high and low Ca pyroxene phase volumes, and the expansion

to more ZO_2-rich compositions of the spinel volume. This is only to be expected, since the olivine solid solution series will not accommodate Fe^{3+}, whereas the other Fe/Mg-bearing solid solution series can take Fe^{3+} into their structure more readily.

Temperatures again decrease, but do not continue to decrease to the MgO-free (X) system. Instead, the spinel volume forms a buffer causing the low temperature region to be at about the FeO/MgO mole ratio of 7. In the join $YO.ZO_2$-$3XO.R_2O_3.3ZO_2$ (En-Gross) the lowest temperatures are about 1150°C, some 80°C higher than at the pO_2 of the Fe/FeO equilibrium.

The liquidus diagrams for the plane $XO.ZO_2$-$YO.ZO_2$-R_2O_3 (CS-MS-A) (figures 6.86-6.90) again show that anorthite and clinopyroxene become the liquidus phases dominant at intermediate FeO/MgO mole ratios. At higher ratios, however, spinel becomes dominant.

2. The position of L. 6 E 4 ol,an,cpx,liq, in projections from $2YO.ZO_2$ (olivine), becomes more R_2O_3-rich as the Fe/Mg ratio increases, as does the associated L. 6 E 3 ol,an,cpx, pig,liq (figures 6.86-6.87). More important from the standpoint of crystallisation histories, mentioned later in section 6.4, is that L. 6 E 4 ol,sp,an,liq becomes less R_2O_3-rich as the Fe/Mg ratio increases. Consequently, in contrast to the behaviour at the pO_2 of the Fe/FeO equilibrium, the extent of L. 6 E 5 ol,an,liq decreases.

3. The olivine reaction relationship present in L. 6 E 5 ol,pyx,liq in the iron-free system (well seen in the join C_3AS_{15}-M)(figure 4.5), and which remained throughout at the

pO_2 of the Fe/FeO equilibrium, gradually alters its nature to one of coprecipitation of olivine+pyroxene. This is to be expected from the analysis of the system $MgO-SiO_2-Fe-O_2$ (section 6.2.2 and figures 6.2-6.3), where olivine+pyroxene coprecipitation most likely occurs at the pO_2 of the Ni/NiO equilibrium. Further discussion of this point is presented in section 6.4.

4. The summary $2YO.ZO_2$ (olivine) projection diagram (figure 6.98) postulates the existence of L. 6 E 2 ol,an,pig,cpx, sp,liq (OAPDML), L. 6 E 2 an,sil,pig,sp,cpx,liq (ASPMDL) and L. 6 E 2 ol,sil,pig,sp,cpx,liq (OSPMDL), their locations in this figure being very speculative. A wollastonite-bearing L. 6 E 2 must also exist, its nature, however, cannot be speculated due to insufficient information.

A number of the compositions used in this study were studied by Clarke and Biggar (1972) in an air atmosphere; the results are represented as Appendix E.3.3 for completeness. A liquidus diagram for the join $3XO.R_2O_3.15ZO_2$-YO (C_3AS_{15}-M) utilising these results (figure 6.99), shows that in air the liquidus phase fields are similar to those at the pO_2 of the Ni/NiO equilibrium, except that the spinel volume now extends to much lower Fe/Mg ratios. The boundary between opx and pen phase fields is only approximate and may be more complex than shown in this figure.

The full effects of changing pO_2 cannot be fully evaluated without considerably more data. However, the effect on some of the sections studied can be mentioned at this stage, and provide further limiting data from which future studies can commence.

The join $YO.ZO_2$-$3XO.R_2O_3.3ZO_2$ (En-Gross) contains sufficient piercing points to speculate on the manner in which the phase fields change with varying pO_2. The L. 6 E 4 data from the diagrams presented for the pO_2 at Ni/NiO and Fe/FeO (figures 6.79 and 6.37) are presented in figure 6.100 as a multi-pO_2 diagram for the join. The interpretation presented predicts the existence of five L. 6 E 3: L. 6 E 3 sil,cpx,pig,ol,liq (SDPOL), L. 6 E 3 sil, cpx,ol,an,liq (SDOAL), L. 6 E 3 sil,an,sp,cpx,liq (SAMDL), L. 6 E 3 sil,cpx,pig,sp,liq (SDPML) and L. 6 E 3 cpx,pig,ol, sp,liq (DPOML), the main influence being the extension of the spinel phase field to much lower Fe/Mg ratios as pO_2 increases.

A multi-pO_2 plot (figure 6.101) of the L. 6 E 4 data from the join $3XO.R_2O_3.15ZO_2$-YO (C_3AS_{15}-M) presented in figures 6.42, 6.81 and 6.99, presents a similar change in the pattern of the equilibria to that presented for the system MgO-SiO_2-Fe-O_2 (figure 6.2). The main feature as pO_2 becomes more reducing is the initial expansion of the pyroxene phase volume until L. 6 E 3 ol,pyx,sp,sil,liq (OPMSL) is reached, followed by slight reduction. Accompanying this change, the pyroxene-bearing equilibria become less ZO_2-rich initially, but become more ZO_2-rich at more reducing conditions.

6.4 Discussion

Previous research on systems involving iron have revealed a difference in residual liquid composition trends depending upon the type of crystallisation involved - equilibrium or fractional - and on the behaviour of pO_2 during crystallisation - a closed or open system relative to oxygen availability.

The study of Anorthite-MgO-SiO_2-Fe-O_2 by Roeder and Osborn (1966) confirmed the general trends found by previous researchers in similar but simpler systems. Namely, either silica enrichment, when crystallisation takes place in a system open to oxygen and a buffering situation exists, or iron enrichment when the system is closed to oxygen, that is, a constant composition type of crystallisation. The type of crystallisation influences the extent to which these enrichments occur - perfect fractional crystallisation producing the most striking effects.

In this study, descriptions of the crystallisation behaviour of individual compositions are extremely difficult, partly due to the many dimensions required for portrayal of the system, but also due to the presence of solid solution in many of the phases, the compositions of these phases in any equilibrium being unknown and not determined at this stage of the study.

However, that these two contrasted enrichment trends still occur, can be seen from the diagrams presented for the plane $3XO.R_2O_3$-YO-ZO_2 (C_3A-M-S), and the section through that plane shown by the join $3XO.R_2O_3.15ZO_2$-YO (C_3AS_{15}-M), at the pO_2 of the Ni/NiO and Fe/FeO equilibria. Thus, at

Ni/NiO the olivine and pyroxene volumes butt against a spinel volume, as in the simpler systems (see, for example, figure 6.2), and any fractionation path must be via pyroxene+spinel-bearing equilibria and involve silica enrichment.

At the pO_2 of the Fe/FeO equilibria, however, the disappearance of a spinel phase volume in that part of the plane of interest, results in olivine being present at all Fe/Mg ratios, again as in simpler systems at like pO_2, and any fractionation path must result in iron enrichment, eventually by olivine+silica-bearing equilibria.

The precise behaviour of all compositions in the system must await analysis of solid solution phase compositions, liquid compositions and a more refined computerised system for studying such multicomponent systems.

It can be stated, though, that because the phases crystallising are solid solutions, under equilibrium crystallisation conditions and any pO_2 conditions, many compositions within the system will solidify in moderately high variance equilibria (6 E 3 or 6 E 4), when the tie plane involving the varying composition of each of the solid phases in the equilibrium in question, uniquely expresses the bulk composition, which may also be varying by gaining or losing oxygen. Under fractional crystallisation, the residual liquids will be those at the lowest temperature that the pO_2 conditions will allow, and again may not necessarily be in a low variance equilibria.

The early characterisation of residual liquid composition from geologically interesting bulk compositions,

during any type of crystallisation can again be influenced by the nature of the equilibrium involving olivine, anorthite and spinel, as discussed in the systems CMAS and CMASN (sections 4.4 and 5.4). However, in the system CMAS-Fe-O_2, at each pO_2 investigated in this study, the equilibrium retains precisely the same nature, that is, one involving spinel reaction with the liquid, as it does in the system CMAS.

Sufficient analysis of an olivine projection diagram showing this reaction was presented in section 4.4 and by O'Hara (1969). The extra dimensions introduced affect the discussion only in the extent to which residual liquids during crystallisation remain within particular equilibria. Thus, there exists a wide range of compositions with variable Fe/Mg ratios which can produce residual liquids either saturated* or undersaturated* in the CIPW norm, depending upon the type of crystallisation involved.

The main effects of different pO_2 on the olivine-bearing equilibria, in terms of distribution of CIPW normative constituents, are:

1. At the pO_2 of the Fe/FeO equilibria, the extent of those areas saturated in the norm which can crystallise spinel decreases as the Fe/Mg ratio increases. Thus, L. 6 E 4 ol,sp, an,liq becomes more anorthite-rich in projection, but less anorthite-rich in the CIPW norm. At the pO_2 of the Ni/NiO equilibria the extent of the saturated areas which can

---

* The term saturated is taken to represent those compositions which would not contain corundum, larnite, and nepheline in the CIPW norm; and undersaturated represents those compositions which would contain corundum, and/or larnite and/or nepheline in the norm.

crystallise spinel increases; L. 6 E 4 ol,sp,an,liq therefore becomes less anorthite-rich in projection and in the CIPW norm, and a wider range of undersaturated compositions can produce either saturated or undersaturated residual liquids.

2. L. 6 E 4 ol,cpx,an,liq, L. 6 E 4 ol,an,pig,liq and L. 6 E 3 ol,an,cpx,pig,liq produce the reverse effect to that mentioned above for L. 6 E 4 ol,sp,an,liq at each pO_2 studied. At the pO_2 of the Fe/FeO equilibria, these residual liquids become less anorthite-rich in projection and in the norm as Fe/Mg ratio increases, but at Ni/NiO become more anorthite-rich in projection and less anorthite-rich in the norm. Thus at Fe/FeO the L. 6 E 5 ol,an,liq increases its extent in projection while at Ni/NiO decreases its extent.

A further interesting crystallisation feature, mentioned in the previous section, is the possibility of olivine+low-Ca pyroxene coprecipitating during crystallisation - equilibrium or fractional - from a range of compositions and over a range of pO_2. The precise delineation of the phase boundaries which allow this feature requires knowledge of phase and liquid compositions.

That it exists, can be seen from the diagram for the simple system MS-Fe-O_2 (figure 6.2), where at low pO_2, Bowen and Schairer (1935) described a range of compositions which achieved this condition. In more oxidising conditions this feature will still be present, but extended initially due to the iron content in L. 6 E 4 ol,sil,pyx,liq increasing. The increase in Fe^{3+} content in the liquid will shrink the olivine and pyroxene solid solution extents,

but only by a small amount, judging by the data for Fe^{2+}/Fe^{3+} ratios from Muan and Osborn (1956). The maximum extent will occur at the pO_2 of L. 6 E 3 ol,sil,pyx,sp,liq (OSPML) and thereafter will shrink more rapidly as the amount of Fe^{3+} increases in the liquid.

Extension from this simple system to Anorthite-M-S-Fe-O_2, reveals that the tangents to L. 6 E 4 ol,an,pyx,liq (OAPL) will probably also enable this equilibrium to retain its coprecipitation nature, both above and below the pO_2 of L. 6 E 2 ol,an,pyx,sil,sp,liq (OAPSML), though to what extent is unknown without data on Fe^{2+}/Fe^{3+} ratios.

Further extension into high-Ca pyroxene-bearing equilibria will occur, but lack of data severely limits the interpretation of how and to what effect.

The equilibria inferred to exist from the data presented at the pO_2 of the Fe/FeO and Ni/NiO equilibria can be further extrapolated to postulate the existence of L. 6 E 1 ol,sil,pyx,an,cpx,sp,liq (OSPADML) at a pO_2 between that of Ni/NiO and Fe/FeO, but at an unknown temperature. The existence of L. 6 E 2 ol,an,sil,cpx,sp,liq (OASDML) has not been previously postulated, but exists by analogy with the situation for low-Ca pyroxene equilibria and the fact that a link to wollastonite-bearing L. 6 E 1 is necessary, the existence of Hedenbergite at atmospheric pressure being unknown in the presence of liquid. The flow diagram (figure 6.102) shows the relationship between the pO_2 studied here and the inferred equilibria, but the relationship between temperature and pO_2 for these equilibria, especially

L. 6 E 2 ol,an,sp,pyx,sil,liq (OAMPSL) and L. 6 E 2 ol,an,sp,cpx,sil,liq (OAMDSL), will be complex due to the pyroxene (pyx) and clinopyroxene (cpx) solid solutions terminating.

CHAPTER 7

THE SYSTEM $CaO-MgO-Al_2O_3-SiO_2-Na_2O-Fe-O_2$

7.1 Introduction

The effects of the addition of both Na_2O and $Fe-O_2$ to the basic synthetic system CMAS, encompasses the three most important oxides in the "minor" fraction of the chemical analysis of an igneous rock, and affects each of the important solid solution series found in such rocks. To study such an addition would require experiments on bulk compositions at several albite/anorthite ratios with varying FeO/MgO ratios. Such a project has not been attempted in this study.

The beginnings of such a study have, however, been attempted by Eggler (1974), by studying a plagioclase saturation surface in the system Albite-Anorthite-MgO-SiO_2-$Fe-O_2$, where the bulk normative albite/anorthite ratio equals 1.0. Such a study is equivalent to the anorthite saturation surfaces described by Roeder and Osborn (1966).

In this Chapter, a brief discussion of the results obtained by Eggler (1974) is presented, plus some predictions of the likely behaviour of compositions in this more complete system, in the light of these data and those for the bounding systems (present above).

7.2 Previous research

Eggler (1974) studied the plagioclase saturation surface for bulk compositions having a normative plagioclase ratio of $An_{50}Ab_{50}$ in the system Albite-Anorthite-MgO-SiO_2-Fe-O_2 at, and slightly more oxidising than, the pO_2 of the Ni/NiO equilibrium, locating the piercing points of two equilibria in this section : L. 7 E 4 ol,plag,pyx,sp,liq (OAPML) and L. 7 E 4 plag,sil,pyx,sp,liq (ASPML).

The analyses of two of the liquids in each of these equilibria within this section, with total iron as FeO as reported, are plotted on the diagram $XO.R_2O_3.2ZO_2$-ZO_2-YO (An-S-M)(figure 7.1), together with the albite-free phase boundaries from figure 6.10. Although only a part of the equilibria are present, it is immediately obvious that the addition of albite has had a similar effect to that seen in the system CMASN with no iron present. Namely, that the liquid compositions in the equilibria are moving to higher potential plagioclase contents as the albite/anorthite ratio increases, which, when projected from $2YO.ZO_2$ (olivine), brings the liquids in the equilibria to more R_2O_3-rich projected positions in the plane $XO.ZO_2$-$YO.ZO_2$-R_2O_3 (CS-MS-A).

The same analyses, plotted as a projection from albite plus anorthite into the plane MgO-FeO-SiO_2, together with the phase boundaries from figure 6.9 where the plagioclase present was anorthite only (figure 7.2), reveal an interesting feature. The field of pyroxene has enlarged relative to the albite-free system, resulting in the projected

position of L. 7 E 4 sil,plag,pyx,sp,liq (SAPML)* becoming much more SiO_2-rich, but the projected position of L. 7 E 4 ol,plag,pyx,sp,liq (OAPML) remains in essentially the same position as when the plagioclase was anorthite. This behaviour is important in relation to the olivine+low-Ca pyroxene coprecipitation mentioned in the albite-free system. Since the projected position has not become more SiO_2-rich, the equilibrium L. 7 E 4 ol,plag,pyx,sp,liq (OAPML) probably still has a portion, though at unknown pO_2, in which olivine+pyroxene crystallise together.

The limited data also show that a spinel phase is present at higher albite/anorthite bulk normative ratios than in the iron-free system. In the system CMASN, spinel was not a liquidus phase in the section Albite-Anorthite-Forsterite for any bulk composition having a bulk normative albite/anorthite ratio more albite-rich than An_{59}, while in CMASN-Fe-O_2, a spinel phase remains at least until An_{50}. This is undoubtedly due to the fact that the spinel composition is now markedly different - previously the spinel was of the composition $MgO.Al_2O_3$, now it is primarily a magnetite.

One surprising result obtained by Eggler is that the temperatures of analogous equilibria, between the bulk normative ratios An_{100} and An_{50} in this system, are only slightly lowered. The temperature-pO_2 plot for the system

---

* In this chapter, to shorten the figure notations for the equilibria mentioned, the following abbreviations have been used for the phases in the equilibria:
O = ol, A = plag, P = pyx, S = sil, M = sp, L = liq.

(figure 7.3) from Eggler (1974) shows the temperatures for L. 7 E 4 plag,ol,pyx,sp,liq (AOPML) and L. 7 E 4 plag,sil, pyx,sp,liq (ASPML) to be only about 10°C lower than the albite-free equilibria. Data for the Ab_{100} equilibria are unknown, the positions in figure 7.3 being inferred, but show that a larger temperature decrease occurs again as in the iron-free system at high albite contents.

The replacement of anorthite by albite, seen in Chapter 5, was a gradual change, no univariant equilibria being reached until high albite ratios are encountered, and all compositions solidify in higher variance equilibria. A similar situation will probably exist in CMASN-Fe-O_2, as portrayed in figure 7.3, with the lowest variance equilibria postulated being L. 7 E 3 plag,ol,sp,pyx,sil,liq (AOPMSL), and the majority of compositions solidifying within this equilibria.

7.3 Discussion

While no experimental results have been obtained for variable albite/anorthite ratios and variable FeO/MgO ratios combined, some inferences on the expected behaviour within the system can be attempted. The results presented for each individual substitution are quite markedly different - addition of albite increases the potential plagioclase content of the liquids to a large extent, while addition of iron alters the proportions of the normative constituents in the liquids only slightly, the precise effect of the latter addition depending on the pO_2. A simple assumption to make in order to consider the combined effect, is to sum the individual effects for particular combinations of ratios of each factor.

Thus, as an illustration, assume the bulk compositions have a normative plagioclase ratio of $An_{50}Ab_{50}$ and FeO/MgO mole ratio of 0.5, and the pO_2 in question is that of the Ni/NiO equilibrium. For this combination, a $2YO.ZO_2$ (olivine) projection into the plane $XO.ZO_2$-$YO.ZO_2$-R_2O_3 (CS-MS-A) can be constructed as follows (figure 7.4): Starting with the projected phase boundaries for the system CMAS (figure 4.3), addition of albite, so that the bulk normative plagioclase ratio is $An_{50}Ab_{50}$, will increase the plagioclase content of the liquids slightly more than that for the ratio $An_{51.5}$ (figure 5.8). From the projected position of these boundaries, addition of iron to the system at this pO_2 will also slightly increase the plagioclase projection content of the liquids (from figure 6.86). Thus the olivine-bearing projected phase boundaries L. 7 E 5 ol,plag,

cpx,liq, L. 7 E 5 ol,plag,pyx,liq and L. 7 E 5 ol,pyx,cpx, liq can be inferred.

That the magnitude of this effect is approximately correct, is confirmed by the data from Eggler (1974), which projects along the join $YO.ZO_2$-$XO.R_2O_3.2ZO_2$:$2YO.ZO_2$ (En-AnFo piercing point). The resultant projection figure should be used only for compositions which, after recalculation using the data reduction scheme (Chapter 3), project in the plane $XO.ZO_2$-$YO.ZO_2$-R_2O_3 (CS-MS-A). In practise, when dealing with natural compositions for example, compositions near the ratios used and which project about the plane can be included without losing much accuracy.

CHAPTER 8

MELTING STUDIES ON NATURAL ROCKS

8.1 Introduction

The approach used so far has been to consider the effect of adding the "minor" oxides on basaltic-type equilibria by concentrating on synthetic systems, modifying a base system by changing one component of the important solid solution series at a time and noting the changes which occur. To continue this approach by adding each of the minor oxides one at a time and then combining them in varying amounts, would be a very large project. In order to determine whether the important minor oxides have been dealt with, it is necessary to have some information on the phase relations of the natural rocks themselves under the same conditions.

Each rock, however, has a different FeO/MgO and Albite/Anorthite ratio, and it is unlikely that more than one rock, randomly selected from widely different geographical locations, will be valid on the same phase diagram. A simplification therefore has to be made: that by studying a series of rocks, assumed to be related by crystallisation at atmospheric pressure, a pseudo phase diagram can be constructed for that series. It should then be possible to compare the results from the synthetic systems with those from the natural rocks.

Two possible sources of natural rocks are available: terrestrial and lunar samples. However, since the lunar samples are restricted in number, and their petrographic

relations in doubt, it is more appropriate to utilise the terrestrial rocks available to form the base for such a study. A great deal of information is already available in the literature on the phase relations of both types of rocks; its value, however, in terms of this study, is very limited because the precise atmospheric conditions of many of the experiments are unknown because of the techniques used. It is also evident that the two groups evolved under very widely different conditions: terrestrial - moderately oxidising; lunar - very low pO_2.

In view of these facts it is, therefore, important to know the phase relations of a series of related natural terrestrial samples under a range of temperature and pO_2 conditions. With this information it will then be possible to compare the natural pseudosystem with the synthetic systems; compare the phase equilibria behaviour of the lunar samples with that of the terrestrial samples; and discuss the possible crystallisation behaviour of natural samples under varying conditions. This is attempted in this Chapter by studying the natural samples from Reunion Island, Indian Ocean.

8.2 Previous melting studies

8.2.1 Terrestrial samples

During the past 20 years, several groups of researchers have determined the phase relations of natural terrestrial samples of various chemical compositions and geographical locations. The basic concept of the majority of the studies has been to allow each sample studied to create its own individual pO_2 in the atmosphere inside its capsule from the Fe_2O_3:FeO ratio of the sample, at each temperature studied. In this way the constant composition equilibrium phase relations of each sample is determined, and by studying a series of rocks of related origin from one volcanic series, an equilibrium constant composition pseudobinary-type diagram can be constructed, by plotting temperature of appearance of each phase against an index which arranges the samples in an evolutionary sequence. The relationship between synthetic and natural studies can then be evaluated.

Two slightly different techniques have been used to achieve this: sealed evacuated capsules (Yoder and Tilley (1962); Tilley, Yoder and Schairer (1963,1964,1965, 1967,1968); Brown and Schairer (1971)) or open capsules in an argon atmosphere (Thompson (1972; summary of individual articles references therein)). The basic technique, however, is open to criticism on the following points. The atmosphere generated by the sample will depend not only on the Fe_2O_3:FeO ratio but also on the amounts of H_2O and CO_2 in the rocks, these gases exerting an oxidising influence on the atmosphere. The rock may also not preserve the

original Fe_2O_3:FeO ratio at the time of its crystallisation because of subsolidus re-equilibration. The magnitude of this effect has not been determined, but it probably occurs because of Mg:Fe re-equilibration in the crystallised phases as occurs in the system $MgO-SiO_2-Fe-O_2$ (Speidel and Osborn (1967)). The samples studied may have been oxidised or reduced after complete cooling and consequently yield an incorrect atmosphere.

The argon atmosphere experiments have the additional criticisms: the oxygen impurity in the argon may be so great as to override that from the sample; and oxygen loss from the open capsule will induce a more reducing atmosphere than intended in long runs. Realising the latter criticism, Thompson conducted short runs, generally only of about one hour duration. However, in such short runs, it is possible that equilibrium would then not have been reached between the atmosphere (which is always changing) and the charge. From the work of Presnall (1966) it is known that at least 3 hours is required to achieve a stable Fe_2O_3:FeO ratio in synthetic compositions run under constant controlled atmosphere conditions.

In spite of these further possible errors, agreement between the two techniques is claimed to be good by Thompson (p.903:1972) because results on samples from Kilauea studied using both techniques yield similar results.

A few melting studies have utilised a different technique: that of controlling the atmosphere at a known pO_2 in each experiment. Temperature : pO_2 diagrams are therefore obtained for each composition studied. Results

on one composition studied by both the argon method and in CO_2/H_2 mixtures have been reported. Sample CM4 (a lava from the Snake River Basalts, Idaho) studied by the argon method (read from Thompson (1972) since the results in Thompson (1970) do not include magnetite appearance), gave plagioclase appearing at 1090°C, olivine+magnetite at 1075°C and clinopyroxene at 1050°C. Using CO_2/H_2 mixtures (Thompson (1973)), such a sequence was found possible, the pO_2 being that of approximately 1.6% H_2 (a slightly more oxidising pO_2 than that of the Ni/NiO equilibrium).

Recent work by Biggar (1974) in this laboratory on the chilled margins of some layered intrusions has also utilised the control of the atmosphere by CO_2/H_2 gas mixtures. The pO_2:temperature results obtained by Biggar are very different to those obtained by Tilley, Yoder and Schairer (1963,1968) on the same rocks samples. It was concluded by Biggar that the experiments of Tilley et al. were very oxidising, probably having the atmosphere controlled more by the H_2O content than the Fe_2O_3:FeO ratio in the rock in question. This would be confirmed by the presence of magnetite in the results of Tilley et al.; these authors however neglected to record the temperature of appearance of magnetite in their charges, although it was noted, in passing, to be present (Tilley, Yoder and Schairer (1963)).

This study by Biggar (1974) showed that as the pO_2 of the atmosphere in the experiment became more oxidising, the temperature of appearance of olivine decreased, plagioclase remained constant until spinel appeared and then rose,

pyroxene increased, and spinel appeared and became the liquidus phase just more oxidising than the pO_2 of the Ni/NiO equilibrium.

Roeder and Emslie (1970) presented pO_2:temperature results on an olivine basalt from Kilauea, Hawaii. The trend of appearance of phases as the pO_2 became more oxidising was similar to that of Biggar (1974). It is notable however that this sample had an olivine or spinel liquidus depending on the pO_2, but encountered plagioclase as the next phase appearing and not clinopyroxene as in the previous melting studies on the Hawaiian rocks. Clinopyroxene was not recorded in any of the results presented. Two further rocks, studied by Hill and Roeder (1974), also revealed similar patterns in phase fields as a function of pO_2.

Samples from Reunion Island, some of which have also been studied in this thesis, have been studied by the argon method by Tilley, Thompson, Wadsworth and Upton (1971). The results of the more Magnesian samples showed olivine as the liquidus phase, followed by plagioclase for a short interval before clinopyroxene appears. Magnetite (read from Thompson (1972)), was always the last phase to appear, but was often not far behind the incoming of clinopyroxene. More differentiated rocks showed a plagioclase liquidus, followed by olivine.

In summary, therefore, a number of melting studies on terrestrial samples have been conducted, generally, however, under unknown atmospheric conditions. It has usually been assumed in these studies that the rocks have generated

the atmosphere under which they crystallised, and that the results obtained describe the equilibrium phase diagram for the natural rock series under the conditions in which they evolved. Whether this assumption is correct will be discussed following the presentation of the results on the Reunion rocks.

8.2.2 Lunar samples

The study of lunar samples has proceeded at a prolific rate, with a variety of techniques being used in the experimental studies. The most favoured technique has been to seal iron capsules and place them in sealed evacuated tubes, usually of silica (Muan, et al.,(1971); Longhi, et al., (1974)). Various refinements to this technique have included placing graphite between a Platinum outer tube and the iron capsules (Ringwood and Essene (1970)), and using molybdenum instead of iron capsules (Walker, Longhi and Hays (1972)). The use of this technique has been considered applicable since iron metal has been thought present during the crystallisation of these rocks.

Each of these techniques, however, suffers from problems associated with the loss or gain of iron in the charge, each having a different measure of success (O'Hara, Humphries and Waterston (1975)). The technique is also only of limited use in that the pO_2 inside the capsule in contact with the charge is unknown. However, the criticisms mentioned in connection with the studies on terrestrial rocks using a similar technique do not apply,

since no Fe_2O_3 or H_2O is present in these rocks.

Experiments have also been conducted on the lunar samples using controlled atmospheres. Walker *et al.* (1973) used iron capsules to study the pO_2 at which iron is stable in Apollo 16 samples, again encountering iron loss/gain problems at the low pO_2 required.

Experiments conducted in this laboratory on many lunar samples (O'Hara, *et al.* (1970); Biggar, *et al.* (1971); Ford, *et al.* (1972)) have utilised molybdenum capsules and a controlled pO_2 at, and just below that of, the Fe/FeO equilibrium, exactly as used in this study. The results from these studies, in which iron loss is negligible, are, therefore, applicable to the present synthetic study, especially since these rocks, unlike terrestrial rocks, evolved under very reducing conditions. The comparison between lunar results and the synthetic systems will therefore reveal any future studies necessary in order to compare more closely natural rocks with synthetic systems under reducing conditions.

8.3 Experimental results

The island of Reunion is composed of two volcanoes, Piton des Neiges and Piton de la Fournaise. The volcanic series has been described by Upton and Wadsworth (1966), the rocks of Piton des Neiges belonging to two series: the Oceanite Series and the younger Differentiated Series. Samples from Piton de la Fournaise indicate that they belong chemically to the Oceanite Series, while Differentiated Series rock types are not present.

The melting studies were conducted on 12 samples from the Oceanite Series (2 of the samples were from Piton de la Fournaise), 11 samples from the Differentiated Series (7 samples were lavas, 4 samples were intrusives), and 2 samples were nodules from Piton des Neiges. Each sample was studied in a similar manner to that for the iron-bearing system, over a wide range of pO_2:temperature conditions. The chemical analyses and petrographic data for these rocks are given in Appendix B.4; the details of the furnace operations involving these compositions in Appendix C.2; details of the atmospheric control in Appendix D; and the results of the experiments in Appendix E.4.

The data for this series of rocks are presented in diagrammatic form in the following ways:

1. As pO_2 versus temperature plots for each rock studied, to show the effect of pO_2 on the order and temperature of appearance of the various phases (figures 8.1-8.25).
2. Utilising the data reduction scheme (Chapter 3), with total iron recast as FeO, projection diagrams from $2YO.ZO_2$

(olivine) into the plane $XO.ZO_2$-$YO.ZO_2$-R_2O_3 (CS-MS-A) and from $XO.YO.2ZO_2$ (clinopyroxene) into the plane $XO.R_2O_3$-YO-ZO_2 (CA-M-S) were drawn, using the data obtained in the experiments at the pO_2 of the Fe/FeO and Ni/NiO equilibria, for each of the rock series - the Oceanite Series and the Differentiated Series (figures 8.26-8.29).

The results obtained confirm the patterns of change found by previous studies in the appearance of the phases as the pO_2 is varied. Thus, from reducing conditions to more oxidising pO_2 and the appearance of magnetite as the liquidus phase, the temperature of olivine appearance decreases, the temperature of plagioclase entry remains constant or increases slightly, and the temperature of clinopyroxene appearance increases. In reducing conditions, the ore mineral appears very late in the crystallisation sequence, and is probably an ilmenite. The temperature of appearance of the ore mineral increases rapidly at, and above the pO_2 of the Ni/NiO equilibria and this mineral eventually becomes the liquidus phase. In those compositions having a plagioclase liquidus over most pO_2 conditions, the magnetite liquidus is limited to higher pO_2 than in other compositions. The change in the phase appearance pattern when magnetite is the liquidus phase is similar to that mentioned, except that plagioclase appearance increases more rapidly.

The projection diagrams presented allow pseudo quaternary phase diagrams to be drawn and the locus of liquids in the equilibrium olivine+clinopyroxene+plagioclase+liquid outlined at the pO_2 of the Ni/NiO and Fe/FeO

equilibria. The majority of the Oceanite Series compositions have an olivine liquidus at both pO_2 with plagioclase, closely followed by clinopyroxene, appearing later. The Differentiated Series rocks, however, generally have a plagioclase liquidus which is followed by olivine, so that an olivine projection can still be drawn for these rocks. The majority of all the compositions plot in the system $XO-YO-R_2O_3-ZO_2$ at slightly lower olivine contents than those in the plane $XO.ZO_2-YO.ZO_2-R_2O_3$ (CS-MS-A), as is seen in the clinopyroxene projections (figures 8.27,8.29).

The effect of pO_2 on the projected phase boundaries can be measured by comparing their positions at the pO_2 of the Ni/NiO and Fe/FeO equilibria. The major change is in the expansion of the plagioclase phase volume, to cover more of the Differentiated Series rocks with increase in pO_2. The Oceanite Series generally still have an olivine liquidus, but the plagioclase second phase field has now moved to slightly higher R_2O_3-rich compositions in projection, some Oceanite Series compositions now having olivine followed by clinopyroxene not plagioclase.

8.4 Discussion

Data are now available for both terrestrial and lunar samples, obtained by the same experimental technique as the synthetic compositions studied here. A comparison of the results from natural and synthetic systems is now possible. Consider first the terrestrial rocks from Reunion, in which the normative plagioclase content of the lavas is approximately $An_{50}Ab_{50}$, and the FeO/MgO mole ratio in the ferromagnesian minerals about 0.50. A $XO.YO.2ZO_2$ (clinopyroxene) projection of these bulk rock compositions into the plane $XO.R_2O_3$-YO-ZO_2 (CA-M-S)(figure 8.30), shows the estimated phase boundary between the liquidus phase fields of olivine and plagioclase for these rocks, compared with the projected phase boundary olivine+plagioclase+clinopyroxene+liquid estimated for the combination of ratios in question from the synthetic system, using the assumption discussed in section 7.3. A comparison is valid since the rocks crystallise clinopyroxene very shortly after the olivine+plagioclase+liquid equilibrium is encountered. The estimated position is based on the clinopyroxene projection (figure 5.15) for albite/anorthite ratios, and from the data for clinopyroxene liquidus compositions in the join Enstatite-Grossular in the system CMAS-Fe-O_2.

From figures 8.27 and 8.30 it can be seen that there is some agreement between the phase boundaries at each pO_2, the disagreement always being that the liquids on the synthetic system boundaries are more olivine-rich than those

on the natural system boundaries. The cause of this discrepancy will be discussed below in connection with the lunar samples. It is also obvious why the majority of the Differentiated Series rocks have a plagioclase liquidus, while the Oceanite Series rocks have an olivine liquidus.

The $2YO.ZO_2$ (olivine) projection into the plane $XO.ZO_2$-$YO.ZO_2$-R_2O_3 (CS-MS-A) (figure 8.26) can also be used to compare the projected position of the equilibrium olivine+plagioclase+clinopyroxene+liquid between natural and synthetic compositions. Once again some agreement can be found, and it is somewhat better than the agreement with the synthetic system CMAS alone. The disagreement is also again consistent at both pO_2, the synthetic boundaries in this projection always being less R_2O_3-rich than the natural boundaries. The cause will be mentioned below.

Considering now the lunar samples from Apollo 11, 12 and 15, the normative plagioclase ratio in each case is about $An_{85}Ab_{15}$ and the FeO/MgO mole ratio in the ferromagnesian minerals about 0.75. A $XO.YO.2ZO_2$ (clinopyroxene) projection into the plane $XO.R_2O_3$-YO-ZO_2 (CA-M-S) (figure 8.31) shows the relationship between the cotectic liquids for the synthetic system at these ratios, estimated as for the terrestrial rocks, and the Apollo 11, 12 and 15 deduced cotectic liquid compositions (Biggar et al. (1971,1972); Humphries, et al. (1972a)). A noticeable disagreement occurs, the displacement from the synthetic boundary increasing as the TiO_2 content of the samples increases. Apollo 11 has the highest TiO_2 content: c.11%; Apollo 12 rocks have c. 4% TiO_2; and Apollo 15 rocks c. 2% TiO_2.

The Apollo samples do not have high K_2O (bulk normative orthoclase) contents (which would shift the boundary in a similar manner to that for albite addition), or any other oxides in large amounts, thus the TiO_2 content must be the dominant influence and account for the discrepancies. The terrestrial samples contained only low TiO_2 contents c. 2-3%, and, as was noted, the natural boundaries were only slightly displaced from the synthetic boundaries, by an amount comparable with the displacement of the Apollo 15 samples.

The $2YO.ZO_2$ (olivine) projection into $XO.ZO_2$-$YO.ZO_2$-R_2O_3 (CS-MS-A) (figure 8.32), shows a similar discrepancy from the synthetic boundaries to that in the terrestrial rocks, the disagreement again increasing with the TiO_2 content of the Apollo samples.

The effect of TiO_2 on the phase boundaries may be more of a projection effect than a real effect, because of the way TiO_2 is handled in the data reduction scheme. Increase in the TiO_2 content of a sample, without altering the molecular proportions of the other oxides, will drive the composition in the reduced system XO-YO-R_2O_3-ZO_2 towards higher R_2O_3 positions, because TiO_2 is summed with R_2O_3. In an olivine projection this will result in a shift towards the R_2O_3-rich apex and away from the $YO.ZO_2$ apex (since TiO_2 is also subtracted from YO); and in the clinopyroxene projection, results in a shift towards $XO.R_2O_3$ and away from YO. This is exactly the shift noted in the diagrams. This projection effect, however, probably does not account for all the change noted.

A comparison between the terrestrial and lunar pseudo quaternary phase diagrams reveals another significant point. The phase boundaries depend to a large degree on the minor oxides present apart from CMAS, and also on the relative proportions of these minor oxides. The phase boundaries for the lunar samples, therefore, do not match the observed phase boundaries for the terrestrial samples, since the minor oxides present are in widely different proportions. It should, therefore, not be expected that the phase boundaries for the terrestrial samples from Reunion should apply to rocks from any other geographical location, unless the chemistry of the rocks is similar.

A further comparison can be made between natural and synthetic results - a comparison of crystallisation histories. If the assumption is made that the natural compositions studied form a related series of fractionated rocks, crystallisation patterns can be constructed by arranging the rocks in an evolutionary sequence. The resulting patterns can then be compared to those obtained in synthetic systems for bulk compositions crystallising similar sequences of phases.

This approach has been made by Thompson (1972), comparing the equilibrium crystallisation patterns of five volcanic series to a pattern obtained by equilibrium crystallisation of a fractionated series of compositions in the system $MgO-SiO_2-Fe-O_2$, the phase boundaries used being those in contact with metallic iron, a reducing condition completely inappropriate in a comparison with natural terrestrial volcanic series. It is, therefore, little

wonder that the patterns obtained in the argon atmosphere experiments, produced some different trends to those expected from the synthetic system.

Two basic melting patterns were found by Thompson (1972) for the equilibrium crystallisation of these series - one in which the temperature of appearance of the second and subsequent phases gradually decreased, but eventually joined the liquidus trend, (figure 8.33a); the other in which the appearance of magnetite was at progressively higher temperatures, while clinopyroxene temperature of appearance decreased and failed to join the liquidus trend (figure 8.33b). The first trend agreed with the simple pattern predicted by Thompson, even though the pO_2 was inappropriate. The second pattern failed to agree, but the discrepancies can be explained by considering a more realistic comparison in the system $MgO-SiO_2-Fe-O_2$.

Assuming that the liquidus phases(s) of the samples studied represent the fractionation trend for the series in question, the two melting patterns can be obtained from the compositional series produced by olivine from the same parent composition, but at two slightly different original pO_2 crystallisation conditions. Equilibrium melting studies on the compositional series produced, using the argon technique, would produce results for equilibrium constant composition crystallisation. The phase boundaries on the original equilibrium crystallisation diagram under which the rocks evolved would then be inappropriate, the boundaries for gradually more reducing pO_2 conditions being required.

The crystallisation patterns so obtained, and the phase diagrams at the original pO_2 fractionation conditions, are shown in figures 8.34,8.35, drawn from the analysis of the system $MgO-SiO_2-Fe-O_2$ illustrated in figure 6.2. In the first case (figure 8.34), the pO_2 (10^{-6}) is above that at which L. 4 E 1 ol,sil,pyx,sp,liq exists, such that pyx+sp is a stable assemblage. The fractionation series has olivine initially on the liquidus, but is later joined by spinel, the fractionation curve being very shallow due to the Fe^{3+} content of the liquids restricting the range of olivine solid solution that is stable. The equilibrium constant composition crystallisation of those compositions in the olivine phase volume will involve a much sharper crystallisation curve, the initial members of the series encountering pyroxene as the second phase. Later members will encounter pyroxene at lower temperatures, eventually spinel becoming the second phase. The temperature of appearance of spinel must then rise to the temperature at which olivine+spinel occurs on the liquidus trend. Further crystallisation of these compositions in 4 E 3 ol,sp,liq will result in liquids in much lower pO_2 regions and, therefore, encountering pyroxene at lower temperatures, that composition on the olivine+spinel phase boundary encountering pyroxene at the lowest temperature. Eventually pyroxene does reach the liquidus trend (unless the pO_2 during crystallisation falls below that of L. 4 E 1 ol,sp,sil,pyx,liq when a silica mineral will appear), it almost doing so in the melting patterns obtained by Thompson (1972). This type of crystallisation history explains the

discrepancies found by Thompson (1972) in the Snake River volcanic series and the Skye lavas, without recourse to other explanations.

In the second case (figure 8.35), the pO_2 (10^{-8}) is below that of L. 4 E 1 ol,sil,pyx,sp,liq, so that pyx+sp is not a stable assemblage. The fractionation trend under these conditions will be much sharper than in the first case, since less Fe^{3+} is contained in the liquids, thus enabling a larger range of olivine solid solutions to be stable. The equilibrium crystallisation pattern produced using the argon atmosphere technique, will be one in which the temperature of appearance of the second and subsequent phases in the crystallisation histories decreases, each phase eventually joining the liquidus trend. This melting pattern is similar to that obtained by Thompson (1972) in his model, but is at more realistic pO_2 conditions, and agrees with that observed for the rocks from Kilauea and Reunion.

The crystallisation pattern obtained is, therefore, a function of the experimental conditions and independent of the original crystallisation conditions. Only by studying the rock series using controlled atmospheres at the pO_2 under which the rock series evolved, can the "true" melting pattern be obtained. Since the pO_2 under which the rocks evolved is unknown, studies at varying pO_2 conditions are essential in the attempt to confirm the petrographic observations and obtain conclusions regarding the evolution of the rocks series.

This point can be further emphasised by comparing the results obtained by Tilley, Thompson, Wadsworth and Upton (1971) on Reunion rocks, with those obtained in this study using controlled atmospheres. The argon atmosphere experiments on the Oceanite Series rocks did not produce a melting pattern consistent with the petrographic interpretation of these rocks - namely, only olivine fractionation producing the variation in the series. Results at controlled pO_2, however, shows that a simple relationship can exist between the Oceanite Series samples, if it is assumed that the pO_2 under which the series evolved, was slightly more oxidising than that of the Ni/NiO equilibrium. A melting pattern produced for that pO_2 (figure 8.36) agrees with the petrographic interpretation, and agrees with the simple synthetic examples discussed previously. The Differentiated Series rocks cannot be related simply at any pO_2 conditions, and probably have evolved under the influence of pH_2O as discussed by Thompson (1972) for evolved rocks having plagioclase as liquidus phase.

The crystallisation histories of natural compositions and simple synthetic analogues are, therefore, similar. While the synthetic examples have pyroxene instead of clinopyroxene, and no plagioclase present, the data on the synthetic system CMAS-Fe-O_2 showed that these changes will not affect the general crystallisation patterns.

CHAPTER 9

CONCLUSIONS

9.1 Summary

The extension of the phase equilibria study of the geologically orientated olivine-bearing equilibria in the system CMAS, by replacing part of the anorthite with molecularly equivalent amounts of albite in the system CMASN, increased the normative plagioclase content of the liquids in equilibrium with the phases forsterite,plagioclase,diopside, and pyroxene. At the same time, the reaction nature of the equilibrium forsterite+spinel+plagioclase+liquid changed to one of coprecipitation. Bulk compositions having albite-rich normative plagioclase ratios, which are also peraluminous in the CIPW norm, are, therefore, unable to produce the wide variations in residual liquids during equilibrium or fractional crystallisation which bulk compositions having anorthite-rich normative plagioclase ratios could produce.

The extension from the system CMAS to the system CMAS-Fe-O_2, by replacing MgO with molecular equivalent amounts of FeO and controlling the pO_2 of the atmosphere of the experiments, had a less marked effect on the ratio of the normative constituents of the liquids in the equilibrium olivine+anorthite+clinopyroxene+liquid. At high FeO/MgO mole ratios however, marked changes in the phase fields occurred, mainly due to the instability of the pyroxenes, but also due to the instability of olivine at the pO_2 of the Ni/NiO equilibrium, in the MgO-free system. The effect

on crystallisation histories was similar to that described by previous studies on simpler parts of the system - both silica and iron enrichment trends remaining possible, depending on the type of crystallisation and the availability of oxygen to the system.

Comparison of the synthetic results with results obtained on terrestrial and lunar samples, showed that while the agreement in phase boundaries is better than if the system CMAS alone is considered, there was still some disagreement, thought mainly to be due to the TiO_2 content of the natural samples.

9.2 Future studies

Since this study only provides a small amount of data for the two subsystems CMASN and CMAS-Fe-O_2, further experiments are required using the present data as a base to explore the lower variance liquids of geological interest. Experiments can then be conducted in the system CMASN-Fe-O_2 at relevant bulk normative plagioclase and FeO/MgO mole ratios. At the same time, analyses of liquids and phase compositions are essential along with a mathematically based computer program to analyse phase diagrams and present the information in convenient form to the researcher for geological analysis.

A study of the effects of adding TiO_2 to the system would also bring the results of synthetic systems much closer to those from natural samples, and enable more accurate predictions to be made of the melting relations of other natural samples, given a suitable chemical analysis.

ACKNOWLEDGEMENTS

The assistance and encouragement of many colleagues of the Grant Institute of Geology, University of Edinburgh is gratefully acknowledged. Special thanks are due to Dr. G.M. Biggar and Professor M.J. O'Hara, for their advice and instruction in the techniques of experimental petrology at atmospheric pressure, and the interpretation of phase equilibrium diagrams.

My thanks also to the typist, Mrs. P. Williams, who exhibited lasting patience and care with the production of this thesis.

The tenure of a 2-year NERC Research Studentship is also acknowledged, during which part of this research was carried out.

REFERENCES

Andersen, O. 1915. The system anorthite-forsterite-silica. Am.Jour.Sci., v.39, pp.407-454.

Anderson, A.T. 1968. The oxygen fugacity of alkaline basalt and related magmas, Tristan da Cunha. Am.Jour.Sci., v.266, pp.704-727.

Biggar, G.M. 1969. Computer program for the calculation of the partial pressure of oxygen in CO_2-H_2 mixtures. Progr. in Exp.Petrol., v.1, pp.105-108.

_____ 1970. Molybdenum as a container for melts containing iron oxide. Bull.Amer.Ceramic Soc., v.49, pp.286-288.

_____ 1971. Phase relationships of bredigite ($Ca_5MgSi_3O_{12}$) and of the quaternary compound ($Ca_6MgAl_8SiO_{21}$) in the system CaO-MgO-Al_2O_3-SiO_2. Cement and Concrete Res., v.1, pp.493-513.

_____ 1972. Diopside, Lithium metasilicate and the 1968 temperature scale. Mineralog.Mag., v.38, pp.768-770.

_____ 1972a. Melilite solid solutions. Progr. in Exp. Petrol., v.2, pp.127-130.

_____ 1974. Phase equilibrium studies of the chilled margins of some layered intrusions. Contr.Mineral. and Petrol., v.46, pp.159-167.

Biggar, G.M. and O'Hara, M.J. 1969a. A comparison of gel and glass starting materials for phase equilibrium studies. Mineralog.Mag., v.37, pp.198-205.

Biggar, G.M. and O'Hara, M.J. 1969b. Temperature control and calibration in quench furnaces and some new temperature measurements in the system $CaO-MgO-Al_2O_3-SiO_2$. Mineralog.Mag., v.37, pp.1-15.

_____ 1969c. Solid solutions at atmospheric pressure in the system $CaO-MgO-SiO_2$ with special reference to the instabilities of Diopside, Akermanite and Monticellite. Progr. in Exp.Petrol., v.1, pp.86-96.

_____ 1972. Eight joins in $CaO-MgO-Al_2O_3-SiO_2$. Progr. in Exp.Petrol., v.2, pp.131-137.

Biggar, G.M., O'Hara, M.J., Humphries, D.J. and Peckett, A. 1972. Maria lavas, mascons, layered complexes, achondrites and the lunar mantle. In "The Moon", Eds. H.Urey and S.K. Runcorn. International Astonomical Union, pp.129-164.

Biggar, G.M., O'Hara, M.J., Peckett, A. and Humphries, D.J. 1971. Lunar lavas and the achondrites: petrogenesis of protohypersthene basalts in the maria lava lakes. Proc. Second Lunar Sci. Conf., Suppl.2, Geochim.et Cosmochim. Acta, v.1, pp. 617-643.

Bowen, N.L. 1913. The melting phenomena of the plagioclase feldspars. Am.Jour.Sci., v.35, pp.577-599.

_____ 1915. The crystallisation of haplobLastic, haplodioritic and related magmas. Am.Jour.Sci., v.40, pp.161-185.

Bowen, N.L. and Schairer, J.F. 1935. The system $MgO-FeO-SiO_2$. Am.Jour.Sci., v.29, pp.151-217.

Bowen, N.L., Schairer, J.F. and Posnjak, E. 1933. The system $CaO-FeO-SiO_2$. Am.Jour.Sci., v.26, pp.193-284.

Brown, G.M. and Schairer, J.F. 1971. Chemical and melting relations of some calc-alkaline volcanic rocks. Geol.Soc.America, Memoir 130, pp.139-157.

Cairns, E.J. and Tevebaugh, A.D. 1964. CHO gas phase compositions in equilibrium with carbon, and carbon deposition boundaries at one atmosphere. J.Chem. and Eng.Data, v.9, pp.453-462.

Campbell, F.E. and Roeder, P. 1968. The stability of olivine and pyroxene in the Ni-Mg-Si-O system. Am.Mineralogist, v.53, pp.257-268.

Cawthorn, R.G., Ford, C.E., Biggar, G.M., Bravo, M.S. and Clarke, D.B. 1973. Determination of the liquid compositions in experimental samples: discrepancies between microprobe analysis and other methods. Earth Planetary Sci. Letters, v.21, pp.1-5.

Chayes, F. and Yoder, H.S,Jr. 1971. Some anomalies in the norms of extremely undersaturated lavas. Carnegie Inst. Washington Yearbook 70, pp.205-206.

Clarke, D.B. and Biggar, G.M. 1972. Calcium-poor pyroxenes in the system $CaO-MgO-Al_2O_3-SiO_2-Fe-O_2$. Lithos, v.5, pp.203-216.

Darken, L.S. and Gurry, R.W. 1945. The system Iron-Oxygen. I. The wustite field and related equilibria. Jour.Amer.Chem.Soc., v.67, pp.1398-1412.

Eggler, D.H. 1974. Application of a portion of the system $CaAl_2Si_2O_8-NaAlSi_3O_8-SiO_2-MgO-Fe-O_2-H_2O-CO_2$ to genesis of the calc-alkaline suite. Am.Jour.Sci., v.274, pp.297-315.

Ehlers, E.G. 1972. The interpretation of geological phase diagrams. Freeman and Co., San Francisco.

Elsdon, R., Hamilton, D.L. and Nolan, J. 1972. The preparation of iron-bearing gels. Progr. in Exp. Petrol., v.2, pp.11-12.

Emslie, R.F. 1971. Liquidus relations and subsolidus reactions in some plagioclase-bearing systems. Carnegie Inst. Washington Yearbook 69, pp.148-155.

Eugster, H.P. and Wones, D.R. 1962. Stability relations of the ferruginous biotite, annite. Jour.Petrology, v.3, pp.82-125.

Ferguson, J.B. and Merwin, H.E. 1919. The ternary system $MgO-CaO-SiO_2$. Am.Jour.Sci., v.48, pp.81-123.

Ford, C.E., Biggar, G.M., Humphries, D.J., Wilson, G., Dixon, D. and O'Hara, M.J. 1972. Role of water in the evolution of the lunar crust; an experimental study of sample 14310; an indication of lunar calc-alkaline volcanism. Proc. Third Lunar Sci.Conf., Suppl.3, Geochim. et Cosmochim. Acta, v.1, pp.207-229.

Ford, C.E. and O'Hara, M.J. 1972. The system $MgSiO_3$-$Ca_3Al_2Si_3O_{12}$-H_2O. Progr. in Exp.Petrol., v.2, pp.150-152.

Fudali, R.F. 1965. Oxygen fugacities of basaltic and andesitic magmas. Geochim. et Cosmochim. Acta, v.29, pp.1063-1075.

Hahn, W.C.,Jr., and Muan, A. 1961. Activity measurements in oxide solid solutions: the systems NiO-MgO and NiO-MnO in the temperature interval 1100-1300°C. J.Phys.Chem.Solids, v.19, pp.338-348.

Hamilton, D.L. and Henderson, C.M.B. 1968. The preparation of silicate compositions by a gelling method. Mineralog.Mag., v.36, pp.832-838.

Hamilton, D.L. and MacKenzie, W.S. 1960. Nepheline solid solution in the system $NaAlSiO_4$-$KAlSiO_4$-SiO_2. Jour.Petrology, v.1, pp.56-72.

Heald, E.F., Reeker, J.R. and Herrington, D.R. 1969. Gel preparation of starting materials in iron-containing silicate systems. Am.Mineralogist, v.54, pp.317-320.

Hill, R. and Roeder, P.L. 1974. The crystallisation of spinel from basaltic liquid as a function of oxygen fugacity. Jour.Geology, v.82, pp.709-729.

Humphries, D.J. 1972. Dicalcium-silicate and spinel saturated equilibria. Progr. in Exp.Petrol., v.2, pp.140-143.

_____ 1972a. Melting behaviour of Reunion Igneous rocks. Progr. in Exp.Petrol., v.2, pp.113-115.

Humphries, D.J., Biggar, G.M. and O'Hara, M.J. 1972. Flow sheet for CaO-MgO-Al_2O_3-SiO_2 at atmospheric pressure. Progr. in Exp.Petrol., v.2, pp.138-139.

_____ 1972a. Phase equilibria and origin of Apollo 15 basalts, etc. In "The Apollo 15 Lunar Samples", The Lunar Science Institute, Houston, Texas, pp. 103-107.

Hytonen, K. and Schairer, J.F. 1960. The system enstatite-anorthite-diopside. Carnegie Inst. Washington Yearbook 59, pp.71-72.

_____ 1961. The plane enstatite-anorthite-diopside and its relation to basalts. Carnegie Inst. Washington Yearbook 60, pp.125-141.

Jamieson, B.G. 1969. Natural rock projection into a pseudo-quaternary system. Progr. in Exp.Petrol., v.1,pp.152-155.

Jamieson, B.G. 1970. Phase relations in some tholeiitic lavas illustrated by the system R_2O_3-XO-YO-ZO_2. Mineralog.Mag., v.37, pp.538-554.

Kushiro, I. 1972. Determination of liquidus relations in synthetic silicate systems with electron probe analysis: the system forsterite-diopside-silica at 1 atmosphere. Am.Mineralogist, v.57, pp.1260-1271.

_____ 1973. Incongruent melting of pure diopside. Carnegie Inst. Washington Yearbook 72, pp.708-710.

Larimer, J.W. 1968. Experimental studies on the system Fe-MgO-SiO_2-O_2 and their bearing on the petrology of chondritic meteorites. Geochim. et Cosmochim. Acta, v.32, pp.1187-1207.

Longhi, J., Walker,D., Grove, T.L., Stolper, E.M. and Hays, J.F. 1974. The petrology of the Apollo 17 mare basalts. Proc. Fifth Lunar Sci. Conf., Suppl. 5, Geochim. et Cosmochim. Acta, v.1, pp.447-469.

Luth, W.C. and Ingamells, C.O. 1965. Gel preparation of starting materials for hydrothermal experimentation. Am.Mineralogist, v.50, pp.255-258.

Merrill, R.B., Williams, R.J. and Akella, J. 1975. The system anorthite-forsterite-fayalite-silica to 2 kilobars with lunar petrologic applications. Lunar Science VI, pp. 557-559.

Muan, A. 1955. Phase equilibria in the system FeO-Fe_2O_3-SiO_2. Trans. AIME, v.203, pp.965-976.

_____ 1957. Phase equilibrium relationships at liquidus temperatures in the system FeO-Fe_2O_3-Al_2O_3-SiO_2. J.Amer.Ceramic Soc., v.40, pp.420-431.

Muan, A. 1963. Silver-palladium alloys as crucible material in studies of low-melting iron silicates. Bull.Amer. Ceramic Soc., v.42, pp.344-347.

Muan, A., Hauck, J. and Löfall, T. 1972. Equilibrium studies with a bearing on lunar rocks. Proc. Third Lunar Sci. Conf., Suppl.3, Geochim. et Cosmochim. Acta, v.1, pp.185-196.

Muan, A., Hauck, J., Osborn, E.F. and Schairer, J.F. 1971. Equilibrium relations among phases occurring in lunar rocks. Proc. Second Lunar Sci. Conf. Suppl.2, Geochim. et Cosmochim. Acta, v.1, pp.497-505.

Muan, A. and Osborn, E.F. 1956. Phase equilibria at liquidus temperatures in the system MgO-FeO-Fe_2O_3-SiO_2. J.Amer.Ceramic Soc., v.39, pp.121-140.

_____ 1965. Phase equilibria among oxides in steelmaking. American Iron and Steel Inst., New York.

Nafziger, R.H. 1970. The join diopside-iron oxide-silica and its relation to the join diopside-forsterite-iron oxide-silica. Am.Mineralogist, v.55, pp.2042-2052.

Nafziger, R.H., Ulmer, G.C. and Woermann, E. 1971. Gaseous buffering for the control of oxygen fugacity at one atmosphere. In "Research techniques for high pressure and high temperature", Ed. G.C. Ulmer, Springer-Verlag, Berlin, pp. 9-41.

O'Hara, M.J. 1968. The bearing of phase equilibria studies in synthetic and natural systems on the origin and evolution of basic and ultrabasic rocks. Earth-Sci. Rev., v.4, pp.69-133.

O'Hara, M.J. 1969. The atmospheric pressure equilibrium and fractional crystallisation of basaltic-like mixtures in the $MgSiO_3$-rich part of the plane $CaSiO_3$-$MgSiO_3$-Al_2O_3, and the nature of thermal divides. Progr. in Exp.Petrol., v.1, pp.129-152.

O'Hara, M.J. and Biggar, G.M. 1969. The join periclase-C_3AS_{15} and its bearing on basalt crystallisation, melting of siliceous marls and firing of magnesia refractories. Progr. in Exp.Petrol., v.1, pp.79-81.

_____ 1969a. Diopside-spinel equilibria, anorthite and forsterite reaction relationship in silica-poor liquids in the system CaO-MgO-Al_2O_3-SiO_2 at atmospheric pressure and their bearing on the genesis of melilitites and nephelinites. Am.Jour.Sci., Schairer vol. 267-A, pp.364-390.

_____ 1970. Phase equilibria aspects of the performance of basic refractories. Trans.British Ceramic Soc., v.69, pp.243-251.

O'Hara, M.J., Biggar, G.M., Richardson, S.W., Ford, C.E. and Jamieson, B.G. 1970. The nature of seas, mascons, and the lunar interior in the light of experimental studies. Proc. Apollo 11 Lunar Sci.Conf., Suppl.1, Geochim. et Cosmochim. Acta, v.1, pp. 695-710.

O'Hara, M.J., Humphries, D.J. and Waterston, S. 1975. Petrogenesis of mare basalts; implications for chemical, mineralogical and thermal models for the moon. Submitted to Proc. Sixth Lunar Sci.Conf., Suppl.6, Geochim. et Cosmochim. Acta.

O'Hara, M.J. and Yoder, H.S.,Jr. 1967. Formation and fractionation of basic magmas at high pressures. Scott.Jour.Geol., v.3, pp.67-117.

Osborn, E.F. and Muan, A. 1960. Phase equilibrium diagrams of Oxide Systems. Am.Ceramic Soc., Columbus, Ohio.

Osborn, E.F. and Tait, D.B. 1952. The system diopside-forsterite-anorthite. Am.Jour.Sci., Bowen vol., pp.413-433.

Phillips, B. and Muan, A. 1959. Phase equilibria in the system CaO-iron oxide-SiO_2 in air. J.Amer.Ceramic Soc., v.42, pp.413-423.

Presnall, D.C. 1964. Deduction of liquid crystallisation paths in a five-component oxide system containing iron. Carnegie Inst. Washington Yearbook 63, pp. 133-135.

_____ 1966. The join Forsterite-diopside-iron oxide and its bearing on the crystallisation of Basaltic and ultramafic magmas. Am.Jour.Sci., v.264, pp.753-809.

Rankin, G.A. and Wright, F.E. 1915. The ternary system $CaO-Al_2O_3-SiO_2$. Am.Jour.Sci., v.39, pp.1-39.

Ringwood, A.E. and Essene, E. 1970. Petrogenesis of Apollo 11 basalts, internal constitution and origin of the moon. Proc. Apollo 11 Lunar Sci.Conf., Suppl. 1, Geochim. et Cosmochim. Acta, v.1, pp.769-799.

Roedder, E. 1965. A laboratory reconnaissance of the liquidus surface in the pyroxene system En-Di-Hd-Fs ($MgSiO_3-CaMgSi_2O_6-CaFeSi_2O_6-FeSiO_3$). Am.Mineralogist, v.50, pp.696-703.

Roeder, P.L. and Emslie, R.F. 1970. Olivine-liquid equilibria. Contr.Mineral. and Petrol., v.29, pp.275-289.

Roeder, P.L. and Osborn, E.F. 1966. Experimental data for the system $MgO-FeO-Fe_2O_3-CaAl_2Si_2O_8-SiO_2$ and their petrologic implications. Am.Jour.Sci., v.264, pp.428-480.

Roy, R. 1956. Aids in hydrothermal experimentation: II. Methods of making mixtures for both "dry" and "wet" phase equilibrium studies. J.Amer.Ceramic Soc., v.39, pp.145-146.

Sato, M. and Wright, T.L. 1966. Oxygen fugacities directly measured in magmatic gases. Science, v.153, pp.1103-1105.

Schairer, J.F. 1942. The system $CaO-FeO-Al_2O_3-SiO_2$. I. Results of quenching experiments on five joins. J.Amer.Ceramic Soc., v.25, pp.241-274.

_____ 1954. The system $K_2O-MgO-Al_2O_3-SiO_2$. I. Results of quenching experiments on four joins in the tetrahedron cordierite-forsterite-leucite-silica and on the join cordierite-mullite-potash feldspar. J.Amer.Ceramic Soc., v.37, pp.501-533.

_____ 1957. The crystallisation of rock-forming minerals from magmas and the nature of the residual liquid. Carnegie Inst. Washington Yearbook 56, pp.217-222.

Schairer, J.F. and Bowen, N.L. 1955. The system $K_2O-Al_2O_3-SiO_2$. Am.Jour.Sci., v.253, pp.681-746.

_____ 1956. The system $Na_2O-Al_2O_3-SiO_2$. Am.Jour.Sci., v.254, pp.129-195.

Schairer, J.F. and Morimoto, N. 1958. Systems with rock-forming olivines, pyroxenes and feldspars. Carnegie Inst. Washington Yearbook 57, pp.212-213.

_____ 1959. The system forsterite-diopside-silica-albite. Carnegie Inst. Washington Yearbook 58, pp.113-118.

Schairer, J.F. and Yoder, H.S., Jr. 1961. Crystallisation in the system nepheline-forsterite-silica at one atmosphere pressure. Carnegie Inst. Washington Yearbook 60, pp.141-144.

_____ 1967. The system albite-anorthite-forsterite at 1 atmosphere. Carnegie Inst. Washington Yearbook 65, pp.204-209.

_____ 1970. Critical planes and flow sheet for a portion of the system $CaO-MgO-Al_2O_3-SiO_2$ having petrological applications. Carnegie Inst. Washington Yearbook 68, pp.202-214.

Shepherd, E.S., Rankin, G.A. and Wright, F.E. 1909. The binary systems of alumina with silica, lime and magnesia. Am.Jour.Sci., v.28, pp.293-333.

Speidel, D.H. and Nafziger, R.H. 1968. $P-T-fO_2$ relations in the system $Fe-O-MgO-SiO_2$. Am.Jour.Sci., v.266, pp.361-379.

Speidel, D.H. and Osborn, E.F. 1967. Element distribution among coexisting phases in the system $MgO-FeO-Fe_2O_3-SiO_2$ as a function of temperature and oxygen fugacity. Am.Mineralogist, v.52, pp.1139-1152.

Taylor, R.W. and Muan, A. 1962. Activities of iron in iron-platinum alloys at 1300°C. Trans. AIME, v.224, pp. 500-502.

Thompson, R.N. 1972. The 1-atmosphere melting patterns of some basaltic volcanic series. Am.Jour.Sci., v.272, pp.901-932.

_____ 1973. One-atmosphere melting behaviour and nomenclature of terrestrial lavas. Contr.Mineral. and Petrol. v.41, pp.197-204.

Tilley, C.E. and Thompson, R.N. 1970. Melting and crystallisation relations of the Snake River basalts of southern Idaho, U.S.A. Earth Planetary Sci. Letters, v.21, v.8, pp.79-92.

Tilley, C.E., Thompson, R.N., Wadsworth, W.J. and Upton,B.G.J. 1971. Melting and crystallisation relations of some lavas of Reunion Island, Indian Ocean. Mineralog. Mag., v.38, pp.344-352.

Tilley, C.E., Yoder, H.S.,Jr. and Schairer, J.F. 1963. Melting relations of basalts. Carnegie Inst. Washington Yearbook 62, pp.77-84.

Tilley, C.E., Yoder, H.S.,Jr. and Schairer, J.F. 1964. New relations on melting of basalts. Carnegie Inst. Washington Yearbook 63, pp.92-97.

_____ 1965. Melting relations of volcanic tholeiite and alkali rock series. Carnegie Inst. Washington Yearbook 64, pp.69-82.

_____ 1967. Melting relations of volcanic rock series. Carnegie Inst. Washington Yearbook 65, pp.260-269.

_____ 1968. Melting relations of igneous rock series. Carnegie Inst. Washington Yearbook 66, pp.450-457.

Turnock, A.C. 1962. Preliminary results on melting relations of synthetic pyroxenes on the diopside-hedenbergite join. Carnegie Inst. Washington Yearbook 61, p. 82.

Upton, B.G.J. and Wadsworth, W.J. 1966. The basalts of Reunion Island, Indian Ocean. Bull.Volc., v.29, pp.7-24.

_____ 1967. A complex basalt-mugearite sill in Piton des Neiges volcano, Reunion. Am.Mineralogist, v.52, pp.1475-1492.

_____ 1972. Aspects of magmatic evolution on Reunion Island. Phil.Trans.R.Soc.Lond.A., v.271, pp.105-130.

Wagman, D.D., Kilpatrick, J.E., Taylor, W.J., Pitzer, K.S. and Rossini, F.D. 1945. Heats, free energies, and equilibrium constants of some reactions involving O_2,H_2,H_2O,C,CO,CO_2 and CH_4. J.Res.Nat.Bureau Stds., v.34, pp.143-161.

Walker, D., Longhi, J., Grove, T.L., Stolper, E. and Hays, J.F. 1973. Experimental petrology and origin of rocks from the Descartes Highlands. Proc. Fourth Lunar Sci.Conf., Suppl.4, Geochim. et Cosmochim. Acta, v.1, pp. 1013-1032.

Walker, D., Longhi, J. and Hays, J.F. 1972. Experimental petrology and origin of Fra Mauro rocks and soil. Proc. Third Lunar Sci.Conf., Suppl.3, Geochim. et Cosmochim.Acta, v.1, pp.797-817.

Wright, T.L. and Doherty, P.C. 1970. A linear programming and least squares computer method for solving petrologic mixing problems. Bull.Geol.Soc.Amer., v.81, pp.1995-2008.

Yang, H.Y. 1973. Crystallisation of iron-free pigeonite in the system anorthite-diopside-enstatite-silica at atmospheric pressure. Am.Jour.Sci., v.273, pp.488-497.

Yang, H.Y. and Foster, W.R. 1972. Stability of iron-free pigeonite at atmospheric pressure. Am.Mineralogist, v.57, pp.1232-1241.

Yoder, H.S.,Jr. and Tilley, C.E. 1962. Origin of basalt magmas: an experimental study of natural and synthetic rock systems. Jour.Petrology, v.3, pp.342-532.

Yoder, H.S.,Jr., Tilley, C.E. and Schairer, J.F. 1963. Pyroxene and associated minerals in the crust and mantle: pyroxene quadrilateral. Carnegie Inst. Washington Yearbook 62, pp.84-95.

APPENDIX A

ABBREVIATIONS

1. Abbreviations used for the oxides in system names, and for formulae of phases:

   A = Al_2O_3 C = CaO K = K_2O M = MgO

   N = Na_2O S = SiO_2 T = TiO_2 F = FeO

2. Abbreviations used for the phase names, with their equivalent symbols on the figures:

   ab = albite (A)

   an = anorthite (A)

   cor = corundum

   cord = cordierite (C)

   cpx = high-Ca pyroxene (D)

   di = diopside (D)

   en = enstatite (P)

   fa = fayalite (O)

   Fe = iron metal (I)

   fo = forsterite (O)

   gross = grossular

   hc = hercynite (M)

   hd = hedenbergite

   hem = hematite (M)

   jd = jadeite

   liq = liquid (L)

   mel = melilite

   mo = monticellite

   ne = nepheline

ol = olivine (O)

opx = orthopyroxene (P)

pen = protoenstatite (P)

per = periclase

pig = pigeonite (P)

plag = plagioclase (A)

pwoll = pseudowollastonite (W)

pyx = low-Ca pyroxene, used when the polymorph is unknown or uncertain (P)

sil = silica (S)

sp = spinel (M)

woll = wollastonite (W)

wu = wustite (W)

3. Abbreviations used for the experimental technique:

Ag = silver

Ag_{40} = $Ag_{40}Pd_{60}$ capsules

Ag_{70} = $Ag_{70}Pd_{30}$ capsules

Au = gold

AWG = Anorthite-Wollastonite-Gehlenite eutectic composition

AWT = Anorthite-Wollastonite-Tridymite eutectic composition

Di = Diopside

emf = electromotive force (in μV)

Fe/FeO = pO_2 of the Fe/FeO equilibrium

L_2S = Lithium metasilicate

M.I. = Melting interval

Mo = Molybdenum

Ni/NiO = pO_2 of the Ni/NiO equilibrium

Pd = Palladium

pO_2 = partial pressure of oxygen

Pt = Platinum

Rh = Rhodium

APPENDIX B

COMPOSITIONS OF STARTING MATERIALS

B.1. Compositions studied in the system $CaO-MgO-Al_2O_3-SiO_2$

a) Anorthite - Diopside - Forsterite

	wt.%			wt.%				
	AN	DI	FO	CaO	MgO	Al_2O_3	SiO_2	Yield (gms)
ADF1	43.5	49.0	7.5	21.46	13.42	15.94	49.18	10.00
ADF2	40.0	55.0	5.0	22.31	13.10	14.66	49.93	10.00
ADF3	40.0	50.0	10.0	21.01	15.04	14.66	49.29	10.00
ADF4	45.0	45.0	10.0	20.72	14.11	16.49	48.68	10.00
ADF5	45.0	50.0	5.0	22.02	12.17	16.49	49.32	10.00

b) Diopside - MAS

	Moles				Wt.%				
	CaO	MgO	Al_2O_3	SiO_2	CaO	MgO	Al_2O_3	SiO_2	Yield (gms)
H13	1.5	2.5	1.0	4.0	15.96	19.12	19.34	45.59	9.99
H14	2.0	3.0	1.0	5.0	17.65	19.03	16.05	47.28	9.99
H4	2.375	3.375	1.0	5.75	18.58	18.98	14.23	48.21	9.99
H5	2.5	3.5	1.0	6.0	18.85	18.97	13.71	48.47	9.97
H6	2.625	3.625	1.0	6.25	19.10	18.96	13.23	48.72	9.97
H15	3.0	4.0	1.0	7.0	19.75	18.92	11.97	49.36	9.99
H16	4.0	5.0	1.0	9.0	20.99	18.86	9.54	50.61	9.96

c) Diopside - $M_5A_3S_5$

	Moles				Wt.%				
	CaO	MgO	Al_2O_3	SiO_2	CaO	MgO	Al_2O_3	SiO_2	Yield (gms)
H17	3.75	8.75	3.0	12.5	12.98	21.77	18.88	46.36	10.00
H18	5.25	10.25	3.0	15.5	15.14	21.25	15.73	47.89	10.00
H1	6.5	11.5	3.0	18.0	16.45	20.92	13.81	48.82	9.98
H2	7.0	12.0	3.0	19.0	16.89	20.82	13.16	49.13	9.97
H3	7.5	12.25 (12.5)	3.0	20.0	17.29	20.72	12.58	49.41	9.96
H19	9.0	14.0	3.0	23.0	18.31	20.47	11.10	50.13	9.99
H20	12.0	17.0	3.0	29.0	19.76	20.12	8.98	51.15	10.02

d) Diopside - $M_7A_3S_7$

	Moles				Wt.%				
	CaO	MgO	Al_2O_3	SiO_2	CaO	MgO	Al_2O_3	SiO_2	Yield (gms)
H21	3.75	10.75	3.0	14.5	11.55	23.80	16.80	47.85	10.00
H22	5.25	12.25	3.0	17.5	13.72	23.01	14.26	49.01	10.00
H23	6.0	13.0	3.0	19.0	14.58	22.71	13.25	49.46	10.00
H24	6.75	13.75	3.0	20.5	15.32	22.44	12.38	49.86	9.96
H25	7.5	14.5	3.0	22.0	15.98	22.20	11.62	50.21	9.99
H26	9.0	16.0	3.0	25.0	17.07	21.81	10.34	50.79	9.98
H27	12.0	19.0	3.0	31.0	18.66	21.23	8.48	51.63	10.02

B.2. Compositions studied in the system $CaO - MgO - Al_2O_3 - SiO_2 - Na_2O$

B.2.1. Anorthite: Albite CIPW normative ratio = 67.97:32.03 Wt. %

a) $XO.YO.2ZO_2 - YO.R_2O_3.ZO_2$ (Diopside - MAS)

	Moles					Wt.%					
	CaO	MgO	Al_2O_3	SiO_2	Na_2O	CaO	MgO	Al_2O_3	SiO_2	Na_2O	Yield (gms)
N19	1.25	3.25	1.25	5.5	0.25	10.39	19.42	18.90	48.99	2.30	9.97
N16	1.5	3.5	1.25	6.0	0.25	11.54	19.36	17.49	49.48	2.13	9.98
N1	1.875	3.875	1.25	6.75	0.25	12.98	19.29	15.74	50.08	1.91	9.98
N2	2.0	4.0	1.25	7.0	0.25	13.40	19.27	15.23	50.25	1.85	9.95
N3	2.25	4.25	1.25	7.5	0.25	14.16	19.23	14.30	50.57	1.74	9.97
N17	3.0	5.0	1.25	9.0	0.25	15.97	19.13	12.10	51.33	1.47	9.99
N18	4.0	6.0	1.25	11.0	0.25	17.66	19.04	10.04	52.04	1.22	9.98

b) $XO.YO.2ZO_2 - 5YO.3R_2O_3.5ZO_2$ ($M_5A_3S_5$)

	Moles					Wt.%					
	CaO	MgO	Al_2O_3	SiO_2	Na_2O	CaO	MgO	Al_2O_3	SiO_2	Na_2O	Yield (gms)
N20	1.0	4.0	1.25	6.0	0.25	7.78	22.37	17.68	50.02	2.15	9.94
N10	1.5	4.5	1.25	7.0	0.25	10.15	21.88	15.37	50.73	1.87	9.98
N11	1.75	4.75	1.25	7.5	0.25	11.11	21.68	14.43	51.02	1.75	9.98
N12	2.0	5.0	1.25	8.0	0.25	11.97	21.50	13.60	51.28	1.65	9.97
N21	2.5	5.5	1.25	9.0	0.25	13.41	21.20	12.19	51.72	1.48	9.94
N22	3.5	6.0	1.25	11.0	0.25	15.55	20.76	10.10	52.36	1.23	10.05

c) $XO.YO.2ZO_2 - 7YO.3R_2O_3.7ZO_2$ (Diopside - $M_7A_3S_7$)

	Moles					Wt.%					
	CaO	MgO	Al_2O_3	SiO_2	Na_2O	CaO	MgO	Al_2O_3	SiO_2	Na_2O	Yield (gms)
N23	0.66	4.666	1.25	6.333	0.25	4.99	25.12	17.02	50.81	2.07	9.96
N24	1.25	5.25	1.25	7.5	0.25	8.01	24.18	14.56	51.48	1.77	9.94
N25	1.5	5.5	1.25	8.0	0.25	9.05	23.85	13.71	51.72	1.67	9.93
N26	1.75	5.75	1.25	8.5	0.25	9.98	23.57	12.96	51.92	1.58	9.94
N27	2.25	6.25	1.25	9.5	0.25	11.56	23.07	11.67	52.28	1.42	9.95
N28	3.0	7.0	1.25	11.0	0.25	13.41	22.50	10.16	52.69	1.24	9.96

B.2.2. Anorthite-albite CIPW normative ratio = 51.48:48.52 Wt.%.

a) $XO.YO.2ZO_2$ - $YO.R_2O_3.ZO_2$ (Diopside - MAS)

	Moles					Wt.%					
	CaO	MgO	Al_2O_3	SiO_2	Na_2O	CaO	MgO	Al_2O_3	SiO_2	Na_2O	Yield (gms)
L19	1.25	4.25	1.5	7.5	0.5	8.00	19.56	17.46	51.44	3.54	9.98
L1	1.75	4.75	1.5	8.5	0.5	9.97	19.45	15.54	51.89	3.15	9.95
L2	2.0	5.0	1.5	9.0	0.5	10.80	19.41	14.73	52.08	2.98	9.97
L3	2.25	5.25	1.5	9.5	0.5	11.55	19.37	14.00	52.24	2.84	9.97
L20	3.0	6.0	1.5	11.0	0.5	13.41	19.27	12.19	52.67	2.47	9.97
L21	4.0	7.0	1.5	13.0	0.5	15.24	19.18	10.39	53.08	2.11	9.99

b) $XO.YO.2ZO_2$ - $5YO.3R_2O_3.5ZO_2$ (Diopside - $M_5A_3S_5$)

	Moles					Wt.%					
	CaO	MgO	Al_2O_3	SiO_2	Na_2O	CaO	MgO	Al_2O_3	SiO_2	Na_2O	Yield (gms)
L22	1.5	14.5	4.5	22.0	1.5	3.31	22.99	18.05	52.00	3.66	10.01
L23	2.5	15.5	4.5	24.0	1.5	5.08	22.65	16.63	52.27	3.37	9.98
L16	3.5	16.5	4.5	26.0	1.5	6.60	22.35	15.42	52.50	3.13	9.96
L17	4.5	17.5	4.5	28.0	1.5	7.91	22.10	14.37	52.71	2.91	9.93
L18	5.5	18.5	4.5	30.0	1.5	9.05	21.88	13.46	52.88	2.73	9.98
L24	7.0	20.0	4.5	33.0	1.5	10.52	21.60	12.29	53.11	2.49	9.98
L25	10.0	23.0	4.5	39.0	1.5	12.80	21.15	10.47	53.46	2.12	9.98

c) $\underline{XO.YO.2ZO_2 - 7YO.3R_2O_3.7ZO_2}$ (Diopside - $\underline{M_7A_3S_7}$)

	Moles					Wt.%					
	CaO	MgO	Al_2O_3	SiO_2	Na_2O	CaO	MgO	Al_2O_3	SiO_2	Na_2O	Yield (gms)
L26	1.0	18.0	4.5	25.0	1.5	1.98	25.59	16.18	52.98	3.28	9.96
L27	2.0	19.0	4.5	27.0	1.5	3.67	25.10	15.03	53.15	3.05	10.01
L28	3.0	20.0	4.5	29.0	1.5	5.15	24.67	14.04	53.31	2.84	9.99
L29	3.75	20.75	4.5	30.5	1.5	6.13	24.38	13.37	53.41	2.71	10.02
L30	4.5	21.5	4.5	32.0	1.5	7.02	24.12	12.77	53.51	2.59	10.01
L31	6.0	23.0	4.5	35.0	1.5	8.59	23.66	11.71	53.67	2.37	9.93
L32	9.0	26.0	4.5	41.0	1.5	11.05	22.94	10.04	53.93	2.04	9.95

B.2.3 Anorthite:albite CIPW normative ratio = 34.66:65.34 Wt.%

a) $XO.YO.2ZO_2 - YO.R_2O_3.ZO_2$ (Diopside - MAS)

	Moles					Wt.%					
	CaO	MgO	Al_2O_3	SiO_2	Na_2O	CaO	MgO	Al_2O_3	SiO_2	Na_2O	Yield (gms)
A16	1.0	6.0	2.0	11.0	1.0	4.58	19.75	16.65	53.96	5.06	9.95
A1	1.5	6.5	2.0	12.0	1.0	6.31	19.66	15.30	54.09	4.65	9.97
A2	2.0	7.0	2.0	13.0	1.0	7.78	19.58	14.15	54.19	4.30	9.98
A3	2.375	7.375	2.0	13.75	1.0	8.75	19.53	13.39	54.26	4.07	9.96
A18	3.5	8.5	2.0	16.0	1.0	11.11	19.40	11.55	54.43	3.51	9.96
A17	5.0	10.0	2.0	19.0	1.0	13.41	19.28	9.75	54.60	2.96	9.97

b) $XO.YO.2ZO_2 - 5YO.3R_2O_3.5ZO_2$ (Diopside - $M_5A_3S_5$)

	Moles					Wt.%					
	CaO	MgO	Al_2O_3	SiO_2	Na_2O	CaO	MgO	Al_2O_3	SiO_2	Na_2O	Yield (gms)
A19	0.5	7.5	2.0	12.0	1.0	2.13	22.95	15.48	54.74	4.71	9.96
A10	1.0	8.0	2.0	13.0	1.0	3.93	22.62	14.31	54.79	4.35	9.96
A11	1.25	8.25	2.0	13.5	1.0	4.74	22.48	13.78	54.82	4.19	9.95
A12	1.5	8.5	2.0	14.0	1.0	5.48	22.34	13.30	54.84	4.04	9.95
A20	2.0	9.0	2.0	15.0	1.0	6.83	22.09	12.42	54.88	3.77	9.97
A21	3.0	10.0	2.0	17.0	1.0	9.05	21.69	10.97	54.96	3.34	9.97
A22	4.0	11.0	2.0	19.0	1.0	10.81	21.37	9.83	55.01	2.99	9.97

This analysis is not An34·66 BOT 20·96.

c) $XO.YO.2ZO_2 - 7YO.3R_2O_3.7ZO_2$ (Diopside - $M_7A_3S_7$)

	Moles					Wt.%					
	CaO	MgO	Al_2O_3	SiO_2	Na_2O	CaO	MgO	Al_2O_3	SiO_2	Na_2O	Yield (gms)
A23	0.5	9.5	2.0	14.0	1.0	1.85	25.23	13.43	55.41	4.08	9.99
A25	1.5	10.5	2.0	16.0	1.0	4.85	24.40	11.76	55.42	3.57	9.97
A27	3.0	12.0	2.0	19.0	1.0	8.17	23.49	9.90	55.43	3.01	9.98

d) Composition used for Na_2O loss determination

	Moles					Wt.%					
	CaO	MgO	Al_2O_3	SiO_2	Na_2O	CaO	MgO	Al_2O_3	SiO_2	Na_2O	Yield (gms)
A7	2.625	4.625	2.0	11.25	1.0	11.54	14.62	15.99	52.99	4.86	9.96

B.3. Compositions studied in the system $CaO-MgO-Al_2O_3-SiO_2-Fe-O_2$

Composition	Moles					Wt%					Yield
	FeO	MgO	CaO	Al_2O_3	SiO_2	FeO	MgO	CaO	Al_2O_3	SiO_2	%
(A) FeO/MgO mole ratio = 0.074											
(i) $3XO.R_2O_3.15ZO_2$-YO (C_3AS_{15}-M)											
0.074-9-3-1-15	0.666	9.000	3.0	1.0	15.0	3.03	22.93	10.63	6.44	56.97	99.36
(B) FeO/MgO mole ratio = 0.125											
(i) $3XO.R_2O_3.15ZO_2$-YO (C_3AS_{15}-M)											
0.125-2-3-1-15	0.250	2.000	3.0	1.0	15.0	1.41	6.35	13.25	8.03	70.96	99.64
0.125-6-3-1-15	0.750	6.000	3.0	1.0	15.0	3.67	16.49	11.47	6.95	61.43	99.80
0.125-8-3-1-15	1.000	8.000	3.0	1.0	15.0	4.59	20.60	10.75	6.51	57.56	99.70
(C) FeO/MgO mole ratio = 0.18											
(i) $XO.YO.2ZO_2$-$YO.R_2O_3.ZO_2$ (Diopside-MAS)											
AF1	0.450	2.550	2.0	1.0	5.0	4.98	15.82	17.26	15.69	46.24	99.70
AF2	0.525	2.975	2.5	1.0	6.0	4.96	15.77	18.44	13.41	47.42	100.25
AF3	0.600	3.400	3.0	1.0	7.0	4.95	15.74	19.32	11.71	48.29	99.65
AF4	0.750	4.250	4.0	1.0	9.0	4.93	15.69	20.54	9.34	49.51	99.75
AF5	0.900	5.100	5.0	1.0	11.0	4.92	15.65	21.35	7.76	50.32	100.00
AF6	1.200	6.800	7.0	1.0	15.0	4.91	15.61	22.35	5.81	51.32	100.00

Composition	Moles					Wt%					Yield
	FeO	MgO	CaO	Al_2O_3	SiO_2	FeO	MgO	CaO	Al_2O_3	SiO_2	%
(ii) $XO.YO.2ZO_2$-$5YO.3R_2O_3.5ZO_2$ (Diopside-$M_5A_3S_5$)											
AF31	1.500	8.500	5.0	3.0	15.0	5.56	17.68	14.47	15.78	46.51	99.80
AF32	1.650	9.350	6.0	3.0	17.0	5.49	17.46	15.58	14.17	47.31	100.00
AF33	1.875	10.625	7.5	3.0	20.0	5.41	17.19	16.88	12.28	48.24	100.00
AF34	2.100	11.900	9.0	3.0	23.0	5.34	16.99	17.88	10.84	48.95	100.00
AF35	2.550	14.450	12.0	3.0	29.0	5.25	16.71	19.30	8.77	49.97	100.00
AF36	3.450	19.550	18.0	3.0	41.0	5.15	16.37	20.97	6.35	51.17	100.20
(D) FeO/MgO mole ratio = 0.20											
(i) $YO.ZO_2$-$3XO.R_2O_3.3ZO_2$ (En-Gross)											
0.2-10-3-1-15	2.000	10.000	3.0	1.0	15.0	8.36	23.46	9.79	5.93	52.45	99.12
0.2-6.6-3-1-11	1.333	6.666	3.0	1.0	11.0	7.39	20.74	12.99	7.87	51.01	97.47
0.2-5-3-1-9	1.000	5.000	3.0	1.0	9.0	6.63	18.59	15.52	9.40	49.87	100.00
0.2-3.3-3-1-7	0.666	3.333	3.0	1.0	7.0	5.48	15.39	19.27	11.68	48.18	99.50
0.2-2.5-3-1-6	0.500	2.500	3.0	1.0	6.0	4.68	13.13	21.92	13.29	46.98	99.60
0.2-1.6-3-1-5	0.333	1.666	3.0	1.0	5.0	3.62	10.15	25.42	15.41	45.40	100.00
(E) FeO/MgO mole ratio = 0.25											
(i) $3XO.R_2O_3.15ZO_2$-YO (C_3AS_{15}-M)											
0.25-2-3-1-15	0.500	2.000	3.0	1.0	15.0	2.79	6.26	13.06	7.92	69.97	99.19
0.25-6-3-1-15	1.500	6.000	3.0	1.0	15.0	7.09	15.90	11.06	6.70	59.25	99.60
0.25-8-3-1-15	2.000	8.000	3.0	1.0	15.0	8.77	19.69	10.27	6.23	55.03	99.31
0.25-9-3-1-15	2.250	9.000	3.0	1.0	15.0	9.53	21.39	9.92	6.01	53.14	98.62

Composition	Moles					Wt%					Yield
	FeO	MgO	CaO	Al_2O_3	SiO_2	FeO	MgO	CaO	Al_2O_3	SiO_2	%
(F) FeO/MgO mole ratio = 0.33											
(i) $YO.ZO_2$-$3XO.R_2O_3.3ZO_2$ (En-Gross)											
0.3-9-3-1-15	3.000	9.000	3.0	1.0	15.0	12.32	20.73	9.62	5.83	51.51	99.41
0.3-6-3-1-11	2.000	6.000	3.0	1.0	11.0	10.91	18.37	12.78	7.74	50.20	99.70
0.3-4.5-3-1-9	1.500	4.500	3.0	1.0	9.0	9.80	16.49	15.29	9.27	49.15	99.31
0.3-3-3-1-7	1.000	3.000	3.0	1.0	7.0	8.13	13.69	19.04	11.54	47.60	99.41
0.3-2.25-3-1-6	0.750	2.250	3.0	1.0	6.0	6.95	11.70	21.70	13.15	46.50	99.31
0.3-1.5-3-1-5	0.500	1.500	3.0	1.0	5.0	5.39	9.07	25.22	15.29	45.04	99.30
(G) FeO/MgO mole ratio = 0.50											
(i) $XO.YO.2ZO_2$-$YO.R_2O_3.ZO_2$ (Diopside-MAS)											
AF11	1.000	2.000	2.0	1.0	5.0	10.77	12.09	16.82	15.29	45.04	99.51
AF12	1.166	2.333	2.5	1.0	6.0	10.74	12.05	17.96	13.06	46.19	99.80
AF13	1.333	2.666	3.0	1.0	7.0	10.71	12.02	18.82	11.40	47.04	99.60
AF14	1.666	3.333	4.0	1.0	9.0	10.68	11.99	20.01	9.09	48.23	99.90
AF15	2.000	4.000	5.0	1.0	11.0	10.66	11.96	20.80	7.56	49.02	99.80
AF16	2.666	5.333	7.0	1.0	15.0	10.63	11.93	21.78	5.66	50.01	99.70

Composition	Moles					Wt%					Yield
	FeO	MgO	CaO	Al_2O_3	SiO_2	FeO	MgO	CaO	Al_2O_3	SiO_2	%
(ii) $XO.YO.2ZO_2$-$5YO.3R_2O_3.5ZO_2$ (Diopside-$M_5A_3S_5$)											
AF41	3.333	6.666	5.0	3.0	15.0	12.00	13.46	14.05	15.33	45.16	99.90
AF42	3.666	7.333	6.0	3.0	17.0	11.85	13.30	15.14	13.76	45.95	99.90
AF43	4.166	8.333	7.5	3.0	20.0	11.68	13.10	16.41	11.93	46.88	100.00
AF44	4.666	9.333	9.0	3.0	23.0	11.55	12.96	17.38	10.53	47.59	99.80
AF45	5.666	11.333	12.0	3.0	29.0	11.36	12.74	18.77	8.53	48.60	99.90
AF46	7.666	15.333	18.0	3.0	41.0	11.13	12.49	20.40	6.18	49.79	99.80
(iii) $YO.ZO_2$-$3XO.R_2O_3.3ZO_2$ (En-Gross)											
0.5-8-3-1-15	4.000	8.000	3.0	1.0	15.0	16.13	18.10	9.45	5.72	50.60	98.82
0.5-5.3-3-1-11	2.666	5.333	3.0	1.0	11.0	14.32	16.07	12.58	7.62	49.41	99.21
0.5-4-3-1-9	2.000	4.000	3.0	1.0	9.0	12.88	14.45	15.08	9.14	48.46	99.11
0.5-2.6-3-1-7	1.333	2.666	3.0	1.0	7.0	10.72	12.02	18.82	11.40	47.04	99.01
0.5-2-3-1-6	1.000	2.000	3.0	1.0	6.0	9.17	10.29	21.48	13.02	46.03	95.25
0.5-1.3-3-1-5	0.666	1.333	3.0	1.0	5.0	7.12	7.99	25.03	15.17	44.69	99.31

Composition	Moles					Wt%					Yield %
	FeO	MgO	CaO	Al_2O_3	SiO_2	FeO	MgO	CaO	Al_2O_3	SiO_2	
(iv) $3XO.R_2O_3.15ZO_2$-YO (C_3AS_{15}-M)											
0.5-1-3-1-15	0.500	1.000	3.0	1.0	15.0	2.88	3.23	13.48	8.18	72.23	99.50
0.5-2-3-1-15	1.000	2.000	3.0	1.0	15.0	5.43	6.09	12.71	7.70	68.08	99.60
0.5-3-3-1-15	1.500	3.000	3.0	1.0	15.0	7.70	8.64	12.02	7.28	64.37	100.00
0.5-4-3-1-15	2.000	4.000	3.0	1.0	15.0	9.73	10.92	11.40	6.91	61.05	99.53
0.5-6-3-1-15	3.000	6.000	3.0	1.0	15.0	13.23	14.85	10.33	6.26	55.33	99.61
0.5-9-3-1-15	4.500	9.000	3.0	1.0	15.0	17.41	19.53	9.06	5.49	48.52	91.46
0.5-12-3-1-15	6.000	12.000	3.0	1.0	15.0	20.66	23.19	8.06	4.89	43.20	99.22
0.5-16-3-1-15	8.000	16.000	3.0	1.0	15.0	24.04	26.97	7.04	4.26	37.69	99.41
(v) $3XO.R_2O_3$-YO-ZO_2 (C_3A-M-S)											
0.5-4-3-1-6	2.000	4.000	3.0	1.0	6.0	15.36	17.23	17.98	10.90	38.52	99.40
0.5-0.6-3-1-5	0.333	0.666	3.0	1.0	5.0	3.85	4.32	27.07	16.41	48.34*	101.20
(H) FeO/MgO mole ratio = 0.55											
(i) $3XO.R_2O_3.15ZO_2$-YO (C_3AS_{15}-M)											
0.55-5-3-1-15	2.750	5.000	3.0	1.0	15.0	12.58	12.83	10.71	6.49	57.38	99.70
(I) FeO/MgO mole ratio = 0.66											
(i) $3XO.R_2O_3$-YO-ZO_2 (C_3A-M-S)											
0.6-6-3-1-7	4.000	6.000	3.0	1.0	7.0	23.56	19.82	13.79	8.36	34.47	99.03

* 1.45% excess SiO_2 added during preparation.

Composition	Moles					Wt%					Yield %
	FeO	MgO	CaO	Al_2O_3	SiO_2	FeO	MgO	CaO	Al_2O_3	SiO_2	
(J) FeO/MgO mole ratio = 0.75											
(i) $3XO.R_2O_3.15ZO_2$ - YO (C_3AS_{15}-M)											
0.75-8-3-1-15	6.000	8.000	3.0	1.0	15.0	22.39	16.75	8.74	5.30	46.82	99.61
(ii) $3XO.R_2O_3$ - YO - ZO_2 (C_3A-M-S)											
0.75-4-3-1-6	3.000	4.000	3.0	1.0	6.0	21.39	16.01	16.70	10.12	35.78	99.70
(K) FeO/MgO mole ratio = 1.00											
(i) $XO.YO.2ZO_2$ - $YO.R_2O_3.ZO_2$ (Diopside-MAS)											
AF21	1.500	1.500	2.0	1.0	5.0	15.78	8.86	16.43	14.93	44.00	99.61
AF22	1.750	1.750	2.5	1.0	6.0	15.74	8.83	17.55	12.76	45.12	99.56
AF23	2.000	2.000	3.0	1.0	7.0	15.70	8.81	18.39	11.14	45.96	99.61
AF24	2.500	2.500	4.0	1.0	9.0	15.65	8.78	19.55	8.89	47.13	99.51
AF25	3.000	3.000	5.0	1.0	11.0	15.62	8.77	20.32	7.39	47.90	100.00
AF26	4.000	4.000	7.0	1.0	15.0	15.60	8.75	20.87	6.33	48.45	99.80
(ii) $XO.YO.2ZO_2$ - $5YO.3R_2O_3.5ZO_2$ (Diopside-$M_5A_3S_5$)											
AF51	5.000	5.000	5.0	3.0	15.0	17.54	9.84	13.69	14.93	44.00	99.71
AF52	5.500	5.500	6.0	3.0	17.0	17.33	9.72	14.75	13.41	44.79	99.80
AF53	6.250	6.250	7.5	3.0	20.0	17.08	9.58	16.00	11.63	45.71	99.61
AF54	7.000	7.000	9.0	3.0	23.0	16.89	9.48	16.95	10.27	46.41	99.71
AF55	8.500	8.500	12.0	3.0	29.0	16.62	9.33	18.31	8.32	47.42	99.90
AF56	11.500	11.500	18.0	3.0	41.0	16.30	9.15	19.92	6.04	48.60	99.71

Composition	Moles					Wt%					Yield
	FeO	MgO	CaO	Al_2O_3	SiO_2	FeO	MgO	CaO	Al_2O_3	SiO_2	%
(iii) $YO.ZO_2 - 3XO.R_2O_3.3ZO_2$ (En-Gross)											
1-6-3-1-15	6.000	6.000	3.0	1.0	15.0	23.37	13.11	9.12	5.53	48.87	99.81
1-4-3-1-11	4.000	4.000	3.0	1.0	11.0	20.83	11.69	12.19	7.39	47.90	98.83
1-3-3-1-9	3.000	3.000	3.0	1.0	9.0	18.78	10.54	14.66	8.89	47.13	98.92
1-2-3-1-7	2.000	2.000	3.0	1.0	7.0	15.70	8.81	18.39	11.14	45.96	99.71
1-1.5-3-1-6	1.500	1.500	3.0	1.0	6.0	13.49	7.57	21.06	12.76	45.12	99.51
1-1-3-1-5	1.000	1.000	3.0	1.0	5.0	10.52	5.90	24.64	14.93	44.00	99.31
(iv) $3XO.R_2O_3.15ZO_2 - YO$ (C_3AS_{15}-M)											
1-1-3-1-15	1.000	1.000	3.0	1.0	15.0	5.60	3.14	13.11	7.94	70.21	100.30
1-2-3-1-15	2.000	2.000	3.0	1.0	15.0	10.30	5.78	12.05	7.31	64.57	99.21
1-3-3-1-15	3.000	3.000	3.0	1.0	15.0	14.29	8.02	11.16	6.76	59.77	99.31
1-4-3-1-15	4.000	4.000	3.0	1.0	15.0	17.74	9.95	10.39	6.29	55.63	99.61
1-5-3-1-15	5.000	5.000	3.0	1.0	15.0	20.74	11.64	9.71	5.89	52.03	98.14
1-8-3-1-15	8.000	8.000	3.0	1.0	15.0	27.78	15.59	8.13	4.93	43.57	99.71
1-12-3-1-15	12.000	12.000	3.0	1.0	15.0	34.25	19.22	6.68	4.05	35.80	98.27
(v) $3XO.R_2O_3 - YO - ZO_2$ (C_3A-M-S)											
1-2.5-3-1-7	2.500	2.500	3.0	1.0	7.0	18.49	10.38	17.32	10.50	43.31	99.31
1-0.5-3-1-5	0.500	0.500	3.0	1.0	5.0	5.73	3.22	26.85	16.27	47.94	99.50

Composition	Moles					Wt%					Yield
	FeO	MgO	CaO	Al_2O_3	SiO_2	FeO	MgO	CaO	Al_2O_3	SiO_2	%
(L) FeO/MgO mole ratio = 2.00											
(i) $YO.ZO_2 - 3XO.R_2O_3.3ZO_2$ (En-Gross)											
2-4-3-1-15	8.000	4.000	3.0	1.0	15.0	30.13	8.45	8.82	5.35	47.25	99.61
2-2.6-3-1-11	5.333	2.666	3.0	1.0	11.0	26.94	7.56	11.84	7.17	46.49	100.00
2-2-3-1-9	4.000	2.000	3.0	1.0	9.0	24.38	6.84	14.27	8.65	45.87	99.51
2-1.3-3-1-7	2.666	1.333	3.0	1.0	7.0	20.43	5.74	17.98	10.90	44.95	99.71
2-1-3-1-6	2.000	1.000	3.0	1.0	6.0	17.64	4.95	20.65	12.52	44.25	99.51
2-0.6-3-1-5	1.333	0.666	3.0	1.0	5.0	13.82	3.88	24.27	14.71	43.33	99.21
(ii) $3XO.R_2O_3.15ZO_2 - YO$ (C_3AS_{15}-M)											
2-1-3-1-15	2.000	1.000	3.0	1.0	15.0	10.60	2.97	12.41	7.52	66.49	99.31
2-2-3-1-15	4.000	2.000	3.0	1.0	15.0	18.67	5.24	10.93	6.62	58.54	99.22
2-3-3-1-15	6.000	3.000	3.0	1.0	15.0	25.01	7.02	9.76	5.92	52.29	99.90
2-5-3-1-15	10.000	5.000	3.0	1.0	15.0	34.35	9.64	8.04	4.88	43.09	99.33
(M) FeO/MgO mole ratio = 3.00											
(i) $YO.ZO_2 - 3XO.R_2O_3.3ZO_2$ (En-Gross)											
3-3-3-1-15	9.000	3.000	3.0	1.0	15.0	33.35	6.24	8.68	5.26	46.48	99.52
3-2-3-1-11	6.000	2.000	3.0	1.0	11.0	29.88	5.59	11.66	7.07	45.81	99.90
3-1.5-3-1-9	4.500	1.500	3.0	1.0	9.0	27.06	5.06	14.08	8.53	45.26	98.93
3-1-3-1-7	3.000	1.000	3.0	1.0	7.0	22.77	4.26	17.77	10.77	44.43	98.93
3-0.75-3-1-6	2.250	0.750	3.0	1.0	6.0	19.65	3.68	20.45	12.40	43.83	99.51
3-0.5-3-1-5	1.500	0.500	3.0	1.0	5.0	15.43	2.88	24.08	14.60	43.01	99.41

Composition	Moles					Wt%					Yield
	FeO	MgO	CaO	Al_2O_3	SiO_2	FeO	MgO	CaO	Al_2O_3	SiO_2	%
(ii) $3XO.R_2O_3.15ZO_2$ - YO (C_3AS_{15}-M)											
3-5-3-1-15	15.000	5.000	3.0	1.0	15.0	43.97	8.22	6.87	4.16	36.78	99.62
(N) FeO/MgO mole ratio = 4.00											
(i) $3XO.R_2O_3.15ZO_2$ - YO (C_3AS_{15}-M)											
4-2-3-1-15	8.000	2.000	3.0	1.0	15.0	31.46	4.41	9.21	5.58	49.33[+]	98.55
4-4-3-1-15	16.000	4.000	3.0	1.0	15.0	46.31	6.50	6.78	4.11	36.31	99.33
(O) FeO/MgO mole ratio = 5.00											
(i) $YO.ZO_2$ - $3XO.R_2O_3.3ZO_2$ (En-Gross)											
5-2-3-1-15	10.000	2.000	3.0	1.0	15.0	36.46	4.09	8.54	5.17	45.74	MIX[x]
(P) FeO/MgO mole ratio = 6.00											
(i) $3XO.R_2O_3.15ZO_2$ - YO (C_3AS_{15}-M)											
6-3-3-1-15	18.000	3.000	3.0	1.0	15.0	50.02	4.68	6.51	3.94	34.86	99.05

[+] 0.49% excess SiO_2 added during preparation.

[x] The mix compositions were prepared by thoroughly mixing and grinding two different gels in the proportions required for each composition.

Composition	Moles					Wt%					Yield
	FeO	MgO	CaO	Al_2O_3	SiO_2	FeO	MgO	CaO	Al_2O_3	SiO_2	%
(Q) FeO/MgO mole ratio = 7.00											
(i) $YO.ZO_2 - 3XO.R_2O_3.3ZO_2$ (En-Gross)											
7-1.5-3-1-15	10.500	1.500	3.0	1.0	15.0	37.98	3.04	8.47	5.13	45.37	MIX
7-1.2-3-1-12.6	8.400	1.200	3.0	1.0	12.6	35.94	2.88	10.02	6.07	45.09	MIX
7-1-3-1-11	7.000	1.000	3.0	1.0	11.0	34.11	2.73	11.41	6.92	44.83	MIX
7-0.75-3-1-9	5.250	0.750	3.0	1.0	9.0	30.96	2.48	13.81	8.37	44.38	MIX
(R) FeO/MgO mole ratio = no MgO present											
(i) $YO.ZO_2 - 3XO.R_2O_3.3ZO_2$ (En-Gross)											
12-X-3-1-15	12.000	0.000	3.0	1.0	15.0	42.40	0.00	8.27	5.01	44.32	98.66
8-X-3-1-11	8.000	0.000	3.0	1.0	11.0	38.17	0.00	11.17	6.77	43.89	MIX
6-X-3-1-9	6.000	0.000	3.0	1.0	9.0	34.71	0.00	13.55	8.21	43.54	98.36
4-X-3-1-7	4.000	0.000	3.0	1.0	7.0	29.38	0.00	17.20	10.42	43.00	98.45
3-X-3-1-6	3.000	0.000	3.0	1.0	6.0	25.47	0.00	19.88	12.05	42.60	99.71
2-X-3-1-5	2.000	0.000	3.0	1.0	5.0	20.12	0.00	23.55	14.27	42.06	99.51

B.4 Natural compositions

All the natural samples studied are from Reunion Island, Indian Ocean.

The calculated $\log_{10}(pO_2)$ was obtained from the equation

$$\log \frac{X_{FeO}}{X_{FeO_{1.5}}} = -0.20 \log (pO_2) - 1.04$$

which relates the amounts of Fe_2O_3 and FeO in a natural sample with the pO_2 at 1200°C, from Roeder and Emslie (1970).

Those rocks which have nepheline in the CIPW norm, have two values given for the anorthite content of the normative feldspar. The value calculated from the norm does not take account of the nepheline content. So that a comparison can be made with non-nepheline normative rocks, a second value is given, in brackets, calculated as if no nepheline were present.

1. Piton des Neiges : Oceanite Series

	Re331	Re75	Re243	Re134	Re171	Re170	Re124	Re607	Re69	Re180
SiO_2	43.57	47.12	46.20	46.78	47.38	47.94	47.35	47.57	48.45	48.40
Al_2O_3	8.10	12.01	11.08	14.30	14.88	14.80	15.27	14.86	14.71	15.57
Fe_2O_3	2.86	1.65	3.06	3.97	4.34	5.32	2.79	2.94	4.42	3.00
FeO	9.58	9.93	8.96	8.59	7.80	7.02	9.14	6.93	7.40	8.96
MgO	26.87	13.88	13.37	9.71	8.80	7.67	6.88	6.74	6.57	5.19
CaO	5.68	9.21	8.82	9.43	10.12	10.10	12.05	11.75	11.06	11.34
Na_2O	1.16	2.15	1.99	2.49	2.98	2.80	2.50	3.11	2.48	2.73
K_2O	0.31	0.59	0.23	0.55	0.79	0.82	0.42	0.99	0.48	0.49
H_2O+	0.24	0.64	2.47	0.95	0.20	0.17	0.56	1.82	1.27	1.05
H_2O-	-	-	1.32	-	-	0.06	-	-	0.25	0.14
TiO_2	1.28	2.02	1.92	2.43	2.51	2.37	2.47	2.77	2.17	2.37
P_2O_5	0.27	0.21	0.28	0.35	0.41	0.46	0.29	0.34	0.37	0.40
MnO	0.23	0.18	0.18	0.20	0.20	0.20	0.20	0.15	0.17	0.18
CO_2	0.04	-	-	0.15	0.12	-	0.13	-	-	-
S	-	-	-	-	-	-	-	-	-	-
E Fe as FeO	12.15	11.41	11.71	12.16	11.71	11.81	11.65	9.58	11.38	11.66
Calc. pO_2	-8.05	-9.33	-7.76	-7.11	-6.70	-6.30	-8.01	-7.29	-6.55	-7.81
Norm plag: An content	57.84	49.65	53.12	51.88	48.15 (45.41)	47.08	55.27	48.18 (42.38)	53.66	52.54
Ferromagnesian FeO/MgO ratio in norm minerals	0.19	0.28	0.30	0.37	0.38	0.42	0.44	0.38	0.45	0.51

2. Piton des Neiges : Differentiated Series

	Lavas							Intrusives			
	Re512	Re332	Re415	Re471	Re538	Re86	Re100	Re2	Re30a	Re27	Re1
SiO_2	45.28	45.85	45.68	45.07	45.89	48.06	59.39	46.50	41.57	50.26	58.46
Al_2O_3	14.78	15.92	16.77	19.49	16.71	21.08	17.98	13.55	13.07	15.26	17.09
Fe_2O_3	4.86	7.89	4.76	5.38	3.06	3.94	1.37	5.21	9.86	5.55	5.17
FeO	6.55	6.82	9.39	6.89	10.09	5.21	4.53	8.76	6.93	4.74	2.17
MgO	10.92	4.81	4.74	4.57	4.11	3.18	0.78	5.56	5.44	3.34	0.98
CaO	12.62	9.51	9.60	11.74	12.51	10.30	3.99	9.15	10.82	4.84	2.65
Na_2O	1.75	3.34	3.39	2.48	2.75	3.44	5.40	3.36	2.58	5.49	6.35
K_2O	0.50	1.19	0.79	0.59	0.75	1.10	3.08	1.20	0.60	2.32	2.92
H_2O+	0.21	0.39	0.38	0.86	0.26	0.58	-	2.96	1.35	2.54	1.40
H_2O-	-	-	-	-	-	-	-	-	-	-	-
TiO_2	1.91	3.76	3.39	2.58	3.04	2.40	1.05	2.97	4.93	2.80	1.00
P_2O_5	0.24	0.48	0.58	0.43	0.33	0.47	0.79	0.40	0.24	0.36	0.43
MnO	0.20	0.22	0.27	0.23	0.18	0.18	0.19	0.18	0.21	0.18	0.21
CO_2	0.39	-	-	0.27	0.46	0.13	0.40	0.65	1.78	2.14	0.99
S	-	-	-	-	-	-	-	-	0.23	0.07	-
E Fe as FeO	10.92	13.92	13.67	11.73	12.84	8.76	5.76	13.45	15.80	9.73	6.82
Calc. pO_2	-6.08	-5.11	-6.90	-5.97	-8.02	-6.04	-8.03	-6.56	-4.66	-5.09	-3.54
Norm plag: An content	67.20 (63.57)	46.78 (41.40)	50.08 (45.82)	63.97 (62.22)	57.45 (52.79)	53.48 (52.14)	15.93	35.31 (34.06)	47.20 (46.79)	11.91	5.44
Ferromagnesian FeO/MgO ratio in norm minerals	0.33	0.56	0.56	0.54	0.58	0.55	0.78	0.53	0.54	0.55	0.78

3.

	Piton des Neiges Nodules		Piton de la Fournaise Lavas	
	Re508	Re505	Re168	Re634
SiO_2	48.21	49.84	47.28	49.15
Al_2O_3	13.07	15.25	14.55	14.79
Fe_2O_3	3.44	5.44	2.45	1.59
FeO	7.44	5.45	9.70	9.96
MgO	10.77	5.49	8.74	6.03
CaO	11.80	11.47	10.03	10.99
Na_2O	2.62	3.01	2.78	2.87
K_2O	0.70	0.94	0.84	0.81
H_2O+	0.18	0.58	0.23	0.14
H_2O-	-	-	0.08	-
TiO_2	1.66	2.38	2.75	2.99
P_2O_5	0.44	0.30	0.44	0.31
MnO	0.17	0.15	0.18	0.18
CO_2	-	-	-	-
S	-	-	-	-
E Fe as FeO	10.54	10.35	11.91	11.39
Calc. pO_2	-7.10	-5.43	-8.42	-9.41
Norm plag: An content	49.83 (45.36)	44.94	47.45 (46.46)	46.31
Ferromagnesian FeO/MgO ratio in norm minerals	0.32	0.46	0.38	0.45

Phenocrysts in Reunion samples studied

1. Piton des Neiges

a) Oceanite Series

Re 331 Olivine + minor opaque spinel.

R 75 Olivine (?? + subordinate plagioclase).

Re 243 Olivine.

Re 134 Olivine. Scarce plagioclase microphenocrysts.

Re 171 Aphyric.

Re 170 Olivine. (some of the plagioclase could be phenocrystic).

Re 124 Olivine, plagioclase, augite.

Re 607 Gabbroic.

Re 69 Olivine. Microphenocrysts of plagioclase and augite.

Re 180 Olivine. Scarce plagioclase and augite microphenocrysts.

b) Differentiated Series:Lavas

Re 512 Olivine, plagioclase, augite.

Re 332 Very scarce microphenocrysts of plagioclase.

Re 415 Plagioclase. Subordinate olivine, augite, magnetite.

Re 471 Plagioclase. Subordinate olivine, augite, magnetite.

Re 538 Olivine, plagioclase.

Re 86 Plagioclase, olivine, augite, magnetite.

Re 100 Plagioclase, olivine, augite, magnetite, apatite.

c) Differentiated Series: Intrusives

Re 2 Aphyric.

Re 30a Plagioclase. (? olivine + augite).

Re 27 Plagioclase, alkali feldspar, augite, hornblende, magnetite.

Re 1 Microphenocrysts of plagioclase.

d) Nodules

Re 508 Gabbroic.

Re 505 Gabbroic.

2. Piton de la Fournaise

Re 168 Olivine.

Re 634 Olivine.

Source of analyses:

Upton and Wadsworth (1966)	:	343,243,170,69,180,168
Upton and Wadsworth (1967)	:	30a,27
Upton and Wadsworth (1972)	:	331,75,134,171,124,512,332, 415,471,538,86,100,2,1,634
Upton (personal comm.)	:	607,505,508 and phenocryst information.

APPENDIX C

DETAILS OF FURNACE OPERATIONS

C.1. Furnace operations involving compositions in the systems $CaO-MgO-Al_2O_3-SiO_2$ and $CaO-MgO-Al_2O_3-SiO_2-Na_2O$ All run charges contained in platinum capsules.

Run No.	Time Hrs.mins.	Recording T/C emf μv	Calculated temp. °C	Calibration value or Calibrant	Corrected temp. °C	Calibration reference
a) Furnace 8						
8-45	2.00	13138	1193.9	L_2S liquid	mean = 1193.0	1
8-46	2.00	13113	1192.1	L_2S solid	i.e. +14.9±0.9 °C	
8-47	2.30	15781	1382.0	Di solid	mean = 1383.7	2
8-48	2.00	15831	1385.5	Di liquid	i.e. +11.6±1.7 °C	
8-49	168.00	14305-14340	1277.8-1280.3	+13.4±1.3	1291.2-1293.7±1.3 °C	(1,2)
8-50	336.00	14496-14522	1291.4-1293.3	+13.2±1.3	1304.6-1306.5±1.3 °C	(1,2)
8-51	216.00	14219-14233	1271.6-1272.6	+13.5±1.2	1285.1-1286.1±1.2 °C	(1,2)
T/C Broken; new probe used						
8-52	2.15	13120	1192.6	L_2S liquid	mean = 1191.0	3
8-53	2.15	13077	1189.5	L_2S solid	i.e. +16.9±1.5 °C	
8-54	2.15	15831	1385.5	Di liquid	mean = 1383.7	4
8-55	2.15	15781	1382.0	Di solid	i.e. +11.6±1.7 °C	
8-56	168.00	13464-13466	1217.4-1217.6	+16.2±1.5	1233.8-1234.0±1.5 °C	(3,4)
8-57	168.00	13715-13718	1235.5-1235.7	+15.7±1.5	1251.2-1251.4±1.5 °C	(3,4)
8-58	240.00	13872-13903	1246.8-1249.0	+15.3±1.4	1262.1-1264.3±1.4 °C	(3,4)
8-59	216.00	13884-13891	1247.6-1248.1	+15.3±1.4	1262.9-1263.4±1.4 °C	(3,4)

Abbreviations: L_2S = Lithium metasilicate; Di = Diopside; AWG = Anorthite-Wollastonite-Gehlenite; Au = Gold; M.I. = Melting interval.

Run No.	Time Hrs.mins.	Recording T/C emf μv	Calculated temp. °C	Calibration value or Calibrant	Corrected temp. °C	Calibration reference
8-60	2.40	13093	1190.7	L_2S liquid	mean = 1190.0 i.e. +17.9±0.6 °C	5
8-61	2.45	13075	1189.4	L_2S solid		
8-62	2.45	13042	1187.0	L_2S solid		
8-63	2.30	15792	1382.7	Di liquid	less than 1382.7 i.e.>+12.6± ? °C	6
8-64	2.30	15800	1383.3	Di liquid		
Furnace burnt out. New element installed.						
8-65	3.30	13069	1188.9	L_2S solid		
8-66	3.30	13095	1190.8	L_2S solid		
8-67	3.30	13193	1197.9	L_2S solid	mean = 1202.1 i.e. +5.8±0.9°C	7
8-68	3.30	13238	1201.2	L_2S solid		
8-69	3.15	13294	1205.2	L_2S liquid		
8-70	3.30	13264	1203.0	L_2S liquid		
8-71 to 8-76 furnace used in the 1065°C region						
8-77	168.00	14165	1267.8	+5.9±0.6	1273.7±0.6 °C	(8,9)
8-78	192.00	13450	1216.4	+5.5±0.8	1221.9±0.9 °C	(8,9)
8-79	2.15	13222	1200.0	L_2S solid	mean = 1202.5 i.e. +5.4±0.8 °C	8
8-80	2.45	13245	1201.7	L_2S solid		
8-81	2.45	13268	1203.3	L_2S liquid		

Run No.	Time Hrs.mins.	Recording T/C emf μv	Calculated temp. °C	Calibration value or Calibrant	Corrected temp. °C	Calibration reference
8-82	2.30	15878	1388.7	Di liquid		
8-83	2.30	15797	1383.1	Di solid	mean = 1388.4	9
8-84	2.30	15900	1390.3	Di liquid	i.e. +6.9±0.3 °C	
8-85	2.30	15869	1388.1	Di solid		
8-86	168.00	13965-13979	1253.4-1254.4	+5.8±0.7	1259.2-1260.2±0.7 °C	(8,9)
8-87	168.00	13612-13618	1228.1-1228.5	+5.6±0.8	1233.7-1234.1±0.8 °C	(8,9)
8-88	2.30	15886	1389.3	Di liquid		
8-89	2.30	15849	1386.7	Di solid	mean = 1388.7	10
8-90	2.30	15870	1388.2	Di solid	i.e. +6.6±0.5 °C	
8-91	2.30	13238	1201.2	L_2S solid	mean = 1202.3	11
8-92	2.30	13270	1203.5	L_2S liquid	i.e. +5.6±1.1 °C	
8-93	168.00	13730-13728	1236.5-1236.4	+5.8±1.0	1242.3-1242.2±1.0 °C	(10,11)
8-94	168.00	13521-13526	1221.5-1221.9	+5.7±1.0	1227.2-1227.6±1.0 °C	(10,11)
8-95	2.30	15853	1387.0	Di solid		
8-96	2.30	15909	1390.9	Di liquid	mean = 1387.8	12
8-97	2.30	15877	1388.7	Di liquid	i.e. +7.5±0.8 °C	
8-98	2.30	13229	1200.5	L_2S liquid	mean = 1199.2	13
8-99	2.30	13194	1198.0	L_2S solid	i.e. +8.7±1.2 °C	
8-100	168.00	13288-13285	1204.7-1204.5	+8.7±1.2	1213.4-1213.2±1.2 °C	(12,13)
8-101	168.00	14121	1264.6	+8.3±1.1	1272.9±1.1 °C	(12,13)
8-102	2.30	15877	1388.7	Di M.I.	mean = 1388.7	14
8-103	2.30	15853	1387.0	Di solid	i.e. +6.6±0.0 °C	

Run No.	Time Hrs.mins.	Recording T/C emf μv	Calculated temp. °C	Calibration value or Calibrant	Corrected temp. °C	Calibration reference
8-104	3.00	13219	1199.8	L_2S solid		
8-105	3.00	13188	1197.5	L_2S solid		
8-106	2.30	13223	1200.1	L_2S solid	mean = 1202.1	15
8-107	2.30	13220	1199.9	L_2S solid	i.e. +5.8±0.7 °C	
8-108	2.45	13243	1201.4	L_2S solid		
8-109	2.30	13263	1202.9	L_2S liquid		
8-110	168.00	13761-13759	1238.8-1238.6	+6.0±0.6	1244.8-1244.6±0.6 °C	(14,15)
8-111	168.00	13826-13835	1243.5-1244.1	+6.0±0.5	1249.5-1250.1±0.5 °C	(14,15)
8-112	2.30	15841	1386.2	Di solid		
8-113	2.45	15872	1388.3	Di liquid	mean = 1388.1	16
8-114	4.30	15867	1388.0	Di solid	i.e. +7.2±0.1 °C	
8-115	3.00	13249	1201.9	L_2S liquid	mean = 1200.9	17
8-116	3.00	13221	1199.9	L_2S solid	i.e. +7.0±1.0 °C	
8-117	168.00	13529-13525	1222.1-1221.8	+7.0±0.9	1229.1-1228.8±0.9 °C	(16,17)
8-118	168.00	14011	1256.7	+7.1±0.7	1263.8±0.7 °C	(16,17)
Assembly changed to Platinum buckets.						
8-119	2.15	15867	1388.0	Di solid		
8-120	2.15	15945	1393.4	Di liquid	mean = 1390.0	18
8-121	2.15	15902	1390.4	Di liquid	i.e. +5.3±0.0 °C	
8-122	2.15	15896	1390.0	Di M.I.		
8-123	3.00	13249	1201.9	L_2S liquid	mean = 1200.9	19
8-124	3.15	13222	1200.0	L_2S solid	i.e. +7.0±0.9 °C	

Run No.	Time Hrs.mins.	Recording T/C emf μv	Calculated temp. °C	Calibration value or Calibrant	Corrected temp. °C	Calibration reference
8-125	168.00	14157-14150	1267.2-1266.7	+6.4±0.6	1273.6-1273.1±0.6°C	(18,19)
8-126	168.00	14350-14365	1281.0-1282.1	+6.3±0.5	1287.3-1288.4±0.5 °C	(18,19)
8-127	3.00	15881	1389.0	Di solid		
8-128	3.00	15899	1390.2	Di solid	mean = 1390.9	20
8-129	3.00	15908	1390.8	Di solid	i.e. +4.4±0.1 °C	
8-130	3.15	15911	1391.0	Di liquid		
8-131	3.15	13243	1201.5	L_2S solid	mean = 1202.7	21
8-132	3.00	13253	1202.2	L_2S solid	i.e. +5.2±0.5 °C	
8-133	3.00	13268	1203.3	L_2S liquid		
8-134	17.30	14306	1277.9	+4.9±0.4	1282.8±0.4 °C	(20,21)
8-135	18.00	14279	1275.9	+4.9±0.4	1280.8±0.4 °C	(20,21)
8-136	18.15	14233	1272.6	AWG liquid +4.9±0.4	1277.5±0.4 °C	(20,21,22)
8-137	18.15	14181	1268.9	AWG solid +4.9±0.4	1273.8±0.4 °C	(20,21,22)
				AWG calib: mean = 1270.9 i.e. +4.9±1.8 °C		22
8-138	2.15	15891	1389.7	Di liquid	mean = 1389.2	23
8-139	2.15	15861	1387.6	Di solid	i.e. +6.1±0.0 °C	
8-140	2.00	15884	1389.2	Di M.I.		
8-141	2.45	13256	1202.4	L_2S liquid	mean = 1200.3	24
8-142	3.15	13236	1201.0	L_2S liquid	i.e. +7.6±0.6 °C	
8-143	3.15	13218	1199.7	L_2S solid		

Run No.	Time Hrs.mins.	Recording T/C emf μv	Calculated temp. °C	Calibration value or Calibrant	Corrected temp. °C	Calibration reference
8-144	168.00	14208-14221	1270.9-1271.8	+7.0±0.4	1277.9-1278.8±0.4°C	(23,24)
8-145	192.00	14153	1266.9	+7.1±0.4	1274.0±0.4°C	(23,24)
8-146	3.00	15877	1388.7	Di M.I.	mean = 1388.7 i.e. +6.6±0.0 °C	25
8-147	6.45	13229	1200.5	L_2S solid	mean = 1201.2 i.e. +6.7±0.7 °C	26
8-148	3.30	13248	1201.9	L_2S liquid		
b) Furnace 6						
6-30	2.15	15939	1393.0	Di M.I.	mean = 1393.0 i.e. +2.3±0.0 °C	27
6-31	2.15	15930	1392.4	Di solid		
6-32	2.15	13272	1203.6	L_2S solid		
6-33	2.15	13313	1206.5	L_2S solid	mean = 1207.6 i.e. +0.3±1.1°C	28
6-34	3.15	13304	1205.9	L_2S solid		
6-35	3.15	13351	1209.3	L_2S liquid		
6-36	3.00	13344	1208.8	L_2S liquid		
6-37	264.00	14612-14640	1299.6-1301.6	+1.3±0.6	1300.9-1302.9±0.6 °C	(27,28)
6-38	168.00	13272-13293	1203.6-1205.1	+0.3±1.1	1203.9-1205.4±1.1 °C	(28)
6-39 to 6-45 Used over a wide temperature range for other work.						
6-46	2.00	13362	1210.1	L_2S liquid	mean = 1208.8 i.e. -0.9±1.3 °C	29
6-47	3.30	13281	1204.2	L_2S solid		
6-48	3.30	13326	1207.5	L_2S solid		

Run No.	Time Hrs. mins.	Recording T/C emf μv	Calculated temp. °C	Calibration value or Calibrant	Corrected temp. °C	Calibration reference
6-49	2.30	15961	1394.5	Di solid		
6-50	3.30	15897	1390.1	Di solid	mean = >1395.7	30
6-51	2.15	15944	1393.4	Di liquid ?	i.e. >-0.2 °C	
6-52	2.30	15977	1395.7	Di solid	taken as +0.0 °C	
6-53	3.30	13408	1213.4	L_2S liquid		
6-54	3.30	13340	1208.5	L_2S liquid		
6-55	3.30	13307	1206.1	L_2S liquid	mean = 1205.8	31
6-56	3.30	13264	1203.0	L_2S solid	i.e. +2.1±0.3 °C	
6-57	3.30	13288	1204.7	L_2S solid		
6-58	3.30	13299	1205.5	L_2S solid		
6-59 to 6-66 used in the range 1065 °C.						
6-67	168.00	13982	1254.6	+2.1±0.3	1256.7±0.3 °C	(31)
6-68 to 6-70 used in the 1300-1400 °C range.						
6-71	2.30	13207	1198.9	L_2S solid		
6-72	2.45	13272	1203.6	L_2S solid	mean = 1204.5	32
6-73	2.30	13299	1205.5	L_2S liquid	i.e. +3.4±0.9 °C	
6-74	2.30	15846	1386.5	Di solid	taken as calibration no 34 33	
6-75	2.30	15928	1392.2	Di solid	i.e. +2.8±0.8 °C	
6-76	168.00	14282-14309	1276.1-1278.1	+3.2±0.9	1279.3-1281.3±0.9 °C	(32,33)
6-77	168.00	13708-13718	1235.0-1235.7	+3.3±0.9	1238.3-1239.0±0.9 °C	(32,33)

Run No.	Time Hrs.mins	Recording T/C emf μv	Calculated temp. °C	Calibration value or Calibrant	Corrected temp. °C	Calibration reference
6-78	2.30	15968	1395.0	Di liquid		
6-79	2.30	15943	1393.3	Di liquid	mean = 1392.5	34
6-80	2.30	15921	1391.7	Di solid	i.e. +2.8±0.8 °C	
6-81	2.30	13300	1205.6	L_2S liquid	mean = 1204.0	35
6-82	2.30	13272	1203.6	L_2S solid	i.e. +3.9±1.0 °C	
6-83	168.00	13873-13881	1246.8-1247.4	+3.7±1.0	1250.5-1251.1±1.0 °C	(34,35)
6-84	168.00	14068-14075	1260.8-1261.3	+3.6±0.9	1264.4-1264.9±0.9 °C	(34,35)
6-85	2.30	15910	1391.0	Di solid		
6-86	2.30	15979	1395.8	Di liquid	mean = 1394.1	36
6-87	2.30	15931	1392.4	Di solid	i.e. +1.2±1.7 °C	
6-88	2.30	13287	1204.7	L_2S M.I.	mean = 1204.7	37
					i.e. +3.2±0.0 °C	
6-89	168.00	14240-14248	1273.1-1273.7	+2.5±0.6	1275.6-1276.2±0.6 °C	(36,37)
6-90	168.00	14390-14397	1283.9-1284.4	+2.4±0.7	1286.3-1286.8±0.7 °C	(36,37)
6-91	2.30	15954	1394.1	Di liquid		
6-92	2.30	15932	1392.5	Di liquid	mean = 1391.9	38
6-93	3.00	15923	1391.9	Di M.I.	i.e. +3.4±0.0 °C	
6-94	3.00	13248	1201.9	L_2S solid		
6-95	2.15	13211	1199.2	L_2S solid	Confirms calib. no. 37	39
6-96	2.30	13247	1201.8	L_2S solid		
6-97	2.45	13271	1203.5	L_2S solid		

Run No.	Time Hrs.mins	Recording T/C emf μv	Calculated temp. °C	Calibration value or Calibrant	Corrected temp. °C	Calibration reference
6-98	168.00	13814-13827	1242.6-1243.5	+3.2±0.0	1245.8-1246.7±0.0 °C	(37,38)
6-99	168.00	14283-14290	1276.2-1276.7	+3.3±0.0	1279.5-1280.0±0.0 °C	(37,38)
6-100	2.30	15920	1391.7	Di solid	mean = 1392.2	40
6-101	2.30	15934	1392.7	Di liquid	i.e. +3.1±0.5 °C	
6-102	2.45	13293	1205.1	L_2S liquid		
6-103	4.30	13284	1204.5	L_2S liquid	mean = 1203.4	41
6-104	3.30	13269	1203.4	L_2S M.I.	i.e. +4.3±0.0 °C	
c) Furnace 3						
3-51	2.15	13180	1197.0	L_2S solid	mean = 1197.8	42
3-52	2.15	13203	1198.6	L_2S liquid	i.e. +10.1±0.8 °C	
3-53	2.45	15915	1391.3	Di liquid		
3-54	2.30	15862	1387.6	Di liquid	mean = 1387.0	43
3-55	2.30	15803	1383.5	Di solid	i.e. +8.3±0.6 °C	
3-56	2.15	15845	1386.4	Di solid		
3-57	264.00	14119-14118	1264.5-1264.4	+9.5±0.7	1274.0-1273.9±0.7 °C	(42,43)
3-58 to 3-60 used at 1300-1400°C for 1 month.						
3-61	192.00	13558-13551	1224.2-1223.7	+16.9±3.0	1241.1-1240.6±3.0 °C	(44)
3-62	3.00	13201	1198.5	L_2S liquid		
3-63	3.00	13151	1194.9	L_2S liquid	mean = 1191.8	44
3-64	2.30	13067	1188.8	L_2S solid	i.e. +16.9±3.0 °C	

C.2 Details of furnace operations involving compositions in the system $CaO-MgO-Al_2O_3-SiO_2-Fe-O_2$ and natural samples.

In order to achieve efficiency of operation of the atmospheric pressure furnaces used for controlled atmosphere experiments, the author shared with Dr. G.M. Biggar the performance of the furnace operations. This enabled compositions from several projects simultaneously in progress to be used to complete the 18 capsules run in each experiment. The technique used by Dr. G.M. Biggar was identical to that used by the author. Those runs not performed by the author are denoted by a + sign after the run number.

Intermediate run numbers involving compositions of no interest here are omitted. All calibrations are included, however.

Abbreviations are given in Appendix A.

Run No.	Time Hrs.mins.	Recording T/C emf μv	Calculated temp. ^{o}C	Calibration value or calibrant	Corrected temp. ^{o}C	Calibration reference	Charge container
a) Furnace 7							
7-60+	2.00	11430	1068.9	Au liquid			
7-61+	2.00	-	-	Au solid	mean = 1063.7	1	
7-62+	2.00	11394	1066.2	Au liquid	i.e. +0.7±2.5 ^{o}C		
7-63+	2.00	11344	1062.5	Au *lost			
7-64+	2.00	11326	1061.2	Au solid			
7-65+	4.00	13231	1200.6	L_2S solid			
7-66+	2.30	13273	1203.7	L_2S solid	mean = 1205.3	2	
7-67+	2.00	13318	1206.9	L_2S liquid	i.e. +2.6±1.6 ^{o}C		
7-68+	3.30	11313	1060.2	Au solid	Confirms calib.no.1		
7-102	2.00	16135	1406.7	Di liquid			
7-103	2.45	15982	1396.0	Di liquid	mean = 1391.4	3	
7-104	2.30	15848	1386.6	Di solid	i.e. +3.9±1.3 ^{o}C		
7-105	2.45	15897	1390.1	Di solid			
7-106	2.15	15936	1392.8	Di liquid			
7-110	3.15	13399	1212.7	L_2S liquid			
7-111	3.00	13319	1207.0	L_2S solid	mean = 1207.8	4	
7-112	3.00	13284	1204.5	L_2S solid	i.e. +0.1±0.8 ^{o}C		
7-113	3.00	13342	1208.6	L_2S liquid			
7-114	2.15	15892	1389.7	Di solid	taken with calib.no 3 data		
7-115	2.15	15925	1392.0	Di solid	mean = 1392.4	5	
7-116	2.15	15892	1389.7	Di liquid?	i.e. +2.9±0.4 ^{o}C		

Run No.	Time Hrs.mins.	Recording T/C emf μv	Calculated temp. °C	Calibration value or calibrant	Corrected Temp. °C	Calibration reference	Charge container
7-118	6.00	12194	1125.3	+4.4±1.1	1129.7±1.1 °C	(4,8)	Mo
7-119	6.00	12915	1177.8	+1.7±0.9	1179.5±0.9 °C	(4,8)	Mo
7-121	6.00	12567	1152.6	+3.0±1.0	1155.6±1.0 °C	(4,8)	Mo
7-122	2.30	15884	1389.2	Di solid	mean = 1392.4	6	
7-123	2.45	15931	1392.4	Di M.I.	i.e. +2.9±0.0 °C		
7-124	3.30	13319	1207.0	L_2S liquid			
7-125	4.00	13262	1202.9	L_2S solid +4.7±0.3	1207.6±0.3 °C	(7)	Mo
7-126	3.30	13270	1203.5	L_2S liquid	L_2S calib: mean = 1203.2	7	
7-127	3.30	13196	1198.1	L_2S solid	i.e. +4.7±0.3 °C		
7-128	4.30	11344	1062.5	Au liquid			
7-129	4.30	11284	1058.1	Au liquid +7.9±1.3	1066.0±1.3 °C	(8)	Mo
7-130	4.30	11251	1055.6	Au solid +7.9±1.3	1063.5±1.3 °C	(8)	Mo
					Au calib: mean = 1056.9	8	
					i.e. +7.9±1.3°C		
7-133	6.15	12175	1123.9	+6.4±0.8	1130.3±0.8 °C	(7,8)	Mo
7-134	6.00	11869	1101.4	+6.9±1.0	1108.3±1.0 °C	(7,8)	Mo
7-135	6.15	14203	1270.5	+4.1±0.2	1274.6±0.2 °C	(7,6)	Mo

Run No.	Time Hrs.mins.	Recording T/C emf μv	Calculated temp. °C	Calibration value or calibrant	Corrected temp. °C	Calibration reference	Charge container
New platinum bucket.							
7-136+	2.00	13226	1200.3	L_2S liquid	mean = 1199.4 i.e. +8.5±0.0 °C	9	
7-137+	2.00	13214	1199.4	L_2S M.I.			
7-138+	3.00	13171	1196.3	L_2S solid			
7-141+	4.00	14600	1298.8	+8.5±0.0	1307.3±0.0 °C	(9)	Mo
7-142+	2.15	11228	1053.9	Au solid	mean = 1055.0 i.e. +9.4±1.1 °C	10	
7-143+	2.15	11259	1056.2	Au liquid			
7-146+	1.45	13103	1191.4	L_2S solid	mean = 1193.5 i.e. +14.4±2.1 °C	11	
7-147+	2.00	13191	1197.8	L_2S liquid			
7-148+	1.45	13161	1195.6	L_2S liquid			
New probe; new weld on T/C							
7-150+	1.35	13230	1200.6	L_2S M.I.	mean = 1200.6 i.e. +7.3±0.0 °C	12	
7-151+	2.00	13210	1199.1	L_2S solid			
7-152+	2.15	13174	1196.5	L_2S solid			
7-153+	2.00	11244	1055.1	Au solid	mean = 1057.9 i.e. +6.5±1.5 °C	13	
7-154+	1.30	11262	1056.4	Au solid			
7-155+	2.15	11302	1059.4	Au liquid			
7-156+	5.00	12720	1163.7	+7.1±0.4	1170.8±0.4 °C	(12,13)	Mo
7-157+	6.00	12667	1159.9	+7.1±0.4	1167.0±0.4 °C	(12,13)	Mo
7-161	6.00	12981	1182.6	+7.2±0.2	1189.8±0.2 °C	(12,13)	Mo
7-163+	2.00	13183	1197.2	L_2S solid	confirms calib. no 12		

Run No.	Time Hrs.mins.	Recording T/C emf μv	Calculated temp. ^{o}C	Calibration value or calibrant	Corrected temp. ^{o}C	Calibration reference	Charge container
7-170	5.45	12335	1135.6	+6.9±0.7	1142.5±0.7 ^{o}C	(12,13)	Mo
7-171	4.00	13215	1199.5	L_2S solid	mean = 1200.7	14	
7-172	4.00	13249	1201.9	L_2S liquid	i.e. +7.2±1.2 ^{o}C		
7-173	3.45	13143	1194.3	L_2S solid			
7-174	4.00	13198	1198.3	L_2S solid +7.2±1.2	1205.5±1.2 ^{o}C	(14)	Mo
7-175	8.00	13531	1222.2	+7.2±1.2	1229.4±1.2 ^{o}C	(14)	Mo
7-177	4.15	11294	1058.8	Au liquid +6.2±0.7	1065.0±0.7 ^{o}C	(15)	Mo
7-178	3.30	11277	1057.5	Au solid	Au calib: mean = 1058.2 i.e. +6.2±0.7 ^{o}C	15	
7-180	7.15	12040	1114.0	+6.6±0.9	1120.6±0.9 ^{o}C	(14,15)	Mo
7-181	7.15	12528	1149.7	+6.8±1.0	1156.5±1.0 ^{o}C	(14,15)	Mo
7-182	3.00	15923	1391.9	Di liquid	mean = 1391.8	16	
7-183	3.15	15922	1391.8	Di M.I.	i.e. +3.5±0.0 ^{o}C		
7-184	7.00	14022	1257.5	+6.1±0.8	1263.6±0.8 ^{o}C	(14,16)	Mo
7-185	6.00	13829	1243.7	+6.4±0.9	1250.1±0.9 ^{o}C	(14,16)	Mo
7-186	6.45	14388	1283.7	+5.6±0.7	1289.2±0.7 ^{o}C	(14,16)	Mo
7-187	7.00	13572	1225.2	+6.7±1.0	1231.9±1.0 ^{o}C	(14,16)	Mo
7-188	5.45	12818	1170.8	+7.0±1.1	1177.8±1.1 ^{o}C	(14,15)	Mo
7-189	7.00	12611	1155.8	+6.9±1.0	1162.7±1.0 ^{o}C	(14,15)	Mo
7-191	5.30	12061	1115.5	+6.6±0.9	1122.1±0.9 ^{o}C	(14,15)	Mo

Run No.	Time Hrs.mins.	Recording T/C emf μv	Calculated temp. °C	Calibration value or calibrant	Corrected temp. °C	Calibration reference	Charge container
7-192	3.00	11295	1058.9	Au liquid			
7-193	7.00	11265	1056.6	Au liquid	mean = 1056.1	17	
7-194	3.30	11251	1055.6	Au solid	i.e. +8.3±0.5 °C		
7-195	3.45	15896	1390.0	Di M.I.	mean = 1390.0	18	
7-196	2.15	15916	1391.4	Di liquid	i.e. +5.3±0.0 °C		
7-197	3.30	13225	1200.2	L_2S liquid			
7-198	4.00	13221	1199.9	L_2S liquid +9.0±1.1	1208.9±1.1 °C	(19)	Mo
7-199	4.15	13191	1197.8	L_2S solid +9.0±1.1	1206.8±1.1 °C	(19)	Mo
					L_2S calib: mean = 1198.9	19	
					i.e. +9.0±1.1 °C		
7-200	7.00	13189	1197.6	+9.0±1.1	1206.6±1.1 °C	(19)	Mo
7-201	6.15	14167	1267.9	+7.7±0.7	1275.6±0.7 °C	(18,19)	Mo
7-202	7.00	13798	1241.4	+8.2±0.9	1249.6±0.9 °C	(18,19)	Mo
7-203	6.30	13831	1243.8	+8.1±0.9	1251.9±0.9 °C	(18,19)	Mo
7-204	6.15	13652	1230.9	+8.4±0.9	1239.3±0.9 °C	(18,19)	Mo
7-205	6.30	13432	1215.1	+8.7±1.0	1223.8±1.0 °C	(18,19)	Mo
7-206	6.30	13394	1212.4	+8.7±1.0	1221.1±1.0 °C	(18,19)	Mo

Run No.	Time Hrs.mins.	Recording T/C emf μv	Calculated temp. °C	Calibration value or calibrant	Corrected temp. °C	Calibration reference	Charge container
7-207	3.15	15876	1388.6	Di solid			
7-208	3.15	15904	1390.6	Di solid	mean = 1391.7	20	
7-209	3.30	15912	1391.1	Di liquid	i.e. +3.6±0.6 °C		
7-210	3.30	15928	1392.2	Di solid			
7-211	3.15	13217	1199.6	L_2S solid	mean = 1200.6	21	
7-212	2.30	13243	1201.5	L_2S liquid	i.e. +7.3±1.0 °C		
7-213	5.30	14002	1256.0	+6.2±0.9	1262.2±0.9°C	(20,21)	Mo
7-216+	5.00	14166	1267.8	+6.0±0.9	1273.8±0.9 °C	(20,21)	Mo
7-217+	5.00	13794	1241.2	+6.5±0.9	1247.7±0.9 °C	(20,21)	Mo
New probe.							
7-218+	3.00	13191	1197.8	L_2S M.I.	mean = 1197.8	22	
7-219+	3.00	13139	1194.0	L_2S solid	i.e. +10.1±0.0 °C		
7-220+	3.00	15921	1391.7	Di liquid			
7-221+	2.30	15863	1387.7	Di liquid +8.8±1.2	1396.5±1.2 °C	(23)	Mo
7-222+	2.30	15829	1385.3	Di solid	Di calib: mean = 1386.5 i.e. +8.8±1.2 °C	23	
7-223+	5.00	13240	1201.3	+10.1±0.0	1211.4±0.0 °C	(22,23)	Mo
7-224	5.15	13657	1231.3	+9.9±0.2	1241.2±0.2 °C	(22,23)	Mo
7-225+	2.00	15829	1385.3	Di solid	confirms calib. no 23		
7-226+	5.00	13606	1227.6	+9.9±0.2	1237.5±0.2°C	(22,23)	Mo

Run No.	Time Hrs.mins.	Recording T/C emf μv	Calculated temp. °C	Calibration value or calibrant	Corrected temp. °C	Calibration reference	Charge container
7-229+	5.00	14145	1266.3	+9.6±0.4	1275.9±0.4°C	(22,23)	Mo
7-230+	5.00	14420	1286.0	+9.5±0.6	1295.5±0.6 °C	(22,23)	Mo
7-231+	3.00	15818	1384.5	Di solid	confirms calib. no 23		
7-232+	72.00	13510	1220.7	+9.9±0.1	1230.6±0.1 °C	(22,23)	Mo
7-233+	5.00	14626	1300.6	+9.4±0.7	1310.0±0.7 °C	(22,23)	Mo
7-234	5.00	13205	1198.8	L_2S solid			
7-235	5.00	13186	1197.4	L_2S solid +7.9±1.2	1205.3±1.2 °C	(24)	Mo
7-236	4.00	13238	1201.2	L_2S liquid	L_2S calib: mean = 1200.0 i.e. +7.9±1.2 °C	24	
New probe.							
7-237	3.30	15909	1390.9	Di liquid	mean = 1388.7 i.e. +6.6±1.2 °C	25	
7-238	3.30	15860	1387.5	Di solid			
7-239	3.45	15893	1389.8	Di liquid			
7-240	3.45	13238	1201.2	L_2S liquid	mean = 1200.4 i.e. +7.5±0.8 °C	26	
7-241	3.45	13216	1199.6	L_2S solid			
7-242	5.00	13209	1199.1	L_2S solid			

Run No.	Time Hrs.mins.	Recording T/C emf μv	Calculated temp. °C	Calibration value or calibrant	Corrected temp. °C	Calibration reference	Charge container
7-247+	3.00	13215	1199.5	L_2S liquid			
7-248+	3.00	13163	1195.7	L_2S solid	mean = 1197.9	27	
7-253+	3.00	13112	1192.0	L_2S solid	i.e. +10.0±1.6 °C		
7-254+	3.00	13171	1196.3	L_2S solid			
7-256+	18.00	13225	1200.2	+10.0±1.6	1210.2±1.6 °C	(27)	Mo
7-257	17.05	13441	1215.8	+9.7±1.6	1225.5±1.6 °C	(25,27)	Mo
7-258	17.05	14098	1262.9	AWG solid +4.7±1.2	1267.6±1.2 °C	(27,28)	Mo
7-259	17.05	14120	1264.5	AWG solid +4.6±1.2	1269.1±1.2 °C	(27,28)	Mo
7-260	17.20	14206	1270.7	AWG solid +4.0±1.1	1274.7±1.1 °C	(28)	Mo
7-261	17.15	14284	1276.3	AWG liquid +4.0±1.1	1280.3±1.1 °C	(28)	Mo
7-262	17.25	14237	1272.9	AWG liquid +4.0±1.1	1276.9±1.1 °C	(28)	Mo
					AWG calib: mean = 1271.8 i.e. +4.0±1.1 °C	28	
New platinum bucket.							
7-264	17.10	14229	1272.4	AWG liquid +5.9±1.2	1278.3±1.2 °C	(29)	Mo

Run No.	Time Hrs.mins.	Recording T/C emf μv	Calculated temp. °C	Calibration value or calibrant	Corrected temp. °C	Calibration reference	Charge container
7-265	17.40	14212	1271.1	AWG liquid +5.9±1.2	1277.0±1.2°C	(29)	Mo
7-266	17.30	14178	1268.7	AWG solid	AWG calib: mean = 1269.9 i.e. +5.9±1.2 °C	29	
7-267	17.40	14579	1297.3	+5.9±1.2	1303.2±1.2 °C	(29)	Mo
7-268	17.20	14547	1295.0	+5.9±1.2	1300.9±1.2 °C	(29)	Mo
7-269	18.55	14576	1297.1	+5.9±1.2	1303.0±1.2 °C	(29)	Mo
New furnace tube; new platinum bucket.							
7-270	4.00	13968	1253.6	AWG solid			
7-271	4.00	14221	1271.8	AWG liquid	mean = 1266.2	30	
7-272	4.45	14191	1269.6	AWG liquid	i.e. +9.6±1.1 °C		
7-273	3.00	14159	1267.3	AWG liquid			
7-274	3.00	14128	1265.1	AWG solid			
7-275	17.35	13774	1239.7	+9.6±1.1	1249.3±1.1 °C	(30)	Mo
7-276	17.40	13756	1238.4	+9.6±1.1	1248.0±1.1 °C	(30)	Mo
7-277	17.50	13757	1238.5	+9.6±1.1	1248.1±1.1 °C	(30)	Mo
7-278	17.50	13798	1241.4	+9.6±1.1	1251.0±1.1 °C	(30)	Mo
7-279	20.00	13800	1241.6	+9.6±1.1	1251.2±1.1 °C	(30)	Mo
New platinum bucket.							
7-280	2.30	13180	1197.0	L_2S liquid			
7-281	3.05	13129	1193.3	L_2S solid	mean = 1195.2	31	
7-282	3.00	13122	1192.8	L_2S solid	i.e. +12.7±1.9 °C		

Run No.	Time Hrs.mins.	Recording T/C emf μv	Calculated temp. °C	Calibration value or calibrant	Corrected temp. °C	Calibration reference	Charge container
7-286	18.00	13503	1220.2	+12.7±1.9	1232.9±1.9 °C	(31)	Mo
7-288	3.20	13200	1198.4	L_2S liquid			
7-289	3.00	13094	1190.7	L_2S solid	mean = 1191.7	32	
7-290	3.15	13171	1196.3	L_2S liquid	i.e. +16.2±1.0 °C		
7-291	3.00	13120	1192.6	L_2S liquid			
7-292	21.25	13286	1204.6	+16.2±1.0	1220.8±1.0 °C	(32)	Mo
7-293	23.15	12829	1171.6	+16.2±1.0	1187.8±1.0 °C	(32)	Mo
7-294	21.50	13568	1224.9	+16.2±1.0	1241.1±1.0 °C	(32)	Mo
New furnace tube.							
7-296+	3.00	13085	1190.1	L_2S solid			
7-299	3.30	13057	1188.1	L_2S solid			
7-300	3.15	13254	1202.3	L_2S liquid			
7-301	17.30	13202	1198.6	L_2S liquid +16.5±1.3	1215.1±1.3 °C	(33)	Mo
7-302	17.30	13122	1192.8	L_2S liquid +16.5±1.3	1209.3±1.3 °C	(33)	Mo
7-303	17.00	13127	1193.1	L_2S liquid +16.5±1.3	1209.6±1.3 °C	(33)	Mo
					L_2S calib: mean = 1191.4 i.e. +16.5±1.3 °C	33	
7-304	17.00	13358	1209.8	+16.5±1.3	1226.3±1.3 °C	(33)	Mo
7-305	18.55	14129	1265.2	AWG liquid +14.4±3.1	1279.6±3.1 °C	(34)	Mo

Run No.	Time Hrs.mins.	Recording T/C emf μv	Calculated temp. °C	Calibration value or calibrant	Corrected temp. °C	Calibration reference	Charge container
7-306	24.00	14515	1292.8	+14.4±3.1	1307.2±3.1 °C	(34)	Mo
7-307	17.00	14870	1317.9	+14.4±3.1	1332.3±3.1 °C	(34)	Mo
7-308	17.15	14033	1258.3	AWG solid +14.4±3.1	1272.7±3.1 °C	(34)	Mo
7-310	2.00	14120	1264.5	AWG liquid	AWG calib: mean = 1261.4	34	
7-311	2.30	13990	1255.2	AWG liquid?	i.e. +14.4±3.1 °C		
7-312	18.15	13710	1235.1	+15.2±2.4	1250.3±2.4	(33,34)	Mo
7-318+	5.00	14093	1262.6	AWG liquid			
7-319+	4.00	14049	1259.4	AWG solid +14.8±1.6	1274.2±1.6 °C	(35)	Mo
					AWG calib: mean = 1261.0	35	
					i.e. +14.8±1.6 °C		
7-320+	3.00	14752	1309.6	+14.8±1.6	1324.4±1.6 °C	(35)	Mo
b) Furnace 6							
Used over a wide temperature range for long periods.							
6-44+	5.30	13324	1207.3	-0.9±1.3	1206.4±1.3 °C	(36)	Ag40
6-45+	18.00	15370	1353.1	-0.9±1.3	1352.2±1.3 °C	(36)	Pt
6-46	2.00	13362	1210.1	L_2S liquid	mean = 1208.8	36	
6-47	3.30	13281	1204.2	L_2S solid	i.e. -0.9±1.3 °C		
6-48	3.30	13326	1207.5	L_2S solid			

Run No.	Time Hrs. mins.	Recording T/C emf μv	Calculated temp. °C	Calibration value or calibrant	Corrected temp. °C	Calibration reference	Charge container
c) Furnace 5							
5-52+	2.00	13260	1202.7	L_2S liquid	mean = 1200.5 i.e. +7.4±2.1 °C	37	
5-53+	2.00	13192	1197.8	L_2S solid			
5-56+	2.00	13200	1198.4	L_2S solid			
5-60+	1.45	13170	1196.2	L_2S solid			
5-63+	24.00	13836	1244.2	+7.4±2.1	1251.6±2.1 °C	(37)	Ag40
5-72+	2.30	13160	1195.5	L_2S solid	confirms calib. no 37		
5-73+	2.00	13205	1198.8	L_2S solid			
5-77+	25.00	13858	1245.8	+7.4±2.1	1253.2±2.1 °C	(37)	Ag40
T/C rewelded.							
5-86+	2.00	13167	1196.0	L_2S solid			
5-108+	6.00	13866	1246.4	? +7.4±2.1	c. 1254 °C		
T/C rewelded.							
5-125+	2.00	11243	1055.0	Au solid	mean = 1057.0 i.e. +7.4±2.0 °C	38	
5-126+	2.00	11297	1059.0	Au liquid			
5-127+	2.00	13149	1194.7	L_2S solid	mean = 1200.4 i.e. +7.5±2.0 °C	39	
5-128+	2.00	13200	1198.4	L_2S solid			
5-129+	2.00	13256	1202.4	L_2S liquid			
5-132+	18.00	12364	1137.7	+7.5±2.0	1145.2±2.0 °C	(38,39)	Ag70
5-133+	18.00	12630	1157.2	+7.5±2.0	1164.7±2.0 °C	(38,39)	Ag70
5-134+	18.00	12760	1166.6	+7.5±2.0	1174.1±2.0 °C	(38,39)	Ag70
5-135+	3.00	12788	1168.6	+7.5±2.0	1176.1±2.0 °C	(38,39)	Ag70

Run No.	Time Hrs.mins.	Recording T/C emf μv	Calculated temp. °C	Calibration value or calibrant	Corrected temp. °C	Calibration reference	Charge container
5-140+	2.00	13219	1199.8	L_2S liquid			
5-141+	2.30	13165	1195.9	L_2S liquid	mean = 1193.7	40	
5-142+	1.45	13108	1191.7	L_2S solid	i.e. +14.2±2.0 °C		
5-143+	2.15	13161	1195.6	L_2S liquid			
5-146+	7.00	13852	1245.3	+14.2±2.0	1259.5±2.0 °C	(40)	Mo
5-147+	1.30	11149	1048.0	Au solid			
5-148+	2.00	11212	1052.7	Au solid	mean = 1054.7	41	
5-149+	2.00	11266	1056.7	Au liquid	i.e. +9.7±2.0 °C		
5-151+	6.00	15238	1343.9	+14.6±3.2	1358.5±3.2 °C	(42)	Mo
5-152+	5.30	12937	1179.4	+14.1±3.1	1193.5±3.1 °C	(41,42)	Mo
5-153+	6.00	14547	1295.0	+14.6±3.2	1309.6±3.2 °C	(42)	Mo
5-154+	1.45	12995	1183.6	L_2S solid	mean = 1193.3	42	
5-155+	2.30	13085	1190.1	L_2S liquid	i.e. +14.6±3.2 °C		
5-157+	6.30	13765	1239.1	+14.6±3.2	1253.7±3.2 °C	(42)	Mo
5-159+	5.30	13030	1186.1	+14.3±3.1	1200.4±3.1 °C	(41,42)	Mo
5-160+	7.00	11623	1083.2	+10.7±2.2	1093.9±2.2 °C	(41,42)	Mo
5-161+	6.00	12328	1135.1	+12.5±2.7	1147.6±2.7 °C	(41,42)	Mo
5-162+	6.00	13794	1241.2	+14.6±3.2	1255.8±3.2 °C	(42)	Ag40
5-163+	5.30	13005	1184.3	+14.3±3.1	1198.6±3.1 °C	(41,42)	Ag40
5-164+	4.30	14283	1276.2	+14.6±3.2	1290.8±3.2 °C	(42)	Pt
5-165+	5.30	12471	1145.5	+12.9±2.8	1158.4±2.8 °C	(41,42)	Ag70
5-166+	2.00	12900	1176.7	L_2S solid	confirms calib. no 42		

Run No.	Time Hrs.mins.	Recording T/C emf μv	Calculated temp. °C	Calibration value or calibrant	Corrected temp. °C	Calibration reference	Charge container
New probe; T/C rewelded.							
5-168+	4.00	11244	1055.1	Au solid	mean = 1057.5 i.e. +6.9±1.7 °C	43	
5-169+	2.30	11254	1055.8	Au solid			
5-170+	2.30	11301	1059.3	Au liquid			
5-171+	4.30	13060	1188.3	L_2S solid	mean = 1194.5 i.e. +13.4±0.7°C	44	
5-172+	2.45	13137	1193.8	L_2S solid			
5-173+	3.00	13156	1195.2	L_2S liquid			
5-177+	5.30	13477	1218.3	+13.4±0.7	1231.7±0.7 °C	(44)	Mo
5-178+	5.30	12050	1114.7	+9.6±1.3	1124.3±1.3 °C	(43,44)	Mo
5-179+	4.00	15799	1383.2	+13.4±0.7	1396.6±0.7 °C	(44)	Mo
5-180+	2.00	13132	1193.5	L_2S solid	mean = 1202.9 i.e. +5.0±2.1 °C	45	
5-181+	3.30	13156	1195.2	L_2S solid			
5-182+	2.00	13233	1200.8	L_2S solid			
5-183+	2.00	13291	1205.0	L_2S liquid			
5-184+	3.30	11314	1060.3	Au solid			
5-185+	5.30	14641	1301.7	+5.0±2.1	1306.7±2.1 °C	(45)	Mo
5-186+	3.00	11368	1064.3	Au liquid	Au calib: mean = 1062.3 i.e. +2.1±2.0 °C	46	
5-187+	3.00	13255	1202.4	L_2S liquid	mean = 1200.7 i.e. +7.2±1.6 °C	47	
5-188+	3.30	13209	1199.1	L_2S solid			
5-189+	5.00	13926	1250.6	+7.2±1.6	1257.8±1.6 °C	(47)	Mo
5-190+	4.30	13183	1197.2	+7.1±1.6	1204.3±1.6 °C	(46,47)	Mo

Run No.	Time Hrs.mins.	Recording T/C emf μv	Calculated temp. °C	Calibration value or calibrant	Corrected temp. °C	Calibration reference	Charge container
New furnace tube.							
5-194+	2.30	13247	1201.8	L_2S liquid	mean = 1200.5 i.e. +7.4±1.2 °C	48	
5-195+	2.30	13212	1199.3	L_2S solid			
5-202+	3.00	13211	1199.2	L_2S solid			
5-203+	5.00	13481	1218.6	+7.4±1.2	1226.0±1.2 °C	(48)	Mo
5-205+	9.30	12745	1165.5	+6.8±1.2	1172.3±1.2 °C	(48,49)	Mo
5-206+	5.00	11320	1060.7	Au solid	mean = 1061.0 i.e. +3.4±1.3 °C	49	
5-207+	5.00	11396	1066.4	Au liquid			
5-208+	4.00	11341	1062.3	Au liquid			
5-209+	4.00	13188	1197.5	L_2S solid	mean = 1198.5 i.e. +9.4±1.0 °C	50	
5-210+	4.00	13214	1199.4	L_2S liquid			
5-212+	5.00	12935	1179.3	+8.6±1.0	1187.9±1.0 °C	(49,50)	Mo
5-216+	3.00	11292	1058.7	Au solid	confirms calib. no 49		
5-217+	4.00	13161	1195.6	L_2S solid	confirms calib. no 50		
5-222	5.00	11947	1107.1	+5.4±1.2	1112.5±1.2 °C	(49,50)	Mo
5-227	3.30	13266	1203.2	L_2S liquid	mean = 1198.4 i.e. +9.5±0.0 °C	51	
5-228	3.45	13201	1198.5	L_2S solid			
5-229	5.00	13199	1198.3	L_2S liquid			
5-230	4.00	11338	1062.1	Au liquid	mean = 1060.4 i.e. +4.0±1.6 °C	52	
5-231	4.00	11294	1058.8	Au solid			

Run No.	Time Hrs.mins.	Recording T/C emf μv	Calculated temp. °C	Calibration value or calibrant	Corrected temp. °C	Calibration reference	Charge container
5-243+	3.00	13179	1196.9	L_2S solid	mean = 1202.0 i.e. +5.9±0.9 °C	53	
5-244+	3.00	13237	1201.1	L_2S solid			
5-245+	4.30	13262	1202.9	L_2S liquid			
5-246+	2.45	11273	1057.2	Au solid	mean = 1061.1 i.e. +3.3±0.0 °C	54	
5-247+	3.00	11325	1061.1	Au M.I.			
5-251+	3.00	11291	1058.6	Au solid	confirms calib. no 54		
5-252+	3.00	13214	1199.4	L_2S solid	confirms calib. no 53		
5-260	17.20	12468	1145.3	+4.9±0.5	1150.2±0.5 °C	(53,54)	Mo
New probe; new platinum bucket.							
5-264	17.40	13233	1200.8	+9.0±1.9	1209.8±1.9 °C	(55)	Mo
5-265	17.20	13233	1200.8	L_2S liquid +9.0±1.9	1209.8±1.9 °C	(55)	Mo
5-266	3.30	13155	1195.1	L_2S solid	mean = 1198.9 i.e. +9.0±1.9°C	55	
5-267+	5.45	13180	1197.0	L_2S solid			
5-268	4.00	11338	1062.1	Au liquid	mean = 1061.6 i.e. +2.8±0.5 °C	56	
5-269	3.00	11283	1058.0	Au solid			
5-270	4.00	11323	1061.0	Au solid			
5-271	18.20	12757	1166.4	+7.5±1.6	1173.9±1.6 °C	(55,56)	Mo
5-272	18.35	12735	1164.8	+7.5±1.6	1172.3±1.6 °C	(55,56)	Mo
5-273	18.00	12750	1165.9	+7.5±1.6	1173.4±1.6 °C	(55,56)	Mo
5-274	17.35	12753	1166.1	+7.5±1.6	1173.6±1.6 °C	(55,56)	Mo
5-275	17.50	12423	1142.0	+6.4±1.3	1148.4±1.3 °C	(55,56)	Mo

Run No.	Time Hrs.mins.	Recording T/C emf μv	Calculated temp. °C	Calibration value or calibrant	Corrected temp. °C	Calibration reference	Charge container
New platinum bucket; new running depth.							
5-277+	3.30	11308	1059.9	+5.3±1.0	1065.2±1.0 °C	(58)	Mo
5-278+	4.00	13195	1198.0	L_2S solid	mean = 1200.3	57	
5-279+	3.30	13257	1202.5	L_2S liquid	i.e. +7.6±2.3 °C		
5-280+	2.30	11285	1058.1	Au solid	mean = 1059.1	58	
5-281+	4.00	11312	1060.1	Au liquid	i.e. +5.3±1.0 °C		
5-282+	17.00	12333	1135.5	+6.5±1.7	1142.0±1.7 °C	(57,58)	Mo
5-283+	18.00	12227	1127.7	+6.4±1.6	1134.1±1.6 °C	(57,58)	Mo
5-284+	4.00	11324	1061.0	Au M.I.	mean = 1061.0	59	
					i.e. +3.4±0.0 °C		
5-286	23.00	12989	1183.2	+7.1±2.0	1190.3±2.0 °C	(57,59)	Mo
5-287	3.00	11312	1060.1	Au M.I.	mean = 1060.1	60	
					i.e. +4.3±0.0 °C		
5-288	21.25	11647	1085.0	+4.9±0.4	1089.9±0.4 °C	(57,60)	Mo
5-289	23.25	11848	1099.9	+5.2±0.7	1105.1±0.7 °C	(57,60)	Mo
New furnace tube.							
5-291+	16.00	11222	1053.4	Au solid	c. 1053 °C		
5-292+	16.00	11321	1060.8	Au solid	c. 1061 °C		
5-293+	12.00	13200	1198.4	L_2S solid	c. 1198 °C		
5-294+	18.00	11361	1063.8	Au solid	c. 1064 °C		
New furnace tube; new probe; new platinum bucket.							
5-297+	3.00	11415	1067.8	Au liquid			

Run No.	Time Hrs.mins.	Recording T/C emf μv	Calculated temp. °C	Calibration value or calibrant	Corrected temp. °C	Calibration reference	Charge container
5-298+	3.00	13236	1201.0	L_2S solid	mean = 1202.1	61	
5-299+	3.00	13267	1203.2	L_2S liquid	i.e. +5.8±1.1 °C		
5-300+	2.00	11363	1063.9	Au liquid	mean = 1062.6	62	
5-302+	2.00	11329	1061.4	Au solid	i.e. +1.8±1.2 °C		
5-305+	3.00	13248	1201.9	L_2S solid	confirms calib. no 61		
5-309+	2.30	13199	1198.3	L_2S solid	confirms calib. no 61		
5-311+	2.15	11319	1060.7	Au solid	confirms calib. no 62		
5-315+	3.00	13212	1199.3	L_2S solid	confirms calib. no 61		
5-317+	17.00	12607	1155.5	+4.5±1.1	1160.0±1.1 °C	(61,62)	Mo
5-322+	19.00	13235	1200.9	L_2S solid	confirms calib. no 61		
5-325	18.40	11322	1060.9	Au solid	confirms calib. no 62		
				+1.8±1.2	1062.7±1.2 °C	(62)	Mo
5-326	17.20	11800	1096.3	+2.8±1.2	1099.1±1.2 °C	(61,62)	Mo
T/C rewelded.							
5-327	18.20	12200	1125.7	+3.5±1.5	1129.2±1.5 °C	(63)	Mo
New platinum bucket.							
5-328	2.30	11302	1059.4	Au solid	mean = 1060.9	63	
5-329	2.00	11343	1062.4	Au liquid	i.e. +3.5±1.5 °C		
5-330	18.00	10978	1035.2	+3.5±1.5	1038.7±1.5 °C	(63)	Mo

Run No.	Time Hrs.mins.	Recording T/C emf μv	Calculated temp. °C	Calibration value or calibrant	Corrected temp. °C	Calibration reference	Charge container
d) Furnace 3							
3-62+	3.00	13201	1198.5	L_2S liquid	mean = 1191.8 i.e. +16.9±3.0 °C	64	
3-63+	3.00	13151	1194.9	L_2S liquid			
3-64+	2.30	13067	1188.8	L_2S solid			
3-65+	6.30	14470	1289.6	+16.9±3.0	1306.5±3.0 °C	(64)	Pt
3-66	5.00	12532	1150.0	+16.9±3.0	1166.9±3.0 °C	(64)	Ag70
3-67	5.30	11818	1097.6	+16.9±3.0	1114.5±3.0 °C	(64)	Ag70
3-68	2.00	13032	1186.3	L_2S solid	taken with 3-63 mean = 1194.5 i.e. +13.4±0.4 °C	65	
3-69	2.00	13068	1188.8	L_2S solid			
3-70	2.00	13082	1189.9	L_2S solid			
3-71	2.00	13097	1190.9	L_2S solid			
3-72	3.00	13104	1191.4	L_2S solid			
3-73	2.00	13141	1194.1	L_2S solid			
3-74	5.45	12161	1122.9	+12.0±0.8	1134.9±0.8 °C	(65,67)	Ag70
3-75	5.45	11680	1087.4	+11.3±0.9	1098.7±0.9 °C	(65,67)	Ag70
3-76	6.00	12342	1136.1	+12.3±0.7	1148.4±0.7 °C	(65,67)	Ag70
3-79	5.45	12846	1172.8	+10.6±0.6	1183.4±0.6 °C	(66,67)	Ag40
3-80	5.30	12842	1172.5	+10.6±0.6	1183.1±0.6 °C	(66,67)	Ag40

Run No.	Time Hrs.mins.	Recording T/C emf μv	Calculated temp. °C	Calibration value or calibrant	Corrected temp. °C	Calibration reference	Charge container
3-81	3.30	13180	1197.0	L_2S solid			
3-82	3.30	13229	1200.5	L_2S liquid	mean = 1197.5	66	
3-83	3.30	13208	1199.0	L_2S liquid	i.e. +10.4±0.5 °C		
3-84	3.30	13170	1196.2	L_2S solid			
3-85	3.15	13194	1198.0	L_2S liquid			
3-86	2.15	11351	1063.0	Au liquid			
3-87	3.00	11242	1054.9	Au liquid			
3-88	3.00	11248	1055.4	Au liquid			
3-89	2.15	11015	1038.0	Au solid	mean = 1053.7	67	
3-90	2.15	11139	1047.2	Au solid	i.e. +10.7±1.1 °C		
3-91	2.15	11186	1050.7	Au solid			
3-92	2.15	11211	1052.6	Au solid			
New furnace tube; new probe; new platinum bucket.							
3-118+	2.00	13214	1199.4	L_2S liquid			
3-119+	3.00	13089	1190.4	L_2S solid	mean = 1191.6	68	
3-123+	3.00	13122	1192.8	L_2S liquid	i.e. +16.3±1.2 °C		
3-124+	3.00	13088	1190.3	L_2S solid			
3-126+	3.00	11209	1052.5	Au liquid			
3-127+	3.00	11198	1051.6	Au liquid	mean = 1049.5	69	
3-128+	4.00	11143	1047.5	Au solid	i.e. +14.9±2.0 °C		
3-137+	2.00	11152	1048.2	Au solid	confirms calib. no 69		
3-138+	4.30	13096	1190.9	L_2S solid	confirms calib. no 68		
3-140+	5.00	12294	1132.6	+15.7±1.5	1148.3±1.5 °C	(68,69)	Ag70

Run No.	Time Hrs.mins.	Recording T/C emf μv	Calculated temp. °C	Calibration value or calibrant	Corrected temp. °C	Calibration reference	Charge container
New furnace element; new platinum bucket.							
3-176+	2.15	13079	1189.6	L_2S solid	mean = 1194.1 i.e. +13.8±1.8 °C	70	
3-177+	2.20	13116	1192.3	L_2S solid			
3-178+	2.45	13166	1195.9	L_2S liquid			
3-179+	19.00	12950	1180.4	+13.6±1.7	1194.0±1.7 °C	(70,71)	Ag40
3-182+	4.20	11111	1045.1	Au solid	mean = 1053.1 i.e. +11.3±1.1 °C	71	
3-183+	3.30	11203	1052.0	Au solid			
3-184+	3.00	11234	1054.3	Au liquid			
New probe.							
3-188+	3.20	11201	1051.9	Au solid	mean = 1053.3 i.e. +11.1±1.4 °C	72	
3-189+	2.45	11240	1054.8	Au liquid			
3-191+	18.00	11511	1074.9	+11.8±1.5	1086.7±1.5 °C	(72,73)	Ag70
3-192+	3.00	12996	1183.7	L_2S solid	mean = 1192.1 i.e. +15.8±2.0 °C	73	
3-193+	3.10	13141	1194.1	L_2S liquid			
3-194+	2.00	13174	1196.5	L_2S liquid			
3-195+	2.15	13086	1190.1	L_2S solid			
New T/C.							
3-255+	18.00	13180	1197.0	L_2S solid +2.9±1.5	1199.9±1.5 °C	(75)	Ag40
3-256+	19.00	13250	1202.0	L_2S solid +2.9±1.5	1204.9±1.5 °C	(75)	Ag40
3-257+	24.00	11306	1059.7	Au solid			

Run No.	Time Hrs.mins.	Recording T/C emf μv	Calculated temp. °C	Calibration value or calibrant	Corrected temp. °C	Calibration reference	Charge container
3-258+	20.30	11340	1062.2	Au solid +0.6±1.6	1062.8±1.6 °C	(74)	Ag70
3-259+	17.00	11384	1065.5	Au liquid	Au calib: mean = 1063.8 i.e. +0.6±1.6 °C	74	
3-263	20.15	11838	1099.1	+1.2±1.6	1100.3±1.6 °C	(74,75)	Ag70
3-264	24.00	13267	1203.2	+2.9±1.5	1206.1±1.5 °C	(75)	Ag40
3-265	17.00	13270	1203.5	L_2S solid	mean = 1205.0 i.e. +2.9±1.5 °C	75	
3-266	17.15	13314	1206.6	L_2S liquid			
3-267	23.00	14334	1279.9	AWG liquid -2.6±1.5	1277.3±1.5 °C	(76)	Pt
3-268	17.15	14292	1276.9	AWG solid -2.6±1.5	1274.3±1.5 °C	(76)	Pt
					AWG calib: mean = 1278.4 i.e. -2.6±1.5 °C	76	
3-269	17.15	13626	1229.1	+0.9±1.5	1230.0±1.5 °C	(75.76)	Pt
3-270	18.15	13852	1245.3	-0.1±1.5	1245.2±1.5 °C	(75,76)	Pt
3-271	18.00	13856	1245.6	-0.2±1.5	1245.4±1.5 °C	(75,76)	Pt
3-272	18.00	14055	1259.9	-1.2±1.5	1258.7±1.5 °C	(75,76)	Pt
3-273	18.00	14301	1277.5	AWG solid -2.6±1.5	1274.9±1.5 °C confirms calib. no 76	(76)	Pt
3-274	19.00	14512	1292.6	-2.6±1.5	1290.0±1.5 °C	(76)	Pt
3-275	21.00	14514	1292.7	-2.6±1.5	1290.1±1.5 °C	(76)	Pt

Run No.	Time Hrs.mins.	Recording T/C emf μv	Calculated temp. °C	Calibration value or calibrant	Corrected temp. °C	Calibration reference	Charge container
3-276	17.00	13298	1205.5	L_2S solid	taken with 3-266		
					mean = 1206.0	77	
					i.e. +1.9±0.5 °C		
3-277+	16.00	13400	1212.8	+1.5±0.6	1214.3±0.6 °C	(76,77)	Ag40
3-279+	17.00	12870	1174.6	+1.9±0.5	1176.5±0.5 °C	(77)	Ag40
3-280+	19.00	12992	1183.4	+1.9±0.5	1185.3±0.5 °C	(77)	Ag40
3-282	17.00	12682	1160.9	+1.9±0.5	1162.8±0.5 °C	(77)	Ag40
3-284	18.00	13279	1204.1	L_2S solid	confirms calib. no 77		
3-289	23.45	14343	1280.5	AWG liquid	1277.9±1.5 °C	(76)	Pt
				-2.6±1.5			
3-290	17.00	14878	1318.5	-2.6±1.5	1315.9±1.5 °C	(76)	Pt
3-291	17.00	13576	1225.5	+0.7±0.8	1226.2±0.8 °C	(76,77)	Ag40
3-292	24.00	14309	1278.1	AWG solid	1275.5±1.5 °C	(76)	Pt
				-2.6±1.5	confirms AWG calib. no 76		
3-293	16.30	14511	1292.5	-2.6±1.5	1289.9±1.5 °C	(76)	Pt
3-294	17.30	13846	1244.9	-0.5±1.0	1244.4±1.0 °C	(76,77)	Pt
3-295	17.30	14723	1307.5	-2.6±1.5	1304.9±1.5 °C	(76)	Pt
3-296	20.15	14722	1307.4	-2.6±1.5	1304.8±1.5 °C	(76)	Pt
3-297	17.15	14085	1262.0	-1.6±1.3	1260.4±1.3 °C	(76,77)	Pt
3-298	18.00	14076	1261.4	-1.5±1.3	1259.9±1.3 °C	(76,77)	Pt

Run No.	Time Hrs.mins.	Recording T/C emf μv	Calculated temp. °C	Calibration value or calibrant	Corrected temp. °C	Calibration reference	Charge container
3-299	17.00	13311	1206.4	L_2S solid +1.4±0.1	1207.8±0.1 °C	(78)	Ag40
					L_2S calib: taken with 3-266		
					mean = 1206.5		
					i.e. +1.4±0.1 °C	78	
3-300	17.10	12989	1183.2	+0.9±0.1	1184.1±0.1 °C	(78,79)	Ag40
3-301	17.35	12644	1158.2	+0.3±0.1	1158.5±0.1 °C	(78,79)	Ag40
3-302	19.00	12325	1134.9	-0.2±0.0	1134.7±0.0 °C	(78,79)	Ag70
3-303	2.35	11345	1062.6	Au solid			
3-304	2.45	11360	1063.7	Au solid	mean = 1066.2	79	
3-305	2.15	11394	1066.2	Au M.I.	i.e. -1.8±0.0 °C		
3-306	2.15	11430	1068.9	Au liquid			
3-307	42.15	12146	1121.8	-0.5±0.0	1121.3±0.0 °C	(78,79)	Ag70
3-309	17.45	13325	1207.4	L_2S solid +0.0±0.5	1207.4±0.5 °C	(80)	Ag40
3-311	2.45	16062	1401.6	Di liquid +0.0±0.5	1401.6±0.5 °C	(80)	Pt
3-312	4.00	14340	1280.3	AWG liquid +0.0±0.5	1280.3±0.5 °C	(80)	Pt
3-313	3.00	13314	1206.6	+0.0±0.5	1206.6±0.5 °C	(80)	Pt
3-314	3.00	15237	1343.8	+0.0±0.5	1343.3±0.5 °C	(80)	Pt

Run No.	Time Hrs.mins.	Recording T/C emf μv	Calculated temp. °C	Calibration value or calibrant	Corrected temp. °C	Calibration reference	Charge container
3-319	3.45	13340	1208.5	L_2S liquid	taken with 3-309		
3-320	3.00	13373	1210.9	L_2S liquid	mean = 1207.9	80	
					i.e. +0.0±0.5 °C		
3-323	3.00	11478	1072.4	Au liquid			
3-324	3.00	11366	1064.1	Au liquid	mean = 1062.1	81	
3-325	3.15	11256	1056.0	Au solid	i.e. +2.3±1.9 °C		
3-326	3.15	11313	1060.2	Au solid			
3-327	3.00	13252	1202.2	L_2S liquid?			
3-328	3.00	13291	1205.0	L_2S solid +1.2±1.7	1206.2±1.7 °C	(82)	Ag40
3-329	3.00	13227	1200.4	L_2S solid	taken with 3-319		
					mean = 1206.7	82	
					i.e. +1.2±1.7 °C		
3-330	4.30	13236	1201.0	+1.2±1.7	1202.2±1.7 °C	(81,82)	Ag40
3-331	4.00	12785	1168.4	+1.5±1.8	1169.9±1.8 °C	(81,82)	Ag40
3-332	4.00	12130	1120.6	+1.9±1.8	1122.5±1.8 °C	(81,82)	Ag70
3-333	3.45	13077	1189.5	+1.2±1.7	1190.7±1.7 °C	(81,82)	Ag40
3-334	4.00	13079	1189.6	+1.2±1.7	1190.8±1.7 °C	(81,82)	Ag40
3-335	4.00	12641	1158.0	+1.5±1.8	1159.5±1.8 °C	(81,82)	Ag70
3-336	4.00	13569	1225.0	+2.7±1.8	1227.7±1.8 °C	(83)	Pt
3-337	3.45	13444	1216.0	+2.7±1.8	1218.7±1.8 °C	(83)	Ag40
3-338	21.30	13323	1207.3	+2.7±1.8	1210.0±1.8 °C	(83)	Ag40

Run No.	Time Hrs.mins.	Recording T/C emf μv	Calculated temp. °C	Calibration value or calibrant	Corrected temp. °C	Calibration reference	Charge container
3-339	3.30	13316	1206.8	L_2S liquid +2.7±1.8	1209.5±1.8 °C	(83)	Pt
3-340	3.20	13270	1203.5	+2.7±1.8	1206.2±1.8 °C	(83)	Pt
3-341	3.00	13266	1203.2	L_2S solid	L_2S calib: mean = 1205.0 i.e. +2.7±1.8 °C	83	
3-342	3.20	13078	1189.6	+2.7±1.8	1192.3±1.8 °C	(81,83)	Pt
3-343	4.15	13090	1190.4	+2.7±1.8	1193.1±1.8 °C	(81,83)	Pt
3-344	4.15	13097	1190.9	+2.7±1.8	1193.6±1.8 °C	(81,83)	Ag40
3-345	4.00	12467	1145.3	+2.5±1.8	1147.8±1.8 °C	(81,83)	Ag70
3-346	47.30	12308	1133.6	+2.5±1.8	1136.1±1.8 °C	(81,83)	Ag70
3-347	21.50	12468	1145.3	+2.5±1.8	1147.8±1.8 °C	(81,83)	Ag70
3-349	67.05	13682	1233.1	+2.7±1.8	1235.8±1.8 °C	(83)	Pt
3-350	17.00	13329	1207.7	+2.7±1.8	1210.4±1.8 °C	(83)	Pt
3-351	18.30	13290	1204.9	+2.7±1.8	1207.6±1.8 °C	(83)	Pt

APPENDIX D

DETAILS OF ATMOSPHERIC CONTROL

Run no.	Calculated $\%H_2$	Katharometer reading	Calibrant result	Calibration correction value	Corrected $\%H_2$	$Log_{10}(pO_2)$
a) Furnace 7						
7-60	67.1	-		-2.4	64.7	-13.80
7-61	67.1	64.5	Fe	-2.4	64.7	-13.80
7-62	60.0	58.0	Fe	-2.4	57.6	-13.53
7-63	62.6	61.0	Fe	-2.4	60.2	-13.70
7-64	64.9	62.5	Fe	-2.3	62.6	-13.82
7-65	64.7	63.0	FeO	-4.0	60.7	-11.79
7-66	69.4	67.0	Fe	-4.1	65.3	-11.97
7-67	72.0	69.5	Fe	-4.1	67.9	-12.05
7-68	69.4	67.0	Fe	-2.3	67.1	-14.04
7-102	72.8	69.5		-6.5	66.3	- 9.80
7-103	72.8	69.5		-6.4	66.4	- 9.91
7-104	72.8	69.5		-6.3	66.5	-10.01
7-105	72.8	69.5		-6.3	66.5	- 9.97
7-106	72.8	69.5		-6.4	66.4	- 9.94
7-110	72.8	69.5		-4.2	68.6	-12.05
7-111	72.8	69.5		-4.1	68.7	-12.12
7-112	72.8	69.5		-4.1	68.7	-12.15
7-113	72.8	69.5		-4.1	68.7	-12.10
7-114	72.8	69.5		-6.3	66.5	- 9.98
7-115	72.8	69.5		-6.3	66.5	- 9.96
7-116	72.9	69.7		-6.3	66.6	- 9.99
7-118	72.9	69.4		-3.2	69.7	-13.17

Run no.	Calculated $\%H_2$	Katharometer reading	Calibrant result	Calibration correction value	Corrected $\%H_2$	$Log_{10}(pO_2)$
7-119	72.9	69.5		-3.8	69.1	-12.48
7-121	73.1	69.9		-3.5	69.6	-12.82
7-122	72.8	69.7		-6.3	66.5	- 9.99
7-123	72.8	-		-6.3	66.5	- 9.96
7-124	72.8	-		-4.1	68.7	-12.06
7-125*	72.8	70.0		-4.1	68.7	-12.11
7-126	73.0	69.9		-4.1	68.9	-12.12
7-127	72.8	69.9		-4.0	68.8	-12.18
7-128	73.0	70.2		-2.4	70.6	-14.06
7-129	72.9	69.9		-2.4	70.5	-14.12
7-130	72.9	70.0		-2.4	70.5	-14.16
7-133	72.9	70.2		-3.2	69.7	-13.16
7-134	73.1	70.1		-2.9	70.2	-13.49
7-135	72.9	69.7		-4.9	68.0	-11.29
7-136	73.0	69.5	Fe	-4.1	68.9	-12.11
7-137	76.4	73.0	Fe	-4.1	72.3	-12.29
7-138	79.2	75.5	Fe	-4.1	75.1	-12.48
7-141	76.8	73.0		-5.3	71.5	-11.11
7-142	76.8	73.2		-2.4	74.4	-14.35

* Partial H_2 failure: $\%H_2$ down to c. 62% during run for a short time

Run no.	Calculated $\%H_2$	Katharometer reading	Calibrant result	Calibration correction value	Corrected $\%H_2$	$Log_{10}(pO_2)$
7-143	76.8	73.7		-2.4	74.4	-14.32
7-146	76.7	72.7		-4.1	72.6	-12.33
7-147	77.0	73.7		-4.1	72.9	-12.27
7-148	76.8	73.0	Fe	-4.1	72.7	-12.29
7-150	76.5	72.7		-4.1	72.4	-12.30
7-151	76.8	73.0		-4.1	72.7	-12.33
7-152	77.0	73.2		-4.0	73.0	-12.38
7-153	76.7	72.7		-2.3	74.4	-14.38
7-154	76.5	72.5		-2.4	74.1	-14.35
7-155	76.5	73.0		-2.4	74.1	-14.30
7-156	76.5	73.0		-3.6	72.9	-12.79
7-157	76.3	73.0		-3.6	72.7	-12.83
7-161	76.4	72.7		-3.9	72.5	-12.53
7-163	76.3	72.7		-4.1	72.2	-12.33
7-170	77.1	74.0		-3.3	73.8	-13.20
7-171	76.7	73.2		-4.1	72.6	-12.32
7-172*	76.8	73.7		-4.1	72.7	-12.30
7-173	76.8	73.7		-4.0	72.8	-12.40
7-174	76.8	73.7		-4.1	72.7	-12.34
7-175	77.1	74.1		-4.4	72.7	-12.05

* Partial H_2 failure: $\%H_2$ down to c. 40% for a short time.

Run no.	Calculated $\%H_2$	Katharometer reading	Calibrant result	Calibration correction value	Corrected $\%H_2$	$Log_{10}(pO_2)$
7-177	77.1	73.9		-2.4	74.7	-14.34
7-178	76.8	73.7		-2.4	74.4	-14.35
7-180	76.9	73.9		-3.0	73.9	-13.51
7-181	77.2	74.1		-3.5	73.7	-13.01
7-182	77.1	74.1		-6.3	70.8	-10.18
7-183	77.1	73.7		-6.3	70.8	-10.18
7-184	76.7	73.7		-4.8	71.9	-11.62
7-185	77.1	74.5		-4.6	72.5	-11.80
7-186	77.1	73.9		-5.1	72.0	-11.34
7-187	76.9	73.7		-4.4	72.5	-12.01
7-188	77.2	74.0		-3.7	73.5	-12.73
7-189	77.1	74.1		-3.6	73.5	-12.92
7-191	77.1	73.9		-3.1	74.0	-13.49
7-192	76.7	73.2		-2.4	74.3	-14.29
7-193	77.1	73.9		-2.4	74.7	-14.35
7-194	76.6	-		-2.4	74.2	-14.34
7-195	76.8	73.2		-6.3	70.5	-10.17
7-196	77.0	73.9		-6.4	70.6	-10.16
7-197	77.0	73.2		-4.1	72.9	-12.31
7-198	76.4	-		-4.1	72.3	-12.28
7-199	76.6	-		-4.1	72.5	-12.32

Run no.	Calculated $\%H_2$	Katharometer reading	Calibrant result	Calibration correction value	Corrected $\%H_2$	$Log_{10}(pO_2)$
7-200*	76.6	-		-4.1	72.5	-12.32
7-201	76.6	-		-4.9	71.7	-11.47
7-202	76.7	73.7		-4.6	72.1	-11.79
7-203	76.6	73.2		-4.6	72.0	-11.75
7-204	76.9	73.9		-4.5	72.4	-11.92
7-205	76.7	73.8		-4.3	72.4	-12.11
7-206	77.0	73.9		-4.3	72.7	-12.15
7-207	76.7	-		-6.3	70.4	-10.19
7-208	76.6	-		-6.3	70.3	-10.17
7-209	76.4	-		-6.3	70.1	-10.15
7-210	76.6	-		-6.3	70.3	-10.15
7-211	76.7	-		-4.1	72.6	-12.32
7-212	77.0	-		-4.1	72.9	-12.31
7-213	76.8	-		-4.7	72.1	-11.64
7-216	76.9	72.5		-4.9	72.0	-11.51
7-217	77.0	73.0		-4.6	72.4	-11.82
7-218	74.9	70.6	Fe	-4.1	70.8	-12.22
7-219	67.3	64.7	Fe	-4.0	63.3	-11.90
7-220	66.8	64.4	FeO	-6.4	60.4	- 9.60
7-221	66.6	63.5		-6.4	60.2	- 9.63
7-222	66.7	-		-6.3	60.4	- 9.66

* CO_2 failure: pure H_2 atmosphere for a short time.

Run no.	Calculated $\%H_2$	Katharometer reading	Calibrant result	Calibration correction value	Corrected $\%H_2$	$Log_{10}(pO_2)$
7-223	67.3	67.5		-4.1	63.2	-11.80
7-224	76.6	72.9		-4.5	72.1	-11.88
7-225	66.9	64.4		-6.3	60.6	- 9.67
7-226	66.7	64.0		-4.5	62.2	-11.44
7-229	66.9	64.2	Fe	-4.9	62.0	-10.99
7-230	66.4	63.2	Fe	-5.1	61.3	-10.73
7-231	64.7	62.0		-6.3	58.4	- 9.57
7-232	64.0	61.3		-4.4	59.6	-11.40
7-233	62.7	60.0	FeO	-5.3	57.4	-10.39
7-234	77.4	-		-4.1	73.3	-12.36
7-235	76.8	72.5		-4.1	72.7	-12.34
7-236	76.8	-		-4.1	72.7	-12.30
7-237	76.8	-		-6.4	70.4	-10.14
7-238	76.7	-		-6.3	70.4	-10.17
7-239	76.2	-		-6.4	69.8	-10.12
7-240	75.7	-		-4.1	71.6	-12.25
7-241	76.6	-		-4.1	72.5	-12.31
7-242	76.4	-		-4.1	72.3	-12.31
7-247	66.0	-	Fe+FeO	-4.1	61.9	-11.77
7-248	68.4	-	Fe	-4.1	64.3	-11.93
7-253	63.6	-	FeO	-4.0	59.6	-11.75
7-254	66.3	-		-4.1	62.2	-11.82

Run no.	Calculated $\%H_2$	Katharometer reading	Calibrant result	Calibration correction value	Corrected $\%H_2$	$Log_{10}(pO_2)$
7-256	66.2	-		-4.1	62.1	-11.77
7-257	66.7	63.7		-4.3	62.4	-11.59
7-258	66.8	63.5		-4.8	62.0	-11.08
7-259	67.4	-		-4.8	62.6	-11.09
7-260	66.3	63.0		-4.9	61.4	-10.97
7-261	67.4	-		-5.0	62.4	-10.95
7-262	67.4	-		-4.9	62.5	-11.00
7-264	67.9	64.4		-4.9	63.0	-11.01
7-265	67.8	64.7		-4.9	62.9	-11.02
7-266	67.6	64.4		-4.9	62.7	-11.03
7-267	68.0	64.7		-5.2	62.8	-10.72
7-268	68.0	65.0		-5.2	62.8	-10.75
7-269	68.0	65.0		-5.2	62.8	-10.72
7-270	68.1	-	Fe	-4.8	63.3	-11.19
7-271	66.2	-	Fe+FeO	-5.0	61.2	-10.88
7-272	64.0	-	FeO	-5.0	59.0	-10.81
7-273	66.1	-		-4.9	61.2	-10.94
7-274	66.0	-		-4.9	61.1	-10.96
7-275	66.3	-		-4.6	61.7	-11.28
7-276	66.0	-		-4.6	61.4	-11.28
7-277	66.2	-		-4.6	61.6	-11.29
7-278	65.7	-		-4.6	61.1	-11.23

Run no.	Calculated $\%H_2$	Katharometer reading	Calibrant result	Calibration correction value	Corrected $\%H_2$	$Log_{10}(pO_2)$
7-279	66.0	-		-4.6	61.4	-11.24
7-280	66.1	-		-4.1	62.0	-11.77
7-281	66.5	-		-4.1	62.4	-11.83
7-282	66.1	-		-4.1	62.0	-11.82
7-286	66.0	-		-4.4	61.6	-11.47
7-288	66.0	-		-4.2	61.8	-11.70
7-289	66.1	-		-4.1	62.0	-11.80
7-290	66.1	-		-4.2	61.9	-11.73
7-291	66.1	-		-4.1	62.0	-11.78
7-292	66.1	-		-4.2	61.9	-11.63
7-293	66.2	-		-3.9	62.3	-12.06
7-294	65.9	-		-4.5	61.4	-11.36
7-296	65.6	67.5	Fe	-4.1	61.5	-11.78
7-299	66.7	-	FeO	-4.1	62.6	-11.86
7-300	68.5	-	Fe+FeO	-4.2	64.3	-11.76
7-301	69.6	-	Fe	-4.2	65.4	-11.86
7-302	66.6	-	FeO	-4.1	62.5	-11.80
7-303	68.6	-	FeO	-4.1	64.5	-11.89
7-304	68.8	-		-4.3	64.5	-11.68
7-305	69.0	-	FeO	-5.0	64.0	-11.04
7-306	72.0	-		-5.3	66.7	-10.87
7-307	72.2	-		-5.6	66.6	-10.60

Run no.	Calculated $\%H_2$	Katharometer reading	Calibrant result	Calibration correction value	Corrected $\%H_2$	$Log_{10}(pO_2)$
7-308	71.9	-	Fe	-4.9	67.0	-11.26
7-310	71.8	-		-4.9	66.9	-11.19
7-311	71.9	-		-4.8	67.1	-11.30
7-312	72.0	-		-4.6	67.4	-11.54
7-318	71.6	-		-4.9	66.7	-11.20
7-319	72.2	69.0		-4.9	67.3	-11.26
7-320	71.7	68.5		-5.5	66.2	-10.66
b) Furnace 6						
6-44	air				-	air
6-45	air				-	air
6-46	air				-	air
6-47	air				-	air
6-48	air				-	air
c) Furnace 5						
5-52	0.0	-			0.0	- 3.81
5-53	0.0	-			0.0	- 3.83
5-56	0.0	-			0.0	- 3.82
5-60	0.0	-			0.0	- 3.83
5-63	air				-	air
5-72	0.0	-			0.0	- 3.84
5-73	0.0	-			0.0	- 3.82
5-77	air				-	air

Run no.	Calculated $\%H_2$	Katharometer reading	Calibrant result	Calibration correction value	Corrected $\%H_2$	$Log_{10}(pO_2)$
5-86	0.0	-			0.0	- 3.83
5-108	air				-	air
5-125	0.0	-			0.0	- 4.53
5-126	0.0	-			0.0	- 4.51
5-127	0.0	-			0.0	- 3.84
5-128	0.0	-			0.0	- 3.82
5-129	0.0	-			0.0	- 3.81
5-132	1.70	1.7	NiO	+0.29	1.99	- 8.35
5-133	1.95	2.0	Ni+NiO	+0.33	2.28	- 8.19
5-134	1.97	1.95	NiO	+0.35	2.32	- 8.08
5-135	1.97	2.0	Ni	+0.35	2.32	- 8.05
5-140	2.10	2.1	Ni+NiO	+0.43	2.53	- 7.62
5-141	1.92	1.95	NiO	+0.42	2.34	- 7.60
5-142	0.0	-			0.0	- 3.82
5-143	0.0	-			0.0	- 3.81
5-146	64.7	64.0		-3.5	61.2	-11.13
5-147	0.0	-			0.0	- 4.56
5-148	0.0	-			0.0	- 4.53
5-149	0.0	-			0.0	- 4.51
5-151	67.7	66.5		-7.4	60.3	-10.01
5-152	66.5	64.0		-0.8	65.7	-12.14
5-153	66.0	66.0		-5.5	60.5	-10.54

Run no.	Calculated $\%H_2$	Katharometer reading	Calibrant result	Calibration correction value	Corrected $\%H_2$	$Log_{10}(pO_2)$
5-154	0.0	-			0.0	- 3.86
5-155	0.0	-			0.0	- 3.83
5-157	68.0	68.0		-3.2	64.8	-11.37
5-159	68.6	68.0		-1.1	67.5	-12.14
5-160	68.6	68.0		+3.1	71.7	-13.77
5-161	68.6	68.0		+1.0	69.6	-12.92
5-162	2.38	2.45		+0.51	2.89	- 7.20
5-163	2.22	2.2		+0.40	2.62	- 7.85
5-164	2.60	2.7		+0.58	3.18	- 6.86
5-165	1.83	1.9		+0.32	2.15	- 8.23
5-166	0.0	-			0.0	- 3.89
5-168	64.1	63.2	Fe	+4.4	68.5	-14.09
5-169	56.3	55.5	FeO	+4.4	60.7	-13.73
5-170	59.6	59.0	FeO	+4.3	63.9	-13.82
5-171	57.1	57.4	Fe+FeO	-1.2	55.9	-11.59
5-172	63.7	62.0	FeO	-1.4	62.3	-11.81
5-173	66.0	64.7	Fe	-1.4	64.6	-11.90
5-177	66.1	65.0		-2.4	63.7	-11.58
5-178	67.2	65.0		+1.9	69.1	-13.22
5-179	66.6	66.0		-9.0	57.6	- 9.50
5-180	67.1	67.0	Fe	-1.0	66.1	-12.10
5-181	65.4	64.2	Fe	-1.1	64.3	-11.99

Run no.	Calculated $\%H_2$	Katharometer reading	Calibrant result	Calibration correction value	Corrected $\%H_2$	$Log_{10}(pO_2)$
5-182	62.5	61.3	FeO	-1.3	61.2	-11.78
5-183	67.2	67.0		-1.5	65.7	-11.94
5-184	60.2	59.7	FeO	+4.4	64.6	-13.90
5-185	67.9	67.0		-5.4	62.5	-10.67
5-186	65.2	64.5	Fe	+4.2	69.4	-14.06
5-187	64.8	63.5		-1.5	63.3	-11.83
5-188	64.0	64.5		-1.4	62.6	-11.84
5-189	66.4	66.5		-3.4	63.0	-11.24
5-190	66.2	65.0		-1.3	64.9	-11.97
5-194	66.4	60.0		-1.5	64.9	-11.91
5-195	66.5	-		-1.4	65.1	-11.95
5-202	67.4	67.0	Fe	-1.4	66.0	-11.99
5-203	67.8	67.0		-2.1	65.7	-11.74
5-205	60.8	61.0	FeO	+0.0	60.8	-12.19
5-206	61.1	61.5	Fe	+4.3	65.4	-13.91
5-207	59.1	57.8	FeO	+4.1	63.2	-13.73
5-208	60.1	59.7		+4.3	64.4	-13.85
5-209	62.2	62.3	FeO	-1.4	60.8	-11.75
5-210	64.7	64.5	Fe	-1.5	63.2	-11.84
5-212	63.4	-		-0.6	62.8	-12.08
5-216	60.6	-	Fe	+4.4	65.0	-13.93
5-217	60.1	59.7	FeO	-1.3	58.8	-11.68

Run no.	Calculated $\%H_2$	Katharometer reading	Calibrant result	Calibration correction value	Corrected $\%H_2$	$Log_{10}(pO_2)$
5-222	63.0	-		+2.4	65.4	-13.21
5-227	63.7	-		-1.6	62.1	-11.74
5-228	63.1	-		-1.4	61.7	-11.78
5-229	63.6	-		-1.4	62.2	-11.80
5-230	63.1	-		+4.3	67.4	-13.97
5-231	62.3	-		+4.4	66.7	-13.99
5-243	60.8	-	FeO	-1.2	59.6	-11.74
5-244	65.7	-	Fe	-1.4	64.3	-11.91
5-245	63.5	-	Fe+FeO	-1.5	62.0	-11.78
5-246	61.9	-	Fe	+4.5	66.4	-14.01
5-247	59.5	-	Fe+FeO	+4.3	63.8	-13.84
5-251	59.7	-		+4.4	64.1	-13.89
5-252	59.5	-		-1.3	58.2	-11.65
5-260	62.0	-		+0.9	62.9	-12.57
5-264	61.7	-		-1.5	60.2	-11.68
5-265	63.3	-		-1.5	61.8	-11.76
5-266	63.1	62.0		-1.3	61.8	-11.83
5-267	60.1	59.7	FeO+(Fe)	-1.3	58.8	-11.67
5-268	58.5	58.2	FeO+(Fe)	+4.3	62.8	-13.79
5-269	62.2	61.0	Fe	+4.5	66.7	-14.02
5-270	62.5	61.3		+4.3	66.8	-13.98

Run no.	Calculated $\%H_2$	Katharometer reading	Calibrant result	Calibration correction value	Corrected $\%H_2$	$Log_{10}(pO_2)$
5-271	62.2	-		-0.1	62.1	-12.23
5-272	63.0	-		+0.0	63.0	-12.29
5-273	62.6	-		-0.0	62.6	-12.26
5-274	62.8	-		-0.0	62.8	-12.26
5-275	62.5	-		+1.0	63.5	-12.63
5-277	59.4	-	FeO	+4.3	63.7	-13.82
5-278	64.9	63.5	Fe+FeO	-1.3	63.6	-11.89
5-279	61.9	61.0		-1.5	60.4	-11.69
5-280	62.1	-		+4.4	66.5	-13.97
5-281	62.1	-		+4.3	66.4	-13.94
5-282	62.9	-		+1.2	64.1	-12.74
5-283	62.0	-		+1.5	63.5	-12.82
5-284	61.6	-		+4.3	65.9	-13.93
5-286	61.8	-		-0.7	61.1	-11.97
5-287	62.0	-		+4.3	66.3	-13.95
5-288	61.4	-		+3.3	64.7	-13.50
5-289	62.0	-		+2.7	64.7	-13.28
5-291	60.7	59.8	Fe	+4.4	65.1	-14.06
5-292	59.0	58.0	Fe	+4.4	63.4	-13.88
5-293	58.9	-	FeO	-1.3	57.6	-11.71
5-294	58.4	57.6	Fe+FeO	+4.4	62.8	-13.80
5-297	57.5	57.1	FeO	+4.1	61.6	-13.66

Run no.	Calculated $\%H_2$	Katharometer reading	Calibrant result	Calibration correction value	Corrected $\%H_2$	$Log_{10}(pO_2)$
5-298	58.9	58.2	FeO	-1.4	57.5	-11.60
5-299	60.3	60.0	FeO	-1.5	58.8	-11.63
5-300	59.6	59.7	Fe+FeO	+4.3	63.9	-13.82
5-302	62.3	61.8	Fe	+4.4	66.7	-13.99
5-305	62.2	62.0	Fe+FeO	-1.4	60.8	-11.74
5-309	64.9	64.2	Fe	-1.3	63.6	-11.91
5-311	58.6	57.8		+4.4	63.0	-13.83
5-315	64.3	62.1	FeO	-1.3	63.0	-11.87
5-317	80.3	80.0		+0.5	80.8	-13.37
5-322	80.6	80.0		-1.4	79.2	-12.69
5-325	62.0	-		+4.4	66.4	-13.98
5-326	61.9	64.7		+2.9	64.8	-13.37
5-327	62.3	-		+1.7	64.0	-12.91
5-328	62.0	-		+4.4	66.4	-13.98
5-329	63.1	-		+4.3	67.4	-13.98
5-330	59.1	-		+5.4	64.5	-14.27
d) Furnace 3						
3-62	air				-	air
3-63	air				-	air
3-64	air				-	air
3-65	air				-	air
3-66	2.03	2.05		+0.11	2.14	- 8.10
3-67	1.71	1.70		-0.00	1.71	- 8.67

Run no.	Calculated $\%H_2$	Katharometer reading	Calibrant result	Calibration correction value	Corrected $\%H_2$	$Log_{10}(pO_2)$
3-68	air				-	air
3-69	2.25	2.275		+0.18	2.43	- 7.74
3-70	air				-	air
3-71	air				-	air
3-72	air				-	air
3-73	air				-	air
3-74	1.82	1.85		+0.04	1.86	- 8.44
3-75	1.63	1.65		-0.04	1.59	- 8.85
3-76	1.92	1.95		+0.07	1.99	- 8.30
3-79	2.10	2.125		+0.14	2.24	- 7.92
3-80	2.01	2.025		+0.14	2.15	- 7.88
3-81	2.25	2.25	Ni+NiO	+0.19	2.44	- 7.67
3-82	2.04	2.05		+0.19	2.23	- 7.54
3-83	2.40	2.475		+0.19	2.59	- 7.70
3-84	1.85	1.8		+0.19	2.04	- 7.52
3-85	1.85	1.8		+0.19	2.04	- 7.50
3-86	1.09	1.1		-0.10	0.99	- 8.83
3-87	1.32	1.25		-0.11	1.21	- 9.13
3-88	1.38	0.85		-0.11	1.27	- 9.17
3-89	1.01	1.0	NiO	-0.15	0.86	- 9.11
3-90	1.64	1.55		-0.13	1.51	- 9.46
3-91	1.45	1.4		-0.12	1.33	- 9.29

Run no.	Calculated $\%H_2$	Katharometer reading	Calibrant result	Calibration correction value	Corrected $\%H_2$	$Log_{10}(pO_2)$
3-92	1.45	1.4		-0.12	1.33	- 9.25
3-118	2.01	1.9	NiO	+0.20	2.21	- 7.47
3-119	2.51	2.45	Ni+(NiO)	+0.19	2.70	- 7.77
3-123	10.69	10.3		+0.19	10.88	- 9.07
3-124	10.69	10.3		+0.19	10.88	- 9.10
3-126	13.66	13.0		-0.11	13.55	-11.37
3-127	11.58	11.0		-0.11	11.47	-11.21
3-128	10.20	10.0		-0.12	10.08	-11.15
3-137	2.28	-	Ni	-0.12	2.16	- 9.69
3-138	2.42	-	Ni+NiO	+0.19	2.61	- 7.73
3-140	2.71	2.7	Ni	+0.07	2.78	- 8.60
3-176	2.63	2.6	Ni	+0.18	2.81	- 7.85
3-177	2.70	2.8	Ni	+0.18	2.88	- 7.84
3-178	2.93	-	Ni	+0.19	3.12	- 7.86
3-179	3.07	3.05	Ni	+0.16	3.23	- 8.10
3-182	3.25	3.2	Ni	-0.14	3.11	-10.13
3-183	2.44	2.35	Ni	-0.12	2.32	- 9.75
3-184	1.93	1.8	Ni+NiO	-0.11	1.82	- 9.50
3-188	1.50	-	NiO	-0.12	1.38	- 9.29
3-189	1.50	-	NiO	-0.11	1.39	- 9.25
3-191	2.49	-	Ni	-0.07	2.42	- 9.41
3-192	2.08	2.0	NiO	+0.17	2.25	- 7.70

Run no.	Calculated $\%H_2$	Katharometer reading	Calibrant result	Calibration correction value	Corrected $\%H_2$	$Log_{10}(pO_2)$
3-193	2.30	2.1	Ni+NiO	+0.19	2.49	- 7.65
3-194	2.36	-	Ni+NiO	+0.20	2.56	- 7.65
3-195	2.40	-	NiO+(Ni)	+0.18	2.58	- 7.74
3-255	1.93	2.15	Ni+(NiO)	+0.17	2.10	- 7.64
3-256	1.71	1.70	NiO	+0.18	1.89	- 7.48
3-257	1.37	1.4	NiO	-0.13	1.24	- 9.24
3-258+	2.19	-		-0.12	2.07	- 9.66
3-259	1.65	-	Ni+(NiO)	-0.11	1.54	- 9.34
3-263	1.58	1.64		-0.03	1.55	- 8.80
3-264*	1.87	1.9		+0.18	2.05	- 7.53
3-265	2.03	2.125		+0.19	2.22	- 7.60
3-266	2.01	2.05		+0.19	2.20	- 7.55
3-267	2.37	2.5	Ni+NiO	+0.33	2.70	- 6.88
3-268	2.39	2.48		+0.32	2.71	- 6.92
3-269	2.17	2.25		+0.23	2.40	- 7.36
3-270	2.24	2.35		+0.26	2.50	- 7.20
3-271	2.22	2.325		+0.26	2.48	- 7.19
3-272	2.32	2.45		+0.29	2.61	- 7.07

+ Partial CO_2 failure: Up to c. 3% H_2 for a short time.

* Partial CO_2 failure: Up to c. 6% H_2 for a short time.

Run no.	Calculated $\%H_2$	Katharometer reading	Calibrant result	Calibration correction value	Corrected $\%H_2$	$Log_{10}(pO_2)$
3-273	2.34	2.45		+0.32	2.66	- 6.89
3-274	2.37	2.45		+0.35	2.72	- 6.73
3-275	2.37	2.5		+0.35	2.72	- 6.73
3-276	1.88	-		+0.19	2.07	- 7.52
3-277	2.24	2.5		+0.20	2.44	- 7.58
3-279	1.33	1.5	NiO	+0.12	1.45	- 7.63
3-280	2.24	2.55	Ni+(NiO)	+0.14	2.38	- 7.94
3-282	2.03	2.1	Ni+NiO	+0.10	2.13	- 8.16
3-284	2.25	2.3	Ni+NiO	+0.18	2.43	- 7.68
3-289	2.51	2.6	NiO	+0.33	2.84	- 6.92
3-290	2.83	2.9		+0.41	3.24	- 6.59
3-291	2.28	2.35		+0.23	2.51	- 7.45
3-292	2.83	2.9		+0.33	3.16	- 7.04
3-293	2.87	2.95		+0.35	3.22	- 6.89
3-294	2.53	2.6		+0.26	2.79	- 7.31
3-295	2.86	2.9		+0.38	3.24	- 6.72
3-296	2.84	2.9		+0.38	3.22	- 6.71
3-297	2.53	2.59		+0.29	2.82	- 7.12
3-298	2.52	2.59		+0.37	2.89	- 6.67
3-299	2.79	2.9	Ni	+0.19	2.98	- 7.84
3-300	2.57	2.65		+0.14	2.71	- 8.08
3-301	2.25	2.3		+0.09	2.34	- 8.30

Run no.	Calculated $\%H_2$	Katharometer reading	Calibrant result	Calibration correction value	Corrected $\%H_2$	$Log_{10}(pO_2)$
3-302	2.16	2.2		+0.04	2.20	- 8.59
3-303	2.02	2.05	Ni	-0.13	1.89	- 9.61
3-304	2.04	2.05		-0.12	1.92	- 9.60
3-305	2.06	2.1		-0.12	1.94	- 9.57
3-306	2.06	2.1		-0.11	1.95	- 9.53
3-307	2.19	2.23		+0.01	2.20	- 8.79
3-309	2.61	2.7		+0.19	2.80	- 7.79
3-311	3.07	3.125	NiO+(Ni)	+0.58	3.65	- 5.78
3-312	2.96	3.0	Ni	+0.33	3.29	- 7.02
3-313	2.54	2.59	Ni	+0.19	2.73	- 7.78
3-314	2.75	2.825	Ni+NiO	+0.46	3.21	- 6.28
3-319	33.83	33.1		+0.19	34.02	-10.50
3-320	1.22	1.24		+0.19	1.41	- 7.14
3-323	1.78	1.83		-0.09	1.69	- 9.28
3-324	9.93	10.4		-0.11	9.82	-11.05
3-325	1.10	1.125		-0.13	0.97	- 9.06
3-326	0.48	0.527		-0.12	0.36	- 8.13
3-327	0.55	-		+0.18	0.73	- 6.67
3-328	2.38	2.475		+0.18	2.56	- 7.73
3-329	1.13	1.16		+0.18	1.31	- 7.20
3-330	2.31	2.39		+0.18	2.49	- 7.76
3-331	2.31	2.41		+0.11	2.42	- 8.17

Run no.	Calculated $\%H_2$	Katharometer reading	Calibrant result	Calibration correction value	Corrected $\%H_2$	$Log_{10}(pO_2)$
3-332	1.93	1.95		+0.02	1.95	- 8.67
3-333	2.36	2.42		+0.15	2.51	- 7.92
3-334	2.32	2.37		+0.15	2.47	- 7.90
3-335	2.20	2.25		+0.09	2.29	- 8.27
3-336	2.38	2.45		+0.23	2.61	- 7.46
3-337	2.33	2.38		+0.21	2.54	- 7.56
3-338	2.18	2.25		+0.19	2.37	- 7.61
3-339	0.52	0.565		+0.19	0.71	- 6.57
3-340	0.0	-			0.0	- 3.82
3-341	0.0	-			0.0	- 3.82
3-342	0.51	0.55		+0.16	0.67	- 6.75
3-343	0.0	-			0.0	- 3.88
3-344	2.20	2.25		+0.16	2.36	- 7.82
3-345	1.97	2.0		+0.07	2.04	- 8.33
3-346	1.92	1.95		+0.04	1.96	- 8.47
3-347	0.0	-			0.0	- 4.09
3-349	0.50	0.525		+0.24	0.74	- 6.27
3-350	0.51	0.56		+0.19	0.70	- 6.55
3-351	0.0	-			0.0	- 3.82

APPENDIX E

RESULTS OF QUENCHING EXPERIMENTS

E.1. Compositions in the system $CaO-MgO-Al_2O_3-SiO_2$

Composition	Run No.	Temperature °C	Result
a) Anorthite-Diopside-Forsterite			
ADF1	8-134	1283	liq
	8-135	1281	liq
	8-136	1278	(an),(fo),liq
	8-144	1278	an,di,(fo),liq
	8-137	1274	an,di,fo,(liq)
ADF2	8-134	1283	di,liq
	8-135	1281	di,liq
	8-136	1278	di,liq
	8-144	1278	di,an,liq
	8-137	1274	di,an,fo,(liq)
ADF3	8-134	1283	fo,(di),liq
	8-135	1281	fo,di,liq
	8-136	1278	fo,di,liq
	8-144	1278	fo,di,an,liq
	8-137	1274	fo,di,an,(liq)
ADF4	8-134	1283	fo,liq
	8-135	1281	fo,liq
	8-136	1278	fo,an,liq
	8-144	1278	fo,an,di,liq
	8-137	1274	fo,an,di,(liq)
ADF5	8-134	1283	an,liq
	8-135	1281	an,liq
	8-136	1278	an,liq
	8-144	1278	an,di,liq
	8-137	1274	an,di,fo,(liq)
b) Diopside - MAS			
H13	8-144	1278	fo,an,liq
	8-118	1264	fo,an,di,liq
H14	6-76	1280	fo,an,di,liq

Abbreviations: ( ) small amount only; * indicates phase(s) which should (+) or should not (-) be present; ? identification questionable; other abbreviations in Appendix A.

Composition	Run No.	Temperature °C	Result
H4	8-50	1306	fo,liq
	8-49	1292	fo,liq
	8-51	1286	fo,liq
	6-76	1280	fo,an,di,liq
	3-57	1274	fo,an,di,liq
H5	8-50	1306	fo,liq
	8-49	1292	fo,liq
	8-51	1286	fo,liq
	6-76	1280	fo,an,di,liq
	3-57	1274	fo,an,di,liq
H6	8-50	1306	fo,liq
	8-49	1292	fo,liq
	8-51	1286	fo,liq
	6-76	1280	fo,an,di,liq
	3-57	1274	fo,an,di,liq
H15	6-76	1280	fo,an,di,liq
H16	6-76	1280	fo,an,di,liq
c) Diopside - $M_5A_3S_5$			
H17	8-144	1278	fo,an,liq
	8-118	1264	fo,an,liq
H18	6-76	1280	fo,an,di,liq
H1	8-50	1306	fo,liq
	8-49	1292	fo,liq
	8-51	1286	fo,liq
	6-76	1280	fo,an,di,liq
	3-57	1274	fo,an,di,liq
	8-58	1263	fo,an,di,liq
H2	8-50	1306	fo,liq
	8-49	1292	fo,liq
	8-51	1286	fo,liq
	6-76	1280	fo,an,di,liq
	3-57	1274	fo,an,di,liq
	8-58	1263	fo,an,di,liq

Composition	Run No.	Temperature °C	Result
H3	8-50	1306	fo,liq
	8-49	1292	fo,liq
	8-51	1286	fo,liq
	6-76	1280	fo,an,di,liq
	3-57	1274	fo,an,di,liq
	8-58	1263	fo,an,di,liq
H19	6-76	1280	fo,an,di,liq
H20	6-76	1280	fo,di,liq
d) Diopside - $M_7A_3S_7$			
H21	8-144	1278	fo,an,liq
	8-118	1264	fo,an,liq
H22	8-144	1278	fo,an,liq
	8-118	1264	fo,an,di,liq
H23	8-144	1278	fo,an,liq
	8-118	1264	fo,an,di,liq
H24	8-144	1278	fo,liq
	8-118	1264	fo,an,di,liq
H25	8-144	1278	fo,di,liq
	8-118	1264	fo,di,an,liq
H26	8-144	1278	fo,di,liq
	8-118	1264	fo,di,an,liq
H27	8-144	1278	fo,di,liq
	8-118	1264	fo,di,an,liq

E.2. Compositions in the system $CaO-MgO-Al_2O_3-SiO_2-Na_2O$

E.2.1. Compositions with CIPW normative anorthite:albite ratio = 67.97:32.03.

Composition	Run No.	Temperature °C	Result
a) $XO.YO.2ZO_2$-$YO.R_2O_3.ZO_2$ (Diopside - MAS)			
N19	8-145	1274	fo,plag,liq
	8-111	1250	fo,plag,liq
N16	8-145	1274	fo,plag,liq
	8-111	1250	fo,plag,liq
	8-93	1242	fo,plag,liq
N1	8-145	1274	fo,plag,liq
	8-59	1263	fo,plag,liq
	8-86	1260	fo,plag,liq
	8-57	1251	fo,plag,liq
	8-93	1242	fo,plag,di,liq
	8-56	1234	fo,plag,di,liq
N2	8-59	1263	fo,liq (*+plag)
	8-86	1260	fo,plag,liq
	8-57	1251	fo,plag,liq
	8-93	1242	fo,plag,di,liq
	8-56	1234	fo,plag,di,liq
N3	8-59	1263	fo,liq
	8-86	1260	fo,liq
	8-57	1251	fo,plag,di,liq
	8-93	1242	fo,plag,di,liq
	8-56	1234	fo,plag,di,liq
N17	8-145	1274	fo,di,liq
	8-86	1260	fo,di,liq
	8-93	1242	fo,di,plag,liq
N18	8-93	1242	fo,di,plag,liq
b) $XO.YO.2ZO_2$-$5YO.3R_2O_3.5ZO_2$ (Diopside - $M_5A_3S_5$)			
N20	8-145	1274	fo,plag,liq
	8-111	1250	fo,plag,pyx,liq
	8-93	1242	fo,plag,pyx,liq
N10	8-145	1274	fo,plag,liq
	8-59	1263	fo,plag,liq
	8-86	1260	fo,plag,liq
	8-57	1251	fo,plag,liq
	8-93	1242	fo,plag,liq
	8-56	1234	fo,plag,di,liq

Composition	Run No.	Temperature °C	Results
N11	8-145	1274	fo,liq
	8-59	1263	fo,plag,liq
	8-86	1260	fo,plag,liq
	8-57	1251	fo,plag,liq
	8-111	1250	fo,plag,(di),liq
	8-93	1242	fo,plag,di,liq
	8-56	1234	fo,plag,di,liq
N12	8-59	1263	fo,liq
	8-86	1260	fo,plag,liq
	8-57	1251	fo,plag,liq
	8-111	1250	fo,plag,(di),liq
	8-93	1242	fo,plag,di,liq
	8-56	1234	fo,plag,di,liq
N21	8-145	1274	fo,di,liq (*-di)
	8-86	1260	fo,di,liq
	8-93	1242	fo,di,plag,liq
N22	8-145	1274	fo,di,liq
	8-111	1250	fo,di,plag,liq
	8-93	1242	fo,di,plag,liq
c) $XO.YO.2ZO_2$-$7YO.3R_2O_3.7ZO_2$ (Diopside - $M_7A_3S_7$)			
N23	8-111	1250	fo,plag,sp,liq
N24	8-145	1274	fo,plag,liq
	8-86	1260	fo,plag,liq
	8-111	1250	fo,plag,liq
N25	8-145	1274	fo,plag,liq
	8-86	1260	fo,plag,liq
	8-111	1250	fo,plag,liq
N26	8-145	1274	fo,liq
	8-86	1260	fo,plag,liq
	8-111	1250	fo,plag,liq
N27	8-86	1260	fo,di,liq
	8-111	1250	fo,di,plag,liq
N28	8-145	1274	fo,di,liq
	8-111	1250	fo,di,plag,liq

E.2.2. Compositions with CIPW normative anorthite:albite ratio = 51.48:48.52

Composition	Run No.	Temperature °C	Results
a) $XO.YO.2ZO_2$-$YO.R_2O_3.ZO_2$ (Diopside - MAS)			
L19	8-145	1274	fo,plag,liq
	6-83	1251	fo,plag,liq
	6-77	1239	fo,plag,liq
	8-117	1229	fo,plag,di,liq
L1	8-77	1274	fo,liq
	6-67	1257	fo,plag,liq
	6-83	1251	fo,plag,liq
	3-61	1241	fo,plag,liq
	6-77	1239	fo,plag,di,liq
L2	8-77	1274	fo,liq
	6-67	1257	fo,plag,liq
	6-83	1251	fo,plag,liq
	3-61	1241	fo,plag,?di,liq
	6-77	1239	fo,plag,di,liq
L3	8-77	1274	fo,liq
	6-67	1257	fo,liq
	6-83	1251	fo,(plag),liq
	8-110	1245	fo,plag,liq
	3-61	1241	fo,plag,di,liq
	6-77	1239	fo,plag,di,liq
L20	8-145	1274	fo,liq
	6-83	1251	fo,di,liq
	8-110	1245	fo,di,liq
	6-77	1239	fo,di,plag,liq
L21	6-83	1251	fo,di,liq
	6-77	1239	fo,di,plag,liq
b) $XO.YO.2ZO_2$-$5YO.3R_2O_3.5ZO_2$ (Diopside - $M_5A_3S_5$)			
L22	8-110	1245	fo,sp,liq
	8-117	1229	fo,sp,plag,liq
L23	6-83	1251	fo,plag,sp,liq
L16	8-145	1274	fo,liq
	6-83	1251	fo,plag,liq
	8-110	1245	fo,plag,liq
	6-77	1239	fo,plag,liq
	8-117	1229	fo,plag,di,liq

Composition	Run No.	Temperature °C	Results
L17	6-83	1251	fo,plag,liq
	6-77	1239	fo,plag,liq
	8-117	1229	fo,plag,di,liq
L18	6-83	1251	fo,liq
	8-110	1245	fo,liq
	6-77	1239	fo,plag,di,liq
L24	8-145	1274	fo,liq
	6-83	1251	fo,di,liq
	6-77	1239	fo,di,plag,liq
L25	8-145	1274	fo,di,liq
	6-83	1251	fo,di,liq
	6-77	1239	fo,di,plag,liq
c) $\underline{XO.YO.2ZO_2}$-$\underline{7YO.3R_2O_3.7ZO_2}$ (Diopside - $\underline{M_7A_3S_7}$)			
L26	8-110	1245	fo,sp,liq
L27	8-110	1245	fo,sp,liq
	8-117	1229	fo,sp,plag,liq
L28	8-110	1245	fo,plag,liq
	8-117	1229	fo,plag,pyx,liq
L29	8-110	1245	fo,plag,liq
	8-117	1229	fo,plag,pyx,liq
L30	8-110	1245	fo,plag,liq
	8-117	1229	fo,plag,di,liq
L31	8-110	1245	fo,liq
	8-117	1229	fo,plag,di,liq
L32	8-117	1229	fo,plag,di,liq

E.2.3. Compositions with CIPW normative anorthite:albite ratio = 34.66:65.34

Composition	Run No.	Temperature °C	Result
a) $ZO.YO.2ZO_2$-$YO.R_2O_3.ZO_2$ (Diopside - MAS)			
A16	8-87	1234	fo,plag,liq
A1	8-87	1234	fo,plag,liq
	8-78	1222	fo,plag,liq
	8-100	1213	fo,plag,di,liq
	6-38	1205	fo,plag,di,?liq
A2	6-98	1246	fo,liq
	8-87	1234	fo,plag,liq
	8-94	1227	fo,plag,di,liq
	8-78	1222	fo,plag,di,liq
	8-100	1213	fo,plag,di,liq
	6-38	1205	fo,plag,di,?liq
A3	6-98	1246	fo,liq
	8-87	1234	fo,di,liq
	8-94	1227	fo,di,plag,liq
	8-78	1222	fo,di,plag,liq
	8-100	1213	fo,di,plag,liq
	6-38	1205	fo,di,plag,?liq
A18	8-87	1234	fo,di,liq
A17	8-87	1234	fo,di,liq
b) $XO.YO.2ZO_2$-$5YO.3R_2O_3.5ZO_2$ (Diopside - $M_5A_3S_5$)			
A19	8-87	1234	fo,sp,liq
	8-94	1227	fo,sp,liq
A10	6-98	1246	fo,plag,liq
	8-87	1234	fo,plag,liq
	8-94	1227	fo,plag,pyx,liq
	8-100	1213	fo,plag,pyx,liq
A11	6-98	1246	fo,plag,liq
	8-87	1234	fo,plag,liq
	8-94	1227	fo,plag,pyx,liq
	8-78	1222	fo,plag,pyx,liq
	8-100	1213	fo,plag,pyx,liq
	6-38	1205	fo,plag,pyx,?liq

Composition	Run No.	Temperature °C	Result
A12	6-98	1246	fo,liq
	8-87	1234	fo,plag,liq
	8-94	1227	fo,plag,pyx,liq
	8-78	1222	fo,plag,pyx,liq
	8-100	1213	fo,plag,pyx,liq
	6-38	1205	fo,plag,pyx,?liq
A20	6-98	1246	fo,liq
	8-87	1234	fo,plag,liq
	8-94	1227	fo,plag,liq
	8-100	1213	fo,plag,di,liq
A21	6-98	1246	fo,di,liq
	8-87	1234	fo,di,liq
c) $\underline{XO.YO.2ZO_2}$-$\underline{7YO.3R_2O_3.7ZO_2}$ (Diopside - $\underline{M_7A_3S_7}$)			
A23	6-98	1246	fo,sp,liq
A25	6-98	1246	fo,plag,liq
	8-94	1227	fo,plag,liq
	8-100	1213	fo,plag,liq
A27	6-98	1246	fo,di,liq
	8-94	1227	fo,di,liq

E.3. Compositions in the system $CaO-MgO-Al_2O_3-SiO_2-Fe-O_2$

E.3.1. Results at the FeFeO equilibrium.

Composition	Run No.	Temperature ^{o}C	Result
(A) FeO/MgO mole ratio = 0.074			
(i) $3XO.R_2O_3.15ZO_2$-YO (C_3AS_{15}-M)			
0.074-9-3-1-15	5-151	1359	ol,pen,liq
	5-153	1310	ol,pig,liq
	5-157	1254	pig,cpx,liq
(B) FeO/MgO mole ratio = 0.125			
(i) $3XO.R_2O_3.15ZO_2$-YO (C_3AS_{15}-M)			
0.125-2-3-1-15	7-319	1274	sil,cpx,liq
0.125-6-3-1-15	5-151	1359	pen,liq
	5-153	1310	pig,sil,liq
	5-157	1254	pig,sil,cpx,liq
0.125-8-3-1-15	5-151	1359	pen,liq
	5-153	1310	pig,liq
	5-157	1254	pig,cpx,liq
(C) FeO/MgO mole ratio $\simeq$ 0.18			
(i) $XO.YO.2ZO_2$-$YO.R_2O_3.ZO_2$ (Diopside - MAS)			
AF1	7-307	1332	ol,liq
	7-306	1307	ol,liq
	7-186	1289	ol,an,liq
	7-135	1275	ol,an,liq
	7-184	1264	ol,an,liq
	7-203	1252	ol,an,cpx,liq
	7-204	1239	ol,an,cpx,(liq)
AF2	7-307	1332	ol,liq
	7-186	1289	ol,liq
	7-135	1275	ol,liq
	7-184	1264	ol,cpx,liq
	7-203	1252	ol,cpx,an,liq
	7-204	1239	ol,cpx,an,(liq)?

Composition	Run No.	Temperature °C	Result
AF3	7-307	1332	ol,liq
	7-186	1289	ol,liq
	7-135	1275	ol,cpx,liq
	7-184	1264	ol,cpx,liq
	7-203	1252	ol,cpx,an,liq
	7-204	1239	ol,cpx,an,liq?
AF4	7-307	1332	(ol),liq
	7-306	1307	ol,cpx,liq
	7-186	1289	ol,cpx,liq
	7-135	1275	ol,cpx,liq
	7-184	1264	ol,cpx,liq
	7-203	1252	ol,cpx,an,liq
	7-204	1239	ol,cpx,an,liq?
AF5	7-307	1332	liq
	7-306	1307	ol,cpx,liq
	7-186	1289	ol,cpx,liq
	7-135	1275	ol,cpx,liq
	7-184	1264	ol,cpx,liq
AF6	7-307	1332	cpx,liq
	7-306	1307	cpx,liq
	7-186	1289	cpx,liq
	7-135	1275	cpx,ol,liq
	7-184	1264	cpx,ol,liq
(ii) $\underline{XO.YO.2ZO_2\text{-}5YO.3R_2O_3.5ZO_2}$ (Diopside-$\underline{M_5A_3S_5}$)			
AF31	7-307	1332	ol,liq
	7-306	1307	ol,liq
	7-186	1289	ol,an,liq
	7-135	1275	ol,an,liq
	7-184	1264	ol,an,liq
	7-203	1252	ol,an,liq
	7-204	1239	ol,an,cpx,liq

Composition	Run No.	Temperature °C	Result
AF32	7-307	1332	ol,liq
	7-186	1289	ol,liq
	7-135	1275	ol,liq
	7-184	1264	ol,liq (*+an)
	7-203	1252	ol,an,cpx,liq
	7-312	1250	ol,an,cpx,liq
	7-204	1239	ol,an,cpx,liq
AF33	7-307	1332	ol,liq
	7-306	1307	ol,liq
	7-186	1289	ol,liq
	7-135	1275	ol,cpx,liq
	7-184	1264	ol,cpx,liq
	7-203	1252	ol,cpx,an,liq
	7-204	1239	ol,cpx,an,liq
AF34	7-307	1332	ol,liq
	7-186	1289	ol,cpx,liq
	7-135	1275	ol,cpx,liq
	7-184	1264	ol,cpx,liq
	7-203	1252	ol,cpx,an,liq
	7-204	1239	ol,cpx,an,liq
AF35	7-307	1332	ol,liq
	7-186	1289	ol,cpx,liq
	7-135	1275	ol,cpx,liq
	7-184	1264	ol,cpx,liq
AF36	7-320	1324	cpx,liq
	7-186	1289	cpx,ol,liq
	7-135	1275	cpx,ol,liq
	7-184	1264	cpx,ol,liq
(D) FeO/MgO mole ratio = 0.20			
(i) $YO.ZO_2$-$3XO.R_2O_3.3ZO_2$ (En-Gross)			
0.2-10-3-1-15	5-151	1359	ol,liq
	5-153	1310	ol,pig,liq
	7-201	1276	ol,pig,liq
	5-157	1254	ol,pig,cpx,liq

Composition	Run No.	Temperature °C	Result
0.2-6.6-3-1-11	7-269	1303	ol,liq
	7-230	1296	ol,liq
	7-201	1276	ol,cpx,liq
	7-213	1262	ol,cpx,liq
	7-202	1250	ol,cpx,liq
0.2-5-3-1-9	7-141	1307	ol,liq
	7-269	1303	ol,liq
	7-230	1296	ol,liq
	7-201	1276	ol,cpx,liq
	7-213	1262	ol,cpx,liq
	7-202	1250	ol,cpx,liq
0.2-3.3-3-1-7	7-269	1303	ol,liq
	7-230	1296	ol,liq
	7-201	1276	ol,cpx,liq
	7-213	1262	ol,cpx,liq
	7-202	1250	ol,cpx,an,liq
0.2-2.5-3-1-6	7-233	1310	liq
	7-269	1303	liq
	7-201	1276	ol,(cpx),liq
	7-213	1262	ol,cpx,liq
	7-202	1250	ol,cpx,an,liq
0.2-1.6-3-1-5	7-201	1276	liq
	7-213	1262	liq
	7-202	1250	an,cpx,liq
(E) FeO/MgO mole ratio = 0.25			
(i) $3XO.R_2O_3.15ZO_2$-YO($C_3AS_{1.5}$-M)			
0.25-2-3-1-15	7-319	1274	sil,cpx,liq
0.25-6-3-1-15	5-151	1359	liq
	5-153	1310	pig,liq
	5-146	1260	pig,sil,liq
	5-157	1254	pig,sil,cpx,liq
0.25-8-3-1-15	5-151	1359	ol,pen,liq
	5-153	1310	ol,pig,liq
	5-146	1260	ol,pig,liq

Composition	Run No.	Temperature °C	Result
0.25-9-3-1-15	5-151	1359	ol,liq
	5-146	1260	ol,pig,liq
	5-157	1254	ol,pig,cpx,liq
(F) FeO/MgO mole ratio = 0.33			
(i) $YO.ZO_2$-$3XO.R_2O_3.3ZO_2$ (En-Gross)			
0.3-9-3-1-15	5-151	1359	ol,liq
	5-153	1310	ol,pig,liq
	7-201	1276	ol,pig,liq
	7-213	1262	ol,pig,liq
	5-157	1254	ol,pig,liq
	7-205	1224	ol,pig,cpx,liq
	5-159	1200	ol,pig,cpx,liq
0.3-6-3-1-11	7-201	1276	ol,liq
	7-213	1262	ol,cpx,liq
	7-202	1250	ol,cpx,liq
	7-205	1224	ol,cpx,liq
0.3-4.5-3-1-9	7-201	1276	ol,liq
	7-213	1262	ol,liq
	7-202	1250	ol,cpx,liq
	7-205	1224	ol,cpx,liq
0.3-3-3-1-7	7-201	1276	ol,liq
	7-213	1262	ol,cpx,liq
	7-202	1250	ol,cpx,liq
	7-205	1224	ol,cpx,an,liq
0.3-2.25-3-1-6	7-201	1276	liq
	7-213	1262	cpx,liq
	7-202	1250	cpx,liq
	7-205	1224	cpx,ol,an,liq
0.3-1.5-3-1-5	7-201	1276	liq
	7-213	1262	liq
	7-202	1250	an,liq
	7-205	1224	an,cpx,liq

Composition	Run No.	Temperature °C	Result
(G) FeO/MgO mole ratio = 0.50			
(i) $XO.YO.2ZO_2$-$YO.R_2O_3.ZO_2$ (Diopside-MAS)			
AF11	7-306	1307	liq
	7-186	1289	ol,liq
	7-305	1280	ol,liq
	7-135	1275	ol,liq
	7-184	1264	ol,liq
	7-203	1252	ol,an,liq
	7-279	1251	ol,an,liq
	7-294	1241	ol,an,liq
	7-204	1239	ol,an,liq
AF12	7-306	1307	liq
	7-186	1289	ol,liq
	7-305	1280	ol,liq
	7-135	1275	ol,liq
	7-184	1264	ol,liq
	7-203	1252	ol,liq
	7-279	1251	ol,(an),liq
	7-294	1241	ol,an,cpx,liq
	7-204	1239	ol,an,cpx,liq
AF13	7-186	1289	liq
	7-305	1280	liq
	7-135	1275	liq
	7-184	1264	ol,liq
	7-203	1252	ol,liq
	7-279	1251	ol,cpx,liq
	7-294	1241	ol,cpx,liq
	7-204	1239	ol,cpx,an,liq
AF14	7-186	1289	liq
	7-305	1280	liq
	7-135	1275	(cpx), liq
	7-184	1264	cpx,liq
	7-203	1252	cpx,liq
	7-279	1251	cpx,liq
	7-294	1241	cpx,ol,liq
	7-204	1239	cpx,ol,liq

Composition	Run No.	Temperature °C	Result
AF15	7-306	1307	liq
	7-186	1289	cpx,liq
	7-305	1280	cpx,liq
	7-135	1275	cpx,liq
	7-184	1264	cpx,liq
	7-203	1252	cpx,liq
	7-279	1251	cpx,liq
	7-294	1241	cpx,liq
	7-204	1239	cpx,liq
AF16	7-306	1307	cpx,liq
	7-186	1289	cpx,liq
	7-305	1280	cpx,liq
	7-135	1275	cpx,liq
	7-184	1264	cpx,liq
	7-203	1252	cpx,liq
	7-279	1251	cpx,liq
	7-294	1241	cpx,liq
	7-204	1239	cpx,liq
(ii) $XO.YO.2ZO_2$-$5YO.3R_2O_3.5ZO_2$ (Diopside-$M_5A_3S_5$)			
AF41	7-279	1251	ol,an,liq
	7-278	1251	ol,an,liq
	7-312	1250	ol,an,liq
	7-185	1250	ol,an,liq
	7-224	1241	ol,an,liq
	7-294	1241	ol,an,liq
	7-187	1232	ol,an,liq
	7-206	1221	ol,an,(cpx),liq
	7-200	1207	ol,an,cpx,liq
AF42	7-279	1251	ol,an,liq
	7-278	1251	ol,an,liq
	7-185	1250	ol,(an),liq
	7-224	1241	ol,an,liq
	7-294	1241	ol,an,liq
	7-187	1232	ol,an,liq
	7-206	1221	ol,an,cpx,liq
	7-200	1207	ol,an,cpx,liq

Composition	Run No.	Temperature °C	Result
AF43	7-279	1251	ol,liq
	7-278	1251	ol,liq
	7-185	1250	ol,liq
	7-224	1241	ol,liq
	7-294	1241	ol,liq
	7-187	1232	ol,cpx,liq
	7-206	1221	ol,cpx,an,liq
	7-200	1207	ol,cpx,an,liq
AF44	7-279	1251	ol,cpx,liq
	7-278	1251	ol,cpx,liq
	7-312	1250	ol,cpx,liq
	7-185	1250	ol,cpx,liq
	7-224	1241	ol,cpx,liq
	7-294	1241	ol,cpx,liq
	7-187	1232	ol,cpx,liq
	7-206	1221	ol,cpx,an,liq
	7-200	1207	ol,cpx,an,liq
AF45	7-279	1251	ol,cpx,liq
	7-278	1251	ol,cpx,liq
	7-312	1250	ol,cpx,liq
	7-185	1250	ol,cpx,liq
	7-224	1241	ol,cpx,liq
	7-294	1241	ol,cpx,liq
	7-187	1232	ol,cpx,liq
AF46	7-279	1251	cpx,liq
	7-278	1251	cpx,liq
	7-312	1250	cpx,liq
	7-185	1250	cpx,liq
	7-224	1241	cpx,ol,liq
	7-294	1241	cpx,ol,liq
	7-187	1232	cpx,ol,liq

Composition	Run No.	Temperature °C	Result
(iii) $YO.ZO_2$-$3XO.R_2O_3.3ZO_2$ (En-Gross)			
0.5-8-3-1-15	7-233	1310	ol,pig,liq
	7-267	1303	ol,pig,liq
	7-258	1268	ol,pig,liq
	5-146	1260	ol,pig,liq
	5-157	1254	ol,pig,liq
	7-275	1249	ol,pig,liq
	7-257	1226	ol,pig,cpx,liq
	5-264	1210	ol,pig,cpx,liq
	5-159	1200	ol,pig,cpx,liq
0.5-5.3-3-1-11	7-267	1303	ol,liq
	7-261	1280	ol,liq
	7-213	1262	ol,liq
	7-202	1250	ol,cpx,liq
	7-276	1248	ol,(cpx),liq
	7-257	1226	ol,cpx,liq
	7-205	1224	ol,cpx,liq
	5-264	1210	ol,cpx,liq
	7-174	1206	ol,cpx,liq
0.5-4-3-1-9	7-267	1303	ol,liq
	7-261	1280	ol,liq
	7-213	1262	ol,liq
	7-202	1250	ol,cpx,liq
	7-276	1248	ol,cpx,liq
	7-175	1229	ol,cpx,liq
	7-257	1226	ol,cpx,liq
	7-292	1221	ol,cpx,liq
	5-264	1210	ol,cpx,an,liq
	7-174	1206	ol,cpx,an,liq
0.5-2.6-3-1-7	7-267	1303	liq
	7-261	1280	(ol),liq
	7-201	1276	ol,liq
	7-213	1262	ol,liq
	7-202	1250	ol,cpx,liq
	7-276	1248	ol,cpx,liq
	7-175	1229	ol,cpx,an,liq

Composition	Run No.	Temperature °C	Result
0.5-2-3-1-6	7-201	1276	liq
	7-213	1262	liq
	7-202	1250	cpx,liq
	7-276	1248	cpx,liq
	7-175	1229	cpx,an,ol,liq
0.5-1.3-3-1-5	7-201	1276	liq
	7-213	1262	liq
	7-202	1250	an,liq
	7-275	1249	an,liq
	7-205	1224	an,cpx,liq
(iv) $\underline{3XO.R_2O_3.15ZO_2}$-$\underline{YO(C_3AS_{15}}$-$\underline{M)}$			
0.5-1-3-1-15	7-286	1233	sil,cpx,liq
	5-286	1190	sil,cpx,liq
	5-273	1173	sil,cpx,liq
0.5-2-3-1-15	7-258	1268	sil,liq
	7-275	1249	sil,cpx,liq
	7-286	1233	sil,cpx,pig,liq
	7-256	1210	sil,cpx,pig,liq
	5-264	1210	sil,cpx,pig,liq
	5-286	1190	sil,cpx,pig,liq
	5-273	1173	sil,cpx,pig,liq
0.5-3-3-1-15	7-267	1303	sil,liq
	7-258	1268	sil,(pig),liq
	7-275	1249	sil,pig,cpx,liq
	7-256	1210	sil,pig,cpx,liq
	5-264	1210	sil,pig,cpx,liq
	5-273	1173	sil,pig,cpx,liq
0.5-4-3-1-15	7-267	1303	sil,liq
	7-258	1268	sil,pig,liq
	5-146	1260	sil,pig,liq
	7-275	1249	sil,pig,liq
	7-257	1226	sil,pig,cpx,liq
	7-256	1210	sil,pig,cpx,liq
	5-264	1210	sil,pig,cpx,liq
	5-273	1173	sil,pig,cpx,liq

Composition	Run No.	Temperature °C	Result
0.5-6-3-1-15	5-151	1359	liq
	7-320	1324	pig,liq
	5-153	1310	pig,liq
	7-267	1303	pig,liq
	7-258	1268	pig,liq
	7-275	1249	pig,liq
	7-257	1226	pig,cpx,liq
	7-256	1210	pig,cpx,liq
	5-264	1210	pig,cpx,sil,liq
	5-273	1173	pig,cpx,sil,liq
0.5-9-3-1-15	5-151	1359	ol,liq
	5-153	1310	ol,liq
	7-267	1303	ol,(pig),liq
	7-258	1268	ol,pig,liq
	7-275	1249	ol,pig,liq
	7-257	1226	ol,pig,cpx,liq
	5-264	1210	ol,pig,cpx,liq
	5-265	1210	ol,pig,cpx,liq
0.5-12-3-1-15	5-151	1359	ol,liq
	7-261	1280	ol,liq
	7-262	1277	ol,liq
	7-265	1277	ol,liq
	7-275	1249	ol,liq
	7-286	1233	ol,cpx,liq
	5-265	1210	ol,cpx,liq
(v) $\underline{3XO.R_2O_3\text{-}YO\text{-}ZO_2(C_3A\text{-}M\text{-}S)}$			
0.5-4-3-1-6	7-261	1280	ol,sp,liq
0.5-0.6-3-1-5	7-259	1269	an,liq

Composition	Run No.	Temperature °C	Result
(H) FeO/MgO mole ratio = 0.55			
(i) $3XO.R_2O_3.15ZO_2$ - YO (C_3AS_{15}-M)			
0.55-5-3-1-15	7-307	1332	liq
	7-306	1307	pig,liq
	7-267	1303	pig,liq
	7-305	1280	pig,liq
	7-258	1268	pig,sil,liq
	5-146	1260	pig,sil,liq
	5-157	1254	pig,sil,liq
	7-275	1249	pig,sil,liq
	7-257	1226	pig,sil,cpx,liq
	5-264	1210	pig,sil,cpx,liq
	5-159	1200	pig,sil,cpx,liq
(I) FeO/MgO mole ratio = 0.66			
(i) $3XO.R_2O_3$-YO-ZO_2 (C_3A-M-S)			
0.6-6-3-1-7	7-261	1280	ol,sp,liq
(J) FeO/MgO mole ratio = 0.75			
(i) $3XO.R_2O_3.15ZO_2$-YO (C_3AS_{15}-M)			
0.75-8-3-1-15	7-259	1269	ol,(pig),liq
	5-159	1201	ol,pig,liq
(ii) $3XO.R_2O_3$-YO-ZO_2 (C_3A-M-S)			
0.75-4-3-1-6	7-261	1280	ol,sp,liq
	7-265	1277	ol,sp,liq
(K) FeO/MgO mole ratio = 1.00			
(i) $XO.YO.2ZO_2$-$YO.R_2O_3.ZO_2$ (Diopside-MAS)			
AF21	7-185	1250	liq
	7-224	1241	liq
	7-187	1232	ol,an,liq
	7-206	1221	ol,an,liq
	7-200	1207	ol,an,cpx,liq

Composition	Run No.	Temperature °C	Result
AF22	7-185	1250	liq
	7-224	1241	liq
	7-187	1232	an,liq
	7-206	1221	an,(ol),liq
	7-200	1207	an,ol,cpx,liq
AF23	7-185	1250	liq
	7-224	1241	liq
	7-187	1232	liq
	7-206	1221	cpx,liq
	7-200	1207	cpx,ol,an,liq
AF24	7-185	1250	liq
	7-224	1241	cpx,liq
	7-187	1232	cpx,liq
	7-206	1221	cpx,liq
	7-200	1207	cpx,ol,an,liq
AF25	7-312	1250	cpx,liq
	7-185	1250	cpx,liq
	7-224	1241	cpx,liq
	7-187	1232	cpx,liq
	7-206	1221	cpx,liq
	7-200	1207	cpx,ol,an,liq
AF26	7-312	1250	cpx,liq
	7-185	1250	cpx,liq
	7-224	1241	cpx,liq
	7-187	1232	cpx,liq
	7-206	1221	cpx,liq
(ii) $\underline{XO.YO.2ZO_2\text{-}5YO.3R_2O_3.5ZO_2}$ ($\underline{Diopside\text{-}M_5A_3S_5}$)			
AF51	7-312	1250	(ol),liq
	7-185	1250	ol,liq
	7-224	1241	ol,liq
	7-187	1232	ol,an,liq
	7-206	1221	ol,an,liq
	7-301	1215	ol,an,liq
	7-200	1207	ol,an,liq

Composition	Run No.	Temperature °C	Result
AF52	7-312	1250	ol,liq
	7-185	1250	ol,liq
	7-224	1241	ol,liq
	7-187	1232	ol,an,liq
	7-206	1221	ol,an,liq
	7-301	1215	ol,liq (*+an)
	7-200	1207	ol,an,liq
AF53	7-185	1250	liq
	7-224	1241	ol,liq
	7-187	1232	ol,liq
	7-206	1221	ol,cpx,liq (*-cpx)
	7-301	1215	ol,liq
	7-200	1207	ol,cpx,an,liq
AF54	7-185	1250	liq
	7-224	1241	liq
	7-187	1232	ol,cpx,liq
	7-206	1221	ol,liq (*+cpx)
	7-301	1215	ol,cpx,liq
	7-200	1207	ol,cpx,liq
AF55	7-312	1250	cpx,liq
	7-185	1250	cpx,liq
	7-224	1241	cpx,liq
	7-187	1232	cpx,liq
	7-206	1221	cpx,liq
	7-301	1215	cpx,ol,liq
	7-200	1207	cpx,ol,liq
AF56	7-312	1250	cpx,liq
	7-185	1250	cpx,liq
	7-224	1241	cpx,liq
	7-187	1232	cpx,liq
	7-206	1221	cpx,liq

Composition	Run No.	Temperature °C	Result
(iii) $YO.ZO_2$-$3XO.R_2O_3.3ZO_2$ (En-Gross)			
1-6-3-1-15	5-153	1310	ol,liq
	7-268	1301	ol,liq
	7-259	1269	ol,pig,liq
	7-213	1262	ol,pig,liq
	5-146	1260	ol,pig,liq
	7-277	1248	ol,pig,liq
	7-226	1238	ol,pig,liq
	7-286	1233	ol,pig,liq
	7-292	1221	ol,pig,liq
	7-174	1206	ol,pig,cpx,liq
	5-159	1200	ol,pig,cpx,liq
	5-286	1190	ol,pig,cpx,liq
	5-271	1174	ol,pig,cpx,liq
1-4-3-1-11	7-141	1307	(ol),liq
	7-268	1301	liq
	7-261	1280	ol,liq
	7-277	1248	ol,liq
	7-226	1238	ol,liq
	7-286	1233	ol,liq
	7-292	1221	ol,cpx,liq
	7-174	1206	ol,cpx,liq
	5-286	1190	ol,cpx,liq
	7-188	1178	ol,cpx,liq
	5-271	1174	ol,cpx,liq
1-3-3-1-9	7-259	1269	liq
	7-213	1262	ol,liq
	7-277	1248	ol,liq
	7-226	1238	ol,liq
	7-286	1233	ol,liq
	5-203	1226	ol,liq
	7-292	1221	ol,(cpx),liq
	7-174	1206	ol,cpx,liq
	5-286	1190	ol,cpx,liq
	7-188	1178	ol,cpx,an,liq
	5-271	1174	ol,cpx,an,liq

Composition	Run No.	Temperature °C	Result
1-2-3-1-7	7-259	1269	liq
	7-277	1248	liq
	7-286	1233	liq
	7-292	1221	cpx,liq
	7-198	1209	cpx,an,(ol),liq
1-1.5-3-1-6	7-259	1269	liq
	7-277	1248	liq
	7-286	1233	liq
	7-292	1221	an,cpx,liq
	7-198	1209	an,cpx,(liq)
1-1-3-1-5	7-259	1269	liq
	7-277	1248	an,liq
	7-286	1233	an,liq
	7-292	1221	an,cpx,liq
	7-256	1210	an,cpx,liq
(iv) $\underline{3XO.R_2O_3.15ZO_2\text{-}YO(C_3AS_{15}\text{-}M)}$			
1-1-3-1-15	7-260	1275	sil,liq
	7-276	1248	sil,liq
	7-292	1221	sil,cpx,liq
	5-265	1210	sil,cpx,liq
	5-272	1172	sil,cpx,liq
1-2-3-1-15	7-260	1275	sil,liq
	7-276	1248	sil,liq
	7-292	1221	sil,pig,cpx,liq
	5-265	1210	sil,pig,cpx,liq
	5-272	1172	sil,pig,cpx,liq
1-3-3-1-15	7-268	1301	sil,liq
	7-259	1269	sil,liq
	7-276	1248	sil,liq
	7-292	1221	sil,pig,cpx?,liq
	5-265	1210	sil,pig,cpx,liq
	5-272	1172	sil,pig,cpx,liq

Composition	Run No.	Temperature °C	Result
1-4-3-1-15	7-268	1301	sil,liq
	7-259	1269	sil,pig,liq
	5-146	1260	sil,pig,liq
	5-157	1254	sil,pig,liq
	7-276	1248	sil,pig,liq
	7-292	1221	sil,pig,cpx?,liq
	5-265	1210	sil,pig,cpx?,liq
	5-159	1200	sil,pig,cpx,liq
	5-272	1172	sil,pig,cpx,liq
1-5-3-1-15	5-153	1310	ol,liq (*-ol)
	7-268	1301	liq
	7-259	1269	pig,liq
	5-146	1260	pig,ol,liq (*-ol)
	5-157	1254	pig,ol,liq (*-ol)
	7-276	1248	pig,liq
	7-292	1221	pig,liq
	5-265	1210	pig,cpx,liq
	5-159	1200	pig,cpx,liq
	5-286	1190	pig,cpx,liq
	5-272	1172	pig,cpx,liq
1-8-3-1-15	7-268	1301	ol,liq
	7-277	1248	ol,liq
	7-292	1221	ol,cpx,liq
	5-286	1190	ol,cpx,pig,liq
	5-272	1172	ol,cpx,pig,liq
(v) $\underline{3XO.R_2O_3\text{-}YO\text{-}ZO_2}$ ($\underline{C_3A\text{-}M\text{-}S}$)			
1-2.5-3-1-7	7-260	1275	liq
1-0.5-3-1-5	7-260	1275	an,liq

Composition	Run No.	Temperature °C	Result
(L) FeO/MgO mole ratio = 2.00			
(i) $YO.ZO_2$-$3XO.R_2O_3.3ZO_2$ (En-Gross)			
2-4-3-1-15	5-153	1310	liq
	7-269	1303	liq
	7-262	1277	liq
	7-260	1275	liq
	5-157	1254	ol,liq
	7-226	1238	ol,liq
	5-203	1226	ol,pig,liq
	7-198	1209	ol,pig,liq
	5-152	1194	ol,pig,liq
	5-274	1174	ol,pig,cpx,liq
	5-161	1148	ol,pig,cpx,liq
2-2.6-3-1-11	7-277	1248	liq
	7-175	1229	ol,liq
	7-174	1206	ol,liq
	7-293	1188	ol,liq
	5-205	1172	ol,cpx,liq
	5-272	1172	ol,cpx,liq
	7-181	1157	ol,cpx,liq
2-2-3-1-9	7-174	1206	liq
	7-293	1188	ol,cpx,liq
	5-271	1174	ol,cpx,liq
	5-205	1172	ol,cpx,liq
	7-181	1157	cl,cpx,(an),liq
2-1.3-3-1-7	5-203	1226	liq
	7-174	1206	cpx,liq
	7-293	1188	cpx,liq
	5-205	1172	cpx,liq
	5-272	1172	cpx,liq
2-1-3-1-6	7-304	1226	an,liq
	7-256	1210	an,liq
	7-293	1188	an,cpx,liq
2-0.6-3-1-5	5-203	1226	an,liq
	7-174	1206	an,cpx,liq
	7-293	1188	an,cpx,liq
	5-205	1172	an,cpx,liq

Composition	Run No.	Temperature °C	Result
(ii) $3XO.R_2O_3.15ZO_2$ - YO (C_3AS_{15}-M)			
2-1-3-1-15	7-260	1275	sil,liq
	7-293	1188	sil,cpx,liq
	5-260	1150	sil,cpx,liq
2-2-3-1-15	7-268	1301	sil,liq
	7-260	1275	sil,liq
	7-293	1188	sil,pig,liq
	5-260	1150	sil,pig,cpx,liq
2-3-3-1-15	7-269	1303	liq
	7-262	1277	sil,liq
	7-260	1275	sil,liq
	7-277	1248	sil,liq
	7-304	1226	sil,pig,liq
	7-293	1188	sil,pig,liq
	5-260	1150	sil,pig,cpx,liq
2-5-3-1-15	7-269	1303	ol,liq
	7-262	1277	ol,liq
	5-146	1260	*Leak
	5-152	1194	ol,cpx,liq
	5-161	1148	ol,cpx,pig,liq

Composition	Run No.	Temperature °C	Result
(M) FeO/MgO mole ratio = 3.00			
(i) $YO.ZO_2$-$3XO.R_2O_3.3ZO_2$ (En-Gross)			
3-3-3-1-15	5-203	1227	(ol),liq
	7-199	1207	ol,liq
	5-152	1194	ol,pig,liq
	5-212	1188	ol,pig,liq
	5-274	1174	ol,pig,liq
	5-161	1148	ol,pig,liq
	5-282	1142	ol,pig,cpx,liq
	5-289	1105	ol,pig,cpx,liq
	5-160	1094	ol,pig,cpx,liq
3-2-3-1-11	7-174	1206	liq
	7-293	1188	liq
	7-189	1163	ol,liq
	5-282	1142	ol,cpx,liq
	7-191	1122	ol,cpx,liq
	5-289	1105	ol,cpx,an,liq
3-1.5-3-1-9	7-198	1209	liq
	7-293	1188	liq
	7-189	1163	cpx,liq
	5-282	1142	cpx,liq
	7-191	1122	cpx,ol,an,liq
3-1-3-1-7	7-174	1206	liq
	7-293	1188	liq
	7-181	1157	an,cpx,liq
	5-282	1142	an,cpx,liq
3-0.75-3-1-6	5-203	1226	liq
	7-198	1209	an,liq
	7-293	1188	an,liq
	7-189	1163	an,cpx,liq
	5-282	1142	an,cpx,liq
(ii) $3XO.R_2O_3.15ZO_2$-$YO(C_3AS_{15}$-M)			
3-5-3-1-15	5-152	1194	ol,liq

Composition	Run No.	Temperature °C	Result
(N) FeO/MgO mole ratio = 4.00			
(i) $3XO.R_2O_3.15ZO_2$-$YO(C_3AS_{15}$-M)			
4-2-3-1-15	7-319	1274	liq
4-4-3-1-15	5-152	1194	ol,liq
(O) FeO/MgO mole ratio = 5.00			
(i) $YO.ZO_2$-$3XO.R_2O_3.3ZO_2$ (En-Gross)			
5-2-3-1-15	7-303	1210	liq
	7-302	1209	liq
	5-317	1160	ol,pig,liq
	5-327	1129	ol,pig,sil,liq
	5-326	1099	ol,pig,sil,liq
(P) FeO/MgO mole ratio = 6.00			
(i) $3XO.R_2O_3.15ZO_2$-YO (C_3AS_{15}-M)			
6-3-3-1-15	5-152	1192	ol,liq
(Q) FeO/MgO mole ratio = 7.00			
(i) $YO.ZO_2$-$3XO.R_2O_3.3ZO_2$ (En-Gross)			
7-1.5-3-1-15	7-303	1210	liq
	7-302	1209	liq
	5-317	1160	ol,(sil),liq
	5-327	1129	ol,sil,pig,liq
	5-326	1099	ol,sil,pig,liq
	5-325	1063	ol,sil,pig,cpx,liq
7-1.2-3-1-12.6	7-303	1210	liq
	7-302	1209	liq
	5-317	1160	liq
	5-327	1129	ol,liq
	5-326	1099	ol,pig,liq
	5-325	1063	ol,pig,cpx,sil,liq
7-1-3-1-11	7-303	1210	liq
	7-302	1209	liq
	5-326	1099	liq
	5-325	1063	ol,cpx,an,liq

Composition	Run No.	Temperature °C	Result
7-0.75-3-1-9	7-303	1210	liq
	7-302	1209	liq
	5-327	1129	liq
	5-326	1099	an,cpx,liq
	5-325	1063	an,cpx,ol?,liq
(R) FeO/MgO mole ratio = no MgO present			
(i) $YO.ZO_2$-$3XO.R_2O_3$.$3ZO_2$ (En-Gross)			
12-X-3-1-15	7-292	1221	liq
	7-199	1207	sil,liq
	7-188	1178	sil,liq
	5-282	1142	sil,liq
	5-289	1105	sil,liq
	5-288	1090	sil,ol,liq
	7-177	1065	sil,ol,liq
	5-325	1063	sil,ol,liq
	5-330	1039	an,sil,ol,woll
8-X-3-1-11	7-303	1210	liq
	7-302	1209	liq
	5-326	1099	liq
	5-325	1063	an,liq
	5-330	1039	an,sil,ol,woll
6-X-3-1-9	7-199	1207	liq
	7-189	1163	liq
	5-282	1142	liq
	7-180	1121	liq
	5-289	1105	(an),liq
	5-288	1090	an,liq
	7-177	1065	an,liq
	5-325	1063	an,liq
	5-330	1039	an,ol,woll,sil?

Composition	Run No.	Temperature °C	Result
4-X-3-1-7	7-304	1227	liq
	7-199	1207	an,liq
	7-293	1188	an,liq
	7-189	1163	an,liq
	5-282	1142	an,liq
	7-180	1121	an,liq
	5-289	1105	an,liq
	5-288	1090	an,woll,liq
	7-177	1065	an,woll,liq
3-X-3-1-6	7-261	1280	liq
	7-199	1207	an,liq
	7-293	1188	an,liq
	7-189	1163	an,liq
	7-180	1121	an,liq
	5-289	1105	an,liq
	5-288	1090	an,woll,liq
	7-177	1065	an,woll,liq

E.3.2. Results at the NiNiO Equilibrium

Composition	Run No.	Temperature °C	Result
A) FeO/MgO mole ratio = 0.074			
i) $3XO.R_2O_3.15ZO_2$ - YO (C_3AS_{15}-M)			
0.074-9-3-1-15	5-162	1256	ol,pig,cpx,liq
B) FeO/MgO mole ratio = 0.125			
i) $3XO.R_2O_3.15ZO_2$ - YO (C_3AS_{15}-M)			
0.125-6-3-1-15	5-164	1291	sil,pig,liq
	5-162	1256	sil,pig,cpx,liq
0.125-8-3-1-15	5-164	1291	pig,liq
	5-162	1256	pig,cpx,liq
C) FeO/MgO mole ratio = 0.18			
i) $XO.YO.2ZO_2$ - $YO.R_2O_3.ZO_2$ (Diopside-MAS)			
AF1	3-290	1316	ol,liq
	3-295	1305	ol,liq
	3-274	1290	ol,an,liq
	3-267	1277	ol,an,liq
AF2	3-274	1290	ol,liq
	3-267	1277	ol,cpx,an,liq
AF3	3-290	1316	ol,liq
	3-295	1305	ol,cpx,liq
	3-274	1290	ol,cpx,liq
	3-267	1277	ol,cpx,an,liq
AF4	3-290	1316	cpx,liq
	3-295	1305	cpx,ol,liq
	3-274	1290	cpx,ol,liq
	3-268	1274	cpx,ol,an,liq
ii) $XO.YO.2ZO_2$ - $5YO.3R_2O_3.5ZO_2$ (Diopside-$M_5A_3S_5$)			
AF31	3-290	1316	ol,liq
	3-295	1305	ol,liq
	3-274	1290	ol,an,liq
	3-293	1290	ol,an,liq
	3-267	1277	ol,an,liq

Composition	Run No.	Temperature °C	Result
AF32	3-290	1316	ol,liq
	3-274	1290	ol,cpx,liq (*-cpx)
	3-293	1290	ol,an,liq
	3-267	1277	ol,cpx,an,liq
AF33	3-290	1316	ol,liq
	3-295	1305	ol,liq
	3-274	1290	ol,liq
	3-293	1290	ol,cpx,liq
	3-267	1277	ol,cpx,an,liq
AF34	3-290	1316	ol,liq
	3-295	1305	ol,cpx,liq
	3-274	1290	ol,cpx,liq
	3-267	1277	ol,cpx,liq
AF35	3-290	1316	ol,cpx,liq
	3-274	1290	ol,cpx,liq
	3-268	1274	ol,cpx,liq
AF36	3-290	1316	ol,cpx,liq
	3-274	1290	ol,cpx,liq
	3-268	1274	ol,cpx,liq
D) FeO/MgO mole ratio = 0.20			
i) $YO.ZO_2$ - $3XO.R_2O_3.3ZO_2$ (En-Gross)			
0.2-10-3-1-15	3-296	1305	ol,pig,liq
	5-162	1256	ol,pig,cpx,liq
0.2-6.6̇-3-1-11	3-296	1305	ol,cpx,(pig),liq
0.2-5-3-1-9	3-296	1305	ol,cpx,liq
0.2-3.3̇-3-1-7	3-296	1305	ol,(cpx),liq
0.2-2.5-3-1-6	3-295	1305	liq
	3-293	1290	(cpx),liq
	3-298	1260	cpx,ol,an,liq
0.2-1.6̇-3-1-5	3-298	1260	an,cpx,liq

Composition	Run No.	Temperature °C	Result
E) FeO/MgO mole ratio = 0.25			
i) $3XO.R_2O_3.15ZO_2$ - YO (C_3AS_{15}-M)			
0.25-6-3-1-15	5-162	1256	sil,pig,cpx,liq
0.25-9-3-1-15	5-162	1256	ol,pig,cpx,liq
F) FeO/MgO mole ratio = $0.3\dot{3}$			
i) $YO.ZO_2$ - $3XO.R_2O_3.3ZO_2$ (En-Gross)			
$0.\dot{3}$-9-3-1-15	5-162	1256	ol,pig,cpx,liq
$0.\dot{3}$-6-3-1-11	3-290	1316	ol,pig,liq
	3-296	1305	ol,pig,cpx,liq
	3-275	1290	ol,pig,cpx,liq
	3-298	1260	ol,pig,cpx,liq
$0.\dot{3}$-4.5-3-1-9	3-290	1316	ol,liq
	3-296	1305	ol,cpx,liq
	3-293	1290	ol,cpx,liq
	3-292	1276	ol,cpx,pig,liq
	3-298	1260	ol,cpx,pig,liq
$0.\dot{3}$-3-3-1-7	3-290	1316	liq
	3-296	1305	(ol),liq
	3-293	1290	ol,cpx,liq
	3-292	1276	ol,cpx,liq
	3-298	1260	ol,cpx,an,liq
	3-294	1244	ol,cpx,an,liq
$0.\dot{3}$-2.25-3-1-6	3-293	1290	liq
	3-292	1276	cpx,liq
	3-297	1260	an,cpx,ol,liq
	3-294	1244	an,cpx,ol,liq
$0.\dot{3}$-1.5-3-1-5	3-293	1290	liq
	3-292	1276	liq
	3-297	1260	an,liq
	3-294	1244	an,cpx,liq

Composition	Run No.	Temperature °C	Result
G) FeO/MgO mole ratio = 0.50			
i) $XO.YO.2ZO_2$ - $YO.R_2O_3.ZO_2$ (Diopside-MAS)			
AF11	3-290	1316	liq
	3-295	1305	(an),(ol),liq
	3-274	1290	an,ol,liq
	3-293	1290	an,ol,liq
	3-268	1274	an,ol,liq
	3-272	1259	an,ol,cpx,liq
	3-271	1245	an,ol,cpx,liq
AF12	3-290	1316	liq
	3-295	1305	liq
	3-274	1290	cpx,liq (*-cpx)
	3-293	1290	liq
	3-268	1274	ol,liq
	3-272	1259	ol,cpx,an,liq
	3-271	1245	ol,cpx,an,liq
AF13	3-290	1316	liq
	3-295	1305	liq
	3-274	1290	(cpx),liq
	3-293	1290	cpx,liq
	3-268	1274	cpx,liq
	3-272	1259	cpx,an,ol,liq
	3-271	1245	cpx,an,ol,liq
AF14	3-295	1305	liq
	3-274	1290	cpx,liq
	3-267	1277	cpx,liq
AF15	3-274	1290	cpx,liq
	3-268	1274	cpx,liq
AF16	3-274	1290	cpx,liq
	3-268	1274	cpx,liq
ii) $XO.YO.2ZO_2$ - $5YO.3R_2O_3.5ZO_2$ (Diopside-$M_5A_3S_5$)			
AF41	3-275	1290	ol,(an),liq
	3-267	1277	ol,an,liq
	3-272	1259	ol,an,(cpx)?,liq
	3-270	1245	ol,an,cpx,liq
	3-269	1230	ol,an,cpx,liq

Composition	Run No.	Temperature °C	Result
AF42	3-295	1305	ol,liq
	3-275	1290	ol,liq
	3-267	1277	ol,(an),liq
	3-272	1259	ol,an,cpx,liq
	3-270	1245	ol,an,cpx,liq
	3-269	1230	ol,an,cpx,liq
AF43	3-295	1305	ol,liq
	3-275	1290	ol,liq
	3-267	1277	ol,cpx,liq
	3-272	1259	ol,cpx,(an),liq
	3-270	1245	ol,cpx,an,liq
AF44	3-295	1305	liq
	3-275	1290	(cpx),(ol),liq
	3-267	1277	ol,cpx,liq
	3-272	1259	ol,cpx,liq
	3-270	1245	ol,cpx,an,liq
AF45	3-295	1305	cpx,liq
	3-275	1290	cpx,liq
	3-267	1277	cpx,ol?,liq
AF46	3-275	1290	cpx,liq
	3-267	1277	cpx,liq

iii) $YO.ZO_2$ - $3XO.R_2O_3.3ZO_2$ (En-Gross)

0.5-8-3-1-15	3-290	1316	pig,(ol),liq
	5-164	1291	pig,ol,cpx,liq
	3-273	1275	pig,ol,cpx,liq
	5-162	1256	pig,ol,cpx,liq
	5-163	1199	ol,(pig),liq **error
0.5-5.$\dot{3}$-3-1-11	3-290	1316	ol,pig,liq
	3-275	1290	ol,pig,cpx,liq
	3-273	1275	ol,pig,cpx,liq
	3-297	1260	ol,pig,cpx,liq
	3-294	1244	ol,pig,cpx,liq

Composition	Run No.	Temperature °C	Result
0.5-4-3-1-9	3-290	1316	ol,liq
	3-296	1305	ol,(cpx),liq
	3-275	1290	ol,cpx,liq
	3-268	1274	ol,cpx,pig,liq
	3-297	1260	ol,cpx,pig,liq
	3-294	1244	ol,cpx,pig,liq
0.5-2.$\dot{6}$-3-1-7	3-296	1305	liq
	3-293	1290	(cpx),liq
	3-273	1275	cpx,liq
	3-297	1260	ol,cpx,liq
	3-271	1245	ol,cpx,an,liq
0.5-2-3-1-6	3-293	1290	liq
	3-268	1274	(cpx),liq
	3-297	1260	cpx,liq
	3-271	1245	cpx,an,liq
0.5-1.$\dot{3}$-3-1-5	3-293	1290	liq
	3-273	1275	(an),liq
	3-297	1260	an,cpx,liq
	3-271	1245	an,cpx,liq
iv) $3XO.R_2O_3.15ZO_2$ - YO (C_3AS_{15}-M)			
0.5-1-3-1-15	3-298	1260	sil,liq
	3-299	1208	sil,cpx,liq
0.5-2-3-1-15	3-298	1260	sil,cpx,liq
	3-299	1208	sil,cpx,pig,liq
0.5-3-3-1-15	3-298	1260	sil,cpx,pig,liq
	3-299	1208	sil,cpx,pig,liq
0.5-4-3-1-15	3-298	1260	sil,cpx,pig,liq
	3-299	1208	sil,cpx,pig,liq
0.5-6-3-1-15	3-296	1305	sil,pig,liq
	3-292	1276	sil,pig,cpx,liq
	3-298	1260	sil,pig,cpx,liq
	3-299	1208	sil,pig,cpx,liq
0.5-9-3-1-15	3-296	1305	ol,pig,liq
0.5-12-3-1-15	3-299	1208	ol,cpx,(sp),liq
0.5-16-3-1-15	3-299	1208	ol,sp,liq

Composition	Run. No.	Temperature °C	Result
H) FeO/MgO mole ratio = 0.55			
i) $3XO.R_2O_3.15ZO_2$ - YO (C_3AS_{15}-M)			
0.55-5-3-1-15	3-296	1305	sil,pig,liq
	5-164	1291	sil,pig,cpx,liq
	5-162	1256	sil,pig,cpx,liq
	5-163	1199	sil,pig,cpx,liq
I) FeO/MgO mole ratio = 0.75			
i) $3XO.R_2O_3.15ZO_2$ - YO (C_3AS_{15}-M)			
0.75-8-3-1-15	5-162	1256	ol,pig,liq
J) FeO/MgO mole ratio = 1.00			
i) $XO.YO.2ZO_2$ - $YO.R_2O_3.ZO_2$ (Diopside-MAS)			
AF21	3-292	1276	an,liq
	3-272	1259	an,liq
	3-270	1245	an,liq
	3-294	1244	an,liq
	3-269	1230	an,cpx,liq
	3-277	1214	an,cpx,ol,liq
	3-255	1200	an,cpx,ol,liq?
AF22	3-297	1260	an,liq
	3-270	1245	(cpx)?,liq
	3-294	1244	an,(cpx),liq
	3-269	1230	an,cpx,liq
	3-277	1214	an,cpx,(ol),liq
	3-255	1200	an,cpx,ol,liq
AF23	3-292	1276	liq
	3-272	1259	cpx,liq
	3-270	1245	cpx,liq
	3-294	1244	cpx,liq
	3-269	1230	cpx,an,liq
	3-277	1214	cpx,an,liq
	3-255	1200	cpx,an,ol,liq

Composition	Run No.	Temperature °C	Result
AF24	3-295	1305	liq
	3-275	1290	(cpx),liq
	3-272	1259	cpx,liq
	3-270	1245	cpx,liq
	3-269	1230	cpx,an,liq
	3-277	1214	cpx,an,liq
	3-255	1200	cpx,an,ol,liq
AF25	3-295	1305	liq
	3-275	1290	cpx,liq
	3-268	1274	cpx,liq
	3-272	1259	cpx,liq
	3-270	1245	cpx,liq
	3-269	1230	cpx,an,liq
	3-277	1214	cpx,an,liq
AF26	3-275	1290	cpx,liq
	3-268	1274	cpx,liq
	3-272	1259	cpx,liq
	3-270	1245	cpx,liq
	3-269	1230	cpx,liq
	3-277	1214	cpx,liq
ii) $XO.YO.2ZO_2$ - $5YO.3R_2O_3.5ZO_2$ (Diopside-$M_5A_3S_5$)			
AF51	3-292	1276	an,liq
	3-297	1260	an,liq
	3-270	1245	an,(ol),liq
	3-294	1244	an,liq
	3-269	1230	an,cpx,ol,liq
	3-291	1226	an,cpx,ol,liq
	3-277	1214	an,cpx,ol,liq
	3-255	1200	an,cpx,ol,liq
AF52	3-297	1260	liq
	3-270	1245	cpx,(an),liq (*-cpx)
	3-294	1244	an,liq
	3-269	1230	an,(ol),(cpx),liq
	3-277	1214	an,ol,cpx,liq
	3-255	1200	an,ol,cpx,liq

Composition	Run No.	Temperature °C	Result
AF53	3-292	1276	liq
	3-297	1260	liq
	3-272	1259	liq
	3-270	1245	cpx,liq
	3-294	1244	cpx,liq
	3-269	1230	cpx,an,liq
	3-277	1214	cpx,an,(ol),liq
	3-255	1200	cpx,an,ol,liq
AF54	3-293	1290	liq
	3-292	1276	cpx,liq
	3-297	1260	cpx,liq
	3-270	1245	cpx,liq
	3-269	1230	cpx,an,liq
	3-277	1214	cpx,an,liq
	3-256	1205	cpx,an,ol,liq
AF55	3-295	1305	(cpx),liq
	3-275	1290	cpx,liq
	3-268	1274	cpx,liq
	3-270	1245	cpx,liq
	3-269	1230	cpx,an,liq
	3-277	1214	cpx,an,liq
	3-256	1205	cpx,an,liq
AF56	3-275	1290	cpx,liq
	3-268	1274	cpx,liq
	3-270	1245	cpx,liq
	3-269	1230	cpx,liq
	3-277	1214	cpx,liq

iii) $YO.ZO_2$ - $3XO.R_2O_3.3ZO_2$ (En-Gross)

1-6-3-1-15	3-296	1305	pig,liq
	3-293	1290	pig,liq
	3-273	1275	pig,liq
	3-297	1260	pig,liq
	3-294	1244	pig,cpx,liq
	3-291	1226	pig,cpx,ol,liq

Composition	Run No.	Temperature °C	Result
1-4-3-1-11	3-296	1305	liq
	3-275	1290	(pig),liq
	3-273	1275	pig,liq
	3-297	1260	pig,cpx,liq
	3-271	1245	pig,cpx,liq
	3-291	1226	pig,cpx,ol,liq
1-3-3-1-9	3-268	1274	liq
	3-297	1260	cpx,liq
	3-271	1245	cpx,(pig),liq
	3-291	1226	cpx,pig,ol,liq
1-2-3-1-7	3-292	1276	liq
	3-297	1260	cpx,liq
	3-271	1245	cpx,liq
	3-291	1226	cpx,an,ol,liq
	3-276	1207	cpx,an,ol,liq
1-1.5-3-1-6	3-292	1276	liq
	3-297	1260	liq
	3-271	1245	cpx,an,liq
	3-291	1226	cpx,an,liq
	3-276	1207	fine grained
1-1-3-1-5	3-296	1305	liq
	3-275	1290	(an),liq
	3-297	1260	*leaked out
	3-271	1245	an,cpx,liq
	3-291	1226	an,cpx,liq

iv) $3XO.R_2O_3.15ZO_2$ - YO (C_3AS_{15}-M)

1-1-3-1-15	3-299	1208	sil,cpx,liq
1-2-3-1-15	3-299	1208	sil,cpx,liq
1-3-3-1-15	3-298	1260	sil,liq
	3-299	1208	sil,cpx,pig,liq
1-4-3-1-15	3-296	1305	sil,liq
	5-162	1256	sil,pig,liq
	5-163	1199	sil,pig,cpx,liq
	5-165	1158	sil,pig,cpx,liq

Composition	Run No.	Temperature °C	Result
1-5-3-1-15	3-296	1305	sil,(pig),liq
	5-164	1291	sil,pig,liq
	5-162	1256	sil,pig,liq
1-8-3-1-15	3-298	1260	ol,pig,liq
	3-299	1208	ol,pig,cpx,liq

K) FeO/MgO mole ratio = 2.00

i) $YO.ZO_2 - 3XO.R_2O_3.3ZO_2$ (En-Gross)

2-4-3-1-15	3-273	1275	sil,liq
	3-298	1260	sil,liq
	3-294	1244	sil,(pig),liq
	3-291	1226	sil,pig,liq
	3-264	1206	sil,pig,liq
	3-300	1184	sil,pig,liq
2-2.$\dot{6}$-3-1-11	3-292	1276	liq
	3-291	1226	liq
	3-264	1206	cpx,pig,liq
	3-300	1184	cpx,pig,liq
2-2-3-1-9	3-291	1226	liq
	3-264	1206	cpx,liq
	3-300	1184	cpx,liq
2-1.$\dot{3}$-3-1-7	3-291	1226	(an),liq
	3-264	1206	an,cpx,liq
	3-300	1184	an,cpx,liq
2-1-3-1-6	3-293	1290	liq
	3-292	1276	liq
	3-298	1260	liq
	3-294	1244	(an),liq
	3-291	1226	an,liq
	3-264	1206	an,cpx,liq
	3-300	1184	an,cpx,liq
2-0.$\dot{6}$-3-1-5	3-275	1290	an,liq
	3-273	1275	an,liq
	3-264	1206	an,cpx,liq

Composition	Run No.	Temperature °C	Result
ii) $3XO.R_2O_3.15ZO_2$ - YO (C_3AS_{15}-M)			
2-1-3-1-15	3-299	1208	sil,liq
	3-301	1159	sil,cpx,liq
2-2-3-1-15	3-298	1260	sil,liq
	3-299	1208	sil,liq
	3-301	1159	sil,cpx,liq
2-3-3-1-15	3-298	1260	sil,liq
	3-301	1159	sil,pig,liq
2-5-3-1-15	3-299	1208	ol,pig,liq
L) FeO/MgO mole ratio = 3.00			
i) $YO.ZO_2$ - $3XO.R_2O_3.3ZO_2$ (En-Gross)			
3-3-3-1-15	3-293	1290	sil,liq
	3-273	1275	sil,liq
	3-294	1244	sil,liq
	3-264	1206	sil,pig,liq
	3-300	1184	sil,pig,liq
	3-301	1159	sil,pig,sp,liq
	5-165	1158	sil,pig,liq
	3-302	1135	sil,pig,sp,liq
3-2-3-1-11	3-264	1206	liq
	3-300	1184	liq
	3-301	1159	pig,cpx,liq
	3-302	1135	pig,cpx,sp,liq
3-1.5-3-1-9	3-291	1226	liq
	3-264	1206	liq
	3-300	1184	liq
	3-301	1159	cpx,(an),liq
	3-302	1135	cpx,an,liq
3-1-3-1-7	3-291	1226	liq
	3-264	1206	liq
	3-300	1184	an,cpx,liq
	3-301	1159	an,cpx,liq
	3-302	1135	an,cpx,sp,liq

Composition	Run No.	Temperature °C	Result
3-0.75-3-1-6	3-298	1260	liq
	3-294	1244	(an),liq
	3-264	1206	an,liq
	3-300	1184	an,liq
	3-301	1159	an,cpx,liq
3-0.5-3-1-5	3-273	1275	an,liq
	3-264	1206	an,liq

M) FeO/MgO mole ratio = 5.00

i) $3XO.R_2O_3.15ZO_2$ - YO (C_3AS_{15}-M)

5-2-3-1-15	3-309	1207	sil,liq
	3-301	1159	sil,pig,sp,liq
	3-302	1135	sil,pig,sp,liq

N) FeO/MgO mole ratio = 7.00

i) $YO.ZO_2$ - $3XO.R_2O_3.3ZO_2$ (En-Gross)

7-1.5-3-1-15	3-309	1207	sil,liq
	3-300	1184	sil,sp,liq
	3-301	1159	sil,sp,liq
	3-302	1135	sil,sp,(pig),liq
7-1.2-3-1-12.6	3-309	1207	liq
	3-300	1184	sil,sp,liq
	3-301	1159	sil,sp,liq
	3-302	1135	sil,sp,liq
7-1-3-1-11	3-300	1184	liq
	3-301	1159	sil,sp,liq
	3-302	1135	sil,sp,liq
7-0.75-3-1-9	3-300	1184	liq
	3-301	1159	liq
	3-302	1135	liq
	3-307	1121	liq
	3-263	1100	cpx,an,sp,liq (fine grained)

Composition	Run No.	Temperature °C	Result
0) FeO/MgO mole ratio = no MgO present			
i) $YO.ZO_2$ - $3XO.R_2O_3.3ZO_2$ (En-Gross)			
12-X-3-1-15	3-296	1305	sil,liq
	3-292	1276	sil,liq
	3-273	1275	sil,sp,liq
	3-264	1206	sil,liq
	3-300	1184	sil,sp,liq
	3-301	1159	sil,sp,liq
	3-302	1135	sil,sp,liq
	3-263	1100	sil,sp,liq
8-X-3-1-11	3-264	1206	liq
	3-300	1184	liq
	3-301	1159	sil,sp,liq
	3-302	1135	sil,sp,liq
	3-263	1100	sil,sp,liq
6-X-3-1-9	3-264	1206	liq
	3-300	1184	liq
	3-301	1159	liq
	3-302	1135	sp,liq
4-X-3-1-7	3-298	1260	liq
	3-294	1244	an,liq
	3-264	1206	an,liq
	3-300	1184	an,liq
	3-301	1159	an,liq
	3-302	1135	an,liq
	3-307	1121	an,liq
3-X-3-1-6	3-292	1276	liq
	3-294	1244	an,liq
	3-264	1206	an,liq
	3-301	1159	an,liq
	3-302	1135	an,liq
	3-307	1121	an,liq
	3-263	1100	an,sp,liq
2-X-3-1-5	3-273	1275	an,liq

E.3.3. RESULTS IN AIR ATMOSPHERE

These results were obtained by Dr. G.M. Biggar on the same compositions used in this thesis, and presented in diagrammatic form by Clarke and Biggar (1972).

All compositions are in the join $3XO.R_2O_3.15ZO_2$ - $YO(C_3AS_{15}-M)$.

Composition	Run No.	Temperature °C	Result
A) FeO/MgO mole ratio = 0.074			
0.074-9-3-1-15	6-45	1352	ol,pen,liq
	5-77	1253	opx,(ol),cpx,liq
	6-44	1206	opx,cpx,an,liq
B) FeO/MgO mole ratio = 0.125			
0.125-6-3-1-15	6-45	1352	(pen),liq
	3-65	1307	sil,opx,liq
	6-44	1206	sil,opx,cpx,liq
0.125-8-3-1-15	6-45	1352	pen,(ol),liq
	3-65	1307	opx,liq
	5-63	1252	opx,cpx,liq
C) FeO/MgO mole ratio = 0.20			
0.2-10-3-1-15	3-65	1307	ol,opx,liq
D) FeO/MgO mole ratio = 0.25			
0.25-6-3-1-15	6-45	1352	pen,liq
	3-65	1307	sil,opx,liq
	5-77	1253	opx,liq (?+sil)
	6-44	1206	opx,cpx,liq (?+sil)
0.25-9-3-1-15	6-45	1352	ol,(pen),liq
	3-65	1307	ol,opx,liq
	5-77	1253	ol,opx,liq
	6-44	1206	opx,cpx,an,liq
E) FeO/MgO mole ratio = 0.33			
0.33-9-3-1-15	6-45	1352	ol,pen,liq
	3-65	1307	ol,opx,pen,liq
F) FeO/MgO mole ratio = 0.5			
0.5-2-3-1-15	5-63	1252	sil,(cpx),liq
0.5-3-3-1-15	6-44	1206	sil,cpx,liq
0.5-4-3-1-15	3-65	1307	sil,liq
	5-108	c.1254	sil,(opx),liq
	6-44	1206	sil,opx,cpx,liq

Composition	Run No.	Temperature °C	Result
0.5-6-3-1-15	6-44	1206	sp,(hem),opx,cpx,liq
0.5-8-3-1-15	5-108	c.1254	sp,opx,ol,liq
	6-44	1206	fine grained
0.5-9-3-1-15	6-45	1352	ol,(pen),liq
	3-65	1307	ol,pen,(sp),liq
0.5-12-3-1-15	3-65	1307	sp,ol,(pen),liq
	5-77	1253	sp,ol,opx,liq
G) FeO/MgO mole ratio = 0.55			
0.55-5-3-1-15	3-65	1307	sil,liq
H) FeO/MgO mole ratio = 0.75			
0.75-8-3-1-15	6-45	1352	liq
	3-65	1307	sp,pen,(ol),liq
	6-44	1206	sp,hem,opx,cpx
I) FeO/MgO mole ratio = 1.0			
1-4-3-1-15	5-108	c.1254	liq
1-8-3-1-15	6-44	1206	hem,sp,cpx,liq
1-12-3-1-15	3-65	1307	ol,sp,liq
	5-63	1252	ol,sp,opx,liq
	6-44	1206	sp,liq + ??
J) FeO/MgO mole ratio = 2.0			
2-2-3-1-15	5-108	c.1254	sil,hem,liq

E.4. Natural Compositions

Composition: Re 331

Run No.	Temperature °C	pO_2	Result
a) FeFeO equilibrium			
5-179	1397	- 9.50	ol,liq
5-185	1307	-10.67	ol,liq
5-189	1258	-11.24	ol,liq
5-190	1204	-11.97	ol,liq
7-161	1190	-12.53	ol,plag,liq
7-119	1180	-12.48	ol,plag,cpx,liq
7-157	1167	-12.83	ol,plag,cpx,liq
7-121	1156	-12.82	ol,plag,cpx,liq
7-133	1130	-13.16	ol,plag,cpx,sp,liq
7-130	1064	-14.16	ol,plag,cpx,sp
b) NiNiO equilibrium			
5-163	1199	- 7.85	ol,liq
3-333	1191	- 7.92	ol,cpx,liq
3-79	1183	- 7.92	ol,cpx,(plag),liq
3-66	1167	- 8.10	ol,cpx,plag,sp,liq
c) other pO_2			
3-349	1236	- 6.27	ol,sp,liq
3-339	1210	- 6.57	ol,sp,liq
3-340	1206	- 3.82	ol,cpx,sp,liq
3-343	1193	- 3.88	ol,cpx,sp,liq
3-342	1192	- 6.75	ol,cpx,sp,liq
3-347	1148	- 4.09	ol,cpx,plag,sp,liq

Composition: Re 75

Run No.	Temperature °C	pO_2	Result
a) FeFeO equilibrium			
7-221	1397	- 9.63	liq
5-185	1307	-10.67	ol,liq
7-264	1278	-11.01	ol,liq
5-189	1258	-11.24	ol,liq
5-177	1232	-11.58	ol,liq
5-190	1204	-11.97	ol,liq
7-161	1190	-12.53	ol,liq
7-119	1180	-12.48	ol,liq
7-157	1167	-12.83	ol,plag,cpx,liq
7-121	1156	-12.82	ol,plag,cpx,liq
7-133	1130	-13.16	ol,plag,cpx,liq
7-130	1064	-14.16	ol,plag,cpx,sp
b) NiNiO equilibrium			
5-163	1199	- 7.85	ol,liq
3-333	1191	- 7.92	ol,(cpx),liq
3-79	1183	- 7.92	ol,cpx,liq
3-66	1167	- 8.10	ol,cpx,plag,liq
3-345	1148	- 8.33	ol,cpx,plag,sp,liq
3-346	1136	- 8.47	ol,cpx,plag,sp,liq
3-332	1123	- 8.67	ol,cpx,plag,sp,liq
c) Other pO_2			
3-349	1236	- 6.27	ol,(sp),liq
3-339	1210	- 6.57	ol,sp,liq
3-340	1206	- 3.82	ol,cpx,sp,liq
3-343	1193	- 3.88	ol,cpx,sp,liq
3-342	1192	- 6.75	ol,cpx,sp,liq
3-347	1148	- 4.09	ol,cpx,plag,sp,liq

Composition: Re 243

Run No.	Temperature °C	pO_2	Result
a) FeFeO equilibrium			
7-221	1397	- 9.63	liq
5-185	1307	-10.67	ol,liq
7-264	1278	-11.01	ol,liq
5-189	1258	-11.24	ol,liq
5-177	1232	-11.58	ol,liq
5-190	1204	-11.97	ol,liq
7-161	1190	-12.53	ol,liq
7-119	1180	-12.48	ol,liq
7-157	1167	-12.83	ol,plag,cpx,liq
7-121	1156	-12.82	ol,plag,cpx,liq
7-133	1130	-13.16	ol,plag,cpx,liq
7-134	1108	-13.49	ol,plag,cpx,sp,liq
7-129	1066	-14.12	ol,plag,cpx,sp
b) NiNiO equilibrium			
5-163	1199	- 7.85	ol,liq
3-333	1191	- 7.92	(* capsule melted)
3-334	1191	- 7.90	ol,(cpx),liq
3-79	1183	- 7.92	ol,cpx,(plag),liq
3-66	1167	- 8.10	ol,cpx,plag,liq
3-345	1148	- 8.33	ol,cpx,plag,sp,liq
3-346	1136	- 8.47	ol,cpx,plag,sp,liq
3-332	1123	- 8.67	ol,cpx,plag,sp,liq
c) other pO_2			
3-349	1236	- 6.27	ol,sp,liq
3-339	1210	- 6.57	ol,sp,liq
3-340	1206	- 3.82	ol,cpx,sp,liq
3-343	1193	- 3.88	ol,cpx,sp,liq
3-342	1192	- 6.75	ol,cpx,sp,liq
3-347	1148	- 4.09	ol,cpx,plag,sp,liq

Composition: Re 134

Run No.	Temperature °C	pO_2	Result
a) FeFeO equilibrium			
7-141	1307	-11.11	liq
7-264	1278	-11.01	liq
5-189	1258	-11.24	ol,liq
5-190	1204	-11.97	ol,liq
7-161	1190	-12.53	ol,liq
5-212	1188	-12.08	ol,(plag),liq
7-119	1180	-12.48	ol,plag,liq
7-157	1167	-12.83	ol,plag,(cpx),liq
7-121	1156	-12.82	ol,plag,cpx,liq
7-133	1130	-13.16	ol,plag,cpx,liq
7-134	1108	-13.49	ol,plag,cpx,sp,liq
7-129	1066	-14.12	ol,plag,cpx,sp
b) NiNiO equilibrium			
3-330	1202	- 7.76	ol,liq
3-333	1191	- 7.92	ol,liq
3-334	1191	- 7.90	ol,liq
3-80	1183	- 7.88	ol,plag,liq
3-331	1170	- 8.17	ol,plag,liq
5-165	1158	- 8.23	ol,plag,cpx,liq
3-76	1148	- 8.30	ol,plag,cpx,liq
3-346	1136	- 8.47	ol,plag,cpx,sp,liq
3-332	1123	- 8.67	ol,plag,cpx,sp,liq
c) other pO_2			
3-349	1236	- 6.27	ol,sp,liq
3-339	1210	- 6.57	ol,sp,liq
3-340	1206	- 3.82	ol,sp,liq
3-343	1193	- 3.88	ol,sp,liq
3-342	1192	- 6.75	ol,sp,liq
3-347	1148	- 4.09	ol,plag,cpx,sp,liq

Composition: Re 171

Run No.	Temperature °C	pO_2	Result
a) FeFeO equilibrium			
7-235	1205	-12.34	ol,liq
5-274	1174	-12.26	ol,plag,liq
5-275	1148	-12.63	ol,plag,cpx,liq
5-283	1134	-12.82	ol,plag,cpx,liq
5-222	1113	-13.21	ol,plag,cpx,sp,liq
b) NiNiO equilibrium			
3-336	1228	- 7.46	(ol),liq
3-337	1219	- 7.56	ol,liq
3-328	1206	- 7.73	ol,liq
3-333	1191	- 7.92	ol,plag,liq
3-331	1170	- 8.17	ol,plag,liq
3-335	1160	- 8.27	ol,plag,cpx,liq
3-345	1148	- 8.33	ol,plag,cpx,sp,liq
3-346	1136	- 8.47	ol,plag,cpx,sp,liq
c) other pO_2			
3-349	1236	- 6.27	sp,liq
3-350	1210	- 6.55	ol,sp,liq
3-351	1208	- 3.82	sp,liq
3-343	1193	- 3.88	ol,plag,sp,liq
3-347	1148	- 4.09	ol,plag,cpx,sp,liq

Composition: Re 170

Run No.	Temperature °C	pO_2	Result
a) FeFeO equilibrium			
7-217	1248	-11.82	liq
7-175	1230	-12.05	ol,liq
5-190	1204	-11.97	ol,liq
7-119	1180	-12.48	ol,liq
7-157	1167	-12.83	ol,plag,liq
7-121	1156	-12.82	ol,plag,liq
7-170	1143	-13.20	ol,plag,cpx,liq
7-133	1130	-13.16	ol,plag,cpx,liq
7-134	1108	-13.49	ol,plag,cpx,sp,liq
7-129	1066	-14.12	ol?,plag,cpx,sp
b) NiNiO equilibrium			
3-336	1228	- 7.46	ol,liq
3-328	1206	- 7.73	ol,liq
3-334	1191	- 7.90	ol,liq
3-80	1183	- 7.88	ol,(plag),liq
3-331	1170	- 8.17	ol,plag,liq
5-165	1158	- 8.23	ol,plag,cpx,liq
3-76	1148	- 8.30	ol,plag,cpx,liq
3-346	1136	- 8.47	ol,plag,cpx,sp,liq
3-332	1123	- 8.67	ol,plag,cpx,sp,liq
c) other pO_2			
3-349	1236	- 6.27	(sp),liq
3-339	1210	- 6.57	ol,sp,liq
3-340	1206	- 3.82	sp,(ol),liq
3-343	1193	- 3.88	ol,sp,liq
3-342	1192	- 6.75	ol,sp,liq
3-347	1148	- 4.09	ol,plag,cpx,sp,liq

Composition: Re 124

Run No.	Temperature °C	pO_2	Result
a) FeFeO equilibrium			
7-175	1229	-12.05	liq
7-223	1211	-11.80	liq
5-190	1204	-11.97	(ol),liq
7-161	1190	-12.53	ol,(plag),liq
7-119	1180	-12.48	ol,plag,liq
7-157	1167	-12.83	ol,plag,liq
7-121	1156	-12.82	ol,plag,cpx,liq
7-133	1130	-13.16	ol,plag,cpx,liq
7-134	1108	-13.49	plag,cpx,sp,liq
7-129	1066	-14.12	plag,cpx,sp
b) NiNiO equilibrium			
3-328	1206	- 7.73	liq
3-333	1191	- 7.92	(plag),(ol),liq
3-80	1183	- 7.88	plag,ol,cpx,liq
3-331	1170	- 8.17	plag,ol,cpx,liq
3-76	1148	- 8.30	plag,ol,cpx,liq
3-346	1136	- 8.47	plag,ol,cpx,liq
3-332	1123	- 8.67	plag,ol,cpx,sp,liq
c) other pO_2			
3-349	1236	- 6.27	liq
3-339	1210	- 6.57	(sp),liq
3-340	1206	- 3.82	plag,sp,liq
3-343	1193	- 3.88	plag,sp,liq
3-342	1192	- 6.75	plag,sp,liq
3-347	1148	- 4.09	plag,ol,cpx,sp,liq

Composition: Re 607

Run No.	Temperature °C	pO_2	Result
a) FeFeO equilibrium			
5-189	1258	-11.24	liq
7-175	1229	-12.05	liq
7-223	1211	-11.80	ol,liq
5-190	1204	-11.97	ol,liq
7-119	1180	-12.48	ol,liq
7-157	1167	-12.83	ol,plag,cpx,liq
7-121	1156	-12.82	ol,plag,cpx,liq
7-133	1130	-13.16	ol,plag,cpx,liq
7-134	1108	-13.49	plag,cpx,liq
7-129	1066	-14.12	plag,cpx,sp
b) NiNiO equilibrium			
3-336	1228	- 7.46	liq
3-337	1219	- 7.56	liq
3-338	1210	- 7.61	liq
3-328	1206	- 7.73	liq
3-344	1194	- 7.82	liq
3-80	1183	- 7.88	ol,plag,cpx,liq
3-331	1170	- 8.17	ol,plag,cpx,liq
5-165	1158	- 8.23	ol,plag,cpx,liq
3-76	1148	- 8.30	ol,plag,cpx,liq
3-346	1136	- 8.47	ol,plag,cpx,liq
3-332	1123	- 8.67	ol,plag,cpx,sp,liq
c) other pO_2			
3-339	1210	- 6.57	liq
3-340	1206	- 3.82	sp,liq
3-343	1193	- 3.88	plag,sp,liq
3-342	1192	- 6.75	(plag),liq
3-347	1148	- 4.09	plag,cpx,sp,liq

Composition: Re 69

Run.No.	Temperature °C	pO_2	Result
a) FeFeO equilibrium			
7-175	1229	-12.05	liq
7-223	1211	-11.80	ol,liq
7-125	1208	-12.11	(ol),liq
7-119	1180	-12.48	ol,liq
7-157	1167	-12.83	ol,plag,liq
7-121	1156	-12.82	ol,plag,cpx,liq
7-133	1130	-13.16	ol,plag,cpx,liq
7-134	1108	-13.49	plag,cpx,sp,liq
7-129	1066	-14.12	plag,cpx,sp
b) NiNiO equilibrium			
3-337	1219	- 7.56	liq
3-338	1210	- 7.61	liq
3-328	1206	- 7.73	(* capsule melted)
3-330	1202	- 7.76	(ol),liq
3-333	1191	- 7.92	(* capsule melted)
3-334	1191	- 7.90	ol,liq
3-80	1183	- 7.88	ol,plag,cpx,liq
3-66	1167	- 8.10	ol,plag,cpx,liq
3-76	1148	- 8.30	ol,plag,cpx,liq
3-346	1136	- 8.47	ol,plag,cpx,liq
3-332	1123	- 8.67	ol,plag,cpx,sp,liq
c) other pO_2			
3-339	1210	- 6.57	(sp),liq
3-340	1206	- 3.82	sp,liq
3-343	1193	- 3.88	sp,liq
3-342	1192	- 6.75	(ol),sp,liq
3-347	1148	- 4.09	ol,plag,cpx,sp,liq

Composition: Re 180

Run No.	Temperature °C	pO_2	Result
a) FeFeO equilibrium			
7-235	1205	-12.34	liq
5-222	1113	-13.21	ol,plag,cpx,sp,liq
b) NiNiO equilibrium			
3-336	1228	- 7.46	liq
3-337	1219	- 7.56	liq
3-328	1206	- 7.73	plag,liq
3-333	1191	- 7.92	plag,(ol),liq
3-331	1170	- 8.17	plag,ol,liq
3-335	1160	- 8.27	plag,ol,cpx,liq
3-345	1148	- 8.33	plag,ol,cpx,liq
3-346	1136	- 8.47	plag,ol,cpx,liq
c) other pO_2			
3-350	1210	- 6.55	liq
3-351	1208	- 3.82	plag,sp,liq
3-343	1193	- 3.88	plag,sp,liq
3-347	1148	- 4.09	ol?,plag,cpx,sp,liq

Composition: Re 512

Run No.	Temperature °C	pO_2	Result
a) FeFeO equilibrium			
7-141	1307	-11.11	liq
7-264	1278	-11.01	(ol),liq
7-216	1274	-11.51	(ol),liq
5-189	1258	-11.24	ol,liq
7-175	1229	-12.05	ol,liq
7-223	1211	-11.80	ol,plag,liq
5-190	1204	-11.97	ol,plag,liq
7-161	1190	-12.53	ol,plag,liq
5-212	1188	-12.08	ol,plag,cpx,liq
7-119	1180	-12.48	ol,plag,cpx,liq
7-157	1167	-12.83	ol,plag,cpx,liq
7-121	1156	-12.82	ol,plag,cpx,liq
7-133	1130	-13.16	ol,plag,cpx,liq
7-134	1108	-13.49	ol,plag,cpx,sp,liq
7-129	1066	-14.12	ol,plag,cpx,sp
b) NiNiO equilibrium			
3-336	1228	- 7.46	ol,liq
3-337	1219	- 7.56	ol,liq
3-338	1210	- 7.61	ol,plag,liq
5-163	1199	- 7.85	ol,plag,cpx,liq
3-79	1183	- 7.92	ol,plag,cpx,liq
3-66	1167	- 8.10	ol,plag,cpx,liq
3-345	1148	- 8.33	ol,plag,cpx,(sp),liq
3-346	1136	- 8.47	ol,plag,cpx,sp,liq
c) other pO_2			
3-349	1236	- 6.27	ol,(sp),liq
3-339	1210	- 6.57	ol,plag,sp,liq
3-340	1206	- 3.82	ol,plag,cpx,sp,liq
3-342	1192	- 6.75	ol,plag,cpx,sp,liq

Composition: Re 332

Run No.	Temperature °C	pO_2	Result
a) FeFeO equilibrium			
7-125	1208	-12.11	liq
7-161	1190	-12.53	liq
7-188	1178	-12.73	plag,liq
7-156	1171	-12.79	plag,liq
7-181	1157	-13.01	ol,plag,liq
7-170	1143	-13.20	ol,plag,liq
5-178	1124	-13.22	ol,plag,sp,liq
7-180	1121	-13.51	ol,plag,liq
7-134	1108	-13.49	ol,plag,cpx,sp,liq
7-129	1066	-14.12	ol,plag,cpx,sp
b) NiNiO equilibrium			
3-336	1228	- 7.46	liq
3-337	1219	- 7.56	liq
3-338	1210	- 7.61	liq
3-330	1202	- 7.76	(plag),liq
3-80	1183	- 7.88	plag,liq
3-331	1170	- 8.17	plag,liq
3-335	1160	- 8.27	plag,liq
3-76	1148	- 8.30	ol,plag,liq
3-74	1135	- 8.44	ol,plag,sp,liq
3-332	1123	- 8.67	ol,plag,(cpx),sp,liq
3-67	1115	- 8.67	ol,plag,cpx,sp,liq
3-75	1099	- 8.85	ol,plag,cpx,sp,liq
c) other pO_2			
3-349	1236	- 6.27	liq
3-339	1210	- 6.57	(plag),sp,liq
3-340	1206	- 3.82	plag,sp,liq
3-342	1192	- 6.75	plag,sp,liq
3-347	1148	- 4.09	plag,cpx,sp,liq

Composition: Re 415

Run No.	Temperature °C	pO_2	Result
a) FeFeO equilibrium			
7-125	1208	-12.11	liq
7-119	1180	-12.48	liq
7-157	1167	-12.83	plag,liq
7-181	1157	-13.01	ol,plag,liq
7-170	1143	-13.20	ol,plag,liq
5-178	1124	-13.22	ol,plag,liq
7-180	1121	-13.51	ol,plag,liq
7-134	1108	-13.49	ol,plag,cpx,liq
7-129	1066	-14.12	ol,plag,cpx,sp
b) NiNiO equilibrium			
3-338	1210	- 7.61	liq
3-344	1194	- 7.82	liq
3-80	1183	- 7.88	plag,liq
3-331	1170	- 8.17	plag,liq
3-76	1148	- 8.30	ol,plag,liq
3-74	1135	- 8.44	ol,plag,sp,liq
3-332	1123	- 8.67	ol,plag,sp,liq
3-67	1115	- 8.67	ol,plag,cpx,sp,liq
3-75	1099	- 8.85	ol,plag,cpx,sp,liq
c) other pO_2			
3-349	1236	- 6.27	liq
3-339	1210	- 6.57	sp,liq
3-340	1206	- 3.82	plag,sp,liq
3-342	1192	- 6.75	plag,sp,liq
3-347	1148	- 4.09	plag,cpx,sp,liq

Composition: Re 471

Run No.	Temperature °C	pO_2	Result
a) FeFeO equilibrium			
7-264	1278	-11.01	liq
7-216	1274	-11.51	(plag),liq
7-217	1248	-11.82	plag,liq
7-232	1231	-11.40	plag,liq
7-175	1229	-12.05	plag,liq
7-125	1208	-12.11	plag,liq
7-119	1180	-12.48	plag,liq
7-157	1167	-12.83	plag,liq
7-181	1157	-13.01	ol,plag,liq
7-170	1143	-13.20	ol,plag,liq
7-118	1130	-13.17	ol,plag,liq
7-180	1121	-13.51	ol,plag,cpx,liq
7-134	1108	-13.49	ol,plag,cpx,sp,liq
7-129	1066	-14.12	ol,plag,cpx,sp
b) NiNiO equilibrium			
3-336	1228	- 7.46	plag,liq
3-328	1206	- 7.73	liq (* error)
3-330	1202	- 7.76	plag,liq
3-80	1183	- 7.88	plag,liq
3-331	1170	- 8.17	plag,liq
3-335	1160	- 8.27	plag,liq
3-76	1148	- 8.30	ol,plag,liq
3-74	1135	- 8.44	ol,plag,sp,liq
3-332	1123	- 8.67	ol,plag,cpx,sp,liq
3-67	1115	- 8.67	ol,plag,cpx,sp,liq
3-75	1099	- 8.85	ol,plag,cpx,sp,(liq)
c) other pO_2			
3-349	1236	- 6.27	plag,liq
3-339	1210	- 6.57	plag,sp,liq
3-340	1206	- 3.82	plag,sp,liq
3-347	1148	- 4.09	plag,cpx,sp,liq

Composition: Re 538

Run No.	Temperature °C	pO_2	Result
a) NiNiO equilibrium			
3-336	1228	- 7.46	plag,liq
3-330	1202	- 7.76	plag,liq
3-333	1191	- 7.92	(* capsule melted)
3-334	1191	- 7.90	(* capsule melted)
3-331	1170	- 8.17	plag,liq
3-335	1160	- 8.27	plag,liq
3-345	1148	- 8.33	plag,ol,sp,liq
b) other pO_2			
3-351	1208	- 3.82	plag,sp,liq
3-350	1210	- 6.55	plag,liq

Composition: Re 86

Run No.	Temperature °C	pO_2	Result
a) NiNiO equilibrium			
3-336	1228	- 7.46	plag,liq
3-330	1202	- 7.76	plag,liq
3-333	1191	- 7.92	(* capsule melted)
3-334	1191	- 7.90	(* capsule melted)
3-335	1160	- 8.27	plag,liq
3-345	1148	- 8.33	plag,sp,liq
3-346	1136	- 8.47	plag,ol,sp,liq
b) other pO_2			
3-350	1210	- 6.55	plag,sp,liq
3-351	1208	- 3.82	plag,sp,liq
3-343	1193	- 3.88	plag,sp,liq

Composition: Re 100

Run No.	Temperature °C	pO_2	Result
a) FeFeO equilibrium			
7-198	1209	-12.28	(plag),liq
5-212	1188	-12.08	plag,liq
7-188	1178	-12.73	plag,liq
7-181	1157	-13.01	plag,liq
7-170	1143	-13.20	plag,liq
7-133	1130	-13.16	plag,liq
7-180	1121	-13.51	plag,liq
7-134	1108	-13.49	plag,liq
7-129	1066	-14.12	plag,cpx or pyx,liq
b) NiNiO equilibrium			
3-337	1219	- 7.56	liq
3-328	1206	- 7.73	plag,liq
3-331	1170	- 8.17	plag,liq
3-332	1123	- 8.67	plag,liq
3-75	1099	- 8.85	plag,sp,liq
c) other pO_2			
3-350	1210	- 6.55	plag,liq
3-351	1208	- 3.82	plag,(sp),liq
3-343	1193	- 3.88	plag,sp,liq
3-342	1192	- 6.75	plag,liq

Composition: Re 2

Run No.	Temperature °C	pO_2	Result
a) FeFeO equilibrium			
7-125	1208	-12.11	liq
7-161	1190	-12.53	liq
7-119	1180	-12.48	(ol),liq
7-121	1156	-12.82	ol,liq
7-170	1143	-13.20	ol,liq
7-118	1130	-13.17	ol,plag,liq
7-180	1121	-13.51	ol,plag,cpx,liq
7-134	1108	-13.49	ol,plag,cpx,liq
7-129	1066	-14.12	plag,cpx,sp
b) NiNiO equilibrium			
3-330	1202	- 7.76	liq
3-331	1170	- 8.17	liq
3-335	1160	- 8.27	liq
3-345	1148	- 8.33	liq
3-74	1135	- 8.44	plag,cpx,sp,liq
3-332	1123	- 8.67	ol,plag,cpx,sp,liq
3-67	1115	- 8.67	ol,plag,cpx,sp,liq
3-75	1099	- 8.85	plag,cpx,sp,ol?,liq
c) other pO_2			
3-349	1236	- 6.27	liq
3-339	1210	- 6.57	sp,liq
3-340	1206	- 3.82	sp,liq
3-347	1148	- 4.09	plag,cpx,sp,liq

Composition: Re 30a

Run No.	Temperature °C	pO_2	Result
a) FeFeO equilibrium			
7-125	1208	-12.11	liq
7-161	1190	-12.53	liq
7-119	1180	-12.48	(plag),liq
7-157	1167	-12.83	plag,liq
7-181	1157	-13.01	ol,plag,liq
7-170	1143	-13.20	ol,plag,liq
5-178	1124	-13.22	ol,plag,sp,liq
7-180	1121	-13.51	ol,plag,cpx,liq
7-134	1108	-13.49	ol,plag,cpx,sp,liq
7-129	1066	-14.12	plag,cpx,sp
b) NiNiO equilibrium			
3-330	1202	- 7.76	liq
3-344	1194	- 7.82	liq
3-80	1183	- 7.88	plag,liq
3-331	1170	- 8.17	plag,liq
3-335	1160	- 8.27	plag,liq
3-76	1148	- 8.30	ol,plag,liq
3-74	1135	- 8.44	ol,plag,sp,liq
3-332	1123	- 8.67	ol,plag,cpx,sp,liq
3-67	1115	- 8.67	ol,plag,cpx,sp,liq
3-75	1099	- 8.85	ol?,plag,cpx,sp,(liq)
c) other pO_2			
3-349	1236	- 6.27	liq
3-339	1210	- 6.57	sp,liq
3-340	1206	- 3.82	plag,sp,liq
3-342	1192	- 6.75	plag,sp,liq
3-347	1148	- 4.09	plag,cpx,sp,liq

Composition: Re 27

Run No.	Temperature °C	pO_2	Result
a) FeFeO equilibrium			
7-125	1208	-12.11	liq
7-161	1190	-12.53	liq
7-156	1171	-12.79	liq
7-181	1157	-13.01	liq
7-170	1143	-13.20	ol,liq
5-178	1124	-13.22	ol,liq
7-180	1121	-13.51	ol,liq
7-134	1108	-13.49	ol,plag,liq
7-129	1066	-14.12	plag,cpx,sp
b) NiNiO equilibrium			
3-80	1183	- 7.88	liq
3-76	1148	- 8.30	liq
3-74	1135	- 8.44	sp,liq
3-332	1123	- 8.67	plag,cpx,sp,liq
3-67	1115	- 8.67	plag,cpx,sp,liq
3-75	1099	- 8.85	plag,cpx,sp,liq
c) other pO_2			
3-349	1236	- 6.27	liq
3-339	1210	- 6.57	sp,liq
3-340	1206	- 3.82	sp,liq
3-347	1148	- 4.09	(plag),(cpx),sp,liq

Composition: Re 1

Run No.	Temperature °C	pO_2	Result
a) FeFeO equilibrium			
7-133	1130	-13.16	liq
7-180	1121	-13.51	(plag),liq
7-134	1108	-13.49	plag,liq
7-129	1066	-14.12	plag,liq
b) NiNiO equilibrium			
3-335	1160	- 8.27	liq
3-346	1136	- 8.47	liq
3-332	1123	- 8.67	plag,liq
3-75	1099	- 8.85	plag,sp,liq
c) other pO_2			
3-350	1210	- 6.55	liq
3-351	1208	- 3.82	sp,liq
3-343	1193	- 3.88	sp,liq
3-342	1192	- 6.75	sp,liq

Composition: Re 508

Run No.	Temperature °C	pO_2	Result
a) FeFeO equilibrium			
7-141	1307	-11.11	liq
7-264	1278	-11.01	(ol),liq
7-216	1274	-11.51	ol,liq
5-189	1258	-11.24	ol,liq
7-175	1229	-12.05	ol,liq
7-223	1211	-11.80	ol,liq
5-190	1204	-11.97	ol,plag,cpx,liq
7-161	1190	-12.53	ol,plag,cpx,liq
7-119	1180	-12.48	ol,plag,cpx,liq
7-157	1167	-12.83	ol,plag,cpx,liq
7-121	1156	-12.82	ol,plag,cpx,liq
7-133	1130	-13.16	ol,plag,cpx,liq
7-134	1108	-13.49	ol,plag,cpx,sp,liq
7-129	1066	-14.12	ol,plag,cpx,sp
b) NiNiO equilibrium			
3-336	1228	- 7.46	ol,liq
3-337	1219	- 7.56	ol,(cpx),liq
3-338	1210	- 7.61	ol,cpx,liq
5-163	1199	- 7.85	ol,plag,cpx,liq
3-79	1183	- 7.92	ol,plag,cpx,liq
3-66	1167	- 8.10	ol,plag,cpx,liq
3-345	1148	- 8.33	ol,plag,cpx,(sp),liq
3-346	1136	- 8.47	ol,plag,cpx,sp,liq
3-332	1123	- 8.67	ol,plag,cpx,sp,liq
c) other pO_2			
3-349	1236	- 6.27	ol,(sp),liq
3-339	1210	- 6.57	ol,cpx,sp,liq
3-340	1206	- 3.82	ol,plag,cpx,sp,liq
3-342	1192	- 6.75	ol,plag,cpx,sp,liq

Composition: Re 505

Run No.	Temperature °C	pO_2	Result
a) FeFeO equilibrium			
7-217	1248	-11.82	liq
7-232	1231	-11.40	plag,liq
7-175	1230	-12.05	(plag),liq
7-125	1208	-12.11	plag,liq
7-119	1180	-12.48	plag,liq
7-157	1167	-12.83	ol,plag,cpx,liq
7-121	1156	-12.82	ol,plag,cpx,liq
7-133	1130	-13.16	ol,plag,cpx,liq
7-180	1121	-13.51	ol,plag,cpx,liq
7-134	1108	-13.49	ol,plag,cpx,sp,liq
7-129	1066	-14.12	plag,cpx,sp
b) NiNiO equilibrium			
3-336	1228	- 7.46	plag,liq
3-337	1219	- 7.56	plag,liq
3-328	1206	- 7.73	plag,liq
3-80	1183	- 7.88	plag,liq
3-331	1170	- 8.17	ol,plag,cpx,liq
5-165	1158	- 8.23	ol,plag,cpx,liq
3-76	1148	- 8.30	ol,plag,cpx,liq
3-346	1136	- 8.47	ol,plag,cpx,liq
3-332	1123	- 8.67	ol,plag,cpx,sp,liq
c) other pO_2			
3-339	1210	- 6.57	plag,liq
3-340	1206	- 3.82	plag,sp,liq
3-343	1193	- 3.88	plag,sp,liq
3-342	1192	- 6.75	plag,liq
3-347	1148	- 4.09	ol?,plag,cpx,sp,liq

Composition: Re 168

Run No.	Temperature °C	pO_2	Result
a) NiNiO equilibrium			
3-336	1228	- 7.46	ol,liq
3-337	1219	- 7.56	ol,liq
3-328	1206	- 7.73	ol,liq
3-333	1191	- 7.92	(* capsule melted)
3-334	1191	- 7.90	ol,liq
3-331	1170	- 8.17	ol,plag,liq
3-335	1160	- 8.27	ol,plag,cpx,liq
3-345	1148	- 8.33	ol,plag,cpx,sp,liq
3-346	1136	- 8.47	ol,plag,cpx,sp,liq
c) other pO_2			
3-349	1236	- 6.27	ol,sp,liq
3-350	1210	- 6.55	ol,sp,liq
3-351	1208	- 3.82	ol,sp,liq
3-343	1193	- 3.88	ol,sp,liq

Composition: Re 634

Run No.	Temperature °C	pO_2	Result
a) FeFeO equilibrium			
7-125	1208	-12.11	liq
5-212	1188	-12.08	liq
7-119	1180	-12.48	(ol),(plag),liq
7-157	1167	-12.83	ol,plag,liq
7-121	1156	-12.82	ol,plag,liq
7-170	1143	-13.20	ol,plag,cpx,liq
7-133	1130	-13.16	ol,plag,cpx,liq
7-134	1108	-13.49	ol,plag,cpx,liq
7-129	1066	-14.12	plag,cpx,sp
b) NiNiO equilibrium			
3-330	1202	- 7.76	liq
3-80	1183	- 7.88	(plag),liq
3-331	1170	- 8.17	plag,liq
5-165	1158	- 8.23	plag,ol,liq
3-76	1148	- 8.30	ol,plag,cpx,liq
3-332	1123	- 8.67	ol,plag,cpx,liq
c) other pO_2			
3-339	1210	- 6.57	liq
3-340	1206	- 3.82	sp,liq
3-343	1193	- 3.88	plag,sp,liq
3-342	1192	- 6.75	(plag),liq
3-347	1148	- 4.09	ol,plag,cpx,sp,liq

APPENDIX F

CALCULATION OF CO-ORDINATES IN PROJECTION DIAGRAMS

The calculation of the projection co-ordinates for a composition, when projected from a specified point into a specified plane in a four component system is a simple procedure. The mechanism of the projection of a composition (X) may be defined as: the composition of the projection point is added to or subtracted from the composition of X until the new projected composition of X can be uniquely recast in terms of the compositions of the end members of the plane desired for the projection.

The general equations for calculating the co-ordinates are developed as follows using molar proportions:

Let X=XO (CaO); Y=YO (MgO); R=R_2O_3 (Al_2O_3); Z=ZO_2 (SiO_2)

Let p,q,s be the molar amounts of the three end members of the plane projected into.

Let n be the molar amount of the projection phase which must be added to or subtracted from the composition.

To obtain the solution, the following equation must be balanced:

$$\underbrace{p\ X_aY_bR_cZ_d + q\ X_eY_fR_gZ_h + s\ X_jY_kR_lZ_m}_{\text{end members of the plane}} + \underbrace{n\ X_tY_uR_vZ_w}_{\text{projection point}} = \underbrace{X_xY_yR_rZ_z}_{\text{composition X}}$$

where each subscript represents the molar proportions of the oxide in question.

To solve this equation, an equation must be set up for each of the oxides involved:

$ap + eq + js + tn = x$ Equation for XO

$bp + fq + ks + un = y$ Equation for YO

$cp + gq + ls + vn = r$ Equation for R_2O_3

$dp + hq + ms + wn = z$ Equation for ZO_2

The matrix thus formed can then be solved by any standard mathematical procedure for solving simultaneous equations, for example, Gaussian elimination. The amounts of p,q,s in the solution are then recast to 100% total. The wt% co-ordinates are calculated from the molecular co-ordinates by multiplying p,q,s by the respective molecular weights of the end members of the plane, and recasting to 100% total.

The value obtained for n will be positive when the composition (X) is on the projection point side of the projection plane, and negative when on the opposite side of the plane.

As an example, consider the projection from the $2YO.ZO_2$ (olivine) composition into the plane $XO.ZO_2$-$YO.ZO_2$-R_2O_3 (CS-MS-A). Omitting the redundant oxides in the general equations, the solution is:

$$p\ XZ + q\ YZ + s\ R + n\ Y_2Z = XYRZ$$

$$(\ p\ CS + q\ MS + s\ A + n\ M_2S = CMAS\ )$$

Therefore

$p = x$

$q + 2n = y$

$s = r$

$p + q + n = z$

Recasting these equations:

$$p = x$$

$$q = 2z - 2x - y$$

$$s = r$$

$$n = x + y - z$$

The solution for the Anorthite composition (x=1;r=1;z=2) is:

$p = 1$ = 25.00 %

$q = 4 - 2 - 0 = 2$ = 50.00 %

$s = 1$ = 25.00 %

$n = 1 + 0 - 2 = -1$ = 25.00 % (from $\frac{n}{p+q+s}$)

Calculation of the original composition from a projected composition is the reverse procedure when the amount of the projection phase (n) is known. When n is unknown, the original composition can still be obtained if the projected composition of the same original composition is known in a different projection. The equation to be solved then is

Projected composition A + Projection phase composition = Projected composition B + Projection phase composition

For example: if the co-ordinates of a composition were known in the $2YO.ZO_2$ (olivine) into $XO.ZO_2$-$YO.ZO_2$-R_2O_3 (CS-MS-A) projection and in the $XO.YO.2ZO_2$ (clinopyroxene) into $XO.R_2O_3$-YO-ZO_2(CA-M-S) projection, the equation to be solved would be:

$XO.ZO_2$-$YO.ZO_2$-R_2O_3 co-ords. + $2YO.ZO_2$ = $ZO.R_2O_3$-YO-ZO_2 co-ords. + $XO.YO.2ZO_2$

Since the co-ordinates will generally not give a perfect solution, a least squares calculation will give the optimum solution. The computer program of Wright and Doherty (1970) will perform such a calculation. The original composition can then be calculated from the proportions of the projected composition and its projection phase composition in the solution.

APPENDIX G

PUBLISHED PAPERS

Batts, B.D., Biggar, G.M., Billetop, M.C.J., Davis, P.R., Eglinton, G., Erents, S.K., Gardiner, L.R., Gowar, A.P., Housley, R.M., Humphries, D.J., Jull, A.J.T., Maxwell, J.R., Mays, B.J., McCracken, G.M. and Pillenger, C.T. 1974. The origin of lunar carbide. Lunar Science V, The Lunar Science Institute, Houston, Texas, pp. 47-49.

Bell, J.D. and Humphries, D.J. 1972. Lakagigar fissure eruption. Progr. in Exp. Petrol., v2, pp.110-112

Biggar, G.M., Ford, C.E., Humphries, D.J., Jamieson, B.G., O'Hara, M.J., Peckett, A. and Richardson, S.W. 1972. Melting relations in maria surface basalts. Progr. in Exp. Petrol., v2, pp. 108-109.

Biggar, G.M., Ford, C.E., Humphries, D.J., Wilson, G. and O'Hara, M.J. 1972. Melting relations of more primitive mare-type basalts 14053 and M (Reid et al., 1972); and of breccia 14321 and soil 14162 (average lunar crust?). Lunar Science III, The Lunar Science Institute, Houston, Texas. pp. 74-76.

Biggar, G.M., Humphries, D.J. and O'Hara, M.J. 1974. Experimental crystallisation and geochemical interpretation of low titanium basalts. Lunar Science V, The Lunar Science Institute, Houston, Texas. pp.60-62.

Biggar, G.M., O'Hara, M.J., Humphries, D.J. and Peckett, A. 1972. Experimental crystallisation of Apollo 11 and 12 lavas - a re-examination. Lunar Science III, The Lunar Science Institute, Houston, Texas, pp. 77-79.

Biggar, G.M., O'Hara, M.J., Humphries, D.J. and Peckett, A. 1972. Maria lavas, mascons, layered complexes, achondrites and the lunar mantle. In "The Moon", Eds. H. Urey and S.K. Runcorn. International Astonomical Union, pp. 129-164.

Biggar, G.M., O'Hara, M.J., Peckett, A. and Humphries, D.J. 1971. Lunar lavas and the achondrites: Petrogenesis of protohypersthene basalts in the maria lava lakes. Proc. Second Lunar Sci. Conf., Suppl. 2, Geochim. et Cosmochim. Acta, v1, pp.617-643.

Ford, C.E., Biggar, G.M., Humphries, D.J., Wilson, G., Dixon, D. and O'Hara, M.J. 1972. Role of water in the evolution of the lunar crust; an experimental study of sample 14310; an indication of lunar calc-alkaline volcanism. Proc. Third Lunar Sci. Conf., Suppl. 3, Geochim. et Cosmochim. Acta, v1, pp. 207-229.

Ford, C.E., Biggar, G.M., O'Hara, M.J., Humphries, D.J. and Spencer, P.N. 1974. Origin of the Lunar Highlands. Lunar Science V, The Lunar Science Institute, Houston, Texas, pp. 239-241.

Ford, C.E., Humphries, D.J., Wilson, G., Dixon, D., Biggar, G.M. and O'Hara, M.J. 1972. Experimental petrology of high alumina basalt, 14310, and related compositions. Lunar Science III, The Lunar Science Institute, Houston, Texas, pp.274-276.

Humphries, D.J. 1972. Melting behaviour of Reunion igneous rocks. Progr. in Exp. Petrol., v2, pp. 113-115.

Humphries, D.J. 1972. Liquids in equilibrium with plagioclase, olivine and augite. Progr. in Exp. Petrol., v2, p. 120.

Humphries, D.J. 1972. Dicalcium-silicate and spinel saturated equilibria. Progr. in Exp. Petrol., v2, pp.140-143.

Humphries, D.J., Biggar, G.M., and O'Hara, M.J. 1972. Flow sheet for $CaO-MgO-Al_2O_3-SiO_2$ at atmospheric pressure. Progr. in Exp. Petrol. v2, pp.138-139.

Humphries, D.J., Biggar, G.M. and O'Hara, M.J. 1972. Phase equilibria and origin of Apollo 15 basalts, etc. In "The Apollo 15 Lunar Samples", The Lunar Science Institute, Houston, Texas, pp.103-107.

Humphries, D.J. and Cox, K.G. 1972. Melting data for volcanic rocks from Aden, South Arabia. Progr. in Exp. Petrol., v2, p. 116.

Jull, A.J.T., Davis, P.R., Eglinton, G., Gardiner, L.R., Maxwell, J.R., Pillinger, C.T., Biggar, G.M., Humphries, D.J. and Batts, B.D. 1975. Simulation of lunar processes: II. Redistribution of carbon in the lunar regolith during meteorite impact. Lunar Science VI, The Lunar Science Institute, Houston, Texas, pp. 457-459.

O'Hara, M.J., Biggar, G.M., Humphries, D.J. and Saha, P. 1974. Experimental petrology of high titanium basalt. Lunar Science V, The Lunar Science Institute, Houston, Texas, pp. 571-573.

O'Hara, M.J., Biggar, G.M., Hill, P.G., Jefferies, B. and Humphries, D.J. 1974. Plagioclase saturation in lunar high-titanium basalt. Earth Planetary Sci. Letters, v21, pp.253-268.

O'Hara, M.J. and Humphries, D.J. 1975. Analysis of composition variations in high titanium basalts and related materials. Lunar Science VI, The Lunar Science Institute, Houston, Texas, pp.616-618.

O'Hara, M.J. and Humphries, D.J. 1975. Armalcolite crystallisation, phenocryst assemblages, eruption conditions and origin of eleven high titanium basalts from Taurus Littrow. Lunar Science VI, The Lunar Science Institute, Houston, Texas, pp.619-621.

Storey, W.C., Humphries, D.J. and O'Hara, M.J. 1974. Experimental petrology of sample 77135. Earth Planetary Sci. Letters, v23, pp.435-438.

Reference:

Reid, A.M., Warner, J., Ridley, W.I., Johnston, D.A., Harmon, R.S., Jakes, P. and Brown, R.W. 1972. The major element compositions of lunar rocks as inferred from glass compositions in the lunar soils. Proc. Third Lunar Sci. Conf., Suppl. 3, Geochim. et Cosmochim, Acta, v1, pp. 363-378.

Proceedings of the Second Lunar Science Conference, Vol. 1, pp. 617–643.
The M.I.T. Press, 1971.

Lunar lavas and the achondrites: Petrogenesis of protohypersthene basalts in the maria lava lakes

G. M. BIGGAR, M. J. O'HARA, A. PECKETT,* and D. J. HUMPHRIES
Grant Institute of Geology, Edinburgh University, Edinburgh EH9 3JW, Scotland

(*Received* 16 *March* 1971; *accepted in revised form* 12 *April* 1971)

Abstract—The crystallization of olivine, chrome spinel, protohypersthene, pigeonite, plagioclase, augite, ulvöspinel, ilmenite, and tridymite in the range 1310–1065°C, $fO_2 \sim 10^{-12.5}$ bar is described and microprobe analyses of the equilibrium olivines, pyroxenes, and residual glasses are presented, for 9 rocks falling into 3 groups: (1) 12038 is close to a low pressure cotectic liquid; 12018, 12020, and 12040 are olivine (spinel and pyroxene) phenocryst-enriched samples of that lava. (2) 12064 is close to a second low pressure cotectic liquid, 12021, 12065, and 12052 being pigeonite (olivine, chrome spinel) phenocryst-enriched samples of that lava. (3) 12022 is an olivine phenocryst-enriched sample of a third lava. Eruption temperatures (1165, 1145°C in groups 1 and 2, respectively) are deduced to have been close to the atmospheric pressure cotectic crystallization temperatures; crystals produced in experiments near the eruption temperature closely match cores to phenocrysts in the natural rocks; margins to phenocrysts and groundmass crystals are not equilibrium products.

Close approach of Apollo 11 basalts also to low pressure cotectic liquid compositions is established by microprobe analyses of equilibrium residual glasses in two natural samples. Cotectic character in these and Apollo 12 basalts combined with geochemical features indicate derivation from underlying lava lakes already far advanced in extreme fractional crystallization. The complementary cumulus has the petrographic character of howardite/eucrite achondrite and the results are combined with those of Duke and Silver to yield a cross section of the lunar maria implying early accumulates of metallic iron (a possible source of mascon effects) overlain by howardite-like, eucrite-like and eventually granophyric products. Volatilization losses of alkalis especially during the first filling of the lava lakes imposed this distinctive trend upon parental magmas which may have been similar to common terrestrial basalts. Nothing can be deduced about the lunar mantle from high pressure phase equilibria studies on Apollo 11 and Apollo 12 samples.

INTRODUCTION

WE SEEK TO ANSWER nine questions: (1) How have the Apollo 12 lavas crystallized? (2) Are the lunar lavas close in composition to atmospheric pressure cotectic liquids? (3) Is that composition the product of fractional crystallization at low pressure? (4) Has the lava composition been significantly modified by volatilization loss on eruption? (5) Has a metal phase been fractionated from the lavas? (6) Are the lunar maria consolidated differentiated lava lakes rather than basins filled by successive flows of lava? This choice makes a 50–100-fold difference to the mass balance problems encountered by geochemists. (7) Are phase equilibria studies carried out on Apollo 11 and Apollo 12 lava compositions valueless as a guide to the mineralogy of the lunar interior? (8) Is it unjustifiable to select a specific hypothesis of lunar origin at present? (9) Have lines of reasoning been applied to lunar basalts which would be rejected if applied equally to randomly selected terrestrial basalts?

In our opinion, the answer to the last eight questions is "yes."

* Geology Department, Durham University, England.

Experimental Technique

All experiments were carried out at 1 atm pressure in CO_2/H_2 atmospheres under conditions described by O'HARA *et al.* (1970), except where noted. About 0.25 bar H_2O pressure exists in the furnace and probably accelerates approach to equilibrium. Unless otherwise stated, the starting material for experiments on all Apollo rocks was the finely ground natural rock powder. For synthetic analogs, the material was a recrystallized "gel."

Simultaneous calibration for temperature (at the melting points of lithium metasilicate, 1203°C, and gold, 1064.5°C) and oxygen fugacity (at the Fe/FeO and Ni/NiO equilibria at each temperature) were carried out. Electron microprobe analyses of the glass in near liquidus runs on 12038 and 12064 confirmed that iron loss is low, and that molybdenum content of the glass is below the limit of detection (0.2%). Phase compositions were determined on the microprobe at the Geology Department, Durham University.

APOLLO 12 SYNTHETIC ANALOGS: NONCOTECTIC CHARACTER OF RANDOM COMPOSITIONS

Twelve synthetic mixtures and the results obtained from them, are set out in Table 1. Errors in the SiO_2 content in the analyses reported by LSPET (1970) mean that the two SiO_2-poor series of compositions (A1–5, B1–4) represent randomly selected compositions bearing no relationship to the actual lava compositions present in the Apollo 12 suite. They neither approach cotectic behavior themselves, nor bracket any composition which exhibits such behavior. The silica-saturated series (C1–4) simulates the compositions of the Apollo 12 lavas. These compositions lie close to the low temperature cotectic liquids in equilibrium with olivine, feldspar, augite, and pigeonite (Figs. 1, 2).

Table 1. Experimental compositions.

Code	Composition (molar) an	di	ilm	ol	geh	Mg/(Mg + Fe) in norm silicate	Liquidus phase and temperature		ΔT°C to 3rd phase entry (neglecting opaque oxides)	2nd phase (not opaque)	3rd phase (not opaque)
A1	1½	1	1	10	1		ol	1300	100	sp	an
A2	1½	3	1	10	1		ol	1300	100	sp	an
A3	3½	1	1	10	1	60%	sp	1300	75	ol	an
A4	1½	1	1	12	1		ol	1300	100	sp	an
A5	1½	1	1	10	3		ol, sp	1250	100	sp	aug
B1	1½	1	1	3½			ol	1275	75	sp	an
B2	1½	3	1	3½		50%	ol	1250	100	an	aug
B3	3½	1	1	3½			sp	1250	40	ol	an
B4	1½	1	1	5½			ol	1300	110	sp	an
				hyp							
C1	3	2	1	8			an	1185	30	ol	pig
C2	3	4	1	8		40%	an	1180	20	aug	ol
C3	5	2	1	8			an	1210	25	ol, aug, pig	
			12038				ol	1160	5	pig, prhy	plag
			12064				pig	1140	30	plag, aug	

Note that only compositions C1/3 show low liquidus temperature and a close approach to atmospheric pressure cotectic liquid character, that the liquidus fields of pigeonite and augite were not directly intersected; and that despite the variations of 2 moles in the amounts of diopside, feldspar, and olivine in each group, no group intersected more than 2 liquidus fields. Mineral abbreviations as in Fig. 2.

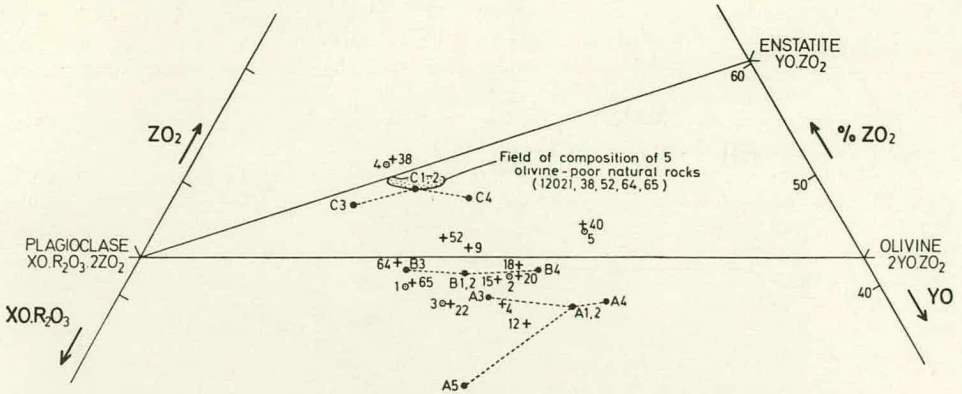


Fig. 1. This figure and Figs. 2, 5, 6, 8, and 9 use a projection system reported by O'HARA (1968), CLARKE (1970), and JAMIESON (1970). Fig. 1 is a projection from diopside ($XO \cdot YO \cdot 2ZO_2$) into the composition plane $XO \cdot R_2O_3$–YO–ZO_2 which includes the plane plagioclase-enstatite-olivine, showing, by crosses, the compositions of Apollo 12 rock samples 12004, 12009, 12015, 12018, 12020, 12022, 12038, 12040, 12052, 12064, and 12065 as reported by LSPET (1970). The compositions of 13 synthetic simulations (A1/5, B1/4, C1/4 filled circles) used by ourselves and lunar simulations 1–5 (numbered circles) used by MUAN *et al.* (1971) are also shown. The composition studied by ANDERSON *et al.* (1971) projects close to B2 in Figs. 1 and 2.

APOLLO 12 SAMPLES: THREE GROUPS, AT LEAST THREE FLOWS

Three types of behavior were distinguished. Group 1. Rocks 12018, 12020, 12038, and 12040 show variable temperatures of entry of olivine and spinel at the liquidus, but behave as four compositions arranged along a control line linking olivine ($cFo_{70}Fa_{30}$) to a liquid of composition close to 12038 (see Figs. 5, 6). Protohypersthene, joined by pigeonite are the first pyroxenes, and these are joined at c.1160°C by calcic plagioclase. Group 2. Rocks 12021, 12052, 12064, and 12065 show less variation in composition. Two have olivine near the liquidus; both show its resorption by reaction with the liquid on cooling. This group shows the nearly simultaneous entry of plagioclase and augite at c. 1140°C. Group 3. Rock 12022 crystallizes abundant spinel and olivine before the entry of pyroxene at c. 1137°C, joined by plagioclase close to 1133°C.

The simplest interpretation is that 12038 is a low pressure cotectic liquid (Fig. 3); 12018, 12020, 12040 are samples of the same lava enriched with cumulus olivine (KUSHIRO and HARAMURA, 1971) plus some pyroxene and chrome spinel. 12064 is close to another low-pressure cotectic liquid; 12021, 12065, and 12052 are samples of the same lava in which principally pigeonite phenocrysts, plus some olivine and spinel have been concentrated (Fig. 4). 12022 is an olivine-enriched sample of a third lava. Located samples of the first lava are from Bench crater; of the second from Head and Surveyor craters (LSPET, 1970). Figs. 3 and 4 and Table 2 present the atmospheric pressure quenching experiment data for the first two groups of rocks, plotted as partial pseudobinary temperature sections along the major axis of chemical

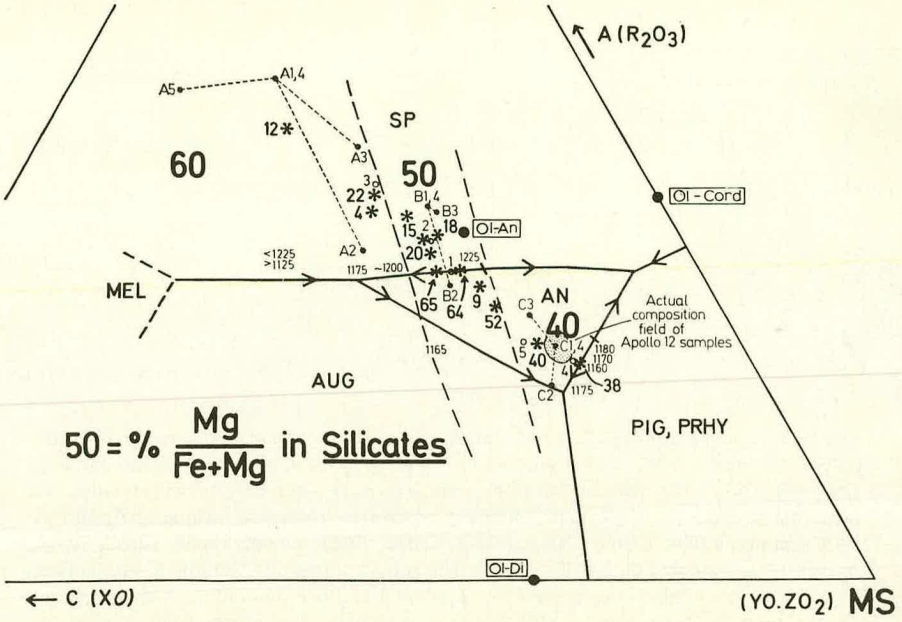


Fig. 2. Projection from olivine ($2YO \cdot ZO_2$) into the composition plane $XO–YO \cdot ZO_2–R_2O_3$ showing the piercing points of the olivine-diopside (Ol-Di), olivine-cordierite (Ol–Cord), and olivine-plagioclase (Ol–An) joins by large filled circles. Other points are shown as in Fig. 1 except that LSPET (1970) analyses are shown by asterisks, not crosses. The phase boundaries drawn are deduced from the quenching data for the 13 synthetic compositions, and represent the projection of the bounding surfaces of the olivine primary phase volume, labeled with the other crystalline phase stable at the liquidus on these surfaces (sp = aluminous spinel, aug = augite, an = anorthite, pig, prhy = pigeonite, protohypersthene, mel = melilite). The Mg/(Mg + Fe) ratio in the silicates varies across the diagram between sample groups A, B, C in the manner shown. Note the very wide spread of apparent compositions, arranged at a high angle to, and mostly far remote from, atmospheric pressure cotectic liquids, and the close approach of the actual composition field of Apollo 12 samples to the deduced low temperature liquid-olivine-pigeonite-plagioclase-cotectic curve.

variation in each group. The TiO_2 content of the spinel does not exceed 10% at temperatures down to 1114°C. The olivine which is present at temperatures of 1180–1114°C has a composition in the range $Fo_{70}Fa_{30}$ to $Fo_{60}Fa_{40}$ (Table 3).

Protohypersthene crystallizes between 1200 and 1160°C and is joined within this range and eventually replaced by pigeonite which persists to the solidus. Protohypersthene, never abundant, is most common in samples 12020 and 12040. Olivine has a reaction relationship with the liquid in 12052, 12065; rocks 12021, 12064 have pyroxene on the silicate liquidus and may have developed by a small degree of fractional crystallization from liquids having an olivine liquidus. Olivine is in reaction relationship with the liquid once calcium-poor pyroxene has begun to crystallize. Complete resorption occurs in 12038, 12052, and 12065 at c. 1135°C. Calcic plagioclase crystallization commences at c. 1160°C in all rocks from group 1. Augite and

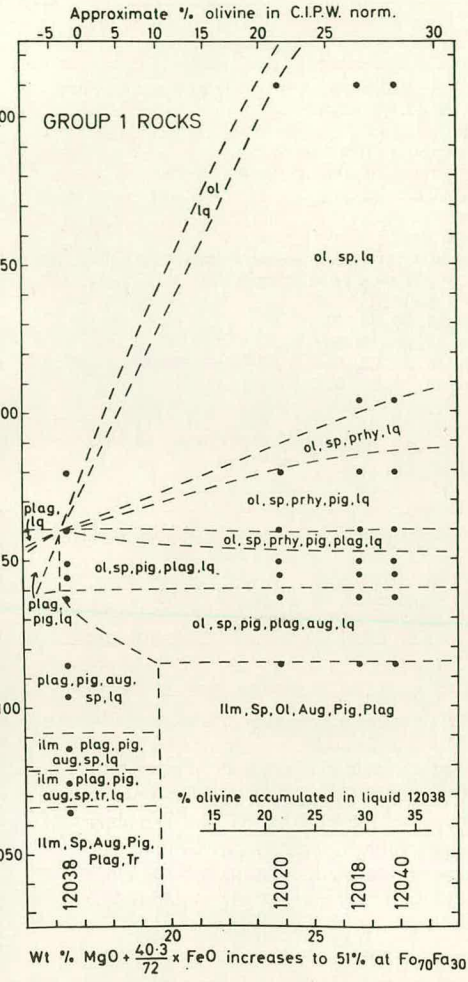


Fig. 3. Quenching experiment results at atmospheric pressure, $fO_2 \sim 10^{-12.5}$ bar on four group 1 rock samples from the Apollo 12 site, plotted and interpreted as a pseudobinary section along the predominant olivine-controlled composition variation. Three composition scales in terms of normative olivine, putative "modal" olivine, and in terms of a simple chemical parameter, are indicated.

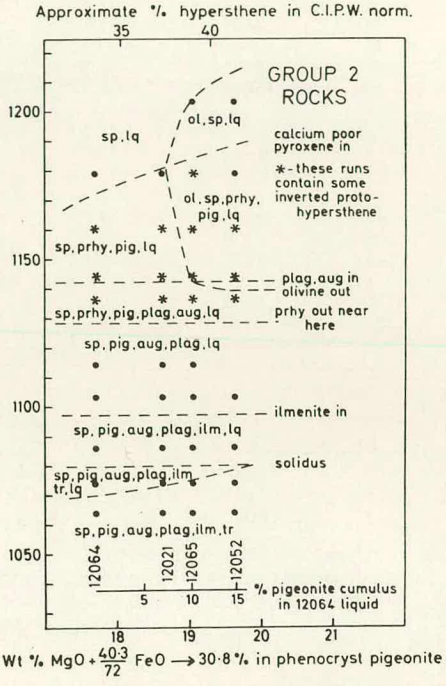


Fig. 4. Quenching experiment results at atmospheric pressure, $fO_2 \sim 10^{-12.5}$ bar on four group 2 rock samples from the Apollo 12 site, plotted and interpreted as a pseudobinary section along the predominant calcium-poor pyroxene-controlled composition variation. 12064 and 12021 lie very close to the olivine primary phase volume, and olivine has been provisionally identified in 12064 at 1160°C. Three composition scales are indicated, in terms of a chemical parameter, putative "modal" pigeonite, and normative hypersthene.

Table 2. Details of experiments on Apollo 12 samples 12018, 20, 21, 22, 38, 40, 52, 64, 65. Results reported in Figs. 3 and 4 of text.

Runs	Temperature °C	$\log_{10} fO_2$	Hours	Comments
14	1310	−10.6	1	All molybdenum capsules, Fe/FeO equilibrium 18, 20, 40, 52 only
9	1203	−11.8	5	not 64, 21, 38
4	1179	−12.1	5	nine rocks olivine in 12064
1	1160	−12.3	5	nine rocks olivine in 12064
18	1149	−12.5	5	18, 20, 38, 40 only
3	1144	−12.6	5	nine rocks
2	1137	−12.7	5	nine rocks
15, 16, 17	1129	−12.8	1½	Using natural rock powder; unannealed glass; glass + 5% rock powder seeds. 22, 38, 52 only.
5	1114	−12.9	5	nine rocks
19	1104	−13.1	5	not 18, 20, 40
12	1086	−13.3	5	not 18, 20, 22, 40
11	1074	−13.5	5	not 18, 20, 22, 40
10	1064	−13.7	5	not 18, 20, 22, 40
6	1250 → 1154	−12.5	1 → 4½	nine rocks } cooling experiments Fe/FeO equilibrium
13	1306 → 1127	−12.8	1 → 1	nine rocks } cooling experiments Fe/FeO equilibrium
7, 8	1159 → 1085	−13.3	7	21, 64, 65 only } cooling experiments Fe/FeO equilibrium
21	1161	− 8.3	4	
20	1150	− 8.3	4	$Ag_{70}Pd_{30}$ capsules, nine rocks Ni/NiO equilibrium
22	1139	− 8.3	4	
24	1180	−17	3¼	Fe capsules 22, 38, 64 only
23	1134	−17	3	Fe capsules 22, 38, 64 only

Table 3. Analyses of olivines from experimental charges.

	12040/4 1179°C $Fo_{68.7}$*	12040/1 1160°C Fo_{66}	12040/2 1137°C $Fo_{63.5}$	12038/1 1160°C $Fo_{66.9}$	12038/2 1137°C $Fo_{60.4}$	12022/4 1179°C $Fo_{66.8}$	12022/15 1129°C $Fo_{60.9}$
SiO_2	37.71	37.28	36.72	37.34	36.73	37.00	36.31
TiO_2	0.08	0.14	0.10	0.14	0.16	0.18	0.24
Cr_2O_3	0.24	0.17	0.15	0.19	0.19	0.21	0.16
FeO	27.45	29.61	31.66	29.00	33.53	29.03	33.37
MnO	0.28	0.28	0.34	0.33	0.43	0.36	0.41
MgO	33.74	32.21	30.95	32.87	28.70	32.76	29.12
CaO	0.48	0.42	0.45	0.47	0.62	0.39	0.45
TOTAL	99.98	100.11	100.37	100.34	100.36	99.93	100.06

* Fo_x = Fo/(Fo + Fa) mole %.

plagioclase apparently begin to crystallize almost simultaneously at a temperature of c. 1140°C from rocks in group 2. Augite (Table 4) is present in rocks of groups 1 and 2 at 1137°C as discrete crystals and persists to the solidus.

The three olivine-rich samples, 12018, 12020, and 12040, have high liquidus temperatures and contain so much olivine that it does not all react with the liquid. These rocks solidify with abundant olivine still present at temperatures close to 1114°C. A little liquid is present at lower temperatures (cf. MUAN *et al.*, 1971) but

brown glass is no longer seen, and equilibrium between the pyroxenes is not established in our runs. Sample 12038 from group 1, and all four samples from group 2 show continued crystallization after the disappearance of olivine by reaction with the liquid. Calcic plagioclase, augite, pigeonite, and spinel are present in the liquid at temperatures below 1114°C. In 12022 the Cr_2O_3 content of the spinel falls sharply from c. 32% at 1129°C to c. 20% at 1103°C, titanium increasing simultaneously from 13% to 22%. 12064 contains a spinel with 29% TiO_2, 13% Cr_2O_3 at 1086°C. No evidence of a *discontinuous* reaction of chrome spinel and liquid to yield ulvöspinel has been found in the experiments on natural samples.

Ilmenite crystallization begins at c. 1095 ± 7°C and persists to the solidus. Ilmenite does not appear to be stable at the "solidus" of the olivine-enriched samples, although this mineral is plentiful in the natural rock. MgO contents of the ilmenites are 3–4.5% and Cr_2O_3 contents 1.2–1.5% in 12038, 12064 at 1086°C; and 12022 at 1103°C. Tridymite begins to crystallize at c. 1080°C less than 10°C above the apparent solidus.

Equilibrium Residual Liquid Evolution 1180–1086°C

In 12038 the cotectic liquid of group 1, silica decreases slightly with falling temperature until 1114°C (Table 5) then increases slightly; TiO_2 increases steadily; Al_2O_3 falls while CaO declines slightly; FeO, MnO rise while MgO and Cr_2O_3 fall sharply. The C.I.P.W. norms show increasing amounts of quartz and orthoclase, declining total feldspar which becomes more sodic, roughly constant total pyroxene in which the Mg/(Mg + Fe) and hypersthene/diopside ratios decrease steadily, and marked increase in normative ilmenite. Between 1180° and 1086°C this residual liquid trend is not leading conspicuously towards acidic products, but rather towards ilmenite ferrogabbros, and it does not lead towards Apollo 11-type liquids.

12040 belongs to the same group, but liquid is consumed much more rapidly between 1180 and 1137°C due to reaction with the excessive amounts of olivine. The decline in Mg/(Mg + Fe) is prevented by the buffering effect of the large amounts of magnesian olivine with which the liquid is reacting, but there is a much accelerated trend of silica depletion, coupled with TiO_2 and ilmenite enrichment, due to the rapid reduction of residual liquid volume. *This trend does in many respects lead towards the development of residual liquids with Apollo 11 characteristics* which raises the outside possibility that those basalts represent either filter pressed interstitial magmas from a horizon of olivine-rich cumulus, or a partial melting product of such a rock.

Rock 12064, close to the cotectic liquid composition of group 2, exhibits similar chemical trends to 12038, but the fall in Al_2O_3 is less marked; consequently there is less decline in total feldspar in the norm (Table 5). The turn towards silica enrichment, displayed by both 12038 and 12064 between 1114°C and 1086°C, may mark the start of the development of acid mesostasis in the residual liquids. Rock 12022, the possible olivine-enriched sample of group 3, shows little change in the liquid character except for a moderate decrease of the Mg/(Fe + Mg) ratio, but the TiO_2 contents of the liquids are ~ 6%, a value otherwise attained only in the residual liquids of 12038, 12064 at c. 1114°C, but in 12040 at 1137°C.

Table 4. Microprobe analyses of

	12040/4 1179°C	12040/4 1179°C	12040/1 1160°C	12040/2 1137°C	12040/2 1137°C
	Protohyp. (Invtd)	Pigeonite	Pigeonite	Pigeonite	Augite
SiO_2	53.44	52.40	53.02	52.37	49.80
TiO_2	0.43	1.00	0.73	0.89	1.91
Al_2O_3	1.08	2.84	1.50	1.46	3.86
Cr_2O_3	0.06	0.50	0.61	0.50	0.87
FeO	16.72	16.62	17.05	18.79	12.67
MnO	0.25	0.25	0.34	0.34	0.30
MgO	23.81	21.12	21.96	20.82	14.62
CaO	3.39	4.84	4.59	5.13	15.71
Total	99.58	99.57	99.80	100.30	99.74

Table 5. Analyses and norms of bulk rocks

	12040,36 Rock[1]	12040,4 1179°C	12040,1 1160°C	12040,2* 1137°C	12038,44 Rock[4]	12038,4 1179°C	12038,1 1160°C	12038,2 1137°C	12038,5 1114°C
SiO_2	43.89	47.23	46.86	44.90	47.13	46.91	46.81	46.24	45.08
TiO_2	2.74	3.76	4.17	6.11	3.28	3.42	3.47	4.35	5.58
Al_2O_3	7.41	10.40	11.50	10.46	13.03	12.39	12.27	11.14	9.97
Cr_2O_3	0.70	0.28	0.17	0.16	—	0.20	0.17	0.17	0.15
FeO	20.84	17.71	17.58	19.03	17.73	17.62	17.69	19.63	21.43
MnO	0.26	0.25	0.20	0.25	0.25	0.24	0.24	0.24	0.28
MgO	16.10	7.53	7.10	6.18	6.60	6.84	6.59	5.66	4.78
CaO	7.87	11.46	11.93	11.56	11.43	11.18	11.16	11.32	10.82
Na_2O	0.20[3]	0.72[3]	0.51[3]	0.73	0.69	0.77	0.74	0.78	0.85
K_2O	0.04	0.02	0.07	0.10	0.06	0.06	0.09	0.10	0.13
P_2O_5	0.07	—	—	—	0.14	—	—	—	—
S	0.06	—	—	—	—	—	—	—	—
Total	97.87	99.36	100.09	99.48	100.34	99.63	99.23	99.63	99.07
Qz	—	1.97	2.35	1.82	1.45	1.07	1.62	1.74	2.07
Ab	1.69	6.13	4.31	6.21	5.82	6.54	6.31	6.62	7.26
An	19.17	25.25	28.86	25.10	32.17	30.12	30.12	26.70	23.22
Or	0.24	0.12	0.41	0.59	0.35	0.65	0.54	0.59	0.78
Di	15.91	26.76	25.36	27.38	19.73	21.44	21.60	25.15	26.42
Hy	31.34	32.16	30.54	26.99	33.95	33.37	32.92	30.66	29.34
Ol	25.14	—	—	—	—	—	—	—	—
Ilm	5.19	7.19	7.91	11.66	6.21	6.52	6.64	8.29	10.70
Cm	1.03	0.42	0.25	0.24	—	0.30	0.25	0.25	0.22
Ap	0.17	—	—	—	0.33	—	—	—	—
Py	0.11	—	—	—	—	—	—	—	—

[1] Analyst, J. Scoon; [2] Total iron as FeO; [3] Apparent inconsistency. Reported as is; [4] Analyst, Lee C. Peck; [5] Analyst, Haramura.

pyroxenes from experimental charges.

12040/5 1114°C	12040/5 1114°C	12038/2 1137°C	12038/5 1114°C	12064/1 1160°C	12064/5 1114°C	12064/5 1114°C
Pigeonite	Augite (see text)	Pigeonite	Pigeonite	Pigeonite	Pigeonite	Augite
51.79	50.48	51.64	51.03	51.10	50.93	49.74
1.07	1.43	0.82	0.96	0.81	0.95	1.56
1.55	1.92	1.88	2.06	1.83	1.59	3.07
0.52	0.48	0.56	0.74	0.62	0.51	0.91
20.31	18.71	20.21	19.86	20.30	21.89	14.08
0.39	0.37	0.33	0.31	0.35	0.36	0.30
19.50	14.58	19.49	18.40	18.66	16.58	13.85
5.34	12.34	5.27	6.11	6.22	7.11	16.10
100.47	100.31	100.20	99.47	99.89	99.92	99.61

and equilibrium residual glasses.

12038,12* 1086°C	12064,38 Rock[1]	12064,1 1160°C	12064,2 1137°C	12064,5 1114°C	12064,12 1086°C	12022,98 Rock[5]	12022,4 1179°C	12022,15 1129°C	12022,19* 1103°C
46.40	46.41	46.35	45.58	45.41	46.38	42.33	44.36	43.77	44.62
5.72	4.14	3.97	4.43	5.50	5.74	4.54	5.81	6.76	6.17
9.07	10.50	10.56	10.59	9.75	8.91	9.12	9.72	9.92	9.91
0.13	0.38	0.20	0.15	0.15	0.12	0.56	0.22	0.12	0.17
23.19	19.95	19.36	20.46	21.68	23.08	22.06	20.78	20.53	22.96
0.33	0.27	0.28	0.30	0.31	0.37	0.26	0.27	0.30	0.31
3.37	6.38	6.57	5.57	4.50	3.46	11.58	7.55	5.72	4.38
10.51	11.71	11.64	11.76	11.15	10.63	9.37	10.93	11.36	10.71
0.72	0.30	0.45	0.78	0.86	1.03	0.29	0.42	0.73	0.66
0.20	0.07	0.07	0.08	0.08	0.21	0.07	0.13	0.13	0.32
—	0.04	—	—	—	—	0.25	—	—	—
—	0.07	—	—	—	—	—	—	—	—
99.64	100.22	99.45	99.70	99.39	99.93	100.43	100.19	99.34	100.21
5.34	2.94	2.11	0.43	2.46	3.67	—	0.07	0.99	1.80
6.11	2.53	3.83	6.62	7.32	8.72	2.45	3.55	6.22	5.57
21.00	27.04	26.73	25.23	22.63	19.08	23.33	24.21	23.56	23.08
1.19	0.41	0.42	0.47	0.48	1.24	0.41	0.77	0.77	1.89
27.06	25.92	26.44	28.27	28.22	29.08	19.06	25.11	28.04	25.65
28.21	32.53	32.60	30.31	28.17	27.12	25.56	34.97	27.32	30.06
—	—	—	—	—	—	19.71	—	—	—
10.90	7.84	7.58	8.44	10.50	10.91	8.60	11.01	12.92	11.69
0.19	0.56	0.30	0.22	0.22	0.18	0.82	0.32	0.18	0.25
—	0.09	—	—	—	—	—	—	—	—
—	0.13	—	—	—	—	—	—	—	—

* The pyroxenes and olivines in these runs were not homogeneous.

Interlaboratory Discrepancies in Atmospheric Pressure Quenching Data on Apollo 12

Our results are in close agreement with those of Muan *et al.* (1971). Like them we find small increases in the amount of the crystalline phases, in most samples, prior to the precipitation of pyroxene and feldspar; and unlike Green *et al.* (1971), who report plagioclase crystallization delayed until c. 1130°C in 12021, 12065, and 12040 when they estimate the compositions to be already c. 40%–70% crystalline. This discrepancy may result from the use of glass as a starting material by Green *et al.* (1971). We have carried out the following relevant studies.

Cooling experiments on Apollo 12 samples using unannealed glass and crystalline starting materials

(1) All nine samples held at 1250°C, 1 hour to destroy pyroxene and plagioclase nuclei, then cooled 50°C in 100 seconds and a total 96°C in 5 minutes, followed by 4½ hours at 1154°C before quenching. Well-formed crystals of chrome spinel were accompanied by skeletal crystals of protohypersthene and olivine. Pigeonite failed to nucleate in all but 12064; plagioclase failed to nucleate in group 1 samples although present in equilibrium runs at similar temperatures.

(2) Three samples (12021, 12064, 12065) held at 1159°C for 1 hour to leave only a few calcium-poor pyroxene crystals; then cooled through 75°C in 6 hours beginning at c. 7°C per hour, ending at c. 15°C per hour, followed by quenching. Prismatic, and some skeletal, pyroxene crystals were formed, showing marked exterior zoning of optical properties, set in abundant glassy matrix containing sheaves or skeletal forms of plagioclase crystals, and occasional spinel octahedra. Despite having been held at temperatures up to 55°C below the incoming of plagioclase crystallization for 4½ hours, plagioclase crystallization was inhibited, less plagioclase and pyroxene being present than is observed in equilibrium runs at the same temperature.

(3) All nine samples were heated one hour at 1306°C, cooled to 1110°C in 9 minutes, heated to 1120°C within next 10 minutes and to 1127°C during a period of 1 hour, after which the run was quenched. Again, 50°C below the equilibrium appearance of feldspar, no plagioclase nucleated in any of the samples and pyroxene nucleation was virtually absent from 12038, 12064 (contrast experiment (2) above). Skeletal crystallization was less marked than in the two preceding experiments. Experiments (2) and (3) yielded textures indicative of faster cooling than affected the natural samples, which must have cooled at less than 12°C/hour.

(4) Feldspar nucleation from glass starting materials was tested when three samples (12022, 12038, 12052) were held at 1300°C for 1 hour and quenched to yield glasses, each of which was then split and reloaded in two capsules, one with a few % of the crushed crystalline rock as seeds, the other without. The six resulting samples were then held for 1½ hours at 1129°C together with three samples of 100% natural rock powder within the equilibrium plagioclase crystallization field of the samples. Where rock powder was present, perfect euhedral crystals of feldspar formed in the products. Glass-containing charges also nucleated a very fine-grained mesh of pyroxene and plagioclase crystals. The strength of the X-ray reflections from feldspar

are weakest relative to pyroxene in the all glass charge, stronger in the seeded run, where there were large crystals of pyroxene and feldspar derived from the seeds, and strongest in the equilibrium run starting from natural rock powder. The fine-grained mesh may have originated by devitrification of the glass during the heating cycle.

The presence of 0.25 bar H_2O pressure in the furnace atmosphere in all the above experiments aids nucleation in glass starting materials and may speed approach to equilibrium.

Onset of rapid cooling: Final eruption temperature of the lavas

The phenocrysts indicate that group 1 lavas were erupted between 1160°C and 1170°C since 12038 contains equant crystals of olivine and pyroxene probably representing a phenocryst generation. Group 2 lavas erupted with pigeonite phenocrysts in all, and olivine in 12052 and 12065. This implies eruption between 1180°C and 1140°C, probably close to 1145°C if protohypersthene phenocrysts are absent from this group, and plagioclase crystals in the groundmass have adopted a trachytic texture (LSPET Apollo 12 Information Catalogue, of 12052, 12064, 12065). The group 3 lava may have been erupted at any temperature in the range 1200–1130°C on present evidence. Group 1 and group 2 lavas thus appear to have been erupted in each case at temperatures close to, but slightly above those appropriate to cotectic crystallization of spinel, olivine, calcium-poor pyroxene, and plagioclase, with the group 2 lava also close to cotectic equilibrium with augite also.

The rims of augite on the natural pigeonite phenocrysts (plus perhaps some of the pigeonite) and of ulvöspinel on the chrome spinel phenocrysts, together with all the groundmass pyroxene, plagioclase, ilmenite, and tridymite/cristobalite probably crystallized from supercooled liquids during the period of rapid cooling; as such they represent quenching products and neither they nor the interstitial residual glasses in the natural rocks can be expected to have equilibrium compositions. The Al_2O_3 content of phenocryst pigeonites reported by BENCE *et al.* (1970) from 12052 are 3–4.5%, and 5–8% in the later crystallized augite whereas *at equilibrium* in experiments on 12038, 12040, and 12064 the pigeonites contain 1–3% and the augites 3–4% Al_2O_3 (Table 4). This observation cannot be used as proof of phenocryst formation at high pressures because some of the phenocrysts display skeletal habit. Rapid growth from supercooled liquids (cf. BENCE *et al.*, 1970) is known to produce metastable clinopyroxene solid solutions with up to twice the equilibrium Al_2O_3 contents (O'HARA and SCHAIRER, 1963, pp. 108–109), which then persist for long periods of time even at high temperatures. However, it is natural to suppose that the phenocrysts were present at eruption and that they are, therefore, derived from a slightly higher pressure region.

Low Pressure Cotectic Character of the Olivine-Poor Basalts

The compositions of some of the rocks, and the probe analyses of residual liquids (Table 5) are compared with each other, and the compositions of coexisting olivines and pyroxenes (Tables 3, 4) in three projections (Figs. 5, 6, and 7). The first two figures utilize the four component projection system involving c. 99% of the rock

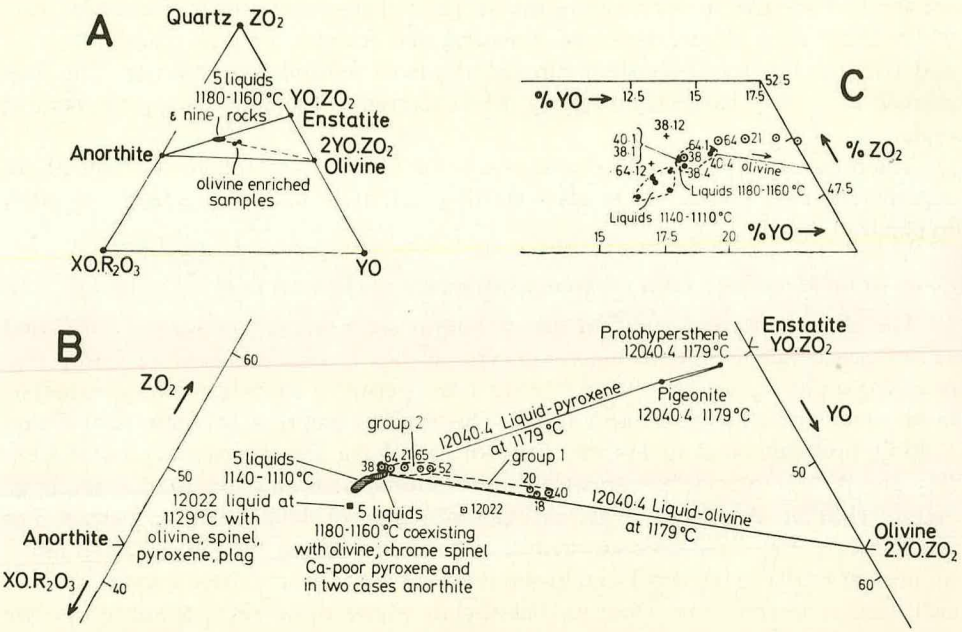


Fig. 5. Chemistry of natural Apollo 12 rock samples and low pressure, experimentally produced equilibrium crystallization cotectic liquid phases compared. The data points have been projected from diopside into the composition plane $XO \cdot R_2O_3$–YO–ZO_2 (Fig. 5A); enlargements of the relationships to show increased detail of the very close grouping of data at five and ten times the scale are shown in Figs. 5B, 5C, respectively, where small filled circles indicate compositions of analysed phases from melting experiments, identified by run number (e.g., 12040.4 or 40.4 = run 4 on composition 12040). Rock analyses are shown by open circles, numbered with the last two digits of the specimen number (e.g., 38 = 12038). Rock analyses from KUSHIRO and HARAMURA (1971), PECK, ROSE, and SCOON (personal communications). Note the predominant olivine control through 12038 and 12040 (Fig. 5B), pigeonite (+olivine) control through 12064 and 12052 (Fig. 5C), and close correspondence between rock compositions and cotectic liquids.

constituents previously used in studies of terrestrial basalt petrogenesis (O'HARA, 1968, Figs. 4–6; CLARKE, 1970; JAMIESON, 1970).

Figs. 5 and 6 illustrate three points: (1) rocks such as 12038 (group 1), 12064 (group 2) have compositions lying very close to those of the liquids in cotectic equilibrium with chrome spinel, olivine, plagioclase, calcium-poor pyroxene, and in the case of 12064, of augite also; (2) olivine basalts such as 12018, 12020, 12040 (group 1) could be related to the cotectic liquid compositions by local accumulation within them of olivine and some calcium-poor pyroxene (12020, 12040) together with some chrome spinel (not apparent from this figure). These three minerals were the phenocryst phases at the temperature of eruption; (3) pigeonite porphyries such as 12052, 12065, and 12021 can be related to the cotectic liquids by a concentration of pigeonite phenocrysts, together with some olivine and spinel.

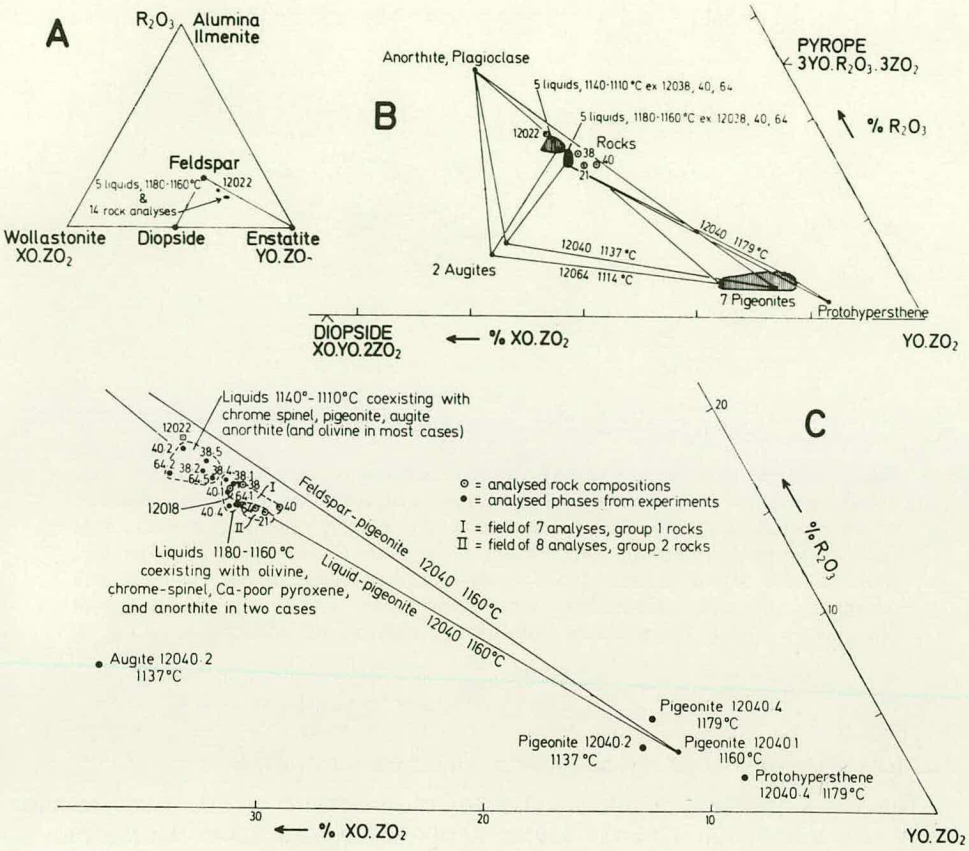


Fig. 6. Chemistry of Apollo 12 rock samples and low pressure experimentally produced equilibrium crystalline phases compared, by same technique and with same indexing and data sources as in Fig. 5, but using a projection from olivine into the plane $XO{\cdot}ZO_2$–$YO{\cdot}ZO_2$–R_2O_3 (Fig. 6A). Olivine-controlled variation is concealed by this projection. Figs. 6B and 6C show increasing detail at 5 and 10 times the scale, of the very close grouping of rock and cotectic liquid analyses, and their relationships to experimentally determined coexisting phase tie-lines.

The projection used in Figs. 5 and 6 conceals differences in Fe/Mg ratio in the silicates. Fig. 7 is a conventional projection from every other component into the system Ca–Mg–Fe. This illustrates the similarity between experimentally produced early crystalline phases ($\sim$ 1140°C) and the phenocryst core compositions. Fig. 7 confirms the three conclusions reached from Fig. 5. There is close correspondence between the bulk normative pyroxene compositions of suggested near cotectic lavas 12038, 12064, and the same parameter of the 1160–1137°C experimental liquid compositions in equilibrium with three, four, or five crystalline phases. Note also the progressive iron-enrichment of residual liquids in 12038, 12064, and the arrested iron-enrichment in the case of 12040 which is controlled by excessive amounts of magnesian olivine.

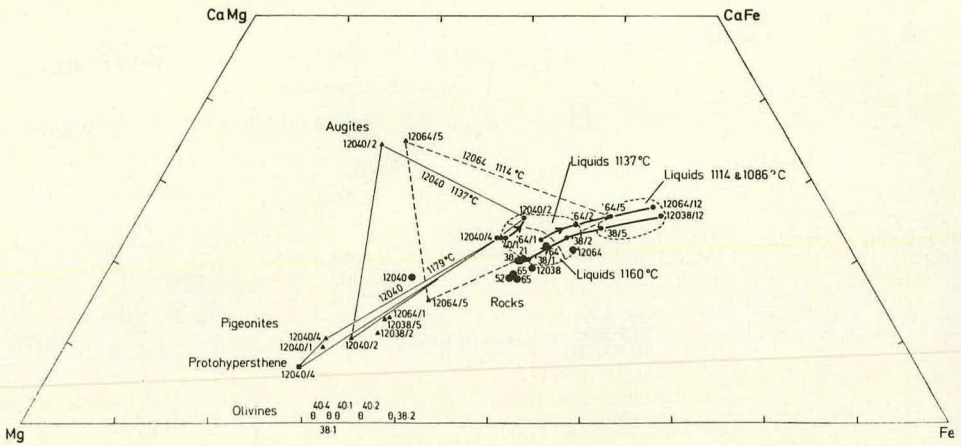


Fig. 7. Chemistry of Apollo 12 rock samples and low pressure experimentally produced equilibrium crystalline phases compared, using a Ca–Mg–Fe molar projection of the experimentally produced pyroxene and olivine compositions, and of the bulk C.I.P.W. normative pyroxene compositions in the natural rocks and analysed equilibrium cotectic liquid phases. Open circles = olivine compositions, squares and triangles = pyroxene compositions, large filled circles = rock compositions, small filled circles = glass compositions from melting experiments. Indexing as in Fig. 5.

Average composition of lavas 1 and 2 on eruption; Parental liquids

The classic problem of interpretation of olivine-phyric picritic basic magmas arises with the Apollo 12 lavas 12018, 12020, 12022, and 12040. In the case of Kilauean tholeiites accumulation of liquidus olivine within a parental lava of much less olivine-normative character has been proved (MURATA and RICHTER, 1966). The phenocryst mineralogy of 12018, 12020, and perhaps 12022 demonstrates eruption at a temperature where most of the normative olivine would have been present as crystals. ROEDDER and WEIBLEN (personal communication) find that the glass inclusions in these olivine crystals have olivine-poor compositions, and that inward zoning of the olivine wall to the glass inclusion (due to further crystallization of olivine in equilibrium with the inclusion) has been reversed below 1200°C. Olivine growth and accumulation within liquids more like 12038 at temperatures close to the low pressure cotectic temperature is indicated; the situation is analogous to that found by MURATA and RICHTER (1966).

AGRELL *et al.* (1971) report no glass fragments of 12018, 12020, 12040, or 12022 composition from the soil, but many approximating to 12038, 12064 in composition. CHAMPNESS *et al.* (1971) report a similar situation among small rock fragments in the soil from this site. The parental magmas to these flows were close to the cotectic liquids in average composition and there is no basis for supposing more olivine-rich liquids were common, or for treating the olivine-enriched samples as crystallization products of primary partial melt magmas.

Low Pressure Cotectic Liquid Character of the Apollo 11 Lavas Re-Examined

O'Hara *et al.* (1970) deduced that Apollo 11 lavas had compositions close to those of liquids simultaneously in equilibrium with olivine, calcium-poor and calcium-rich pyroxene, plagioclase, and one or more titanium oxide-rich phases. Anderson *et al.* (1970), Ringwood and Essene (1970), Weill *et al.* (1970), and Tuthill and Sato (1970) all reported substantial crystallization of titanium oxide-rich phases, olivine, and pyroxene before the precipitation of plagioclase, whence Ringwood (1970) and Tuthill and Sato (1970) deduced that the lava compositions were in fact well removed from true low pressure cotectic liquid compositions. A decision between these two interpretations is fundamental to much that follows. Precisely what was done by each experimental group must first be appreciated.

O'Hara *et al.* (1970) studied 2 natural Apollo 11 samples and 13 synthetic analogs. The other four groups each used a single synthetic analog, those of Anderson *et al.* (1970), and Weill *et al.* (1970) being significantly enriched in potential olivine and pyroxene relative to the average composition of the natural samples (Figs. 8, 9). In view of the compositions they used we would be surprised if these two groups found them to be close to cotectic compositions. The Ringwood and Essene (1970) composition lay very close to the average composition of the natural rocks but their experiments were conducted for relatively short times (1–2 hours).

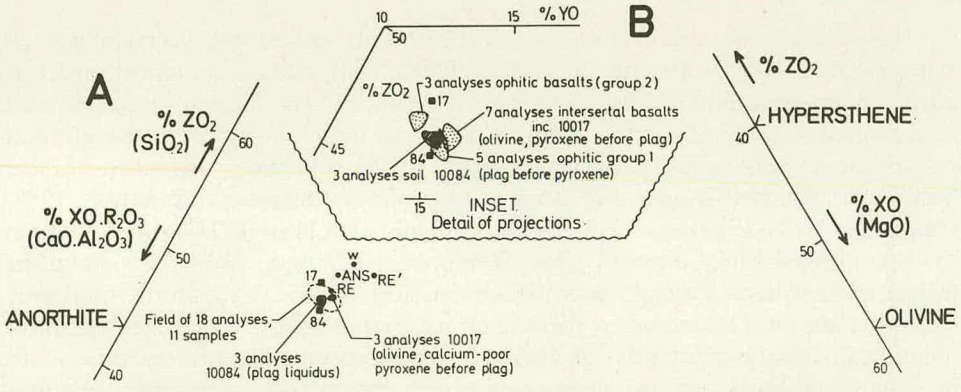


Fig. 8. Comparison of Apollo 11 basalt and soil analyses with details of crystallization sequence of feldspar, olivine, and pyroxene (Fig. 8A) based on experiments on 10017, 10084 indicated on the diagram. Projection as Fig. 5. Detail of projection at twice the scale in Fig. 8B implies that ophitic basalts may have nucleated plagioclase before pyroxene, and the intersertal group pyroxene before plagioclase. All experimental data were obtained at or close to saturation with spinel and ilmenite also. Rock analyses from Agrell *et al.* (1970), Compston *et al.* (1970), Engel *et al.* (1970), and Maxwell *et al.* (1970). Filled circles represent the synthetic compositions investigated by Anderson *et al.* (1970), ANS; Ringwood and Essene (1970), RE (and RE', $+10\%$ $MgSiO_3$), Weill *et al.* (1970), W, and (in Fig. 10 only) Tuthill and Sato (1970), TS. Filled squares represent cotectic liquid compositions from 10017,17 and 10084,84 as in Table 6.

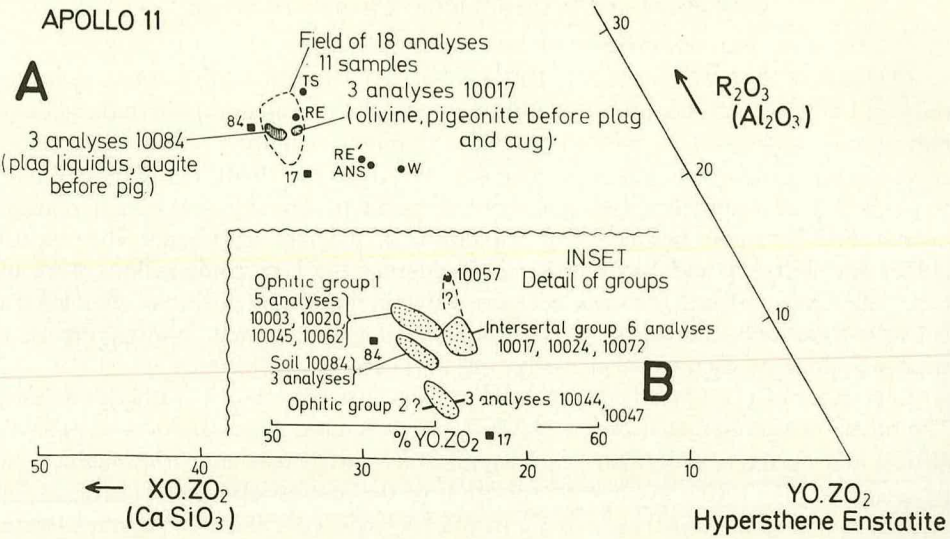


Fig. 9. Comparison of Apollo 11 basalt and soil analyses with details of crystallization sequence of feldspar, pigeonite, and augite based on experiments on 10017, 10084. Projection as in Fig. 6. Detail of projection at twice the scale in Fig. 9B showing the two apparent ophitic groups. Data as in Fig. 8.

The samples used by O'HARA *et al.* (1970) were either wholly crystalline (13 synthetics and 10017) or partly crystalline (10084, soil), and all contained nuclei of all the major crystalline phases at the start of each run. The other four groups used unannealed glasses prepared by fusion at 200°C or more above that of equilibrium plagioclase crystallization. Unannealed glass has been avoided by most workers because of the well-known difficulties of attaining equilibrium (SCHAIRER, 1959; CHALMERS, 1964). Experience with the diopside-spinel problem (O'HARA and BIGGAR, 1969) confirmed using annealed glass (SCHAIRER and YODER, 1970) shows that our technique does lead to a close approach to equilibrium, and this is further indicated by the perfect form developed by the plagioclase crystals at their highest temperatures of survival. The use of unannealed glass as a starting material inhibits the appearance of plagioclase while perhaps encouraging excess precipitation of simpler structures such as spinel and olivine. We can demonstrate this effect in the case of Apollo 12 samples; ROEDDER and WEIBLEN (1970, pp. 808/9) report it for liquid inclusions in olivines from Apollo 11 rocks.

To illustrate the close approach to low pressure cotectic character of the Apollo 11 rocks, two data projections (Figs. 8, 9) are shown. Following JAMES and JACKSON (1970) and TUTHILL and SATO (1970), the textural difference between the intersertal and ophitic groups of Apollo 11 indicate a change in the order of nucleation of plagioclase and pyroxene. Table 6 contains some probe analyses of phases produced in runs on samples 10017 and 10084 which demonstrate that there has been only a small change of magma composition prior to the entry of five crystalline phases

Table 6. Probe analyses of equilibrium residual (cotectic) glasses in 10017 at 1133°C; 10084 at 1162°C, $fO_2 \sim 10^{-12.5}$ bar, compared with the average compositions of the intersertal and ophitic group lavas and soil (from COMPSTON *et al.*, 1970, Table 4) and with a single analysis of 10047 (COMPSTON *et al.*, 1970, Table 1) belonging to ophitic group 2 (Figs. 8, 9).

	Group 1 intersertal	Group 2 ophitic	10017/51 1133°C[1]	10047	10084/16 1162°C[2]	10084 soil
SiO_2	40.28	40.47	44.09	42.16	41.91	42.03
TiO_2	11.88	10.32	8.31	9.43	9.24	7.50
Al_2O_3	8.95	10.41	10.09	9.89	10.52	13.84
Cr_2O_3	—	—	0.09	—	0.16	—
FeO	19.21	18.72	18.13	19.11	17.23	15.76
MnO	0.24	0.27	0.28	0.28	0.34	0.21
MgO	7.60	6.66	5.92	5.67	7.03	7.87
CaO	10.53	11.48	11.07	12.15	11.62	11.98
Na_2O	0.64	0.49	0.62	0.45	0.83	0.45
K_2O	0.31	0.09	0.59	0.11	0.16	0.14
TOTAL	99.64	98.91	99.19	99.25	99.23	99.78

[1] With ilmenite, augite, olivine Fo_{66}; plagioclase about to crystallize; [2] With plagioclase, augite, ilmenite, spinel and olivine Fo_{75} (identified by microprobe).

(olivine, pyroxene, ilmenite, spinel, and plagioclase). Calculations from the analyses on the assumption that the small sample (O'HARA *et al.*, 1970, p. 697) of 10017,51 available was truly representative, suggest c. 24% crystallization prior to the entry of plagioclase below 1133°C, cotectic crystallization of chrome ulvöspinel, ilmenite, augite, and olivine *already* being observed from the liquid prior to that stage. We measure 8.3 and 9.1% TiO_2 in appropriate residual liquids from the natural rocks, confirming the indications from experiments on nine synthetic compositions (O'HARA *et al.*, 1970, Fig. 2) at oxygen fugacities of 10^{-8}–$10^{-12.5}$ bar.

Petrographic evidence of cotectic character from Apollo 11 rocks

The careful petrographic account of the Apollo 11 basalts by JAMES and JACKSON (1970, p. 5799) makes clear that the ophitic group fine-grained members were precipitating plagioclase before all the olivine had formed (maximum 6–8%) at which stage spinel ($\sim$ 0.5%) had already crystallized and some ilmenite was already present. Ilmenite, which precipitates over a long temperature interval, amounts to only 14% of the final crystallization products. 3½% ilmenite precipitation would be sufficient to lower the TiO_2 content from the starting value to that observed in the cotectic liquids (Table 6). It is reasonable to estimate that these basalts contained less than 10% crystalline material when plagioclase began to precipitate, and it is further clear from JACKSON and JAMES (1970, p. 5799) that augite and/or pigeonite also began to precipitate at almost the same stage—i.e., 6 crystalline species were present as microphenocrysts after c. 10% solidification. This evidence from the natural rocks conflicts with RINGWOOD's (1970, pp. 6455, 6465) estimate of more than 30–50% in experiments on synthetic simulations of the Apollo 11 basalts, and we have ascribed this to delayed nucleation consequent on use of unannealed glass as a starting material. The large number of phases present at low degrees of solidification in the natural rocks, and their variable order of appearance, clearly indicate that the original

compositions lay just within the primary phase volume of chrome spinel, virtually at its junction with the primary phase volumes of olivine and ilmenite, and only a short distance from their simultaneous junctions with the primary phase volumes of pigeonite, augite, and plagioclase. This is what we call cotectic character. Furthermore, it is clear from the phenocryst assemblages that these magmas, like the Apollo 12 lavas, were erupted with temperatures, as well as compositions, close to that of the atmospheric pressure cotectic equilibrium.

Close approach to low pressure cotectic liquid character reaffirmed; departures discussed

The Apollo 11 lavas have compositions close to atmospheric pressure cotectic liquids. Apollo 12 lavas, while displaying some sorting of phenocrysts after eruption, are even closer in composition to atmospheric pressure cotectic liquids. They had eruption temperatures close to these equilibria. Small discrepancies between the crystallization behavior of Apollo 11 and Apollo 12 lavas and true atmospheric pressure cotectic character indicate that cotectic character was imposed on the magmas under slightly different conditions from those accompanying eruption.

An increase in pressure in compositions similar to the lunar maria lavas is known to suppress the liquidus fields of olivine, spinel, ilmenite, and armalcolite. O'HARA *et al.* (1970, Table 7 and Fig. 2) report suppression of the titanium oxide phase liquidus in synthetic composition 9 (11.1% TiO_2) at less than 2 kb. A further fall in pressure on eruption will lead to a small displacement of the liquid composition away from olivine, spinel, and titanium oxide phase compositions; hence these phases will crystallize early from the erupted magmas. Any volatilization losses will displace the erupted magma composition towards these mineral compositions rather than away from them. These are precisely the types of departure from atmospheric pressure cotectic character which are displayed by Apollo 11 and Apollo 12 lavas.

LAVA LAKES AND FIRE FOUNTAINS

The topographic form of lunar maria is that of a lava lake, roofless lopolith, or a hollow filled by a succession of thin fluid flows of lava. In the lava lake or roofless lopolith situation, filling of the hollow by a relatively small number of magma pulses is implied, and indicated if a major impact is accepted as the triggering mechanism. Fire fountaining is commonly observed during eruption of such magmas.

The choice between the lava lake (O'HARA *et al.*, 1970) and the multiple eruption lava field (KANE *et al.*, 1969; ESSENE *et al.*, 1970) is critical to discussions of mass balance in the moon. If the last lava to be poured out is very rich in incompatible elements, then all the underlying lavas must be as rich or richer in these elements if direct incipient partial melting is their origin. But if the last lava represents a spill from the final few % of residual liquid in an underlying lava lake, then the high incompatible element concentrations will be found only in the topmost 1–2% of the basic igneous maria filling, thus reducing *by nearly two orders of size* either the volume of lunar mantle which must be depleted in partial melting, or alternatively the initial concentration of incompatible elements required to meet the mass demands within a particular partly melted volume.

Experimental proof of volatilization effects: Petrogenetic effects

DE MARIA *et al.* (1971) have measured the vapor pressure over samples 12022 and 12065. These samples still develop vapor pressures of Na, K, Fe, and O_2 at their liquidus temperatures which are greatly in excess of lunar surface pressures, confirming in principle our own experiments (O'HARA *et al.*, 1970) carried out on an alkali-enriched simulated lunar magma at 1200°C. SMALES *et al.* (1964) also report ready volatilization of K, Rb, and Cs at temperatures lower than those accompanying eruption. SATO and HELZ (1971) calculate that in the absence of sulphur, volatilization losses of oxygen on eruption would have been sufficient to reduce the oxygen fugacity to within one order of size of that observed in the lunar basalts, with the appearance of metallic iron. Sulphur is present and may account for the further reduction in oxygen fugacity.

The lunar lavas established an atmosphere by selective volatilization of Na, K, O_2. Equilibrium was not reached, but losses may have been substantial during fire fountaining or if the flow is thin and widespread. Loss of oxygen leads to metallic iron precipitation, to a less olivine-normative character, to increase in the amount of hypersthene, and to a lower Fe/Mg ratio in the silicates (eq. (1)):

$$Fe_2SiO_4 + Mg_2SiO_4 = 2MgSiO_3 + 2Fe + O_2 \qquad (1)$$

Loss of Na increases hypersthene at the expense of olivine, and decreases the amount of diopside as anorthite is formed (eq. (2))

$$\underbrace{3NaAlSi_3O_8 + 3CaAl_2Si_2O_8}_{\text{labradorite-andesine}} + 5Mg_2SiO_4 + CaMgSi_2O_6$$

$$= \underbrace{4CaAl_2Si_2O_8 + NaAlSi_3O_8}_{\text{bytownite}} + 11MgSiO_3 + 2Na + O \qquad (2)$$

LARIMER (1967) suggests that SiO_2, as sodium silicate, might also have been volatile, in which case silica enrichment would be less marked.

The effect of volatilization losses upon tholeiitic magmas would be a trend of crystallization marked by low oxygen fugacity, early metallic iron precipitation, inhibited Fe/Mg enrichment in remaining silicates (relative to the build up of incompatible elements), excessive calcium-poor pyroxene precipitation, and excessively calcic feldspar development. All these mineralogical-geochemical features are found in the calcium-rich achondrite igneous series (MOORE, 1962; MASON, 1962; and DUKE and SILVER, 1967) and in the lunar maria lavas, pointing to the importance of volatilization-fractionation (O'HARA *et al.*, 1971) as a petrogenetic process on small planets. Volatilization losses prevent lunar basalts being treated as primary magmas to deduce lunar mantle compositions.

Incompatible element concentrations indicate late stage residual liquids

High concentration of the incompatible elements in basic magmas can result in (1) a primary magma formed by a very small degree of incipient partial melting (say 1%) of a source rock with more normal chemistry; (2) the late residual liquid of

extreme fractional crystallization of a primary or parental magma body originally formed by c. 20–30% partial melting of the same source rock; or (3) a primary or parental magma seriously contaminated by previously differentiated crustal material. Only in the first case is the resultant composition valid for high pressure experiments to determine the mineralogy of the lunar interior. Partial melting *followed* by extreme fractionation of the resultant magma body can yield much higher concentrations of "incompatible" elements than direct partial melting (no matter how small the amount) of the same source rock (BOWEN, 1928, p. 35); the concentration of the incompatible element enriched basalt into a single small magma body is an inevitable by-product of the fractional crystallization hypothesis. In the Skaergaard intrusion enrichments of the rare earth elements comparable with those seen in the Apollo 11 and Apollo 12 basalts develop at a very late stage of the crystallization (HASKIN and HASKIN, 1968).

Apollo 11 basalts should be envisaged as residual liquids after 98% or more crystallization of the original magma body in the light of their REE concentrations. The REE concentrations would support a later than 90% stage of fractionation for the Apollo 12 basalts. The Apollo 12 basalts have Mg/(Mg + Fe) consistent with the residual liquids at the 80% crystallization stage in terrestrial layered intrusions, perhaps a later stage in the lunar case where iron-enrichment may have been inhibited by the early precipitation of metallic iron. Because of the large amount of calcic plagioclase suspected to have fractionated a europium deficiency is to be expected, and enhanced because, at low oxygen fugacity and low confining pressure europium oxide is so volatile relative to other REE that it can be distilled by the kilogram in short times (ACHARD, 1966).

Evidence of low oxygen fugacity throughout low-pressure fractionation

Low fO_2 inhibits early precipitation of Cr^{3+}, V^{5+}, Fe^{3+} as spinel; consequently Cr and V will be concentrated in residual liquids until a late stage of crystallization (contrast RINGWOOD, 1970) provided fO_2 was low throughout.

A distinctive geochemical feature of the Apollo 11 and Apollo 12 lavas is their depletion in siderophile elements *relative to terrestrial basalts and carbonaceous chondrites* (MASON and MELSON, 1970; ANDERS *et al.*, 1971). This implies equilibration of the system with a metal phase *followed by* separation of the silicate (liquid) from the metal. If equilibration and separation of the metal phase occurred during near surface fractional crystallization, concentrations of dense iron should occur near the base of some maria fillings, consistent with the deduced location of observed mass-concentrations.

Rb–Sr data: Extent of Volatilization and a Possible Metamorphism

The ophitic group of Apollo 11 lavas and all the Apollo 12 rocks have the Rb/Sr characteristics of systems which have suffered no fractionation of Rb from Sr since 4.5 b.y. (PAPANASTASSIOU and WASSERBURG, 1970). Neither volatilization, fractional crystallization nor partial melting can have affected these rocks since 4.5 b.y. ago because all three processes would have fractionated Rb relative to Sr (cf. UREY *et al.*, 1971). The igneous events connected with maria formation must have occurred

4.5 b.y. ago, and the isochron ages of 3.7–3.3 b.y. obtained from the Apollo 11 and Apollo 12 rock samples must represent widespread metamorphic events (SILVER, 1970).

Nature of the underlying cumulus from Apollo 12 lavas

The Apollo 12 basalts, prior to eruption, were in equilibrium with calcic plagioclase and pigeonite or protohypersthene, the Mg/(Fe + Mg) of the silicates being 0.70. Olivine is in reaction relationship with the liquid. Its presence, like that of chrome spinel, may be due to expansion of the liquidus field with falling pressure but it would *not* form a significant part of the accumulating crystalline phases in the lava lake. That cumulus would have consisted of calcic plagioclase, pigeonite (liable to recrystallize to hypersthene and augite on slow cooling), and perhaps minor chrome spinel; any trapped interstitial liquid might subsequently crystallize to yield spinel, ilmenite, and tridymite as accessory phases.

There is a well-known rock type having this mineralogy—the howardite group of the achondrites. (The mineralogy deduced for these underlying cumulates is such that if fragments were observed to fall as meteorites, their finder would classify them with the howardites or eucrites. No more specific correlation is intended. The term *norite*, which is being applied to certain fragments in the lunar regolith, and in particular the type A norites (WOOD *et al.*, 1971), describes a rock type somewhat similar to that envisaged here *except for* the P_2O_5 and minor element contents). Further fractionation of the minerals with accompanying cryptic variation would lead to the formation of essentially calcic plagioclase-pigeonite (Mg/(Mg + Fe) ~ 60) rocks, in which the pigeonite is more likely to be preserved on cooling, yielding a mineralogy analogous to the eucrite group of the achondrites.

Ultimately this fractionation trend must lead to the precipitation of calcium-rich clinopyroxene in addition to, or instead of pigeonite. Lack of depletion in the light REE indicates that calcium-rich pyroxene has not played a prominent part in the early fractionation sequences (contrast GAST and HUBBARD, 1970). The increasing TiO_2 content of the liquid will at some stage result in the precipitation of ilmenite, ulvöspinel, or armalcolite. The late stage cumulus might include bytownite-ilmenite norite or gabbro. In the very late stages of fractional crystallization of layered intrusions the concentrations of elements such as K, P grow high enough for K-feldspar and apatite or, in the case of volatile depleted rocks, whitlockite to join the accumulating phases. K-feldspar removes K, Rb, Cs, and Ba from the liquid; whitlockite reduces the P, REE, Y, Zr. These reductions of "incompatible" elements in the residual liquid would be accompanied by a further fall in the Mg/(Mg + Fe) ratio.

Material answering some of the geochemical requirements of this very late stage cumulus has been reported from the Sea of Tranquillity and the Ocean of Storms (ALBEE and CHODOS, 1970, Luny Rock 1; FUCHS, 1970, fragment A; DRAKE *et al.*, 1970; HUBBARD and GAST, 1970, dark portion 12013; GAST and HUBBARD, 1970, KREEP). The final stages of fractionation of large terrestrial layered intrusions terminates with the formation of diminutive volumes of granophyres. MASON *et al.* (1971) report the finding of hedenbergite-fayalite-granophyres which they compare with the late stage products of terrestrial layered intrusions.

Relationship between the two lava groups of Apollo 11

The ophitic group has lower Mg/(Mg + Fe), lower K, Rb, Cs, Ba, REE, Y, and Zr, than the intersertal group (COMPSTON *et al.*, 1970). These are the changes expected in the late stage residual liquids, just prior to the development of granophyric liquids, except that neither K nor P has a sufficient concentration in the lavas to have saturated the liquid with feldspar or whitlockite. However, both these elements are volatile at low pressures and low oxygen fugacities; they could have been lost from the lavas after final eruption.

Achondrites, mesosiderites, and lunar maria lavas

HESS and HENDERSON (1949) identified the igneous cumulative texture of the Moore County eucrite; MOORE (1962), MASON (1962, 1967), and DUKE and SILVER (1967) all recognized the mesosiderite, pallasite, hypersthene achondrite, howardite, and eucrite groups of the meteorites as having a possible igneous fractionation interrelationship and the last authors suggested that these meteorites might have formed in layered igneous masses on the surfaces of small planetary bodies, specifically mentioning the lunar maria in this context. The lavas returned by the Apollo 11 and Apollo 12 missions qualify as complementary liquids to such a cumulus sequence; hence we support the DUKE and SILVER (1967) model, and suggest that the lunar maria are each underlain by layered sequences of mesosiderite-like, hypersthene achondrite-like, howardite-like, and eucrite-like igneous rocks (without implying specific identity with the particular sources of known achondrite falls). Fig. 10 illustrates the way in which the DUKE and SILVER (1967) model for achondrite meteorite formation and our model of lunar basalt petrogenesis can be married to yield a possible geological section for the lunar maria.

INTERGROUP AND INTRAGROUP CONNECTIONS BETWEEN THE APOLLO 12 LAVAS

In previous sections we have, implicitly or explicitly, proposed that the following relationships are true:

$$\begin{gathered}12038 + \text{olivine} + \text{chrome spinel} + \text{pigeonite} \\ \text{(low pressure phenocrysts)} \\ = 12040 \\ \text{phenocryst enriched lava}\end{gathered} \tag{1}$$

$$\begin{gathered}12064 + \text{pigeonite} + \text{olivine} + \text{chrome spinel} \\ \text{(low pressure phenocrysts)} \\ = 12052 \\ \text{(phenocryst enriched lava)}\end{gathered} \tag{2}$$

and

$$\begin{gathered}12064 + \text{calcic plagioclase} + \text{(exsolved) pigeonite} + \text{? chrome spinel} \\ \text{(“howardite” cumulus in underlying magma chamber)} \\ = 12038 \\ \text{earlier cotectic liquid}\end{gathered} \tag{3}$$

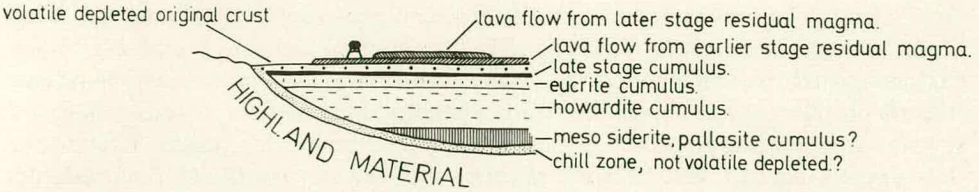


Fig. 10. Hypothetical cross-section of lunar maria illustrating disposition of rock types consistent with experimental and petrological observations, topography, and the Duke and Silver interpretation of achondrite relationships.

Table 7. Results of calculations.

	12040	12038(54.0%) + A(46.0%)	A	12052	12064(84.4%) + B(15.6%)	B	12038	12064(79.7%) + C(20.3%)	C	D	Bununu howardite
SiO_2	43.59	43.88	40.2	46.33	46.26	47.2	46.98	46.99	50.5	50.6	50.63
TiO_2	2.48	1.96	0.5	3.17	3.36	0.9	3.22	3.17	0.6	0.7	0.11
Al_2O_3	7.34	7.71	2.6	10.26	10.17	6.0	12.11	12.08	16.6	8.3	9.23
Cr_2O_3	0.70	0.67	1.1	0.55	0.55	1.6	0.34	0.42	0.6	0.5	0.58
FeO	20.87	21.37	25.4	19.87	19.73	19.4	17.89	17.88	10.4	16.1	16.69
MnO	0.26	0.28	0.3	0.27	0.27	0.3	0.24	0.25	0.2	0.3	0.55
MgO	16.66	16.43	27.4	8.42	8.48	18.6	7.08	7.16	9.4	15.6	14.77
CaO	7.90	7.31	2.5	10.79	10.89	5.9	11.45	11.65	11.0	7.6	7.04
Na_2O	0.16	0.39	0.1	0.28	0.27	0.2	0.64	0.38	0.8	0.3	0.35
K_2O	0.05	0.04	—	0.07	0.06	—	0.07	0.06	—	—	0.04
P_2O_5	0.02	0.02	—	0.03	0.02	—	0.02	0.02	—	—	—

Results of calculations to test petrogenetic relationships proposed in text. All analyses normalized to 100%. Mineral compositions used in obtaining solutions were plagioclase. An_{85}(calc.), pigeonite from experimental run 12038/2 at 1137°C (Table 4), olivine from run 12038/1 at 1160°C (Table 3), and chrome spinel from 12064,6 (HAGERTY and MEYER, 1970). Columns A, B, C represent the calculated extract compositions, their mineral ratios being A = $pig_{22.6}ol_{69.8}plag_{5.5}sp_{2.1}$; B = $pig_{68.4}ol_{15.8}plag_{12.8}sp_{3.0}$; C = $pig_{63.9}ol_{-9.4}plag_{44.8}sp_{0.7}$. The appearance of plagioclase in the extracts A and B reflects the use of a pigeonite in calculation which is poorer in Al_2O_3 than the modal phase; the appearance of negative olivine in extract C implies that the best source liquid for derivation of 12064 by "howardite" crystallization would be 12038 + c. 2.5% extra dissolved olivine. D = $pig_{80}plag_{20}$ is a further mixture for comparison with the Bununu meteorite silicate phase composition (MASON, 1967).

These propositions have been tested (Table 7) using the program written by WRIGHT and DOHERTY (1970). Rock 12038 contains exceptionally large amounts of Na_2O among lunar rock samples and may have escaped some of the volatilization losses affecting the lavas generally. Na_2O is the only component not to yield a satisfactory fit in the solutions, and reduction of Na_2O from 0.64% to c. 0.40% (or increasing Na_2O slightly in 12064 or 12040) greatly improves the fit. The possibility of adcumulus growth in 12040 (WAGER and BROWN, 1968, p. 227) means that the suggested relationship cannot be rejected on grounds of unbalance among the minor elements. The solutions obtained indicate that the essential chemical difference between the compositions of lava groups 1 and 2 is expressible in terms of extraction of a calcium-poor pyroxene + calcic plagioclase cumulus. The differences within each lava group are reasonably explained in terms of the sorting of the phenocryst phases now present.

RESTATEMENT OF THE FRACTIONATED LAVA-LAKE HYPOTHESIS

The working hypothesis which best fits the available information involves, for all the maria, (1) partial melting and extraction of c. 10–30% partial melt from a lunar mantle about whose detailed mineralogy and chemistry very little can be deduced; (2) eruption of these parental magmas into the maria basins to form large

lava lakes. Volatilization losses to the lunar atmosphere depleted the magmas in all volatile constituents among which the alkalis and europium were prominent. A low oxygen fugacity was imposed on the magma at this stage; it is not possible to deduce the pre-eruption oxygen fugacity or water content; (3) formation of a crust, followed by slow and extreme fractional crystallization of the underlying magma. Due to the low oxygen fugacity, metallic iron, together with olivine, "pallasite" (mesosiderite) was a significant constituent of the early cumulates (mascon formation). The low oxygen fugacity reduced the activity of the higher oxides of iron, chromium, and vanadium, preventing early chrome spinel or magnetite precipitation and subsequently delaying iron-titanium oxide precipitation. Cr, V contents of the liquids, therefore, increased gradually until very late stages of crystallization were reached and Ti enrichment also continued to later stages and more extreme values than would have occurred at higher oxygen fugacities. At the same time early extraction of a metal phase depleted the magma in Fe, Ni, Co, and other siderophile elements such that attainment of a particular Mg/(Fe + Mg) ratio in the residual liquids and their precipitates was reached at a later stage than would have been the case at higher oxygen fugacities. Loss of alkalis by volatilization released additional Al_2O_3 from potential alkali feldspar in the magma, thereby increasing the likelihood of anorthite precipitation and suppressing augite precipitation; the additional silica released by the same process contributed to the formation of hypersthene at the expense of olivine. Substantial volumes of olivine-hypersthene and hypersthene cumulus and hypersthene + calcic plagioclase (howardite) accumulates were succeeded by lesser pigeonite + calcic plagioclase (eucrite) accumulates, and finally by very small volumes of rocks in which augite, ilmenite, ulvöspinel, apatite, and biotite were cumulus phases.

(4) Periodic foundering of the crust or penetration by impact and release of the residual magmas permitted formation of lava flows and further release of alkalis and other volatiles. The lava flows sampled from the Ocean of Storms and the Sea of Tranquillity represent samples of the underlying liquids at the greater than 80% solidified stage.

As noted previously (O'HARA *et al.*, 1970, p. 709), this type of hypothesis permits, *but does not demand*, derivation of the whole sequence from familiar terrestrial source magmas, and is consistent with several plausible lunar mantle compositions. Development of the magmas within each lake followed independent but broadly similar lines.

Nature of the lunar interior in the light of experimental studies

The evidence that extensive low pressure fractionation and volatilization has modified the composition of the parental magmas supplied to the maria is overwhelming. *Nothing* can be deduced about the mineralogy of the lunar interior from experimental studies until those fractionation effects have been unravelled and reversed to obtain a realistic estimate of the parental magma composition.

SUMMARY OF CONCLUSIONS

Protohypersthene-crystallizing basic lavas from the Ocean of Storms were erupted as low pressure cotectic residual liquids from an underlying magma body, already as

much as 80% crystallized. The lunar maria are differentiated lava lakes, filled by rock types familiar among the achondrites, floored by early metal precipitates which form mass concentrations, and capped by lava flows representing the late residual liquids of the fractionation sequence. The distinctive geochemical and petrographic characteristics of this magmatic kindred relative to terrestrial experience were controlled by volatilization losses during eruption and crystallization. The igneous events leading to maria formation may have been very early and were triggered by major impacts. Subsequent metamorphism may have yielded the apparent 3.3–3.7 b.y. ages of the rocks.

Acknowledgments—The Natural Environment Research Council (U.K.) supported this research. We thank particularly S. O. Agrell, G. M. Brown, I. Kushiro, and D. B. Stewart for their help during the work, and our long-suffering referees during preparation of this paper.

References

Achard J. C. (1966) Reduction et volatilisation des oxydes de terres rares. *Rev. Hautes Temper. et Refract.* **3,** 281–289.

Agrell S. O., Scoon J. H., Muir I. D., Long J. V. P., McConnell J. D. C., and Peckett A. (1970) Observations on the chemistry, mineralogy, and petrology of some Apollo 11 lunar samples. *Proc. Apollo 11 Lunar Sci. Conf., Geochim. Cosmochim. Acta* Suppl. 1, Vol. 1, pp. 93–128. Pergamon.

Agrell S. O., Long J. V. P., and Reed S. J. B. (1971) A comparison of glasses from the Apollo 11 and 12 missions. Second Lunar Science Conference (unpublished proceedings).

Albee A. L. and Chodos A. A. (1970) Microprobe investigations on Apollo 11 samples. *Proc. Apollo 11 Lunar Sci. Conf., Geochim. Cosmochim. Acta* Suppl. 1, Vol. 1, pp. 135–157. Pergamon.

Anders E., Laul J. C., Keays R. R., Ganapathy R., and Morgan J. W. (1971) Elements depleted on lunar surface: Implications for origin of moon and meteorite influx rate. Second Lunar Science Conference (unpublished proceedings).

Anderson A. T., Crewe A. V., Goldsmith J. R., Moore P. B., Newton J. C., Olsen E. J., Smith J. V., and Wyllie P. J. (1970) Petrologic history of moon suggested by petrography, mineralogy, and crystallography. *Science* **167,** 587–589.

Anderson A. T., Newton R. C., and Smith J. V. (1971) Mineralogy and petrology of some Apollo 12 samples: General comments on petrology of the moon. Second Lunar Science Conference (unpublished proceedings).

Bence A. E., Papike J. J., and Prewitt C. T. (1970) Apollo 12 clinopyroxenes: Chemical trends. *Earth Planet. Sci. Lett.* **8,** 393–399.

Bowen N. L. (1928) *The Evolution of the Igneous Rocks.* Dover (reprint 1956), 251 pp.

Chalmers B. (1964) *Principles of Solidification.* J. Wiley.

Champness P. E., Dunham A. C., Esson J., Fyfe W. S., Gibb F. G. F., MacKenzie W. S., Stumpfl E. F., and Zussman J. (1971) Some aspects of the mineralogy and petrology of Apollo 12 rocks. Second Lunar Science Conference (unpublished proceedings).

Clarke D. B. (1970) Tertiary basalts of Baffin Bay: Possible primary magma from the mantle. *Contrib. Mineral. Petrol.* **25,** 203–224.

Compston W., Chappell B. W., Arriens P. A., and Vernon M. J. (1970) The chemistry and age of Apollo 11 lunar material. *Proc. Apollo 11 Lunar Sci. Conf., Geochim. Cosmochim. Acta* Suppl. 1, Vol. 2, pp. 1007–1028. Pergamon.

De Maria G., Balducci G., Guido M., and Piacente V. (1971) Mass spectrometric investigation of the vaporization process of lunar samples. Second Lunar Science Conference (unpublished proceedings).

Drake M. J., McCallum I. S., McKay G. A., and Weill D. F. (1970) Mineralogy and petrology of Apollo 12 sample No. 12013: A progress report. *Earth Planet. Sci. Lett.* **9,** 103–123.

Duke M. B. and Silver L. T. (1967) Petrology of eucrites, howardites, and mesosiderites. *Geochim. Cosmochim. Acta* **31,** 1637–1665.

ENGEL A. E. J. and ENGEL C. G. (1970) Lunar rock compositions and some interpretations. *Proc. Apollo 11 Lunar Sci. Conf., Geochim. Cosmochim. Acta* Suppl. 1, Vol. 2, pp. 1081–1084. Pergamon.

ESSENE E. J., RINGWOOD A. E., and WARE N. G. (1970) Petrology of the lunar rocks from Apollo 11 landing site. *Proc. Apollo 11 Lunar Sci. Conf., Geochim. Cosmochim. Acta* Suppl. 1, Vol. 1, pp. 385–397. Pergamon.

FUCHS L. H. (1970) Orthopyroxene-plagioclase fragments in the lunar soil from Apollo 12. *Science* **169,** 866–868.

GAST P. W. and HUBBARD N. J. (1970) Rare earth abundances in soil and rocks from the Ocean of Storms. *Earth Planet. Sci. Lett.* **10,** 94–101.

GREEN D. H., RINGWOOD A. E., WARE N. G., HIBBERSON W. O., MAJOR A., and KISS E. (1971) Experimental petrology and petrogenesis of Apollo 12 basalts. Second Lunar Science Conference (unpublished proceedings).

HAGGERTY S. E. and MEYER H. A. O. (1970) Apollo 12: Opaque oxides. *Earth Planet. Sci. Lett.* **9,** 379–387.

HASKIN L. A. and HASKIN M. A. (1968) Rare earth elements in the Skaergaard intrusion. *Geochim. Cosmochim. Acta* **32,** 433–447.

HESS H. H. and HENDERSON E. P. (1949) The Moore Country meteorite: A further study with comment on its primordial environment. *Amer. Mineral.* **34,** 494–507.

HUBBARD N. J. and GAST P. W. (1970) Rare earth, alkaline and alkali metal and $^{87/86}Sr$ data for subsamples of lunar sample 12013. *Earth Planet. Sci. Lett.* **9,** 181–184.

JAMES O. B. and JACKSON E. D. (1970) Petrology of the Apollo 11 ilmenite basalts. *J. Geophys. Res.* **75,** 5793–5824.

JAMIESON B. G. (1970) Phase relations in some tholeiitic lavas illustrated by the system R_2O_3–XO–YO–ZO_2. *Min. Mag.* **37,** 537–554.

KANE J., CARUCCI G., TURNER B., and MCENTEE J. (1969) Mascons, maria, and sinuous rilles—a postulated igneous origin. *Nature* **224,** 164.

KUSHIRO I. and HARAMURA H. (1971) *Science* (in press).

LARIMER J. W. (1967) Chemical fractionations in meteorites, I. Condensation of the elements. *Geochim. Cosmochim. Acta* **31,** 1215–1238.

LSPET (Lunar Sample Preliminary Examination Team) (1970) *Apollo 12 Preliminary Science Report*, NASA, Washington, D.C.

MASON B. (1962) *Meteorites.* John Wiley.

MASON B. (1967) The Bununu meteorite, and a discussion of the pyroxene-plagioclase achondrites. *Geochim. Cosmochim. Acta* **31,** 107–115.

MASON B. and MELSON W. G. (1970) *Lunar Rocks.* John Wiley.

MASON B., MELSON W. G., HENDERSON E. P., JAROSEWICH E., and NELEN J. (1971) Mineralogy and petrography of Apollo 12 samples. Second Lunar Science Conference (unpublished proceedings).

MAXWELL J. A., PECK L. C., and WIIK M. B. (1970) Chemical composition of Apollo 11 lunar samples 10017, 10020, 10072, and 10084. *Proc. Apollo 11 Lunar Sci. Conf., Geochim. Cosmochim. Acta* Suppl. 1, Vol. 2, pp. 1369–1374. Pergamon.

MOORE C. B. (1962) The petrochemistry of the achondrites. *Researches on Meteorites.* John Wiley.

MUAN A., OSBORN E. F., and SCHAIRER J. F. (1971) Equilibrium relations among phases occurring in lunar rocks. Second Lunar Science Conference (unpublished proceedings).

MURATA K. J. and RICHTER D. H. (1966) The settling of olivine in Kilauean magma as shown by lavas of the 1959 eruption. *Amer. J. Sci.* **264,** 194–203.

O'HARA M. J. (1968) The bearing of phase equilibria studies in synthetic and natural systems on the origin and evolution of basic and ultrabasic rocks. *Earth-Sci. Rev.* **4,** 69–133.

O'HARA M. J., BIGGAR G. M., RICHARDSON S. W., JAMIESON B. G., and FORD C. E. (1970) The nature of seas, mascons, and the lunar interior in the light of experimental studies. *Proc. Apollo 11 Lunar Sci. Conf., Geochim. Cosmochim. Acta* Suppl. 1, Vol. 1, pp. 695–710. Pergamon.

O'HARA M. J., BIGGAR G. M., RICHARDSON S. W., FORD C. E., and JAMIESON B. G. (1971) The nature of seas, mascons, and the lunar interior in the light of experimental studies, II. *Phys. of the Earth Planet. Interiors* **4** (in press).

O'HARA M. J. and BIGGAR G. M. (1969) Diopside and spinel equilibria, anorthite and forsterite reaction relationships in silica-poor liquids in the system $CaO–MgO–Al_2O_3–SiO_2$ at atmospheric pressure and their bearing on the genesis of melilitites and nephelinites. *Amer. J. Sci.* **267A,** 364–390.

O'HARA M. J. and SCHAIRER J. F. (1963) The join diopside-pyrope at atmospheric pressure. *Yearb. Carnegie Inst. Wash.* **62,** 107–115.

PAPANASTASSIOU D. A. and WASSERBURG G. J. (1970) Rb–Sr ages from the Ocean of Storms. *Earth Planet. Sci. Lett.* **8,** 269–278.

RINGWOOD A. E. (1970) Petrogenesis of Apollo 11 basalts and implications for lunar origin. *J. Geophys. Res.* **75,** 6453–6479.

RINGWOOD A. E. and ESSENE E. (1970) Petrogenesis of Apollo 11 basalts, internal constitution and origin of the moon. *Proc. Apollo 11 Lunar Sci. Conf., Geochim. Cosmochim. Acta* Suppl. 1, Vol. 1, pp. 769–799. Pergamon.

ROEDDER E. and WEIBLEN P. W. (1970) Lunar petrology of silicate melt inclusions, Apollo 11 rocks. *Proc. Apollo 11 Lunar Sci. Conf., Geochim. Cosmochim. Acta* Suppl. 1, Vol. 1, pp. 801–837. Pergamon.

SATO M. and HELZ R. T. (1971) Oxygen fugacity values of Apollo 12 basaltic rocks. Second Lunar Science Conference (unpublished proceedings).

SCHAIRER J. F. (1959) Phase equilibria with particular reference to silicate systems. In *Physicochemical Measurements at High Temperatures* (editors J. O'M. Bockris, J. L. White, and J. D. Mackenzie), pp. 117–134. Butterworths.

SCHAIRER J. F. and YODER H. S. (1970) Critical planes and flow sheet for a portion of the system $CaO–MgO–Al_2O_3–SiO_2$ having petrological applications. *Yearb. Carnegie Inst. Wash.* **68,** 202–214.

SILVER L. T. (1970) Uranium-thorium-lead isotopes in some Tranquillity Base samples and their implications for lunar history. *Proc. Apollo 11 Lunar Sci. Conf., Geochim. Cosmochim. Acta* Suppl. 1, Vol. 2, pp. 1533–1574. Pergamon.

SMALES A. A., HUGHES T. C., MAPPER D., MCINNIS C. A. S., and WEBSTER R. K. (1964) The determination of rubidium and caesium in stony meteorites by neutron activation analysis and by mass spectrometry. *Geochim. Cosmochim. Acta* **28,** 209–233.

TUTHILL R. L. and SATO M. (1970) Phase relations of a simulated lunar basalt as a function of oxygen fugacity, their bearing on the petrogenesis of the Apollo 11 basalts. *Geochim. Cosmochim. Acta* **34,** 1293–1302.

UREY H. C., MARTI K., MEI-KAO L., and HAWKINS J. W. (1971) Suggested model history of the moon. Second Lunar Science Conference (unpublished proceedings).

WAGER L. R. and BROWN G. M. (1968) *Layered Igneous Rocks.* Oliver and Boyd (Edinburgh).

WEILL D. F., MCCALLUM I. S., BOTTINGA Y., DRAKE M. J., and MCKAY G. A. (1970) Mineralogy and petrology of some Apollo 11 igneous rocks. *Proc. Apollo 11 Lunar Sci. Conf., Geochim. Cosmochim. Acta* Suppl. 1, Vol. 1, pp. 937–955. Pergamon.

WOOD J. A., MARVIN U. B., REID J. B., TAYLOR G. J., POWELL B. N., DICKEY J. S., and BOWER J. F. (1971) Sources of anorthositic and other light-colored particles in the Apollo 12 soil samples. Second Lunar Science Conference (unpublished proceedings).

WRIGHT T. L. and DOHERTY P. C. (1970) A linear programming and least squares computer method for solving petrologic mixing problems. *Bull. Geol. Soc. Amer.* **81,** 1995–2008.

Proceedings of the Third Lunar Science Conference
(Supplement 3, *Geochimica et Cosmochimica Acta*)
Vol. 1, pp. 207–229
The M.I.T. Press, 1972

Role of water in the evolution of the lunar crust; an experimental study of sample 14310; an indication of lunar calc-alkaline volcanism

C. E. Ford, G. M. Biggar, D. J. Humphries, G. Wilson, D. Dixon, and M. J. O'Hara

Grant Institute of Geology,
West Mains Road,
Edinburgh EH9 3JW,
Scotland

Abstract—Intersertal feldspar-phyric high alumina basalt, 14310, from the Fra Mauro formation has anorthite as liquidus phase at approximately 1310°C at pressures to as much as 12 kb (~ 250 km depth) where it is replaced first by spinel, and then by garnet at pressures greater than approximately 17 kb (~ 350 km depth). Olivine is the next silicate to crystallize at low pressures (~ 1230°C), but is replaced in this role by one or more pyroxenes at pressures greater than 4 kb. Olivine reacts out on cooling at atmospheric pressure, calcium-poor pyroxene being the product at temperatures between 1200°C and 1160°C. The present bulk composition of 14310 contains too little oxygen to keep all the iron oxidized as FeO, or to maintain a Fe^{2+}/Mg^{2+} ratio in the liquid high enough to precipitate the relatively iron enriched pigeonites formed during the natural crystallization, and late stage loss of oxygen by volatilization is evident. The highly aluminous phases present on the liquidus are unsuitable as major residual constituents of the lunar mantle and 14310 cannot be a primary magma from that source. Water and alkalis may also have been lost by posteruption volatilization: addition of these components to 14310 produces a magma nearly cotectic with the minerals of spinel-troctolite at low pressures (~ 250 bars) and such rocks are observed in the breccias. We deduce that 14310 is a volatile depleted sample of liquid from a shallow seated fractionating magma chamber containing a liquid of calc-alkaline affinities.

Introduction

Six groups (Ford *et al.*, 1972; Kushiro, 1972; Muan *et al.*, 1972; Ridley *et al.*, 1972 (unrevised abstract); Ringwood *et al.*, 1972; Walker *et al.*, 1972) presented phase equilibria data for rock 14310 or related compositions. Atmospheric pressure results, though variable between groups, are shown to be broadly reconcilable, assuming differing oxygen contents of the charges recovered. The present composition of 14310 has suffered posteruption volatilization losses of O_2; significant losses of Na_2O and K_2O have also been claimed (Brown and Peckett, 1971, but challenged by Ridley *et al.*, 1972). We argue that water has also been lost; that water played a vital role in the origin of 14310 and the lunar crust in general, and re-emphasize that the reduced, volatile-depleted character of lunar surface rocks is no guide to lunar chemistry as a whole but is a consequence of exposure over many hours at ~ 1200°C to a vacuum of $\sim 10^{-13}$ bars. Sample 14310 has not suffered significant near-surface fractional crystallization but may have evolved by fractional crystallization of spinel-bearing troctolites in magma chambers situated within 5 km of the lunar surface.

Data for 14053, 14162, 14321, and four preferred glass compositions in the soils, are also presented, both with and without restoration of alkalis that may have been volatilized.

Rock 14310: a feldspar-phyric endogenic high alumina lunar basalt

This rock contained about 8% plagioclase phenocrysts on eruption (Brown and Peckett, 1971). This rock may be an impact melt and as such may have no direct crystal-liquid connection with the lunar interior. However, the thermal histories of impact melted rocks are marked by superheating followed by rapid chilling under which conditions plagioclase *in particular* is very reluctant to nucleate or grow (Biggar *et al.*, 1972a, table 8, section C). Terrestrial impact melts crystallize to phenocryst-free rocks (Dence, 1971) and commonly retain inhomogeneous xenolithic textures. Brown and Peckett (1971) found no xenoliths in 14310, in contrast with other descriptions (LSPET, 1971; Walter *et al.*, 1972).

Clasts of this rock type occur in the Apollo 14 breccias (Wilshire and Jackson, 1972). Any resemblance between the compositions of 14310 and the subsequently formed soils at the Apollo 14 site merely testifies to the volumetric significance of high alumina, relatively magnesian basaltic rocks in the Imbrian target area. We assume 14310 to be a fragment of the solidified eruptive fraction of an endogenic magma, the problem of whose origin lies at the heart of a major question of lunar petrogenesis: *How is an early, relatively magnesian, and highly feldspathic crust derived from a lunar mantle that subsequently yielded mare basalts of relatively iron-rich, much less feldspathic character?*

Three hypotheses have been offered to explain a generally noritic-anorthositic lunar crust now thought to be about 50–65 km thick (Toksöz *et al.*, 1972). The first two hypotheses hold to a model of volatile-depleted moon. The third requires the presence initially of *substantial* amounts of water in the moon: (1) The last material accreted to the moon was more calcic and aluminous and poorer in Fe (Gast and McConnell, 1972) than all earlier material. The proponents of such hypotheses must explain convincingly how the anorthite rich material formed in space, or why such refractory material accumulated so late, and why such material is now so scarce among the meteorites. (2) The outermost layers of the moon were partly melted early in lunar history and during their recrystallization plagioclase floated to form the observed crust (Smith *et al.*, 1970; Wood *et al.*, 1970). Plagioclase is not observed to behave in this manner in terrestrial magmas, nor in experiments on lunar lavas (O'Hara *et al.*, 1970). The model presupposes either an outer layer of at least 200 km of the lunar mantle that is exceptionally rich in CaO and Al_2O_3 [see (1) above], or the formation of a surface layer, about 200 km thick, of *basaltic* melt followed by differentiation of much of its plagioclase to form a 60–70 km thick crust. In the latter case 130 km of complementary basic igneous rock (crystallized by some to eclogite, S.G. $\sim$ 3.7) would then underlie the anorthositic crust. (3) The lunar mantle underwent two major differentiating events: In the first, massive partial melting under high water vapor pressures produced magnesian melts whose condensed compositions were exceptionally rich in plagioclase. On eruption these outgassed, crystallized, and differentiated to form the lunar crust. Few hydrous minerals would have been stable in these magmas at depths less than 50 km (but see Mason *et al.*, 1972). In the second event, drier magnesian partial melts were derived from the largely dehydrated mantle, erupted into the maria, and there strongly fractionated to yield cumulus sequences of

achondritic composition and iron-enriched late residual liquids (mare surface basalts). Enrichment of iron relative to magnesium was not pronounced during lunar crustal fractionation because plagioclase was the major phase separating. This model is summarized in Fig. 1. It interprets both 14310 and the mare surface basalts as late

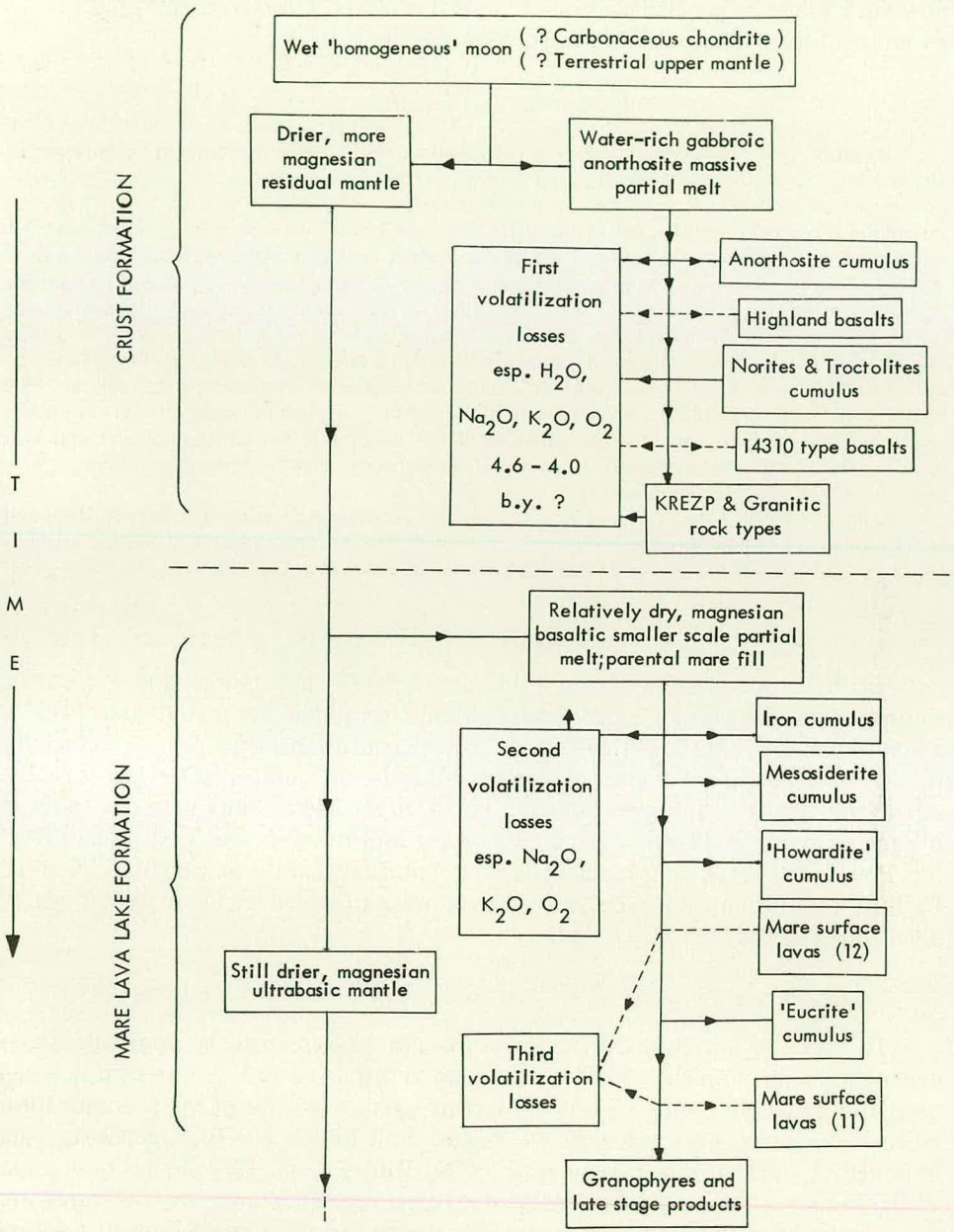


Fig. 1. Possible evolution and interrelationships of important lunar rock types.

stage residual liquids from high level fractional crystallization processes, thereby accommodating their high rare element concentrations without recourse to primary magmas derived from incipient partial melting events (an hypothesis leading to severe mass balance problems, Biggar *et al.* (1971, 1972a), and leaving unexplained how such magmas penetrate as much as two hundred kilometers of "cold" rocks without enforced differentiation en route to the surface).

Experimental Techniques

Atmospheric pressure techniques have been described, calibrated for temperature and oxygen fugacity, and checked for objectivity, reversibility, reproducibility, composition control, and attainment of equilibrium (Biggar *et al.*, 1972a, and references traceable thereby). Experiments between 1 and 10 kb were carried out in internally heated vessels (Ford, 1972). Dry experiments were carried out in sealed iron tubes using argon as the external pressure medium. Buffered water-bearing charges were contained in sealed $Ag_{70}Pd_{30}$, or Pt capsules inside larger sealed Pt tubes containing the buffer with sufficient water added to completely oxidize the buffer should all the hydrogen be lost, and run with an argon-hydrogen mixture as the external pressure medium to prolong the life of the buffer. Experiments in the range above 10 kb were carried out in piston-cylinder solid media equipment (Boyd and England, 1963) that has been extensively calibrated (O'Hara *et al.*, 1971; Herzberg and O'Hara, 1972) against five equilibria in the range 8–33 kb, 900–1700°C. No proven differences exist between our pressure/temperature scales for the solid media results and those quoted for similar work by the Geophysical Laboratory. Sealed platinum tubes were used in short exploratory experiments and sealed iron tubes in longer definitive experiments. Charges were dried in a nitrogen furnace before sealing.

Additions of alkalis to a 14310 sample were made by weighing and mixing in Analar Na_2CO_3 and K_2CO_3 followed by 4 hours heating at 1000°C at $f_{O_2} \sim 10^{-15}$ bars. In some of the wet melting experiments Na_2O was added in solution as NaOH (see Table 1).

Experimental Data

Conditions and results of quenching experiments on 4 natural and 4 synthetic samples, with and without added oxygen, water, and alkalis, are presented in Table 1, and interpreted in Figs. 2, 3, 4, 6, 7, and 8. Note that all atmospheric pressure data refer to charges that had an oxygen content imposed by the controlled oxygen fugacity. All dry melting data at higher pressures on 14310 refer to a composition too poor in oxygen to maintain all iron as FeO, except perhaps those in which Na_2O and K_2O had been added to the sample and the material preheated at the oxygen fugacity of the Fe/FeO equilibrium. All wet melting data were obtained at an oxygen fugacity determined by the FeO/Fe_3O_4 buffer.

Atmospheric Pressure Equilibrium Crystallization Data for 14310

The effect of variations in temperature and oxygen fugacity upon the phase assemblages stable in the 14310 composition is displayed in Fig. 4, which is based upon our own data points as shown, together with knowledge of the probable form of such diagrams from the work of Roeder and Emslie (1970). Quenching data obtained by other groups (Muan *et al.*, 1972; Ridley *et al.*, 1972; Ringwood *et al.*, 1972; Walker *et al.*, 1972) at unstated oxygen fugacities and low pressures are consistent with their charges having equilibrated at variable oxygen fugacities within the limited range $\sim 10^{-14}$ to 10^{-12} bars at about 1200°C, reflecting perhaps differing

Table 1

A. Runs in Atmospheric Pressure Equipment

Run No.	Time (hr)	$-\log_{10} f_{O_2}$	Temp. (°C)	Result	Run No.	Time (hr)	$-\log_{10} f_{O_2}$	Temp. (°C)	Result
14310, rock powder, 1 atm, Fe/FeO equilibrium ($CO_2 + H_2$), molybdenum capsules[1]									
020	5	10.6	1310	(plag) 1	009	5	11.7	1211	plag crsp ol 1
016	5	10.8	1295	plag 1	004	11	11.8	1200	plag crsp ol (pig) 1
006	5	11.0	1274	plag 1	010	5	12.1	1189	plag crsp ol pig 1
007	5	11.3	1248	plag 1	005	9	12.2	1173	plag crsp ol pig 1
011	5	11.5	1237	plag crsp 1	008	5	12.6	1142	plag crsp pig (ol) 1
018	72	11.5	1231	plag crsp 1	017	5	13.2	1097	plag pig pk (1)
003	5	11.6	1226	plag crsp (ol) 1	002	7	13.7	1065	solid[2]
14310, glass starting material,[3,4] 1 atm, Fe/FeO equilibrium ($CO_2 + H_2$) molybdenum capsules									
720	5	10.6	1310	(plag) 1	609	5	11.7	1211	plag crsp ol 1
716	5	10.8	1295	plag 1	504	11	11.8	1200	plag crsp pig 1
506	5	11.0	1274	plag 1	610	5	12.1	1189	plag crsp pig 1
507	5	11.3	1248	plag 1	505	9	12.2	1173	plag crsp ol pig 1
711	5	11.5	1237	plag crsp (ol) 1	508	5	12.6	1142	fine grained[2]
718	72	11.5	1231	plag crsp 1	717	5	13.2	1097	very fine grained[2]
503	5	11.6	1226	plag crsp ol 1					
14310, rock powder + $1\frac{1}{2}\%$ Na_2O + $\frac{1}{2}\%$ K_2O,[5] 1 atm, Fe/FeO equilibrium, molybdenum capsules									
914	5	11.0	1276	(crsp) 1	912	5	11.6	1225	plag ol crsp 1
913	5	11.2	1255	plag crsp 1					
14310, rock powder, 1 atm, 90% H_2 10% CO_2, $f_{O_2} \approx 10^{-14}$, Fe and Mo capsules; Ni/NiO equilibrium AgPd capsules[6]									
071	5	≈14(Mo)	1197	plag ol opx m 1	042	5	7.8	1207	plag ol sp 1
072	5	≈14(Fe)	1197	plag ol opx m 1	043	5	8.3	1161	plag ol sp opx 1
14321, breccia powder,[7] 1 atm, Fe/FeO equilibrium ($CO_2 + H_2$), molybdenum capsules									
016	5	10.8	1295	1	010	5	12.1	1189	ol plag pk 1
006	5	11.0	1274	ol 1	005	9	12.2	1173	ol plag opx pk 1
007	5	11.3	1248	ol 1	021	5	12.3	1163	ol plag opx pk 1
011	5	11.5	1237	ol 1	008	5	12.6	1142	ol plag pig pk 1
003	5	11.6	1226	ol sp 1	017	5	13.2	1097	trace liquid[2]
009	5	11.7	1211	ol sp 1	002	7	13.7	1065	solid[2]
004	11	11.8	1200	ol plag sp 1					
14321, breccia powder, 1 atm, 90% H_2 10% CO_2, $f_{O_2} \approx 10^{-14}$, Fe and Mo capsules; NiNiO equilibrium Ag Pd capsules[6]									
071	5	≈14(Mo)	1197	ol plag pig 1	042	5	7.8	1207	plag ol crsp 1
072	5	≈14(Fe)	1197	ol plag m 1	043	5	8.3	1161	plag pig ol crsp 1

Table 1 (continued)

A. Runs in Atmospheric Pressure Equipment (continued)

Run No.	Time (hr)	$-\log_{10} f_{O_2}$	Temp. (°C)	Result	Run No.	Time (hr)	$-\log_{10} f_{O_2}$	Temp. (°C)	Result
14053, powder, 1 atm, FeFeO equilibrium (CO_2 + H_2) molybdenum capsules									
011	5	11.5	1237	qu-pk 1	021	5	12.3	1163	ol plag pig crsp 1
003	5	11.6	1226	crsp ol 1	008	5	12.6	1142	ol plag pig crsp 1
009	5	11.7	1211	ol crsp 1	019	5	12.9	1122	ol plag pig pk 1
004	11	11.8	1200	ol crsp 1	017	5	13.2	1097	ol plag pig pk (1)[2]
010	5	12.1	1189	ol plag crsp 1	002	7	13.7	1065	solid[2]
005	9	12.2	1173	ol plag crsp 1					
14053, powder, 1 atm, NiNiO buffer AgPd capsules;[6] 90% H_2 10% CO_2 $f_{O_2} \approx 10^{-14}$ iron capsules									
042	4	7.8	1207	qu-pk 1	072	5	≈14	1197	ol plag pig m 1
044	5	8.3	1150	plag pig ol pk 1					
14053, glass,[3] 1 atm, Fe/FeO equilibrium (CO_2 + H_2) molybdenum capsules									
511	5	11.5	1237	qu-sp 1	505	9	12.2	1173	pig plag ol crsp 1
503	5	11.6	1226	qu-sp 1	521	5	12.3	1163	pig plag ol pk 1
509	5	11.7	1211	crsp (ol) 1	508	5	12.6	1142	pig plag ol pk 1
504	11	11.8	1200	crsp ol 1	719	5	12.9	1122	pig plag ol pk 1
510	5	12.1	1189	crsp ol (plag) 1	717	5	13.2	1097	very fine grained (1)[2]
14162, soil powder, 1 atm, Fe/FeO equilibrium (CO_2 + H_2) molybdenum capsules									
007	5	11.3	1248	1	010	5	12.1	1189	plag ol crsp 1
011	5	11.5	1237	(plag) (crsp) 1	005	9	12.2	1173	plag ol crsp pig !
018	72	11.5	1231	plag crsp 1	008	5	12.6	1142[2]	
003	7	11.6	1226	plag crsp (ol) 1	019	5	12.9	1122[2]	
009	5	11.7	1211	plag crsp ol 1	017	5	13.2	1097[2]	
004	11	11.8	1200	plag crsp ol 1	002	7	13.7	1065[2]	
Synthetic composition, Apollo Soil Survey (1971) Type E. 1 atm, Fe/FeO equilibrium (CO_2 + H_2) Mo capsules									
020	5	10.6	1310	plag 1	009	5	11.7	1211	plag ol 1
006	5	11.0	1274	plag 1	010	5	12.1	1189	plag sp ol 1
007	5	11.3	1248	plag ol 1	021	5	12.3	1163[2]	
011	5	11.5	1237	plag ol 1	008	5	12.6	1142	solid[2]
Synthetic composition, Apollo Soil Survey (1971) Type E, doped[5] with Na_2O, K_2O, 1 atm, Fe/FeO equilibrium									
(i) plus 1% Na_2O plus ½% K_2O					(ii) plus 2% Na_2O plus ½% K_2O				
914	5	11.0	1276	plag sp 1	914	5	11.0	1276	plag sp 1
913	5	11.3	1255	plag ol sp 1	913	5	11.3	1255	plag sp 1
912	5	11.6	1225	plag ol sp 1	912	5	11.6	1225	plag ol sp 1

Table 1 (continued)

A. Runs in Atmospheric Pressure Equipment (continued)

Run No.	Time (hr)	$-\log_{10} f_{O_2}$	Temp. (°C)	Result	Run No.	Time (hr)	$-\log_{10} f_{O_2}$	Temp. (°C)	Result
Synthetic composition, Apollo Soil Survey (1971) Type C, 1 atm, Fe/FeO equilibrium									
006	5	11.0	1274	l	010	5	12.1	1189	plag ol pk l
007	5	11.3	1248	(plag) l	021	5	12.3	1163	plag pig ol pk l
011	5	11.5	1237	plag l	008	5	12.6	1142	plag pig ol pk l
018	72	11.5	1231	plag l	019	5	12.9	1122	fine grained (1)[2]
009	5	11.7	1211	plag (ol) l	017	5	13.2	1097	fine grained (1)[2]
Synthetic composition, Apollo Soil Survey (1971) Type C, doped[5] with Na_2O, K_2O, 1 atm, Fe/FeO equilibrium									
(i) plus 1% Na_2O plus ½% K_2O					(ii) plus 2% Na_2O plus ½% K_2O				
913	5	11.3	1255	l	913	5	11.3	1255	l
912	5	11.6	1225	(plag) l	912	5	11.6	1225	(plag) l
Synthetic composition, Apollo Soil Survey (1971) Type B, 1 atm, Fe/FeO equilibrium									
006	5	11.0	1274	l	009	5	11.7	1211	plag ol l
007	5	11.3	1248	plag (ol) l	010	5	12.1	1189	plag ol pig l
011	5	11.5	1237	plag ol l	008	5	12.6	1142	plag ol pig (l)
018	72	11.5	1231	plag ol l	019	5	12.9	1122	fine grained (1)[2]
Synthetic composition, Apollo Soil Survey (1971) Type B,[5] doped with Na_2O, K_2O, 1 atm, Fe/FeO equilibrium									
(i) plus 1% Na_2O plus ½% K_2O					(ii) plus 2% Na_2O plus ½% K_2O				
914	5	11.0	1276	l	914	5	11.0	1276	(ol?) l
913	5	11.3	1255	ol l	913	5	11.3	1255	ol l
912	5	11.6	1225	ol plag l qu-sp	912	5	11.6	1225	ol l qu-sp
Synthetic composition, Apollo Soil Survey (1971) Mare type, 1 atm, Fe/FeO equilibrium									
011	5	11.5	1237	ol l	008	5	12.6	1142	ol pig plag pk l
009	5	11.7	1211	ol l	019	5	12.9	1122	ol pig plag pk l
010	5	12.1	1189	ol l	017	5	13.2	1097	ol pig plag pk l
021	5	12.3	1163	ol plag (pig) pk l					

Table 1 (continued)

B. Runs in Internally Heated Gas Media Equipment

Run No.	Time (hr)	Pressure (kb)	Temp. (°C)	Result	Run No.	Time (hr)	Pressure (kb)	Temp. (°C)	Result
14310, rock powder dried at 800°C and sealed in Fe tubes[6]									
143	4.5	2	1225	1 plag (ol) m qu-px	131	17	5	1201	1 plag cpx opx m
140	7	2	1200	1 plag ol m (sp) px	142	3.5	10	1336	1
146	3	3	1220	1 plag ol qu-px	138	3.5	10	1322	1 plag qu-px
147	6	3	1175	1 plag cpx opx m	137	3.5	10	1312	1 plag m qu-px
144	3.75	4	1221	1 plag opx cpx m	134	4	10	1290	1 plag m qu-px
132	4.25	5	1311	1 v[8]	136	3.5	10	1276	1 plag cpx m qu-px
130	18.5	5	1290	1 plag m qu-px	135	4.25	10	1260	1 plag cpx opx qu-px
126	17.5	5	1277	1 plag m qu-cpx	139	15.25	10	1226	1 plag cpx opx m
120	>0.25	5	1275	1 sp (plag) m qu-px[9]	141	88	10	1175	1 plag cpx opx m pk
129	4	5	1250	1 plag m qu-px	133	14	$10 \rightarrow \frac{1}{2}$	1250	1 plag m
127	17.5	5	1223	1 plag cpx opx m					
14310, rock powder dried at 110°C and sealed in Pt tubes									
111	0.17	10	1304	1 plag (sp) qu-cpx[4]	109	0.17	10	1228	1 plag cpx sp pk qu-px[4]
14310, rock powder + c. 10% H_2O sealed in $Ag_{70}Pd_{30}$ tubes and run at the FeO/Fe_3O_4 buffer									
108	0.5	2	1126	1 plag (sp) qu-amph v[10]	118	22	5	1075	1 sp qu-amph qu-mica v
					114	0.17	5	1074	1 plag sp qu-amph v[11]
124	21	2	1075	1 plag sp ol qu-amph v	115	0.5	5	1026	1 ol plag sp qu-amph v[11]
110	0.5	2	1076	1 plag ol sp qu-cpx qu-mica v[11]	121	>0.25	5	1025	1 ol sp qu-amph v
106	1	2	1025	1 plag (ol) cpx sp qu-mica v	117	17	5	1000	1 plag cpx ol sp qu-amph qu-mica v
105	1	2	952	plag cpx ilm v	122	>1.5	5	951	1 plag ol ilm cpx amph sp qu-mica v
119	16	5	1075	1 sp qu-amph v					
14310, rock powder + c. 10% H_2O sealed in Pt tubes and run at FeO/Fe_3O_4 buffer									
107	0.17	2	1199	1 (sp) qu-amph v	103	0.33	2	1051	1 plag ol sp pk qu-amph v[12]
102	0.17	2	1173	1 (sp) qu-amph v	104	1	2	1000	1 plag ilm ol cpx (?qu-ru) v
112	0.17	2	1150	1 plag (sp) qu-amph v[11]	116	0.17/ 0.17	2	1200/ 1025	1 sp plag qu-amph v[4]
101	0.17	2	1100	1 plag (sp) qu-amph v					
14310, rock powder + $1\frac{1}{2}$% Na_2O + $\frac{1}{2}$% K_2O dried at 800°C and sealed in Fe tubes[5]									
148	21.5	5	1260	1 plag m[4]	150	17.75	10	1302	1 plag[4,13]
155	1	7.5	1281	1 (plag) m qu-px					
14310, rock powder + $1\frac{1}{2}$% Na_2O + $\frac{1}{2}$% K_2O[5] + c. 10% H_2O sealed in $Ag_{70}Pd_{30}$ and run at the FeO/Fe_3O_4 buffer									
149	18	2	1090	1 sp qu-amph qu-mica v	153	18.5	2	1060	1 ol sp qu-amph qu-mica v
152	21	2	1075	1 ol sp qu-amph qu-mica v	154	16	2	1041	1 ol sp plag qu-amph qu-mica v

Table 1 (continued)

B. Runs in Internally Heated Gas Media Equipment (continued)

Run No.	Time (hr)	Pressure (kb)	Temp. (°C)	Result	Run No.	Time (hr)	Pressure (kb)	Temp. (°C)	Result
14310, rock powder + NaOH solution to give c. + 1½% Na_2O + c.10% H_2O sealed in $Ag_{70}Pd_{30}$ tubes and run at the FeO/Fe_3O_4 buffer[4]									
123	22	2	1100	1 sp qu-amph v					
124	21	2	1075	1 ol plag sp qu-amph v	125	19	2	1049	1 plag ol sp qu-amph v
14321, rock powder dried at 800°C and sealed in Fe tubes[7]									
143	4.75	2	1225	1 ol	127	17.5	5	1223	1 plag opx cpx (ol) m
140	7	2	1200	1 ol (plag) (cpx) sp m qu-px	131	17	5	1201	1 plag opx cpx ol m
146	3	3	1220	1 ol plag m qu-px	142	3.5	10	1336	1 opx qu-px m
145	4.75	2.8	1210	1 ol opx plag m qu-px	138	3.5	10	1322	1 opx qu-px m
144	3.75	4	1221	1 ol opx plag cpx m qu-px	137	3.25	10	1312	1 opx qu-px m
132	4.25	5	1311	1 m (qu-px)	134	4	10	1290	1 opx qu-px
128	4	5	1301	1 (ol) m qu-px	136	3.75	10	1276	1 opx m
130	18.5	5	1290	1 ol	135	4.25	10	1260	1 ol plag opx cpx m qu-px
126	17.5	5	1277	1 ol m	139	15.25	10	1229	1 cpx plag opx m
120	>0.25	5	1275	1 ol sp m[9]	141	88	10	1175	plag cpx opx pk m
129	4	5	1250	1 ol m	133	4	10 → ½	1250	1 ol m qu-px
14321, rock powder dried at 110° and sealed in Pt tubes									
111	0.17	10	1304	1 qu-px	109	0.17	10	1278	1 plag opx qu-cpx[11]
14321, rock powder + c. 10% H_2O sealed in $Ag_{70}Pd_{30}$ tubes and run at the FeO/Fe_3O_4 buffer									
108	0.5	2	1126	1 ol sp qu-amph qu-mica v	119	16	5	1075	1 ol sp qu-amph qu-mica v
106	1	2	1025	1 plag ol cpx sp qu-mica v	121	>0.25	5	1025	1 ol sp qu-mica v
105	1	2	952	plag ilm cpx ol sp v	117	17.25	5	1000	1 ol plag sp (pk) qu-mica qu-cpx v
113	0.17	5	1100	1 ol sp qu-amph qu-mica v	122	>1.5	5	951	1 ol plag ilm cpx amph sp qu-mica v
114	0.17	5	1074	1 ol sp qu-amph qu-mica v					
14321, rock powder + c.10% H_2O sealed in Pt tubes and run at the FeO/Fe_3O_4 buffer									
107	0.17	2	1199	1 sp qu-amph qu-pk v	103	0.33	2	1051	1 sp ol qu-amph v
102	0.17	2	1173	1 sp ol (pk) qu-amph v	116	0.17/ 0.17	2	1200/ 1025	1 sp ol cpx qu-cpx qu-amph qu-mica v
101	0.17	2	1100	1 sp ol pk v	104	1	2	1000	1 sp ol plag cpx ilm (ru) v
14321, rock powder + NaOH solution to give c. + 1½% Na_2O + 10% H_2O sealed in $Ag_{70}Pd_{30}$ capsules and run at the FeO/Fe_3O_4 buffer									
123	22	2	1100	1 ol sp qu-amph v	125	19	2	1049	1 ol sp qu-amph qu-mica v
124	21	2	1075	1 ol sp qu-amph v					

Table 1 (continued)

B. Runs in Internally Heated Gas Media Equipment (continued)

Run No.	Time (hr)	Pressure (kb)	Temp. (°C)	Result	Run No.	Time (hr)	Pressure (kb)	Temp. (°C)	Result
14053, rock powder + c.10% H_2O sealed in $Ag_{70}Pd_{30}$ tubes and run at the FeO/Fe_3O_4 buffer									
108	0.5	2	1126	1 sp qu-amph v[10]	119	16	5	1075	1 (ol) pk sp qu-amph v
110	0.5	2	1076	1 ol sp (pk) cpx v	114	0.17	5	1074	1 sp ol pk cpx qu-amph v
106	1	2	1025	1 ol cpx ilm sp plag qu-amph qu-mica v	115	0.5	5	1026	1 ol cpx pk qu-amph v
105	1	2	952	plag ilm cpx (sp) v	117	17.25	5	1000	1 ol cpx pk sp qu-amph qu-mica v
113	0.17	5	1100	1 sp ol pk m qu-amph v	122	>1.5	5	951	1 plag ol ilm cpx sp qu-cpx qu-mica v
14053, rock powder + c.10% H_2O sealed in Pt tubes and run at the FeO/Fe_3O_4 buffer									
107	0.17	2	1199	1 sp pk qu-amph v	103	0.3	2	1051	1 ol cpx ilm sp qu-amph v
102	0.17	2	1173	1 sp ilm qu-cpx qu-amph v	116	0.17/ 0.17	2	1200/ 1025	1 ol cpx sp pk qu-amph v
101	0.17	2	1100	1 ol pk sp qu-amph v	104	1	2	1000	1 plag sp ilm cpx (ru) v

C. Runs in Solid Media Equipment

Run No.	Time (hr)	Pressure (kb)	Temp. (°C)	Result	Run No.	Time (hr)	Pressure (kb)	Temp. (°C)	Result
14310, rock powder dried at 800°C, sealed in platinum tubes									
205	0.17	15	1250	plag gr cpx m (1)	206	0.17	20	1350	gr (cpx) m 1
202	0.17	15	1225	plag gr cpx (1) (?opx)	204	0.17	20	1275	gr cpx plag pk ru (1)[14]
14310, rock powder dried at 800°C, sealed in iron tubes									
254	2.5	10	1125	(gr) cpx plag opx m	231	1	20	1350	gr (cpx) m 1
235	1	15	1350	(sp) m 1	222	1	20	1317.5	gr cpx plag m 1
238	1	15	1335	(sp) m 1	223	1	20	1317.5	gr cpx plag m 1
228	1	15	1325	gr cpx plag m 1 (sp)					
227	1	15	1300	gr cpx plag m 1	219	1.25	20	1310	gr cpx plag m 1
215	1	15	1275	gr cpx plag m 1	236	1	25	1450	gr m 1
213	1	15	1250	gr cpx plag m (1) (?opx)	230	1	25	1425	gr (cpx) m 1
253	4	15	1175	gr cpx plag opx m (?1)	224	1	25	1400	gr cpx m 1
240	1	17.5	1370	((gr)) m 1	220	1	25	1375	gr cpx m 1
234	1	20	1400	1	218	1	25	1350	gr cpx m 1
239	1	20	1390	(gr) m 1					

Table 1 (continued)

C. Runs in Solid Media Equipment (continued)

Run No.	Time (hr)	Pressure (kb)	Temp. (°C)	Result	Run No.	Time (hr)	Pressure (kb)	Temp. (°C)	Result
14310, rock powder + 1½% Na_2O + ½% K_2O,(5) dried at 800°C, sealed in iron tubes									
243	1	15	1325	m l	249	1	17.5	1275	cpx plag gr m l
244	1	15	1300	sp m l	250	1	18	1300	cpx plag gr m sp l
246	1	15	1300	sp m l	247	1	20	1375	(cpx) m sp l
248	1	15	1285	sp cpx m l	245	1	20	1360	cpx ((gr)) sp m l
					242	1	20	1315	gr cpx plag m l (?sp)
14321, rock powder, dried at 800°C, sealed in platinum tubes									
205	0.17	10	1300	opx (sp) l(4)					
203	0.17	15	1350	opx (sp) l(4)	204	0.17	20	1400	gr (opx) l
201	0.17	15	1325	opx (cpx) l	202	0.17	20	1375	gr opx cpx l qu-cpx
14321, rock powder, dried at 800°C, sealed in iron tubes									
231	1	15	1375	l	227	1	20	1425	l
234	1	15	1365	opx m l	233	1	20	1400	(gr) opx m l qu-cpx
225	1	15	1335	opx qu-cpx l	215	1	20	1375	gr opx m l qu-cpx
222	1	15	1325	opx m l	236	1	25	1440	gr cpx l qu-cpx
232	1	15	1225	opx gr cpx plag (?sp)	223	1	25	1425	gr (opx) cpx m l qu-cpx
230	3	15	1150	plag cpx opx gr (?ilm)	229	1	25	1250	gr cpx (opx) (ru) (?sp) (?qz) (pk)

Key (additional to that in Fig. 2):

m = metal (iron)
pig = pigeonite
pk = opaque phase (ilmenite, spinel)
px = pyroxene undistinguished
qu = quenching product
qz = quartz
ru = rutile
( ) = very small amount
? = doubtful identification

Where liquid is recorded, glass or quenching products were observed. Charges were dried in oxygen-free nitrogen at stated temperatures. Runs 120, 121, 122 in internally heated vessels were quenched by fuse blowing overnight. Durations were less than 18 hours.

(1) Molybdenum capsules were made by welding sheet supplied by Murex Ltd., Essex.
(2) Equilibrium probably not attained in these runs due to small proportion of liquid present.
(3) Glasses previously prepared at 1350–1400°C, 1–2 hours in molybdenum capsules at Fe/FeO equilibrium in CO_2:H_2 atmosphere.
(4) These results not used in constructing Figs. 2 or 3.
(5) Alkalis added as carbonates and sintered at 1000°C, Fe/FeO equilibrium in CO_2:H_2 atmosphere.
(6) Iron capsules for solid media work made up from stock containing 180 ppm C, 190 ppm S, 180 ppm Mn, 1230 ppm Cu, supplied by New Metals and Chemicals Ltd. $AG_{70}Pd_{30}$ capsules were used up to 1170°C, $Ag_{40}Pd_{60}$ at higher temperatures in all runs using silver-palladium alloy containers.
(7) Results presented for 14321 supersede those shown by Biggar *et al.*, 1972b in a diagram containing some errors.
(8) Composition and source of vapor unknown.
(9) Dried at 110°C.
(10) Capsule partly melted.
(11) There may not have been sufficient time to dissolve plagioclase.
(12) Opaque phase assumed to be residual.
(13) Incompatible with solid media results if temperature scales are identical.
(14) Opaque phase and rutile fields not shown in Fig. 2.

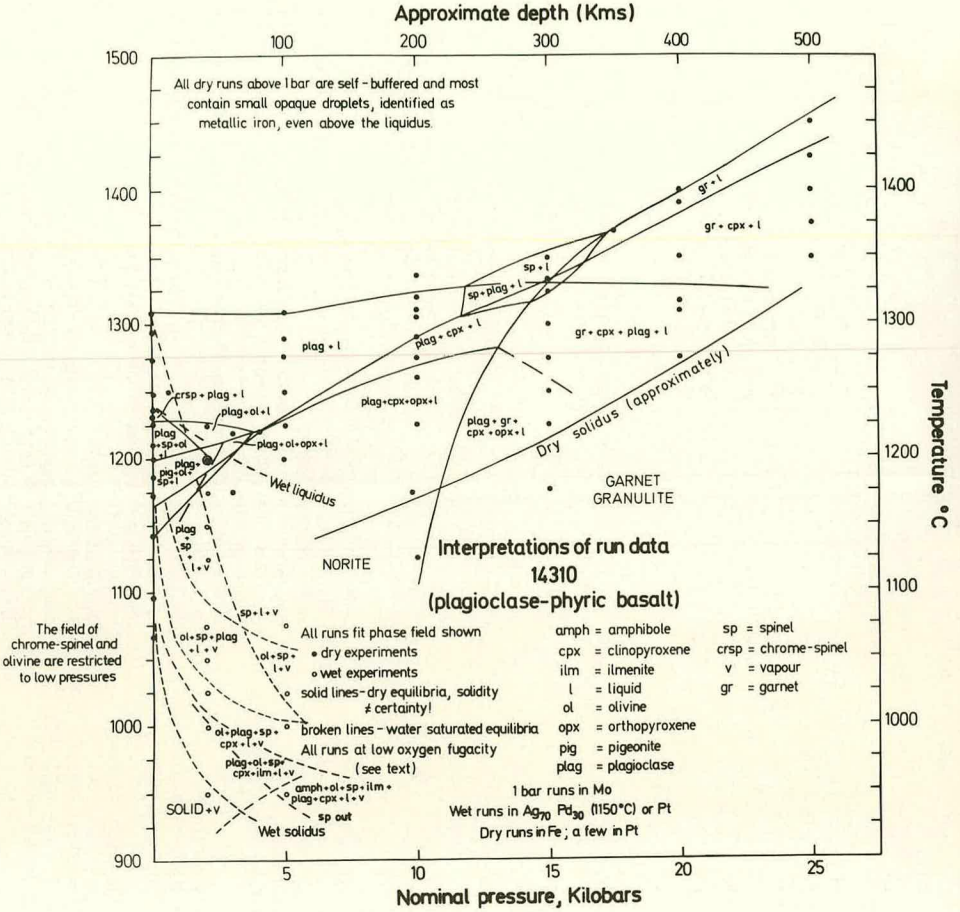


Fig. 2. Pressure–temperature section interpreting run data for 14310, with and without the addition of water and oxygen. Note that dry high-pressure runs on unmodified 14310 composition refer to a composition depleted in oxygen relative to *all* other experiments shown. (Revised from Ford *et al.*, 1972.)

degrees of success in controlling the charge composition as well as possible differences in oxygen content between subsamples ($\sim \pm 0.3\%$ O_2). Estimates of differences in oxygen content are based upon known, or assumed changes in the amounts of Fe metal, FeO, and Fe_2O_3 in the charges. Ringwood *et al.* (1972) seem to have attained oxygen fugacities intermediate between those achieved by Walker *et al.* (1972) and ourselves. Charges contain $\sim 1.1\%$ more O_2 at the highest f_{O_2} investigated by us than the samples do at the lowest f_{O_2}.

The compositions of 14310, its residual glasses and certain other investigated compositions lie almost in the plagioclase-olivine-silica plane, and are shown projected from diopside into that plane (Fig. 6). An internally consistent pseudo-ternary phase diagram can be drawn for the low pressure phase equilibria data, and

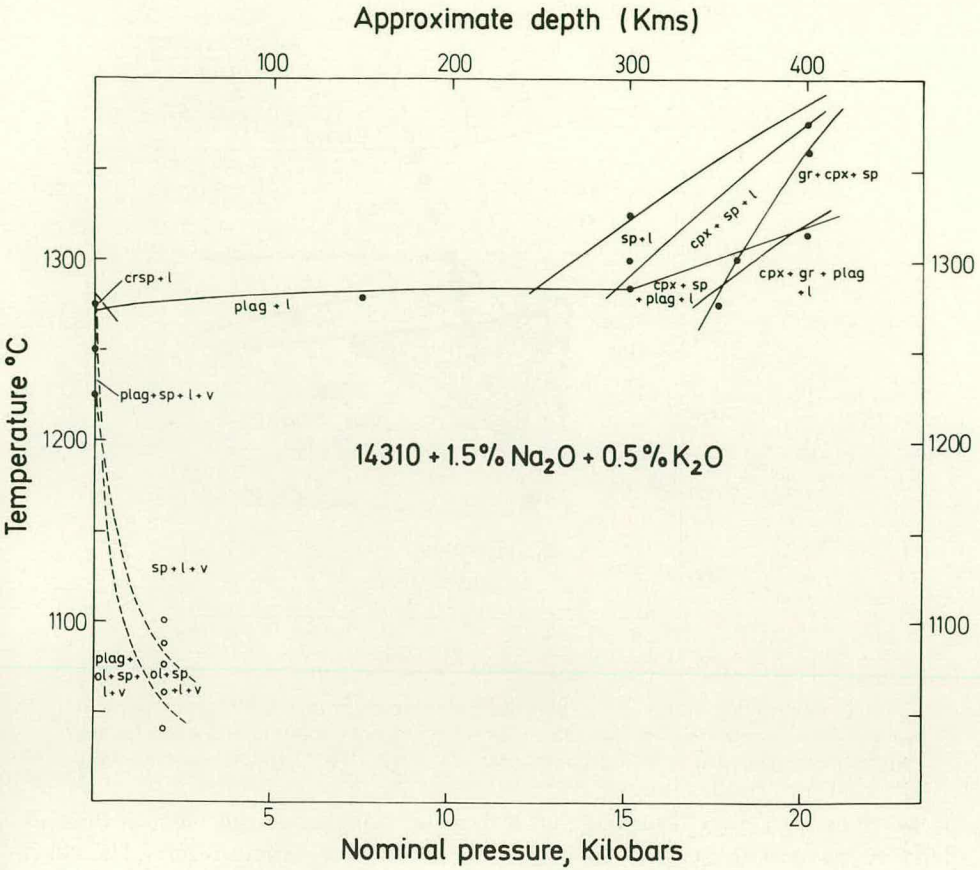


Fig. 3. Partial pressure–temperature section for 14310 plus alkalis, oxygen, and water. Key as in Fig. 2.

even contoured for the plagioclase liquidus temperature. Note the implied high liquidus temperature, abundant plagioclase crystallization and subsequent lengthy olivine crystallization interval predicted for "highland basalts."

Oxygen Content of 14310: Late Volatilization Loss

Our subsample 14310,141 when dried and sealed in iron or platinum capsules and run at high pressures almost always produced iron droplets. Microprobe analyses of glass in near-liquidus runs at 5 and 10 kb show substantial loss of iron by reduction to metal indicating about 0.7% deficiency of oxygen relative to that necessary to keep the iron oxidized as FeO (Table 2). Iron did not, however, form early in the crystallization of 14310 (Ridley *et al.*, 1972).

Had iron ever formed in equilibrium with a liquid of 14310 composition, its rapid loss by sinking would be anticipated, and nickel should be severely depleted in this rock, but it is not. Moreover, the earlier pyroxenes observed to have crystallized from

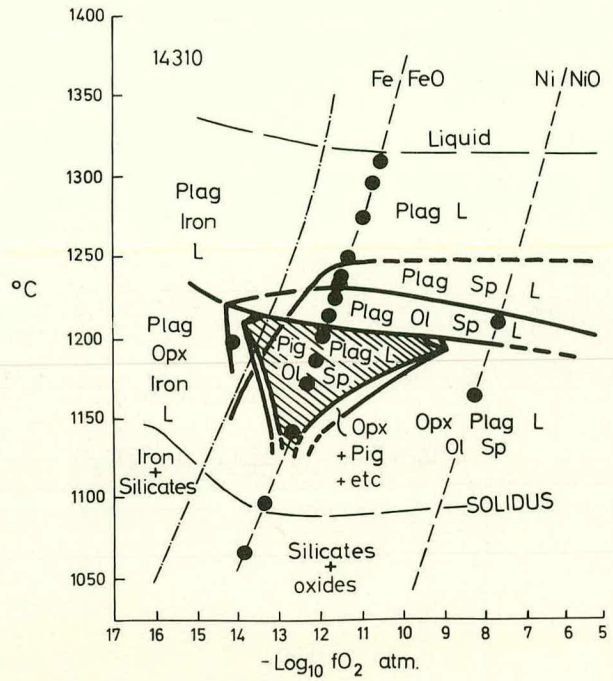


Fig. 4. Temperature versus log f_{O_2} plot of phases present in the 14310 composition at atmospheric pressure showing the critical effect of f_{O_2} upon the appearance of iron, chrome-spinel, and orthopyroxene versus pigeonite near 1200°C, $f_{O_2} \sim 10^{-13}$ bars in this composition.

the 14310 magma (Fig. 7) suggest that it then had a higher complement of FeO and therefore was not as oxygen depleted as the present bulk composition. The effects observed imply genuine loss of oxygen from the bulk rock, not merely a decline in oxygen fugacity with falling temperature (which also occurred). It follows that substantial losses of oxygen accompanied the eruption and consolidation of this rock, and its present oxygen content is not that appropriate to its previous evolution.

"Primitive" Character of the 14310 Magma

Rock 14310 originally crystallized with most of its iron as FeO in relatively iron-rich pigeonite. At atmospheric pressure substantial (~20–25%) plagioclase crystallization precedes the appearance of olivine, which is later joined by pigeonite, the plagioclase + olivine + pyroxene cotectic being reached at ~1200°C when the charge is about 45–50% crystalline (by construction from Fig. 6; visual estimate in Ford *et al* (1972) of 30% crystallinity at olivine entry prior to pyroxene also is in accord with Fig. 6). The composition is not specially related to the cotectic liquids at atmospheric pressure. The probability of so distant a relationship to the cotectic liquid occurring by coincidence in a random liquid composition derived from some higher pressure is 0.94 (see Biggar *et al.*, 1972a, Table 6, calculated using $C = 8$, $P^* = 3$, $X = 0.5$). This magma composition is, therefore, more primitive than those

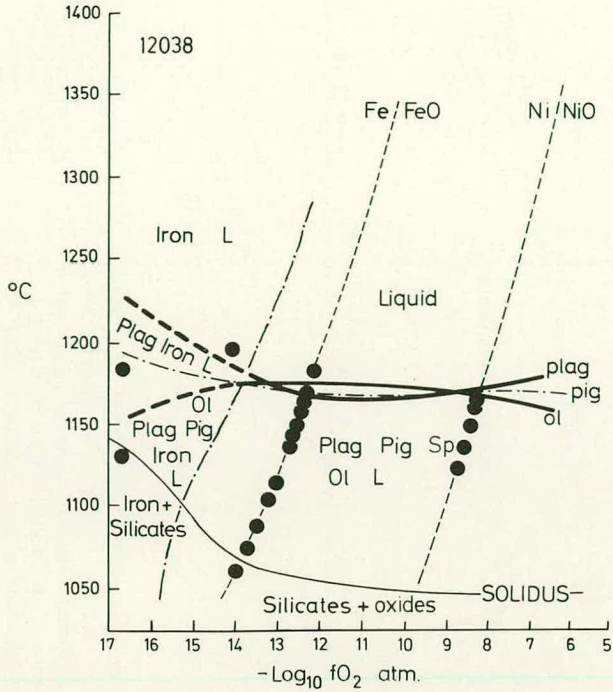


Fig. 5. Similar diagram to Fig. 4 but drawn for sample 12038, a near cotectic composition. The interchange of plagioclase and olivine entries is based upon visual observation of abundant plagioclase and very scarce olivine in the highest temperature run at the Ni/NiO equilibrium. The spinel entry boundary has not been included for the sake of clarity but lies close to the silicate liquidus between the Fe/FeO and Ni/NiO equilibria.

of the mare basalts, which have been established (Biggar *et al.*, 1971, 1972a) as being specially related to atmospheric pressure cotectic liquids. In the case of 14310, we differ from the interpretation of Walker *et al.* (1972), because the special relationship that they observe (plagioclase enrichment relative to the olivine + pyroxene + plagioclase cotectic) is a coincidence due to iron depletion in their closed system charges consequent on late stage oxygen loss from the natural rock (Figs. 6 and 7). Furthermore, if the 8% plagioclase phenocrysts are interpreted as equilibrium products of dry, near surface crystallization, the eruption temperature was about 60°C above that of the cotectic. (If the rock is interpreted as a wet magma of lower liquidus temperature whose groundmass was quenched by volatile loss, see below, further argument with regard to atmospheric pressure dry cotectic liquids is irrelevant).

Sample 14310, Though "Primitive" is not a Primary Magma

Posteruption oxygen loss has been demonstrated for 14310; substantial loss of alkalis has been claimed by Brown and Peckett (1971), and the case for substantial water loss will be argued below. Sample 14310, therefore, is not a primary magma from the lunar interior and any attempt to treat it as such leads inexorably toward

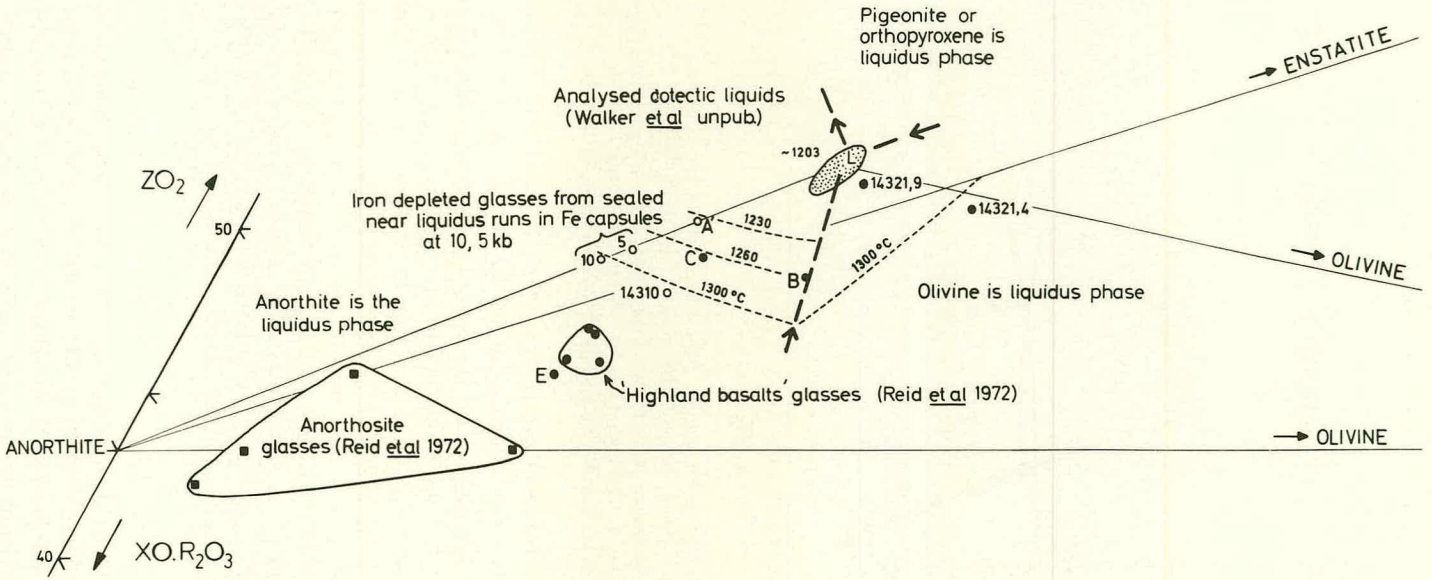


Fig. 6. Projection from "diopside" into the plagioclase-olivine-silica plane of the system XO-YO-R_2O_3-ZO_2 (Biggar *et al.*, 1971, Fig. 1) showing preferred glass compositions B, C, E (Apollo Soil Survey, 1971) and the compositions of "highland basalt" and "anorthosite" glasses from Apollo 14 and other soils (Reid *et al.*, 1972) and the analyses of two subsamples of breccia 14321 and of sample 14310 (shown as A; used by Ridley *et al.*, 1972, unrevised abstract, for experiments) from LSPET (1971). A more recent analysis of 14310 (LSPET 1972) is also shown, together with the compositions of glasses from near liquidus experiments in equilibrium with iron droplets and plagioclase in sealed tube experiments at 5 and 10 kb (Table 2). Approximate boundaries between the liquidus fields of anorthite, olivine, and calcium-poor pyroxene are shown, meeting at the cotectic liquid compositions found by Walker *et al.* (1972) (field *L*). Approximate thermal contours on the plagioclase and olivine surface are shown.

Table 2. Phase compositions (wt %) from experiments on 14310.

Run No.	010	130	111	134	208
Container	Mo	Fe	Pt	Fe	Pt
Conditions	(1 bar, 1189°C, Fe/FeO)	(5 kb, 1290°C dry)	(10 kb, 1304°C dry)	(15 kb, 1200°C)	(15 kb, 1300°C)
Plagioclases:					
SiO_2	47.05	45.47		45.84	45.72
TiO_2	0.08	0.04		0.08	0.08
Al_2O_3	32.36	34.57		34.07	34.36
FeO	0.72	0.32		0.46	0.43
MgO	0.23	0.30		0.28	0.25
CaO	17.27	18.56		18.33	17.54
Na_2O	1.06	0.64		0.94	1.23
K_2O	0.46	0.18		0.29	0.22
TOTAL	99.23	100.08		100.29	99.83
An	87.6	93.2		90.0	87.6
Ab	9.7	5.8		8.3	11.1
Or	2.7	1.0		1.7	1.3
Glasses:					
SiO_2	50.13	51.13	50.47		46.96
TiO_2	2.26	1.46	1.45		1.24
Al_2O_3	13.97	19.87	20.18		20.37
Cr_2O_3	n.d.	n.d.	n.d.		n.d.
FeO	10.82	5.21*	5.22*		8.04
MnO	n.d.	n.d.	n.d.		n.d.
MgO	7.46	9.27	8.52		7.83
CaO	13.24	12.27	12.19		12.31
Na_2O	0.90	0.88	0.80		0.76
K_2O	0.64	0.67	0.64		0.47
TOTAL	99.42	100.76	99.47		97.97

* Iron droplets present.

hypotheses of derivation by partial melting of anorthosite at shallow depths, or of spinel or garnet rocks at greater depths (inadmissible on grounds of density).

Effect of Pressure and Water Vapor Pressure on the Crystallization of 14310, 14321

Figure 6 locates the approximate boundary between the liquidus fields of plagioclase, olivine, and calcium-poor pyroxene in compositions close to the anorthite-olivine-silica plane, in which to a first approximation, Apollo 14 rock and soil compositions fall. Figure 8 reproduces this boundary in relation to the compositions of 14310 (LSPET, 1972, analysis), and breccia 14321 (LSPET, 1971, analyses). It shows, in sketch form, the effect of increased dry pressure in contracting the olivine liquidus field. Contrast this with the effect of addition of water to the system, where the olivine field expands into silica-saturated compositions of high normative plagioclase content, and a spinel-field also becomes prominent. Liquids in equilibrium with olivine and plagioclase at 1–3 kb water vapor pressure lie well inside the plagioclase liquidus field if pressure is released and the water lost. Similar effects are well-known from relevant synthetic systems (Yoder, 1968, 1969). These relationships may be rephrased in the statement that partial melting of plagioclase- or spinel-peridotites in the presence of water yields liquids of relatively high normative plagioclase content, which are quartz-normative if orthopyroxene was a phase in the crystalline residuum.

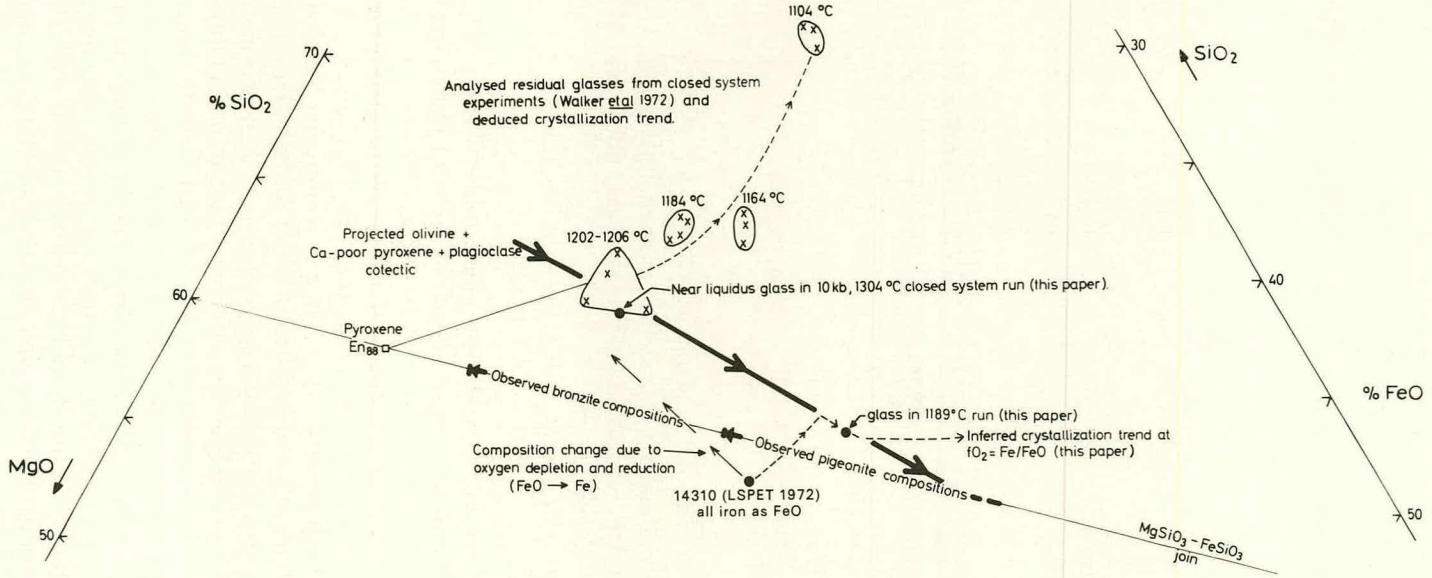


Fig. 7. Projection from $CaSiO_3$, normative feldspars, apatite, Cr_2O_3, and TiO_2 into the system MgO-FeO-SiO_2 (Kushiro *et al.*, 1971, Fig. 5), showing (heavy line) the effective boundary between olivine and calcium-poor pyroxene as liquidus phase; the bulk composition of 14310 (LSPET, 1972) and (short dashed lines) the inferred evolution of its residual liquids during equilibrium crystallization in our experiments: and the oxygen and metallic iron depleted residual liquid compositions achieved or retained from the natural starting material in sealed system experiments on 14310 by ourselves and Walker *et al.* (1972) in relation to Walker *et al.* experimentally produced orthopyroxene and the ranges of pyroxene composition reported from the natural rock. The observed natural pigeonites appear to be more iron-rich than those that form during closed system crystallization of the present oxygen-depleted 14310 natural rock powder.

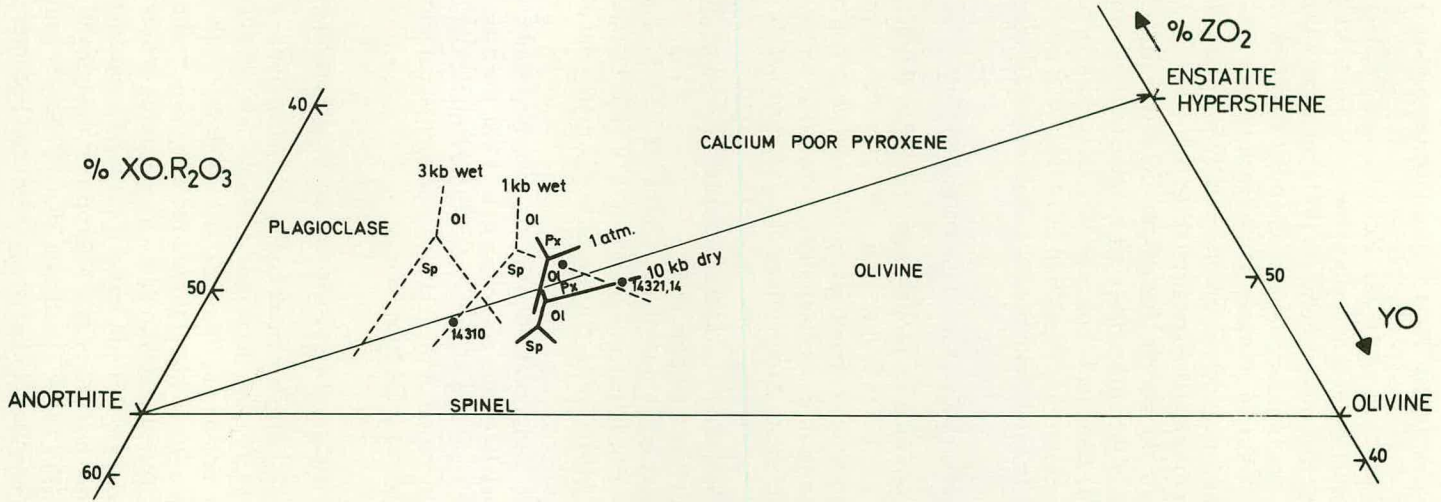


Fig. 8. Projection as in Fig. 6, but to smaller scale, showing the effect of pressure and water content upon the extent of the olivine, spinel, and calcic plagioclase liquidus fields in Apollo 14 compositions.

Affinities and Origin of 14310; The Complementary Spinel Trocolites

Brown *et al.* (1972), Drever *et al.* (1972), Roedder and Weiblen (1972) report spinel-troctolite or spinel and troctolite as clasts in the breccias and soils and comment on their cumulus textures. Brown and Peckett (1971) interpret 14310 as liquid extracted from a high-level fractionating magma chamber (perhaps elutriating some plagioclase phenocrysts). Addition of water and oxygen (at the FeO/Fe_3O_4 buffer) to 14310 brings olivine and plagioclase simultaneously into equilibrium with the liquid after trivial amounts of spinel precipitation (Fig. 2) at ~1075°C, 3 kb (~55 km). Restoration of lost alkalis to the sample changes this condition (Fig. 3) to ~1175°C, ~0.25 kb (~5 km). Some of the spinel observed in these experiments is of primary, equilibrium crystallization; some may, however, be a quenching product. A magma matching the deduced pre-eruption composition of 14310 could, evidently, have been in equilibrium with spinel-troctolite cumulus in a shallow-seated magma chamber.

The Natural Crystallization of 14310

Olivine has not been reported by groups studying 14310 (Hollister *et al.*, 1972; Kushiro, 1972; Ridley *et al.*, 1972; Walter *et al.*, 1972), yet it was prominent in the atmospheric pressure equilibrium crystallization histories observed between 1230°C and ~1190°C by four groups of experimentalists; below that temperature it is consumed by reaction with the liquid. At least three interpretations of the mineralogy are admissible:

(i) The dry magma cooled slowly enough after eruption to allow all olivine to react (unusual in terrestrial experience perhaps).

(ii) The dry magma was equilibrated at ~1260°C, with 8% plagioclase phenocrysts, erupted as a porphyritic liquid and quenched to ~1150°C, then annealed long enough for the liquid to crystallize to the plagioclase + pyroxene assemblage, and then further cooled.

(iii) The 14310 magma, containing about 1–2% dissolved water at, for example, 1150°C, 250 bars escaped from an approximately 5 km deep magma chamber, carrying with it the 8% plagioclase phenocrysts. Rapid boiling out of H_2O, Na_2O, K_2O, and O_2 led to crystallization of the relatively cool magma at and below 1150°C, where olivine would not be expected to appear.

Alkali Loss and Restoration; Plagioclase Compositions in 14310

Brown and Peckett (1971) with whom we concur, deduced significant posteruption loss of Na_2O, K_2O from 14310 from the zoning of plagioclase phenocrysts (An_{94-67}), the groundmass feldspar not having the expected alkali-rich bulk composition to represent potential feldspar in the liquid during the sodic rim crystallization. Ridley *et al.* (1972) however, interpret the relationships as indicating xenocrystal derivation for some of the plagioclase, yet this still leaves a problem regarding the more sodic liquid required to provide the sodic rims. Microprobe analyses of experimentally produced crystals in 14310 (Table 2) indicate that in the dry state near-liquidus plagioclase has composition An_{88} (15 kb), An_{94} (5 kb) and becomes more calcic with

lower pressure. Even after plagioclase crystallization has proceeded for more than 100°C at atmospheric pressure and at 10 kb, feldspar compositions have advanced only to An_{88} and An_{90}, respectively. Simplistic interpretation is, however, impossible, because (i) the high pressure data refer to oxygen and iron depleted material and (ii) elevated water pressures are suspected to promote excessively calcic plagioclase crystallization from terrestrial calc-alkali magmas of relatively high Na/Ca ratio (Wager, 1962; Baker, 1968; Yoder, 1968, 1969).

We have restored Na_2O and K_2O to 14310 in lesser amounts than Kushiro (1972), finding this to lower liquidus temperatures, enhance olivine and spinel crystallization, and reduce the water vapor pressure required to suppress plagioclase as the liquidus phase (Fig. 3). The additions made were not, however, sufficient to alter the qualitative character of the phase equilibria.

If the analysis of 14310 is adjusted to restore Na_2O, K_2O, oxygen and water a composition remarkably similar to high alumina basalts of terrestrial calc-alkaline provinces is obtained (and vice versa; see Table 3).

Table 3

	SiO_2	TiO_2	Al_2O_3	FeO	MnO	MgO	CaO	Na_2O	K_2O	P_2O_5
I	49.38	0.86	19.89	9.14	0.18	6.79	12.81	0.52	0.35	0.08
II	47.82	1.26	20.41	8.49	0.11	7.98	12.45	0.64	0.50	0.34

I. Basalt cinders (14802) from Mansion pyroclastics, St. Kitts (Baker, 1968) recalculated to 100% after arbitrary "volatilization" of 1.81% Na_2O, 0.46% O_2 and all water. In its original alkali-rich state this type of material precipitated about $Fo_{77} + An_{70}$ *after* eruption and water loss but was apparently precipitating $Fo_{77} + An_{90-93}$ in a relatively shallow seated wet magma chamber immediately before eruption.

II. 14310 (LSPET, 1972) from Fra Mauro formation, normalized to 100%. Carries phenocryst cores of An_{94}, suggested here to form in water-bearing magma chamber when liquid contained about 1.5% more Na_2O; the groundmass plagioclase formed after water loss *and* Na_2O loss and is An_{93}. Liquidus plagioclase in experiments on present dry, Na_2O-poor composition is about An_{94}.

Differences in Reported Results on 14310 at High Pressures

Four groups (Ford, *et al.*, 1972; Kushiro, 1972; Ringwood *et al.*, 1972; Walker *et al.*, 1972) reported high-pressure data for 14310 composition that are in broad agreement on one point: Plagioclase is the liquidus phase to pressures in excess of 10 kb, then it is replaced by spinel, and at even higher pressures by garnet. Kushiro (1972) reported a much greater spinel field than shown in Fig. 2; from our own experience this *might* reflect the accession to the charge of a *small* amount of water through the permeable graphite capsules that he used; but it is also probable that his data refer to different oxygen contents of the charges. Most of our high pressure data can be reconciled with those of Walker *et al.* (1972), although our interpretation of the phase diagram differs somewhat, and we cannot accommodate 14310 as a primary melting product of any type of dry pyroxenite source region. Ringwood *et al.* (1972) found olivine present at 10 kb, but we observe no olivine above 4 kb.

Summary and Conclusions

Evidence presented or reviewed in this paper establishes that the present bulk composition of 14310 is not that of a primary magma from the lunar interior. Whether

14310 represents an endogenous partial melt or residual liquid from the lunar interior, or an exogenous impact melt, is largely immaterial to the major problem of the origin of anorthite-rich materials in the outer layer of the moon. We suggest that the anorthositic layer originated by early stage partial melting of a wet lunar interior, giving rise to liquids of calc-alkaline affinities (of which 14310 may represent a late stage derivative). Subsequent melting of the dehydrated residual mantle yielded the parental magmas of the maria suites.

References

Apollo Soil Survey (1971) Apollo 14; nature and origin of rock types in soil from the Fra Mauro formation. *Earth Planet. Sci. Lett.* **12**, 49–54.

Baker P. E. (1968) Petrology of Mt. Misery volcano, St. Kitts, West Indies. *Lithos* **1**, 124–150.

Biggar G. M. O'Hara M. J. Peckett A. and Humphries D. J. (1971) Lunar lavas and the achondrites: Petrogenesis of protohypersthene basalts in the maria lava lakes. *Proc. Second Lunar Sci. Conf., Geochim. Cosmochim. Acta*, Suppl. 2, Vol. 1, pp. 617–643. M.I.T. Press.

Biggar G. M. O'Hara M. J. Humphries D. J. and Peckett A. (1972a). Maria lavas, mascons, layered complexes, achondrites and the lunar mantle. In *The Moon* (editors H. Urey and S. K. Runcorn, IAU. In press.

Biggar G. M. Ford C. E. Humphries D. J. Wilson G. and O'Hara M. J. (1972b) Melting relations of more primitive mare-type basalts 14053 and M (Reid 1971); and of breccia 14321 and soil 14162 (average lunar crust?) In *Lunar Science—III* (editor C. Watkins), pp. 74–76, Lunar Science Institute Contr. No. 88.

Boyd F. R. and England J. L. (1963) Effect of pressure on the melting of diopside, $CaMgSi_2O_6$, and albite, $NaAlSi_3O_8$, in the range up to 50 kb. *J. Geophys. Res.* **68**, 311–323.

Brown G. M. and Peckett A. (1971) Selective volatilization on the lunar surface: Evidence from Apollo 14 feldspar-phyric basalts. *Nature* **234**, 262–266.

Brown G. M. Emeleus C. H. Holland J. G. Peckett A. and Phillips R. (1972) Mineral fractionation patterns between Apollo 14 primitive feldspathic rocks and Apollo 15 and other basalts (abstract). In *Lunar Science—III* (editor C. Watkins), pp. 95–97, Lunar Science Institute Contr. No. 88.

Dence M. R. (1971) Impact melts. *J. Geophys. Res.* **76**, 5552–5565.

Drever H. I. Johnston R. and Gibb F. G. F. (1972) A note on three Imbrium spinels, and a twinned pigeonite in high alumina basalt 14310 (abstract). In *Lunar Science—III* (editor C. Watkins), pp. 186–188, Lunar Science Institute Contr. No. 88.

Ford C. E. (1972) Furnace design, temperature distribution, calibration and seal design in internally heated pressure vessels. *Progress in Experimental Petrology*, Second Rept. Natural Environment Research Council (in press).

Ford C. E. Humphries D. J. Wilson G. Dixon D. Biggar G. M. and O'Hara M. J. (1972) Experimental petrology of high alumina basalt, 14310, and related compositions (abstract). In *Lunar Science—III* (editor C. Watkins), pp. 274–276, Lunar Science Institute Contr. No. 88.

Gast P. W. and McConnell R. K. Jr. (1972) Evidence for initial chemical layering of the moon (abstract). In *Lunar Science—III* (editor C. Watkins), pp. 289–291, Lunar Science Institute Contr. No. 88.

Herzberg C. and O'Hara M. J. (1972) Temperature and pressure calibration and reproducibility of pressure in solid media equipment. *Progress in Experimental Petrology*, Second Rept. Natural Environment Research Council (in press).

Hollister L. Trzcienski W. Dymek R. Kulick C. Weigand P. and Hargraves R. (1972) Igneous fragment 14310,21 and the origin of the mare basalts (abstract). In *Lunar Science—III* (editor C. Watkins), pp. 386–388, Lunar Science Institute Contr. No. 88.

Kushiro I. (1972) Petrology of lunar high-alumina basalt (abstract). In *Lunar Science—III* (editor C. Watkins), pp. 466–468, Lunar Science Institute Contr. No. 88.

Kushiro I. Nakamura Y. Kitayama K. and Akimoto S. (1971) Petrology of some Apollo 12 crystalline rocks. *Proc. Second Lunar Sci. Conf., Geochim. Cosmochim. Acta*, Suppl. 2, Vol. 1, pp. 481–495. M.I.T. Press.

LSPET (1971) (Lunar Sample Preliminary Examination Team) *Apollo 14 Preliminary Science Report*, NASA SP-272, 309 pp., Washington, D.C.

LSPET (1972) (Lunar Sample Preliminary Examination Team) A preliminary description of the Apollo 15 lunar samples. *Science* (in press).

Mason B. Melson W. G. and Nelen J. (1972) Spinel and hornblende in Apollo 14 fines (abstract). In *Lunar Science—III* (editor C. Watkins), pp. 512–514, Lunar Science Institute Contr. No. 88.

Muan A. Hauck J. and Löfall T. (1972) Equilibrium studies with a bearing on lunar rocks (abstract). In *Lunar Science—III* (editor C. Watkins), pp. 561–563, Lunar Science Institute Contr. No. 88.

O'Hara M. J. Biggar G. M. Richardson S. W. Ford C. E. and Jamieson B. G. (1970) The nature of seas, mascons and the lunar interior in the light of experimental studies. *Proc. Apollo 11 Lunar Sci. Conf., Geochim. Cosmochim. Acta*, Suppl. 1, Vol. 1, pp. 695–710. Pergamon.

O'Hara M. J. Richardson S. W. and Wilson G. (1971) Garnet-peridotite stability and occurrence in crust and mantle. *Contr. Mineral. Petrol.* **32**, 48–68.

Reid A. M. Warner J. Harmon R. S. and Brett R. (1972) Chemistry of highland and mare basalts as inferred from glasses in the lunar soils (abstract). In *Lunar Science—III* (editor C. Watkins), pp. 640–642, Lunar Science Institute Contr. No. 88.

Ridley W. I. Williams R. J. Brett R. and Takeda H. (1972) Petrology of lunar basalt 14310 (abstract). In *Lunar Science—III* (editor C. Watkins), pp. 648–650, Lunar Science Institute Contr. No. 88.

Ringwood A. E. Green D. H. and Ware N. G. (1972) Experimental petrology and petrogenesis of Apollo 14 basalts (abstract). In *Lunar Science—III* (editor C. Watkins), pp. 654–656, Lunar Science Institute Contr. No. 88.

Roedder E. and Weiblen P. W. (1972) Petrographic and petrologic features of Apollo 14, 15 and Luna 16 samples (abstract). In *Lunar Science—III* (editor C. Watkins), pp. 657–659, Lunar Science Institute Contr. No. 88.

Roeder P. L. and Emslie R. F. (1970) Olivine-liquid equilibrium. *Contr. Mineral. Petrol.* **29**, 275–289.

Smith J. V. Anderson A. T. Newton R. C. Olsen E. J. Crewe A. V. Isaacson M. S. Johnson D. and Wyllie P. J. (1970) Petrologic history of the moon inferred from petrography, mineralogy and petrogenesis of Apollo 11 rocks. *Proc. Apollo 11 Lunar Sci. Conf., Geochim. Cosmochim. Acta*, Suppl. 1, Vol. 1, pp. 897–926. Pergamon.

Toksöz M. N. Press F. Anderson K. Dainty A. Latham G. Ewing M. Dorman J. Lammlein D. Sutton G. Duennebrier F. and Nakamura Y. (1972) Velocity structure and properties of the lunar crust (abstract). In *Lunar Science—III* (editor C. Watkins), pp. 758–760, Lunar Science Institute Contr. No. 88.

Wager L. R. (1962) Igneous cumulates from the 1902 eruption of Soufriere, St. Vincent. *Bull. Volcanol.* **29**, 93–99.

Walker D. Longhi J. and Hays J. F. (1972) Experimental petrology and origin of Fra Mauro rocks and soils (abstract). In *Lunar Science—III* (editor C. Watkins), pp. 770–772, Lunar Science Institute Contr. No. 88.

Walter L. S. French B. M. and Doan A. J. (1972) Petrographic analysis of lunar samples 14171 and 14305 (breccias) and 14310 (melt rock) (abstract). In *Lunar Science—III* (editor C. Watkins), pp. 773–775, Lunar Science Institute Contr. No. 88.

Wilshire H. G. and Jackson E. D. (1972) Petrology of the Fra Mauro formation at the Apollo 14 landing site (abstract). In *Lunar Science—III* (editor C. Watkins), pp. 803–805, Lunar Science Institute Contr. No. 88.

Wood J. A. Dickey J. S. Jr. Marvin U. B. and Powell B. N. (1970) Lunar anorthosites and a geophysical model of the moon. *Proc. Apollo 11 Lunar Sci. Conf., Geochim. Cosmochim. Acta*, Suppl. 1, Vol. 1, pp. 965–988. Pergamon.

Yoder H. S. Jr. (1968) Experimental studies bearing on the origin of anorthosites. In *Origin of Anorthosite and Related Rocks* (editor Y. W. Isachsen), pp. 13–22, Univ. State New York Mem. 18.

Yoder H. S. Jr. (1969) Calcalkalic andesites: Experimental data bearing on the origin of their assumed characteristics. In *Proc. Andesite Conf.* (editor A. R. McBirney), pp. 77–89, Oregon Dept. Geol. Mineral. Res., Bull. 65.

MARIA LAVAS, MASCONS, LAYERED COMPLEXES, ACHONDRITES AND THE LUNAR MANTLE

G. M. BIGGAR, M. J. O'HARA and D. J. HUMPHRIES
Grant Institute of Geology, University of Edinburgh, Scotland

and

A. PECKETT
Department of Geology, University of Durham, England

Abstract. Experimental data show Apollo 11 and 12 lava compositions to be controlled by fractional crystallization close to the lunar surface, in a process which yields achondrite-like igneous rocks as underlying complementary crystal accumulates. Volatilization losses during eruption can account for most other chemical differences between lunar lavas and common terrestrial magmas. No specific hypotheses of the composition, mineralogy, or origin of lunar interior can be sustained until the extent of these processes is known. A terrestrial upper-mantle-type lunar interior cannot yet be excluded. The assumption that maria surface lavas are primary partial melts is unjustified and leads to a postulated lunar interior with too low Mg/Mg+Fe to serve as a source for Apollo 14 and other igneous liquids. Other workers' uncontrolled visual estimates of crystallinity in experimental charges, purporting to show that maria lavas were not modified by low pressure fractionation, are irreconcilable with the chemistry of the residual liquids developed in our 'reversed' equilibrium experiments. The undesirability of using glass as a starting material for this type of experiment is re-emphasized.

1. Introduction and Statement

The preferred interpretation (Biggar *et al.*, 1971) of available lunar samples involves at least the following sequence of events:

(1) Lunar accretion.

(2) Primordial differentiation to yield crust by partial melting of interior.

(3) Continued but rapidly declining rate of meteoritic impacts, including formation of maria basins.

(4) Triggered release of further partial melts from the interior to fill maria basins with *lakes* of lava. (see 8)

(5) Slow consolidation of the lava lakes with strong fractional crystallization in each liquid body. (see 12)

(6) Random or intermittent eruption of underlying residual differentiated liquid through the crusts of the lava lakes to form the surface lavas sampled by Apollo 11 and 12 missions.

The age of these events is ~4.5 b.y. Apparent younger Rb/Sr isochron ages date one or more metamorphic events. *

Significant facets of this interpretation are that:

(7) There is no evidence that the lunar interior, or the *primary* partial melts derived from it, differ significantly in composition from those present in the *outer* parts of the Earth: there is some evidence that the two groups of materials are similar.

(8) Fire fountaining during initial lava eruption (see 4) led to small droplet forma-

* See footnote, p. 137.

Urey and Runcorn (eds.), The Moon, 129–164. *All Rights Reserved.*
Copyright © 1972 by the IAU.

tion and selective volatilization of elements, as well as fall in oxygen fugacity to the point where metallic iron began to separate. Two of the four major chemical peculiarities of maria lavas (great depletion in all the volatile elements, and most siderophile elements) result directly from the loss of vapour phase at stage (4) coupled with the settling out of a layer of metal phase at the floor of the lava lake after fire fountain droplets had fallen back into the lake.

(9) The extent of metal phase production determines the mass concentration effects.

(10) Prolonged fractional crystallization, just as in large terrestrial lava bodies, greatly reduced the residual liquid volume while concentrating the remaining FeO, the TiO_2, and rare-Earth elements (REE) in that reduced volume, thus producing the third chemical peculiarity of maria surface lavas.

(11) Volatilization losses of Na_2O (in particular) at stage (4) caused excessive precipitation of calcium-poor pyroxenes accompanied by very calcic plagioclase from the differentiating lava lake. Prolonged plagioclase extraction aided by volatilization produced the fourth chemical peculiarity, the marked europium deficiency in the late residual liquids, which occasionally spilled out over the crust as lava flows.

(12) The petrographic character of the crystal accumulates in the underlying maria structure is such that fragments of them observed to fall upon the Earth would be classified as achondrites, irons or stony irons. The essence of the interpretation is conveyed in Figure 1.

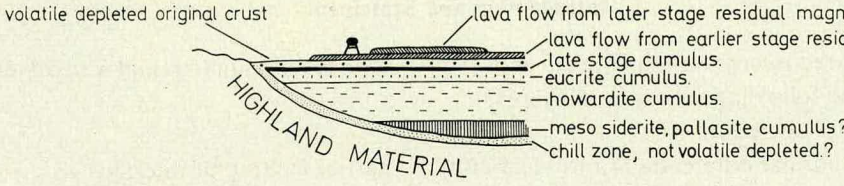


Fig. 1. Hypothetical cross section of lunar maria illustrating disposition of rock types consistent with experimental and petrological observations, topography, and Duke and Silver's (1967) interpretation of the achondrites (reproduced from Biggar *et al.*, 1971, Figure 10). Because both the chill zone and the first crust on the lake are formed from magma which may have fire-fountained on eruption, they will have suffered some volatilization losses, and iron precipitation, but not fractional crystallization. Impact melted glasses of howardite/eucrite-like composition are reported from soils at some sites (Marvin *et al.*, 1972).

This paper summarises the arguments demonstrating (i) that the maria are fractionated lava lakes, and not piles of successive individual flows. (ii) That their surface lavas represent strongly fractionated residual liquids from those lakes. (iii) That selective volatilization was a significant event. (iv) That the true age of the major igneous events is 4.5 b.y.* and (v) that the Mg/Fe+Mg of the lunar interior closely resembles that of the Earth's upper mantle.

The obscuring effect of the near-surface events which modify lunar rock compositions make it difficult to place any valid constraints on the nature of the lunar interior beyond those already imposed by inference from astronomical observations. Firm

* See footnote p. 137.

choice between early fission, capture and conjugate birth as the origin of the Moon is impossible, as yet, on the strength of petrological or chemical data.

The interpretation presented above is founded upon certain observations of phase equilibria produced in our laboratory. Much of this paper is concerned with establishing the accuracy, sufficiency and relevance of these data. Experimental data from another laboratory have been alleged to invalidate our conclusions; some attention is given below to identifying serious discrepancies both within, and between those data and our own results, and to understanding the reasons for the discrepancies.

2. Maria Surface Lavas Are not Primary Partial Melts of Lunar Interior; Lunar Maria Are Sites of Extreme Fractional Crystallization

Strom (1971 and pers. comm.) reports stratigraphic sequences of very extensive thin flows emanating from wrinkle ridges in Mare Imbrium. The older lava flows are 'red', and the upper later flows are 'blue', indicating increase in TiO_2. Final effusions from the fractures appear to be small volumes of very viscous light coloured lava. The telescopic evidence for differentiation increasing with passage of time in a mare surface eruption sequence is strong.

Large lakes or chambers of magma undergo *extreme* differentiation by fractional crystallization during their solidification (Wager and Brown, 1968). At a late stage a very small fraction of the original liquid volume becomes grossly enriched in those rare elements selectively rejected by the crystals forming and sinking to the floor of the body to form cumulates. Periodic escape of such residual liquids onto the surface (due to foundering or impact fracturing of the lava-lake crust) will then give chemical sequences inverted with respect to those expected in a direct partial melting sequence, the latest lava flows being the most enriched in rare elements.

The elements which are selectively rejected by crystalline or immiscible liquid, phases separating at an early stage from basaltic magmas and which might, therefore, be expected to become enriched in the residual liquids developed during consolidation of the lava-lakes, may be subdivided as follows:

(i) *Volatile* e.g. H_2, O_2, H_2O, CO_2, F, Cl, Br, I, S, Se, Na, K, Rb, Cs, Zn, Cd, Hg, B, In, Tl, N, P, As, Sb, Te, Bi, Pb. These, however, will not reach high concentrations in residual liquids if a gaseous phase has separated at low pressure.

(ii) *Chalcophile* These include some of the volatile group, and will not reach high concentrations in residual liquids if a sulphide phase (crystal or liquid) has separated.

(iii) *Siderophile* e.g. Co, Ni, Pd, Pt, Os, Rh, Ag, Au. These will not reach high concentrations in residual liquids if oxygen fugacity has been low enough to cause the separation of an iron-rich metal phase.

(iv) *Lithophile* Any Fe remaining oxidised in the liquid after filling of the lava-lake will thereafter be strongly concentrated by fractional crystallization into the residual liquids together with Li, Sr, U, Th, Ce, Nb, Ba, Y, R.E.E., Ti, Zr, V, Cr. These will be progressively concentrated in the residual liquids regardless of volatilization, sulphide or metal phase precipitation, subject to the following provisos:

(a) Fe, Cr and V will remain high or be progressively concentrated provided there has not been precipitation of spinel (chromite, magnetite) or abundant Ca-rich pyroxene (diopside, augite).

(b) The light and heavy REE elements will be comparably concentrated provided that large amounts of Ca-rich pyroxene have not precipitated.

(c) Europium will not be concentrated if abundant plagioclase feldspar has precipitated, and *may have been selectively volatilized.*

The chemistry of maria surface lavas is marked by high concentration of Fe, Ba, Y, REE, Ti, Zr, V, Cr, without marked relative fractionation of the REE, but with a spectacular relative depletion of Eu. Extreme fractional crystallization and separation of calcic plagioclase and calcium-poor pyroxene, with little spinel or Ca-rich pyroxene is indicated.

In maria lavas great depletion of siderophile elements indicates extraction of a metal phase. Allowing for the initial Fe depletion caused by this, the present Fe/Mg ratio and high concentrations of REE, Ti, Zr, are such as might be generated in the final 1–2% of liquid in a consolidating lava lake.

The fractionated lava lake hypothesis *predicts* that the very high concentrations of elements such as Ti will be found in less than 2% of the total mass of the maria, and that these concentrations will increase in the surface lava flows from any one lava lake as they become younger, consistent with Strom *et al.*'s observation of increasing 'blueness' with passage of time, at least until a late stage when Ti-rich mineral begins to crystallize. Essene *et al.*'s (1970) hypothesis of successive flows of primary partial melts, each representing a very small fraction (less than 1%) of the source lunar mantle requires on the contrary (i) that concentrations of titanium should decrease, rather than increase with passage of time, and (ii) that huge volumes of the Moon's interior should have been 'worked over' and depleted of a minute fraction of partial melt, the mechanics of whose flow and collection into a few lava reservoirs presents severe problems. The mass balance problem is a principal objection to the successive lava flow hypothesis – it does not arise in the fractionated lava lake hypothesis because only 1–2% as much lunar mantle needs to be processed to yield the observed element concentrations in the last extreme differentiate of the lava lake.

One of the very minor but characteristic late stage rocks produced by extreme crystal fractionation in large terrestrial lava bodies is a hedenbergite-granophyre (Wager and Brown, 1968). Mason *et al.* (1971) now report a fragment of hedenbergite-granophyre from regolith at the Apollo 12 site.

3. Lunar interior; High Mg/Mg+Fe

Phase equilibria data from Apollo 11 samples did not exclude the possibility of a lunar mantle of terrestrial upper mantle composition (O'Hara *et al.*, 1970). Figure 2 summarises available relevant information on the partition of Mg and Fe between coexisting olivines and liquids, and the inferences which may be drawn from them about the Mg/Mg+Fe of the source regions of the liquids. The solid curve represents

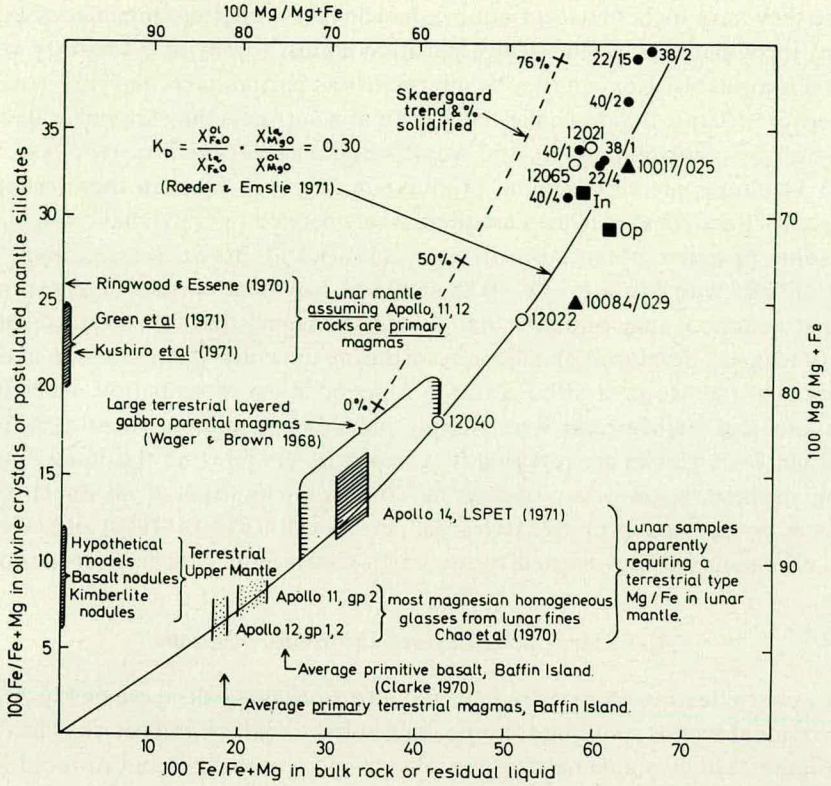


Fig. 2. Fe/Mg distribution between olivine crystals, or postulated lunar mantle and liquid, for Apollo 11, 12 and 14 samples; small filled circles and triangles from experimental data of Biggar *et al.* (1971); open circles from liquidus data of Green *et al.* (1971), filled squares from petrographic observation (James and Jackson, 1970) of the first olivines in the Apollo 11 intersertal (In) and ophitic (Op) group lavas.

an empirical partition function found to fit most terrestrial data. It is seen to fit data from quenching experiments on Apollo 11 samples (Biggar *et al.*, 1971, triangles), Apollo 12 samples (Biggar *et al.*, 1971, filled circles), liquidus olivine compositions quoted for four rocks (Green *et al.*, 1971, open circles) and phenocryst core compositions (James and Jackson, 1970 filled squares) in two groups (Op, ophitic; In, intersertal) of Apollo 11 lavas, plotted against average compositions of these groups (Compston *et al.*, 1970).

On the *assumptions* that Apollo 11 and Apollo 12 lavas represented primary partial melts, Ringwood (1970) and three other groups of workers have deduced relatively low Mg/Mg+Fe (0.75–0.80) in the silicates of the lunar mantle, as noted on the left side of the figure.

However, Apollo 14 samples have much higher Mg/Mg+Fe than the maria surface lavas, implying equilibration against silicates with Mg/Mg+Fe$\sim$0.87. These lavas cannot be interpreted as more advanced partial melts of some more iron-rich mantle

because they have higher concentrations, than do lavas collected from maria-surfaces, of some incompatible elements which partition almost wholly into whatever volume of liquid is available. Nor can they be interpreted as partial melts depleted in metallic iron because relative to lavas collected from maria surfaces, they are richer in nickel, which dissolves preferentially in, and would be eliminated with a metal phase. These Apollo 14 liquids are clearly more primitive in Mg/Mg+Fe than those erupted at the Apollo 11 and 12 sites, which are presumably derived by fractional crystallization from some primitive parent. Brown *et al.* (1971) and Brown (pers. comm. 1971) report olivines with Mg/Mg+Fe ~ 0.88–0.90 and comment on their implications for the lunar mantle. It may transpire that Apollo 14 magmas have the characteristics of primary magmas developed on a large scale during the initial differentiation and crust formation of the Moon (LSPET 1971) in a period when incompatible element concentrations and Fe/Mg ratio were sharply reduced in the lunar mantle. Still more magnesian basic glasses are reported by Chao *et al.* (1970) from the lunar fines, requiring a source region whose silicates have Mg/Mg+Fe ~ 0.91–0.94 similar to that demanded by the most primitive terrestrial partial melts (Clarke 1970) and evidenced in the ultramafic nodules blasted to the Earth's surface in kimberlite eruptions.

4. Lunar Maria, Layered Intrusions, Mascons

The distinctive feature of terrestrial layered intrusions is the decrease of Mg/Mg+Fe in the residual liquids resulting from prolonged fractional crystallization. The dashed line (Figure 2) links points for cumulus olivine and coexisting liquid deduced for the successive residual liquids of the Skaergaard intrusion at various percentages of solidification of the original parental liquid (from Wager and Brown, 1968, Figure 119).

O'Hara *et al.* (1970) and Biggar *et al.* (1971) have proposed that solidification of the lunar maria lava lakes proceeds in a manner analogous to that seen in large terrestrial layered intrusions, with the modification that early precipitation of metallic iron has depleted siderophile elements and inhibited equivalent decrease of Mg/Mg+Fe in the liquid until larger percentages of the parental liquid have solidified. Early precipitation of c. 3.7% of the initial magma as metallic iron would inhibit the evolution of a Skaergaard-type trend so that more than 90% crystallization would be necessary for the liquid to reach the Mg/Mg+Fe ratios of lunar maria surface lavas.

The extent of metallic iron precipitation, and the resulting excess mass in the early stages of maria filling will vary with volatilization losses and hence with the mechanics of the first eruption process, and will, therefore, vary from one mare to another. This is only one of many possible internal explanations of mascons (O'Hara *et al.*, 1971), but the one which is supported by the experimental and petrological data (Biggar *et al.*, 1971).

If circumstances were such that a constant hydrostatic head and constant *volume* of liquid were maintained in the maria basins (possible if the level of the surface is maintained by a 'water-table' effect reflecting *widespread* partial melting at some depth) the process of densification of the erupted magma by loss of O_2, Na_2O and K_2O with

accompanying precipitation of metallic iron might lead to c. 5% extra mass being consolidated in the basin. An excess mass $\sim 10^5$ g cm^{-2}, is required beneath the maria to yield observed mascon effects, equivalent to an extra 6% mass present in what would otherwise have been a gabbro column c. 6 km deep (well within the depth range possible in the lunar maria, and evident in terrestrial layered bodies e.g. Stillwater complex 5.2 km; Bushveld complex 7.3 km, with lateral extent of 300×400 km). Thus far, therefore, we find no constraints which exclude the possibility of a lunar interior and derived liquids comparable with those present in the Earth's upper mantle, and some evidence which points to considerable similarities.

All other factors being equal, the above hypothesis predicts that surface lavas from maria with larger mascons should exhibit higher non-volatile incompatible element concentrations at the same Fe/Mg ratio. The information required to test this prediction will take time to accumulate. It also predicts that lunar volcanic rocks will show some positive correlation between higher alkali retention and lesser depletion of siderophile elements (e.g. Ni) – this is true of Apollo 14 igneous rocks compared with Apollo 11 and 12 materials.

5. Selective Volatilization from Lunar Lavas

The rate of mass loss of Na_2O from a basic magma which is necessary to extract 1% Na_2O by weight from the liquid is readily calculated.

During fire fountaining, droplet surfaces will not be rapidly cooled because they are surrounded by other equally hot droplets. Assuming an ejection velocity of $\sim 10^4$ cm s^{-1}, flight time $\sim 10^2$ s and a droplet size of $\sim 10^{-2}$ cm, a loss rate of $\sim 2.5 \times 10^{-6}$ g cm^{-2} s^{-1} at 1500 K would suffice. Loss rates of 10^{-4} to 10^{-5} g cm^{-2} s^{-1} are required for similar losses from thin sheets of liquid flowing up to a hundred kms across the lunar surface, or fire fountain droplets averaging up to 1 cm in size.

Experiments on a terrestrial iron-rich tholeiite magma near its liquidus temperature are summarised in Table I. The mass loss rate of Na_2O is $> 10^{-5}$ g cm^{-2} s^{-1} at ~ 1450 K and $fO_2 \sim 10^{-11}$ to 10^{-15} bar and is appreciably higher than reported by O'Hara *et al.* (1970) when $fO_2 \sim 10^{-8}$ to 10^{-9} bar. This directly measured loss rate is similar to those inferred by application of the Langmuir equation (rate $= P_v \sqrt{(\text{mol } wt/2\pi RT)}$, vaporization coefficient of 1) to De Maria *et al.*'s (1971) vapour pressures, or by assuming a rate $\sim 10^2$ times greater than for pure SiO_2 or bulk tektite compositions (Chapman and Scheiber 1969). The lower loss rates for K than Na presumably reflect the lower activity of potassium in the melt.

Selective loss of Na_2O at least *must have occurred during eruption* of lunar lavas, and the gross depletion of these rocks in all volatile elements points to the general nature of this conclusion.

Restoration of alkalis and other volatiles including oxygen to the lunar lava compositions leads, among many other possible parents, to compositions familiar among terrestrial basalts. It is unsafe to assume that the present lava compositions are those

TABLE IA

Volatilization study on Scourie iron-rich tholeiite dike; $fO_2 \sim 10^{-12}$ bar

	Time h	Temp °C	Pressure (torr)	Comments	Na_2O wt %	K_2O wt %
Start	–	–	–		2.38 + [a]	0.92 + [a]
V.63	1	1150–60	10^{-4}	part devitrified bubbled surface, black glass powder	1.93	0.88
V.62	5	1160	10^{-4}	part devitrified bubbled surface, brown glass powder	1.51	0.97
V.64	24	1160	1.5×10^{-4}	trace devitrification smooth surface, brown glass powder	0.60	0.91
V.57	60	1175	2×10^{-5}	trace devitrification smooth surface, brown glass powder	0.16	0.25
V.58	240	1175	2×10^{-5}	trace devitrification smooth surface, brown glass powder	0.13	0.12
V.59	430	1175	$\sim 5 \times 10^{-5}$	trace devitrification smooth surface, brown glass powder	0.20	0.21

[a] Not adjusted for H_2O, Fe_2O_3 in rock sample. Alkalis determined by flame photometer. Surface area of sample exposed ~ 2.9 cm^2

TABLE IB

	I	II	III	IV
SiO_2	50.49	51.29	53.43	52.19
TiO_2	2.87	2.81	2.82	2.97
Al_2O_3	12.48	12.44	12.96	12.91
FeO	16.57	16.28	16.03	17.13
MnO	0.26	(0.26)	(0.26)	0.27
MgO	4.85	4.84	4.92	5.02
CaO	8.89	8.97	9.24	9.19
Na_2O	2.41	2.13	0.09	0.09
K_2O	0.93	0.98	0.25	0.25
P_2O_5	0.25	–	–	–
	100.00	100.00	100.00	100.02

I – Scourie dike, 10727 from thin vein at Geodh Eanruig (O'Hara, 1961; Table III, locality II, p. 856, plate XVIII), recalculated less H_2O and with all iron as FeO, from complete wet method analysis by M. R. Saunders.

II – Same material after 2 h at 1200 °C in molybdenum capsule at $pO_2 \sim 10^{-12.0}$ bar, recalculated to 100% less P_2O_5 from microprobe analyses of glass fragments.

III – Same material as I after 60 h at 1175 °C in molybdenum crucible at low pO_2 and total pressure of 2×10^{-5} torr. Electron microprobe analysis.

IV – Analysis I recalculated less P_2O_5 and appropriate alkalis to compare with III.

Note: alkali loss apparent between I and II; apparent loss of FeO from glass III (? reduced and reacted with crucible) and pick-up of SiO_2 (? from cracking of silicones oil of diffusion pump).

of the pre-eruption liquids, let alone the primary partial melts, and premature to ascribe their volatile-poor characteristics to the Moon as a whole on the strength of that assumption.

The feldspar phenocrysts in samples 14073, and 14310 record pre-eruption levels of Na_2O and K_2O in the liquids *at least* 2–3 times higher than the levels on final consolidation of these lavas (Brown and Peckett, 1971). Restoration of the missing alkalis and c. 0.25% O_2 to the present composition of 14310 leads to a composition quite familiar among *inter alia* the Kamchatka calcalkaline volcanics.

Volatilization which would have accompanied eruption and which selectively separates Rb from Sr, would have destroyed the orderly 4.5 b.y. model ages and the 4.5 b.y. isochron defined by the different bulk rock samples collected at the Apollo 11 (ophitic group) and Apollo 12 sites. Therefore, no igneous event can have affected these rocks since 4.5 b.y. (compare Urey *et al.*, 1971) and the internal mineral isochrons from individual rocks may date devitrification or other metamorphic events. 3.3–3.7 b.y. ago. (Liquids low in volatiles, alkalies and Fe^{3+} such as were produced in the experiments of Table I, were very slow to nucleate and some did not devitrify even in cooling times of 1 h from 1175 °C to 700 °C.)*

6. Accuracy Precision and Significance of the Experimental Data

Experiments performed on lunar samples and related compositions define, at various pressures, the (liquidus) crystalline phases stable with a liquid of the sample composition. This information can then be used to deduce the crystalline species present in the solid material with which the liquid last equilibrated *provided that* the pressure of that last equilibration is indicated by other information, or can be reliably estimated.

If that pressure is *assumed*, provisional conclusions only can be reached (O'Hara *et al.*, 1970); but addition of 10% of what you fancy to produce a more convenient liquidus phase is less than objective.

We have presented experimental evidence that maria surface lava compositions have low pressure cotectic character, controlled by crystal-liquid equilibria at low pressure, leading to the preceding interpretation of maria structure and origin. Others claim there is no evidence of significant low pressure control; go further in claiming that there has been no control of particular lunar lava compositions at any pressure other than that of genesis by partial melting of the lunar mantle; and assume the depth of that partial melting process. From this basis they deduce a model of a volatile depleted, strongly reduced pyroxenite or olivine-pyroxenite lunar interior. If our experimental observations are correct, maria surface lavas are not primary magmas and the model developed by Ringwood and Essene (1970), Ringwood (1970) and Green *et al.* (1971) is a chimera.

The controversy centres on the accuracy of our observation of close approach to cotectic character at low pressure, which has been criticized by Ringwood (1970) and

* Wasserburg and Papanastassiou (1971) suggest crustal or soil contamination of the lavas, vitiating this argument and most petrogenetic discussion based on minor element chemistry.

Green *et al.* (1971), on the strength of their visual estimates of crystallinity, in their products obtained from starting material long deprecated for its propensity to yield metastable products. Moreover, much information necessary for the evaluation of their statements was not presented by Green *et al.* (1971). The temperatures and durations of individual experiments were not given, nor is it clear which experiments used natural and which used synthetic materials (p. 602*). Without these data, claims to have produced the same result by different techniques are insubstantial. Details of the containers, atmospheres, temperatures and durations used in the initial glass preparations are needed to define the nature of the starting material. No calibration of the temperature or oxygen fugacity actually achieved in the charges was reported, and the pressure of some experiments is apparently unspecified (p. 610*). There were no data to establish the precision achieved in their visual estimates of percent crystallinity (Figure 2 caption*) which yield unrealistic residual liquid compositions.

There seem to be several inconsistencies in the data which were reported. For example, 12040 is given as showing plagioclase entry between 1120 and 1140 °C (Figure 1*), near 1140 °C (p. 603*), or between 1150 °C and (presumably) 1140 °C (p. 607*; but no 1150 °C run is shown in their Figure 1). The percentage of crystals when plagioclase first appears in 12040 is reported variously as 70% (Figure 2*) or 50–60% (text on same page). There are no runs (Figure 1*) to substantiate the remark (p. 603*) that ilmenite enters at close to 1100 °C in 12040. The percentage of crystals at plagioclase entry in 12021 and 12065 are given as 40% and 45% (Figure 2*), but as 20–30%, and 30–40%, respectively, in the text (p. 607*). It was claimed (p. 611*) that 12021 could be derived by extraction of olivine, spinel and minor pigeonitic pyroxene from 12009, yet the data (Figure 2*) indicate that a pyroxene olivine ratio of 3/1 would be required in the extract from 12009 to yield a residuum with the phase behaviour of 12021 at temperatures of c. 1160 °C. Unlisted experiments of unknown bracket width and duration, which were apparently no more than syntheses from different starting materials *as loaded*, (see Figure 18, sequence 5 below) were presented (p. 608*) and claimed as reversals, and the reader is not told which compositions were used for these experiments.

Green *et al.* (1971) exploit small composition differences between experimental and natural minerals to stress the importance of 'direct supporting evidence from each sample'; but surely there is a prior need to place the experimental observations on a quantitative and objective basis.

Ringwood and Green (1972) have published a further criticism of our results which is disappointing for its misrepresentation of our statements, and for its reliance yet again on subjective visual estimates of crystallinity as a basis for criticism of our quantitative data. We have *never* stated that plagioclase was liquidus phase in natural Apollo 11 or 12 basalts**, nor that the rocks were *on* the plagioclase-precipitating cotectic under the conditions encountered on the lunar surface, nor have we 'qualified' our original position that the lavas have compositions *close to* the 1 atmosphere cotectic (too close

* All page and figure references are to Green *et al.* (1971a).

** 10084 was a soil sample.

for this to be a coincidence). Our position is adequately stated by Biggar *et al.* (1971), p. 634, para 2. We did not *claim* that other workers results were invalid because of the use of glass as a starting material; we have *suggested* that it may have had something to do with the discrepancies in observations between ourselves and Ringwood and Essene (1970) while clearly recognizing that the other two groups whom Ringwood and Green (1972) introduce into the argument worked on compositions substantially removed from those under discussion (Biggar *et al.*, 1971, p. 631, para 2). The reader must judge for himself, in the light of the following remarks, however, how much of the actual disagreement stems from the choice of starting material, how much from inadequate calibration of techniques, and how much from uncertainties in more subjective observations. The loss of alkalis was not "claimed to cause an expansion of the primary fields of crystallization of mafic minerals": no variation in an intensive variable can change the extent of primary phase fields, and, therefore, of cotectic liquid compositions in a system of fixed composition. The effect of the loss of alkalis and oxygen is to shift the composition of the remaining condensed system towards ferromagnesian minerals as claimed by Biggar *et al.* (1971, p. 634) who showed (ibid, p. 635, Equation (2)) a reaction in which the plagioclase declines from 64% to 55.5% consequent on alkali loss. The key question is whether the change in normative feldspar composition from An_{50} to An_{80}, combined with the increase in pyroxene at the expense of olivine will offset the reduction in total plagioclase; and problems raised by possible reduction of iron oxides further complicate the issue.

The reader may want more proof that addition of alkalis suppresses rather than enhances the initial appearance of plagioclase than the difference between the two approximate visual estimates of 40–50% (at 1125 ± 5 °C) and 35–50% (at 1115 ± 5 °C) crystallinity at plagioclase entry with or without alkalis respectively, given by Ringwood and Green (1972, Table II; what the alkali addition does to the *temperature* of plagioclase or other phase entries is, of course, irrelevant). We cannot yet provide a definitive answer for the iron rich composition of maria basalts; for the more magnesian compositions of Apollo 14 samples addition of alkalis *alone* undoubtedly lowers the temperature of plagioclase appearance and (visual estimates!) moves the composition towards the cotectic liquid composition *from* the plagioclase liquidus field. Raising or lowering fO_2 opposes this effect.

Contrary to Ringwood and Green's (1972) suggestion, nothing in any of the reported phase data, nor any conceivable data for effusive rocks could ever support the view that certain basalts were derived from regions below those at which plagioclase was a stable phase in the lunar interior. Such an interpretation depends upon totally different criteria. Their statement is only valid if 'residual' is inserted after 'stable' and the magmas are truly primary.

This disagreement is becoming long on immoderate wording and adrenalin, rather than on discussion of scientific data and techniques; we must, however, thank Ringwood and Green (1972) for pointing out our error in drawing of one of our figures from our data table. Biggar *et al.* (1971, p. 633) carries an error (9.1% TiO_2) in the text. 9.2% is correct; in Table IV, column 1, $Cr_2O_3 = 0.46\%$, not 0.06%.

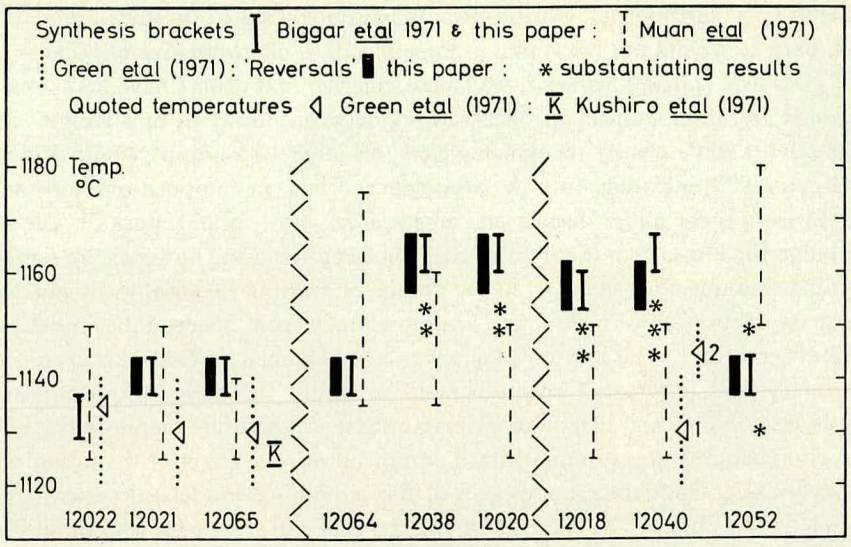


Fig. 3. Comparison of atmospheric pressure quenching data on the temperature of plagioclase appearance for 9 rocks reported on by four laboratories. Results substantiating one side of a bracket are shown where relevant by asterisks. Muan *et al.* (1971) finally reported plagioclase entry at 1125–1150 °C in 12052: Green *et al.* (1971b) now concede ± 5° control precision and ± 10 °C accuracy in their data. See Table IX, footnote (h).

TABLE II

Results of calculations of crystallinity contrasted with visual estimates[a]

100 % rock =	%	residual liquid + %	sp	ol	pig	plag	Estimated % crystals at plagioclase entry	% crystals visual estimates Green *et al.* (1971)
12040[b]	60	cotectic glass 1160	1	29	9	–	40	50 to 60 (text)
12040[b]	54	12038 rock	1	32	10	3	46	70 (Figure 2)
12052[c]	74	12064 cotectic glass at 1137 °C	1	3	17	6	< 25	
12065[c]	77	Plagioclase already fairly common	1	4	12	6	< 20	~ 40 (text)
12021[c]	80		tr	1	14	5	< 15	~ 45 (Figure 2)
12064[c]	88		tr	1	7	4	~5	~ 30 to 40 (text) ~ 40 (Figure 2)
12022[c]	71	cotectic glass 1129 °C	1	23	0	5	< 25	~45 (Figure 2)

[a] These and subsequent calculations are advanced to show a *major* discrepancy between estimates of crystallinity by different methods. Quibbling over the choice of mineral compositions for the calculations could be endless, but would not lead to large changes in the final results.

[b] Calculation in Table III.

[c] These calculations used chrome spinel (Table IV, note 5), plagioclase (An_{85}), and pigeonite and olivine from 12038/2 (Biggar *et al.*, 1971, Tables III, IV).

TABLE III

Solutions to calculations for 12040

	12040[a]		12038 +	12040	12040	
	(Kushiro and Haramura, 1971)	(Scoon, 1971)	46% crystals[b]	1160 °C glass + 40% crystals[c]	liquid at plagioclase entry Calculated[d]	Actually[e]
SiO_2	43.59	43.82	43.88	44.02	37.93	46.86
TiO_2	2.48	2.74	1.96	2.70	8.30	4.17
Al_2O_3	7.34	7.40	7.71	7.22	27.40	11.50
Cr_2O_3	0.70	0.70	0.67	0.76	−0.05	0.17
FeO	20.87	20.81	21.37	21.19	11.15	17.58
MnO	0.26	0.26	0.28	0.24	tr	0.20
MgO	16.66	16.08	16.43	15.83	−8.48	7.10
CaO	7.90	7.86	7.31	7.73	22.79	11.93
Na_2O	0.16	0.20	0.39	0.31	0.67	0.51
K_2O	0.05	0.04	0.04	0.05	0.21	0.07
P_2O_5	0.02	0.07	0.02	–	0.08	–

[a] Normalised to 100%.

[b] 32.1% olivine (Fo_{66} 12040, 1160 °C), 10.4% pigeonite (12040, 1160 °C Biggar *et al.*, 1971) 1.0% spine, (12009, Green *et al.*, 1971) and 2.5% An_{85} calculated to fit Kushiro and Haramura analysis.

[c] 29.3% olivine (Fo_{66}), 9.2% pigeonite, 1.2% spinel; calculated to fit Scoon analysis.

[d] Extracting 30% olivine, 45% pigeonite (1136 °C, Biggar *et al.*, 1971), 1% spinel (12009, 1150 °C, Green *et al.*, 1971); mineral proportions measured from Green *et al.* (1971, Figure 2 first version issued at Houston conference, showing plagioclase entry at c. 1130 °C as per their Figure 1. Later revised values dealt with in Table IV). Note the extraordinary values of CaO, Al_2O_3, very low SiO_2 and excessive depletion in ferromagnesian constituents.

[e] From Biggar *et al.* (1971, Table V).

[f] Biggar *et al.* (1971, p. 619) required at least three lava flows for the simplest admissible explanation of their experimental data. Precise calculations by James and Wright (unpublished) convince us that a more complicated model, involving a greater number of flows is required to explain the detailed geochemistry.

We emphasize that:

(1) The data of Biggar *et al.* (1971) establish significantly higher temperatures of plagioclase entry (Figure 3) than those claimed by Green *et al.* (1971). Muan *et al.* (1971), also using natural rock powder as starting material, could compromise with Biggar *et al.* (1971) on plagioclase entry at 1140–1160 °C in most cases. Green *et al.* (1971) and Kushiro *et al.* (1971), both using glass as a starting material, would select a temperature in the 1120–1140 °C range, but also agree with Muan *et al.* (1971).

(2) Calculations of percent crystallinity based on analyses of the coexisting phases in experimental products from Apollo 12 rocks (Tables II to IV) indicate much less crystallization at observed plagioclase entry (Figure 4) than claimed by Green *et al.* (1971) if levels of MgO, Al_2O_3, SiO_2 in the liquids are to be realistic.

(3) Products obtained from glass starting materials can be so fine grained (plate I) that percent crystallinity and crystalline-phase ratios are difficult to estimate, microprobe analysis of the residual glass is nearly impracticable, phases such as plagioclase are very difficult to detect in small amounts, and augite becomes difficult to distinguish optically from pigeonite.*

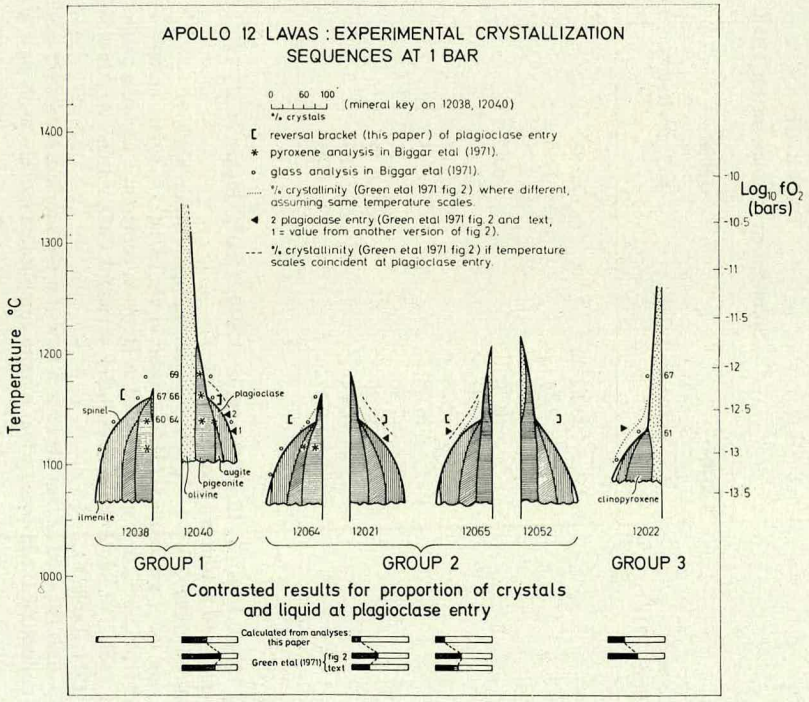


Fig. 4. Graphical representation of co-variation in fO_2, temperature, phase assemblage and percentage crystallinity in Apollo 12 rock compositions (after Green *et al.*, 1971, Figure 2, but with percent crystallinity based on calculations, and the calcium-rich and calcium-poor clino-pyroxenes distinguished except in 12022; note contrast between our calculated, and Green *et al.*'s estimated crystallinity at plagioclase entry, shown by proportional length of black bars).

* Green *et al.* (1971b) refer to this problem, but were confident they could distinguish pigeonite from inverted protohypersthene!

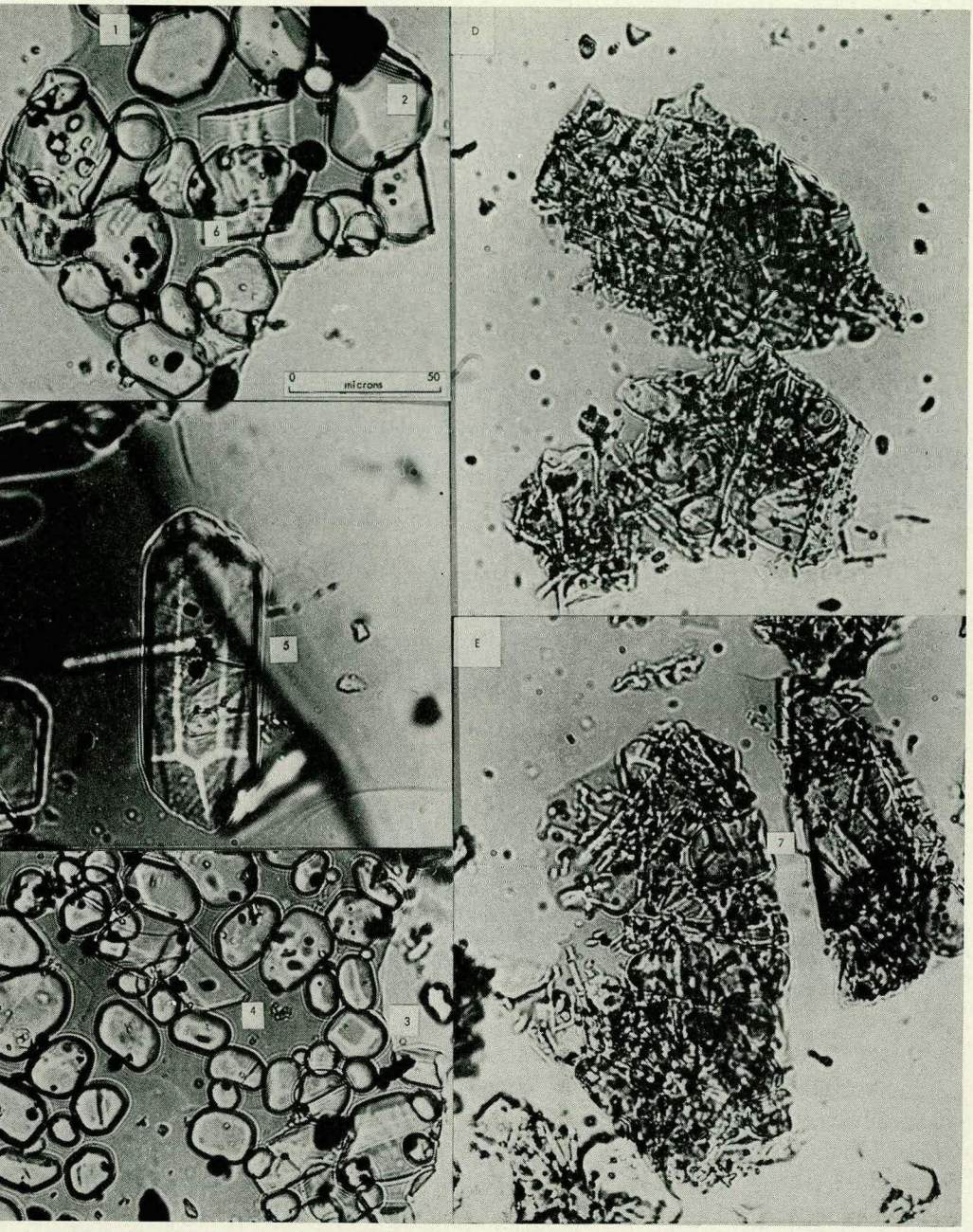


Plate I. Microphotographs (all same scale, see A) of products from reversal experiments on 12040 at 1162°/1153°C; A, B, C from rock powder starting material (experiment 035) showing euhedral olivines (1–3), pyroxene (4) and, again, with curving crack (5), plagioclase (6) and opaque spinel in glass. D, E from largely glass starting material (experiment 117) containing large olivines (7) as in A, C, but interlocking mesh of acicular pyroxenes whose minuscule width makes phase identification, estimation of crystallinity and microprobe analysis extremely difficult.

TABLE IV

Results of extract calculations, using Green *et al.*'s (1971, Figure 2) visual estimates of crystallinity, compared with the actual analysed cotectic liquid compositions

	12021 −40% (A)	12065 −45% (B)	12040 −70% (C)	12040 −50% (D)	12009 −50% (E)	Observed real values 12038, 40, 64 cotectic liquids	12022 −43% (F)	12022/15 observed 1129 °C
SiO_2	43.16	41.77	37.68	41.06	42.33	46 ± 1	48.15	43.77
TiO_2	5.09	5.30	6.71	4.29	4.91	4 ± 0.5	−2.62	6.76
Al_2O_3	16.56	18.29	22.08	13.63	15.67	11.4 ± 1	15.20	9.92
Cr_2O_3	−0.56	−0.55	−0.08	0.37	−0.28		0.53	0.12
FeO	21.09	21.78	20.33	20.64	18.75	19 ± 1.5	17.20	20.53
MnO	0.23	0.22	0.37	0.21	0.25		0.14	0.30
MgO	−2.14	−3.56	−6.69	6.68	4.64	6.1 ± 0.5	5.84	5.72
CaO	15.89	16.18	18.83	12.56	12.88	11.5 ± 0.4	14.51	11.36
Na_2O	0.54	0.40	0.53	0.32	0.46		0.51	0.73
K_2O	0.12	0.13	0.17	0.10	0.13		0.12	0.13
P_2O_5	0.02	0.04	0.07	0.04	0.14		0.43	

Extracts, all obtained from measurement of Green *et al.* (1971, Figure 2). Slightly lower figures are indicated in their text, and these reduce, but do not cure, the discrepancies..

A pigeonite[1] 39%, spinel[2] 1%; B pigeonite[1] 44%, spinel[2] 1%; C olivine[3] 26%, pigeonite[4] 43%, spinel[5] 1%; D olivine[3] 18.6%, pigeonite[4] 30.7%, spinel[5] 0.7%; E olivine[6] 7%, pigeonite[7] 42%, spinel[2] 1%; F olivine[8] 13%, pigeonite[9] 19%, ilmenite[10] 11%.

1 = 12021, 1150 °C; 2 = 12009, 1150 °C; from Green *et al.* (1971).
4 = 12040/2, 1137 °C; 7 = 12064/5, 1114 °C; 8 = 12022/15, 1129 °C; 9 = 12040/2, 1137 °C; from Biggar *et al.* (1971).
3 = Fo_{65} + 0.5 Cr_2O_3, 0.3 CaO; 5 = 12064, 6 (Haggerty and Meyer, 1970).
6 = Fo_{55}; 10 = 12022, 1103 °C (unpublished).

Note that all solutions based on Green *et al.* (1971) visual estimates have attained *conspicuously* higher Al_2O_3, CaO concentrations than the analysed cotectic liquids which are already saturated with these components (as plagioclase). This results from gross overestimation of percentage of olivine, pyroxene. Solutions to 12021, 12040 and 12065 show excessive depletion in SiO_2, MgO because estimates of the amount of pyroxene present are excessive. In 12022, high SiO_2, low FeO and negative TiO_2 result from excessive ilmenite extract. Negative Cr_2O_3 values are not significant.

(4) Green *et al.*'s (1971) visual estimates of crystallinity yield values which are too high overall, and too high in pyroxene/olivine ratio, to apply to our experimental products. Residual liquid compositions, calculated by extracting their estimated percentages of crystals at plagioclase entry, frequently have negative components (Tables III and IV) have plagioclase-forming oxides well in excess of measured values in plagioclase-saturated cotectic residual liquids (Table IV), and are either grossly depleted, or are excessively rich in SiO_2 relative to the analysed residual liquids (Table IV). These discrepancies place the calculated liquids, when in positive composition space at all, in regions where plagioclase is likely to crystallize first and for some interval before the appearance of olivine or pyroxene (Figures 5 and 12).

(5) Similar criticisms apply to Ringwood's (1970) estimate of 30–50% crystallization

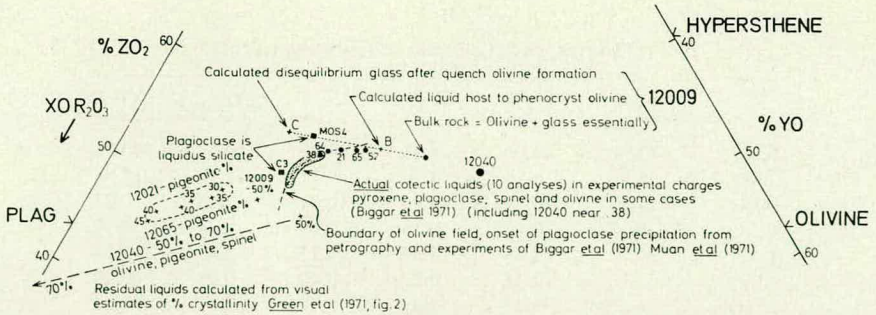


Fig. 5. Projection from diopside into the plagioclase-olivine-hypersthene-(silica) plane, of selected experimentally investigated natural and synthetic Apollo 12 materials, and analysed plagioclase-saturated liquids, to contrast with alleged plagioclase-saturated liquids, calculated by subtracting visual estimates of percentages of crystals in experimental charges. MOS 4 is from Muan *et al.* (1971). Calculated compositions with negative MgO plot within the figure provided there is sufficient FeO to compensate. The result would be unaffected by altering the Fe/Mg ratio in the pyroxene or olivine extracted *in this projection.*

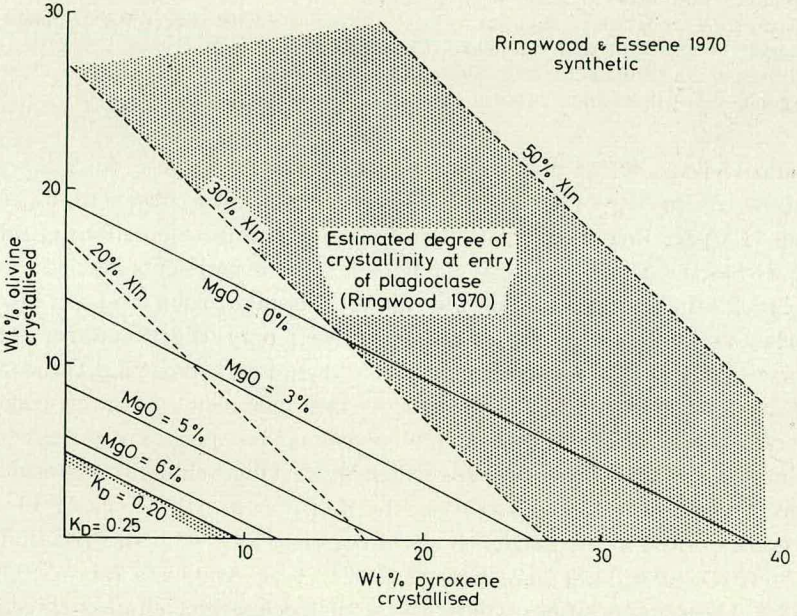


Fig. 6. Graphical presentation of results of extraction of 3% armalcolite (which reduces TiO_2 to cotectic levels at acceptable K_D and MgO figures) and variable combinations of olivine and pyroxene (Ringwood and Essene, 1970; Tables I(i), II(iii) and III, col. 1) from a synthetic Apollo 11 composition, contoured for resultant K_D olivine-liquid distribution coefficients, residual MgO in liquid, and total percentage of crystalline material present. High crystallinity is incompatible with acceptable K_D values and observed MgO contents of 6–7% (Biggar *et al.*, 1971; Table VI).

TABLE V

Apollo 11 lavas, cotectic liquid composition calculations

	I	II	III	IV	V	VI
SiO_2	42.60	43.00	44.89	44.09	40.69	40.76
TiO_2	8.86	8.76	8.25	8.31	11.92	11.98
Al_2O_3	11.01	10.31	9.95	10.09	7.78	7.84
Cr_2O_3	0.12	0.12	0.15	0.09	0.34	0.39
FeO	17.78	17.68	16.83	18.13	19.49	19.54
MnO	0.28	0.31	0.22	0.28	0.28	0.29
MgO	6.12	6.47	5.39	5.92	7.51	7.56
CaO	12.41	11.34	12.73	11.07	10.76	10.81
Na_2O	0.43	0.72	0.66	0.62	0.51	0.45
K_2O	0.09	0.37	0.39	0.59	0.30	0.43
P_2O_5	0.12		0.24		0.18	
S	0.18				0.23	

I – Apollo 11 ophitic group average (Compston *et al.*, 1970) minus 5% ilmenite, 4% olivine, 0.5% spinel.

II – Cotectic liquids, average from 10017, 10084 (Biggar *et al.*, 1971, Table VI); note CaO, Al_2O_3 *lower* than in I.

III – Apollo 11 intersertal group average, (Compston *et al.*, 1970) minus 10% ilmenite, 4% olivine, 4% pigeonite, 4% augite.

IV – 10017 residual liquid at 1133 °C (Biggar *et al.*, 1971), note CaO, *lower* than in III.

V – Apollo 11, 10017 rock (Compston *et al.*, 1970).

VI – Best fit to V using 10017 liquid at 1133 °C plus 0.8% olivine (Fo_{65}), 0.2% spinel (10020–40 Haggerty *et al.*, 1970), 10.1% ilmenite (10020–40), 19.8% augite (10024 – 23/grain 14 Kushiro and Nakamura 1970) and – 2.6% pigeonite (10024 – 23/grain 14): K_D ol – lq = 0.26. Negative pigeonite shows that a more calcic augite should have been used.

of Apollo 11 lavas before plagioclase entry (Figure 6); excessive depletion, in MgO and, above all, in MgO relative to FeO result. Petrological observation (James and Jackson 1970; see Biggar *et al.*, 1971, p. 637) and various calculations (Table V and Figure 7) based on analysed residual liquids from experiments carried out on the natural rock samples, indicate that the Apollo 11 ophitic group (B) lavas precipitated plagioclase and 4 or 5 other crystalline phases when only 10% crystalline. The Apollo 11 intersertal group (A) lavas were nearer 25% crystalline on reaching the same condition. New data (Prinz *et al.*, 1971) for the average composition of lithic fragments at the Apollo 11 site yield more representative average compositions of the high potassium and low potassium lavas groups which are strikingly close in composition to the average of two cotectic liquids analysed by Biggar *et al.* (1971), Table VI. Selected oxide figures, listed in the above sample order, are: SiO_2 42.8, 42.9, 43.0; TiO_2 9.6, 8.7, 8.8; Al_2O_3 10.6, 11.8, 10.3; FeO 18.0, 17.0, 17.7; MgO 7.0, 7.2, 6.5; CaO 10.7, 11.4, 11.3. These compositions will reach the plagioclase-precipitation cotectic at still lower amounts of crystallization.

(6) Primary magmas produced by partial melting of unknown source rocks at an elevated pressure are randomly chosen compositions with respect to the low pressure phase equilibria. The probability of such compositions exhibiting the close approach to low pressure cotectic character actually observed in Apollo 11 and 12 lavas by

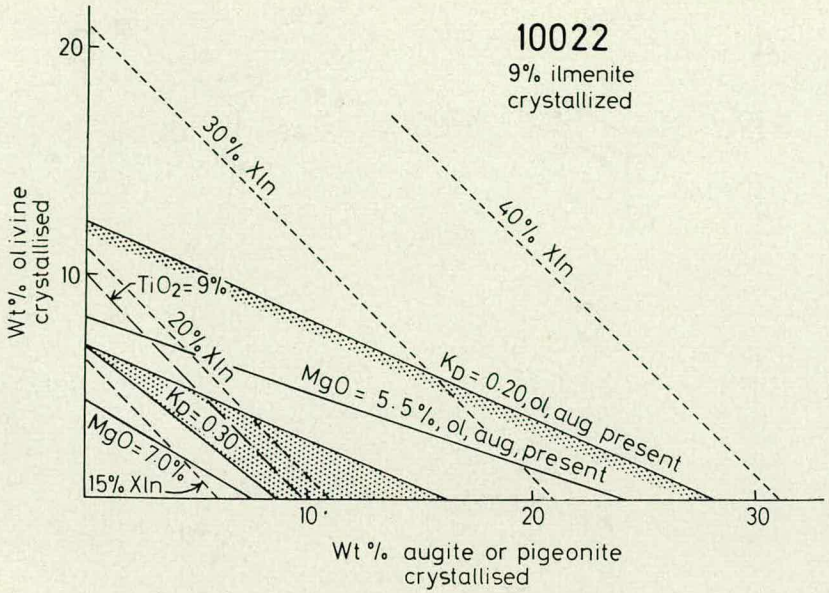


Fig. 7. Similar presentation to Figure 6 for rock 10022, using analysed mineral (core) compositions (Kushiro and Nakamura 1970) showing (shaded field) a range of acceptable MgO contents in the residual liquid at acceptable K_D values consistent with 15–25% crystallization. Results with $K_D < 0.20$ are deemed unacceptable. Alternative sets of K_D and MgO contours result from the choice of pigeonite or augite as the pyroxene crystallizing.

TABLE VI

Probabilities, ϕ, of observed approaches to cotectic behaviour being coincidence

Source	Laki 1783 Iceland			Kilauea Hawaii			Apollo 11				Apollo 12	
							Ophitic		Intersertal		12038	12064
P^*		3			3		6		6		4	5
X		0.10			0.05		0.10		0.25		0.05	0.10
C	4	6	10	4	6	10	7	9	7	9	8	8
ϕ	0.028	0.033	0.22	0.007	0.022	0.071	0.00005	0.0004	0.0046	0.027	0.0036	0.0027

Calculated from the relationship

$$\phi = \sum_{P=P^*}^{P=C} \frac{(C-1)!}{(P-1)!\,(C-P)!} \cdot X^{(P-1)}\,(1-X)^{(C-P)}$$

where C = number of significant components, P^* = number of crystalline phases present, X = weight fraction present as crystals. This relationship is approximately true provided liquid loci are not strongyl curved.

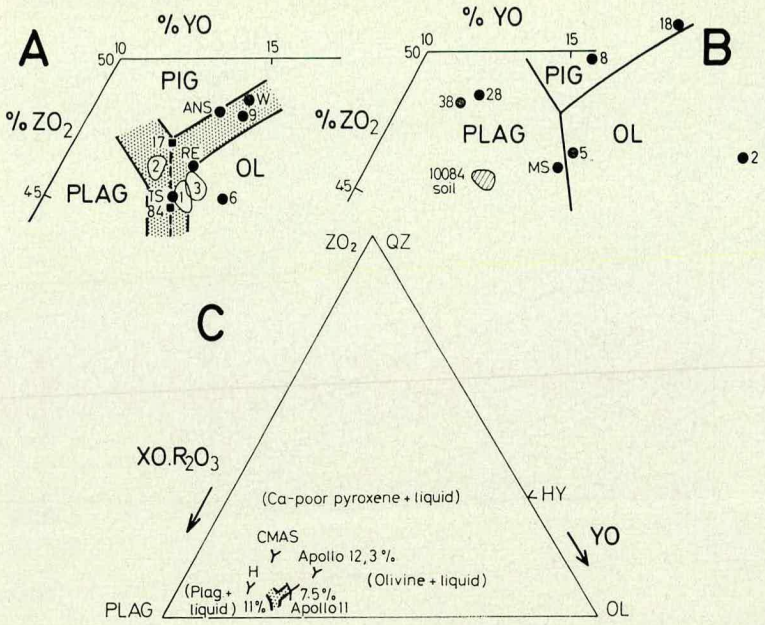


Fig. 8. Projection (O'Hara, 1968; Jamieson, 1970) from diopside into the plane plagioclase-olivine-hypersthene (quartz) showing the boundaries between the primary liquidus phase volumes of plagioclase, pigeonite and olivine as deduced from experimental and petrographic data for (A) synthetic and natural compositions of high TiO_2 content, ($\sim 11 \pm 1\%$) making no allowance for TiO_2-rich phase crystallization at liquidus, and for (B) intermediate TiO_2 content ($\sim 7.5 \pm 1.5\%$). Compositions 2, 5, 6, 8, 9, 18, 28, 38 from O'Hara *et al.* (1970); ANS from Anderson *et al.* (1970); MS from Muan and Schairer (1971); RE from Ringwood and Essene (1970); TS from Tuthill and Sato (1970); W from Weill *et al.* (1970). Numbered fields enclose analyses of lavas of ophitic groups 1, 2; intersertal group 3, and 10084 soil as in Biggar *et al.* (1971, Figure 8), while 17,84 mark the analysed residual liquids of rocks 10017, 10084 at the $8.75 \pm .5$ TiO_2 level (Biggar *et al.*, 1971, Table VI). Figure 7c compares the deduced cotectic liquid compositions with the analogous cotectic liquids in the Apollo 12 rocks at $\sim 3\%$ TiO_2; in Hawaiian tholeiitic lavas (H); and in the iron, sodium and titanium free system CaO-MgO-Al_2O_3-SiO_2 (CMAS).

coincidence is measured in parts per ten thousand to parts per hundred at best (Table VI). When the new average compositions of Apollo 11 lavas (Prinz *et al.*, 1971), and the near coincidence of cotectic temperature and eruption temperature is taken into account these probabilities decline still further.

(7) Cotectic liquid compositions are best established by bracketing, i.e. by finding closely related compositions lying in different primary liquidus phase volumes. This has been done for Apollo 11 compositions (O'Hara *et al.*, 1970, Figures 2, 3; Biggar *et al.*, 1971, Figures 8, 9; and this paper Figures 8, 9 and 10). A bracket on plagioclase entry was established by two laboratories from synthetic compositions resembling Apollo 12 lavas (Figure 5). Cotectic character can also be established by analysing the cotectic liquids and other experimentally produced phases, and thence proving low percentage crystallinity by calculation, as done here (Tables II, III and V). Least

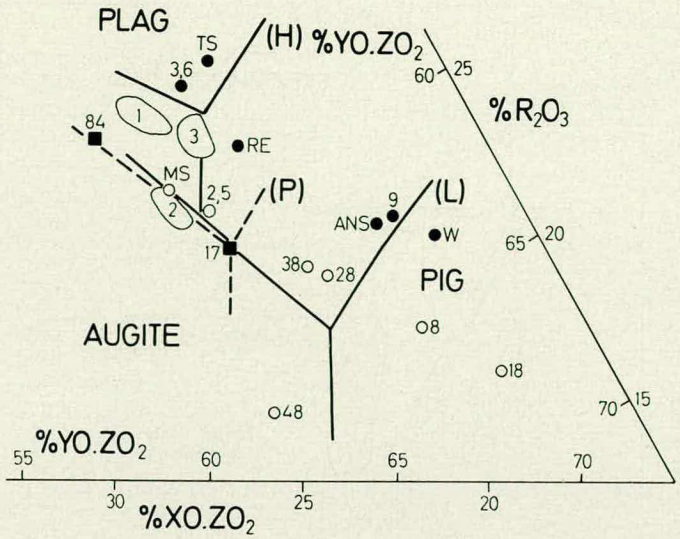


Fig. 9. Part of the projection from olivine into the plane hypersthene ($YO.ZO_2$)-wollastonite ($XO.ZO_2$)-R_2O_3, treating the same data as in Figure 8 to deduce the apparent boundaries between the plagioclase, augite and pigeonite crystallization fields at saturation with olivine, when TiO_2 contents are high ($\sim 11 \pm 1\%$; boundaries (H), solid circle data points and natural rock, fields 1,3; drawn without allowance for TiO_2-rich phase crystallization), or low ($\sim 7.5 \pm 1.5\%$, boundaries L, open circle data points), and the preferred position (P) at simultaneous saturation with TiO_2-rich oxides and the silicates, $TiO_2 \sim 8.75 \pm 0.5\%$ from probe analyses of experimentally produced residual liquids, and ophitic lavas group 2 (compare Biggar *et al.*, 1971, Figure 9). 10084 soil (not shown) falls in the plagioclase field of the (L) boundaries between MS, 84 and 1.

satisfactory is the indirect method of estimating, visually or otherwise, the percentage of crystals present on reaching cotectic crystallization, because it carries no internal check on consistency, and is susceptible to subjective and systematic errors in arriving at the estimates, particularly in fine grained products (plate I; D, E).

Close approach to cotectic composition is often, but not necessarily, accompanied by the appearance of many crystalline phases within a narrow temperature interval. However, neither the size of the temperature interval over which a number of crystalline phases appear, nor the size of the temperature interval between liquidus and solidus are criteria of closeness to cotectic composition. O'Hara *et al.* (1970) were incorrectly criticized (Ringwood, 1970, p. 6455) directly or by implication for the use of such criteria, but neither the abstract from which Ringwood drew his quotations, nor the full statement (O'Hara *et al.*, 1970, pp. 695, 704), is written in terms which excuse such a misrepresentation. The only authors who, to our knowledge, have attempted to utilize the size of the temperature interval as a criterion in this respect are Green *et al.* (1971, p. 608), in search of criticisms of Biggar *et al.* (1971), and Ringwood and Green (1971).

(8) The techniques used in the Edinburgh laboratory did not reveal a spuriously close approach to cotectic character in the random compositions represented by

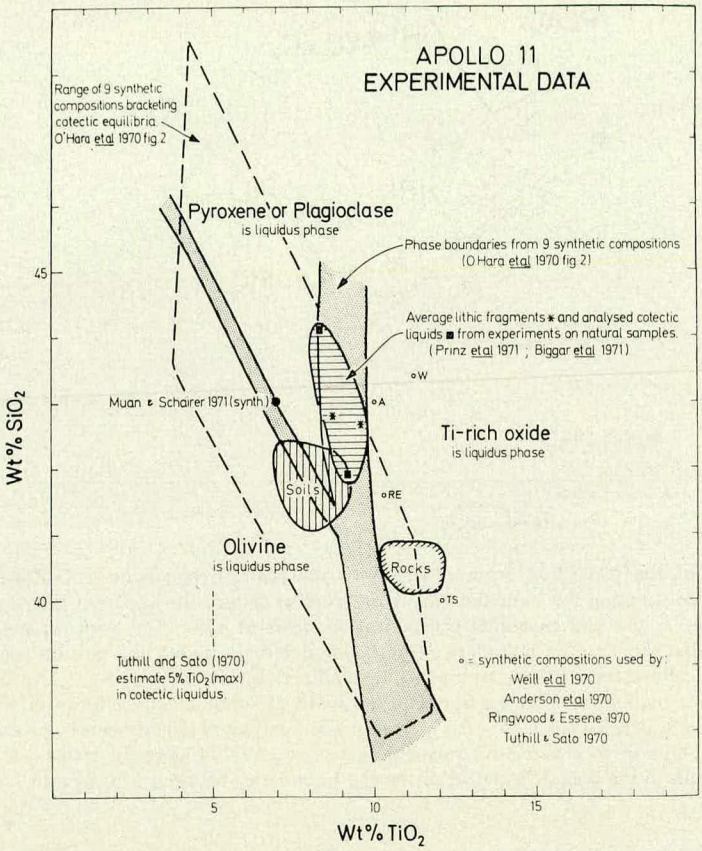


Fig. 10. Simplistic SiO_2 v. TiO_2 representation of liquidus fields, average rock compositions and cotectic liquid compositions encountered in Apollo 11 natural rocks and synthetic simulations. (N. B. Use of a higher oxygen fugacity caused plagioclase to appear as liquidus phase at the centre of the figure).

erroneous Apollo 12 analyses (Biggar *et al.*, 1971), nor has it revealed it in a suite of Reunion lavas known to depart somewhat from low pressure cotectic liquid compositions in their natural crystallisation (D. J. Humphries, in press). These techniques do, however, determine cotectic liquid compositions and temperatures identical (e.g. Figure 11) with those reported by other laboratories also engaged in long-term programs of atmospheric pressure experiments in systems of industrial and geological interest. With these techniques we also observe a close approach to cotectic character in the Laki fissure eruption (J. D. Bell and D. J. Humphries, in press) whose petrography demonstrates eruption with three phenocryst species when as little as 5% crystalline. Similar demonstrations of objectivity and applicability to natural circumstances are available for the technique used by Muan *et al.* (1971), these authors also remarking on the low degree of crystallinity at plagioclase entry.

(9) Available data from relevant synthetic systems (Figure 12) supports the bound-

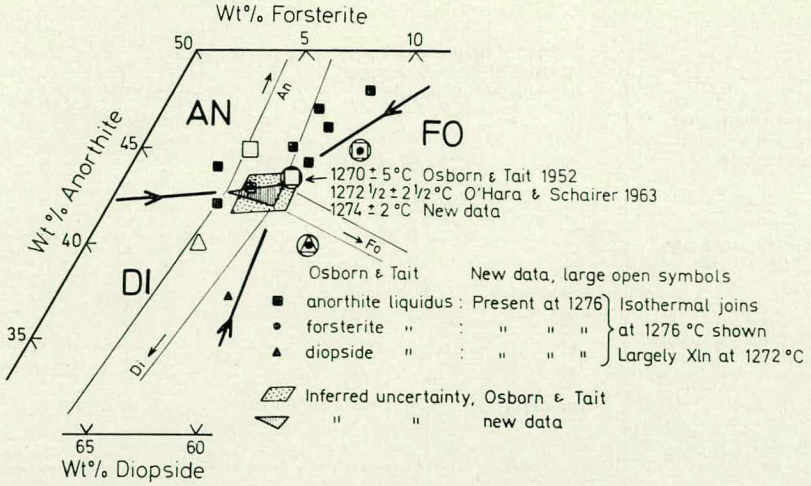


Fig. 11. Part of the plane anorthite-diopside-forsterite comparing atmospheric pressure phase boundaries (Osborn and Tait, 1952), and results for five compositions made and run in the Edinburgh laboratory illustrating close interlaboratory agreement on cotectic composition and temperature.

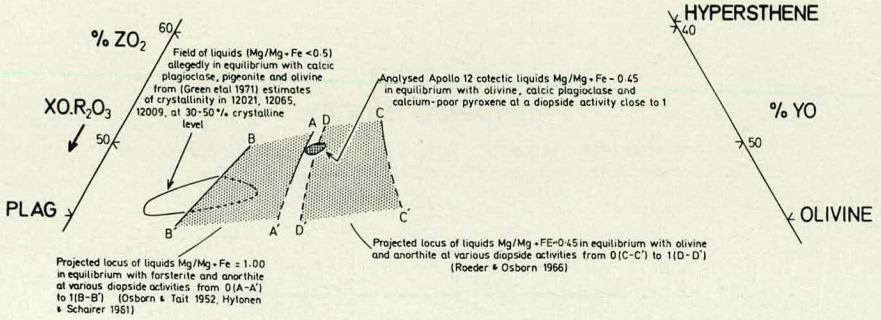


Fig. 12. Projection from diopside (as in Figure 6) into the plane plagioclase-olivine-hypersthene (silica) showing the loci of liquids in equilibrium in synthetic systems with olivine, plagioclase and one or two pyroxenes. Diopside activity has been set at zero in the olivine-plagioclase-silica plane, and at 1 when calcium-rich clinopyroxene coexists with olivine and plagioclase.

ary marking onset of plagioclase crystallisation found by Biggar *et al.* (1971) and Muan *et al.* (1971) in Apollo 12 compositions.

(10) Interpretation of the phase equilibria and lava chemistry turns on the *average* rock composition at the Apollo 12 site (Figures 13, and 14). The fundamental implications of this decision for lunar petrogenesis are illustrated by Figure 15. The hypothesis that 12009 or 12040 represent the parental magma at this site is untenable. The compositions of the average fines; average basaltic lithic fragments from the solls; impact melted glass fragments least affected by alkali depletion; and even the weighted average of the large rocks distributed for analysis (liable to bias towards extreme

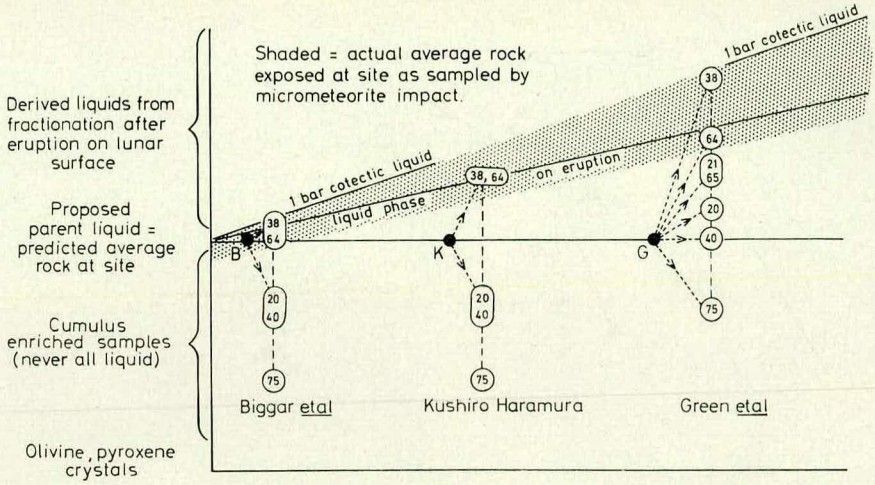


Fig. 13. Graphical summary of alternative interpretations of Apollo 12 site petrogenesis and their implications. The status of 12009, also regarded by Green *et al.* (1971) as possible parental liquid is discussed in the text. The alternative status of Apollo 12 rock samples (indicated by final two digits of sample numbers) in the three interpretations is apparent.

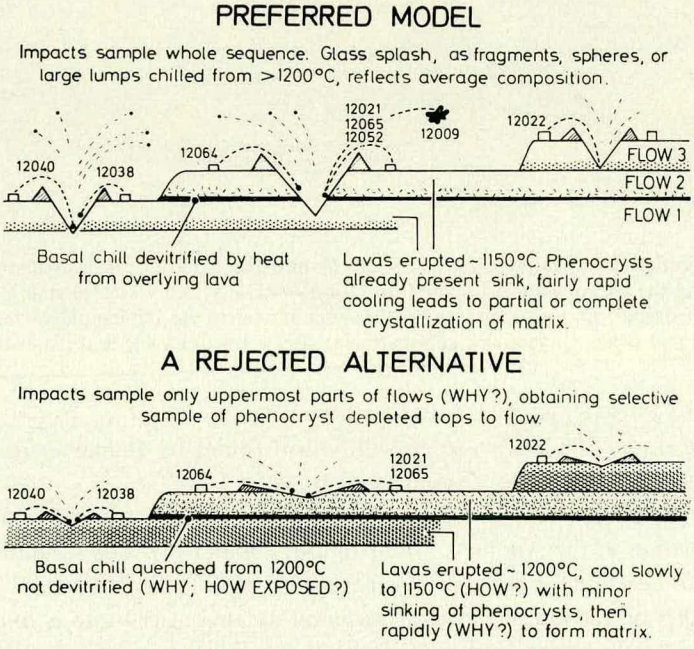


Fig. 14. Schematic cross-sections corresponding with two extreme alternatives from Figure 13, illustrating their implications for Apollo 12 site geology. Individual globs of impact melt depart from average rock composition, but on average short travelled material reflects rock average.

compositions) all fall much closer to the analysed low pressure cotectic liquids (Figure 16, Table VII) than to 12009 or 12040. The average composition of materials exposed near this site resembles that of sparsely porphyritic rocks such as 12038, and 12064, identified by Biggar *et al.* (1971) as the parental magmas, close to cotectic composition at atmospheric pressure and truly cotectic at a slightly higher pressure and volatile content that prevailed within the lava lake.

(11) The phenocrysts probably formed prior to eruption from the lava lake and precipitated at a pressure higher than atmospheric. Changes in alkali content and oxygen fugacity accompanied eruption, and atmospheric pressure experiments do not exactly reproduce the conditions of phenocryst formation. Too much should not be

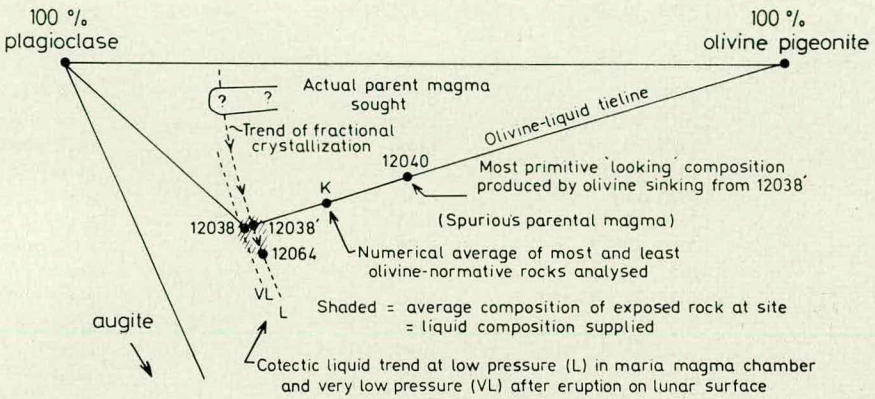


Fig. 15. Simplified phase diagram illustrating the experimental significance of the alternative interpretations of Figure 13, and their implications for studies of the lunar interior.

TABLE VII

	SiO_2	TiO_2	Al_2O_3	Cr_2O_3	FeO	MgO	CaO	Na_2O	K_2O
(1) Average basaltic lithic fragments[a]	47.2	3.0	14.0	tr	15.8	8.0	10.9	0.5	0.2
12038 rock[b]	47.1	3.3	13.0	–	17.7	6.6	11.4	0.7	0.1
(2) K10 glass[a]	40.3	3.5	7.1	0.6	23.2	16.6	8.0	tr	tr
12040 rock[b]	43.9	2.7	7.4	0.7	20.8	16.1	7.9	0.2	tr
(3) K9 glass[a]	43.1	4.4	8.5	0.3	23.0	11.0	9.4	0.4	0.2
12009? impact vitrophyre[c]	45.0	2.9	8.6	0.5	21.0	11.5	9.4	0.2	0.1

[a] Keil *et al.* (1971); [b] Kushiro and Haramura (1971); [c] Compston *et al.* (1971).

(1) Comparison of average of 28 basaltic lithic fragments in Apollo 12 soil with rock 12038 (suggested parental cotectic liquid to eruptive sequence) showing similarity; average fragments are *not* similar to 12040, 12009, below, in SiO_2, Al_2O_3, Cr_2O_3, MgO or CaO.
(2) Comparison of impact melted glass fragment in Apollo 12 soil, with rock 12040, a coarsely crystalline potential target rock formed by crystal accumulation.
(3) Comparison of impact melted glass fragment in Apollo 12 soil with rock 12009, a largely glassy sample with thermal history more akin to that of impact melts than to the great majority of the igneous rock samples.

Summary of experimental data relevant to

Run No.	Samples	Temperatures °C	Time (h)	Starting materi loaded
A. *Reversals*				
031	12021, 38, 52, 64, 65	1144; 1137	5; 5	rock powder
032	12018, 20, 38, 40	1167; 1156	5; 5	rock powder
033	12018, 20, 38, 40	1166; 1153	4; 12[a]	rock powder
035	12018, 20, 38, 40	1162; 1153	4½[g]; 16	rock powder
111	12020	1167; 1156	5; 5	glass (1340, 1⅓ h
112	12020, 12038	1166; 1153	4; 12[a]	glass (1340, 1⅓ h
117	12018, 20, 38, 40	1162; 1153	4½[g]; 16	glass (1330 1¼ h
B. *Syntheses from 'different' starting materials (pseudoreversals)*				
030	12038	1167	5	rock powder
034	12018, 20, 38, 40	1153	6½	rock powder
036	12018, 20, 38, 40	1153	72	rock powder
113	12020, 12038	1300; 1153	24; 6½	glass[b, c]
114	12020 only	1340; 1153	1⅓; 6½	glass[b, c]
116	12018, 20, 38, 40	1153	72	glass[b, c]
015	12022, 38, 52	1129	1½	rock powder
016	12022, 38, 52	1300; 1129	1; 1½	glass[b, c]
017	12022, 38, 52	1300; 1129	1; 1½	glass + 5% rock
109	12052	1300; 1041	24; 0.16	glass[b]
110	12020, 38, 52, 64	1340; 1041	1; 0.16	glass[b]
?	n. d.	n. d.	n. d.	glass[c, d]
?	n. d.	n. d.	n. d.	glass[c, d]
?	n. d.	n. d.	n. d.	devitrified glass
?	n. d.	n. d.	n. d.	devitrified glass
C. *Charges converted to liquid, or mainly liquid then temperature lowered substantially*[f]				
006	18, 20, 21, 22, 38, 40, 52, 64, 65	1250; 1154	1; 4½	rock powder
013	18, 20, 21, 22, 38, 40, 52, 64, 65	1306; 1110–1127	1; 1	rock powder
101	12022, 38, 64	1228; 1121	1,24	rock powder
102	12022, 38, 64	1225; 1119	1,1	rock powder
104	12022, 38, 64	1320; 1116	2,1	rock powder
Muan and Schairer (1971)	Apollo 11 synthetic	1200; 1090	n. d.	devitrified glass
Roedder and Weiblen (1970)	Inclusions in olivine	> 1200; 1125/ 1065	many hours	glass

All Edinburgh experiments carried out at fO_2 of Fe/FeO equilibrium.

[a] held 3 h each at 1159, 1156 during temperature reduction.

[b] glass prepared, quenched, then reloaded. Picritic samples still retain some olivine.

[c] glass may have devitrified while coming up to temperature (see 109, 110).

ase and use of glass as starting material

nts

ase destroyed except in 12038; renucleated in all.
ase destroyed; renucleated 20, 38 only.
ase destroyed; renucleated 12038 only.
ase destroyed; renucleated in all four samples (less than in 034)

ase renucleated
ase renucleated in both
ase renucleated in all samples

ivine only
tributed scarce plagioclase
tributed scarce plagioclase
ase present in 12038
ase present
ase present, pyroxene with multiple twinning
ases present in all;
ase less abundant in products from
aring starting materials
devitrified on reaching 1041 °C;
spent 9 mins > 1000 °C; 17 mins > 700 °C;
ase in some. See text.
et al. (1971) "confirmed temperature
pearance of
ase": claimed as reversal.

gioclase; large pyroxene prisms regenerated, showing curving cracks, some polysynthetic
g, in 12020, 40, 65
rystals free from cracks had straight extinction

gioclase; little pyroxene in 38, 64 (2–50 °C below
ium entry).
gioclase in 12022 (contrast 016)
gioclase in 12022,64 (10–20 °C below equilibrium)
gioclase in any (10–45 °C below equilibrium)
gioclase (90 °C below equilibrium entry)

gioclase or pyroxene renucleation.

prepared by few minutes heating at high temperature (Green, pers. comm).
tions of devitrification not stated.
were kept in the furnace and not quenched, merely lowered to the second temperature
d, and finally quenched.
at 1160, then 2 h at 1162, lowered in 1½ h to 1153.

made out of small differences in composition between experimentally produced liquidus phases and natural phenocryst cores, least of all when the phase in question is in reaction relationship with the liquid and effects leading to excessively magnesian residual compositions can come into play (O'Hara, 1963 p. 42). Those effects are likely to be most marked in rocks such as 12065 where the ratio of olivine resorbed to olivine precipitated is highest, and the occurrence of the most magnesian olivines within the reaction product (pigeonite; Green *et al.*, 1971, p. 605) underlines the need for caution.

(12) A liquid such as 12064 *can* be derived by pigeonite + plagioclase dominated fractionation from liquid such as 12038 (Biggar *et al.*, 1971, Table VII). Green *et al.* (1971, p. 611) have not examined the data sufficiently closely in reaching their conclusions.

(13) 12009 existed as a liquid plus c. 9% olivine crystals at the lunar surface, and even that olivine may be a quenching product if Green *et al.* (1971 p. 601) are correct in identifying it as skeletal. This vitrophyre was very rapidly cooled from temperatures of c. 1200 °C or possibly considerably higher, whereas most other rocks at the site were cooled more slowly, and from temperatures of c. 1140–1170 °C. The distinctive thermal history of 12009 * also characterises impact melted glasses, and impact melted glass spatter is prominent in samples 12017, 12030 and 12054 (LSPET 1970). Impact-melted glasses approaching 12009 and 12040 in composition have been reported (Figure 16, Table VII) as required by our interpretation of 12009 as a fragment of

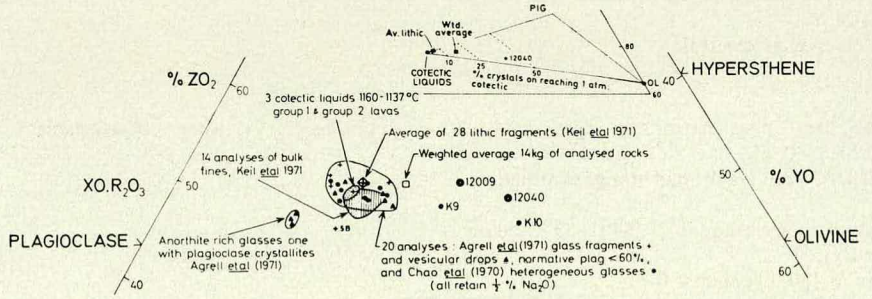


Fig. 16. Projection from diopside into the plane plagioclase-olivine-hypersthene (quartz) (analogous to Figures 6, 12) contrasting Green *et al.*'s (1971) suggested parental magmas 12009, 12040 with the analysed experimental cotectic liquids (Biggar *et al.*, 1971); the compositions of glass fragments and particles little affected by alkali, or silica depletion, taken to approximate to the average rock composition exposed near the site; and the weighted average composition of 14 kg. of 16 rock samples analysed from this site. The average of 28 lithic basaltic fragments in the soil from this site is also shown.

Two impact melted glass spheres conspicuously poorer in SiO_2 or richer in potential ferromagnesian minerals than the majority are indicated, to support the contention that vitrophyres such as 12009 may represent larger globs of impact melted phenocryst-rich target rock.

* The rapid heating and cooling make preservation of pre-existing chemistry, even of alkalis, unremarkable.

TABLE IX

Details of furnace assembly calibration

Carried out between run and run		Calibration point	Width of bracket solid-liquid °C	Date carried out 1970/1971	Correction to be applied temperature from e.m.f. (a) (b)
(initial calibrations)		Au	5.1	13 Oct. 19 Oct.	+0.8
		L_2S	3.2	21 Oct. 22 Oct.	−2.1
003	004	L_2S	3.5	5 Nov. 5 Nov.	−1.0 (c)
including	009	L_2S	2.0 (d)	25 Nov.	−1.6
including	010	Au	Solid (e)	26 Nov.	(+0.8)
019	020	L_2S	2.0 (d)	17 Dec.	−1.5
020	021	L_2S	Solid (f)	24 Dec.	(−1.5)
after 024		Diopside	2.7	4,5 Feb.	+1.5
Furnace used for other calibrated work at higher temperatures					
initial calibration, then					
101	102	L_2S	(d)	22 Apr. 1971	+3.6
102	103	Au	2.3	30 Apr. 1 May	+9.5
104	105	L_2S	4.4	10 May 11 May	+9.6
used for 106, 107, 108 (glass production) and the replaced by new thermocouple junction.					
initial calibrations		L_2S	2.0 (d)	19 May	+4.0
		L_2S	(g)	20 May	
then used for 030, 031, 109, 110, 032, 111, 033, 112		Au	3.0	24 May 25 May	+6.6
033	034	L_2S	(g)	4 June	+4.0

(a) These are the corrections applied to the measured e.m.f. to calculate the temperatures quoted by O'Hara *et al.* (1970), Biggar *et al.* (1971), and this paper.
(b) A further linear interpolation between 0 °C at 1064.4 °C and 4.9 °C at 1208 °C must be added to these quoted temperatures to convert them to the International Practical Temperature Scale of 1968. This further correction mainly results from the redetermination of the melting point of lithium metasilicate as 1208 °C on IPTS 1968 (Biggar, in press).
(c) Based on the wide bracket (3.5 °C). The next line of the table involved a smaller bracket and for greater accuracy the value −1.0 should be replaced by the value between −1.6 (the later and better result) and −2.1 (the value used earlier).
(d) In melting interval known to be less than 2° (Biggar and O'Hara, 1969).
(e) Thermocouple drift cannot have been greater than 0.8°.
(f) Confirmed solid at 3.1° below the melting interval result of line 4. Therefore downward drift of thermocouple emf has not been greater than 3.1° in fact previous correction of −1.5 continued in use.
(g) Confirmed solid at 2.0 °C below result of 19th May.
(h) Control precision is better than ±0.5 °C (Biggar and O'Hara, 1969); accuracy relative to stated scales is ±2.5 °C. Contrast Green *et al.* (1971b) who give ±5.0 °C, ±10 °C respectively.

impact-melted target material from the phenocryst-enriched base of one of the flows (Figure 14).

(14) Results presented here (Table VIII) and by Biggar *et al.* (1971) were obtained from close temperature brackets in thermally explored and properly calibrated furnaces

(Biggar and O'Hara, 1969; and Table IX, Figure 17 this paper), at controlled, known, and calibrated oxygen fugacities (Figure 5; Biggar *et al.*, 1971, Table II), in containers which do not react with the charges (Table X). All temperatures quoted in this and our previous work must be *raised* 2–5 °C to correspond with the International Practical Temperature Scale (1968) and our revised melting point for Li_2SiO_3 (1208 °C; IPTS, 1968) N.B. The emf of a thermocouple indicates nothing more than the temperature of the thermocouple tip (Figure 17). Sample preparation techniques do not

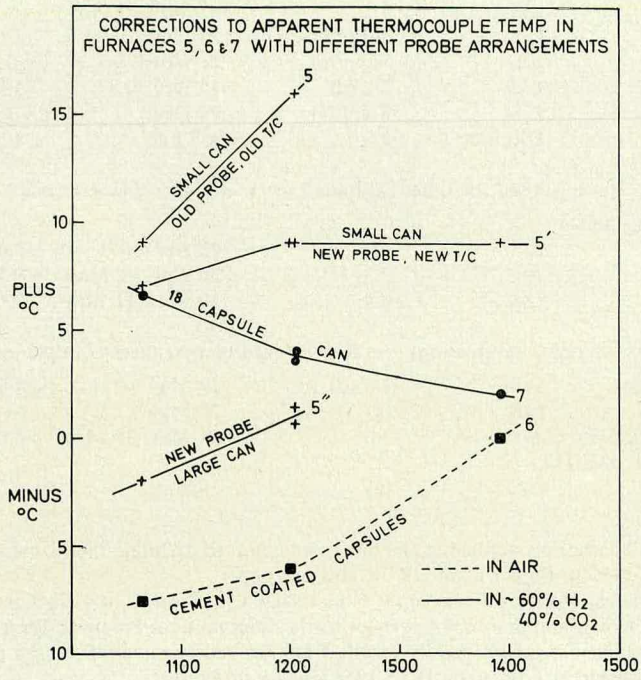


Fig. 17. Plot of corrections to be added to apparent thermocouple temperature as a function of temperature in furnaces of the type used in the studies at Edinburgh.

TABLE X

	SiO_2	TiO_2	Al_2O_3	FeO	MgO	CaO
12038 Rock	47.1	3.3	13.0	17.7	6.6	11.4
12038 1179 °C, 5 h 0% crystals	46.9	3.4	12.4	17.6	6.8	11.2
12038 1160 °C, 5 h <5% crystals[a]	46.8	3.5	12.3	17.7	6.6	11.2
12064 Rock	46.4	4.1	10.5	19.9	6.4	11.7
12064 1160 °C, 5 h <5% crystals	46.4	4.0	10.6	19.4	6.6	11.6

[a] cotectic liquid, plagioclase, olivine, spinel and two pyroxenes.

Table X, comparing glass analyses from all liquid, or nearly all liquid experiments with bulk rock composition, to illustrate composition control, absence of sampling errors conducive to premature plagioclase crystallization, and absence of iron loss. Data from Biggar *et al.* (1971) Table V.

bias the charge compositions, least of all towards excessive potential plagioclase (Table X).

The quenching and microprobe data refer to assemblages of homogeneous equilibrium phases, the apparent variation ($< \pm 2\%$ Fo in olivine; $< \pm 3\%$ Wo, 2–4% En in pyroxene; and ± 1–4% major oxides in the glasses, equivalent to $\pm$ c. 1% olivine in the norm) not greatly exceeding the precision of the method, and arising principally from the difficulty of ensuring that the volume sampled is located exclusively within one phase (c.f. Gibb, 1971) even in the relatively coarse-grained products from rock powder (plate I). No such check could be carried out on the much finer grained products from glass. Total reconstruction of the loaded natural minerals is of course

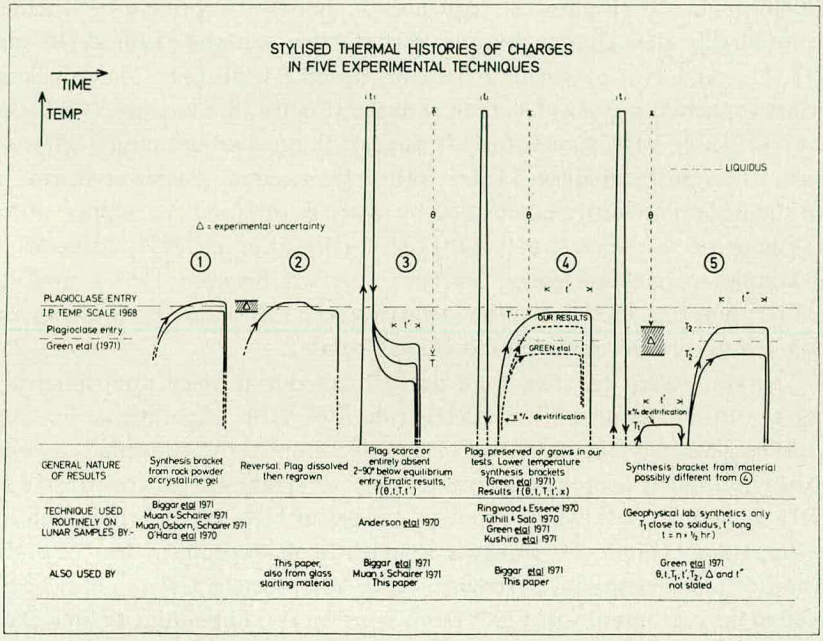


Fig. 18. Diagrammatic representation of thermal sequences used in various experiments.

TABLE XI

Microprobe analysis of cotectic plagioclase-bearing liquids in reversal experiments 1162 °C/1153 °C showing similarity of results from two starting materials

	SiO_2	TiO_2	Al_2O_3	Cr_2O_3	FeO	MnO	MgO	CaO	Na_2O	K_2O	Total
12038/035 (powder)	47.27	3.49	12.12	0.25	17.35	0.31	6.31	11.39	0.62	0.13	99.24
12038/117 (glass)	47.10	3.51	12.47	0.19	16.68	0.28	6.41	11.70	0.62	0.13	99.09
12040/035 (powder)	46.53	4.64	11.33	0.19	16.94	0.22	6.95	12.11	0.46	0.13	99.50
12040/117 (glass)[a]	47.21	4.06	10.46	0.28	17.17	0.25	7.94	11.42	0.33	0.13	99.25

[a] Minute crystal size may mean that some pyroxene lay within sample area.

proved by the reduced Al_2O_3 content of the pyroxenes, and the destruction of the zoning.

(15) The only effects likely to arise from the presence of 0.25 bar H_2O in our furnace atmospheres are accelerated reaction rates, and a slight movement of the total liquid composition towards the primary phase volumes of olivine and pyroxene, which would diminish, not enhance, the appearance of cotectic character.

(16) Thermal sequences used by various workers on Apollo samples or synthetic simulations in different types of experiment are summarised in Figure 18. The entry of plagioclase has been 'reversed'* (Figure 18, sequence 2) in group 2 rocks 12021, 12052, 12064 and 12065 between 1144 and 1137 °C (Table VIII, run 031). Plagioclase has been demonstrated to be present in products of group 1 rocks 12018, 12020, 12038 and 12040 at 1153 °C (Figure 18, sequences 1 and 4), irrespective of whether rock powder or largely glass charges were used as starting material (Table VIII, runs 034, 036, 113, 114, and 116) or whether the runs lasted 6 h or 72 h. The appearance of plagioclase in these four rocks has been reversed (Figure 18, sequence 2) between 1162 and 1153 °C (Table VIII, runs 035, 117) using rock powder and largely glass starting materials. Microprobe analyses (Table XI) of the residual glasses conform, in each case, to the trend previously established by analyses of liquids developed in 5 h syntheses (Figure 18, sequence 1) at 1160, 1137 °C (Biggar *et al.*, 1971, Table V). In two of the samples plagioclase entry has been reversed between 1167 °C and 1156 °C (Table VIII, runs 032, 033) but in the other two even this small extent of superheating was sufficient to prevent renucleation of plagioclase.

(17) Charges loaded as glass may devitrify in our furnace atmospheres before arriving at run temperature (Table VIII, runs 109, 110). Experiments loading glass or devitrified glass may, therefore, arrive at temperature as the same phase assemblages and do not necessarily demonstrate even so much as syntheses from contrasted starting materials. Experiments in which liquid is created at high temperature, then lowered to run temperature (Figure 18, sequence 3) are particularly prone to delayed or deferred nucleation of plagioclase and pyroxene (Table VIII, section C), an effect beautifully displayed in the petrography of 12009 (see Figure 5). It is imperative to limit the superheating used in the first stage of glass preparation for 'reversal' experiments. Other experiments (Table VIII, runs 015, 016, 017) indicate that charges loaded as glass may yield less plagioclase than is obtained from rock powder under the same conditions. The two effects discussed last might be enhanced when dry atmospheres are used.

(18) Nucleation from glass does not always lead immediately, nor even rapidly, to stable phase assemblages (Ostwald, 1897; Volmer, 1939). Products are sensitive to the previous thermal history of the glass (Table VIII, sections B, C). When glasses have been prepared by the several (half-hour) fusions at very high temperature necessary to guarantee homogeneity (Schairer, 1959), and are then used without prior devitrification or annealing, difficulties must be expected. The accumulated experience of the past is worth repeating lest it be altogether overlooked,

* An absolutely valid reversal of an equilibrium involving a phase (e.g. glass) capable of inheriting a metastable internal structural state from the previous thermal treatment is very difficult to devise.

Nearly all silicate glasses readily undercool. Unless crystals are present in the glass before attempts are made to study phase changes with temperature erratic results and metastable equilibrium may be obtained.... In most silicate systems the determination of the appearance of a crystalline phase at equilibrium practically requires that that phase be present in the starting material. (Schairer 1959).

In glasses which devitrify to olivine, pyroxenes and plagioclase, metastable assemblages may form in minutes and persist for weeks unless devitrification is carried out close to the solidus (O'Hara and Schairer, 1963); these metastable crystals may subsequently enter into metastable crystal-liquid equilibria.

Summarising, then, we consider the assertions and criticisms by Ringwood (1970) and Green *et al.* (1971) concerning the atmospheric pressure phase equilibria to be unsubstantiated and somewhat authoritarian. We welcome any discussion of atmospheric pressure data on lunar or terrestrial materials which is based on fully reported, quantitative data obtained by well described techniques in calibrated equipment, preferably not relying solely on glass as a starting material.

Sparsely porphyritic rocks like 12038, 12064 *are* close in composition to low pressure cotectic liquids precipitating plagioclase, spinel, two pyroxenes, and olivine. The plausibility of the choice of these compositions as the parental magmas to local post-eruption differentiation at the Apollo 12 site must be judged by the reader in the light of two facts: The average rock exposed to meteorite bombardment resembles the sparsely porphyritic lavas (Figure 16): When erupted these lavas were in that early stage of crystallization which permits the creation of a small proportion of compositions such as 12040, 12052 by sinking of the dense crystals through the low viscosity liquid.

Whether vitrophyres, like 12009, with its extreme composition and distinctive thermal history which allies it directly with impact melted materials, can safely be interpreted as anything but impact 'splash' must also be judged by the reader.

Even neglecting the *certainty* of alkali and other element losses by volatilization during eruption, which must be restored before any lunar lava can be treated as a primary magma, it is our opinion that *none* of the rocks taken from the Apollo 11 or 12 sites represents even a volatile depleted primary magma from the deep lunar interior; the only identifiable parental magmas bear the stigmata of composition control by low pressure fractional crystallisation.

7. Summary of Conclusions

Protohypersthene *-crystallizing basic lavas from the Ocean of Storms were erupted as low pressure cotectic residual liquids from an underlying magma body, already as much as 80–98% crystallized. The lunar maria are differentiated lava lakes, filled by rock types familiar among the achondrites, floored by early metal precipitates which form mass concentrations, and capped by lava flows representing second-stage extrusion of the late residual liquids of the fractionation sequence. The distinctive geochemical and petrographic characteristics of this magmatic kindred relative to terrestrial ex-

* See addendum.

perience were controlled by volatilization losses during eruption and crystallization. The igneous events leading to maria formation may have been very early and triggered by major impacts.

Acknowledgements

The Natural Environment Research Council (U.K.) supported this research. We thank G. M. Brown, J. E. Dixon, P. L. Roeder and W. C. Storey for their critical reading of this paper.

References

Agrell, S. O., Long, J. V. P., and Reed, S. J. B.: 1971, 'A comparison of Glasses from the Apollo 11 and 12 Missions' (unpublished).

Anderson, A. T., Crewe, A. V., Goldsmith, J. R., Moore, P. B., Newton, J. C., Olsen, E. J., Smith, J. V., and Wyllie, P. J.: 1970, *Science* **167**, 587.

Biggar, G. M. and O'Hara, M. J.: 1969, *Mineral. Mag.* **37**, 1.

Biggar, G. M., O'Hara, M. J., Peckett, A., and Humphries, D. J.: 1971, *Proc. Second Lunar Sci. Conf., Geochim. Cosmochim. Acta Suppl. 2*, Vol. 1, 617.

Brown, G. M., Emeleus, C. H., Holland, J. G., Peckett, A., and Phillips, R.: 1971, *Proc. Second Lunar Sci. Conf. Geochim. Cosmochim. Acta Suppl.* 2, Vol. 1, 583.

Brown, G. M. and Peckett, A.: 1971, *Nature* **234**, 262.

Chapman, D. R. and Scheiber, L. C.: 1969, *J. Geophys. Res.* **74**, 6737.

Chao, E. C. T., Boreman, J. A., Minkin, J. A., James, O.B., and Desborough, G. A.: 1970, *J. Geophys. Res.* **75**, 7445.

Clarke, D. B.: 1970, *Contrib. Mineral. Petrol.* **25**, 203.

Compston, W., Chappell, B. W., Arriens, P. A., and Vernon, M. J.: 1970, *Proc. Apollo 11 Lunar Sci. Conf., Geochim. Cosmochim. Acta Suppl. 1*, Vol. 2, 1007.

Compston, W., Berry, H., Vernon, M. J., Chappell, B. W., and Kaye, M. J.: 1971, *Proc. Second Lunar Sci. Conf., Geochim. Cosmochim. Acta Suppl. 2*, Vol. 2, 1471.

De Maria, G., Balducci, G., Guido, M., and Piacente, V.: 1971, 'Mass Spectrometric Investigation of the Vaporization Process of Lunar Samples', *Second Lunar Sci. Conf., Geochim. Cosmochim. Acta Suppl. 2*, Vol. 2, 1367.

Duke, M. B. and Silver, L. T.: 1967, *Geochim. Cosmochim. Acta* **31**, 1637.

Essene, E. J., Ringwood, A. E., and Ware, N. G.: 1970, *Proc. Apollo 11 Lunar Sci. Conf., Geochim. Cosmochim. Acta Suppl. 1*, Vol. 1, 385.

Gibb, F.: 1971, *Contr. Mineral. Petrol.* **30**, 103.

Green, D. H., Ringwood, A. E., Ware, N. G., Hibberson, W. O., Major, A., and Kiss, E.: 1971a, *Proc. Second Lunar Sci. Conf., Geochim. Cosmochim. Acta Suppl. 2*, Vol. 1, 601.

Green, D. H., Ware, N. G., Hibberson, W. O., and Major, A.: 1971b, *Earth Planetary Sci. Letters* **13**, 85.

Haggerty, S. E. and Meyer, H. A. O.: 1970, *Earth Planetary Sci. Letters* **9**, 379.

Hytonen, K. and Schairer, J. F.: 1961, *Yearb. Carnegie Inst. Wash.* **60**, 125.

James, O. B. and Jackson, E. D.: 1970, *J. Geophys. Res.* **75**, 5793.

Jamieson, B. G.: 1970, *Mineral. Mag.* **37**, 537.

Keil, K., Prinz, M., and Bunch, T. E.: 1971, *Proc. Second Lunar Sci. Conf., Geochim. Cosmochim. Acta Suppl. 2*, Vol. 1, 319.

Kushiro, I. and Haramura, H.: 1971, *Science* **171**, 1235.

Kushiro, I. and Nakamura, Y.: 1970, *Proc. Apollo 11 Lunar Sci. Conf. Geochim. Cosmochim. Acta Suppl. 1*, Vol. 1, 607.

Kushiro, I., Nakamura, Y., Kitayama, K., and Akimoto, S.: 1971, *Proc. Second Lunar Sci. Conf., Geochim. Cosmochim. Acta Suppl. 2*, Vol. 1, 481.

LSPET (Lunar Sample Preliminary Examination Team): 1970, *Apollo 12 Preliminary Science Report*, NASA, Washington, D.C.

LSPET (Lunar Sample Preliminary Examination Team): 1971, *Apollo 14 Preliminary Science Report*, NASA, Washington, D.C.

Marvin, U. B., Reid, J. B. Jr., Taylor, G. J., and Wood, J. A.: 1972, *Abstracts 3rd Lunar Sci. Conf.*, NASA Houston.
Muan, A., Hauck, J., Osborn, E. F., and Schairer, J. F.: 1971, *Proc. Second Lunar Sci. Conf., Geochim. Cosmochim. Acta Suppl. 2*, Vol. 1, 497.
Muan, A. and Schairer, J. F.: 1971, *Yearb. Carnegie Inst. Wash.* **69**, 243.
O'Hara, M. J.: 1961, *Mineral. Mag.* **32**, 848.
O'Hara, M. J.: 1963, *Amer. J. Sci.* **261**, 32.
O'Hara, M. J.: 1968, *Earth Sci. Rev.* **4**, 69.
O'Hara, M. J., Biggar, G. M., Richardson, S. W., Jamieson, B. G., and Ford, C. E.: 1970, *Proc. Apollo 11 Lunar Sci. Conf., Geochim. Cosmochim. Acta Suppl. 1*, Vol. 1, 695.
O'Hara, M. J., Biggar, G. M., Richardson, S. W., Ford, C. E., and Jamieson, B. G.: 1971, *Phys. Earth Planetary Int.* **4**, 181.
O'Hara, M. J. and Schairer, J. F.: 1963, *Yearb. Carnegie Inst. Wash.* **62**, 107.
Osborn, E. F. and Tait, D. B.: 1952, *Amer. J. Sci.* **250A** (Bowen vol.) 413.
Ostwald, W.: 1897, *Z. Phys. Chem.* **22**, 289.
Prinz, M., Bunch, T. E., and Keil, K.: 1971, *Contrib. Mineral. Petrol.* **32**, 211.
Ringwood, A. E.: 1970, *J. Geophys. Res.* **75**, 6453.
Ringwood, A. E. and Essene, E.: 1970, *Proc. Apollo 11 Lunar Sci. Conf., Geochim. Cosmochim. Acta Suppl. 1*, Vol. 1, 769.
Ringwood, A. E. and Green, D. H.: 1972, 'Crystallization of Plagioclase in Lunar Basalts and Its Significance' (in press).
Roedder, E. and Weiblen, P. W.: 1970, *Proc. Apollo 11 Lunar Sci. Conf., Geochim. Cosmochim. Acta Suppl. 1*, Vol. 1, 801.
Roeder, P. L. and Emslie, R. F.: 1971, *Contr. Mineral. Petrol.* **29**, 275.
Roeder, P. L. and Osborn, E. F.: 1966, *Amer. J. Sci.* **264**, 428.
Schairer, J. F.: 1959, in J. O'M. Bockris, J. L. White, and J. D. Mackenzie (eds.), *Physico-Chemical Measurements at High Temperatures*, Butterworths, 117.
Scoon, J.: 1971, *Proc. Second Lunar Sci. Conf., Geochim. Cosmochim. Acta Suppl. 2*, Vol. 2, 1259.
Strom, R. G.: 1971, *Mod. Geol.* **2**, 133.
Tuthill, R. L. and Sato, M.: 1970, *Geochim. Cosmochim. Acta* **34**, 1293.
Urey, H. C., Marti, K., Mei-Kao, L., and Hawkins, J. W.: 1971, *Proc. Second Lunar Sci. Conf., Geochim. Cosmochim. Acta Suppl. 2*, Vol. 2, 987.
Volmer, M.: 1939, *Kinetik der Phasenbildung*, Steinkopff, Dresden.
Wager, L. R. and Brown, G. M.: 1968, *Layered Igneous Rocks*, Oliver and Boyd, Edinburgh.
Wasserburg, G. J. and Papanastassiou, D. A.: 1971, *Earth Planetary Sci. Letters* **13**, 97.
Weill, D. F., McCallum, I. S., Bottinga, Y., Drake, M. J., and McKay, G. A.: 1970, *Proc. Apollo 11 Lunar Sci. Conf., Geochim. Cosmochim. Acta Suppl. 1*, Vol. 1, 937.

Addendum. Green *et al.* (1971b) doubt our finding of protohypersthene on the strength of their experiments carried out under appreciably different conditions. The facts to bear in mind are: (i) Biggar *et al.* (1971) analysed inverted protohypersthene from 12040 ($Ca_7Mg_{67}Fe_{26}$) and observed inverted orthorhombic phase present in the range 1160–1200 °C, and 1135–1160 °C in 12021. Eruption temperatures lay within these ranges, hence inverted protohypersthene is to be expected in the rocks, all other factors being equal. (ii) Ross *et al.* (1971, Abstract, *2nd Lunar Science Conf.*) reported inversion of calcium-poor pigeonite cores ($Ca_9Mg_{63}Fe_{28}$) from 12021 to orthorhombic structures (? space group) at 1160–1215 °C, in their heating experiments. (iii) Hollister *et al.* (1971, *Proc. 2nd Lunar Sci. Conf.*, p. 529–557) report orthorhombic cores in pigeonite from 12065. Aspects of their analysis 9-1-6 ($Ca_6Mg_{66}Fe_{28}$) are compared with our inverted protohypersthene (12040/4) TiO_2 0.43, 0.43; Al_2O_3 1.01, 1.08; Cr_2O_3 0.77, 0.46 (misprint in earlier text); CaO 2.90, 3.39; FeO 17.96, 16.72; MgO 23.50, 23.81. (iv) Brown *et al.* (1971), Gay *et al.* (1971, *Proc. 2nd Lunar Sci. Conf.*, p. 377–392) suggest that curving cracks in pigeonite phenocryst cores of 12040, 12065 may reflect the $C2/c \rightarrow P2_1/c$ inversion in pigeonite; Ross *et al.* (1971) did not report C2/*c* structure formation but Prewitt *et al.* (1971, *Proc. 2nd Lunar Sci. Conf.*, p. 59) did for material of this general composition at 1000 °C. A few cracks are present in the larger prisms of pigeonite in our runs, and the $C2/c \rightarrow P2_1/c$ inversion may also have occurred. Gay *et al.* (1971) comment on unusual pyroxene trends in 12065, matched by a terrestrial

protohypersthene precipitating rock. (v) Yoder, Tilley and Schairer (1964, *Yearb. Carnegie Instn. Wash.* **63**, 121–129) reported an orthorhombic calcium-poor pyroxene stable at these relevant compositions and temperatures, identified as protohypersthene by the same authors (1963, *Yearb. Carnegie Instn. Wash.* **62**, 84–95) with detailed discussion (1963, p. 90). (vi) Low-calcium-pyroxene cores comparable with Biggar *et al.*'s (1971) analysed protohypersthene form a smaller part of the rock powder as loaded, than do the large crystals with curving cracks which we interpret as inverted protohypersthene. Furthermore, had our protohypersthene been undissolved residual phenocryst cores it should have been more abundant in, not absent from, the lower temperature experiments. (vii) Finally we refer to results in Table VIII, run 006 which seem to eliminate worries about unmelted residual material.

Earth and Planetary Science Letters, 23 (1974) 435–438
© North-Holland Publishing Company, Amsterdam – Printed in The Netherlands

EXPERIMENTAL PETROLOGY OF SAMPLE 77135

W.C. STOREY, D.J. HUMPHRIES and M.J. O'HARA

Grant Institute of Geology, Edinburgh (Scotland)

Received July 29, 1974

The matrix of 77135 would not be a liquid at less than 1280°C, 1 atm pressure. The petrography and lack of evidence of crystallization in the 1280–1150°C interval suggest that the matrix is either a devitrified, shock-melted and supercooled glass, or a devitrified, depressurised liquid whose liquidus temperature had been depressed by the presence of a small amount of water at pressures attainable in the upper part of the lunar crust. Devitrification fronts would have advanced faster than 1 mm min^{-1} in 77135 glass at 1050°C under lunar surface conditions.

Results of melting experiments sample 77135,80 described initially as vesicular tan grey matrix and subsequently as fragment-laden pigeonite-feldspathic basalt, are reported in Table 1, and related to results [1] for other highland materials in Fig. 1. 77135 matrix is considered to represent a relatively young enveloping magma of internal lunar origin in the overall stratigraphy of boulder 7 [4]. Spinel is an early crystallizing phase in many highland compositions under the conditions of our experiments; the major mineralogy is, however, well represented in the ternary system calcic plagioclase–olivine–silica. We have, therefore, projected all compositions from spinel into the system feldspar–olivine–silica (Fig. 1). Also shown in Table 1 and Fig. 1 are results for a synthetic glass (77135 CG) supplied by E.C.T. Chao, having a composition close to that of the sample analysed by NASA (see [4]; 77135,2) while also plotted in Fig. 1. is the composition of the 77135,77 matrix, corrected for the presence of 1.5% olivine and 14.3% plagioclase xenocrysts (in [4]).

The phase equilibria behaviour of subsample 77135,80 indicates that its bulk composition lay intermediate between the corrected matrix composition, and the composition of the tan grey matrix as represented by the NASA analysis (Fig. 1). Above

TABLE 1
Results of 1-atm quenching experiments (oxygen fugacity of the Fe/FeO equilibrium, molybdenum capsules)

Run No.	Temp. (°C)	Phases present		
		77135 CG (original glass)	77135 CG (devitrified 972°C ~ 24 hr)	77135/80 (rock powder)
125	1326.2	liq	liq	liq
126	1281.3	liq	liq	(sp), liq
132	1273.5	liq	liq	ol, sp, liq
133	1260.2	liq	liq	ol, sp, liq
127	1253.2	ol, plag, liq	ol, plag, liq	ol, plag, sp, liq
128	1228.9	ol, liq	ol, plag, liq	ol, plag, sp, liq
129	1201.5	ol, plag, pyx, liq	ol, plag, pyx, liq	ol, plag, pyx?, sp, liq
130	1177.2	ol, plag, pyx, liq	ol, plag, pyx, liq	ol, plag, pyx, sp, liq

Abbreviations: sp = spinel, ol = olivine, plag = plagioclase, pyx = pyroxene, liq = liquid.

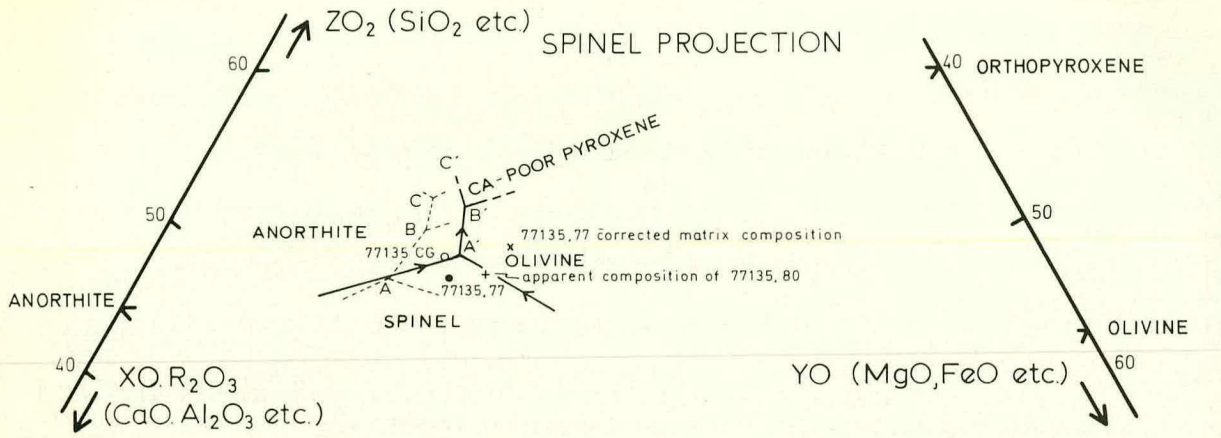


Fig. 1. Projection from spinel into the olivine–silica–anorthite composition plane using the projection scheme described by Jamieson [2]. Solid boundaries separate liquidus phase fields which describe the crystallization of samples 77135, 62295, 60035 and 60315 (unpublished data). The pyroxene–plagioclase cotectic lies between B' and C'. Light dashed lines link the analysed cotectic glasses A, B, C defining similar boundaries from the work of Walker et al. [3], which do not accurately describe our quenching data.

1260°C the spinels are pale in colour; below 1260°C they become scarce and progressively darker in colour. Residual liquids evolve in composition due to the precipitation of olivine and plagioclase until at some temperature about 1200°C calcium-poor pyroxene begins to precipitate and olivine is partly resorbed by reaction with the liquid. Pyroxene and plagioclase are the only crystalline phases identifiable by X-ray diffraction in the 77135 CG samples devitrified at 830–970°C. We estimate from the geometry of Fig. 1 that the samples would be 30–50% by weight crystalline at the first appearance of pigeonite, with as much as 15% by weight of olivine crystals present. 77135,80 is so extensively crystalline at temperatures below 1200°C that it is very difficult to ascertain the relative amounts of pyroxene and olivine. Neither the actual crystallization of the two samples, not their projected compositions in relation to the phase equilibria boundaries which we have determined from Apollo 16 samples suggests that the matrix composition in 77135 falls close to the pyroxene–plagioclase cotectic at low pressures.

If the matrix of 77135 represented and all-liquid magma at the surface of the moon, its temperature was greater than 1280°C. The absence of partially resorbed spinel phenocrysts cannot be used as a criterion for saying that it never was at such temperatures, because spinel crystallization at the liquidus may be suppressed at oxygen fugacities below those of our experiments. However, partial melting of the troctolite clasts, with the appearance of spinel, should have occurred at temperatures greater than ca. 1280°C and for this there is no petrographic evidence. There is little petrographic evidence of crystallization through the 1280–1200°C interval in which excess olivine should have formed, later to react with the liquid to yield pyroxene, although O.B. James (personal communication) finds fine-grained patches with above average amounts of small olivine crystals in the 77135 samples. Slow cooling in the ca. 1200°C range at least would have to be supposed for most of this rock to allow complete resorbtion of the excess olivine, but it is difficult to reconcile such an hypothesis with the texture of the matrix of 77135, which seems to indicate rapid crystallization, and the evidence from terrestrial lavas where excess olivine is persistently preserved under the cooling conditions accompanying eruption.

The solution to this problem may lie in recognising that the texture of 77135 is due to relatively rapid crystallization at less than 1200°C of the glassy matrix. That matrix might have cooled too rapidly through the 1280–1200°C interval for nucleation and growth to occur. This model is consistent with an impact-melting origin of the glass and with the absence of partial melting of the troctolite clasts, glass

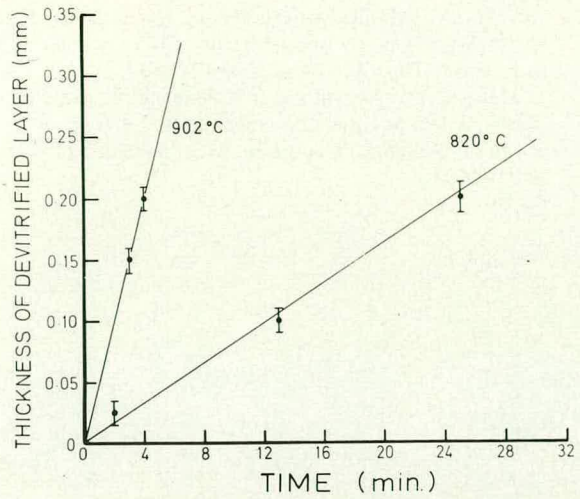


Fig. 2. Typical crystalline layer thickness versus time relations for 77135 CG.

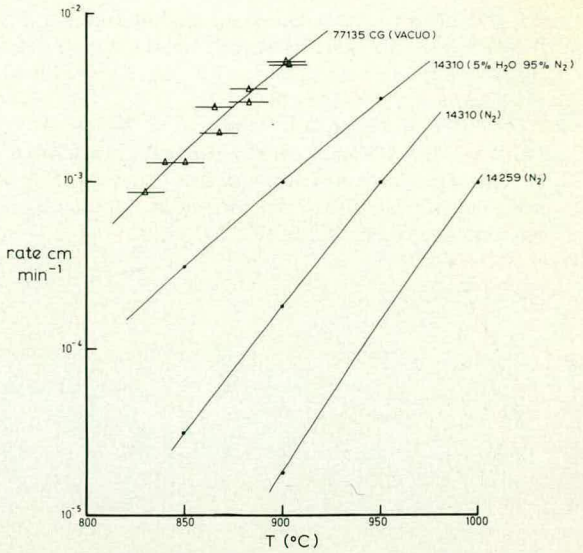


Fig. 3. Growth rate versus temperature relations for 77135 CG in vacuo, 14310 in an N_2 atmosphere and 5% H_2/95% N_2 atmosphere [7] and 14259 in an N_2 atmosphere [7].

and clasts becoming mingled and compacted only at temperatures below 1200°C. It is, however, difficult to reconcile with the behaviour of volatile-poor lavas on the lunar surface. Alternatively, the glassy matrix might have been created at less than 1200°C by the rapid depressurization (and probable explosive fragmentation) of a melt whose liquidus temperature had previously been depressed by the presence of some dissolved water at moderate depth within the moon. The problem, and this particular solution to it, are analogous to that which was encountered with 14310 [5] and is consistent with the model of internal origin for the 77135 matrix magma.

Experiments have also been carried out on the nucleation and crystallization of the synthetic glass 77135 CG provided by E.C.T. Chao. Cut slices, 1 mm thick, which had suffered no devitrification during cutting, were heated in vacuo at $\sim 10^{-6}$ torr for short periods in the furnace described previously [6]. Devitrification commenced from the surfaces and proceeded inwards at constant speeds (Fig. 2) which increased with the temperature of devitrification (Fig. 3). The rate of advance of the devitrification front in 77135 CG in vacuo (where the ambient atmosphere is probably composed largely of H_2 and CO) was much faster than that observed in 14310 or 14259 glass at atmospheric pressure (Fig. 3) [7], where the rate of devitrification was also a function of gas composition. The viscosity of 77135 CG, 14310 and 14259 glasses should not differ greatly and the differences in the rates of devitrification are probably controlled primarily by the oxygen fugacity.

Under conditions similar to those likely to have been encountered during the aggregation of sample 77135, devitrification fronts would have advanced at 1 cm in 3 hours at 900°C, but (by extrapolation of Fig. 3) at rates nearer to 1 mm per minute at 1050°C. If the matrix of 77135 were formed by the aggregation of small glass shards of a diameter less than 1 cm, whatever their origin, at a temperature close to the solidus, crystallization of the bulk of the material would have been very rapid indeed.

References

1 C.E. Ford, G.M. Biggar, M.J. O'Hara, D.J. Humphries and P.N. Spencer, Origin of the lunar highlands, in: Lunar Science V (Lunar Science Institute, Houston, 1974) 239–242.

2 B.G. Jamieson, Phase relations in some tholeiitic lavas illustrated by the system R_2O_3–XO–YO–ZO_2, Min. Mag. 37 (1970) 535–554.

3 D. Walker, T.L. Grove, J. Longhi, E.M. Stolper and J.F. Hays, Origin of lunar feldspathic rocks, Earth Planet. Sci. Lett. 20 (1973) 325–336.

4 E.C.T. Chao and J.A. Minkin, The petrogenesis of 77135, a fragment laden pigeonite feldspathic basalt – a major highland rock type, in: Lunar Science V (Lunar Science Institute, Houston, 1974) 112–114.
5 C.E. Ford, G.M. Biggar, D.J. Humphries, G. Wilson, D. Dixon and M.J. O'Hara, Role of water in the evolution of the lunar crust; an experimental study of sample 14310; an indication of lunar calc-alkaline volcanism, Geochim. Cosmochim. Acta Suppl. 3, 1 (1972) 207–229.
6 W.C. Storey, Volatilization studies on a terrestrial basalt and their applicability to volatilization from the lunar surface, Nat. Phys. Sci. 241 (1973) 154–157.
7 G. Scherer, R.W. Hopper and D.R. Uhlmann, Crystallization behaviour and glass formation of selected lunar compositions, Geochim. Cosmochim. Acta Suppl. 3, 3 (1972) 2627–2637.

Earth and Planetary Science Letters, 21 (1974) 253–268
© North-Holland Publishing Company, Amsterdam – Printed in The Netherlands

GRANT INSTITUTE OF GEOLOGY
Publication
No.....
UNIVERSITY OF EDINBURGH

PLAGIOCLASE SATURATION IN LUNAR HIGH-TITANIUM BASALT

M.J. O'HARA, G.M. BIGGAR, P.G. HILL, B. JEFFERIES and D.J. HUMPHRIES
Grant Institute of Geology, Edinburgh (Scotland)

Received 3 July 1973
Revised version received 16 November 1973

High-titanium basalt collected at the Apollo 11 site was sparsely porphyritic on eruption. Phenocrysts of anorthite are reported for the first time, and were present with a few phenocrysts of olivine, pigeonite, augite, ilmenite and spinel in the liquid. That liquid has a composition which closely resembles the average rock at the site, and also closely resembles new analyses of the liquids produced in equilibrium with anorthite, olivine, pigeonite, augite, ilmenite and spinel in melting experiments at low pressure on samples 10020, 10062 (which are the first of the more abundant low-potassium group lava to have been studied). We deduce that the Apollo 11 basalt was erupted with the temperature and composition of a liquid in cotectic equilibrium at low pressure with these six phenocryst mineral species. This condition is a mandatory consequence of the hypothesis that the lunar maria are slowly consolidated giant lava lakes. It is incompatible with the hypothesis that these mare surface basalts, are unaltered partial melts extracted from the deep lunar interior. Attention is drawn to the consequences of the nearly eutectic character of the crystallization of the high-titanium basalts.

1. Introduction

Two flows of high-titanium basalt have been identified in materials returned from the Apollo 11 site in Mare Tranquilitatis. These are similar in major-element composition, but one is significantly richer than the other in potassium. The Apollo 17 mission to Taurus Littrow has returned high-titanium basalts similar to the low-potassium group from Mare Tranquilitatis.

2. Contrasted interpretations of high-titanium basalts

In one interpretation it is claimed that the high-titanium basalts has a composition close to that of a liquid in simultaneous (cotectic) equilibrium at low pressure with many different crystalline species. This characteristic would be mandatory in the late residual liquids which might develop during the extreme fractional crystallization of large bodies of basalt magma situated at high levels in the lunar crust. Such a process is known to have occurred in large lava lakes on the earth's surface, and the topography of the lunar maria resembles that of a frozen lake of lava [1–3]. If this interpretation is correct, the chemistry of the mare surface basalts has been greatly modified by the preferential removal of crystal cumulates which now compose the deeper parts of the material filling the mare basins. The study of the chemistry and low-pressure phase equilibria of the lavas can, however, indicate the nature of those underlying crystal cumulates. Due to the modification of the liquid composition, which results from extreme fractional crystallization, it is impossible to deduce anything about the lunar interior from the chemistry or high-pressure phase equilibria in these magmas.

In another interpretation it is claimed that the high-titanium basalts had compositions far removed from those of liquids in cotectic equilibrium at low pressure with many crystalline species [4]. It was then possible to assume that the basalts were primary magmas, derived unaltered in chemistry from a small-scale partial melting process occurring at 200–400 km depth within the moon [4]. If this assumption is correct, an experimental study of phase equilibria in these basalts at high pressure will indicate the nature

of the crystalline phases present in the residual lunar mantle at the source of these basalts (provided that the partial melting is not assumed to have been a disequilibrium process). This reasoning could lead on to hypotheses concerning the chemical composition of the lunar interior and the moon's origin.

The two contrasted interpretations arise from a fundamental disagreement about the phase equilibria in the high-titanium basalt compositions at low pressure.

3. Plagioclase-saturation: the key to the problem

The controversy surrounding the low pressure phase equilibria has centered around what percentage of the original magma was crystalline when plagioclase, olivine, pyroxenes, ilmenite and spinel were all present together in the liquid for the first time.

Because plagioclase was the last of these crystal species to appear during the crystallization of individual samples prepared by most investigators, particular attention has been focussed on the percentage crystallinity at first appearance of plagioclase crystals. The question is fundamental because extreme low-pressure fractional crystallization of basaltic magma, as envisaged in the first interpretation, typically leads to the extraction of large amounts of plagioclase-bearing cumulates, which would form the deeper parts of the mare-filling. The anomalous depletion of europium relative to the other rare earth elements in the high-titanium basalts would be a predictable consequence of this extensive plagioclase extraction [5], but such a model requires that the high-titanium basalts were plagioclase-saturated liquids on eruption, i.e. it requires that the average magma composition develops plagioclase crystals in low-pressure experiments when only a few percent crystalline, and it virtually requires that phenocrysts of plagioclase (and several other minerals) should have been present in the magma when it was only sparsely porphyritic.

Petrographic accounts [6] indicate that plagioclase was crystallizing from the low-potassium magma when the rock samples were less than 10% crystalline (olivine, spinel, ilmenite, pyroxene already being present). This does not, however, prove that phenocrysts of plagioclase were present on eruption and there is a risk that the hand specimen samples differ in composition from the average magma composition in a way which either brings forward or retards the stage of crystallinity at which plagioclase appears.

4. Average magma composition

The field relationships at the Apollo 11 site are not known and a few minutes only were spent in collection of samples from the surface of the regolith. Models of how the regolith develops by meteorite bombardment [7] of the original lava flows indicate that larger blocks lying on the surface will have been excavated relatively recently from the floors of larger craters which penetrated the existing regolith. Once exposed at the surface larger blocks tend to be broken up by further impacts and added to the fine soil as small fragments. The upper layers of the original rock will have suffered this process at an earlier period. Large hand specimens, therefore, preferentially sample the material which was originally situated a few metres below the surface. If the regolith thickness and the depth of the lava flow are comparable, it is possible that the hand specimens are sampling the base of an original lava flow into which denser phenocrysts had been concentrated by crystal sinking.

Table 1 summarises the chemical data for materials from the Apollo 11 site. The averages of hand specimen compositions (Table 1, row 7, 8) are poorer in SiO_2 and richer in FeO and TiO_2 than the average composition of the magma, determined by analysing small lithic fragments of high-titanium basalt in the soil (Table 1, row 5). Lithic fragments of low-potassium lavas apparently form by far the greater proportion of the population [9]. At this stage of the discussion we do not attempt to distinguish too sharply between them because the soil is formed from a weighted average of the average composition of each lava flow, and the differences between average magma composition and the average hand specimens is much greater than the differences between the two groups of hand specimens. It is argued that these are a more representative sample of the total rock which has been converted to regolith than are the large hand specimens. Nevertheless, there are some large hand specimens whose compositions closely approach the

TABLE 1
Rock compositions at Apollo 11 site, to show bias in hand specimen samples due to crystal accumulation

	SiO_2	TiO_2	FeO	MgO	Al_2O_3	CaO	Na_2O
(1) Crushed putative basalt	43.0	5.8	14.0	8.1	16.0	12.0	
(2) (60–66%) in soils [11]	42.6	6.8	14.8	8.1	15.0	12.4	0.40
(3) Soil average [8]	42.0	7.5	15.8	7.9	13.8	12.0	0.45
(4) Breccia [8]	41.7	8.9	16.4	7.5	12.4	11.8	0.2
(5) Average ophitic magma [9]	42.9	8.7	17.0	7.2	11.8	11.4	0.6
(6) 10044 [10]	42.5	9.2	18.2	6.0	10.2	12.2	0.5
(7) Hand specimens (ophitic) [8]	40.5	10.3	18.7	6.7	10.4	11.5	0.5
(8) Hand specimens (intersertal) [8]	40.3	11.9	19.2	7.6	9.0	10.5	0.6

average (Table 1, row 6). Independent confirmation of the difference between the hand specimen samples and the magma composition is provided by the average compositions of the soils and breccias (Table 1, rows 3, 4) which are much poorer in TiO_2 than the hand specimens. Both soils and breccias are contaminated by the introduction of a small percentage (3.6–5.0%) of anorthite-rich highland material [7, 12] but two independent calculations have shown that the composition of the regolith at the Apollo 11 site requires a substantial contribution (60–65%) from a basalt much poorer in TiO_2 and FeO, than the large hand specimens (Table 1, rows, 1, 2). Such material is actually present among the lithic fragments as revealed by the ranges of the analyses reported by Prinz et al. [9]. (The contamination of the soils by highland anorthosite is reflected in the appearance of anorthite before ferromagnesian silicates or ilmenite in the crystallization history of soil 10084 [1] and a range of Apollo 17 soils (unpublished).)

We conclude that the hand specimens at the Apollo 11 site are preferentially derived from a phenocryst-enriched flow base and most, but not all, show significant phenocryst enrichment. Ilmenite, $FeTiO_3$, appears to have been the *most important* crystal species to have accumulated into the flow base. This mineral was present as a phenocryst and has a high density, much higher than that of the liquid. The addition of only 3–6% by weight of ilmenite to the average magma composition would produce the lower SiO_2 and higher TiO_2, FeO of the average hand specimen compositions, and we suggest that petrographic evidence for such accumulative introduction may be masked by the large amount of ilmenite crystallizing from the liquid itself. Within each hand specimen group the variation in the amount of ilmenite required to have accumulated is ~ ± 60% *of the amount accumulated* but only ~ ± 15% of the total opaque oxide in the final rock.

5. Liquid composition at plagioclase saturation in laboratory experiments

Our original experiments [1] on thirteen synthetic simulations of Apollo 11 materials were designed to test whether or not they lay close to a liquid in simultaneous cotectic equilibrium at low pressure with several different crystalline species. A network of compositions was set up, displaced about the average rock and soil compositions to cater for the possibility of non-representative sampling. This network of compositions embraced regions in which plagioclase (anorthite), olivine, pigeonite, augite, ilmenite, ulvöspinel or armalcolite were the liquidus phases. From these data limits can be set on the composition of a liquid in *simultaneous* equilibrium at low pressure with anorthite, olivine, two pyroxenes and iron-titanium oxides (Table 2, column 1).

This compositions closely resembles the average magma compositions derived from analyses of lithic fragments in the breccias and soils (Table 2, columns 2, 3) and again closely resembles the plagioclase-saturated cotectic liquids produced from three natural Apollo 11 samples in our experiments (Table 2, columns 4–6), two of which (10020, 10062) are samples of the ophitic group which has not previously been studied in this way.

There is independent confirmation from the natural rock 10020 that these determinations of the plagioclase-saturated liquid compositions are realistic. Roedder and Weiblen [13] report a liquid inclusion

TABLE 2
Experimentally produced plagioclase-saturated cotectic liquid compositions in synthetic and natural materials compared with average magma, individual rock and trapped liquid inclusion compositions at the Apollo 11 site, and a quenched Apollo 11 basalt groundmass containing anorthite phenocrysts*

	1	2	3	4	5	6	7	8	9	10	11	12	13
SiO_2	42.5 ± 1.0	42.9	42.8	44.09	42.49	44.02	40.8	43.98	42.46	42.16	43.4	43.8	44.7
TiO_2	9.25 ± 0.5	8.7	9.6	8.31	8.93	8.23	9.8	9.07	9.18	9.43	8.8	7.9	7.4
Al_2O_3	10.5 ± 1.0	11.8	10.6	10.09	9.70	9.55	9.8	10.42	10.21	9.89	10.2	8.8	12.6
Cr_2O_3		0.29	0.26	0.09	0.08	0.08		0.08	0.21	0.18	0.2	–	–
FeO	18.0 ± 1.0	17.0	18.0	18.13	18.91	19.17	20.7	17.17	18.24	19.11	17.6	18.3	15.2
MnO		0.18	0.19	0.28			0.24		0.28	0.28	0.3	–	–
MgO	7.5 ± 1.0	7.2	7.0	5.92	5.95	6.01	7.0	6.53	5.96	5.67	6.6	7.5	6.5
CaO	11.5 ± 0.7	11.4	10.7	11.07	11.45	11.58	11.1	10.94	12.25	12.15	12.2	12.7	13.0
Na_2O		0.56	0.63	0.62	0.43	0.40	0.2	0.55	0.48	0.45	0.5	0.4	0.4
K_2O		0.07	0.36	0.59		0.12	0.05	0.10	0.11	0.11	0.1	0.1	0.1

* It is claimed that these analyses are similar to each other.

1 = Multiphase cotectic liquid composition, saturated with anorthite, olivine, two pyroxenes and one or two iron-titanium oxides, from synthetic system [1].
2 = Average ophitic group (low-potassium) lava from lithic fragments**; Prinz et al. [9].
3 = Average intersertal group (high-potassium) lava from lithic fragments**; Prinz et al. [9].
4 = Nearly plagioclase saturated cotectic liquid in 10017, 1133°C [2].
5 = Cotectic liquid in 10020, 1133°C with olivine, two pyroxenes, anorthite, ilmenite and chromium ulvöspinel.
6 = Cotectic liquid in 10062, 1120°C with olivine, clinopyroxene(s), anorthite, ilmenite and (?) spinel.
7 = Liquid inclusion in early olivine of 10020, homogenised at 1210°C (13).
8 = Cotectic liquid in synthetic mixture to analysis of column 3, run at 1145°C.
9 = Natural rock sample 10044 (Agrell et al. [10]).
10 = Natural rock sample 10047 (Compston et al. [8]).
11 = Quenched basalt groundmass from felsparphyric lithic fragment** (Table 4, row 7).
12 = Quenched basalt groundmass from felsparphyric lithic fragment** (Table 4, row 11).
13 = Quenched basalt groundmass from feldsparphyric lithic fragment** (Table 4, row 17).
** Defocussed bean analyses are believed to be subject to positive errors in Al_2O_3 and negative errors in FeO, MgO. Errors of + 1% Al_2O_3, – 1% FeO in columns 2, 3 and 11 would not materially affect the validity of this table.
The analyses represented by columns 12 and 13 represent, on account of their much shorter length, less satisfactory samples of the host liquid composition than does column 11.

in olivine from this rock (Table 2, column 7) which represents a sample of the magma at or shortly before the first appearance of plagioclase [7]. However, these workers homogenised this inclusion in its olivine container at 1210°C which is substantially above the probable eruption temperature, hence some allowance must be made for increased FeO, MgO and decreased SiO_2 due to the excessive resolution of olivine.

Further confirmation that the average magma composition lay close to that of a plagioclase-saturated liquid is obtained from an analysis of the residual plagioclase-saturated cotectic liquid (Table 2, column 8) developed in a synthetic mixture made up to the average composition of the high-potassium basalt group (Table 2, column 3).

Analyses of two natural ophitic group samples are reproduced in Table 2, columns 9 and 10, to demonstrate that there are some large hand specimens which closely approach the composition of the experimentally produced liquids which are simultaneously saturated with plagioclase (anorthite), olivine, pigeonite, augite and iron-titanium oxides at low pressure.

6. Percentage crystallinity at plagioclase entry: a red herring

The data in Table 2 establish that the magmas erupted at the Apollo 11 site had compositions close to those of the low-pressure plagioclase, olivine, pigeonite, augite, ilmenite and spinel-saturated liquids. How much crystallization of individual hand specimens, which are *not* representative of the average composition, has occurred when plagioclase first appears in experimental products may be calculated using a least squares program [14] to fit the sample composition to an assemblage of the analysed cotectic liquid and the analysed or reasonably assumed compositions of the crystal species identified in the experimental charges. Results are set out in Table 3.

Results obtained for the ophitic group samples are in excellent agreement with the petrography of the natural rocks.

In the case of three synthetic mixtures made up to simulate average hand specimen analyses, only visual estimates of crystallinity at plagioclase entry were published by the original workers. In one case we have attempted to calculate the result assuming the residual liquid composition to match that which we obtain in our experiments and obtained a lower result.

A similar calculation for a natural rock of the intersertal group 10022 also yielded a much lower figure for crystallinity at the *equilibrium* appearance of plagioclase. Petrographic accounts indicate that plagioclase did not nucleate during the rapid cooling of this natural sample until it was about 60–70% crystalline, but this estimate refers to conditions under which supercooling and delayed nucleation of plagioclase are known to occur [3].

Natural sample 10017, also of the intersertal group has been studied by ourselves, and a synthetic mixture of this composition has been studied by Ringwood and Green [19]. Their visual estimate of crystallinity at plagioclase entry is much higher than we obtain by calculation.

The high petrographic estimate of crystallinity at plagioclase nucleation in 10022, and the high visual estimates of crystallinity contained in the bottom row of Table 3, have been used [4, 18] to argue that the Apollo 11 magmas are far removed from the compositions of plagioclase-saturated liquids. We reject this reasoning because: (1) these estimates refer to hand specimen compositions which depart significantly from the average magma composition; and (2) visual estimates of crystallinity emanating from the Canberra laboratory have been shown to be much too high, and incorrect as to relative mineral proportions, in the case of the Apollo 12 magmas [3] and a similar discrepancy now appears in the Apollo 11 work (Table 3). No control or calibration of their technique for visual estimation has been reported except that afforded by the interlaboratory comparison of the lunar basalt data. In our opinion visual estimation of crystallinity in experimental charges is a subjective, qualitative technique which has little place in science because it too easily leads to an illusion of quantitative certainty.

The important question to be answered is not, however, how much crystallinity individual hand specimens display at plagioclase entry, but whether or not the natural magma was plagioclase saturated and sparsely porphyritic on eruption.

TABLE 3

Percentage crystallinity in Apollo 11 hand specimen compositions at first plagioclase appearance

Method	Ophitic			Hand specimen analyses			Intersertal	
	10020	10062	average [6]	ANS [15]	TS [16]	RE [3, 4]	10022 [3, 17]	10017 [2, 3, 18]
From petrographic study			< 10				60–70	
By calculation from analyses	9*					~ 25	< 25	28–32
By visual estimate in experimental charges (Edinburgh)	< 10	< 10						~ 25
By visual estimates (other laboratories)				30–70**	~ 17**	30–50**		40–50

* In the calculations from experimental data for analysed cotectic liquid compositions in charges where substantial plagioclase was already present, total calculated crystallinity was reduced by (3.2 × wt.% plagioclase) to obtain the percentage crystallinity at first plagioclase entry, 1/3.2 being the weight ratio of plagioclase to total crystals which form from the cotectic liquid (determined by inspection of the C.I.P.W. norm).

** With one exception, other laboratories visual estimates of crystallinity at plagioclase entry are much higher than can be reconciled with analytical data for the phases present. Calculation from the one low visual estimate implied less than 5% TiO_2 in the cotectic liquid [16] but subsequent work has shown that there was 8.0–8.5% TiO_2 in the glass at plagioclase entry, and probably only 8–10% crystallinity (personal communication, R.T. Helz, 1973).

7. Plagioclase phenocrysts in Apollo 11 basalt

The breccias and soils from the Apollo 11 site contain many lithic fragments, some of which are fine-grained plumose-textured aggregates of (principally) pyroxene and skeletal ilmenite. The texture of these closely resembles the quenching products produced in experiments during the rapid cooling (slower than normal quenching) of a liquid, and in common with other petrographers, we ascribe their texture to this cause. Plumose-textured fragments of this type are commonly aphyric, but examination of a large number of samples has disclosed the presence of a *small proportion of microphenocrysts* (forming perhaps 1–2% of this material). Phenocrysts of olivine, pyroxene, ilmenite and chromian ulvöspinel have been identified. Three fragments also contain unambigous plagioclase phenocrysts (Fig. 1C). These phenocrysts are anorthite (An_{93}) and have a uniform composition (Table 4). The groundmass of one of these fragments, representing the liquid phase in which the phenocrysts were carried, has been analysed by a defocussed beam technique, with results presented in Table 4. They are clearly high-titanium basalts, and their analyses have been reproduced in Table 2, columns 11, to demonstrate that they are essentially similar to the average magma composition at the Apollo 11 site, and to the analysed experimentally produced liquids in simultaneous cotectic equilibrium with anorthite, olivine, pigeonite, augite, ilmenite and spinel *at low pressure.*

It follows that the Apollo 11 magma had both the temperature and the composition of a low-pressure multiphase cotectic liquid, saturated *inter alia* with anorthite, when it was erupted.

One of the fragments in question is shown in Fig. 1C. Informed by this observation it is possible to recognise probable phenocrysts in other, more slowly cooled materials (Fig. 1A, B). Analyses of the larger crystals in the latter fragments show them again to be anorthite (An_{93-94}) but the smaller surrounding or groundmass crystals are more sodium-rich, as are the rims to the proposed phenocrysts.

8. Interpretation of the low-pressure multiphase cotectic character of the high-titanium basalts

Low-pressure multiphase cotectic character with respect to both composition and temperature may be asribed to coincidence between a high-pressure partial melt composition and the composition of the special liquids in equilibria of very limited degrees of freedom at low pressure. The probability of such a coincidence arising can be estimated [3, table 6]. In the present instance this probability can be measured in parts per thousand or less, and we discount such an explanation.

Any process, operating at low pressure, which involves the generation of the magma in contact with all six crystalline phases with which it is just saturated will produce the observed effect, i.e. a process in which the magma composition is controlled by events taking place close to the lunar surface. Correct interpretation can greatly increase understanding of near surface lunar processes. Four possible processes are:

(1) Incipient partial melting of a rock consisting of anorthite, moderately iron-rich olivine, pigeonite, augite and ilmenite and spinel in an environment close to the lunar surface. We reject this because the requisite thermal regime is inexplicable, no adequate mechanism exists for the aggregation of that incipient melt into a single lava flow, and the required source rocks are not known to exist close to the lunar surface.

(2) Filter pressing of trappped interstitial liquid from some high-level crystal cumulus. This solves the problems of the thermal regime and the source rock mentioned in (1) but leaves the problem of the cause of filter pressing, there being little evidence of tectonic action in the maria.

(3) Continuous cooling and loss of crystalline material either by sinking or freezing to the side wall of the conduit during the uprise of some primitive magma. This process is known to occur in terrestrial magmas, but we incline away from it in the present instance because it has never been demonstrated to produce such an extreme multiphase cotectic character in a terrestrial magma, and there is on the moon no evidence of the large volcanic superstructure relative to normal land surface in which such processes appear to operate most efficiently on the earth.

(4) Extreme fractional crystallization in a high-level body of some primitive parental magma composition (derived from the lunar interior). This process is widely observed in shallow-seated sheet-like bodies of magma on the earth, and in lava-lakes once a crust has formed [19]. The lunar maria look like consolidated lava lakes, and at least one terrestrial body, the Bushveld complex, has mare-like dimensions

TABLE 4

Phenocryst and groundmass compositions in lithic fragments (These analyses are presented in order to establish the composition of the phenocrysts, and their identity with early crystallizing phases in the more slowly cooled basalts; and to demonstrate that the quenched groundmass was a high-titanium basalt liquid.)

	SiO_2	TiO_2	Al_2O_3	Cr_2O_3	FeO	MnO	MgO	CaO	Na_2O	K_2O	Total
From section 10019,15, fragment one (Fig. 1C)											
(1)	45.13	0.09	34.36	0.03	0.46	0.00	0.27	18.87	0.80	0.05	100.06
(2)	42.72	6.66	8.07	0.41	11.62	0.25	11.09	17.67	0.12	0.00	98.61
(3)	0.14	54.15	0.16	0.75	41.76	0.39	1.74	0.41	0.01	0.00	99.51
(4)	37.85	9.33	9.48	0.23	15.91	0.26	5.93	10.63	0.45	0.13	90.20
(5)	41.59	6.79	9.24	0.17	16.54	0.28	5.81	11.14	0.50	0.14	92.20
(6)	40.31	8.23	9.46	0.20	16.17	0.27	6.61	11.96	0.47	0.14	93.82
(7)	43.4	8.8	10.2	0.2	17.6	0.3	6.6	12.2	0.5	0.1	99.9
From section 10019,15, fragment two: feldspar phenocryst and liquid											
(8)	45.53	0.17	33.59	0.00	0.51	0.00	0.19	18.43	0.72	0.06	99.20
(9)	43.23	8.00	9.12	0.20	17.81	0.27	6.65	12.40	0.47	0.09	98.24
(10)	43.37	7.55	8.19	0.20	18.48	0.27	8.27	12.74	0.30	0.08	99.45
(11)	43.8	7.9	8.8	0.2	18.3	0.3	7.5	12.7	0.4	0.1	100.0
From section 10021,26, fragment two: feldspar phenocrysts and liquid											
(12)	45.52	0.15	33.96	n.d.	0.47	n.d.	0.28	18.54	0.71	0.04	99.67
(13)	45.40	0.14	33.61	n.d.	0.34	n.d.	0.30	18.51	0.77	0.05	99.12
(14)	45.53	0.15	33.68	n.d.	0.48	n.d.	0.27	18.62	0.66	0.03	99.42
(15)	46.20	6.13	11.07	n.d.	13.63	n.d.	7.49	13.28	0.36	0.08	98.24
(16)	4036	8.20	13.47	n.d.	15.85	n.d.	5.17	11.99	0.45	0.11	95.61
(17)	44.7	7.4	12.6	n.d.	15.2	n.d.	6.5	13.0	0.4	0.1	99.9
From section 10019,15, fragment three (Fig. 1A): probable feldspar phenocryst											
(18)	45.53	0.14	33.34	n.d.	0.42	n.d.	0.27	18.15	0.88	0.04	98.77
(19)	47.31	0.14	32.14	n.d.	0.69	n.d.	0.29	17.11	1.26	0.07	99.01
From section 10021,26, fragment one: olivine, pyroxene and ilmenite phenocrysts											
(20)	38.08	0.31	0.08	0.26	25.58	0.26	36.51	0.31	0.03	0.02	101.44
(21)	38.22	0.27	0.05	n.d.	26.62	n.d.	35.52	0.36	0.05	0.03	101.12
(22)	48.01	4.16	4.66	0.78	10.79	0.20	13.61	17.71	0.14	0.03	100.09
(23)	0.14	52.59	0.20	n.d.	43.12	n.d.	1.90	0.26	0.05*	0.04*	98.30
(24)	0.72	51.29	0.43	0.59	44.37	0.34	0.92	0.31	0.04*	0.03*	99.04
From section 10018,20, fragment one: olivine, ilmenite phenocrysts and groundmass											
(25)	37.71	0.09	0.06	0.12*	25.23	0.24*	35.66	0.30	0.03*	0.01*	99.45
(26)	36.88	0.11	0.07	0.06*	29.06	0.26*	32.15	0.35	0.03*	0.03*	99.00
(27)	0.17	21.35	5.77	20.33	47.08	0.38	2.73	0.11	0.01*	0.03*	97.96
(28)	0.07	53.86	0.13	0.72*	42.73	0.41*	2.26	0.09	0.04*	0.03*	100.34
(29)	43.5	7.9	11.8	0.3*	15.8	0.3*	6.9	12.9	0.5	0.1	100.0

From section 10019,15 fragment one (Fig. 1C):

1 = Mean of 6 analyses of plagioclase phenocrysts. The composition (An_{93}) is non-stoichiometric as are other lunar feldspars.
2 = Pyroxene in groundmass.
3 = Ilmenite in groundmass.
4–6 = Defocussed beam traverse analyses of groundmass to the phenocrysts as indicated in Fig. 1. Beam width was 20 μm, scan length 300 μm, counting times 600 sec. Totals are generally low probably due to the presence of cracks and small holes filled with araldite within the area scanned. No significance is claimed for the final figure.
7 = Average of 4, 5, 6, rescaled to 100%, representing a possible composition of the liquid phase in which the feldspar phenocrysts were carried. This analysis is reproduced in Table 1, column 11 for comparison

From section 10019,15, fragment two:

8 = Plagioclase phenocryst, $An_{93.4}$.
9, 10 = Defocussed beam traverse analyses (beam 20 μm, scan length 150 μm, counting time 300 sec) of groundmass.
11 = Average of 9, 10, rescaled to 100%.

From section 10021, 26, fragment one:

12 = Average of 16 analyses in plagioclase phenocrysts, $An_{93.5}$, range $An_{91.3-95.2}$. The most sodic analysis comes from the core of the largest phenocryst, and the most calcic analysis from its rim.
13 = Average of 4 analyses in the core of the largests phenocryst, $An_{93.0}$, range $An_{91.3-94.2}$.
14 = Average of 6 analyses in the rim of the largest phenocryst, $An_{94.0}$, range $An_{92.8-95.2}$. Note the higher FeO, and higher FeO/MgO ratio, combined with the lower Na_2O and K_2O (the ranges of FeO do not overlap). The results are consistent with a loss of alkalis from the liquid between the crystallization of the core and the outermost rim on the plagioclase phenocrysts, suggesting that phenocryst growth bridges an eruptive episode. Calculation, assuming a constant alkali/lime distribution coefficient between plagioclase and liquid indicates as mush as 15% of the Na_2O and 40% of the K_2O in the magma (amounting to 0.06% Na_2O; 0.03% K_2O) were lost by volatilization during eruption.
15, 16 = Defocussed beam transverse analyses, beam width 20 μm, scan length 150 μm, counting time 300 sec.
17 = Average of 15, 16, rescaled to 100%, representing a possible composition of the liquid phase in which the phenocrysts were carried.

From section 10019,15, fragment three (Fig. 1A):

18 = Mean of two analyses in core of largest plagioclase lath, and one analysis each of cores of medium sized laths displaced NW and NE from centre of firts lath by about one lath length, An_{92}, range $An_{90.2-93.4}$. These are possible phenocrysts, but may include some subsequent plagioclase.
19 = Mean of two analyses in the rim of the large lath, plus one analysis each in the small offshoot laths extending to the ENE, S, and SW from the main lath, An_{88}, range $An_{85.2-89.6}$. The increased iron and potassium are also characteristics of these later crystallized plagioclases, which are more sodic than any phenocryst-like plagioclase in the previous three fragments.

From section 10021,62, fragment one:

20 = Core of olivine phenocryst, Fo_{72}. This analysis is as magnesian as the most magnesian olivines reported from the crystalline rocks, e.g. 10045 [10].
21 = Average of two analyses in rim of same phenocryst, Fo_{70}.
22 = Average of cores of three pyroxene microphenocrysts; note low Al_2O_3, high Cr_2O_3, MgO/FeO (marginal pyroxene on these phenocrysts contain lower Cr_2O_3, MgO/FeO and up to 80% more Al_2O_3. This composition compares closely with core pyroxenes from 10045 [10] but not quite as poor in iron.
23 = Average of two analyses of "stumpy" microphenocrysts of ilmenite: note the relatively high MgO (asterisk denotes one determination only).
24 = Average of two analyses of elongated ilmenite in the groundmass, probably of quenching origin; note the low MgO.

From section 10018,20 fragment one:

25 = Average of two analyses of core of olivine phenocryst, $Fo_{71.5}$.
26 = Average of three analyses of rim of same phenocryst, Fo_{66}.
27 = Average of three analyses of three titanian chromite microphenocrysts embedded in the rim of the olivine phenocryst.
28 = Average of two analyses of ilmenite microphenocrysts; note the relatively high MgO.
29 = Average of three defocussed beam traverse analyses of the groundmass, one of 600 μm, two of 300 μm, weighted according to length, rescaled to 100%.

(300 X 400 km; 7 km depth). Characteristic features of such bodies are: (a) the creation of great thickness of cumulus rocks (principally gabbros) which are poor in incompatible elements, and (b) the generation at a late stage of a residual liquid very rich in incompatible elements which is precipitating many different crystalline species (5 in the case of the Bushveld at the ca. 80–90% crystalline stage). We prefer this interpretation of the origin of the low-pressure multiphase cotectic character of the lunar high-titanium basalts because it accords perfectly with a well-established geological process, it is wholly compatible with the topographic environment of eruption, and the magma was generated as an already aggregated body of late residual liquid from a much larger volume of parental magma very close to the lunar surface, where the residual magma is readily available for tapping (e.g. by meteorite impact penetrating or breaking the crust of the lava lake). Moreover, the achondrite meteorites have petrographic and chemical characteristics indicating that they might represent samples of the predicted cumulates [20] and we have been able [2, 3] to identify less extremely fractionated lunar magmas (such as those from the Apollo 12 site) as the cognate liquid for such accumulates in the middle and late stages of such a process.

9. Confirmatory chemical evidence

Extreme fractional crystallization of a parental magma imposes predictable chemical characteristics on the residual liquids, provided the nature of the successive crystal extracts is known.

All likely crystal extracts from a parental basic magma will, however, progressively enrich the rare-earth elements (REE) in the residual liquid. The lunar high-titanium basalts have exceptionally high concentrations of the REE [5]. If, however, plagioclase had been a major member of the crystal assemblages extracted, there should be a profound depletion of europium relative to the other REE, because this element (as Eu^{2+}) is preferentially extracted by plagioclase, particularly at low-oxygen fugacities which favour a high Eu^{2+}/Eu^{3+} ratio [21]. The lunar mare lavas have low-oxygen fugacities and extreme europium depletion relative to other REE [5] and plagioclase saturation of the high-titanium basalts indicates that plagioclase had been a cumulus phase.

The light REE are not strongly depleted relative to the heavy REE in the high-titanium basalts, implying that calcium-rich pyroxene had not been a major crystal extract during the fractional crystallization. Although the high-titanium basalt is augite saturated, the less fractionated magmas from Apollo 12 were not and the achondrites contain little augite. Further fractionation once augite has begun to precipitate should deplete light REE relative to heavy, while still increasing the overall concentrations. The high-potassium/ high-titanium basalts have these characteristics relative to the low-potassium group [5].

Other features of the high-titanium basalts which are best explained by an extreme fractional crystallization model are the high concentrations of those other incompatible elements which are non-volatile (titanium, zirconium, and barium in particular), the high absolute concentration of FeO and its high concentration relative to MgO. In all these respects the lunar high-titanium basalts differ from "normal" basaltic chemistry. Extreme fractional crystallization of a more advanced partial melt can produce much higher concentrations of incompatible elements, (and, moreover, automatically concentrates the liquid product) than can incipient partial melting of the same source rock.

10. Apparently conflicting chemical data integrated with the model

Aspects of the chemistry of chromium, vanadium, rubidium, strontium and barium [4, 8] have been claimed to invalidate the interpretation of high-titanium basalts as products of extreme fractional crystallization, particularly with respect to the possible derivation of the high-potassium group from the low-potassium group at the Apollo 11 site. Acceptance of the fractional crystallization model awaits a satisfactory answer to these points. These answers follow:

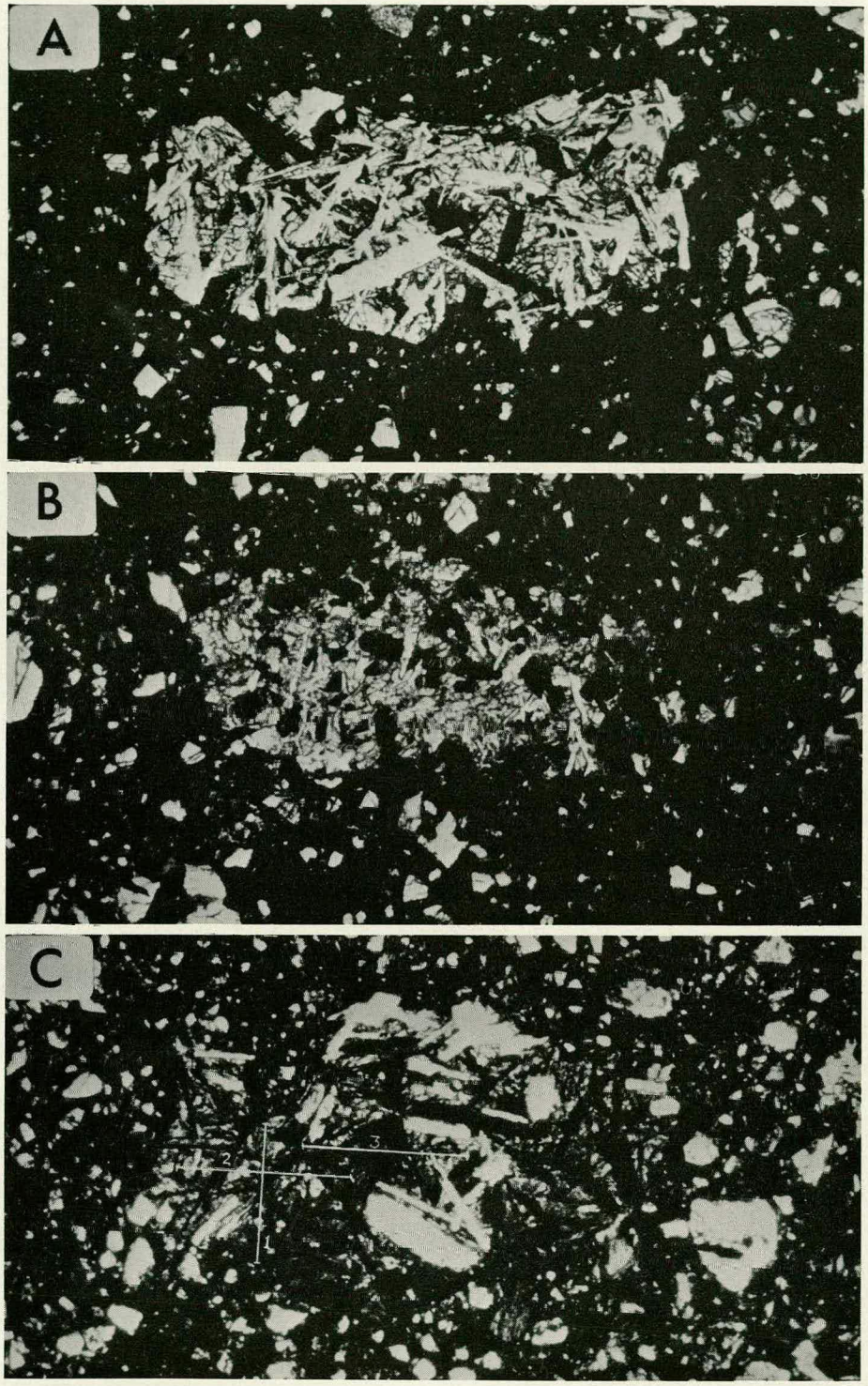


Fig. 1. Lithic fragments containing anorthite phenocrysts from breccia sample 10019,15, showing position of defocussed beam traverses. A Ophitic group fragment, 2 mm long with apparent phenocryst of feldspar in a lower centre. B. Fine-grained lithic fragment, 1 mm long, with texture approaching that of intersertal group, and distinct larger plates of feldspar. C. Plumose-textured fragment, 1 mm long, with abundant phenocrysts of feldspar.

10.1. Near-eutectic character of high-titanium basalt crystallization and the preservation of major-element chemistry during fractionation

The assemblage of anorthite, olivine, augite, pigeonite, ilmenite and spinel which crystallises at the liquids of the high-titanium basalt magma can closely approximate to the bulk composition of the liquid itself in respect of all the major oxide components although the continuing enrichment of iron relative to magnesium in the liquid is only partly suppressed by ilmenite and spinel crystallization. (No comparable situation involving and requiring so many phenocryst phases, has yet been reported from terrestrial rocks to the authors' knowledge.) These are the circumstances in which a near approach to eutectic crystallization may occur, large amounts of crystallization occurring without major change of the residual liquid composition. Electron microprobe analyses confirm that there is little change in the residual liquid composition between 1145 °C and 1108 °C in the natural samples, anorthite, olivine, pyroxene, ilmenite and spinel coexisting with the liquid throughout this interval, and more than 50% of the original liquid becoming crystalline (see Table 5). (This situation does *not* preclude strong fractionation occurring during the *disequilibrium* crystallization of the groundmass in a particular sample under conditions of rapid cooling.)

During near-eutectic crystallization incompatible elements will undergo many-fold enrichment in the residual liquid without any great changes in the major oxide composition occurring. There is a many-fold enrichment of certain incompatible elements in the high-potassium group lava relative to the low-potassium group lava [8]. Far from being an argument against near surface fractional crystallization [8] this features is, in the light of the experimentally determined phase equilibria, one of the stronger arguments in favour of extreme late stage fractional crystallization.

11. Rubidium/strontium systematics

The high-potassium group lava at the Apollo 11 site, which we must interpret as the later residual liquid, has an Rb/Sr ratio so high that its $^{87}Sr/^{86}Sr$ would have evolved from 0.69898 (BABI) in the last 3.93×10^9 years, and therefore this is unlikely to have been a closed system for a longer period [22]. Both high- and low-potassium lavas crystallized at $3.65 \pm 0.7 \times 10^9$ years ago [8] and a whole rock isochron drawn between them indicates that if they are related, Rb and Sr were fractionated between them ca. 3.8×10^9 years ago [8]. Making allowance for interlaboratory discrepancies, it appears that three events were almost contemporaneous at ca. 3.7×10^9 years ago: (1) fractionation of Rb and Sr between the sources of the two lava batches; (2) creation of the high-potassium group lava; and (3) eruption of both lava batches.

This is entirely in accord with the extreme fractional crystallization model. Rubidium may have behaved as a totally incompatible element throughout the fractional crystallization, but strontium will have been extracted by plagioclase especially. The Rb/Sr ratio will, therefore, have been increasing in the residual liquid throughout the crystallization of the lava lake, but the rate of increase of this ratio will have risen sharply and progressively during the late stages of fractionation. The marked rise in Rb/Sr ratio between the low- and high-potassium/high-titanium basalts, combined with the small change in major element composition, again points to the origin of these liquids during the late stages of extreme fractional crystallization. This explanation avoids the problems contained in the alternative postulate of two independent source regions within the moon, one of which had acquired a high Rb/Sr ratio by an unexplained process shortly before production of the two basalts.

12. Chromium and vanadium

It has been claimed [4] that augite and spinel extract so much chromium, and armalcolite so much vanadium that the present high levels of Cr and V in the magmas could not have survived substantial fractional crystallization.

This argument would have been correct if augite, spinel and armalcolite had formed the major part of the crystal extract, as indeed they do during the early crystallization of some of the individual hand specimens and synthetic mixtures. However, the separation

TABLE 5
Summary of new and a few old results of quenching experiments on Apollo 11 materials in molybdenum capsules

	Ophitic group			Intersertal group	
Temp (°C)	10020	10062	Average low-K[1] lithic fragments	10017	average high-K[1] lithic fragments
1177[2]		(ol)gl		(ol) (sp)gl	
1170	gl	ol, gl			
1168			gl(ore)	ol, sp, gl	
1163[2]	sp, gl	ol, sp, gl	pl, sp, gl	ol, sp, ilm, gl	gl
1160	ol, sp, gl	ol, sp, gl	pl, ol, gl, (ore)		(ol) (ilm) (ore)gl
1156			pl, ol, gl(ore)		
1153	ol, sp, gl			ol, sp, ilm, px, gl	
1152[2]		ol, sp, gl	pl, ol, sp, gl		ol, sp, ilm(arm)gl
1151	ol, sp, pl, ilm, gl				
1149[2]	ol, sp, pl, ilm, gl	ol, sp, gl		ol, sp, ilm, px, gl	
1145	ol, sp, pl, ilm, px, gl	ol, sp, gl		ol, sp, ilm, px, gl	*ol (pl) ilm(arm)gl
1142	ol, sp, pl, ilm, px, gl	pl, ol, sp, gl[4]		ol, sp, ilm, px, gl	ol (pl) ilm(arm)gl[9]
1140[2]	ol, sp, pl, ilm, px, gl		pl, ol, sp, ilm(pig)gl	ol, sp, ilm, px, gl	(pl)ol, sp, ilm, gl
1133	(ol)sp, pl, ilm, pig, aug, gl[3]	ol, pl, sp, px(ilm) arm? gl[5]	pl, ol, ilm, px, gl	ol, sp, ilm, aug, pig, gl[7]	pl, ol, px, ilm, gl
1129[2]		ol, sp, pl, px, ilm(arm)gl	pl, px, ilm(gl)	ol, pl, sp, ilm, aug, pig, gl	pl, ilm, aug, pig, gl
1120	sp, pl, ilm, aug, pig, gl	ol, sp, pl, aug, pig, ilm, gl[6]	pl, px, ore, (gl)	sp, pl, ilm, aug, pig, gl	
1108	sp, pl, ilm, aug, pig, gl	(ol)pl, px, ilm(gl)	solid	sp, pl, ilm, aug, pig, gl[8]	pl, px, ore(gl)

Key: arm = armalcolite; aug = augite; gl = glass; ilm = ilmenite; ol = olivine; ore = undifferentiated opaque, possibly including quench products; pig = pigeonite; pl = plagioclase; px = pyroxene; sp = spinel.

[1] Synthetic charges made up to compositions listed in Table 2, column 2, 3.

[2] These experiments conducted at an oxygen fugacity one power of ten lower than that of the Fe/FeO equilibrium. No quench ore forms in these experiments and identification of the opaque phases is more satisfactory than in the other experiments which were conducted at the oxygen fugacity of the Fe/FeO equilibrium.

[3] Glass analysis in Table 2, column 5; glass, ilmenite, plagioclase, augite, pigeonite and spinel analyses in Table 6.

[4] Glass analysis in Table 6.

[5] Glass analysis in Table 2, column 6, and Table 6.

[6] Glass, olivine, plagioclase, augite and ilmenite analyses in Table 6.

[7] Glass analysis in Table 2, column 3.

[8] Ilmenite, augite, plagioclase and glass analyses in Table 6.

[9] Glass analysis in Table 2, column 8.

TABLE 6
Analyses of phases from experimental charges (see Table 5)

	SiO_2	TiO_2	Al_2O_3	Cr_2O_3	FeO	MnO	MgO	CaO	Na_2O	K_2O	Totals
From 10020 (1133°C)											
(1)	42.48	8.93	9.70	0.08	18.91	n.d.	5.94	11.45	0.43	n.d.	97.92
(2)	45.55	0.27	33.67	n.d.	0.95	n.d.	0.30	17.97	0.77	n.d.	99.48
(3)	51.62	1.39	1.06	0.31	15.81	n.d.	21.24	6.21	0.02	n.d.	97.66
(4)	49.41	2.49	3.17	0.47	15.01	n.d.	15.52	14.67	0.07	n.d.	100.81
(5)	0.12	54.67	0.38	1.34	35.80	n.d.	7.03	0.51	n.d.	n.d.	99.85
(6)		18.1		7.3	39.7						
From 10062 (1142°C, 1133°C and 1120°C)											
(7)	43.31	7.62	10.19	0.13	18.29	n.d.	6.13	11.76	0.44	n.d.	97.87
(8)	44.02	8.23	9.55	0.08	19.17	n.d.	6.01	11.58	0.40	0.12	99.16
(9)	42.64	7.97	9.53	0.04	20.32	n.d.	5.28	11.06	0.45	n.d.	97.29
(10)	44.28	0.15	34.23	0.01	0.74	n.d.	0.17	18.75	0.77	n.d.	99.10
(11)	46.72	4.36	4.63	0.61	12.26	n.d.	12.69	17.77	0.10	n.d.	99.14
(12)	35.87	0.35	0.14	0.06	34.88	n.d.	28.23	0.56	nil	n.d.	100.09
(13)	0.24	55.37	0.36	0.77	37.26	n.d.	5.40	0.69	0.01	n.d.	100.10
From 10017 (1108°C)											
(14)	46.00	6.72	10.35	0.05	18.49	0.21	4.40	10.69	0.74	0.59	98.24
(15)	48.64	0.36	32.44	n.d.	0.97	n.d.	0.20	16.29	1.59	0.20	100.69
(16)	50.21	2.51	2.64	0.60	11.80	0.19	15.35	16.40	0.11	0.01	99.82
(17)	0.34	55.09	0.31	1.05	37.97	0.33	5.05	0.60	n.d.	n.d.	100.74

From 10020, 1133°C: 1 = glass, 2 = plagioclase An_{93}, 3 = pigeonite, 4 = augite, 5 = ilmenite, 6 = spinel.

From 10062: 7 = glass, 1142°C, 8 = glass, 1133°C, 9 = glass, 1120°C, 10 = plagioclase, An_{93}, 11 = augite, 12 = olivine, Fo_{59}, 13 = ilmenite, 10–13 = all from 1120°C run. The spinel has a high Ti/Cr ratio.

From 10017, 1108°C: 14 = glass, 15 = plagioclase, An_{85}, 16 = augite, 17 = ilmenite.

General points to note are the relatively small degree of evolution of the liquid compositions with falling temperature; the very high MgO in ilmenites, which compare with the highest reported from rock 10045 [10]; the calcic plagioclase An_{93} at 1133°C and 1120°C, comparing closely with the reported phenocrysts, and the high FeO and MgO contents of these feldspars; the relatively calcic feldspar (An_{85}) in 10017 at 1108°C, still appreciably more calcic than the majority of feldspar in this rock; and the relatively iron-rich olivine (Fo_{59}) present at 1020°C in 10062, considerably less magnesian than the reported phenocrysts which presumably grew at higher temperatures.

of these minerals from the *average* magma composition is accompanied by that of anorthite, olivine, calcium-poor pyroxene, and ilmenite, all of which contain relatively low concentrations of Cr and V. The total crystal extract does not contain conspicuously more of either element than do the liquids themselves. At earlier stages, when augite, armacolite and spinel would not have been accumulating phases, Cr and V might have been *increasing* in the residual liquids during fractionation.

In our experiments chromium is indeed rapidly depleted in the residual liquid, principally due to its high concentration in the spinel formed in our experiments. This effect is a direct product of the relatively high-oxygen fugacity of our experiments (that of the iron-wüstite equilibrium). At the slightly lower

oxygen fugacities, which prevailed during the evolution of the lunar rocks, high Cr^{2+}/Cr^{3+} ratio will be met and the extraction of chromium in both spinel and pyroxene consequently reduced. Unfortunately we have not yet devised a suitable routine experimental technique for operating at lower oxygen fugacities with reliable control over the charge composition, and cannot quantify this effect. Inspection of the chromium content and relative proportions of the phases which first formed from the liquid in the natural situation is, however, sufficient to demonstrate that chromium would not be depleted in the residual liquid.

13. Summary

Plagioclase (An_{93}) phenocrysts were present in the Apollo 11 high-titanium basalt magma on eruption. Although the percentage of phenocrysts was low, anorthite, olivine, pyroxenes, ilmenite and spinel were all present. The liquid which carried these phenocrysts had the same composition as the average rock exposed at the site, and the same composition as the experimentally produced low-pressure cotectic liquids in equilibrium with anorthite, olivine, pyroxene, ilmenite and spinel. It follows that the lavas had the compostion *and* temperature of low-pressure cotectic liquids when they were erupted. Ilmenite and spinel sinking (and possible plagioclase flotation) produced a marked composition gradient within the lava flow. Subsequent regolith formation has not entirely destroyed this effect, the large hand specimens which were preferentially derived from a relatively deep level being enriched in the constituents of ilmenite and spinel, relative to the average magma composition. The study of phase equilibria in these phenocryst-enriched hand specimen compositions on the assumption that they represent the average magma leads to an impression of significant departure from low-pressure cotectic character, although the departure is much less than suggested by uncontrolled visual estimates of crystallinity in experimental charges. Experimental crystallization of two new samples of the ophitic, low-potassium group lava confirms the low-percentage crystallinity at plagioclase appearance indicated from the petrography.

The simultaneous saturation of the high-titanium basalt magma with six crystalline species at low-percentage crystallinity is best explained by derivation of the magmas from the very late residual liquid in a strongly fractionated high-level igneous body, lava lakes of mare dimensions being the obvious possibility. High TiO_2, high FeO, high Fe/Mg ratio, high rare-earth elements, extreme europium anomaly, high zirconium and other non-volatile incompatible elements in the magma are all by-products of this process. Neither chromium nor vanadium would be rapidly depleted during the fractional crystallization of the average magma composition, because the high concentrations noted in some of the minerals are diluted in the total crystal extract by the larger amount of chromium- or vanadium-poor minerals which crystallise simultaneously.

Crystallization of the high-titanium basalt approximates to that of an eutectic liquid; large amounts of crystallization being possible without large changes in the major-element composition of the residual liquid, although incompatible elements increase many-fold in concentration in the remaining liquid. The high- and low-potassium/high-titanium basalts at the Apollo 11 site are related as later and earlier liquids in such a process, which also offers a coherent explanation of the differing rubidium/strontium systematics of the two groups.

The last stages in the fractional crystallization of the Mare Tranquilitatis lava lake occurred about 3.7 by ago. Neither the time of the original filling of the lava lake, nor the composition of the parental magma which filled the basin can be inferred directly from available data.

In a situation likely to arise in the early stages of exploration of any planet, where field relationships were lacking and no in situ samples collected, the techniques of experimental petrology were successful in identifying the unusual petrologic character of the magmas yielding a conclusion otherwise reached only by those studying the rare-earth elements. Plagioclase phenocrysts, which were not positively identified in the early petrographic studies, were found during a detailed search instigated by the following reasoning:

The average magma was cotectic, with both plagioclase and ilmenite (inter alia) saturated in the liquid. Ilmenite crystals could not be present in such a liquid, nor sink to enrich the base of the flow in TiO_2, unless plagioclase crystals were also present. In these

P.74

MELTING RELATIONS OF MORE PRIMITIVE MARE-TYPE BASALTS 14053 AND M (REID 1970); AND OF BRECCIA 14321 AND SOIL 14162 (AVERAGE LUNAR CRUST?).

Biggar, G.M., Ford, C.E., Humphries, D.J., Wilson, G. and O'Hara, M.J.
Grant Institute of Geology, Edinburgh University, EH9 3JW, Scotland.

The olivine-poor basalt, 14053, has Mg/Mg + Fe ~ 0.48 (contrast .40-.38 for near cotectic Apollo 12 basalts) and represents a more primitive, less differentiated type than previous mare basalts. After opaque spinel, olivine is the liquidus silicate (1230°C), plagioclase beginning to crystallize at c. 1190° when the charge is c. 5% crystalline, pyroxene and an opaque phase also being present 15°C lower when the charge is perhaps 20% crystalline. Using glass (1400°C) as a starting material the entries of olivine and plagioclase were c. 10°C lower, but that of pyroxene higher. M is a more olivine-rich composition (Mg/Mg + Fe ~ 0.52), and shows substantial olivine crystallization prior to plagioclase entry, which occurs at a lower temperature than in 14053. The relationship between Mg/Mg + Fe, and cotectic crystallization temperatures in Apollo 11, 12 and 14 basalts is summarised in figure 1. 14053 is not conspicuously close to a low pressure 4-phase cotectic liquid composition, and differs from previous mare surface basalts in having plagioclase as second silicate (cf. Apollo 15 samples). It may be an earlier stage liquid, suitable as a parent for a fractionation trend leading towards Apollo 12 lavas. Owing to its relatively low Mg/Mg + Fe it cannot be a primary magma derived from a mantle which had earlier yielded magmas of high Mg/Fe + Mg (e.g. majority of Apollo 14 samples inc. 14310).

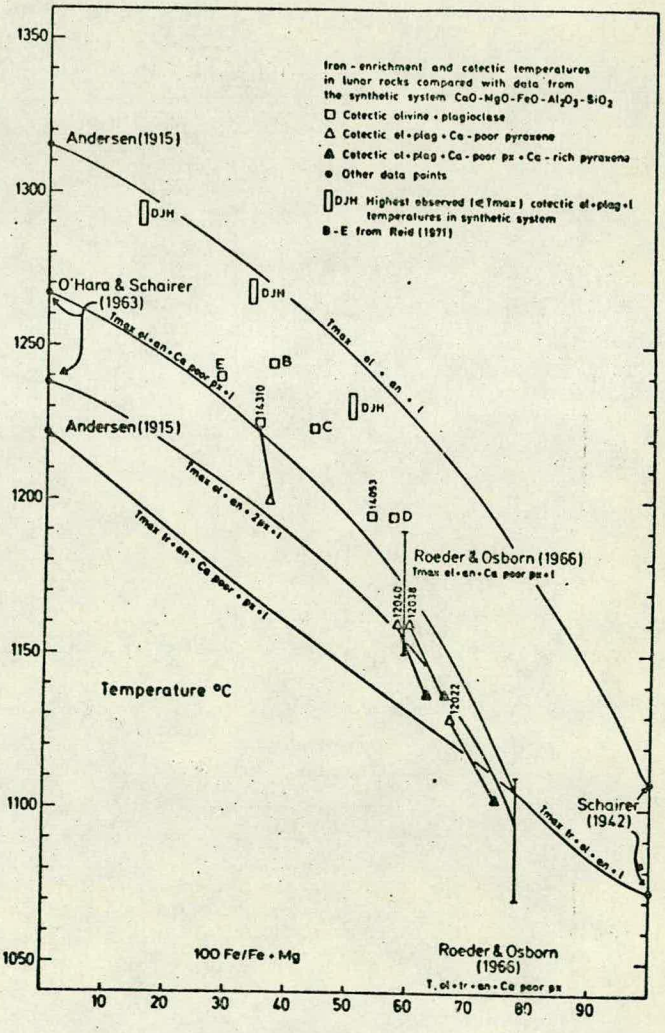


Fig. 1

Interpretation of phase relations in 14321 (breccia) and 14162 (soil) can be attempted via at least three naive assumptions; that the samples represent(1) average lunar crust (2) average parental magma of some intra-crustal preImbrian igneous series (3) some linear and meaningful mixture of crust and uppermost mantle from the site of Mare Imbrium.

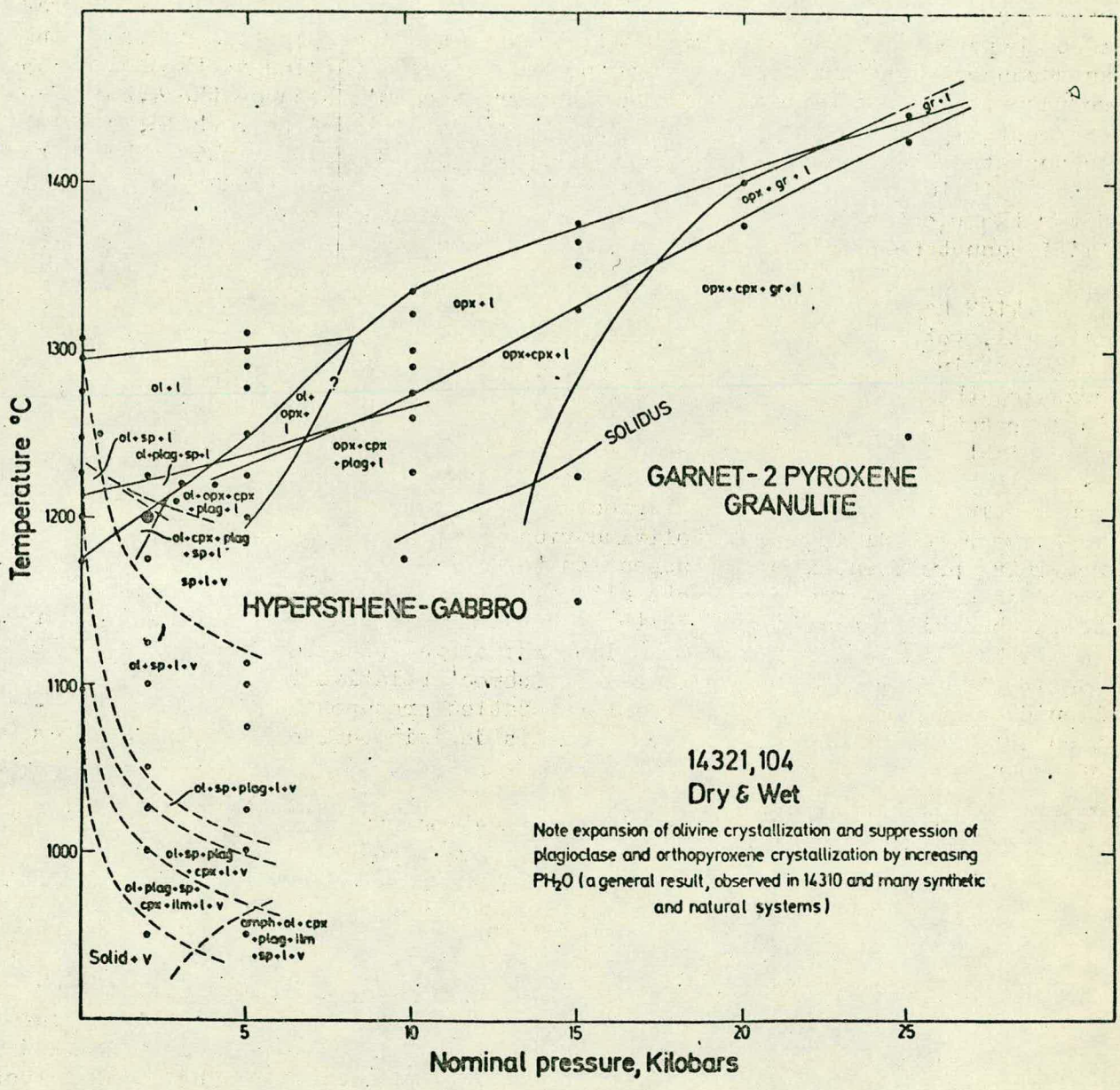


Fig. 2

MELTING RELATIONS 14053, 14321

Biggar, G.M.

P.76

14321 shows extensive olivine and spinel precipitation before plagioclase entry at 1 atmosphere. Increase of pressure suppresses the olivine liquidus, replacing it first by orthopyroxene, then by garnet (fig. 2). Under water vapour pressures of c. 1 kb, spinel replaces olivine as liquidus phase. Whichever assumption is adopted, an ultimate uppermost lunar mantle, of $Mg/Mg + Fe > 0.87$ would be indicated. On assumptions (1) or (2) the magma would either have to be directly derived from great depth (>160 kms if orthopyroxene is to be a residual phase in the lunar mantle) or represent an advanced partial melt of its source rock leaving olivine as the sole residuum. Such considerations are, however, academic because the 4.26 gm fragment, 14321, is probably not representative of 14321 as a whole; and because the breccias are known to contain clasts of feldspar-phyric basalts such as 14310, 14073, which are in turn known to have suffered alkali loss after their extrusion and before incorporation in the breccias. Data on 14321 cannot be meaningfully interpreted by any of the three assumptions.

14162 has a greater claim to be regarded as a fair average of Fra Mauro material, yet it must be contaminated by mare-type basalts (Reid 1971) and must contain a contribution from rocks which suffered alkali loss after reaching the lunar surface. Data for this sample are equally unsuitable for interpretation by hypotheses (1) and (3), but might lend themselves to approximate interpretation by hypothesis (2). At 1 atm., plagioclase is the liquidus phase, rapidly followed by olivine. As a near cotectic liquid in equilibrium with olivine and plagioclase at 1 atm. it could serve as a low pressure parental liquid for olivine-rich precipipitates, plagioclase remaining preferentially in suspension to yield feldspar-phyric basalts. Remixing of these two components with a bias towards the olivine component could then yield a mixture with the properties of 14321. However, feldspar-phyric basalt 14310 contains much less phenocryst plagioclase than would be required to explain the plagioclase enrichment relative to the cotectic liquid, or to 14162, hence this interpretation presuposes extensive resorption of phenocrysts against which there is definite evidence in the results of Brown and Peckett (1971).

We conclude, therefore, that interpretation of the relationships between samples 14162, 14321 and the lunar crust and mantle requires more sophisticated assumptions than are entertained here.

P.77

EXPERIMENTAL CRYSTALLIZATION OF APOLLO 11 AND 12 LAVAS - A RE-EXAMINATION, Biggar, G.M., O'Hara, M.J., Humphries, D.J., and Peckett, A., Grant Institute of Geology, Edinburgh University, Scotland.

Reexamination was aimed at resolving inter-laboratory discrepancies in data and interpretation of Apollo 12 basalts. Plagioclase remains in 12018, 12020, 12038 and 12040 at 1153°C in 3-day runs whether rock powder or glass is used as starting material. Reversal of plagioclase entry by holding 4-5 hours at upper temperature, then 5-16 hours at lower, has been accomplished on 8 samples (figure 1). Cotectic liquid compositions obtained from glass or rock powder were very similar in 12038, 12040. Temperatures are calibrated at m.p. of gold 1064°C and Li_2SiO_3 (1203°C).

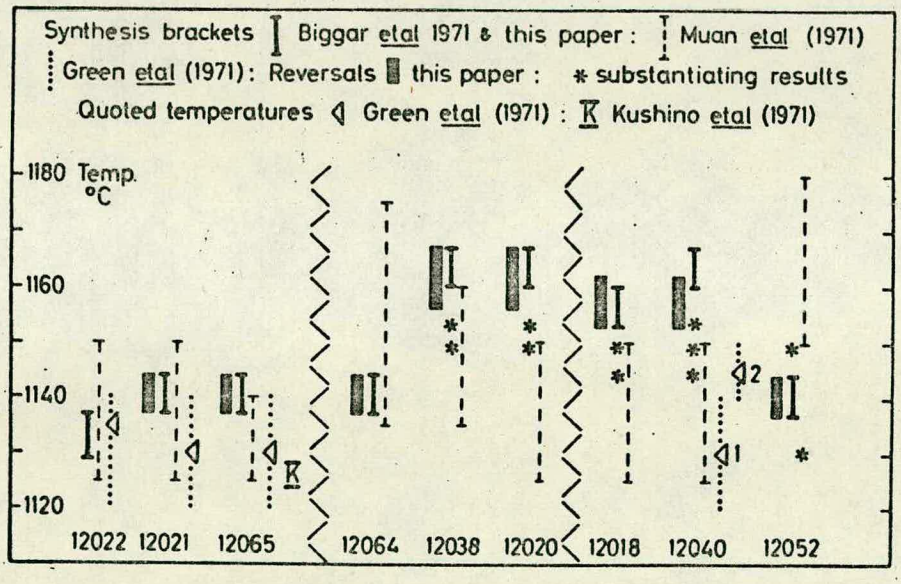


Fig. 1. Comparative results for plagioclase entry

Calculation, from analysed glass and crystal phase composition, of percentage crystals present at plagioclase entry yields values as low as one half of those quoted by other workers relying on visual estimation. Calculation of the putative residual cotectic liquids, by extracting the visually estimated amount of crystals, yields liquids which are enriched in potential plagioclase, and depleted in potential hypersthene relative to the analysed liquids (figure 2); substantial negative MgO, and some normative nepheline (in 'presence' of pigeonite crystals) appear in some of these calculations.

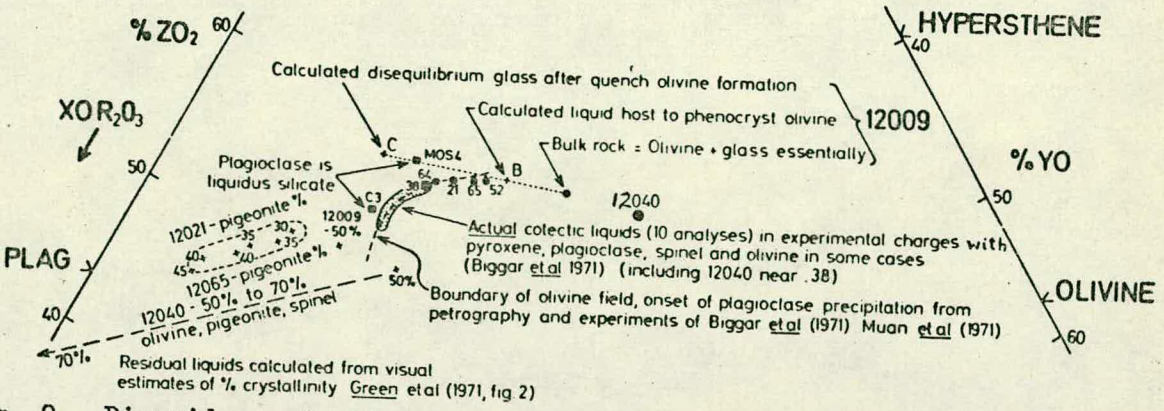


Fig. 2. Diopside projection contrasting analysed and calculated cotectic liquids

The composition of the basaltic magma supplied to the surface at the Apollo 12 site is best sampled by glass and lithic fragments in the soil, or by the bulk soil; or even by averaging the total weight of rocks distributed for chemical analysis (biased towards extremes? N.B. also that glass analyses will not include iron reduced by impact heating in vacuum). These compositions resemble the analysed cotectic liquids but differ from phenocryst-enriched mixtures like 12040 (figure 3). K9, K10 are impact produced glass fragments as rich in potential olivine as the phenocryst-enriched rocks. The glassy sample 12009 shares the thermal history (rapid chilling from > 1200°C) of the impact glasses, but differs from that of most other rock samples (slower cooling from c. 1170°C-1150°C). 12009 may represent a splash of impact remelted phenocryst-enriched lava.

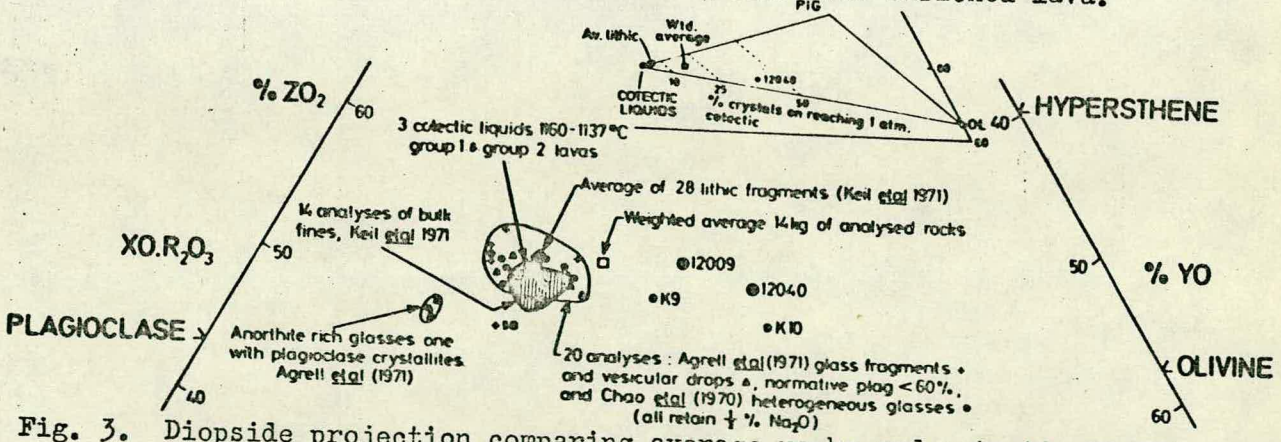


Fig. 3. Diopside projection comparing average rocks and cotectic liquids

The probability of the observed close approach of erupted lava compositions to low pressure cotectic liquid compositions being due to coincidence with a higher pressure primary magma composition is ~ 3 in 1000; in Apollo 11 ophitic group it is ~ 5 in 10,000, but reaches ~ 3 in 100 in the intersertal group. It is more probable that crystal-liquid fractionation at low pressures has controlled the observed lava compositions.

P.79

Prinz et al. (1971 Contrib. Mineral. Petrol. 32, 211-230) reported average composition for Apollo 11 basalts based on analyses of 21 low potassium and 18 high potassium lithic fragments in the soil. These are significantly lower in Ti, Fe, Mn and higher in Si, Al, than averages of analysed rock specimens, and accordingly much closer to the experimentally produced cotectic liquid compositions (cf. Apollo 12 lithic fragments, fig. 3). Selected figures for comparison are:-

	SiO_2	TiO_2	Al_2O_3	FeO	MgO	CaO
High K fragments	42.8	9.6	10.6	18.0	7.0	10.7
Low K fragments	42.9	8.7	11.8	17.0	7.2	11.4
Cotectic liquid (Biggar et al. 1970; average of 2)	43.0	8.8	10.3	17.7	6.5	11.3

The larger rock samples may have been selectively derived from the base of a flow into which ilmenite had accumulated. The average soil is yet more feldspathic than these averages and may reflect the overlying and complementary pole of the differentiation, now fragmented to form regolith.

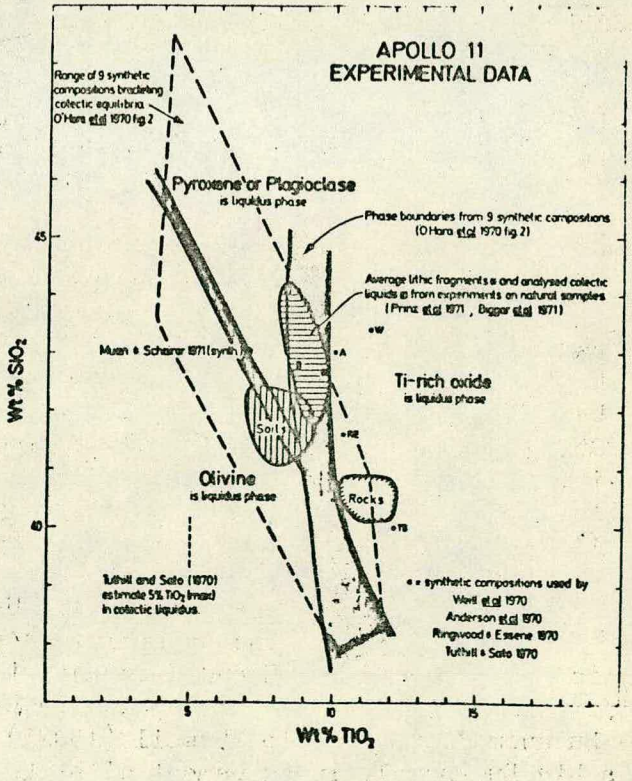


Fig. 4

SiO_2-TiO_2 plot of phase data for synthetic and natural Apollo 11 compositions.

P.274

EXPERIMENTAL PETROLOGY OF HIGH ALUMINA BASALT, 14310, AND RELATED COMPOSITIONS. C.E. Ford, D.J. Humphries, G. Wilson, D. Dixon, G.M. Biggar and M.J. O'Hara. Grant Institute of Geology, West Mains Road, Edinburgh EH9 3JW, Scotland.

At atmospheric pressure anorthite is liquidus silicate phase, joined by spinel, then by olivine when c. 30% crystalline (the chance of this happening in a random high pressure liquid is > 0.67) and subsequently by pyroxene (fig. 1). The composition of 14310 is far removed from atmospheric pressure cotectic liquids and develops iron as a separate phase near or above the silicate liquidus; had this happened and the iron been separated, the relatively high Ni content of 14310 would not have been maintained. 14310 cannot have suffered appreciable fractional crystallization as a system with the present water and alkali contents within, say, 1 km of the lunar surface, nor as a system with its present oxygen content under any conditions. This, and its high Mg/Mg + Fe relative to Apollo 11 and 12 basalts, show 14310 is a more primitive material from the lunar interior than any previously investigated by us. As pressure is increased, however, anorthite, spinel or garnet are the liquidus oxide or silicate phases; none of these phases is suitable as the crystalline residuum from partial melting of the lunar mantle, hence 14310 is not a primary magma. In the presence of water vapour the plagioclase liquidus is rapidly suppressed and replaced by spinel. Olivine supercedes plagioclase as the first silicate at c. 3 kb, equivalent to c. 55 kms depth. The 8% plagioclase phenocrysts in 14310, therefore, indicate derivation from strictly limited pre-eruption temperature and pressure conditions (fig. 2). Restoration of volatilized alkalis (Brown and Peckett 1971) and probable losses of H_2O, O_2, to the present composition of 14310 leads to compositions similar to terrestrial high alumina basalts. Restoration of alkalis lowers the plagioclase liquidus and in the presence of water vapour at c. 0.25-0.5 kb (5-10 kms) the resultant composition is nearly cotectic with respect to olivine, spinel and plagioclase (spinel-troctolite), and could have been derived from a fractionating magma chamber (Brown and Peckett 1971) precipitating those crystalline phases, whose liquid would contain c. 0.25-0.5% H_2O. Derivation of such a calc-alkaline magma from a terrestrial-type lunar upper mantle, with Mg/Mg + Fe $>$ 0.87, cannot be excluded.

The compositions B, C, D and E, identified by Reid (1971) as constituents of lunar soil, resemble 14310 and also have plagioclase as liquidus phase at atmospheric pressure, most displaying extensive feldspar crystallization before the appearance of olivine. Chemical differences between the compositions are not, however, explicable solely in terms of plagioclase fractionation. Any effective fractionation scheme to link these compositions presupposes circumstances under which the plagioclase liquidus field is much

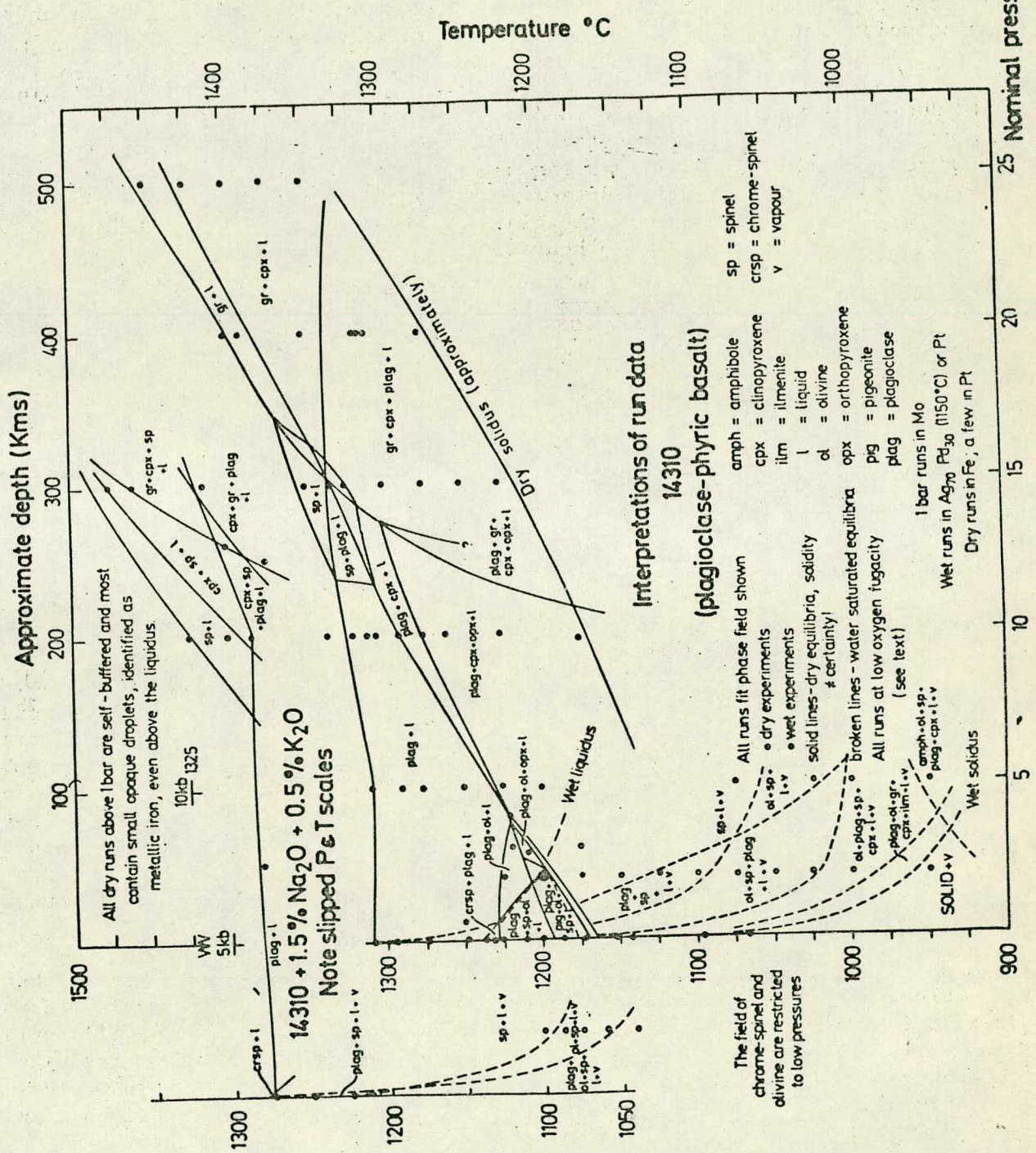
EXPERIMENTAL PETROLOGY 14310

C.E. Ford

P.275

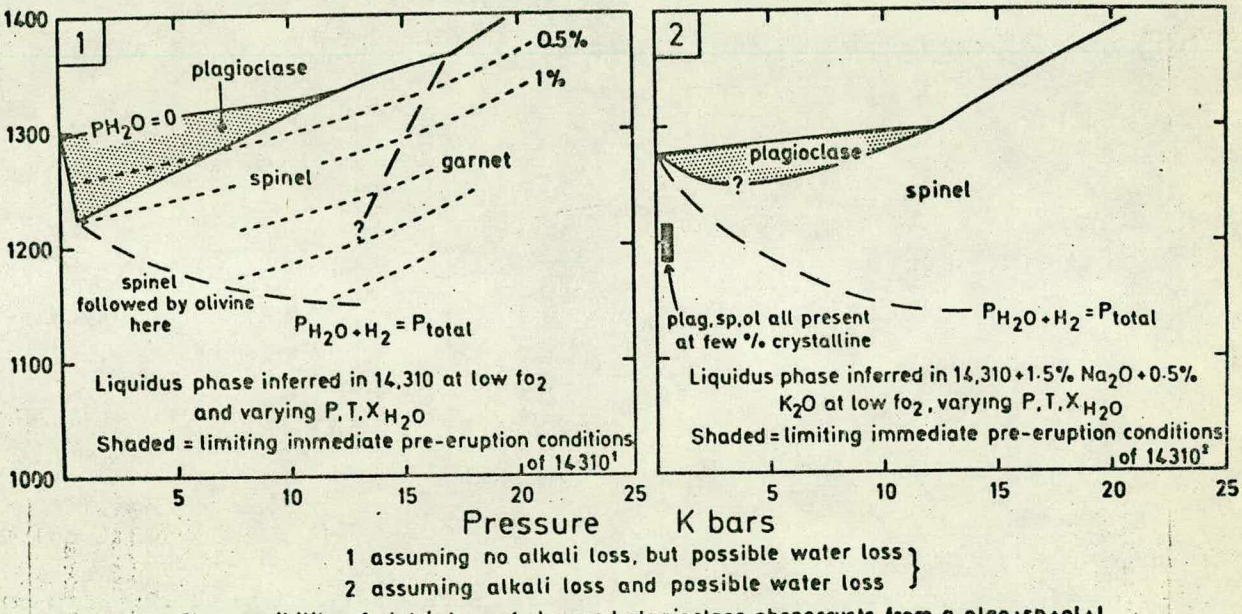
Fig. 1

Experimental data for 14310



reduced - i.e. much higher pressure (>300 kms!); or presence of water combined with a moderate increase of pressure (>10 kms); or some combination of these factors. Restoration of alkalis to compositions B, C, D and E does not greatly change the situation, plagioclase being retained as a near liquidus phase in C, D and E and spinel crystallization enhanced (cf. 14310) with additions of 0.5% K_2O + 1% or 2% Na_2O. In B the near simultaneous appearance of plagioclase and olivine is replaced by an olivine liquidus.

Using glass (1400°C) as starting material, near liquidus plagioclase in 14310 nucleated in sprays and could be misinterpreted as quench growths; olivine and pyroxene were encountered at slightly higher temperatures than when rock powder was used as starting material, but essentially similar atmospheric pressure quenching data were obtained in each case. The higher temperature entry of olivine in the glass starting material was eliminated by increasing run lengths from 5 hours to 3 days.



1 assuming no alkali loss, but possible water loss
2 assuming alkali loss and possible water loss

The possibility of elutriation of observed plagioclase phenocrysts from a plag+sp+ol+l situation has NOT been taken into account here.

Fig. 2

THE APOLLO 15 LUNAR SAMPLES

EDITED BY

J. W. CHAMBERLAIN
AND
C. WATKINS

Reproduced and Distributed by
The Lunar Science Institute
3303 NASA Rd. 1
Houston, Texas 77058

1972

PHASE EQUILIBRIA AND ORIGIN OF APOLLO 15 BASALTS ETC. D.J.Humphries, G.M. Biggar and M.J.O'Hara. Grant Institute of Geology, Edinburgh University.

Samples 15058, 15076, 15499 of types I and II show little or no olivine crystallization before pigeonite entry, olivine reacting out before anorthite entry, at which point the charges are substantially crystalline (fig. 1).

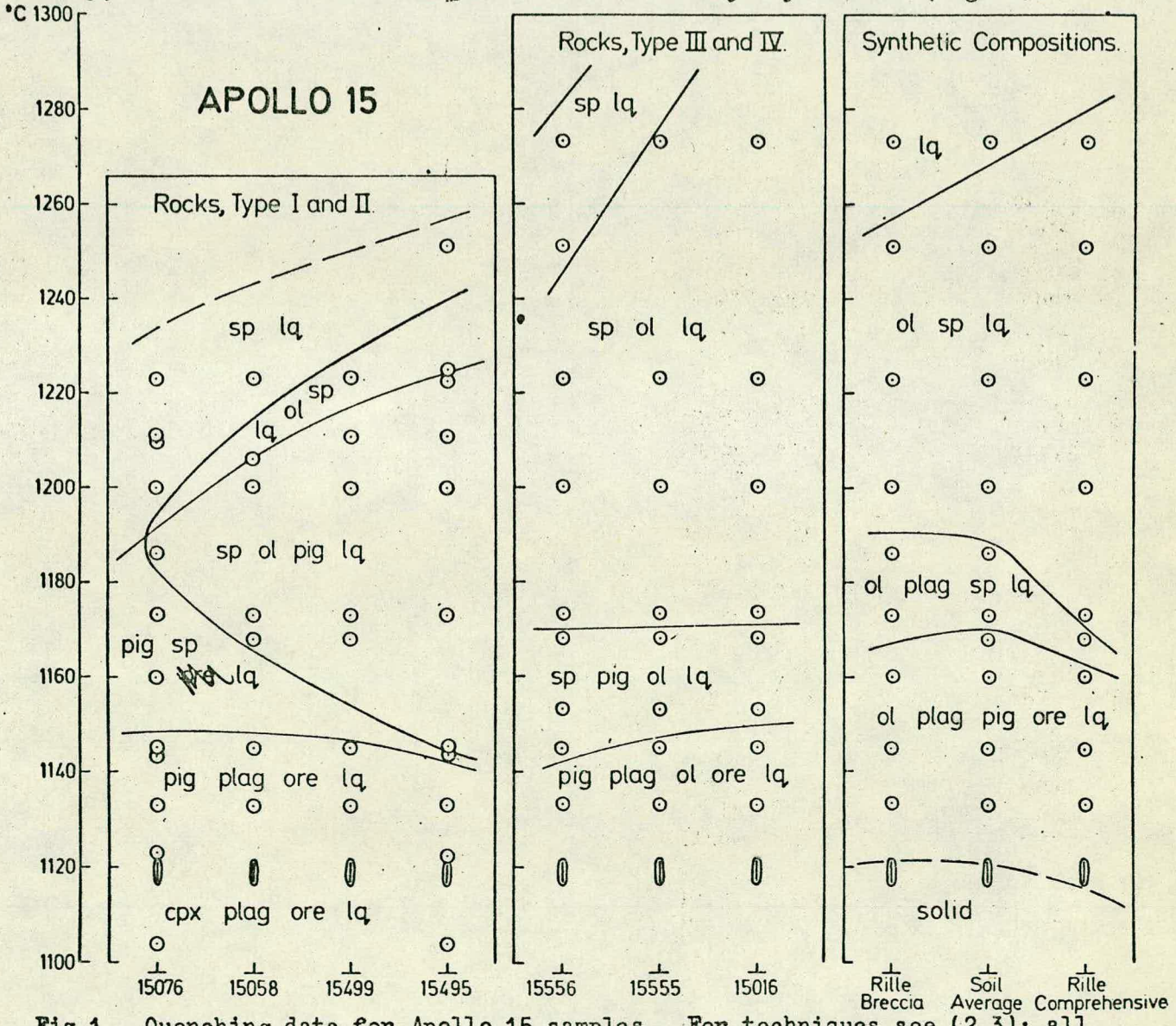


Fig 1. Quenching data for Apollo 15 samples. For techniques see (2,3); all refer to fO_2 = Fe/FeO equilibrium, temperature to IPTS 1968 scale. Abscissa has no scale significance.

PHASE EQUILIBRIA AND ORIGIN OF APOLLO 15 BASALTS ETC.

D.J. Humphries

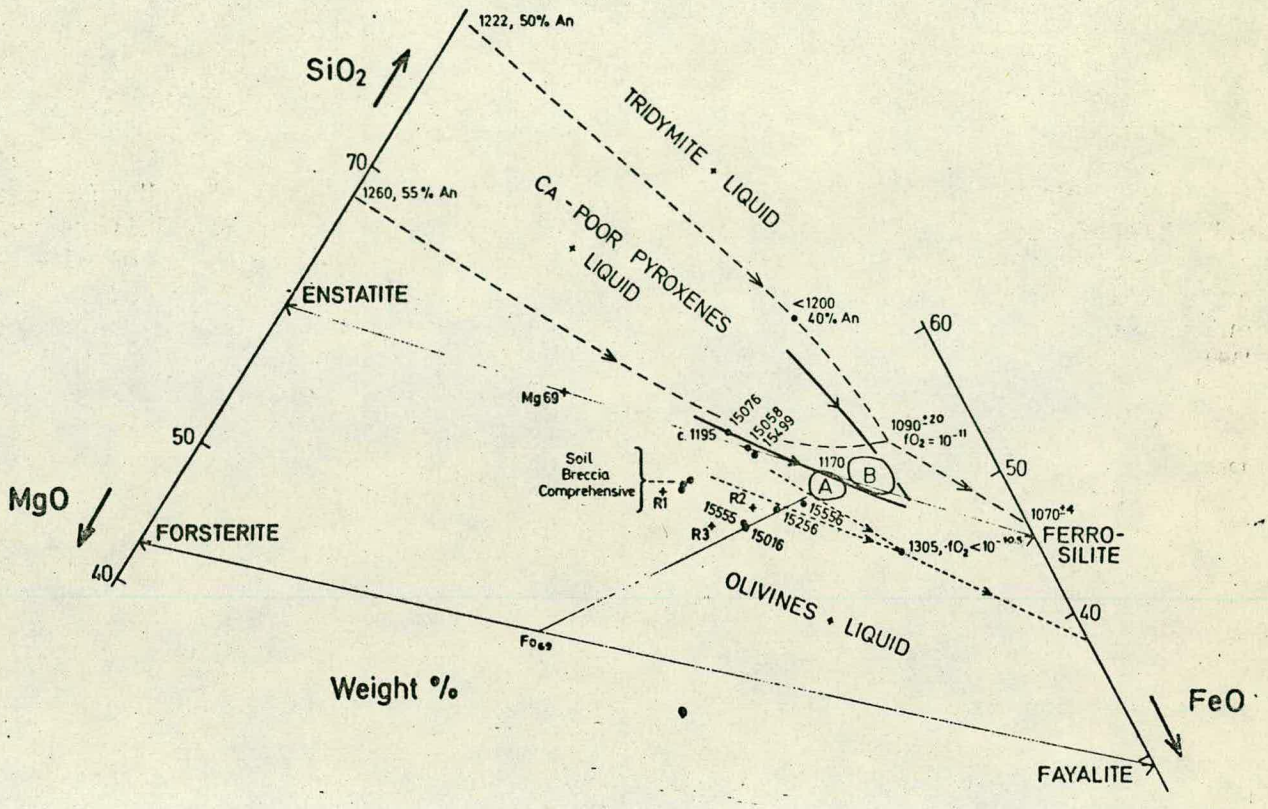


Fig 2. Projection into MgO-FeO-SiO2 from albite, orthoclase, anorthite, $CaSiO_3$, TiO_2, Cr_2O_3, showing phase boundaries in equilibrium with metallic iron in pure system MgO-FeO-SiO2 (5) as fine broken lines; phase boundaries at anorthite saturation at $fO_2 = 10^{-11}$ atm. in MgO-FeO-Fe_2O_3-$CaAl_2Si_2O_8$-SiO2 (6) as coarse broken lines, marked with temperatures and normative anorthite content of liquids. Investigated natural and synthetic Apollo 15 compositions are shown, with phase boundaries (solid lines) and temperatures consistent with our data at fO2 = Fe/FeO, quite close to anorthite saturation. Fields A, B are estimates of liquid composition on eruption in types III, IV and types I, II lavas respectively consistent with petrography (1). An olivine control from Fo69 through types III, IV samples is indicated. The compositions of preferred mare-type glass compositions (7) at site shown by crosses.

Samples 15016, 15555, 15556 of types III and IV show high temperature olivine liquidus followed by pigeonite (fig 1). Types III and IV are related essentially by possible olivine accumulation or fractionation (4) and are substantially crystalline at anorthite entry. Data are also reported for 15495. Synthetic mixtures of the compositions of the Rille Comprehensive 15601, Rille breccia 15558, and an average of soil 15471 and 15501 samples (1) display olivine liquidus joined by anorthite before pigeonite, and at a higher temperature than in the lava samples (fig 1).

Fig 2 interprets these phase equilibria data in terms of Mg/Fe variation and silica saturation showing the estimated composition of the liquid phases in the lavas on eruption. Relative to bedrock, the comprehensive, breccia and soil appear enriched in an Mg-pyroxene bearing component.

PHASE EQUILIBRIA AND ORIGIN OF APOLLO 15 BASALTS ETC.

D.J. Humphries

Fig 3 interprets the same data in terms of variation in olivine, pigeonite and anorthite crystallization, again showing olivine control through types III, IV samples, and the estimated liquid composition in these lavas on eruption. Comprehensive, breccia and soil samples as well as the mare-type glasses are seen to be significantly enriched in anorthite relative to bedrock i.e. in a relatively magnesian norite or pyroxene-anorthosite component (see above).

All four lava types are samples of a consolidated mixture of dense phenocrysts (olivine, pigeonite) in liquids which were close in composition and

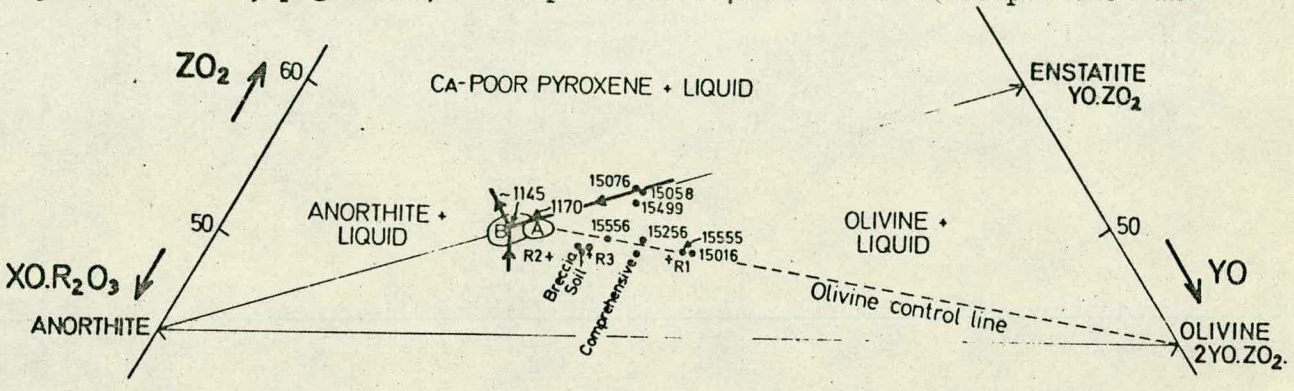


Fig 3. Projection from diopside into anorthite-olivine-silica (see 2) showing investigated samples, three preferred mare-type basalt compositions (7), and liquidus phase boundaries consistent with data of fig 1. Fields A,B as in fig 2.

temperature to those in cotectic equilibrium at low pressure with olivine, pigeonite and plagioclase. Phenocryst assemblages indicate eruption temperatures ~ 1170°C (types III,IV) and ~ 1150°C (types I,II) and far below the liquidus temperatures of many of the samples. At the Apollo 12 site, rock samples were markedly biased from the average magma compositions towards those of the dense phenocrysts (3,8). The same may prove true at the Apollo 15 site. If the average lava compositions are identical with those of the rock samples studied, a satisfactory explanation why the low viscosity magmas were erupted fully equilibrated to the low pressure cotectic and richly porphyritic, yet display only minor accumulation of the dense crystals is hard to devise. Crystal sinking could not have removed olivine without pyroxene from a parental magma common to all four lava types; at least two parental lava flows are required to explain the differences in phenocrysts, and eruption temperature between lava types I, II and types III, IV.

Fig 4 displays the same data as figs 2, 3 to show relationships between components other than olivine, which confirms the addition of an anorthite + pigeonite component to produce comprehensive, breccia and soil samples from bedrock, and combined with figs 2, 3 indicates that any relationship between types I and II lavas on the one hand, and types III, IV on the other must be dominated by pyroxene-liquid equilibria, with possible participation of olivine or silica.

One possible relationship is illustrated in figs 5,6. Parental magma A of types III, IV gave rise by essential anorthite + pigeonite fractionation at some slightly elevated pressure within the lava lake (broken phase boundaries apply) to parental magma B of types I, II. An escape of some of the liquid A

PHASE EQUILIBRIA AND ORIGIN OF APOLLO 15 BASALTS ETC.

D.J. Humphries

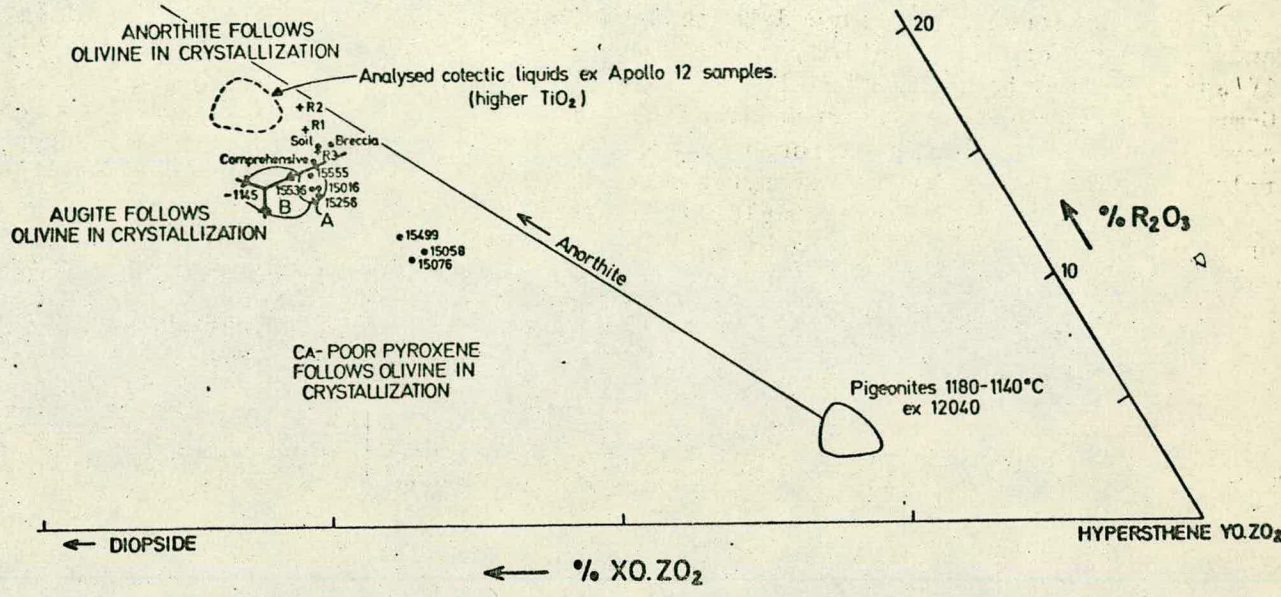


Fig 4. Projection from olivine into hypersthene-diopside-alumina etc. (see 2, fig 6) showing the investigated compositions, and fields A, B as in fig 2. Low pressure phase boundaries for Apollo 15 samples show small displacement relative to more TiO2 rich Apollo 12 results (see 2).

gave rise to the earlier, lower flow unit; expansion across composition A of the olivine liquidus volume because of the pressure release (solid phase boundaries apply) led to precipitation and local accumulation of olivine to yield samples such as 15016, 15555, 15556, in liquid fraction A'. On escape of liquid B, the olivine liquidus volume did not expand sufficiently to cover this composition, which precipitated pigeonite, yielding liquid B' as matrix to local accumulations of crystals, as in samples 15078, 15076, 15499.

A second interpretation involves fractionation at low pressure only. Fractionation and accumulation of crystals within parental magma A yields samples of types III, IV character until residual liquid A' is reached. Thereafter evolution is by pigeonite fractionation and accumulation only,

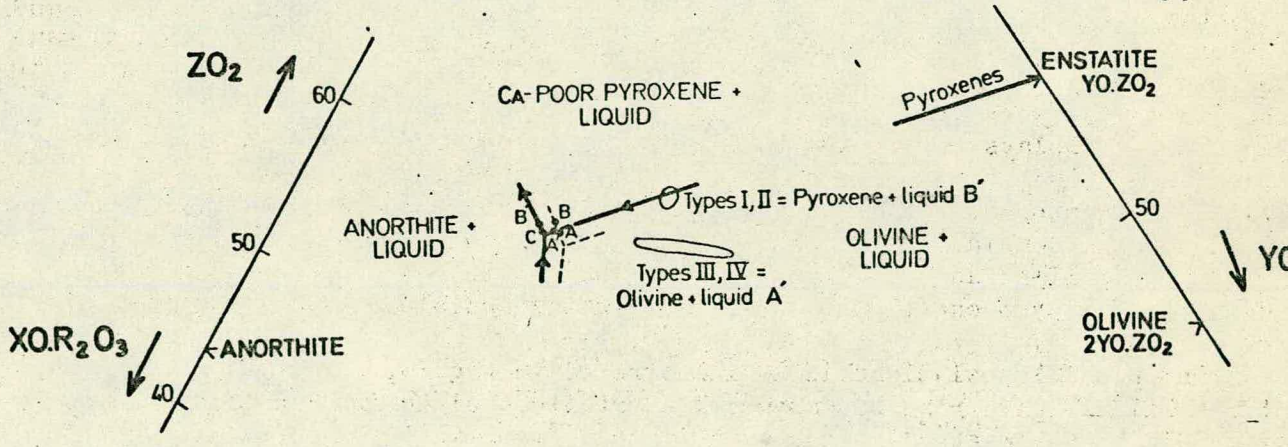


Fig 5. Diopside projection into anorthite-olivine-silica. See text.

PHASE EQUILIBRIA AND ORIGIN OF APOLLO 15 BASALTS ETC.

D.J. Humphries

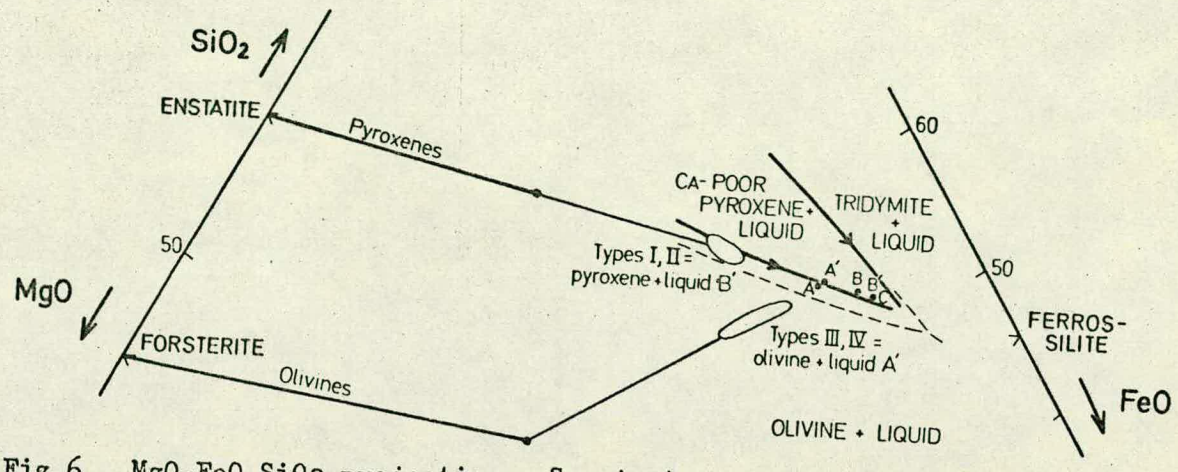


Fig 6. MgO-FeO-SiO2 projection. See text.

yielding types I, II samples, and residual liquid C. The process could scarcely have operated within a single lava flow, and requires the existence of at least a shallow-seated magma chamber.

Both explanations requires types III, IV to be stratigraphically older than types I, II, and both are apparently inconsistent with data of Brown et al. (this volume).

A third alternative, derivation of liquids C, A', A as progressive partial melts of a pyroxenite or olivine-pyroxenite source mantle predicts the reversed stratigraphic relationship, but still requires extensive post eruption crystal accumulation to explain the compositions.

Creation of primary magmas with the compositions of the investigated rock specimens by progressive partial melting of the same source mantle composition is impossible, even making allowances for pressure differences at the scenes of partial melting (Fe/Mg relations, see fig 5 especially).

References

(1) LSPET 1971. Lunar sample information catalog, Apollo 15. NASA Manned Spacecraft Center.

(2) Biggar, G.M., O'Hara, M.J., Peckett, A. and Humphries, D.J. 1971. Geochim. Cosmochim. Acta Suppl. 2 Proc. 2nd Lunar Sci. Conf. 1, 617-643.

(3) Biggar, G.M., O'Hara, M.J., Humphries, D.J. and Peckett, A. 1972. Maria lavas, mascons; layered complexes, achondrites and the lunar mantle. in The Moon ed. H.H. Urey, S.K.Runcorn I.A.U. (in press).

(4) O'Hara, M.J. and Biggar, G.M. A point of phase equilibria interpretation in connection with lavas from the Apollo 12 site. Earth Planet. Sci. Letters (in press).

(5) Bowen, N.L. and Schairer, J.F. 1935. Amer. J. Sci. 229, 151.

(6) Roeder, P.L. and Osborn, E.F. 1966. Amer. J. Sci. 264, 428-480.

(7) Reid, A.M., Warner, J., Ridley, W.I. and Brown, R.W. 1972. Major element composition of glasses in three Apollo 15 soils (preprint).

(8) Biggar, G.M., O'Hara, M.J., Humphries, D.J. and Peckett, A. 1972. in Lunar Science IJJ 77-79 ed. C. Watkins Lunar Science Institute Contrib. 88.

LUNAR SCIENCE V

ABSTRACTS OF PAPERS
SUBMITTED TO THE

FIFTH LUNAR SCIENCE CONFERENCE

SPONSORED BY NASA THROUGH
THE LUNAR SCIENCE INSTITUTE
AND
THE JOHNSON SPACE CENTER
MARCH 18-22, 1974

Compiled by
The Lunar Science Institute
3303 NASA Road 1
Houston, Texas 77058
1974

THE ORIGIN OF LUNAR CARBIDE.

B.D. Batts[1], G.M. Biggar[2], M.C.J. Billetop[3], P.R. Davis[3], G. Eglinton[3], S.K. Erents[4], L.R. Gardiner[3], A.P. Gowar[3], R.M. Housley[5], D.J. Humphries[2], A.J.T. Jull[3], J.R. Maxwell[3], B.J. Mays[3], G.M. McCracken[4] and C.T. Pillinger[3].

1. Macquarie University, Australia.
2. Grant Institute of Geology, Scotland.
3. University of Bristol, England.
4. U.K.A.E.A., Culham Laboratory, England.
5. North American Rockwell Science Center, U.S.A.

The concentration of carbide in lunar fines (estimated as CD_4 from DCl dissolution) is related to both solar wind exposure history (1) and Fe^{II} content (2) of the sample. The $CD_4/^{36}Ar$ ratio is proportional to the content of Fe^{II} (calculated as FeO) in fines from the A11, A12, A14, A15 and A16 missions (2). Current results show that carbide in A17, L16 and L20 fines has the same exposure and Fe^{II} dependence. Limited data suggest that the key iron species implicated in the relationship is superparamagnetic iron, $Fe^{o}sp$ (2). An understanding of the role of $Fe^{o}sp$ is now being sought by acid dissolution studies and Mössbauer spectroscopic measurements (3) of a variety of soils selected on the basis of Fe^{II} concentrations and solar wind exposure histories.

We have previously suggested that the finest (< 10 μm) soil grains represent the main site for initial synthesis of carbon compounds and that the reactions occurring in these non-aggregated fine grains are important in understanding lunar carbon chemistry (4). Subsequent redistribution of carbon species and any further reactions which occur during the recycling (5) of material *via* the formation and comminution of complex particles, such as glassy agglutinates and microbreccias, must be considered separately. Primary synthesis of $Fe^{o}sp$ and carbide in finest fines could be the result of solar wind ion implantation and/or meteorite impact cloud reactions (*inter alia*, 2,4,6-8). Each of the two basic processes may take place by one or more mechanisms. Solar wind ions could reduce silicate Fe^{II} to Fe^{o} by (i) preferential sputtering of the more electronegative elements (e.g. oxygen) or (ii) chemical reactions occurring during diffusion of implanted species, particularly hydrogen, with or without heating or other activation. Carbide synthesis might occur in each case from simultaneously implanted carbon atoms. Reduction of silicate Fe^{II} to Fe^{o} might occur in the hot base surge accompanying a meteorite impact. The reducing gas cloud could be (i) predominantly hydrogen and CO released by pyrolysis of the soil, or (ii) the gas mixture in (i),with a greatly increased proportion of CO, if the meteorite is a carbonaceous chondrite. The presence of carbon species in the gas cloud might be expected to lead to the simultaneous formation of carbide.

The feasibility of each mechanism is being investigated by simulation studies using Fe^{II}-rich glass samples (Fe^{II} in the range 0-20% FeO, supplied by P.S. Irlam, Pilkington Bros. Ltd.) under the appropriate reaction conditions. The DCl dissolution method is used to detect the formation of either Fe^{o} or Fe^{o} with associated carbide. In a preliminary study, glass

THE ORIGIN OF LUNAR CARBIDE

Batts, B.D. et al.

containing 4% Fe^{II} and 7% Fe^{III} was implanted with $^{13}C^+$ ions. No conclusive evidence for the formation of Fe^o or carbide was found, even after heating at temperatures up to 1000°C. However, during the pyrolysis ^{13}CO and $^{13}CO_2$ were released, indicating that ^{13}C-implanted iron-rich glasses exhibit some characteristics of lunar soils (9,10). A suite of samples irradiated by D_2^+ ions is now under investigation.

To simulate the effects of meteorite impact gas clouds, powdered glass samples (average particle size less than 20 μm) have been equilibrated at fixed temperatures (in the range 500°C - 1000°C) in controlled H_2/CO or CO/CO_2 atmospheres. These experimental conditions are probably more favourable for the reduction and carbide synthesis reactions than those prevailing at the lunar surface. However, preliminary results from samples heated in CO/CO_2 at 1000°C show no measurable Fe^o or carbide. Similarly, neither species has been detected in samples of $^{13}C^+$-implanted glass which had been heated in a stream of H_2 at 500°-700°C.

After the initial formation of Fe^o in fine lunar grains, carbide could be generated by (i) subsequent implantation of solar wind carbon, or (ii) gas cloud reactions in which CO chemisorbed on exposed metal is catalytically decomposed. Indeed, laboratory studies have already shown both processes to be possible (11,12).

Any Fe^o synthesized in lunar soil by solar wind ion bombardment should be distributed only in the range of penetration of the ions:e.g. 2000 ± 500Å for hydrogen (13). The proportion of Fe^o exposed at the "very surface" should be small. Conversely, reactions occurring in a gas cloud would be expected to generate only "very surface" material. Housley et al (14) have shown the presence of iron particles (presumably Fe^osp) within the surface region and we are attempting to establish the relationship between these particles and the species which produce CD_4 on DCl dissolution. Preliminary results with a variety of surface-specific reagents suggest that most of the Fe^o and carbide is not directly accessible to these reagents. About 90% of the Fe^o is not attacked without concurrently destroying part of the silicate matrix, implying that solar wind implantation is the major mechanism for Fe^o reduction.

Precise location studies should prove informative in regard to the redistribution processes occurring during the formation of complex particles from finer material. The carbide and CH_4 contents of a series of fractions obtained by disaggregating glassy agglutinates are being measured.

References

1. Cadogan, P.H.,et al., Geochim.Cosmochim.Acta, Suppl.3, 2, 2069 (1972).
2. Pillinger, C.T., et al., Nature Phys.Sci., 245, 3 (1973).
3. Housley, R.M., et al., Geochim.Cosmochim.Acta, Suppl.3, 1, 1065 (1972).
4. Cadogan, P.H., et al., Proc. 4th Lunar Science Conf., in press.

5a. Cadogan, P.H., et al., Nature Phys.Sci., 241, 81 (1973).

5b. Des Marais, D.J., et al., Nature Phys.Sci., 246, 65 (1973).

6. Grant, R.W., et al., Lunar Science IV, 315 (1973).

7. Pearce, G.W., et al., EPSL 17, 95 (1972).

8. Yin, I., et al., J. Geophys. Res., 77, 1360 (1972).

9. Holland, P.T., et al., Geochim.Cosmochim.Acta, Suppl. 3, 2, 2131 (1972).

10. Gibson, E.K. and Moore, G.W., Geochim.Cosmochim.Acta, Suppl.3, 2, 2029, (1972).

11. Pillinger, C.T., et al., Nature Phys.Sci., 235, 108 (1972).

12. Renshaw, G.D., et al., J. Catal., 18, 164 (1970).

13. Leich, D.A., et al., EPSL 19, 305 (1973).

14. Housley, R.M., Proc. 4th Lunar Science Conf., in press.

EXPERIMENTAL CRYSTALLIZATION AND GEOCHEMICAL INTERPRETATION OF LOW TITANIUM BASALTS

G.M. Biggar, D.J. Humphries and M.J. O'Hara. Grant Institute of Geology, Edinburgh University, EH9 3JW

An effective argument in favour of primary origin of picritic low titanium magmas at the Apollo 12 and 15 sites and against their derivation by olivine enrichment in lower temperature cotectic liquids would appear to be that the experimentally produced liquidus olivine composition matches that observed in the cores of natural 'phenocrysts' and is more magnesian than that observed in experiments conducted at the cotectic temperature (1,2). The equilibrium olivine composition which will crystallize from a picrite basalt (e.g. 12040) at a given temperature reaches a minimum Fo content at a critical oxygen fugacity just below that of Fe/Feo equilibrium (fig. 1). Above that critical fO_2, $d(Fo)/d(fO_2)$ is low, and control of the experiment easy. Below that fO_2, metallic iron appears, Fo content of olivine rises rapidly, and $d(Fo)/d(fO_2)$ becomes very large, making precise control of experiment very difficult. Unfortunately the lunar basalts appear to have crystallized below the critical fO_2; we (3, 4) have experimented at just above the critical fO_2 for technical reasons of control of charge composition thus our experimentally produced olivines will be more iron-rich than would form in the natural rock at the same temperature. Where the charge has been run in a sealed, pure iron capsule after conversion of the sample to glass at some unspecified fO_2 (1), reaction between capsule and charge will occur, oxidising and dissolving the container until an fO_2 is attained where iron metal is in equilibrium with the melt, which will, however, be FeO enriched, and precipitate too iron-rich an olivine at any given temperature, as well as showing suppression of the crystallization temperature of anorthite. Unless fO_2 and charge composition have been very precisely and accurately controlled, a direct comparison between experimental and natural olivine is not significant (fig. 2).

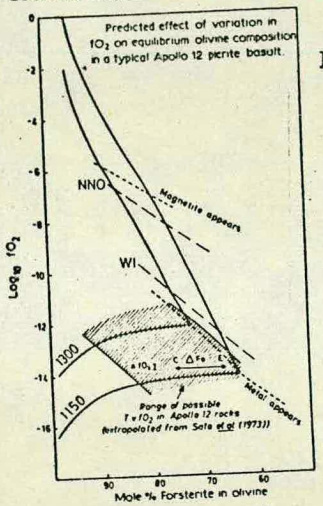


Fig 1

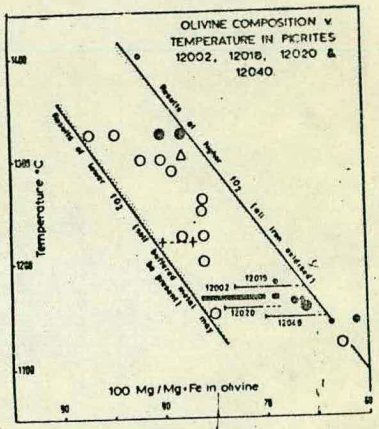


Fig 2

Fig. 1. Olivine composition as a function of oxygen fugacity at 1150, 1300°C (stylized) and relation to nickel-nickel oxide (NNO) and Fe/FeO(WI) equilibria and actual oxygen fugacity in Apollo 12 basalts.

Fig. 2. Variation of olivine composition in natural rocks (horizontal bars) compared with experimental results a Fe/FeO oxygen fugacity (3, solid blobs), oxidised in sealed iron capsule (1, small open circle 12040) and sealed in molybdenum (2, large open circles 12002) and in contact with melting natural olivine container (12020, crosses Large open circles refer to non depleted charges at unknown fO_2(2).

Moreover, during cooling, iron metal is in reaction relationship with iron-bearing silicate melts (5, 6) whi at that stage contain some Fe^{3+}. Thus $Mg/Mg+Fe^{2+}$ of the silicate system decreases during crystallization. It therefore, invalid to take either the Mg/Mg + total Fe (as in 2) or $Mg/Mg+Fe^{2+}$ in the solidified hand specimen, a use a determined K_D to predict the equilibrium liquidus olivine composition - the true equilibrium liquidus olivi could be as much as ~5% Fo more magnesian.

When olivine crystals gro during rapid cooling of basaltic liquids, the effective distribution coefficient appears to be ~0.18 ± 0.03 (7). lower than K_D (~0.335) and causing more magnesian olivine to form than would be t case at equilibrium.

Grove et al have provided microprobe data (pers comm) which enable composition control during crystallization Apollo 12 picrites to be evaluated further (figs. 3, 4). Fig. 3 illustrates the effect of loss or gain or iron bulk sample, liquid and olivine compositions obtained from natural olivine-basalt samples 12002 (2) and 12040 (B et al unpublished). The shaded field encloses all analyses of Apollo 12 olivine basalts, except that of 12002 Grove et al (cross, 02'). The compositions of natural samples 12040 (8) and 12002 (9) are indicated. Willis et analyses of 12002 is used in preference to Grove et al's (1973) analysis, which was made on a residue from other periments, and yields a bulk composition which is incapable of yielding the results of Grove et al's (2) experim 51, 56 at 1325°C (because the charges cannot have gained iron, and hence moved downwards in the diagram, in the technique used). The discrepancy might, however, be due to inhomogeneous sampling of the material available.

The analysed compositions of olivine and liquid from four different experiments (56, 51, 28, 18) at 1325°C plotted, together with the bulk compositions of the charges, A, B, C, D inferred on the assumption that the actu charges consist of olivine and glass only, and that the bulk compositions differ from 12002 only by loss of FeO.

The techniques used (2) were to enclose the charges in molybdenum or iron capsules enclosed in evacuated s silica glass tubes or to run at a controlled oxygen fugacity in a molybdenum container. At the low inherent o

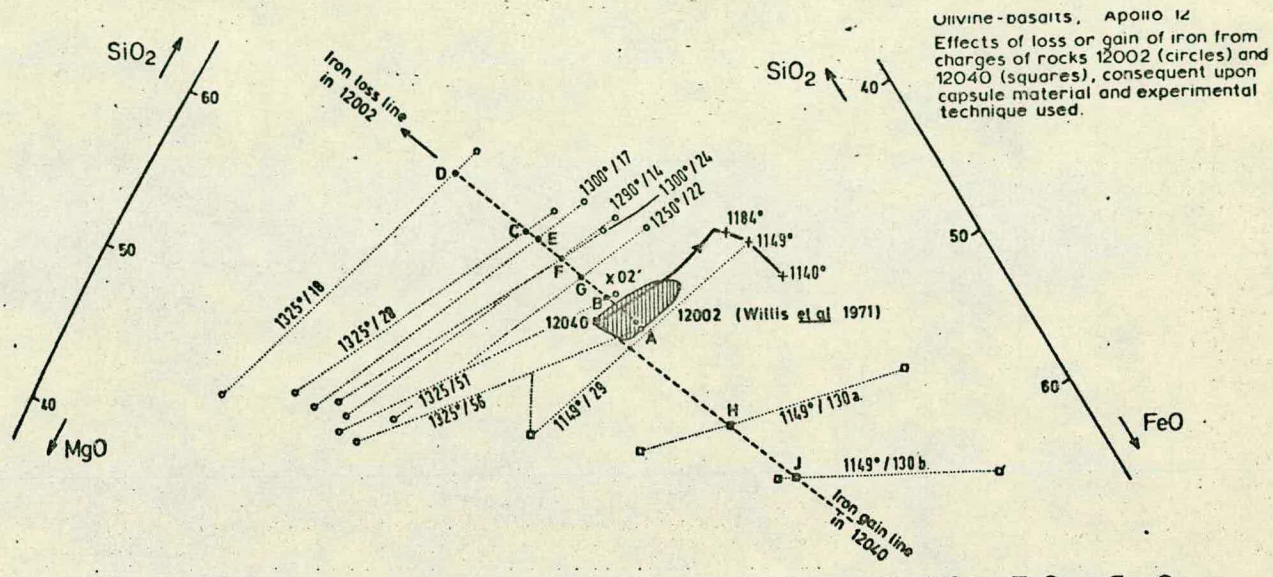


Fig 3. Projection from anorthite, albite, orthoclase, $CaSiO_3$, TiO_2, Cr_2O_3 into $MgO-FeO-SiO_2$. See text.

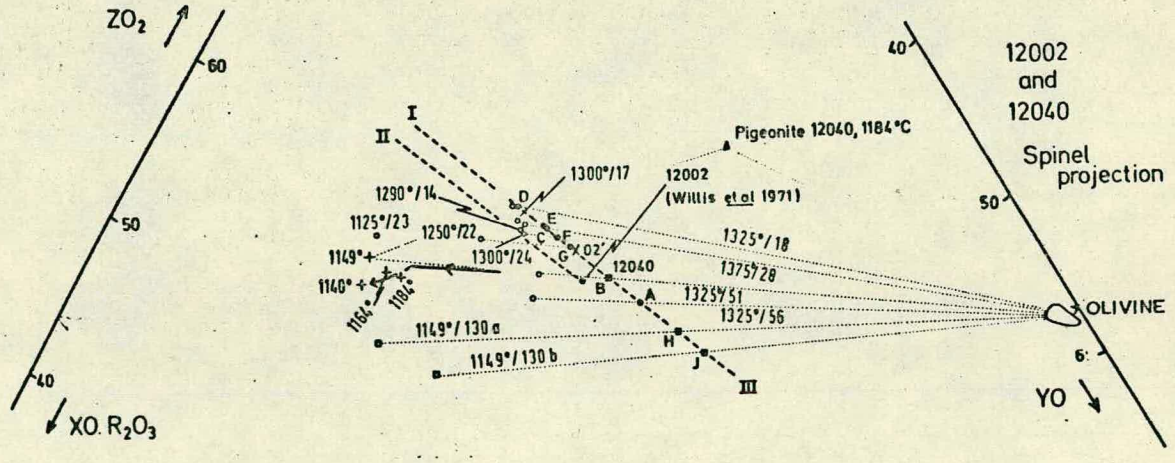


Fig 4. Projection from 'spinel' into the section $XO.R_2O_3$ - $YO-ZO_2$ (includes anorthite-olivine-silica).

LOW TITANIUM BASALTS

BIGGAR, G.M. et al.

fugacity of the charges, in which the activity of metallic iron is close to one, iron is very soluble in the molybdenum capsules. Iron is lost from the charge to the capsule and oxygen is released to the atmosphere inside the capsule, raising the oxygen fugacity until the iron activity is reduced to the point where no further iron dissolves in the molybdenum. The size of this effect will be, to an extent, time dependent, but it will also depend upon the size and configuration of the charge, and the extent to which released oxygen can escape from the molybdenum capsule.

Even greater losses of iron from the charge may occur when a similar technique is utilized but an iron capsule is substituted for the molybdenum. If the iron contains any carbon (not normally reported in analyses) even more extensive reduction of the charge may occur than in the previous case.

Also shown are analysed olivine-liquid assemblages from experiments at 1300°C (runs 17, 24), 1290°C (run 14) and 1250°C (run 22) and their respective inferred bulk charge compositions, E, F, F and G. A consequence of iron loss from the charges is that the olivine/calcium-poor pyroxene liquidus interface is likely to be encountered by the residual liquids at a higher temperature than would have otherwise been the case, and the same is true for the first appearance of plagioclase when the residual liquids meet The equilibrium residual liquids from charges in which all iron has been retained as FeO are represented here by the heavy curves expressing the evolution of residual liquids in 12040 (from ref. 3).

Contrasting with the severe loss of iron which resulted in the sealed tube experiments with iron capsules reported above, the opposite is liable to occur where iron capsules are used in experiments at controlled oxygen fugacities. The effect of iron gain from iron capsules is shown by experiments 129 and 130 on sample 12040 at 1149°C Run side by side in the same controlled atmosphere furnace at an oxygen fugacity of $10^{-12.5}$ atmospheres experiment 129 used a molybdenum capsule. Because the oxygen fugacity is a power of ten lower than that of the Fe/FeO equilibrium, a small amount of iron dissolves in the molybdenum capsule. Metallic iron is not produced from the charge until lower oxygen fugacities are attained.

Experiment 130 used an iron capsule. Metallic iron is not in equilibrium with charge 12040 at this oxygen fugacity, hence oxygen from the gas atmosphere reacts with iron from the capsule to produce FeO which dissolves in the silicate liquid. Two olivine-liquid tie lines (130a, 130b) from experiment 130, and two inferred bulk composition (H, J) are shown, the more iron-rich presumably coming from a part of the charge which was closer to the capsule wall.

Figure 4 is a projection from spinel into the system XO-R_2O_3-ZO_2-YO (which contains the section anorthite-olivine-silica) of the data for samples 12002 and 12040. The field occupied by all hand-specimen analyses of Apollo 12 olivine basalts (shaded) is shown, as are the compositions of 12002 and 12040 as well as the analysis (cross O2') of 12002 provided by Grove et al (2)

Iron-loss lines, radiating from the YO apex of this projection, have been drawn through the two initial bulk compositions (Grove et al; Willis et al) given for sample 12002 (I and II respectively).

Liquid compositions in the four experiments on 12002 at 1325°C, experiments 18, 28, 51 and 56 are shown by appropriately numbered small circles. Tie lines linking these compositions to olivine should intersect the iron-loss line drawn through the original bulk composition of the material used for the experiments at points corresponding in this projection with the bulk compositions labelled D, C, B and A respectively in fig. 3. Again, it appears that the material analysed by Grove et al as 12002 cannot be representative of the material loaded into the capsules because the products of runs 51 and 56 are again inexplicable, requiring a starting material which, in mineralogical terms, would have been significantly depleted in pigeonite relative to feldspar in relation to the aliquot taken for bulk chemical anlysis. From Fig. 3 run 56 should contain very little olivine, while runs 51 and 28 will contain significantly more yet from fig. 4 there is no single choice of a bulk composition and associated iron-loss line which would make such mineral proportions a reality - any single choice would lead to the prediction that the amount of olivine present in run 56 exceeds that in run 51, and that in turn exceeds the amount present in run 28. These results can be explained if the inhomogeneous nature of the sampling of the powder of rock 12002 extends to at least some of the aliquots taken for experimental charges.

The residual liquid developed at the lowest temperature (run 23 at 1125°C) is also shown in relation to the trend of residual liquid evolution deduced from the crystallization of rock 12040 under conditions where no iron is lost and where all available evidence, including microprobe analysis of all glass or nearly all glass products, is consistent with reasonably homogeneous sampling of the powder provided. Run 129, which contains some pyroxene, has clearly lost some iron to the capsule.

An iron-gain line (III) has been drawn from the composition of 12040 towards the YO apex. The compositions of two glasses obtained from a run (130) in an iron capsule at a controlled oxygen fugacity have been plotted and joined to olivine by dotted tie lines. Their intersections with the iron-gain control line mark the compositions of two of the glass compositions H, J, which were generated in this manifestly inhomogeneous run product.

Detailed discussion of equilibrium crystallization paths of individual hand specimens may, however, be superfluous. All hand specimen compositions at the Apollo 12 and 15 sites can be interrelated by

$$\text{rock}_1 = \text{rock}_2 \pm \text{'phenocryst' cores} \pm \text{phenocryst 'rims'}$$

indicating that chemical differentiation has involved the movement of the material in the rims of the crystals as well as the cores. The rim materials must be quenching products, since they are of compositions which are never in equilibrium with the liquid in the absence of abundant anorthite crystals. Phenocryst cores also are frequently skeletal suggesting quenching rather than equilibrium phenocryst growth. It follows that individual hand specimen compositions represent neither liquid compositions nor any composition relatable to the real liquid composition in terms of equilibrium crystal-liquid processes.

References (1) Green, D.H. et al. 1971, Proc. 2nd Lunar Sci. Conf. 1, 661; (2) Grove et al. 1973, Proc. 4th Lunar Sci. Conf., in press; (3) Biggar et al. 1971, Proc. 2nd Lunar Sci. Conf. 1, 617; (4) Biggar et al. 1972, The Moon ed. Urey, Runcorn, pp 129-164; (5) Barren, N.L. and Schairer, J.F. 1935, Amer. J. Sci. 229, 151; (6) Muan, A. 1958, Amer. J. Sci. 256, 171-207; (7) Cawthorn et al. in press; (8) Kushiro, I. and Haramura, H. 1971, Science 171, 1235; (9) Willis et al. 1971, Proc. 2nd Lunar Sci. Conf. 2, 1123.

ORIGIN OF THE LUNAR HIGHLANDS; C.E. Ford, G.M. Biggar, M.J. O'Hara, D.J. Humphries & P.N. Spencer, Grant Institute of Geology, Edinburgh University

The Apollo 16 rocks range from crystallised igneous liquids and cumulates to brecciated, remelted and recrystallised types. In melting experiments at atmospheric pressure (Table 1) the range of chemical composition represented by the Apollo 16 rocks is consistent with a pseudo-ternary system comparable to the An-Fo-SiO_2 system (Fig 1). All the rock compositions lie close to the plane $XO.R_2O_3$-YO-ZO_2.

All of the rocks have a temperature interval from about 1300°C to 1200°C during which spinel is first precipitated either alone or with plagioclase or olivine and subsequently resorbed when olivine and plagioclase occur together whereas plagioclase + spinel and olivine + spinel cumulates could be expected but have not been found, the reported olivine+plagioclase+spinel cumulates should not occur. None of the lunar rocks retain a chemical memory of appreciable spinel fractionation. Many of them do not even retain a memory of crystallisation through the stability field of spinel. Those rocks which do contain spinel, notably 62295 and the spinel-troctolites, are perhaps best explained as remelted troctolite cumulates in which the spinel, which is formed on initial remelting, subsequently fails to re-equilibrate.

The major element chemistry fits very closely a fractionation model dominated by the accumulation of plagioclase:-

60025 (37.6%) + 60335 (62.4%) = 68415 ($\Sigma r^2 = 1.457$)

60025 (58.6%) + Avge Hi-Al basalt (Prinz)(41.4%)= 68415 ($\Sigma r^2 = 0.187$)

or plagioclase + olivine:-

Avge spinel troctolite (20.45%) + 62235 (79.55%) = Avge Hi-Al basalt (Σr^2=0.8)

Avge spinel troctolite (46.8%) + glasses in 14310 at 1211° (53.2%) = Avge Hi-Al basalt (Σr^2=2.5)

These equations do not require any specific rock to be genetically related to any other rock, merely that the rock types as represented by the returned lunar highland samples can be interrelated by crystal-liquid processes.

The key questions now to be answered are (1) What point in the chemical sequence represents the parent magma? (2) How did fractional crystallisation of this magma manage to avoid the involvement of spinel? (3) Where did the parent magma come from?

The recognition of apparent phenocrysts in rocks such as 68415, 68416 and the texture suggestive of crystallisation from a near all liquid state indicate that any parent magma must be at least as anorthositic as these rocks. The close similarity of the soil compositions also suggest the volumetric significance of this composition. Such a parent liquid is capable of fractionation to give about 60% anorthosite cumulus and 40% derivative high alumina basalts. A parent liquid located at the mafic end of the observed rock sequence would require the existence of large volumes of 'unseen' derivative liquid and necessitates unproven plagioclase flotation which would in turn prevent troctolite accumulation.

HIGHLAND ORIGIN

Ford, C.E. et al.

The lack of memory of a spinel 'event' can be explained if under some other conditions of crystallisation spinel did not occur in the crystallisation sequence. Spinel occurs under all experimental conditions examined so far. One sequence of events could bypass the stability field of spinel and lead to some fractional crystallisation. At moderate water vapour pressures the Apollo 16 rocks are rendered all liquid at temperatures below 1200°C. Depressurisation at constant temperature below the stability range of spinel leads to fairly rapid growth of plagioclase which could fractionate provided that olivine nucleation and growth was delayed. Separation of a vapour phase and temperature adjustments due to latent heat effects might provide the ideal stirring mechanism required to explain volatilisation losses of water, alkalis, oxygen and other volatiles, and re-melt previous accumulations of troctolite.

High water pressure suppresses the plagioclase liquidus temperature in favour of ferromagnesian minerals. A pressure somewhat over 5 kb is required to produce olivine crystallisation before plagioclase in 68415 which is close to a possible parent magma composition. Liquids like 68415 can be produced by partial melting of a lunar interior in the presence of water vapour. In the absence of water vapour the same lunar interior could provide mare type basalts.

Table 1

Atmospheric pressure experiments at $fo_2 \equiv$ Fe/FeO, Mo capsules

T°/Rock	60025	68415	60335	62295	60315
1370	p,l	p,l	p,l	s,l	
1330	p,l	p,l	p,l	s,l	l
1300	p,l,ore	p,s,l	p,s,l	s,l	s,l
1276	p,l,ore	p,s,l	p,s,l	o,p,s,l	o,s,l
1256		p,s,l	p,o,s,l		o,s,p,l
1227		p,o,s,l	p,o,s,l	o,p,l	o,s,p,l
1216		p,o,s,l	p,o,s,l	o,p,l	o,s,p,l
1200	solid	p,o,l	p,o,l	o,p,l	o,p,l

Higher pressure/depressurisation experiments on 60335 + 10% H_2O at $fo_2 \equiv$ FeO/Fe_3O_4, Pt capsules.

T	P_1 kb	t_1 hrs	P_2 kb	t_2 hrs	Result
1250	1	0.5			s,l
1250	1	0.5	0	0	s,p,l q-pyroxene
1250	1	0.5	0	1	s,p,l

Abbreviations p = plagioclase, s = spinel, o = olivine, l = liquid

EXPERIMENTAL PETROLOGY OF HIGH TITANIUM BASALT

O'Hara, M.J., Biggar, G.M., Humphries, D.J. and Saha, P., University of Edinburgh

Table 1 contains experimental results for 28 synthetic compositions related to high Ti-basalt run in molybdenum capsules at the fO_2 of the Fe/FeO equilibrium. Primary liquidus fields of olivine, pigeonite, augite, anorthite, ilmenite and armalcolite are found, and the six fields must come close to conjuction in a cotectic liquid whose composition lies intermediate between 528 and 89, all six phases appearing almost simultaneously at the liquidus in such a liquid, at a temperature of close to 1145°C. Phase equilibria data for some Apollo 17 soils in table 2 show early crystallization of anorthite after olivine and iron-titanium oxides. The orange soil 74220 has a very high liquidus temperature, and extensive early olivine crystallization before the entry of other phases. Apollo 17 high TiO_2 rock compositions (table 2) show early crystallization of iron-titanium oxides and ferromagnesian silicates before anorthite appearance. The compositions of Apollo 17 rocks and soils resemble those of Apollo 11 materials, but are poorer in silica, and higher in Mg/Mg + Fe. The average rock composition erupted at the Apollo 11 site was that of a liquid in simulataneous equilibrium with many crystalline phases (including anorthite). Phenocrysts of anorthite, olivine, ilmenite, spinel and pyroxene were all present in small amounts in evidently rapidly quenched matrix among the lithic fragments in soils and breccias (O'Hara et al. in press EPSL).

The chemical characteristics of the high titanium basalts and soils are best accounted for if the original magma was derived from the residual liquid in a high level magma chamber in which there was well advanced extreme fractional crystallization of anorthite-bearing cumulates. Eruption was followed by enrichment of the flow base in olivine and iron-titanium oxides relative to the upper parts. If such a model is adopted for Apollo 17 the orange soil must be regarded as an impact melt, an interpretation supported by the liquidus temperature which is exceptionally high for a magma of internal origin.

Figure 1A shows variation of liquidus phase in 24 of the 26 synthetic network samples studied as a function of SiO_2 and TiO_2 content. Fields in which pigeonite (PIG), anorthite (AN), olivine (OL), or titanium-rich oxide (TI-OXIDE) are the liquidus phases are indicated. Anorthite does not appear as a liquidus phase at this low oxygen fugacity in the compositions 1-9, 23, 56, 59, 69, 89 but its liquidus field lies very close to the surface defined by those compositions. Samples 28 and 38 both display anorthite liquidus as do samples 838, 538 and 528 which are intermediate between 8 and 38, 5 and 38 and 5 and 28 respectively. The narrow anorthite field indicated between the olivine and pigeonite fields thus expresses the composition region in which anorthite will most readily crystallize from TiO_2-rich magmas in the presence of olivine and pigeonite. Figure 2A shows the variation of liquidus phase in the same range of synthetic compositions as a function of SiO_2 and $CaO+Al_2O_3$ content.

TABLE 1

Compn.	1	2	23	3	4	5	56	6	58	59	69	7	9
	ol, an > 1164; aug, pig, ilm 1148 ± 15	ol > 1205; an, aug, ilm 1170	ol > 1205; aug (1160), an 1165	ol > 1205; an, ilm 1165	ol > 1215; an 1193 ± 20; aug 1153, pig ± 20; ilm 1121 ± 10	ol > 1220; an 1210; aug 1160; ilm 1145	ol > 1190; an 1172; ilm 1161; cpx 1150	ol > 1200; arm, an, ilm 1170; aug 1155	ol > 1180; an 1165; aug 1155; pig 1150; ilm 1145	ol 1170; an 1160; pig, arm 1155; ilm 1145	arm, ol 1165; an, ilm, pig 1150	pig 1205±8; aug 1185±12; an 1167±5	pig 1195; ol 1170; aug 1160; an 1155; ilm 1135
SiO_2	43.5	40.5	39.2	37.9	41.9	41.3	40.3	38.3	43.0	41.5	40.0	48.5	44.8
TiO_2	3.8	7.2	8.7	10.1	6.6	6.5	10.1	11.7	8.2	9.8	11.4	4.3	7.9
Al_2O_3	9.8	9.2	8.8	8.5	11.7	10.8	10.4	10.0	10.6	10.1	9.7	11.0	10.2
FeO	19.8	21.7	22.5	23.4	16.6	19.0	20.0	21.1	18.5	19.5	20.6	15.5	17.9
MgO	12.2	11.4	11.0	10.6	9.3	8.5	8.2	7.9	8.1	7.9	7.6	8.7	8.0
CaO	10.8	10.1	9.8	9.4	12.9	11.9	11.5	11.0	11.5	11.2	10.7	12.1	11.2
	89	9	838	538	38	28	528	548	48	848	828	818	18
	pig 1170; arm 1165; an, ilm 1145	arm, pig 1177; ilm 1156; an 1145	an > 1190; cpx 1165; ilm 1136	an > 1190; ol (1180); aug 1165; pig 1148; ilm 1136	an > 1190; cpx 1177; ol 1173; ilm 1136	an 1185; pig 1151; aug 1148; ilm 1135	an, ol, aug 1170; ilm, pig 1135	aug, ol 1195; an 1156; pig 1145	aug 1197; an 1154; pig 1145; ilm(1120)	pig(1175); an 1150; ilm 1130	pig 1160; aug, an 1154; ilm 1136	pig > 1195; ol; an 1146; ilm 1136	pig, ol > 1218; an 1146; ilm 1140
SiO_2	43.3	41.7	44.6	42.9	44.5	43.8	42.5	43.8	46.2	45.5	44.3	45.2	45.6
TiO_2	9.5	11.1	7.1	7.5	6.2	9.0	8.8	7.5	6.5	7.2	8.4	7.5	7.1
Al_2O_3	9.8	9.4	13.0	13.4	15.9	11.4	11.1	9.5	8.3	9.3	10.8	9.7	9.1
FeO	19.0	20.0	16.0	16.5	14.0	16.7	17.8	18.1	17.1	17.5	17.3	18.4	18.8
MgO	7.7	7.4	7.1	7.4	6.3	6.5	7.5	8.4	8.4	8.2	7.2	8.6	9.2
CaO	10.8	10.4	12.2	12.5	13.1	12.6	12.2	12.8	13.6	12.4	11.9	10.6	10.0

Temperatures of appearance of phases are probably ± 5°C. Those in brackets (1195) are ± 10°C. In many samples armalcolite reacts out after the appearance of ilmenite and olivine reacts out after the appearance of pigeonite.

TABLE 2. Preliminary atmospheric pressure, Fe/FeO oxygen fugacity data for Apollo 17 samples

Temp °C	70017	70181	71501	74220	74241	74261	75061	75081
1279	g	g	g	ad 2g's	g	(d)g	g	(d)g
1207	acdg	adg	adg	ad(e)g	adg	adg	adg	acdg
1177	acdg	abdg	adeg	adeg				
1163	acdeg	abdg	abcdefg	adeg	abdfg	abdg	abcdg	abcdg
1140	abeg	abefg	abefg	adefg	abefg	abeg	abeg	abdefg
1129	abefg	abefg	abefg	abefg	abef	abefg	abefg	abefg

a=olivine; b= plagioclase; c=armalcolite; d=spinel; e=ilmenite; f=clinopyroxene; g=glass
Other results 74220 1352=a,2g's; 1325=a,d,2g's; 1152=adeg; 74261 1325=g

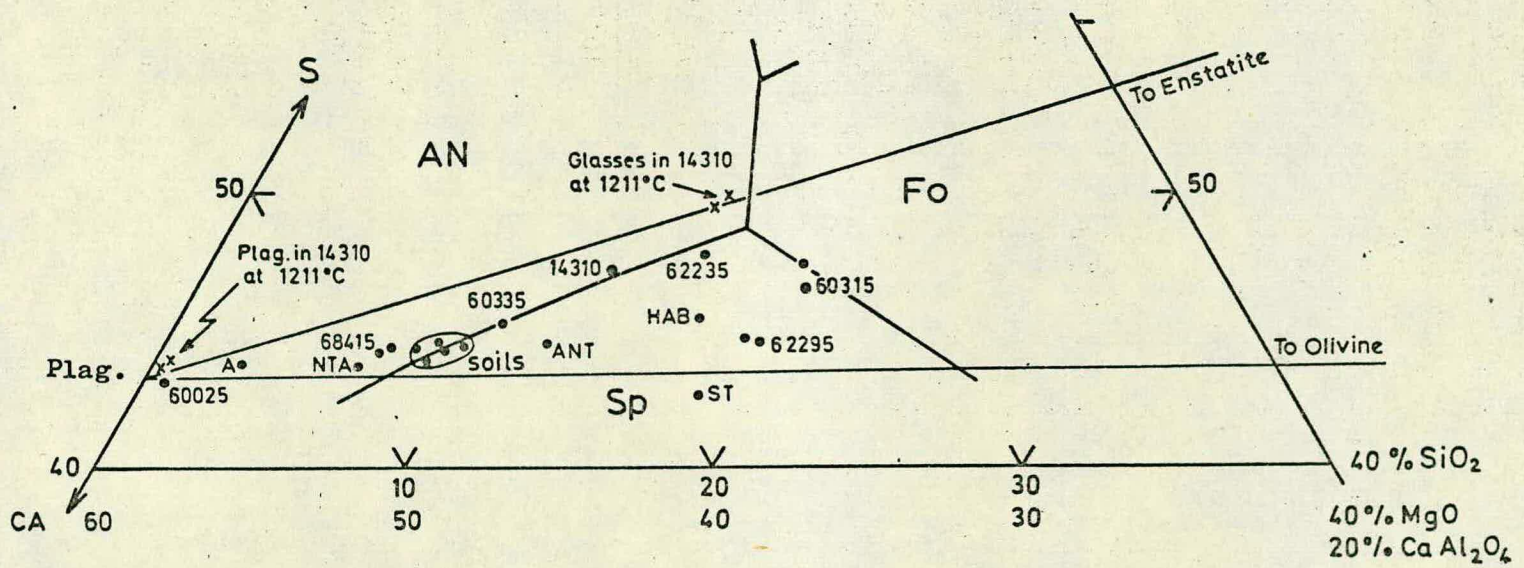


Fig. 1 Spinel projection into $CaAl_2O_4$ - MgO - SiO_2 ($XO.R_2O_3$ - YO - ZO_2)

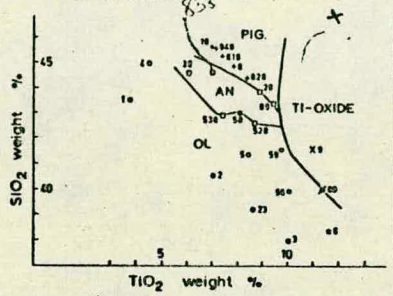
Field boundaries are those of the pseudo-ternary system An-Fo-SiO_2 at atmospheric pressure. The location of several rock compositions at the boundary of the spinel field is fortuitous since in this projection crystallisation of spinel would not alter the apparent course of liquids also crystallising other phases. The suggested crystal-liquid trend is Average Anorthosite (cumulus) ⟵ Soils (parent liquid) ⟶ Average High Alumina Basalt (derivative liquid). The latter gives rise to a second sequence consisting of Average troctolite (cumulus) ⟵ Average High Alumina Basalt ⟶ 62235 (KREEP-like derivative liquids).

HIGH TITANIUM BASALT

O'HARA, M.J. et al.

Figures 1B, 2B compare natural high-titanium basalt data (attached key) with the phase boundaries deduced from figs. 1A, 2A. Figures 1C, 2C compare Apollo 17 rock and soil compositions with the same phase boundaries. The other important aspect of the chemistry variation of these rocks, Mg/Fe ratio as a function of silica-saturation level, is displayed in the MgO-FeO-SiO_2 plots (figs. 3A-D). Figure 3A shows the synthetic net (table 1) and the deduced region of anorthite-saturated multiphase cotectic liquid composition (large circle). Figure 3B shows the relationships of various natural Apollo 11 high titanium basalts to that composition, while figure 3C follows the trends of liquid evolution in the experimental equilibrium crystallization of some of the samples at an fO_2 slightly but significantly higher than in the natural rocks. Figure 3D shows the compositions of Apollo 17 soils and rocks in relation to the synthetic nets and Apollo 11 rock data.

Fig 1A



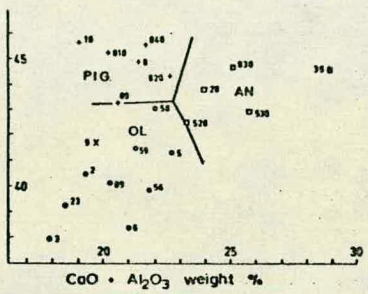
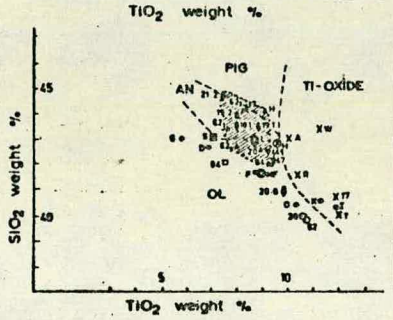


Fig 2A

Fig 1B



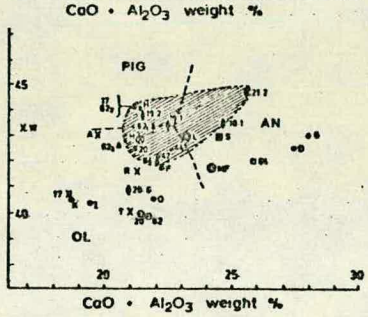
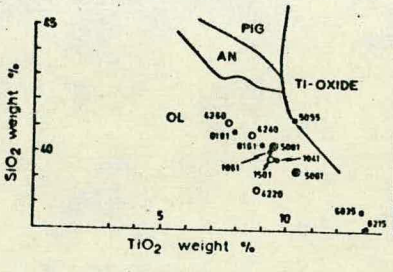


Fig 2B

Fig 1C



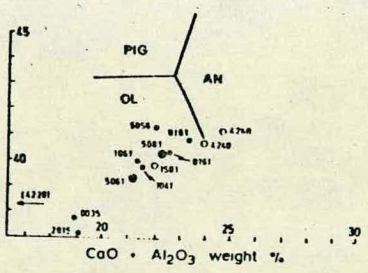


Fig 2C

Key to figures 1-3

(1) Points in figures 1A-2A & 3A are identified by the numbers in table 1, and symbolised in 1A, 2A, by liquidus phase in atmospheric pressure experiments as listed in (2).

(2) Figures 1B,2B,3B and 3C

Liquidus phase (excluding spinel) is:- O = olivine; + = pigeonite; □ = anorthite; X = titanium-rich oxide, in the following compositions (groups C-F). ● indicates a composition for which no phase equilibria data are available.

A. Liquids produced in experiments from natural rocks, soil or synthetics made up to natural rock compositions, which are in or close to equilibrium with olivine, plagioclase, pyroxene(s) and titanium-rich oxide.

▲17 = from 10017, 1133°C; ▲62$_1$ = from 10062, 1142°C
▲20 = from 10020, 1133°C; ▲62$_2$ = from 10062, 1133°C
▲84 = from 10084, 1160°C; ▲62$_3$ = from 10062, 1120°C
▲H = from lithic fragment average, high potassium group.
(Data from Biggar et al 1971, O'Hara et al 1974)

B. Natural rock, groundmass or glass compositions believed, from petrographic evidence, to represent liquids close to saturates with olivine, anorthite pyroxene and iron-titanium oxide.

◆19.1 = groundmass to anorthite phenocrysts in 10019/15; fragment one
◆19.2 = groundmass to anorthite phenocrysts in 10019/15; fragment two
◆21.2 = groundmass to anorthite phenocrysts in 10021/26; fragment two
◆18.1 = groundmass to olivine, spinel, ilmenite phenocrysts in 10018/20; fragment one
◆20.0 = trapped liquid in olivine phenocryst, 10020
(Data from Roeder and Weiblen 1970; O'Hara et al 1974)

C. Average compositions of rock types.

O L = average low K_2O lithic fragments in soil (Prinz et al 1971);
O H = average high K_2O lithic fragments (see A above)(Prinz et al 1971);
● F = average of hand-picked microgabbro fragments in soil (Frondel et al 1970)
● K = average of hand picked vesicular basalt in soil (Frondel et al 1970)
● O = average of hand specimens of low K_2O (ophitic group) basalts, (Compston et al 1970) referred to precipitate anorthite when less than 10% crystalline (from James and Jackson 1971).
● I = average of hand specimens of high K_2O (intersertal group) basalts (Compston et al 1970)
● D)= inferred more feldspathic basalt component, required to be mixed
● G) with hand specimen averages to explain soil compositions (Duke et al 1970; Goles et al 1970)

D. Individual hand specimen analyses

X17 = 10017 intersertal, high K_2O group
O20 = 10020)
O62 = 10062) ophitic, low K_2O group
●44 = 10044 ophitic group rocks, judged to lie relatively close to
●47 = 10047 anorthite saturated compositions (Biggar et al 1971)
Chemical analyses from Agrell et al (1970); Compston et al (1970)
Experimental data from O'Hara et al (1974).

E. Synthetic mixtures made up to particular 'rock' compositions

X A = Anderson et al (1970)
X R = Ringwood and Essene (1970)
X T = Tuthill and Sato (1970)
X W = Weill et al (1970)
+ S = Schairer and Muan (1971)
O MF = High titanium basalt glass (Reid et al 1971) from Mare Fecunditatis, experimental data in this paper.

F. Soil samples, viewed here as representing average magma plus c 3.5% of highland derived anorthosites etc.

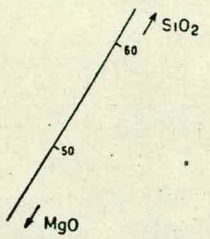
□ 84 = soil sample 10084 (O'Hara et al 1970)

(3) Figures 1C, 2C, 3D. Apollo 17 rock and soil compositions are indicated by the final four digits of the specimen numbers, coded for liquidus phase as in previous figures.

HIGH TITANIUM BASALT

O'HARA, M. J. et al.

Figure 3. Projections from anorthite, albite, orthoclase, $CaSiO_3$, TiO_2, Cr_2O_3 etc. into MgO-FeO-SiO_2



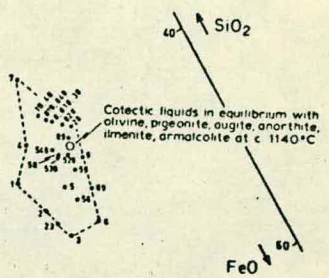
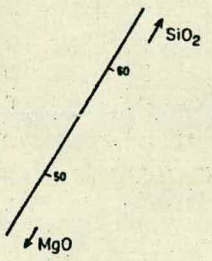


Fig 3A
synthetic net



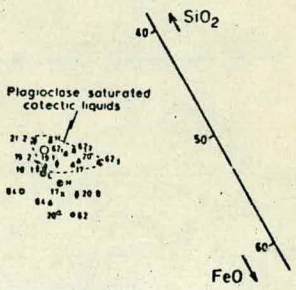
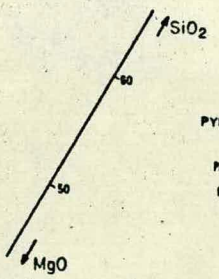


Fig 3B
Natural rock data
Apollo 11



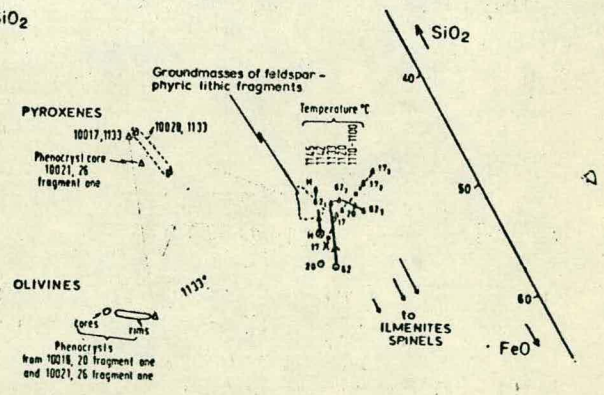
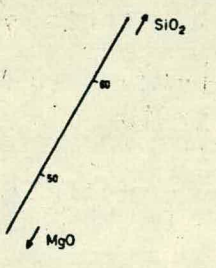


Fig 3C
Crystallization of Apollo 11



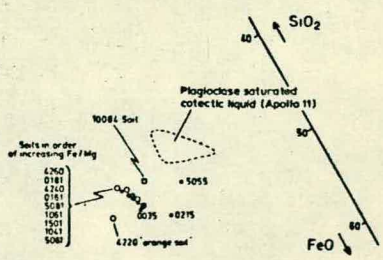


Fig 3D
Apollo 17 results

LUNAR SCIENCE VI

ABSTRACTS OF PAPERS
SUBMITTED TO THE
SIXTH LUNAR SCIENCE CONFERENCE

SPONSORED BY NASA THROUGH
THE LUNAR SCIENCE INSTITUTE
AND
THE JOHNSON SPACE CENTER
MARCH 17-21, 1975

PART I

Compiled by
The Lunar Science Institute
3303 NASA Road 1
Houston, Texas 77058
1975

SIMULATION OF LUNAR PROCESSES: II. REDISTRIBUTION OF CARBON IN THE LUNAR REGOLITH DURING METEORITE IMPACT. A.J.T. Jull, P.R. Davis, G. Eglinton, L.R. Gardiner, J.R. Maxwell, C.T. Pillinger (University of Bristol); G.M. Biggar, D. Humphries (Edinburgh University); B.D. Batts (Macquarie University).

In a companion paper (1) we discuss the possible role of solar wind ion implantation with respect to the formation in the lunar soil of finely-divided metallic iron and associated carbon species, which give rise to deuterocarbons during DCl dissolution. It has been suggested that meteorite impact heating may be necessary to initiate reduction of Fe^{II} by implanted hydrogen and/or to stimulate the migration of carbon and iron during the grain growth of free metal (2). Meteorites could also contribute quite independently to both the formation of metal (3) and acid-hydrolysable carbon (2). For example, the decomposition on impact of carbonaceous chondrites would lead to CO, CO_2 and hydrocarbon gases which would be trapped for a finite time in the pore spaces of the ejecta blanket. The same species, plus H_2 and other gaseous molecules, could also be derived by the concomitant pyrolysis of the lunar soil. This carbon, unless isotopically different, would be indistinguishable from the meteoritic carbon. Gas will be lost to space but some carbon might be retained via chemical reactions involving iron. The processes involved should be more efficient than direct condensation of carbon onto surfaces (4) or re-implantation from the lunar atmosphere (4,5). The original source of the carbon will be obscured. However, some meteoritic species presumably will be among the proportion retained.

To evaluate the role of gas cloud reactions in the redistribution of lunar carbon, we are considering as a starting point simulated samples formed under equilibrium conditions in the systems Fe-C-H-O or Fe-C-O. Although Fe^{II} in the lunar soil is in the form of ferrous silicates and the regolith is not a closed system, these experiments constitute a useful basis for an evaluation of the behaviour of carbon during a meteorite impact. A simplified phase diagram of the equilibrium Fe-C-O system, indicating the various solids containing carbon which can exist, is shown in the Fig. Under certain conditions it is possible to have either α-, γ- or δ-Fe together with carbon in solid solution. The carbide cementite (Fe_3C) is also possible and under non-equilibrium conditions other carbides such as Hägg carbide (probably Fe_2C) and Fe_7C_3 may exist.

Since our original conception of the deuterated acid dissolution technique (7) we, and others, have variously described the carbon species in lunar soil giving rise to deuterocarbons as: 'probably carbide', 'carbide', 'carbide-like', or 'material reacting like carbide'. In order to characterise better this species we have undertaken to study a number of the above carbon-containing iron phases by the DCl method. Preliminary results are given in Table 1. We have classified the samples analysed into two categories, according to the yield of deuterocarbons released. The two samples of cementite made during this investigation, and also the specimen of cohenite, liberated very small amounts of carbon as deuterocarbons. The yields from cementite 3 and Hägg carbide were somewhat higher but the proportion of the total carbon accounted for is still minor. In contrast, the steel samples and the

SIMULATION OF LUNAR PROCESSES: II.

Jull, A.J.T. et al.

austenite are characterised by higher yields of C_1 and C_2 deuterocarbons.

It has been suggested that iron carbides are relatively unreactive towards mineral acids and, in fact, dilute acid etching has been used as a method of isolating cementite from steel or cohenite from iron meteorites (9). Since steels may contain both austenite and cementite, we conclude that it is most likely carbon in solid solution which has reacted to produce deuterocarbons. Indeed, at least one third of the carbon in cementite 3 is not as carbide (8) and it is possible that even the moderate deuterocarbon yields from this sample and from Hägg carbide may be from impurities. The limited data do not yet show whether the carbon species in lunar soil giving rise to CD_4 on DCl treatment is predominantly carbon in solid solution in iron. Such a phase could be formed by any of the mechanisms (involving both meteorite impact and solar wind implantation) so far proposed for the generation of free Fe^o and associated hydrolysable carbon (2). During the reduction and carburisation reactions taking place in the lunar soil, carbide precipitates and carbon/iron solid solutions could coexist. Thus, the total carbon content of the iron could be quite substantial, with the unreactive carbide accounting for the descrepancy between the carbon released by acid dissolution and that measured by pyrolysis. The absolute amounts and the relative proportions of the gases released from the steels are highly variable. Thus, either the samples are inhomogenous or there is a complicated dependence on reaction parameters, sample formation conditions, carbon content and the presence of other metallic elements.

We are continuing our parallel investigation of the reaction of synthetic iron-rich glasses of approximate lunar composition with carbonaceous reducing atmospheres at temperatures up to 900°C, as a simulation of the gas cloud effects of meteorite impact. We hope to relate the Fe-C phases formed to standard Fe-C phases, by comparing DCl reaction products and measuring total carbon by pyrolysis. None of the samples so far examined has released in excess of 1.8 µg/g and we are unable to define the gas cloud conditions most suitable for the formation of acid-hydrolysable carbon. A high proportion of the samples already studied were prepared under conditions which would be expected to produce predominantly cementite and the low deuterocarbon yields may be a result of these conditions.

References

1. Davis, P.R. et al., this volume.
2. Pillinger, C.T. et al., (1974).Proc.Fifth Lunar Sci.Conf., V.2,1949-1961.
3. Pearce, G.W. et al., (1972). Earth Planet.Sci.Lett., 17, 95-104.
4. Bibring, J.P. et al., (1974). Proc.Fifth Lunar Sci.Conf., V.2, 1763-1784.
5. Hayes, J.M., (1972). Space Life Sciences, V.3, No.4, 474-483.
6. Elliot, (1963). Thermochemistry for Steelmaking, V.2.
7. Abell, P.I., et al., (1970). Nature, 226, 251-252.
8. Freel, J., et al., (1968). Trans.Faraday Society, No.568, V.66, Part 4, 1015-1024.
9. Krapf, G., et al., (1972). Thermochim.Acta, 4, 257-271.

SIMULATION OF LUNAR PROCESSES: II.

Jull, A.J.T. et al.

Table 1. The proportion of carbon released as deuterocarbons from various iron/carbon samples by deuterated acid dissolution.

DEUTEROCARBON YIELD							
LOW				HIGH			
sample	total C µg/g	%C released by DCl as CD_4	%C released by DCl as CD_4 + C_2d/cs^5	sample	total C µg/g	%C released by DCl as CD_4	%C released by DCl as CD_4 + C_2d/cs^5
cementite Fe_3C							
1*	6.67	1.6	n.m.	austenite*	$>1x10^4$	49	71
2*	6.67	0.5	n.m.	British std. steels			
3†	9.2††	12.2	15.5	#9	$1.09x10^4$	72	95
cohenite** $(FeNi)_3C$	$6.7x10^4$	1.0	2.0	#5	$6.5x10^3$	53	77
Hägg† carbide Fe_2C	$1x10^5$	10.9	15.5	steel 1045**	$4.7x10^3$	55	79
				steel 1095**	$9.5x10^3$	32	48

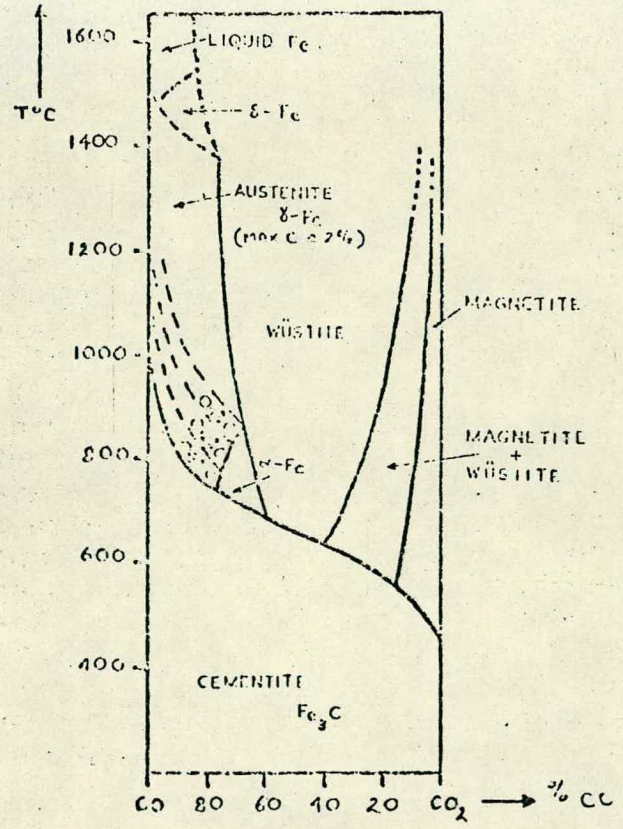
N.B. 10086 fines - total carbon 140-230 µg/g release 18.6 µg/g CD_4 and ca 25 µg/g of CD_4 + C_2d/cs

Footnotes § calibration based on response to C_1 deuterocarbons, * prepared synthetically this work, † ex Dr.A.K.Galwey, ** ex Dr.R.Brett, n.m. not measured

†† 8.5% of the carbon not as carbide (3)

THE Fe-C-O PHASE DIAGRAM

adopted from Elliot et al 1963 (6)



ANALYSIS OF COMPOSITION VARIATIONS IN HIGH TITANIUM BASALTS AND RELATED MATERIALS. M.J. O'Hara and D.J. Humphries, Grant Institute of Geology, Edinburgh University.

A projection to display composition relationships in high titanium basalts has been devised. Six basic coordinates are (all oxide symbols=number of moles):- F=71.846×(MgO+FeO+MnO+NiO+Cr_2O_3+Fe_2O_3); A=101.961×(Al_2O_3+Na_2O+K_2O); C=56.08×(CaO+2Na_2O-3⅓P_2O_5); K=94.203×(2xK_2O); T=TIT=79.90 (TiO_2+Cr_2O_3+Fe_2O_3); S=60.085 (SiO_2-2Na_2O-2K_2O). The F-TIT-S-C and C-K-A-S subfigures of the hypervolume are shown in figs 1 and 2 to illustrate the mineral phases which are represented. The projection provides for the independent representation of the major TiO_2-bearing phases and for the independent treatment of orthoclase from plagioclase, although the C and K components may be combined, when plagioclase and orthoclase are superimposed in a single component (FELS). The subvolume FEM-TIT-SIL-DIOPS-FELS is of particular relevance to the high titanium basalts, where FEM=71.846 (F^*+A^*-C^*-K^*); SIL=60.085 (S^*-2C^*-2K^*); DIOPS=248.1 (C^*+K^*-A^*) and FELS=278.2(A^*), where A*, C* refer to the molar sums used in the basic coordinates, and all coordinates represented in any projection must of course be rescaled to 100%.

Two representative subprojections within the hypervolume are illustrated in figs 3 and 4 (larger prints available on request).

The figures illustrate:- (1) effective discrimination (other than in K_2O) between hand specimens from two Apollo 11 and perhaps two Apollo 17 flows, A, B (see preceeding abstract); (2) the high TiO_2 content of Fe-Ti oxide saturated (low alkali) liquids; (3) close correspondence between phase equilibria in the simple system C-M-F-A-T-S (see ref 1) and those in natural rocks; (4) cotectic liquids from simple system ≙ plagioclase saturated cotectic liquids from natural rocks ≙ groundmasses quenched around phenocrysts of plag, etc in Apollo 11 soils ≙ average target rock compositions from lithic fragments in soils (Apollo 11) or preferred Mare glass composition in soil (Apollo 17) ≙ some hand specimens; (5) liquids saturated simultaneously with ol, pig, aug, plag, ilm, (arm) sp (metal?) change little in major element composition during crystallization, which is pseudo-eutectic. Incompatible elements may however be enriched many times; (6) most hand specimen compositions fall in region olivine+iron titanium oxides±pyroxenes? (dense phenocrysts)+plagioclase saturated cotectic liquids. Their compositions agree better with phenocryst accumulation into such liquids (allowing some variability and according with petrography (ref 2) than with derivation by fractional crystallization of parental liquid P? (If P?, where are the complementary cumulates, especially when at least top flow appears to have been penetrated in regolith formation?); (7) the melt inclusion in olivine from 10020 must have been entrapped early (<7% olivine in rock). It lies on the line between cotectic plagioclase-saturated liquid and olivine itself, and indicates the magma composition from which the olivine crystallized; (8) floor soils can be orange soil+highland soil+cotectic liquid or orange soil+highland soil+hand specimens in terms of projections. Only former answers low proportion of highland derived materials (ref 2) and is consistent with similar mare-wide effect (ref 3); (9) samples of 75035 distributed for analysis and experiment were severely inhomogeneous.

ANALYSIS OF COMPOSITION VARIATIONS

M.J. O'Hara and D.J. Humphries

Fig 1

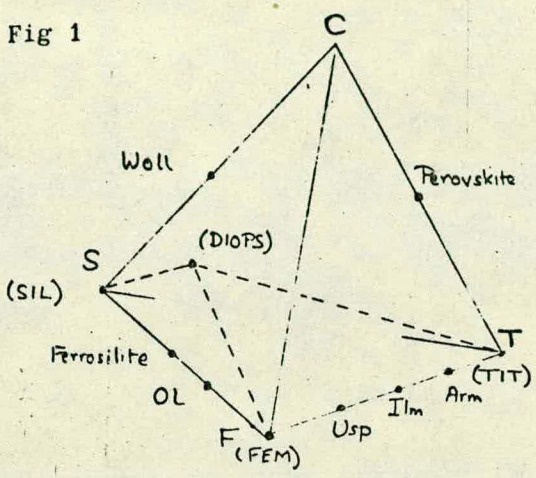
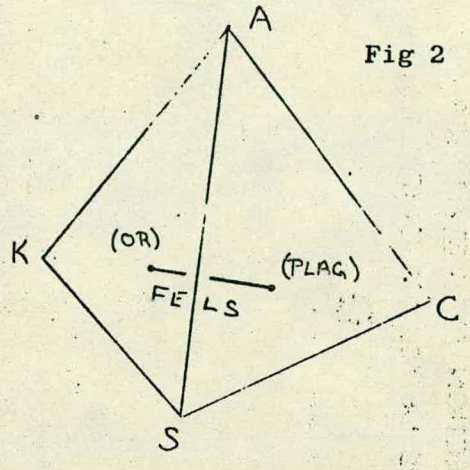
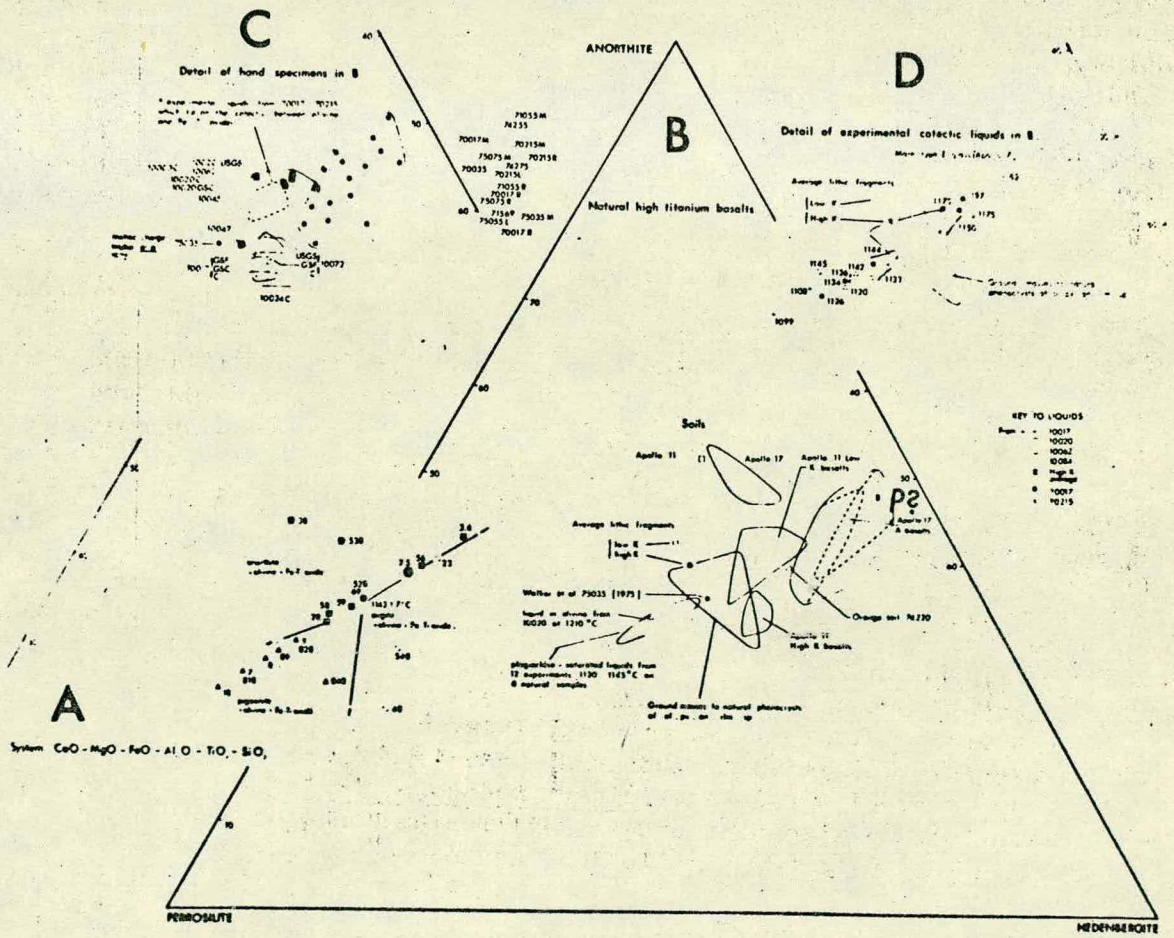


Fig 2

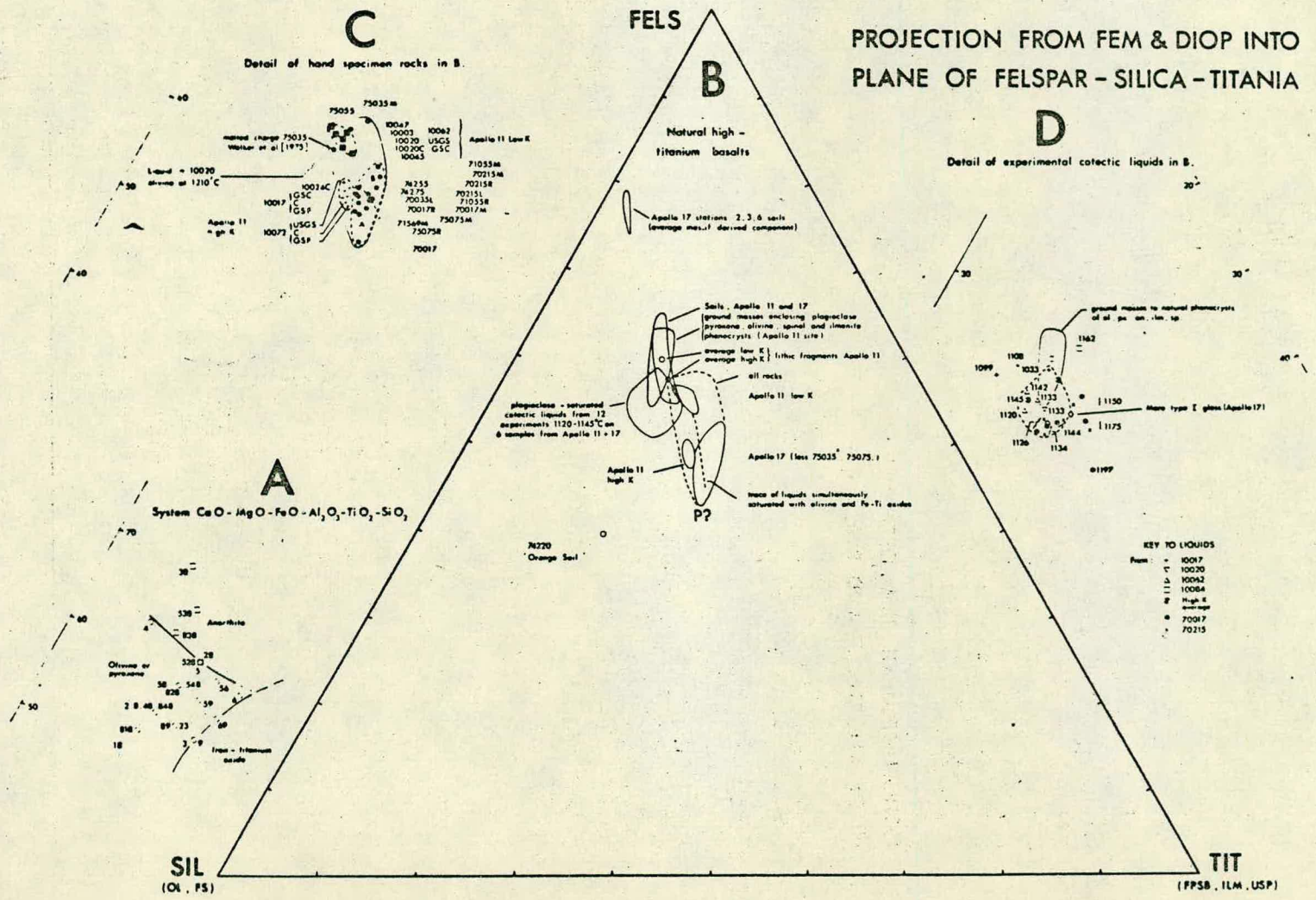


PROJECTION FROM OL, ILM, ORTH INTO PLANE OF ANORTHITE AND PYROXENES.

Figure 3



FS = DIOPS



M.J. O'Hara and D.J. Humphries

ANALYSIS OF COMPOSITION VARIATIONS

References (1) O'Hara et al. 1974. Earth Planet Sci Letters 21, 253-268. (2) Heiken and McKay 1974. Lunar Science V, 319-321. (3) Reid and Ridley 1973. EOS 54, 607-609.

ARMALCOLITE CRYSTALLIZATION, PHENOCRYST ASSEMBLAGES, ERUPTION CONDITIONS AND ORIGIN OF ELEVEN HIGH TITANIUM BASALTS FROM TAURUS LITTROW

M.J. O'Hara and D.J. Humphries, Grant Institute of Geology, Edinburgh University, Scotland.

Table 1 presents phase equilibria data for 12 samples of high titanium basalt. Table 2 presents results exploring the effect of varying the oxygen fugacity at a temperature of 1140±3°C. Fig. 1 shows the general form of equilibrium in relation to the run conditions for an idealised sample.

Two lava groups may be distinguished by the abundance of armalcolite in the one and its scarcity in the other at 1140°C. 71569 has intermediate character (cf ref 1). We find no obvious support for this in available analyses (but see next abstract).

Pyroxene appears with, or at a higher temperature than plagioclase in every sample other than 70275 (contrast ref 2), except in a run in iron capsules at 1140°C, fO_2 $10^{-13.86}$ atm where a small amount of FeO was almost certainly added to most of the charges by oxidation of the capsule.

Relative stability of armalcolite, spinel, ilmenite or karooite (ferri-pseudobrookite) is strongly influenced by oxygen fugacity, especially in the range most likely to apply to these rocks on the lunar surface.

Armalcolite is present with pyroxene, plagioclase and spinel at c 1140°C, in every sample, including 70017 and 70215, provided the oxygen fugacity has an appropriate value (contrast ref 2). The run at 1140°C, $fO_2=10^{-13.85}$ atm, which may have gained iron is again conspicuous in showing no armalcolite in the presence of pyroxene and plagioclase.

75035 is close in composition to a cotectic liquid simultaneously saturated with olivine, two pyroxenes, plagioclase, ilmenite and armalcolite, all these phases being observed in charges which were only a few percent crystalline (cf and contrast ref 1).

70275,6 and 70275,11 are unique, developing metal at a higher oxygen fugacity than any other samples and containing plagioclase at c 1160°C, at least 15°C above the highest temperature reported in other samples. Plagioclase is more abundant than olivine or oxide phases in the interval 1156-1137°C. If derived from the same flows as other samples, 70275 must represent material either enriched in plagioclase primocrysts, or contaminated by ANT. Section 70275,32 is a variolitic, porphyritic rock with large phenocrysts of olivines (100-1500μ), part of which may be quench, and of opaque minerals. Obvious plagioclase phenocrysts are absent, but in addition to the long lath like radially arranged feldspar crystals with cores of glass, pyroxene etc (which are obviously quenching products) there is a generation of small (70-250μ) blocky laths which contain no inclusions, and display marked zoning about a euhedral core. Their size is similar to that of anorthite phenocrysts in lithic fragments at the Apollo 11 site (ref 3) and they may represent feldspar phenocrysts in the magma. Similar crystals are absent from thin sections of 70215, 71569, 74235, 74275, four other rocks which have otherwise comparable textures.

74235, the most rapidly quenched sample, contains c 10% each of microphenocrysts of olivine and armalcolite. Texture resembles that of patches in 70215 and 71569 (where microphenocrysts of olivine and oxide phases are also recognisable: contrast 1,2) which are interstitial between spherulitic patches of pyroxene which appear to have formed during quenching, perhaps around

ARMALCOLITE CRYSTALLIZATION ETC.

O'Hara, M.J. and Humphries, D.J.

Table 1. Results in Mo capsules in 80% H_2 20% CO_2 atmosphere, or as stated

	GROUP A					?	GROUP B					
T°C	70017	74235	74255	74275	75075	71569	70215	71055	70275,6	70275,11	72135	75035
1281	KEY			z						m=iron		
1269	a=armalcolite				z					o=olivine		
1253	c=clinopyroxene (any)			sz	sz		z	z		p=plagioclase		
1229	i=ilmenite			osz	sz		sz	sz		s=spinel		
1202	k=pseudobrookite (ferri)			osz	aosz		sz	sz		z=liquid		
*1178	aiosz	aiosz	aiosz	aiosz	aiosz	aiosz	iosz	aiosz	isz	aisz	aiosz	z
1177	aosz			aosz	aiosz		osz	iosz			aiosz	
1156/7	aiosz	aioz	aiosz	aiosz	aiosz	aiosz	iosz	iosz	aiopz	aipsz	iosz	iz
1147	aiosz			aiosz			iosz	iosz			aiosz	
1144		aiosz	aciopsz		aciosz				ciopz	ciopz		ciopz
1139	aciopz			aciopsz	aciopsz		ciopsz	ciopz			aciopsz	
1124	aciopz			aciopz	aciopz		ciopz	cipz			acipz	
1110	cipz			ciopz	aciopz		cipz	cipz			cipz	
1097	cip			ciop	ciop		cip(z)	cip(z)				

*At 73% H_2 27% CO_2. **At 86.5% H_2 in Fe capsule. All optical identifications.

Table 2 Results at 1140±3°C, varying containers and oxygen fugacities. Key in table 1.

Cont	T°C	$Log_{10} pO_2$ atm	Phases present: all charges contain ciopz, ± those shown (eg ø - no pyroxene). All numbers to be prefixed 7											
			0017	4235	4255	4275	5075	1569	0215	0275,6	0275,11	1055	2135	5035
Fe^1	1140	-14.2	am	am	am	am	am	am	am	amø	amøø	am	am	amøø
Fe^1	1141	-14.1	am	asø	ams	am	am	amø	am	am	am	am	am	amø
Fe^2	1140	-13.86	asøø	søøø	søø	s	s	s	as	møø	møø	✓	sø	ø
Mo^3	1143	-13.85	as	aøøø	as	aø	a	aø	aø	a	as	asø	aøø	✓
Mo^3	1140	-13.7	as	as	as	as	as	aø	as	s	asøø	as	s	✓
Mo^4	1139	-13.4	a	-	-	as	as	-	s	-	-	✓	as	-
$Mo^4{}_5$	1139	-12.9	s	s	s	as	s	as	s	s	s	s	s	sø
$Ag_{80}Pd_{20}$	1137	- 8.2	ks	ks	ks	ks	ks	ks	ks	ksø	ksø	ks	ks	ksø

Notes to Table 2 (✓= ciopz only; - = no data)

(1) Iron metal formed from all charges; Fe^{2+}/Mg in silicates falling tends to reduce ilmenite, favour armalcolite. Reduced FeO+MgO favours pyroxene over olivine. (2) All but 70275 contained no metal,.·. have probably picked up some Fe as FeO with effects opposite to (1), and seemingly also favouring spinel appearance. (3) Iron loss to container significant. Favours armalcolite, but higher fO_2 favours spinel. (4) Iron loss to container slight. Rising fO_2 favours spinel, disfavours armalcolite. (5) Karooite (ferripseudobrookite) present. Spinel abundant, non-magnetic. Rising Fe^{3+}/Fe^{2+} disfavours olivine.

References

(1) Walker et al. Geochim Cosmochim Acta (in press)
(2) Longhi et al 1974. Proc 5th Lunar Sci Conf Geochim Cosmochim Acta Suppl 5.
(3) O'Hara et al 1974. Earth Planet Sci Letters 21, 253-268.
(4) Reid and Ridley 1973. EOS 54, 607-609.
(5) Heiken and McKay 1974. Lunar Science V, 319-321.

ARMALCOLITE CRYSTALLIZATION ETC.

O'Hara, M.J. and Humphries, D.J.

original pyroxene microphenocrysts (tentatively identified in 71569). Clinopyroxene formed readily during quenching of experimental charges from c 1140°C.

74275, the sample with the most conspicuous and abundant olivine phenocrysts, retains olivine to a higher temperature than any other sample studied.

Conditions of eruption of the lavas may be estimated from observed presence of microphenocrysts (primocrysts) of plagioclase, pyroxene ?(both sparse), ilmenite (inc 70215) olivine (most rapidly cooled samples) and armalcolite as c 1145-1147°C and their oxygen fugacity from relative abundance of spinel, paucity of armalcolite in group B samples, as c $10^{-13.5}$ - $10^{-12.5}$ atm.

Average magma composition must have been closer to that of 75035, the liquid phase in experiments at c 1145°C, and the average mare glass I (ref 4; see next abstract) than to that of most hand specimens, if soil compositions are to be explained in terms of target rock + orange soil + massif derived component in observed proportions (ref 5). The suggestion that substantial evolution of the liquids took place within the flow after its arrival at the site, with development of plagioclase saturated liquids only in the upper portion, which then preferentially formed the soils (ref 1) cannot be sustained when complete penetration of at least one flow unit is required to account for the age and exposure age of the orange soil, 74220. The thermal regime required is, in detail, implausible. Besides, all rapidly cooled hand specimen samples of more mafic materials show presence of phenocrysts of olivine and iron titanium oxides, and do not represent real liquid compositions (contrast refs 1,2).

Petrogenesis. Hand specimens were derived by crystal sinking and ?floating within a plagioclase saturated average magma composition. The average magma was saturated with olivine, pyroxenes, plagioclase, spinel, ilmenite and armalcolite and perhaps metal at low pressure, and could therefore have evolved as a residual liquid during previous low pressure fractional crystallization of any combination of these phases. Prior fractionation of plagioclase provides the only satisfactory explanation of the europium anomaly. The chemistry of Cr, V, Rb, Sr and other incompatibles in these rocks is no impediment to such a model, and indeed supports it (ref 3).

Orange soil 74220. Data shown in table 3. The possibility that this type of composition represents distillate or residue during gas escape at top surface of flow is being investigated (the rocks are vesicular).

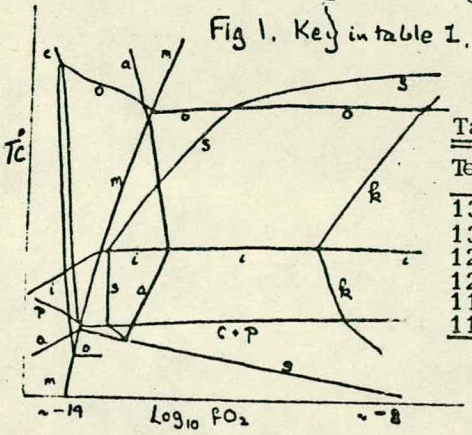


Table 3. Data for 72220

Temp°C	Log_{10} fO_2 atm	Phases	Temp	fO_2	Phases	Temp	fO_2	Phases
1352	-11.2	oz	1163	-13.3	iosz	1140[3]	-13.7	aciosz
1325	-11.5	osz	1152	-13.5	iosz	1139[4]	-12.9	ciosz
1279	-12.0	osz	1140	-14.2	acimopsz[1]	1137	-8.2	cikosz
1207	-12.8	osz	1141	-14.1	acimosz[1]	1129	-13.8	ciopz
1178	-12.8	iosz						
1177	-13.1	iosz	1140	-13.86	iosz[2]			

Key in table 1; Notes as table 2

NATURAL ENVIRONMENT RESEARCH COUNCIL

PROGRESS IN EXPERIMENTAL PETROLOGY

SECOND PROGRESS REPORT OF RESEARCH SUPPORTED BY N.E.R.C. AT EDINBURGH AND MANCHESTER UNIVERSITIES, 1969–1971

EDITORS
C. M. B. HENDERSON and D. L. HAMILTON

The Natural Environment Research Council
Publications Series D No. 2 1972

MELTING RELATIONS IN MARIA SURFACE BASALTS

G. M. Biggar, C. E. Ford, D. J. Humphries, B. G. Jamieson,[1]
M. J. O'Hara, A. Peckett[2] and S. W. Richardson[3]

Our experimental work carried out on samples collected by the first two manned lunar landings, and on synthetic analogues, has been published (O'Hara *et al.*, 1970; Biggar *et al.*, 1971). The studies covered the pressure range 10^{-8} to $3{\cdot}7 \times 10^{4}$ bars at temperatures from 1000-1500°C and at oxygen fugacities ranging from 10^{-17} to 10^{-7} bar.

Combined where appropriate with petrographic data from the natural rocks these experiments have yielded information about the eruption temperatures, cooling rates and orders of crystallization on eruption. Several groups of lavas can be recognised at the Apollo 12 site on the basis of crystallization behaviour. Reaction relationships involving spinels, armalcolite and olivine have been demonstrated and are evidenced in the petrology. Analyses of crystals formed at appropriate temperatures in the experimental charges compare closely with those observed as natural phenocrysts. Equilibrium residual liquid trends have been established.

The major observational result from the work has been the demonstration that both sets of samples have compositions close to those of liquids in cotectic equilibrium at low pressure with 5 or 6 crystalline species, protohypersthene being prominent in the Apollo 12 group.

The cotectic character is controlled by extreme fractional crystallization in underlying lava lakes over whose crusts the magmas have erupted. The complementary cumulus is deduced to be mineralogically and chemically similar to the howardite-achondrites; the hypothesis of achondrite development by igneous differentiation in the lunar maria is thus strongly supported by these results.

Volatilisation, of alkalis particularly, was demonstrated to be a significant effect (see before) when lunar lavas erupt into hard vacuum, and may have been responsible for imposing the low content of all volatile elements and the low oxygen fugacity upon less distinctive parental liquid compositions. Reduction consequent on volatilisation losses may have caused early precipitation of metallic iron at the base of the maria structures, and may be an important factor in mascon formation (Biggar *et al.*, 1971; O'Hara *et al.*, 1971). The possibility of early ilmenite cumulus forming and causing mascon effects

[1] Natural Environment Research Council, London.
[2] Department of Geology, University of Durham.
[3] Department of Geology, University of Oxford.

was briefly entertained in the light of Apollo 11 data but did not survive the results from Apollo 12.

Apollo 11 and 12 samples could not represent average lunar composition because of the eclogite forming reaction which would lead to too high a density for the moon as a whole (this conclusion is general for any basic igneous rock).

Due to the unassessable influence of near surface fractionation and volatilisation on the returned lava samples, it has been impossible to justify any conclusions concerning the detailed mineralogy or chemistry of the lunar interior.

LAKAGIGAR FISSURE ERUPTION

J. D. BELL[1] AND D. J. HUMPHRIES

Between early June 1783 and early February 1784 in southern Iceland c. 12·5 km^3 (Thorarinsson, 1970) of barely quartz-normative tholeiitic flood basalt erupted from a S.W.–N.E. trending fissure 25 km in length and rarely more than 10 m. in width. This was the largest eruption of lava ever observed in historical times. Assuming no significant variation in width, with time or depth, of the fissure, the magma could have filled it to a depth of 50 km prior to eruption. Based on the same assumptions an average vertical flow-rate would be about 0·2 mm/sec which seems too fast for crystal settling to have occurred, if the movement were uniform. *Surface* flow rates were not uniform, for in the first 50 days of the eruption 10 km^3 lava was extruded from the S.W. section of the fissure, a rate of $2{\cdot}2 \times 10^3$ m^3/sec (Thorarinsson, 1970, p. 913), indicating a vertical flow rate of 1 mm/sec. For the last 200 days of the eruption activity was virtually confined to the N.E. section of the fissure whence erupted 2·5 km^3 lava at an average rate of $1{\cdot}2 \times 10^2$ m^3/sec, indicating a vertical flow rate of 0·25 mm/sec, i.e. similar to the overall average figure above.

The presence of normative quartz combined with the presumably low initial water content (<0·5 wt.%), nevertheless suggest that the magma could not have been derived by direct partial melting of a peridotite source at pressures greater than 2-5 kbars.

Previous descriptions of the flow and the extensive sampling on which the present work is based show that the lava is remarkably uniform in chemical composition and petrography over its 565 km^2 outcrop. Phenocrysts and microphenocrysts form 3-26 vol.% of the samples with plagioclase especially prominent and accompanied by clinopyroxene and olivine in that order. Occasional 1 cm glomeroporphyritic clusters of these three phases (olivine gabbro) are present.

The composition and temperature of eruption of this lava clearly approximated closely to those of a liquid in cotectic equilibrium with plagioclase, olivine and clinopyroxene, at or near atmospheric pressure because the phenocrysts either formed, or survived, in mobile lava at or near the surface for some weeks.

This report concerns results on 10 of the 100 samples collected in August 1970. The experiments were carried out at atmospheric pressure in molybdenum capsules at the oxygen fugacity of the Fe/FeO equilibrium in an

[1] Department of Geology, University of Oxford.

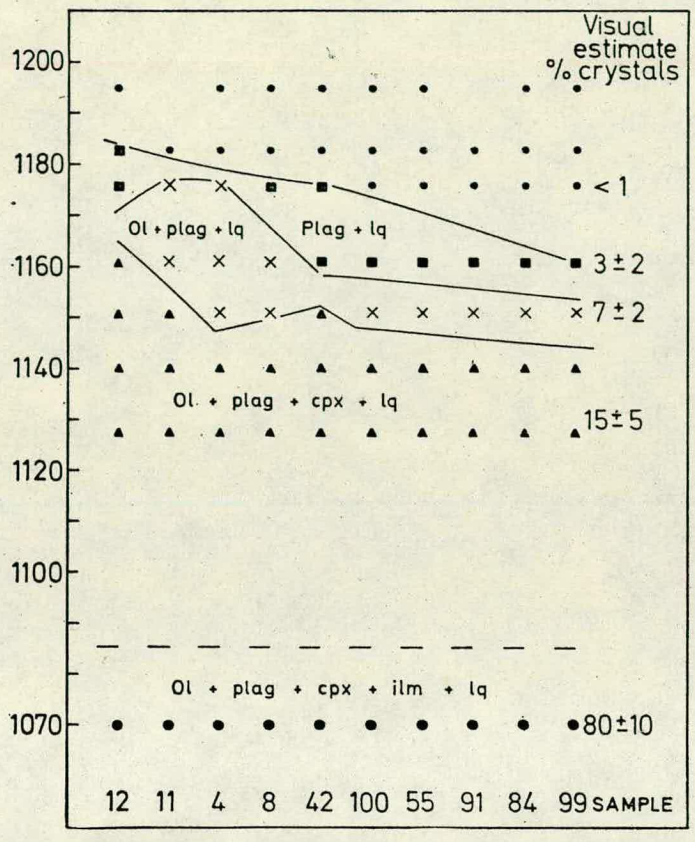


FIG. 31. Melting relations of basalts from Iceland determined at the f_{O_2} of the Fe:FeO buffer at atmospheric pressure in molybdenum capsules.

atmosphere also containing c. 0·25 bar H_2O. The charges were held at constant temperature for periods of 3 to 6 hours. Plagioclase is the liquidus phase, encountered between 1185°C and 1161°C (fig. 31). It is joined a few degrees lower by olivine when the samples were estimated visually to be 1-5% crystalline. The third phase to enter is clinopyroxene at temperatures between 1162°C and 1140°C. Small variations in temperature cannot be correlated unambiguously with small variations in chemical composition. Cotectic crystallization is encountered when the samples are estimated to be 2-10% crystalline. It may be deduced that the lava was erupted at a temperature of 1150° ± 10°C.

Three outstanding questions to be answered are: (i) why is plagioclase on the liquidus? (ii) what is the mechanism of eruption and the immediate source of the lava which permit imposition of low pressure cotectic character on such a large and uniform body of magma? (iii) how widely applicable to the situation in Iceland—and elsewhere—might such processes be?

It may be noted that other investigations (Tilley *et al.*, 1964) of the melting

behaviour of lava from a prehistoric Icelandic fissure eruption, that of Eldgja-Katla which runs parallel with, and some 7 km N.W. of, the Lakagigar, showed that plagioclase was again the liquidus phase either alone at 1120°C, or with clinopyroxene at 1140°C and that cotectic character was achieved within a temperature fall of 10-20°C. Our own investigation of a sample of the Eldgja lava collected in 1970 shows olivine and plagioclase present on the liquidus at 1140°C, joined by clinopyroxene at about 1130°C. Analyses of the Eldgja lava show it to be chemically more variable than the Lakagigar flow while remaining virtually aphyric throughout its extent. Our sample is less siliceous and more magnesian than those quoted by Tilley *et al.* (1964) and was also melted under conditions of different oxygen fugacity.

The total volume of the Lakagigar eruption is about 2·5% of the volume of the Skaergaard intrusion, considered to have been emplaced as a single intrusive event. Tilley *et al.* (1964, 1965) have shown the liquidus phase for the Skaergaard chilled marginal gabbro is plagioclase (1230°C), followed by olivine (1200°C) and clinopyroxene (1190°C), the order usually observed in the Lakagigar samples.

The oceanite series has olivine as liquidus phase at temperatures ranging from 1200°-1450°C, possibly reflecting olivine accumulation within less olivine-rich liquids. All show the appearance of plagioclase, quickly joined by clinopyroxene, at temperatures generally between 1190°C and 1150°C. Ilmenite does not begin to crystallize until ~1115°C, and the samples were effectively solid by 1065°C. Eruption temperatures, deduced from phenocryst assemblages appear to have been 1165°C to somewhat greater than 1190°C, apparently a little lower in rocks of higher Fe/Fe+Mg. A projection of these compositions from olivine (fig. 33) shows them to be grouped on, or to the plagioclase-rich side of, the atmospheric pressure olivine-plagioclase-clinopyroxene cotectic locus, astride the olivine gabbro thermal divide. The deduced position of the locus from these compositions (all Fe as FeO) is nearly identical with that deduced from Hawaiian lavas (Jamieson, 1970; original Fe_2O_3 retained, experiments probably at higher f_{O_2}). A projection from diopside (fig. 34) illustrates the strong olivine control dominating the spread of compositions and causing the high liquidus temperatures in samples 331, 243, 75.

The differentiated series have predominantly higher Fe/Fe+Mg, except for 512, which differs from the majority of oceanite series rocks in having plagioclase entry above 1200°C, following olivine, and the series as a whole is distinguished by having plagioclase either on the liquidus or following

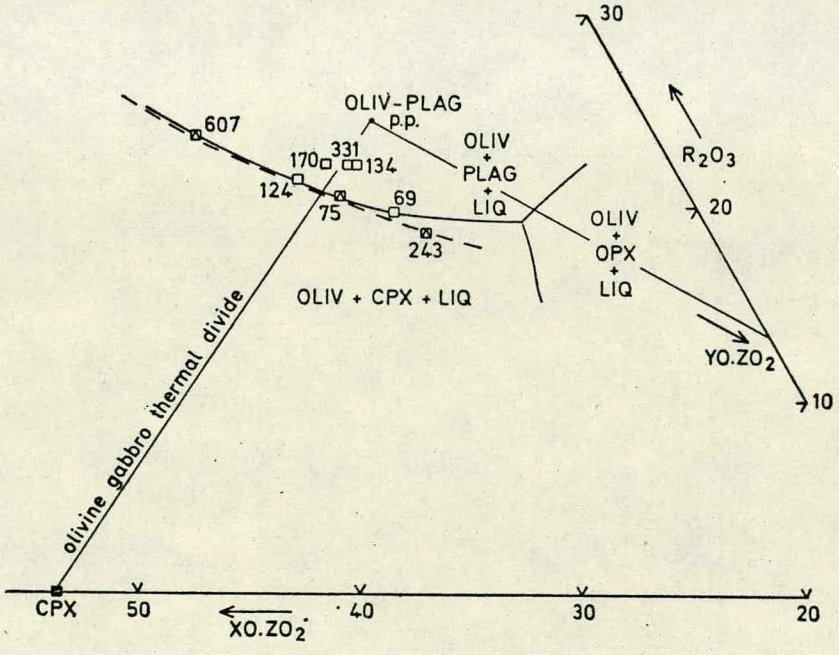


FIG. 33. Olivine projection into the plane $YO.ZO_2$–$XO.ZO_2$–R_2O_3 of Reunion melted rocks. Olivine first phase, followed by either plagioclase □ or plagioclase+clinopyroxene ⧄. Solid phase boundaries from Jamieson (1970); dashed boundary that of Reunion rocks.

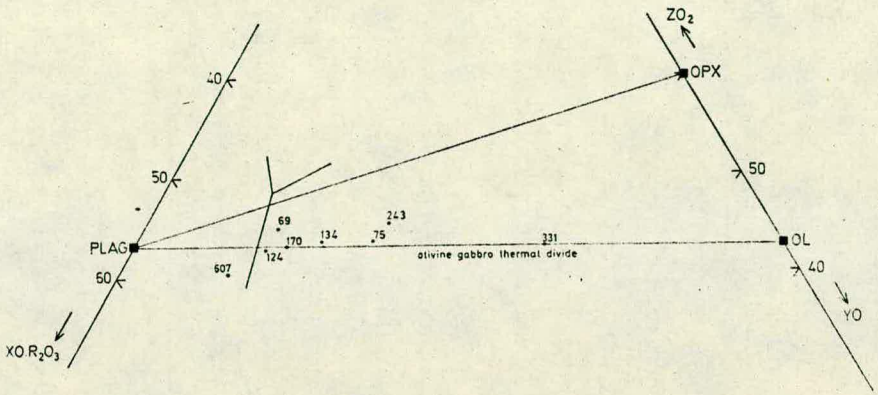


FIG. 34. Clinopyroxene projection into the plane $XO.R_2O_3$–YO–ZO_2 of Reunion melted rocks.

shortly upon olivine with clinopyroxene appearance significantly delayed, i.e. the sample compositions are appreciably displaced from the atmospheric pressure cotectic locus, and if the differentiation involved gabbroic fractionation, it may have occurred at some appreciably higher pressure. This conclusion can only be tentative in view of the uncertainties about the appropriate f_{O_2} to use for experimentation. Upton & Wadsworth (1970) suggest a floor for the chamber in which differentiation occurred barely 5 km ($\sim 1\frac{1}{2}$ kbars) below the surface. A pressure increase of this magnitude, particularly if accompanied by a rise of H_2O content, might be sufficient to produce the required shift of the cotectic liquid locus towards what is the plagioclase primary phase volume at atmospheric pressure.

MELTING DATA FOR VOLCANIC ROCKS FROM ADEN, SOUTH ARABIA

D. J. HUMPHRIES AND K. G. COX

The Aden volcanics (Cox *et al.*, 1970) are currently receiving intensive petrographic and chemical study by P. G. Hill. Quenching experiments are being carried out on 15 rocks ranging from basalt to trachyte in composition. Provisional results are given in fig. 35. The majority of the rocks show a substantial interval of plagioclase crystallization before the entry of other phases. This is consistent with the conclusion reached by Hill (unpublished thesis) that most of them are enriched in cumulus plagioclase during low-pressure crystallization. However, three aphyric rocks (trachyte 828 and mugearitic trachybasalts 833 and 847) also have plagioclase on the liquidus, though over what temperature range is still uncertain. It may be necessary to postulate the fractionation of the appropriate magmas under conditions of elevated water pressure to account for the observed phase relations.

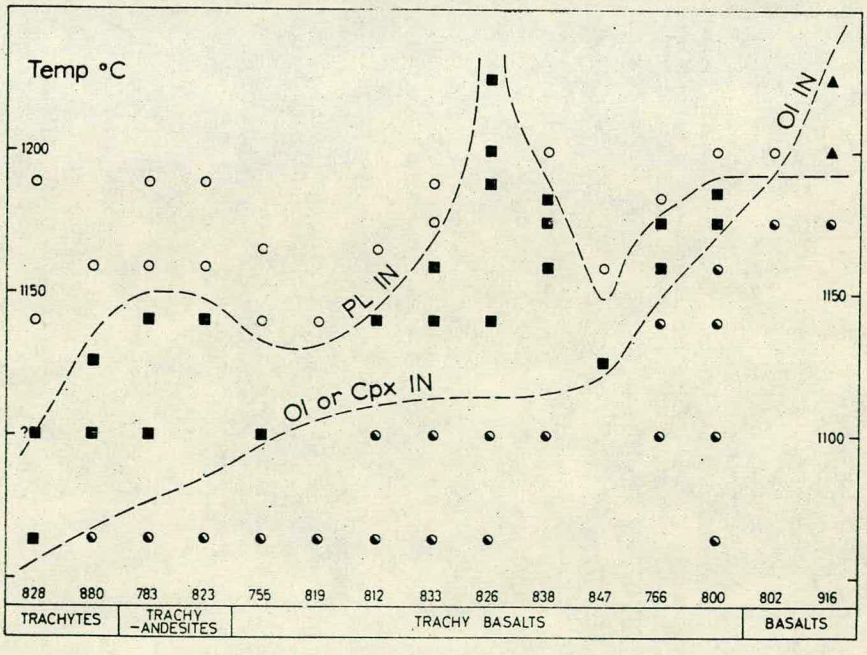


FIG. 35. Melting relations at atmospheric pressure of Aden volcanic rocks, at the f_{O_2} of the Fe:FeO buffer, samples contained in molybdenum capsules.

LIQUIDS IN EQUILIBRIUM WITH PLAGIOCLASE, OLIVINE AND AUGITE

D. J. HUMPHRIES

The curvilinear locus of liquids in 4 2 **E** fo, di, an, lq at atmospheric pressure was described in a projection from forsterite (N.E.R.C. Rept. 1, pp. 129-152). The analogous pseudo-linear locus of Liquid in C F **E** ol, cpx, plag, lq in natural basalt systems have also been described (Jamieson, 1970). The location of the piercing curve of the locus of Liquid in 5 3 **E** fo, di, plag, lq in the diopside-forsterite-plagioclase volume of CaO–MgO–Al_2O_3–SiO_2–Na_2O has been studied using compositions made up to be just within the forsterite primary phase volume. The technique used has been calibrated (Biggar *et al.*, in press), and all runs were made at atmospheric pressure in platinum capsules in air, using runs of 7 days or more.

Results are presented as a projection from forsterite (fig. 36), illustrating the extent of the lowering of the cotectic temperature, and the increased plagioclase/clinopyroxene ratio in the cotectic liquid compositions as the bulk normative feldspar becomes more sodic.

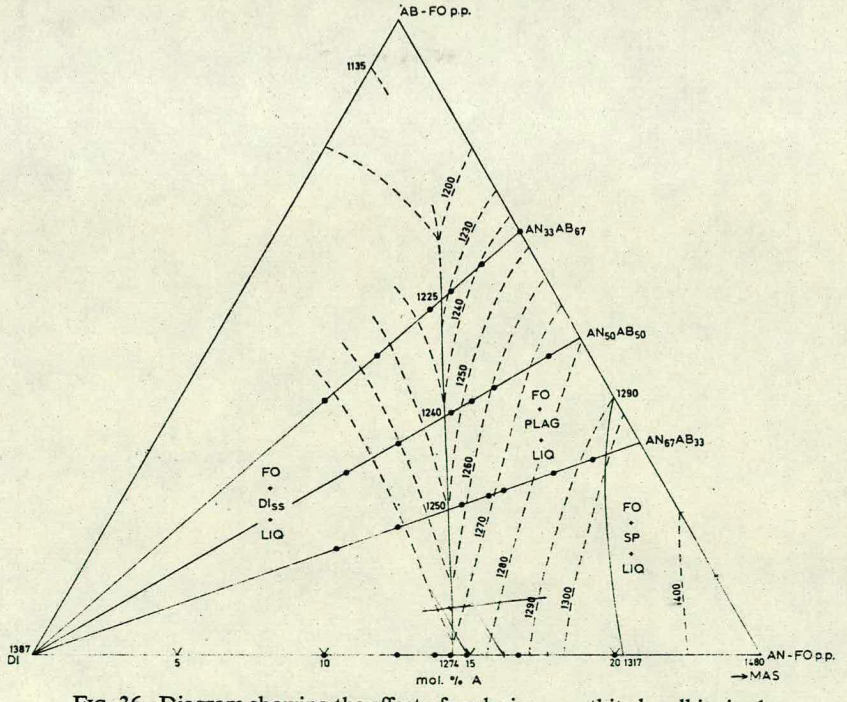


FIG. 36. Diagram showing the effect of replacing anorthite by albite in the equilibrium olivine–plagioclase–augite–liquid, plotted in the join Diopside –MAS of the olivine projection into CS–MS–A (Rept. 1, p. 130).

FLOW SHEET FOR $CaO–MgO–Al_2O_3–SiO_2$ AT ATMOSPHERIC PRESSURE

D. J. Humphries, G. M. Biggar and M. J. O'Hara

Our latest understanding of subsolidus assemblages, isobaric invariant and univariant equilibria in the system $CaO–MgO–Al_2O_3–SiO_2$ at atmospheric pressure is summarised in the flow sheet in fig. 56 which incorporates a number of changes from that published by Osborn *et al.* (1969, fig. 4). These relate to the following regions of the system:—

(1) anorthite–sapphirine is recognised as a stable assemblage introducing 3 invariant points to replace D of Osborn *et al.* (1969).

(2) diopside–spinel is recognised as a stable assemblage instead of anorthite–forsterite–melilite (O'Hara & Biggar, 1969), introducing 3 invariant points to replace 11 and 17 of Osborn *et al.* (1969).

(3) bredigite (C_5MS_3) is recognised as a distinct phase stable in the subsolidus and at least to 1400°C, preventing merwinite (C_3MS_2) coexisting with C_2S (Biggar, 1971). This introduces 4 new invariant points replacing 28 and 37 of Osborn *et al.* (1969).

(4) the quaternary phase C_6A_4MS is recognised as stable with gehlenite, C_2S, spinel, periclase, CA, $C_{12}A_7$, and C_3A_2M, the last of these also being recognised as a phase for the first time in drawing the flow sheet. These changes introduce 10 new invariant points, replacing 35, 36, 42 of Osborn *et al.* (1969).

(5) while 6, 7, 9, 10 of Osborn *et al.* (1969) have been retained, the possibility that the join $diopside_{ss}$–pseudowollastonite is stable instead of anorthite–wollastonite–melilite and/or anorthite–wollastonite–tridymite has been entertained. If true this would introduce 3 or 6 new invariant points replacing 2 or 4 of those listed by Osborn *et al.* (1969). This possibility depends upon the solid solutions in diopside being markedly poor and/or rich in silica with respect to the wollastonite–enstatite–alumina plane. This problem is still under investigation.

Useful information can be extracted from this figure concerning the melting and crystallization of basic refractories (periclase-bearing equilibria); cements (C_3S, C_2S-bearing equilibria); firebricks (corundum, mullite-silica and CA_6 bearing equilibria); slags (melilite-bearing equilibria); simplified basalts (forsterite; diopside and anorthite-bearing equilibria) and partial melting during thermal metamorphism of shales (cordierite, spinel and sapphirine-bearing equilibria).

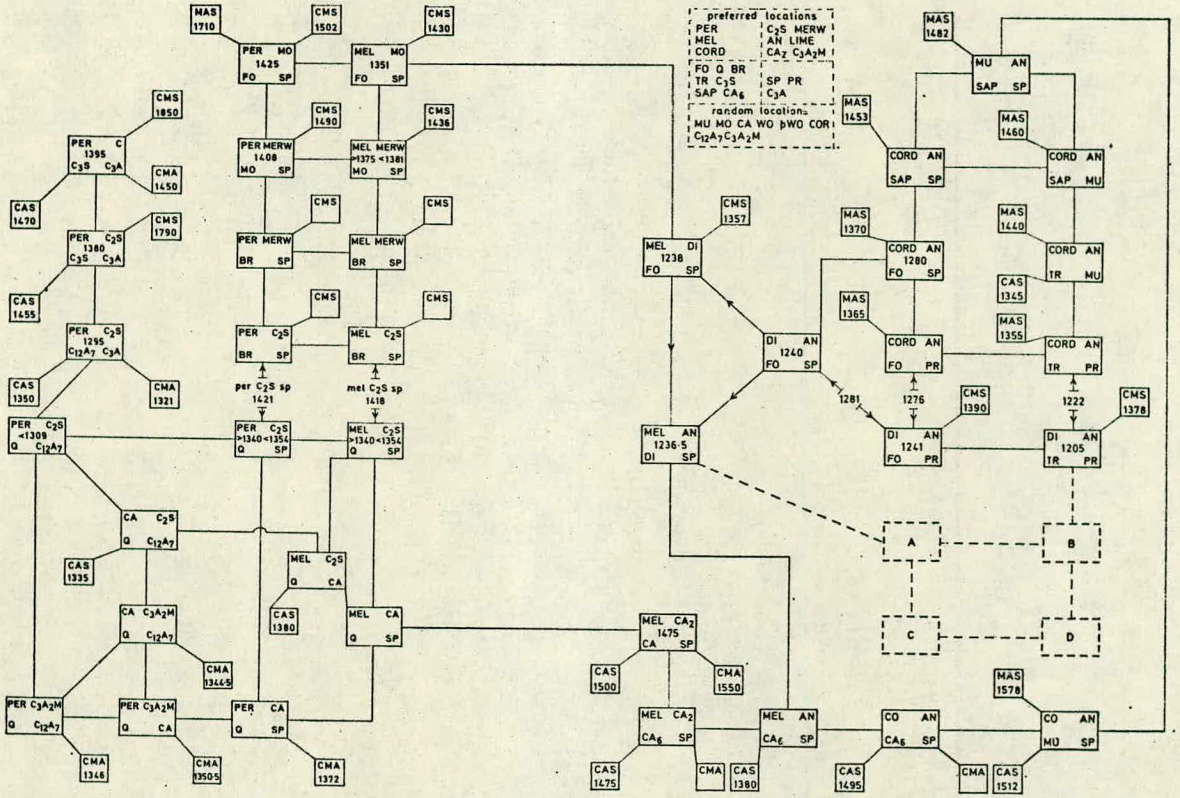


FIG. 56. Atmospheric pressure flow diagram for subsolidus equilibria in the system C–A–M–S. In the larger boxes are listed the phases present in divariant equilibria and the temperature at which they develop liquid and become univariant. Smaller boxes represent terminations of quaternary equilibria in ternary systems.

As far as possible the phases are listed in specific locations to facilitate the finding of particular sets of equilibria. Thus all the equilibria containing periclase have PER in the top left hand corner. An inset shows the preferred positions of these phases. The positions of the ternary boxes relative to the quaternary ones are also fixed, for example all CMS equilibria are shown to the top right of the quaternary box. Boxes ABCD contain wollastonite and pseudowollastonite bearing equilibria.

DICALCIUM-SILICATE AND SPINEL SATURATED EQUILIBRIA

D. J. HUMPHRIES

Treatment of crystal-liquid equilibria in multicomponent systems presents many problems. In the case of 4-component systems, such as CaO–MgO–Al_2O_3–SiO_2 some of the problems can be overcome by projecting from the composition of an important crystalline phase all the liquid compositions with which that phase can be in equilibrium. These projections may be made into any convenient plane or planes.

Such projections, showing subsolidus, polythermal liquidus and isothermal data have already been prepared for the periclase-saturated equilibria, and their application in basic refractories technology outlined (O'Hara & Biggar, 1970). A similar projection for the geologically important forsterite-saturated equilibria was presented and discussed in detail in the previous report (Rept. 1, pp. 129-152).

In this report projections of the C_2S and spinel saturated equilibria are presented (figs. 57, 58) with little accompanying text because sufficient has already been published about the projections from periclase, forsterite, and part of that from C_2S relevant to cement technology (Biggar, 1971) to indicate how they can be read. This type of diagram, like the flow sheet above, collects and condenses a vast amount of phase equilibria information.

On the enlarged portion of the spinel projection (fig. 59), data points from Schairer & Yoder (1970) only have been plotted to elucidate the geometrical relationships of the diopside+spinel-bearing isobaric invariant points to their subsolidus tetrahedra. The following conclusions can be drawn (Rept. 1, 114-120):—

(i) The isobaric invariant point $an+di_{ss}+sp+mel+liq$ is a eutectic.

(ii) The isobaric invariant point $mel+di_{ss}+sp+fo_{ss}+liq$ is a reaction point involving $forsterite_{ss}$ reaction with the liquid.

(iii) The isobaric invariant point $di_{ss}+an+sp+fo_{ss}+liq$ is a double reaction point involving anorthite and $forsterite_{ss}$ reaction relationships with the liquid. Consequently, there can be no maximum on $di_{ss}+sp+fo_{ss}+liq$ as suggested by Schairer & Yoder (1970), unless anorthite is not the third phase in those compositions richer in spinel than $diopside_{75}$ $spinel_{25}$ on the diopside–spinel join (cf. Schairer & Yoder, 1970, fig. 8).

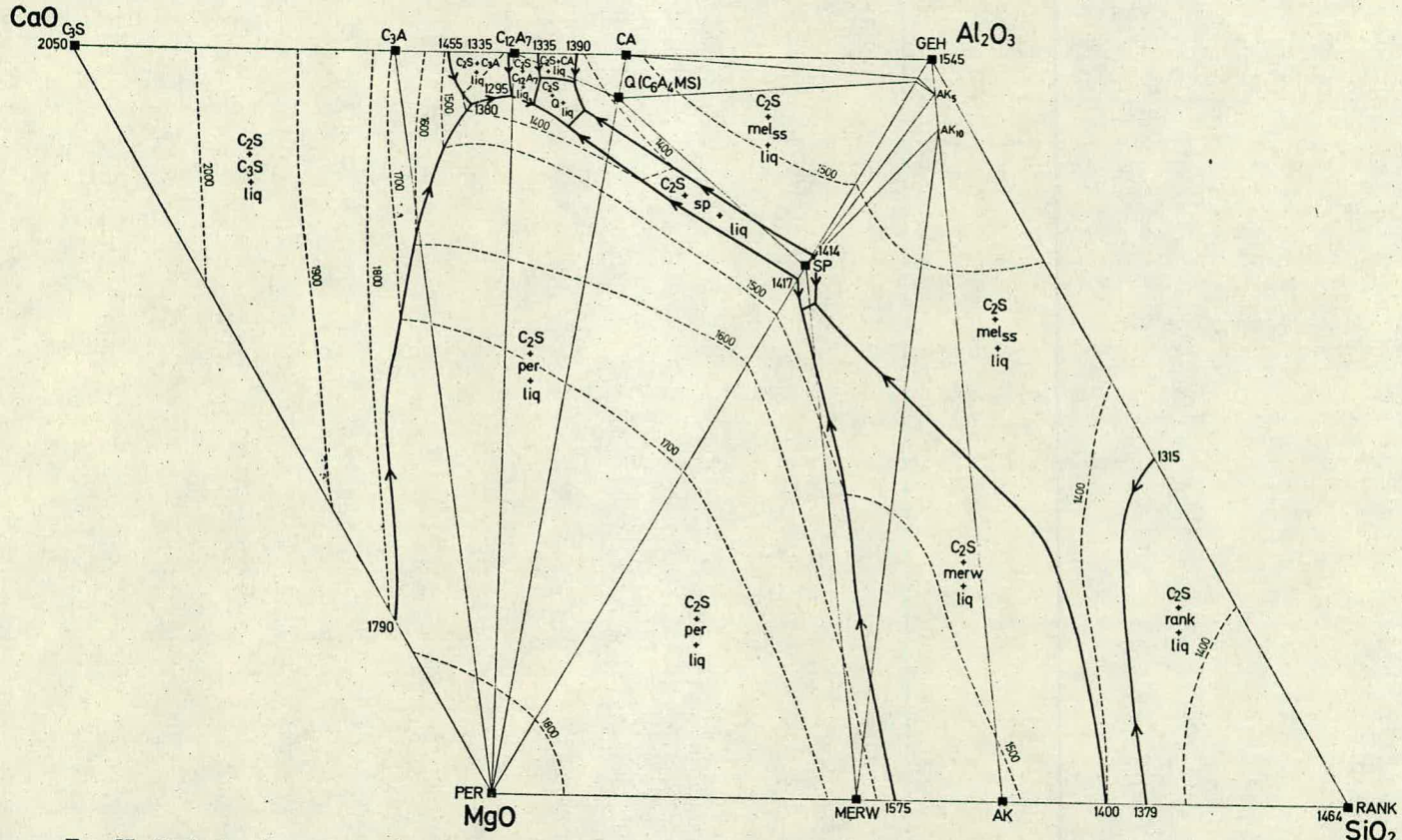


FIG. 57. Projection from C_2S into the planes C–M–A and M–A–S of the C_2S primary phase volume, boundaries from previously published data.

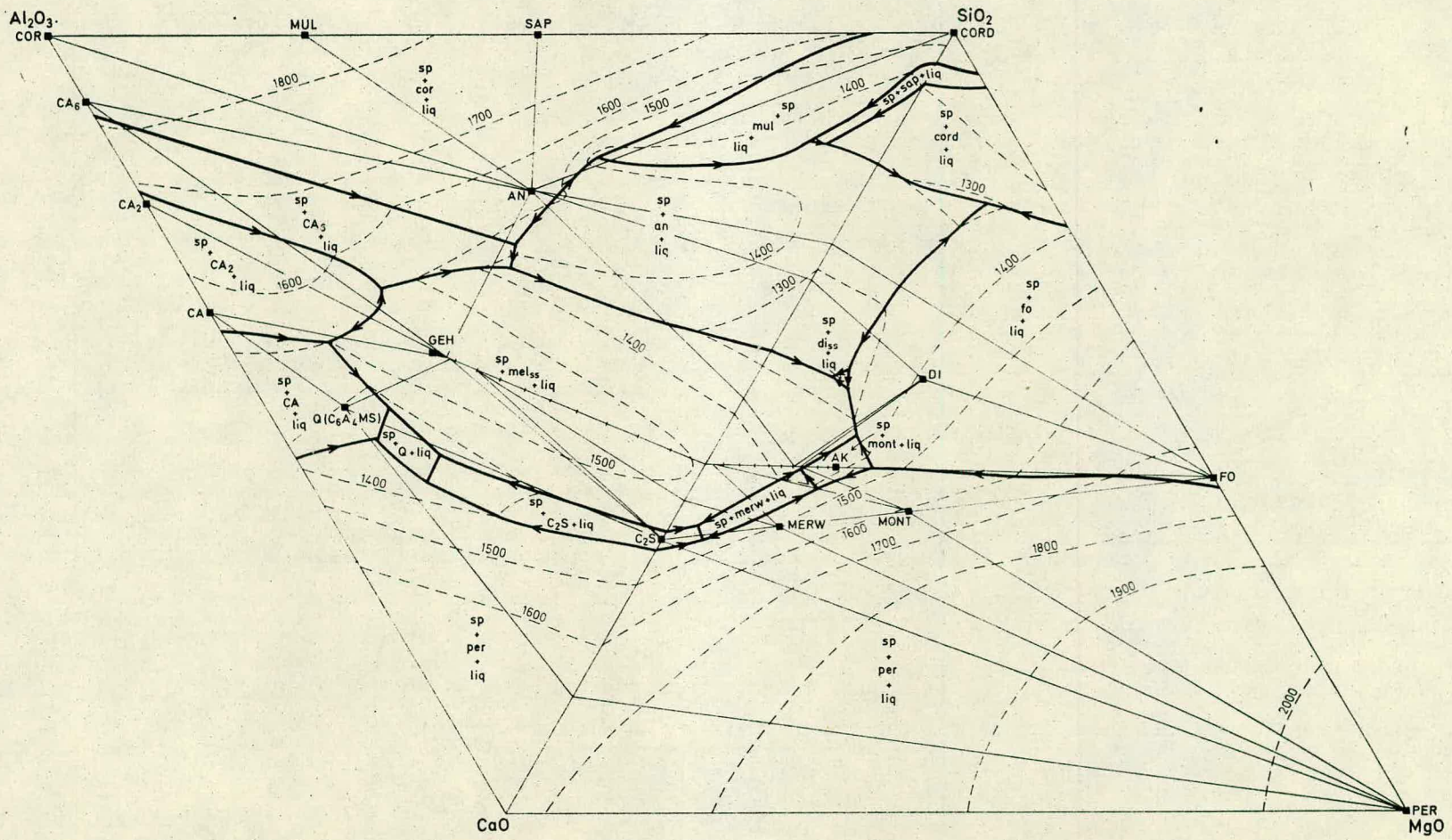


FIG. 58. Projection from spinel into the planes A–S–C and C–S–M of the spinel primary phase volume, boundaries from previously published data.

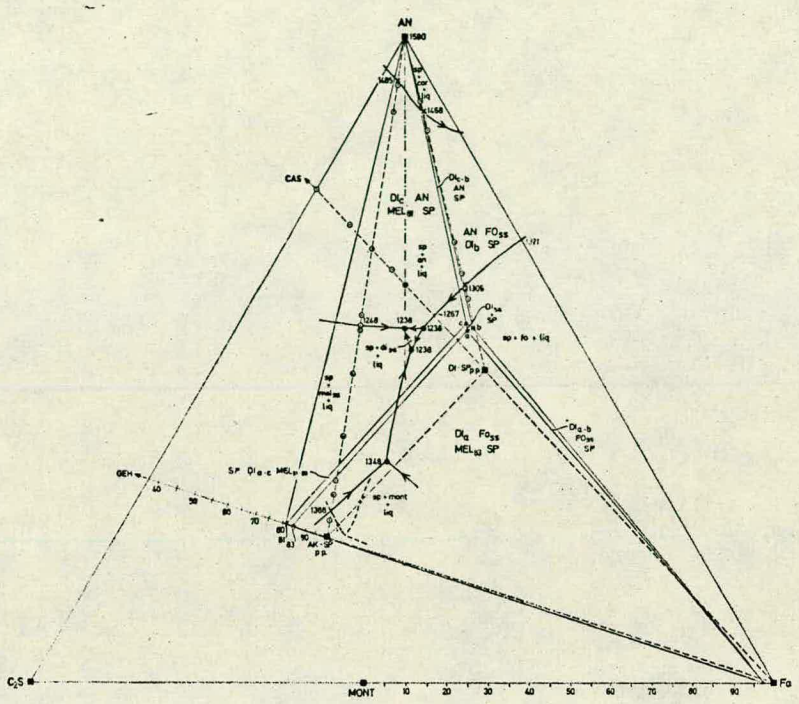


FIG. 59. Projection of the spinel primary phase volume from spinel into the plane C_2S–AN–FO based on the data of Schairer & Yoder (1970). Diopside compositions are from (Rept. 1, p. 97-104), forsterite$_{ss}$ values (unpublished), melilite$_{ss}$ values from (Rept. 2, p. 127-130) and the position of the univariant equilibrium sp + mont + mel$_{ss}$ + fo$_{ss}$ + liq is from (Rept. 2, p. 131-137). The univariant equilibrium sp + di$_{ss}$ + an + mel$_{ss}$ + liq must lie along the dot-dash line. Heavy dash lines are inferred boundaries of Schairer & Yoder (1970).